DESIGN AND DEVELOPMENT OF ELECTROCHEMICAL GAS SENSORS

by

ROBERT YATSHEIN CHAN-HENRY

A thesis submitted to CITY UNIVERSITY, in the Department of Chemistry, in part fulfilment of the requirements for the Degree

of

DOCTOR OF PHILOSOPHY

This investigation was mainly carried out
at CITY TECHNOLOGY LIMITED

December 1992

VOLUME 2

Carbon Monoxide Sensor Reports

Volume 1 : Linking Summary
Volume 2 : Carbon Monoxide Sensor Reports

CONTENTS

COMMERCIAL IN CONFIDENCE

This thesis is based on proprietary work undertaken at City Technology in collaboration with British Coal and is the subject of several patents. The thesis will therefore be lodged in the Library of City University under restricted circulation and no disclosures may be made without the express, written permission of:

BRITISH COAL CORPORATION
Ashby Road, Stanhope Bretby,
Burton-on-Trent, Staffs. DE15 0QD

Telephone: Burton (0283) 550500
Telegrams: Coalboard Burton
Fax: (0283) 550500 ext. 31118

HEADQUARTERS TECHNICAL DEPARTMENT

and

CITY TECHNOLOGY LIMITED
Walton Road
Portsmouth PO6 1SZ
England

Telephone: 44 705 325-511
Fax: 44 705 386-611

CITY TECHNOLOGY CENTRE

Report No. 79/31/002
September 1979.

City Technology Ltd.,
The City University,
Northampton Square,
London, EC1 OHB.

10. CARBON MONOXIDE SENSOR FOR USE IN COAL MINES

Phase 1.

A.D.S. Tantram
R. Chan-Henry
B.S. Hobbs

Mr. L.R. Cooper,
National Coal Board,
Mining R & D Establishment,
Stanhope Bretby, Staffs.

NCB Contract Ref. Y 135007/09/21
CTL Project No. 94.95.31.

ABSTRACT

This report presents the results of the first phase of a program to develop a carbon monoxide sensor for use in coal mines. The overall objective of this phase was to examine the feasibility of combining the principles demonstrated by the NCB (Yorkshire) CO detector with the basic gas sensor technology developed by City Technology Limited for oxygen sensors.

Achievement of this objective required the devotion of a considerable proportion of the effort in the following areas:

- basic electrochemical measurements to gain a sound understanding of the mode of operation of the NCB cell.

- development and assessment of electrode fabrication techniques.

- evaluation of alternative electrocatalytic materials and electrolyte systems.

These studies established an acid electrolyte, platinum electrocatalyst as the favoured system for further development, although there remains a final choice of acid type and concentration and whether Pt or Pt/Au electrocatalysts are employed. Alkaline electrolytes resulted in high carbon monoxide signals from gold electrodes but suffered from interference by carbon dioxide. Neutral salt electrolytes were free of carbon dioxide interference but the electrocatalysts studied lacked sufficient activity towards CO oxidation.

Experimental prototype sensors were made, using sulphuric acid electrolytes, platinum or platinum/gold electrodes and plastic hardware. These sensors embodied a number of novel features compared to conventional CO sensor designs, including a "close sandwich", wicking electrolyte arrangement and a gaseous diffusion barrier. Initial performance tests were very encouraging. Sensor resolutions were better than 1 ppm with a stable linear response of about 0.1μA per ppm and low temperature coefficients (0.2 to 0.4 % per ^{o}C). The design had very good attitude stability which was virtually unaffected by gas bubbles in the electrolyte reservoir caused by water evaporation.

Longer term testing has necessarily been restricted to periods of several weeks. The all .platinum systems have demonstrated stable baselines and signals over this time and one sensor had completed 3 months at the time of reporting. Platinum/gold sensors were similarly very stable up to 5 weeks but were beginning to show signs of deterioration at 6 weeks.

Future development work will need to be primarily devoted to producing suitable acid resistant hardware for production prototype sensors and the evolution of a production process for electrode manufacture.

CONTENTS

LIST OF TABLES

LIST OF FIGURES

1. BACKGROUND.

The overall objective of this project was to combine the principles demonstrated by the NCB (Yorkshire Laboratories) carbon monoxide detector to the basic gas sensor technology developed by City Technology Limited (CTL) for oxygen sensors. It was also hoped that it might prove possible to shorten the hardware development stage by making use of the CTL oxygen sensor hardware.

The CTL oxygen sensor is of the self-powered, diffusion limited, metal-air battery type. It embodies an aqueous electrolyte and a lead anode coupled with an air cathode at which oxygen ingress is restricted by a diffusion barrier. This barrier ensures that all the oxygen is consumed as it reaches the cathode, where its concentration approaches zero. The rate at which oxygen diffuses through the barrier is then solely dependant on its concentration in the atmosphere and therefore, a direct link exists between oxygen concentration and the limiting current, which is the signal from the sensor.

Other oxygen sensors of this general type have used very thin plastic membranes for the diffusion barrier. Such membranes not only suffer handling and stability problems, but also inevitably result in high temperature and pressure coefficients. The CTL sensor uses a gaseous diffusion barrier which can take the form of a simple capillary hole. This not only provides an extremely robust and stable barrier but entirely different diffusion laws apply with the following important practical consequences:

(a) Temperature coefficients at least an order of magnitude less than those of solid membranes. For many purposes temperature compensation is unnecessary.

(b) Sensor measures oxygen concentration directly, compared to solid membranes which depend on partial pressure.

The CTL oxygen sensor hardware makes full use of well-proven nickel-cadmium battery component designs and production technology with resulting benefits in robustness, integrity, reliability, cost and suitability for volume production.

In principle the basis of the CTL oxygen sensor is applicable to any gaseous substance which can be caused to react electrochemically at an electrode. Car bon monoxide undergoes anodic oxidation at suitably catalysed electrodes as follows (see Appendix 1.):

$$CO + H_2O \longrightarrow CO_2 + 2H^+ + 2e.$$

Thus a carbon monoxide analyser can be envisaged comprising the essential elements of the CTL oxygen sensor except that now the reactant gas is fed to an electroactive ANODE with the cell being completed by a counter electrode which supports a cathodic reaction. The cathode could consist of a standard battery electrode material such as NiOOH, PbO_2, MnO_2 etc. which maintains the sensing electrode at a sufficiently high anodic potential to effect CO oxidation. Alternatively, a matched pair of electrodes could be employed which are electroactive to both carbon monoxide oxidation and oxygen reduction, as in the NCB detector. In this case both electrodes are maintained at CO-oxidation potentials by oxygen adsorbing onto their surfaces. The sensing electrode is exposed to the atmosphere and oxidises completely any carbon monoxide diffusing to its surface. Oxygen in the air fed to the sensing anode, dissolves in the electrolyte and transports to the counter electrode, situated inside the cell body. This electrode does not"see" any carbon monoxide and therefore sets up a slightly more anodic potential. The two electrodes are connected via an external load which allows electrons generated at the anode to cathodically reduce an equivalent amount of oxygen at the inner, counter electrode.

The balanced reactions for the two types of cell are as follows:

<u>Lead dioxide cathode/sulphuric acid electrolyte.</u>

Anode: $CO + H_2O = CO_2 + 2H^+ + 2e$

Cathode: $PbO_2 + 2H_2SO_4 + 2e = PbSO_4 + SO_4^{2-} + 2H_2O$

Overall Reaction: $CO + PbO_2 + H_2SO_4 = CO_2 + PbSO_4 + H_2O$

Nickel hydroxide cathode/alkaline or neutral electrolyte.

Anode: $CO + H_2O = CO_2 + 2H^+ + 2e$

Cathode: $NiOOH + 2H_2O + 2e = 2Ni(OH)_2 + 2OH^-$

Overall Reaction: $2NiOOH + CO + H_2O = 2Ni(OH)_2 + CO_2$

Matched pair oxygen electrodes. (NCB SYSTEM)

Anode: $CO + H_2O = CO_2 + 2H^+ + 2e$

Cathode: $\frac{1}{2}O_2 + 2H^+ + 2e = H_2O$

Overall Reaction: $CO + \frac{1}{2}O_2 = CO_2$

Clearly with the matched pair design there must be a sufficient oxygen supply for the counter electrode, but at the signal levels envisaged this should not presentany particular problems. The cell current, being determined solely by the transport of carbon monoxide to the sensing electrode, will be a direct measure of carbon monoxide concentration in the atmosphere. This has been demonstrated by the NCB (Yorkshire) Laboratory. At higher carbon monoxide concentrations the cell oxygen demand could become limiting, necessitating the use of battery cathode systems, or reducing the sensor's signal sensitivity to carbon monoxide (i.e. increasing diffusion barrier resistance).

Access of the reacting gas to the sensing anode would be restricted by means of a capilliary diffusion barrier, as for the CTL oxygen sensor, such that this electrode operates in the limiting current mode. An idea of the required orifice dimensions can be obtained from the following basic equation [1].

$$i = 1.116.10^{-5}\, nFd^2\, Dpl^{-1} \qquad \ldots\ldots(1.1.)$$

i is the sensor current (amps)

n is the number of electrons per mole gas reacted.

F is the Faraday (96494 coulombs mole^{-1}).

d is the capillary diameter (cm).

l is the capillary length (cm).

D is the gas diffusion coefficient (cm^2 s^{-1})

p is the gas partial pressure (atm.)

Assuming the diffusion coefficient for CO in air is similar to that for O_2 (0.21 cm^2 s^{-1}) and with n = 2:

$$i_{CO} = 1.48 p_{CO} d^2 l^{-1}$$

or $$d = \sqrt{0.676\ lS}$$

where S is the sensor sensitivity in μA per ppm CO.

With a capillary length of 2.5 mm (currently used for the oxygen sensor) the following hole diameters are obtained from the above equation:

Sensitivity,	1μA per ppm CO	4 mm dia. hole.
	0.1μA per ppm CO	1.3 mm dia. hole.
	0.01μA per ppm CO	0.4mm dia. hole.

The present oxygen sensor design uses a 0.2 mm hole which can easily be enlarged to the size required for the CO device. Thus the same basic components could be used for either assembly.

Research investigations into the following areas are necessary to fully achieve the objective of developing the carbon monoxide sensor described above:

1.1. Operational mode of the NCB prototype.

Basic electrochemical measurements are required to establish the operational limits of the NCB electrode current-potential characteristics and ensure that the cell operates in a carbon monoxide limiting current condition. Identification of the origin of carbon monoxide diffusion limitations in the NCB cell

would aid design of the capillary/electrode combination for the CTL hardware.

1.2. Electrolyte.

The NCB cell utilises an aqueous sulphuric acid electrolyte which is incompatible with the nickel-plated steel container used for the CTL oxygen sensor. Plastic hardware could be adapted, using techniques established for sealed lead-acid battery manufacture. However, full exploitation of the present oxygen sensor technology demands an alkaline or near neutral pH. Alkaline systems may suffer from signal interference and carbonation by atmospheric carbon dioxide which must be assessed. "Carbon dioxide rejecting", neutral salt solutions might be used provided solubility is high enough to depress the solution vapour pressure and prevent undue water loss. Anions such as chloride and strong metal complexing agents (e.g. many organic acid anions) cause depassivation and corrosion of nickel and steel and must be avoided.

1.3. Electrode Fabrication.

Platinum black, gas diffusion electrodes are used in the NCB design. These were taken from commercially available sensors and it will be necessary to develop an independant electrode manufacturing capability to serve any significant production of sensors. Also, other electrocatalyst materials may be preferred to platinum black; for example gold offers the possibility of comparable CO-oxidation activity combined with much lower hydrogen sensitivity relative to platinum, platinum-gold mixtures or supported gold may provide higher intrinsic CO-oxidation activity (Appendix 1.) which could prove particularly important when measurements are required in high CO concentrations (> 200 ppm), or if a reduction in electrode size is necessary.

1.4. Electrode Performance.

High intrinsic activity towards anodic oxidation of carbon monoxide is an obvious prerequisite for any electrode/electrolyte combination. The electrode activity reserve (i.e. CO-oxidation signal obtained from an open electrode) should be at least 10 times greater than the corresponding capillary current to ensure a stable sensor signal over long periods of time, with minimal temperature dependence.

Other important electrode parameters are:

- background corrosion currents and passivation effects at the operating potentials.
- oxygen reduction activity, particularly if a "matched pair", counter/sensing electrode system is used as for the NCB cell.
- carbon dioxide sensitivity.

Sensitivity towards other contaminants, particularly hydrogen, is also important but was not included within the scope of this initial study.

The above characteristics are affected by the following system variables:

- Electrolyte composition and pH.
- nature and composition of the electrocatalyst.
- electrode structure, namely catalyst/PTFE ratio and catalyst loading.
- electrode potential.

Interactions between these variables may be significant. For example electrode activity, measured as a CO-oxidation current at a fixed potential, varies with the catalyst wetting characteristics and achieves a maximum at some optimum value of PTFE/catalyst ratio, depending on the relative aggregate sizes of these materials. This optimum ratio will alter with any changes in the electrolyte surface tension which in turn is a function of electrolyte composition and pH. The CO-oxidation reaction is strongly influenced by the nature and extent of surface films of oxygen and oxides on noble metal catalysts (Appendix 1) which in turn are governed by the catalyst

and electrolyte compositions and electrode potential.

An exhaustive investigation into all these factors is beyond the scope of the present study but sufficient data should be accumulated to enable a provisional selection to be made of an electrode/electrolyte combination for prototype sensor development.

2. PRELIMINARY TESTS WITH THE NCB CELL

2.1. Experimental.

NCB use a modified "ECOLYSER" cell for the Yorkshire Laboratories Instrument in which a porous bronze filter replaces the plastic moulding containing channels for pumping the test gas across the electrode face. Exposure to a gas mixture containing 50 ppm CO in air resulted in similar outputs from both arrangements - the NCB cell was simply immersed in a chamber purged with the test gas, whereas the "Ecolyser" arrangement required a flow of about 100 to 200 ml per minute through the sensing electrode chamber. It was concluded therefore that the bronze filter on the NCB cell presents little diffusional resistance and that both arrangements are governed by processes occuring within the electrode itself, which comprises a porous PTFE film, coated on the electrolyte side with a layer of Pt black catalyst. Since the "Ecolyser" cell was more convenient to use, particularly with regard to its exposure to the test gases, this arrangement was used in these preliminary tests.

The test gas was a certified mixture of 49.2 ppm carbon monoxide in air, contained in an aluminium cylinder, from Rank Hilger Limited. A needle valve controlled the gas flow which was calibrated by means of a bubble flowmeter. To avoid back diffusion, the exhaust from the cell was passed through a water bubbler.

A dynamic hydrogen reference[4] electrode (DHE) in the same electrolyte as the cell was introduced by means of an electrolyte bridge through the filler hole (see Figure 2.1.). This electrode enabled the sensing and counter electrode potentials to be monitored separately when the cell was operated on a fixed load resistor and also facilitated electronic control for the potentiostatic i-E measurements (section 2.1.2. below).

The "Ecolyser" cell electrolyte was analysed and found to contain about 30 ml of 6.84N (3.22M) sulphuric acid. This

concentration of sulphuric acid was used for most of these preliminary tests, but some measurements were also made with 4M NaOH and 4M potassium acetate/acetic acid mixtures. It was found necessary to contact the electrodes with electrolyte for 3 or 4 days before testing in order to obtain reproducible results, particularly when changing from one electrolyte system to another.

2.1.1. Measurements with fixed load resistor.

A 47 ohm load resistor was soldered between the sensing and counter electrodes and the following measurements made:

- Background current (μA) and sensing/counter electrode potentials in air from a compressed air cylinder at flow rates between 0 and 200 ml per minute.

- same measurements with the air/CO test gas at flow rates between 0 and 240 ml per minute

- signal variations with temperature between 18 and 24 ^{o}C with the air/CO test gas flow at 100 ml per minute.

2.1.2. Steady State Potentiostatic i-E curves.

A potentiostat was used to hold the sensing electrode at fixed potentials (E) with respect to the D.H.E. reference electrode and the resulting steady state currents (i) flowing between the sensing and counter electrodes were measured. Comparison of the derived i-E characteristics obtained in compressed air and the air/CO test gas (both at flow rates of 100ml per minute) enabled an estimate to be made of the intrinsic electrocatalytic CO-oxidation activity of the sensing electrode.

The test was commenced with the potentiostat set to the air rest potential. The background current was monitored until a steady value was reached, then the gas was changed to the air/CO test gas. The new steady state current was noted and the gas switched back again to compressed air. When the current had returned to the steady air value, the potentiostat setting was altered by a 50 mV increment in the cathodic direction and the procedure repeated. At 0.800 volts with respect to D.H.E.

(about 0.25 volts below the air rest potential) the voltage scan was reversed and each point checked on the backward sweep. In general the currents were reproducible on the forward and backward potential sweeps, provided sufficient time was allowed to enable the system to obtain a steady state condition.

On returning to the air R.P. value the scan was continued in the anodic direction until a value of 1.300 volts was reached on the D.H.E. Scale. Above this potential the background corrosion currents were high and the steady state was approached very slowly. At this point the test was stopped.

Below the air R.P. (i.e. cathodic to R.P.) the sensing electrode supports mixed processes of CO-oxidation and oxygen reduction which give rise to steady state currents. Transient currents occur due to the formation or dissolution of surface films of platinum oxide or oxygen which eventually settle to steady background levels. These films can take several days to equilibrate particularly at more anodic potentials, but in most instances during cathodic polarisation, reasonably stable currents were observed within 10 to 30 minutes. Assuming that the oxygen reduction and background currents are identical in air and the CO test gas, the CO-oxidation i-E characteristic can be obtained for the sensing electrode by subtracting the air and test gas i-E curves. Platinum is a very active electrocatalyst for oxygen reduction and the derived net CO-oxidation current, being the difference between two large quantities, was probably subject to some significant error.

A more exact procedure at these potentials would have been to carry out measurements in nitrogen and nitrogen/CO test gases. In this way the CO-oxidation could have been obtained directly, without involving the above assumption regarding the competitive oxygen reduction reaction. The only other possible process would be the small background from the Pt-O film currents. However, it would not have been possible to exclude oxygen completely from the "Ecolyser" cell and it was considered better to operate

under the air saturated conditions described, rather than use semi-anaerobic conditions which may be subject to variations during the test run. Tests in nitrogen mixtures were conducted in the later catalyst work using a modified cell in which air leaks could be more efficiently reduced.

Oxygen reduction interference is absent above the air R.P. and CO-oxidation currents are obtained directly, except for subtraction of the small background Pt-O film oxidation currents. At high anodic overpotentials however, oxygen evolution currents become important and the Pt-O film processes take increasingly long times to achieve a steady state. However, this region is not of direct interest in the CO sensor and can only be utilised if a potential biasing circuit, or battery cathode system, are employed (see Appendix 1.).

2.2. RESULTS AND DISCUSSION.

2.2.1. 6.84 N Sulphuric Acid / 47Ω load tests.

The digital voltmeter (d.v.m.) connected across the load indicated a zero current for a 10 day period operating on compressed air at various flow rates between 0 and 200 ml min^{-1}. The d.v.m. discriminated to 10μV and therefore background current levels were below 0.2μA. The potential of the counter/sensing electrode combination with respect to the D.H.E. reference reached 1.032 volts by the end of the first day and rose to a steady state value of 1.050 volts $\pm$ 5 mV by the second day.

On switching to the air/CO test gas (49.2 ppm CO) an electron current flowed from the sensing to the counter electrode, indicating an oxidation at the sensing electrode and a reduction at the counter. At a given gas flow rate, the current output reached the steady values given in figure 2.2. within 10 to 30 seconds. The cell response was fairly insensitive to flow rate above about 80 ml per minute, producing about 1μA per ppm carbon monoxide. The active electrode cross sectional area was about 5 cm^2, so the electrode CO sensitivity was 0.2μA/ cm^2/ppm CO.

The sensing electrode potential in the air/49.2 ppm test gas at 100 ml per minute, 18°C was 0.930 volts versus D.H.E. and the counter about 1 mV more anodic.

The cell output at 100 ml per minute air/CO increased with temperature as shown in figure 2.3., with a measured temperature coefficient of 3 to 4% per °C.

2.2.2. 6.84 N Sulphuric Acid/Steady state potentiostatic i-E curves.

The i-E curves for the sensing electrode in compressed air and the air /49.2 ppm CO test gas are shown in figure 2.4. The total CO-oxidation current as a function of potential, obtained by subtracting the curves in figure 2.4., tended to a limiting value of 130μA above about 0.9 volts on the D.H.E. scale (figure 2.5.). Considering the cell geometry and the above temperature coefficient measurement, this limiting current very likely arises from a controlling process of diffusion through an electrolyte film within the electrode. Any diffusion control through gaseous barrier such as the PTFE backing tape would result in much lower temperature coefficients as for the CTL oxygen sensor.

With the air-cathode counter electrode arrangement used in the "Ecolyser" and the NCB cells, the sensing electrode operating potential lies in a cathodic region relative to the air R.P. Measured potentials on the D.H.E. scale in section 2.2.1. above were 1.05 volts in air and 0.93 volts with a 49 ppm CO in air mixture. Under the latter conditions the sensing electrode supports both CO-oxidation and oxygen reduction reactions and these couple to form a parasitic local cell which consumes a significant proportion of the total CO-oxidation current, (see Appendix 1.). Thus the "Ecolyser" cell signal with the test gas, using a 47Ω load, measured in section 2.2.1. was only about 49μA (at 20°C) instead of the 122μA indicated in figure 2.5. at the operating potential of 0.93 volts.

An estimated cell signal at 0.93 volts can be obtained from the data in figures 2.4. and 2.5. and compared with the measured value of 49μA from section 2.2.1. as follows.

The sensing electrode rest potential in the air/CO test gas is 0.92 volts which corresponds to the intersection point of the CO-oxidation i-E curve (figure 2.5.) and the air/oxygen reduction curve (figure 2.4.), as redrawn in figure 2.6. The current value of 117μA at this intersection is the local cell current at open circuit in the test gas. An air counter electrode connected via an external load causes the potential of the sensing electrode to rise from 0.92 to 0.93 volts. The local cell oxygen reduction current reduces to 83μA (point B, figure 2.6.), the total CO-oxidation current increases slightly to 121μA (point C. figure 2.6.) and the difference of 38μA appears as a cathodic, oxygen reduction current on the counter electrode which represents the sensor signal (I_s). The correlation between this value and the measured value of 49μA is quite good, considering the errors expected in deriving the curve in figure 2.5. (see section 2.1.2.).

The i-E curve of the counter electrode was not measured, but it is evident that polarisation is greater than for oxygen reduction at the sensing electrode. (A likely curve is sketched in figure 2.6.). This originates from a greater contribution from oxygen diffusion resistance through the cell electrolyte at this electrode compared to the sensing electrode.

The use of a non-polarisable counter electrode such as battery cathode materials to hold the sensing electrode near the air R.P. would suppress the local cell at the sensing electrode and the total CO flux would appear as current in the sensor signal thus increasing sensitivity (see Appendix 1.). Alternatively, a third, unpolarised reference electrode could be included to hold the sensing electrode at or above the air R.P. by means of a potentiostatic control circuit, a provision for this is included in the "Ecolyser" cell design which incorporates a split counter electrode arrangement.

2.2.3. Tests with 4 M NaOH electrolyte,

A steady air R.P. of 1.192 volts versus D.H.E. was achieved after 4 days contact with the electrolyte. The cell output with a 47 ohm load, air/49.2 ppm CO test gas at 100 ml per minute was

about $-2\mu A$. Steady state i-E curves in air and in the test gas were virtually identical indicating complete inactivity of the platinum electrode towards CO-oxidation.

The oxide/oxygen surface films on platinum, which are all important to the CO-oxidation mechanism (see Appendix 1.), are reportedly similar in nature, regardless of the electrolyte pH.[2] However, in alkaline electrolyte, hydroxide anions also form an adsorption film from potentials of about 0.3 volts upwards which may interfere with the CO-oxidation process.[2]

2.2.4. Tests in 4M potassium acetate electrolyte.

4M potassium acetate has a pH of about 8.6 and the Ecolyser platinum electrode displayed a similar lack of activity towards CO-oxidation as for 4M NaOH. Using a 47Ω load, and 100 ml per minute air/49.2 ppm CO test gas, an initial response of $4\mu A$ was obtained, but this rapidly decayed to $< 2\mu A$.

Addition of acetic acid to reduce the pH to 5 resulted in a stable $12\mu A$ response to the air/49.2 ppm CO test gas, but this system, and one adjusted to pH7, were incompatible with the nickel-plated steel hardware of the oxygen sensor, so the investigation was not pursued any further.

2.3. CONCLUSIONS.

- The NCB, platinum black catalysed electrodes exhibited a high, stable activity towards carbon monoxide oxidation and oxygen reduction in 6.84N sulphuric acid electrolyte.

- the electrode CO-oxidation current was probably controlled by diffusion through an electrolyte film within its structure and had a limiting value under the conditions tested ($20^{o}C.$, 100 ml per minute gas flow rate) of about $0.5\mu A$ per ppm CO per cm^2 electrode area.

- with the NCB cell arrangement, the sensing electrode operates at about 0.93 volts (D.H.E. scale) in a test gas containing 49.2 ppm CO in air. At this potential part of the electrode output is consumed by a local cell involving CO-

oxidation coupled with O_2 reduction. Consequently the cell sensitivity to CO under the test conditions was only 0.2μA per ppm per cm^2.

- the NCB electrode was inactive towards CO-oxidation in strong alkaline electrolytes. This is very likely an intrinsic property of platinum, originating from changes in the electrosorbed surface film, when the pH is altered.

- the NCB platinum electrode exhibited a similar lack of activity in 4M potassium acetate (pH 8.6) but gave some response when the pH was adjusted to about 5 by adding acetic acid. However, the acidic acetate system was incompatible with the nickel plated steel hardware and a less aggressive anion system is required at near neutral pH's.

Three possible options exist for the development of a preproduction prototype sensor as follows:

A. Acidic Electrolyte.

PTFE bonded platinum electrodes may be used produced by foil transfer techniques as for the silver electrodes used in the CTL oxygen sensor. Some studies of alternative catalysts could be productive, particularly gold and supported gold which possesses poorer activity towards hydrogen oxidation than platinum.

A more dilute acid electrolyte may be desirable, being less corrosive but NCB work has shown that this results in increased interference from hydrogen. Neutral salts may be added to the acid electrolyte to lower vapour pressure and reduce water loss, but effects of any new ions on the electrocatalytic activity should be assessed.

The main development work involves the production of suitable corrosion resistant plastic hardware and assembly methods. The nickel-cadmium battery hardware used for the CTL oxygen sensor could only be employed if reliable protective coatings could be applied.

B. Alkaline Electrolyte.

Alternative catalysts to platinum will need to be developed. Gold based systems may be suitable. Carbon dioxide interference must be assessed and controlled.

The CTL oxygen sensor hardware could be used, possibly with minor modifications, and less development will be required than with an acid system

C. Near Neutral Electrolytes.

Platinum activity is very low at neutral pH's and alternative catalysts will need to be developed. There would be no incentive to use such electrolytes unless they were both compatible with the CTL oxygen sensor hardware and insensitive to carbon dioxide interference. pH's of 5 to 8 may meet these requirements if soluble salts of non-complexing anions are used, e.g. sulphates, perchlorates, borates, phosphates. Organic acids and halides (chloride, bromide, iodide) are likely to cause corrosion of the nickel-plated steel hardware.

High water solubility of the neutral salt electrolyte is essential to minimise water evaporation. In this respect, sodium perchlorate is a promising candidate (Table 2.1.). Other perchlorates (except potassium and ammonium) and the salts Na_2HPO_4, $MgSO_4$, Sodium and potassium nitrates also have reasonably high solubilities.

3. ELECTROCATALYST TESTS IN ALKALINE ELECTROLYTE.

3.1. Preliminary Screening of Possible Materials and Electrode Preparation Techniques.

3.1.1. Electrode Fabrication.

Two methods were assessed based on direct deposition of precious metal catalysts onto a porous PTFE membrane and a foil transfer method as for the CTL oxygen sensor silver electrode.[3]

(i) Direct Deposition: a porous PTFE disc (20 mm diameter) was attached to the bottom of a vertical glass tube. An aqueous chloride salt solution of precious metal was poured into the tube and the PTFE disc exposed to formaldehyde vapour (figure 3.1.) The Organic vapour permeated the PTFE and reduced the metal salt in the pores on the liquid side, forming a conducting, noble metal film.

Films of platinum, palladium and gold were produced in this way using the salts H_2PtCl_6, $PdCl_2$ and $AuCl_3$ respectively. Mixed gold-platinum and gold-palladium films were prepared from solutions containing chloride salts of both noble metal compounds.

(ii) Foil Transfer: the spray technique described for the oxygen sensor silver electrodes was too wasteful of catalyst due to "overspray" losses to be used with precious metals such as gold and platinum. A modified procedure was therefore developed. A PTFE-coated aluminium foil was pressed onto a steel plate containing a nickel foil ring stuck to its surface. The aluminium foil formed a depression into the ring about 1 mm deep and 20 mm diameter. A weighed amount of metal catalyst was mixed with a measured quantity of PTFE aqueous dispersion (I.C.I. Fluon GP1 dispersion) and slurried with sufficient water to form a paste which could be easily transferred to fill the depression in the aluminium foil. The quantities used were calculated to give a metal/PTFE ratio of 10:3 and a catalyst loading of 50-60 mg per cm^2.

The transferred mix was dried with a hair dryer and the foil cut around the outer edge of the nickel ring. The catalyst coated foil disc was then removed and heat cured at 280 - 290°C. in a circulated air oven for 1 hour. The cured catalyst layer was transferred to a porous PTFE disc using an hydraulic press[3]. The PTFE disc was weighed before and after transfer to enable an estimate to be made of catalyst loading. In this way electrodes were prepared containing the catalysts, gold, gold-ferric oxide (3 to 1 by weight), gold-palladium (1:1 mixture) and gold-platinum (1:1 mixture). Noble metal powders were obtained from Johnson Matthey (all 99% purity) and the ferric oxide from Koch Light (99.995%).

3.1.2. Electrode Testing.

The test cell arrangement is shown in figure 3.2. The counter electrode was a floating oxygen cathode with free access to ambient air. Compressed air or air/50 ppm CO test gas were fed to the gas compartment behind the sensing electrode sealed into the bottom of the cell which had a catalyst/electrolyte projected area of 3.142 cm^2. The cell was filled with 5M KOH electrolyte and the electrodes connected externally via a 47 ohm load resistor. The background corrosion current and CO-oxidation activity of the sensing electrodes were assessed by measuring the load resistor current with air acid test gas fed respectively to the sensing electrodes.

3.1.3. Results of electrode tests.

The electrode test results are summarised in Table 3.1. The carbon monoxide oxidation currents on the deposition electrodes were considerably less than those on the corresponding foil transfer electrodes. This could have been due to low surface area with the deposition catalysts or electrolyte flooding. The latter is a more likely cause since corrosion currents were of a similar order for both types of electrode. In view of these results, the foil transfer technique was adopted as standard for all further work.

Of the foil transfer electrodes, plain gold exhibited the highest CO-oxidation activity, with a background corrosion current of about 1 ppm CO equivalent per cm^2 electrode. As expected Pt was inactive, but the low activity of Pt/Au was surprising. Palladium-gold possessed some CO-oxidation activity, but background corrosion currents were relatively high at about 10 ppm CO equivalent. A mesh electrode containing Au/Fe_2O_3 catalyst was tested in case any synergic effect in the foil transfer electrode had been masked by conductivity effects. However, although the activity of the mesh electrode was higher, it was still below that of the pure gold, foil transfer electrode and the Fe_2O_3 appeared merely to dilute the gold activity under the test conditions.

As a result of these tests, pure gold was selected as the electrocatalyst for detailed studies in alkaline and near neutral electrolytes.

3.2. Detailed Electrochemical Testing of Gold Electrodes in Alkaline Electrolytes.

3.2.1. Experimental.

The glass cell shown in figures 3.3. was designed to exclude air totally so that accurate measurements of CO-oxidation activity could be made in anaerobic conditions below the air rest potential (see section 2.1.2.). Potentiostatic i-E scans were made using white-spot, compressed nitrogen to obtain background behaviour. CO-oxidation activity was assessed using a nitrogen/ 56 ppm CO mixture. In practice a small oxygen reduction background was evident which probably arose from impurities in the gases, or leaks in the connections of the gas lines.

Electrochemical measurements were made according to the following sequence:

(a) Electrode contacted with electrolyte and left in static air overnight.

(b) Air rest potential noted and system purged with nitrogen. Gas flow to rear of electrode was 200 ml per minute.

(c) Electrode potentiostatted at 0.5 volts on the D.H.E.

scale for 1 hour when the current settled to a small steady cathodic value (~ 50 - 60 μA) deriving from traces of oxygen in the gas or system leaks.

(d) Background current noted and gas switched to N_2/CO mixture at the same flow rate. Response was measured on a recorder and was normally rapid, reaching a steady value within 1 minute. The difference between the nitrogen and N_2/CO currents was taken as the CO-signal.

(e) Gas was switched back to nitrogen and the current allowed to return to the original nitrogen value.

(f) Potentiostat control potential was increased by 50 mV in the anodic direction and the above procedure repeated.

(g) The potential was increased in 50mV steps and the above measurements made over the potential range 0.5 to about 1.3 volts on the D.H.E. scale.

On completing the anaerobic scan the oxygen electrode activity was measured by taking i-E readings in air from the rest potential to about 0.5 volts on the D.H.E. scale.

Carbon monoxide response using an air/50ppm CO gas mixture was checked against the N_2/CO response at potentials above the air rest potential where oxygen interference is absent. Correlation was very good between these two mixtures.

Carbon dioxide interference was assessed in the above aerobic i-E scans above the air R.P. by exposing the electrode to air/0.5% CO_2 and air/5.0% CO_2 gas mixtures after the CO-response measurement at each potential increment. Carbon dioxide response was essentially independant of potential over the range investigated.

3.2.2. Results with Gold Electrodes in 8M NaOH.

"i-E carbon monoxide scans for three gold electrodes, differing in their gold:PTFE catalyst ratio, are shown in figure 3.4. Corresponding backgrounnd currents are shown in figure 3.5. together with the oxygen reduction i-E curve for the 1:1 gold:PTFE electrode in air.

An optimum activity was obtained with a 1:1 gold:PTFE catalyst ratio; limiting CO oxidation current was 0.23 to 0.27μA per ppm CO per cm^2 between 0.7 and 1.15 volts on the D.H.E. scale. The 10:3 and 1:1.7 gold:PTFE electrodes exhibited CO-oxidation limiting currents of 0.04 to 0.07μA per ppm per cm^2 and 0.14 to 0.17 A per ppm per cm^2 respectively over a similar potential range. The decline in activity above 1.15 volts was probably due to the formation an inactive oxide film with high surface coverage. Below about 0.7 volts the gold surface is clean when the CO-oxidation reaction would be inhibited by a strongly bound , high coverage CO-adsorption film.

The CO time response for all electrodes was very sharp and typical of those shown in figure 3.6. The oxidation currents were unaffected after several hours at the air rest potential (1.15 to 1.17 volts).However, there was some loss in activity following an overnight stand in air when the limiting current on the 1:1 electrode decayed from 38 to 28μA (0.22 to 0.16μA per ppm per cm^2). The original activity was restored by cathodisation at 0.5 volt for $\frac{1}{2}$ hour and the decay was therefore, probably caused by surface oxidation. No further deactivation was noticed for longer periods of up to 1 week on stand at the air R.P., and the 28μA (0.16μA per ppm per cm^2) appeared to be a reasonably stable value.

CO-oxidation activity was very low after the electrodes had been operated at potentials above 1.3 to 1.4 volts. The activity slowly recovered at lower potentials as the surface oxide was removed by cathodisation, but complete recovery was only achieved by cathodisation at about 0.5 volts.

Oxygen reduction activity was very high with very little polarisation over the CO-oxidation current density range studied.

Carbon dioxide interference was a serious aspect in 8M NaOH. A typical response to a $\frac{1}{2}$% CO_2 in air gas mixture at the air rest potential (1.17 volts) is shown in figure 3.7.

Switching from air to the test gas resulted in a cathodic current at the sensing electrode of about 15μA (about -34 ppm CO equivalent with this electrode) which increased steadily over a 3 minute period to 60μA (cathodic) when the gas was switched to compressed air. The electrode then restored to its original air rest condition after about 2 minutes. No tests were made with the air/5% CO_2 gas mixture.

3.2.3. Results with Gold Electrodes in 4M NaOH.

"i-E" scans for CO-oxidation and background currents in nitrogen are shown in figure 3.8. for two electrodes having a 10:3 and 1:1.7 gold:PTFE catalyst ratio. A 1:1.2 gold:PTFE catalyst electrode gave a similar output to the 1:1.7 electrode, but the response was slower (figure 3.9.).

CO-oxidation activity was much higher than with the 8M NaOH electrolyte, but otherwise i-E curves had similar profiles. The 1:1.2 and 1:1.7 Au:PTFE electrodes were more active than the 10:3 electrode with limiting CO-oxidation currents of 60 to 70 μA (0.34 to 0.40μA per ppm per cm^2) over the potential range 0.8 to 1.2 volts. Air rest potentials were a bit lower compared to 8M NaOH at about 1.10 to 1.15 volts and surface oxidation of the gold was apparent at slightly higher potentials.

CO-oxidation activity declined sharply above 1.2 volts due to surface oxidation but little hysteresis was observed on the reverse scan, provided the potential did not exceed 1.4 volts. There was no decline in the CO-oxidation response after standing for 1 week at the air R.P. as was observed in the 8M NaOH electrolyte. The 1:1.7 Au:PTFE electrode after these tests was retested in 8M NaOH. The CO-oxidation currents at the air rest potential (1.15 volts) reduced from 64 to 28μA and further declined to 25μA after standing overnight at the air R.P. in 8M NaOH.

Carbon dioxide interference was again very serious in this electrolyte at the $\frac{1}{2}$ and 5% levels in air - figure 3.10. The response was independant of electrode potential in the range investigated of 1.0 to 1.3 volts. The 5% CO_2 mixture produced a very high cathodic

transient of several hundredμA which quickly decayed to a steady current of about 50 to 60μA (cathodic). The $\frac{1}{2}$% CO_2 mixture produced a less sharp cathodic transient current of about 90μA which decayed over about 2 minutes to about 60μA when air was readmitted.

3.2.4. Results with Gold Electrodes in 4M potassium acetate (pH 8.6) and acetate/acetic acid electrolyte.

The i-E scans for CO-oxidation and background currents in nitrogen are given in figure **3.11.** for an electrode having a 1:1.7, Au:PTFE catalyst ratio. There was no well defined CO-oxidation limiting current as for the NaOH solutions and some sort of poisoning/progressive inhibition was evident, with the N_2/CO and air/CO gas mixtures. The CO-response at 1.2 volts in a 50 ppm CO in air mixture shown in figure 3.12. was typical - an initial rapid rise to a current peak resulted on first exposure to the gas, followed by a gradual decay in the CO-oxidation current. On switching back to the CO-free gas (air or nitrogen) the current rapidly returned to its baseline with no "overshoot". The same CO-response profile was obtained on switching back to the CO test gas mixture.

CO_2 interference was evident with this electrolyte; figure 3.13. shows the response to an air/$\frac{1}{2}$% CO_2 mixture admitted to an electrode at the air R.P. (1.20Volts). Adjustment of the solution pH to 7 with acetic acid removed all CO_2 interference but the electrode had no CO-oxidation activity over a potential range of 0.85 to 1.30 volts and this solution also corroded the nickel-plated steel hardware of the oxygen sensor. The lack of CO-oxidation activity was probably due to a poisoning effect of the acetate ion or acetic acid, since higher activities (20-30μA) could be obtained at pH 7 using electrolytes such as sodium perchlorate at 1.2 volts (see section 5). Unlike the acetate ion or acetic acid molecule the perchlorate ion has a virtually unpolarisable electronic charge and therefore does not form coordination compounds or strong surface adsorption complexes.

3.3. Conclusions - Alkaline Electrolyte Systems.

The gold electrodes studied exhibited a high, stable, CO-oxidation activity in NaOH solutions. The current was controlled by CO diffusion through an electrolyte film and had a limiting value over the operating potential range of about 0.8 to 1.2 volts on the D.H.E. scale. The best response, 0.34 to 0.40 μA /ppm/cm^2, was obtained with 4M NaOH and a catalyst ratio of 1:1, Au:PTFE. This is comparable to the intrinsic activity of the "Ecolyser" Pt electrode in 6.84 N sulphuric acid - 0.5μA /ppm/cm^2 (Section 2.3.). Stable activities in 8M NaOH were much lower at aboute 0.14μA/ppm/cm^2. Formation of a gold oxide film above about 1.3 volts deactivates the electrode towards CO-oxidation.

The gold electrode had good oxygen reduction activities and air R.P.'s were in the range 1.15 to 1.17 volts.

The main problem in NaOH electrolytes is CO_2 interference which produces large negative (cathodic) responses at concentrations of $\frac{1}{2}$% and 5%. It would be essential to remove the CO_2 before the gas reaches the sensing electrode. External scrubbing of the gas supply would be a serious disadvantage but it may be possible to remove the CO_2 internally using the sensor electrolyte (see Appendix 4.).

Acetate/ acetic acid electrolytes cause poisoning of the gold electrode CO-oxidation activity, probably as a result of anion adsorption. 4M potassium acetate would be compatible with nickel plated steel hardware but suffers from CO_2 interference. Acetic acid additions remove CO_2 interference but also deactivate the electrode towards CO-oxidation and cause corrosion of nickel hardware. These electrolytes are therefore totally unsuitable.

4 . ELECTROCATALYST TESTS IN ACID ELECTROLYTE.

4.1. Gold in Acid Electrolyte.

The main attraction of gold compared to platinum in acid media; is that it possesses a lower intrinsic activity towards hydrogen and hydrocarbon oxidation.

Two electrolytes were studied, sulphuric acid and perchloric acid. The latter should have minimal anion effects.

Electrodes contained a 1:1 Au:PTFE catalyst prepared by the foil transfer method described in section 3.1.1.

Electrochemical measurements were made with the cell described in section 3.1.2.

4.1.1. Gold in 6.84 N Sulphuric Acid.

The air rest potential was 0.72 volts (D.H.E. scale). No CO-oxidation current was observed until the potential was increased to 1.1 volts when a rather poorly defined current $<2\mu A$ was observed. At 1.28 volts the CO-oxidation current was $5\mu A$ (about $0.03\mu A/ppm/cm^2$). At higher potentials the activity tended to decrease, probably through the formation of a surface oxide film. The low activity of gold at this pH is probably due to the surface being virtually clean of any Au-O surface film, which is important to the CO-oxidation mechanism. The background currents however, were quite high ($15\mu A$, $4.77\mu A/cm^2$ at 1.28 volts) and it is likely that gold corrosion occured via a soluble species, rather than surface oxide products.

As expected, 5% CO_2 in air produced no response at the electrode.

4.1.2. Gold in 0.1N Sulphuric Acid (pH.1).

The air rest potential was somewhat unstable in this electrolyte; the initial value was 1.03 which steadily decreased overnight to 0.98 volts. CO-oxidation activity was higher than the stronger sulphuric acid, but still, measurable currents were only obtained

above 1.1 volts.

Potential	1.1 volts	1.28 volts
CO-oxidation	9μA (0.05μA/ppm/cm^2)	37μA (0.21μA/ppm/cm^2)
Background	4μA (1.27μA/cm^2)	12μA (3.82μA/cm^2)

The activity at 1.28 volts was comparable to the "Ecolyser" Pt electrode, but operation at this potential would require a sensor incorporating a non-polarisable counter electrode (e.g. PbO_2) or a third, unpolarised, reference oxygen electrode.

4.1.3. Gold in Acid Perchlorate media.

Two electrolyte compositions were examined:

(i) 4M $NaClO_4$, 0.1M $HClO_4$ pH0.

(ii) 4M $NaClO_4$, 0.01M $HClO_4$ pH1.

No CO-oxidation activity was obtained below 1.1 volts in the pH 0electrolyte. The following results were obtained at 1.18 and 1.28 volts:

Potential	1.18 volts	1.28 volts
CO-oxidation	20μA (0.11μA/ppm/cm^2)	27μA (0.15μA/ppm/cm^2)
Background	10μA (3.18μA/cm^2)	18μA (5.73μA/cm^2)

The air R.P. was 0.8 volts and, as with the 0.1N H_2SO_4 electrolyte, the pH 0 electrolyte would require a sensor incorporating a non-polarisable counter on third reference electrode.

The pH 1 electrolyte had a low pH-buffer capacity (see section 5). The D.H.E. reference generates alkali at its surface and if the electrolyte buffer capacity is low we will be effectively measuring the sensor potential in acid against the D.H.E. in a much higher pH. This results in much higher apparent air rest potentials. At steady state the air R.P. on the D.H.E. scale was 1.48 volts. Consequently CO-oxidation activities were compared with the pH 0 electrolyte at the same overpotentials with respect to the D.H.E., rather than

the same potentials.

CO-oxidation activity in the pH 1 electrolyte was similar to the pH 0 electrolyte. No CO response was obtained until an overpotential of 0.30 volts was reached above the air R.P. (i.e. 1.1 volts in the pH 0 electrolyte 1.78 volts in the pH 1 electrolyte). At 0.38 volts overpotential the CO-current was 26μA (0.15μA/ppm/cm^2), background 2μA (2.23μA/cm^2) and at 0.48 volts overpotential 31μA (0.18μA/ppm/cm^2), background 15μA (4.77μA/cm^2).

4.2. Platinum in Acid Electrolyte.

No open electrode tests have yet been made on platinum or platinum-containing electrodes in acid electrolytes. However, platinum and platinum-gold electrodes have been prepared by the foil transfer technique and incorporated into experimental CO sensors (section 7). These sensors have maintained a reasonably stable response over several months, with low temperature coefficient (about 0.2% per ^{o}C), implying that the open electrode activity is at least near the requirement of about 1μA/ppm on a 3cm^2 electrode, i.e. about 10 times the capilliary diffusion sensitivity of 0.1μA/ppm.

Tests are in hand to measure actual open electrode performances of these electodes in sulphuric and perchloric acid electrolytes of various concentrations.

4.3. Conclusions - Acid Electrolyte Systems.

Gold is not a suitable electrocatalytic material for acid electrolyte systems. CO-oxidation only occurs at high anodic potentials, well above the air rest potential, background corrosion currents are high in the active potential region, particularly in the stronger acid solutions.

Although no open electrode tests have been made with platinum or platinum/gold electrodes, they have been produced by the foil transfer method and used successfully in experimental CO-sensors for periods of several months. The inference is that their intrinsic activities are at least of the order

0.3 - 0.4μA/ppm/cm^2 which is comparable with the "Ecolyser" electrode activity of 0.5μA/ppm/cm^2.

5. ELECTROCATALYST TESTS IN pH 4 to 7 ELECTROLYTE.

5.1. Selection of Electrolyte System.

5.1.1. Basic System.

The electrolyte would consist of a dissolved neutral salt to provide ionic conductivity and depress the water vapour pressure, together with small amounts of added acid or alkali to adjust the solution pH.

The neutral salt should have high solubility and consist of anions and cations which are compatible with the nickel-plated steel hardware and do not adversely affect the CO-oxidation reaction. In these respects sodium perchlorate is among the most soluble salts (Table 2.1.) and should exhibit minimal anion adsorption effects on the CO-reaction. Other candidates are lithium, magnesium, calcium and barium perchlorates, magnesium sulphate and sodium nitrate. Organic anions are likely to interfere with the CO-oxidation as noted with potassium acetate in section 3.2.4. and halides (chlorides, bromides and iodides) are incompatible with the hardware.

5.1.2. pH Buffers.

Initial studies with 4M $NaClO_4$, at pH's between 4 and 7 (adjusted by additions of $HClO_4$ or NaOH), gave poorly reproducible CO-oxidation i-E curves and CO_2 responses which depended on the previous history of the electrode. Electrodes, previously checked for activity in 4M NaOH, exhibited strong CO_2 sensitivity even after several days soaking in a pH 4 $NaClO_4$ solution, indicating the presence of residual alkali in the electrode structure. Cathodisation treatments of fresh electrodes produced localised alkaline pH's which modified the CO/CO_2 response and persisted for several days.

Sodium perchlorate is a salt formed by the neutralisation of a strong acid ($HClO_4$) with a strong base (NaOH). When NaOH

solution is titrated into a perchloric acid solution the pH increases as the neutralisation proceeds and a curve of pH against ml base added is obtained having the general shape shown in figure 5.1. Thus, 0.1 M $HClO_4$ is virtually completely ionised and has a pH of about 1; as 1M NaOH is added the pH increases only slightly, reaching a value of 2 when 90% of the acid has been neutralised (i.e. equivalent to 10% acid remaining which is 0.01M). Thereafter, the pH increases steeply with further alkali additions through the neutralisation point (pH 7) and up to pH 11. Above pH 11 the curve levels out again and tends to a limiting value, equivalent to the pH of 1M NaOH.

As a result of the titration curve shape for a strong acid/strong base, the pH of neutral salt solutions will be very sensitive to traces of alkali or acid. The salt solutions are said to have low "pH-buffer capacity"; conversely solutions of strong acids or strong bases have high "buffer capacities". Thus an electrode, operated in an ostensibly neutral, CO_2-rejecting, $NaClO_4$ solution would only require a fractional change in the OH^- ion concentration at its surface to raise the pH into a CO_2 sensitive region. This could occur as a result of relatively small cathodic currents or ingress of trace alkaline impurities.

The addition of 4M sodium perchlorate to perchloric acid shifted the acid end of the titration curve to lower pH values. (figure 5.2.). However, the general shape, and hence pH sensitivity at the neutral point remained unchanged. Lithium, barium and calcium perchlorates produced similar shaped titration curves to figure 5.2.

Magnesium perchlorate showed a steeply rising curve at the equivalent point which levelled out at pH 7 (figure 5.3.). This was caused by precipitation of $Mg(OH)_2$ on further alkali addition above pH 7. The addition of 4M $NaClO_4$ to the 2M $Mg(ClO_4)_2$ resulted in a pH plateau at the slightly lower value of about pH 6.4, and the system was therefore selected for further electrochemical testing (section 5.2.).

The sharp S-shape of the titration curve for strong acids/strong bases arises from the virtually complete dissociation of the substances in solution. For example aqueous perchloric acid consists almost totally of the separate ions:

$$HClO_4 \longrightarrow H^+ + ClO_4^-$$

Weak acids (or bases) however are only partially ionised and significant concentrations of the unionised acid (or base) exist in an aqueous solution, e.g. boric acid,

$$H_3BO_3 \rightleftharpoons H_2BO_3^- + H^+$$

The undissociated acid does not contribute to the solution pH, but as alkali is titrated into the solution it acts as an acid reserve by dissociating to replace the hydrogen ions neutralised. The effect on the titration curve is to cause a more gradual change in pH at the equivalence point.

Weak acids and bases, and their salts, are called pH buffer electrolytes and can be added to neutral solutions to stabilise the pH. Three possible candidates were considered for the CO-sensor using 4M $NaClO_4$ electrolyte.

phosphoric acid/sodium phosphates.

boric acid/sodium borates.

phthalic acid/sodium phthalates.

The titration curves are shown in figure 5.4. and show that each system buffers over slightly different pH ranges as follows:

phosphate buffer range	pH 4 to 6 with a second plateau above pH9.
borate buffer range	pH 6 to 8
phthalate buffer range	pH 4 to 4.5

From these results, borate was selected from the three as the best all-purpose buffer in the range 6 to 7 for the CO-sensor.

5.2. Gold Electrodes in Magnesium Perchlorate Buffered Solutions (pH 7).

A 1:1 Au:PTFE electrode was prepared according to section 3.1.1.

and tested as detailed in section 3.2.1. The air rest potential was initially at about 1.09 volts on the D.H.E. scale, but tended to drift downwards, reaching about 1.02 volts after 4 days. The i-E scans in nitrogen and nitrogen/50 ppm CO mixture are given in figure 5.5. The electrode had a CO-oxidation limiting current of about 10μA (0.64μA/ppm/cm^2) over the potential range 0.8 to 1.2 volts. Above 1.2 volts the CO-oxidation activity decreased, probably because of surface oxidation. Background corrosion currents were low over the limiting current potential range at about 1μA (0.32μA/cm^2). The electrode did not respond to an air/5% CO_2 gas mixture over the entire potential range studied. The electrode was tested in 4 M NaOH and found to give a CO response similar to that given in section 3.2.2. for a 1:1 Au:PTFE electrode. On returning to the $Mg(ClO_4)_2$ electrolyte and soaking overnight, the electrode remained unresponsive to CO_2 and gave a similar CO i-E curve to figure 5.8. Hence the buffering action of $Mg(ClO_4)_2$ is sufficient to maintain a stable, reproducible electrode performance.

The electrode was tested for oxygen reduction performance in 2M $Mg(ClO_4)_2$ solution. The initial response is plotted in figure 5.5. At currents up to about 30μA, the performance remained fairly steady but at higher current levels a progressive decay was observed. For example the initial current at 0.8 volts was 340μA, at 0.700 volts the current suddenly dropped to 125μA and decayed over a period of 4 hours to 12μA. On the return scan the current at 0.8 volts was only 4μA. CO-oxidation activity had also completely dissappeared. Acid washing completely restored the original electrode performance and it is likely that the high cathodic current densities had generated sufficient OH^- ions to cause blockage of the electrode surface by the $Mg(OH)_2$ precipitate. The mode of buffer action with Mg^{++} ions could therefore, cause problems at the counter electrode of a CO-sensor and other buffer systems, such as borates, are more attractive in this application.

5.3. Gold Electrodes in Sodium Perchlorate, Boric Acid Buffered Solutions.

5.3.1. The Electrolyte.

The basic solution consisted of 4M $NaClO_4$ to which boric acid was added and the pH adjusted to the required value by adding NaOH solution. Boric acid has a solubility ranging between 0.32 M at $0^{o}C$ to 6.3 M at $100^{o}C$. (Table 2.1.). However, as the solution pH is increased, the acid is converted to sodium tetraborate which has a much lower solubility, ranging between 0.074 M at $0^{o}C$. and 0.44 M at $100^{o}C$. The highest pH likely to be used in the sensor is about 7.5, since above this value the system becomes increasingly sensitive to CO_2. Solubility tests in ambient temperatures (15-$20^{0}C$.) at pH 7.5 indicated that 15 g/l (0.24 M) was the maximum boric acid content and this concentration was used in all tests described in this section.

5.3.2. Gold Electrode Behaviour as a Function of Au:PTFE ratio at pH 7.

Fresh electrodes having Au:PTFE ratios of 1:1.7, 1:1 and 2:1 were completely inactive for CO-oxidation. This was ascribed to poor wetting at the electrode by the electrolyte. The electrodes exhibited high activity when tested in 4M NaOH solution and on washing and returning to the pH 7 electrolyte gave performances typified by that given in Table 5.1. None of the electrodes exhibited any CO_2 response to a 5% CO_2 in air gas mixture after 24 hours soaking in the neutral, buffered electrolyte.

Three further electrodes were prepared with Au:PTFE ratios of 5:1, 10:1 and 15:1. All these exhibited comparable electrochemical performance without any exposure to 4M NaOH. The CO-oxidation activity and background current data are listed in Table 5.2. All these electrodes underwent considerable activation after anodising at 1.8 volts. This activation remained stable after an overnight stand period at air

R.P. with the 5:1 electrode, but tended to decay to a somewhat lower value with the other two electrodes.

None of the electrodes were sensitive to a 5% CO_2 in air gas mixture at any potential or any stage of the test.

5.3.3. Gold Electrode behaviour as a Function of pH with a 10:1 Au:PTFE ratio.

The 10:1 Au:PTFE electrode above was tested in $NaClO_4$ / borate electrolytes adjusted to the pH's 4.3, 6.3 and 8.25. The CO-oxidation activity was similar to that in the pH 7 electrolyte with very little activity ($< 2\mu A$ in 50 ppm CO in air on a 3.142 cm^2 electrode) below 1.2 volts and a maximum of about $20\mu A$ at 1.6 volts, after anodising at 1.8 volts. The pH 8.25 electrolyte imparted slight CO_2 sensitivity with a 5% CO_2 in air gas mixture - about-$1\mu A$.

5.3.4. Electrochemical Tests with mixed Precious Metal Catalysts in pH 7 $NaClO_4$/borate electrolyte.

Gold mixtures with Pt, Pd and Fe_2O_3 were prepared; metal:metal ratios were 1:1 and Au:Fe_2O_3 was 10:1. These powders were fabricated into 10:1 catalyst:PTFE electrodes and tested for CO-oxidation activity. In all cases the maximum CO-oxidation currents were below corresponding pure gold values. Typical maximum CO-oxidation currents were $5\mu A$ in a 50 ppm CO in air gas mixture on a 3.142 cm^2 electrode.

5.4. Conclusions - Neutral Salt Electrolytes.

- Carbon dioxide interference is absent at pH's below about 8.

- gold electrodes only exhibit measurable CO-oxidation activities in pH 7, borate, sodium perchlorate electrolytes at potentials about 150 mV more anodic than the air R.P., i.e. above about 1.2 volts on the D.H.E. scale. Even at these potentials, best electrode activities were only about $0.13\mu A/ppm/cm^2$. compared to $0.5\mu A/ppm/cm^2$ for the "Ecolyser" Pt electrode in 6.84 N H_2SO_4 and 0.34 to $0.4\mu A/ppm/cm^2$ for gold electrodes in 4M NaOH.

Attempts to activate gold at lower potentials by admixing with Pd, Pt and Fe_2O_3 were unsuccessful.

- magnesium perchlorate electrolyte resulted in higher activities at lower potentials than $NaClO_4$/borate, but maximum currents ($\sim 0.064 \mu A/ppm/cm^2$ at 1 volt on D.H.E. Scale) were still too low. Precipitation of $Mg(OH)_2$ by reaction products at the counter may also cause problems.

6. PRODUCTION AND TESTING OF EXPERIMENTAL CARBON MONOXIDE SENSORS.

6.1. Hardware.

6.1.1. Constructional Materials.

The electrode/electrolyte investigations of the previous sections established a strong preference for an acidic electrolyte system. Consquently, all materials in contact with the electrolyte had to be acid resistant which precluded the CTL Oxygen Sensor materials. The experimental sensor bodies used for this work were made from machined perspex and sealing effected by means of a neoprene O-ring. Gold or platinum foils were used for current collection and platinum black was the primary electrocatalyst for both the counter and sensing electrodes. Electrodes consisted of PTFE-bonded catalyst layers, foil transferred to a porous PTFE backing tape. Webril separator material, as used in the CTL Oxygen Sensor, proved compatible with the cell electrolytes used, over a period of several months.

Components not in direct contact with the electrolyte, e.g. gas diffusers, external electrical connections, clamping bolts etc., were made from nickel or nickel plated steel.

6.1.2. General Cell Design Features.

The construction of the cell design is shown in figure 6.1. The sensing and counter electrodes were held in a close sandwich arrangement, and separated by a pair of Webril discs which "wicked" electrolyte from a reservoir contained behind the counter electrode. A single neoprene O-ring sealed the edges of both electrodes.

This configuration offers the following advantages over other designs, such as the Ecolyser cell:

-oxygen diffusion path to the counter electrode is minimised and hence polarisation of this electrode under load will be less.

-gas bubbles resulting from water evaporation from the electrolyte form in the reservoir and do not interfere with the sensor operation.

-sealing areas are at a minimum.

6.1.3. Design of Gas Diffusion Restriction.

The sensor top cap assembly, controlling diffusion of the test gas to the sensing electrodes was designed to achieve a high degree of signal current distribution over the electrode cross section. To this end a pattern of 9 holes was drilled in the perspex end plate as shown in figure 6.1. and a nickel mesh, coupled with an additional porous PTFE disc, were located in a recess between the sensing electrode and capillary holes to act as a gas "spreader".

Each capillary hole was 1.2 mm diameter and 3.68 mm long. The hole sensitivity, calculated from equation 1.3., section 1 (assuming diffusion coefficients for O_2 and CO in air are the same - 0.21 $cm^2\ sec^{-1}$) is 0.057μA/ppm CO. And for 9 holes the overall sensitivity should be 0.51μA/ppm CO. Measured sensitivities on actual sensors were only 0.10 to 0.11μA/ppm CO for the whole electrode/top cap assembly and obviously the capillary holes only constituted some 20 to 25% of the total diffusional resistance to the incoming gas. Since temperature coefficients were only about 0.2 to 0.4% per ^{o}C (section 6.2.), the additional diffusional resistance probably originated predominantly from gaseous diffusion barriers such as the PTFE tapes and nickel mesh, rather than through liquid films present in the electrode structure.

With the CTL Oxygen Sensor, in ambient air, the concentration gradients are considerably larger. Consequently the required capillary hole size is much smaller and it provides essentially all the diffusion restriction. The "spreading" diffusion resistance,downstream of the capillary is then relatively insignificant.

6.1.4. Electrodes and Electrolytes.

Three experimental sensors were built and tested, comprising the following electrodes and electrolytes:

Sensor P5. This was the first sensor made and its constructional details were somewhat different from the other two:

- capillary	single 3.175 mm dia. hole 5 mm length.
- gas spreader,	single Webril disc
- current collectors,	gold foil
- sensing and counter electrodes,	platinum black
- electrode projected area,	1.13 cm^2
- electrolyte,	7 N H_2SO_4

The estimated hole sensitivity was 0.27μA/ppm and measured value 0.067μA/ppm. An additional PTFE membrane was stuck to the capillary inlet to act as a dust protection which reduced the sensor sensitivity to 0.03μA/ppm.

Sensor P9.

-capillary	9 hole x 1.2 mm dia. x 3.68 mm length as described (section 6.1.3.)
- gas spreader,	nickel mesh + PTFE disc
- current collectors,	gold foil
- sensing electrode,	platinum black and gold powder (1:1) intimately mixed plus gold flake to improve conductivity
- counter electrode,	platinum black with gold flake
- electrode projected area,	3.142 cm^2
- electrolyte,	1 N H_2SO_4.

Sensor P18.

- capillary and gas spreader,	as for sensor P9.
- current collectors,	platinum foil
- sensing and counter electrodes,	platinum black
- electrode projected area,	3.142 cm^2
- electrolyte,	7 N H_2SO_4

6.1.5. Electronic Control.

Two methods were used:

- 100 ohm load resistor.
- 47 ohm load with potentiostatic bias potential across the cell to maintain the sensing electrode at about 5 mV more anodic relative to the counter electrode.

The fixed load resistor resulted in slightly negative or positive baseline currents flowing between the counter and sensing electrodes (figure 6.4.). This was effectively removed by the external potentiostatic cell potential. It was also found that the potentiostatic control circuit improved the baseline hysteresis when CO cycling.

When setting the cell zero the capillary holes were blocked off to ensure that the sensor was in a CO-free atmosphere. Ambient air and compressed air were found to give variable responses, equivalent to a few ppm CO relative to the blocked capillary setting, depending on the time of day (figures 6.4. and 6.7.) The ambient air response is due to daily variations in the atmospheric CO concentration.

6.2. Sensor Testing.

6.2.1. Response of Sensors to Carbon Monoxide.

All sensors required a settling-in period of about 1 week during which the response progressively reduced to a stable limiting value when exposed to a 55 ppm CO in air test gas. The signals and response times of the fully settled sensors were as follows:

SENSOR	P5*	P9	P18
Signal 55 ppm CO in air (μA)	1.7	6.0	5.3
Sensitivity (μA/ppm CO)	0.03	0.109	0.096
Response time 80% change (sec)	-	16	24
Response time 90% change (sec)	-	24	35

* Constructional details of sensor P5 differed from the other two - see section 6.1.4.

Sensors P18 and P9 were cycled on the 55 ppm CO in air test gas. Over the first two cycles there occurred a slight decrease in signal amplitude of about 0.05μA or 0.5 ppm CO equivalent and a shift in air baseline of

similar magnitude. The sensor responses appeared to stabilise on further cycling.

The ambient laboratory and street level air signals of sensors P9 and P18 were continuously monitored over several days. The results of two 24 hour test periods are given in figures 6.5. and 6.7. respectively. Figure 6.6. shows the effect on sensor signal at a higher chart speed when changing from a street to a laboratory location. The apparently much noisier street trace was obviously largely due to real variations in CO concentration with very little electronic noise, apart from the occasional interference spike. Figure 6.4. gives the results of a baseline monitor over 24 hours on sensor P19 with a blocked capillary This shows an apparent +0.025 $\pm$ 0.005μA signal (0.25 ppm CO equivalent) on a 100 ohm fixed load resistor which may be at least partly due to some incomplete sealing of the capillary block.

Two further platinum catalyst sensors have recently been made, confirming the general behaviour described above with fresh sensors, but no longer term monitoring results are yet available. Figure 6.3. shows the response of one of these sensors on a 100 ohm fixed load resistor.

The results depicted in figures 6.2. to 6.7. clearly demonstrate that the sensors are capable of a fast, stable and reproducible CO response, with a discrimination of better than 0.5 ppm.

6.2.2. Longer Term Effects.

The sensors have been in operation at the time of reporting for the following periods:

P5	3 months
P9	6 weeks
P18	4 weeks

During these times the sensor signals from P5 and P18 to the 55 ppm CO in air test gas have remained constant. Sensor P9 however, had shown some decrease in its signal during week 5 when a value of 5.9μA was measured which had further reduced to 5.5μA by the end of week 6.

Sensors P9 and P 18 were operated with the 5 mV potentiostatic control system, whereas P5 had a fixed load resistor. The latter's baseline in ambient air over the 3 month period has been at -0.25μA; the other two sensors have maintained a zero baseline on blocked capillaries ($\pm$ 0.1μA), over their lifetimes to date.

6.2.3. Linearity.

Sensors P9 and P18 were tested in a 9.5 ppm CO in air gas to check

their linearity to CO concentration in the range 0 to 50 ppm. The results were as follows:

Sensor	P9	P18
Signal 55 ppm CO (μA)	6.00	5.30
Signal 9.5 ppm CO (μA)	1.10	0.93
Calculated signal in 9.5 ppm CO assuming perfect linearity (μA)	1.04	0.92

6.2.4. Temperature Coefficients.

Signals in 55 ppm CO in air test gas were measured over the temperature range 20 to 40^{o}C and temperature coefficients obtained of 0.24 and 0.39% per ^{o}C for sensors P9 and P18 respectively.

6.2.5. Attitude Stability.

180^{o} inversion gave no detectable change in the baseline signal (i.e. o.5 ppm CO equivalent), even with sensor P9 which had an air bubble of about 1.5 ml in the electrolyte reservoir due to water evaporation.

6.2.6. Water Loss.

Sensors P5 and P18, using 7 N H_2SO_4, lost less than 0.5 ml water over their 3 month and 4 week periods respectively. Sensor P9 with 1N H_2SO_4 had lost about 1.5 ml over the first 6 weeks.

6.3. Discussion.

The sensor test results indicate that the design is capable of a fast, stable and reproducible, linear response to carbon monoxide in the concentration range 0 to 55 ppm CO in air, discriminating to better than 0.5ppm with a stable, zero current, baseline using the potentiostatic control circuit.

The P9 sensor incorporating a platinum/gold electrocatalyst in 1N H_2SO_4 had a much smaller temperature coefficient than the P18 sensor with a plain platinum electrocatalyst and 7N H_2SO_4 electrolyte. The measured values of 0.24% per ^{o}C and 0.39% per ^{o}C. for sensors P9 and P18 respectively compare with 0.17% per ^{o}C. for a sensor output totally governed by gaseous diffusion. These results suggest that the P9 sensor electrode/electrolyte system had a higher intrinsic CO-oxidation activity than the P18 system. This needs to be confirmed in open electrode tests (see sections 3,4 and 5) but improved

characteristics may result through optimisation of the electrode structure and composition and suitable choice of electrolyte type and concentration.

Although the addition of gold to the electrocatalyst may increase the activity of platinum electrodes towards CO-oxidation, the studies on gold electrodes in acid media (section 4.1.) indicate that corrosion rates will be too high at high acid concentrations at or above 1N (or pH 0). This may explain the serious decline in CO-response of the P9 sensor after 6 weeks operation. Gold may be employed in 0.1N acid systems with added salts such as $MgSO_4$ or $NaClO_4$ to reduce water evaporation, but an all platinum system is likely to be necessary at higher acid concentrations. In either case improved intrinsic performance might be obtained through optimisation of the catalyst, PTFE ratio.

With regard to the choice of electrolyte system, options exist other than plain H_2SO_4. The dilute acid with dissolved salts has already been mentioned, and perchloric acid may replace sulphuric. Final selection should be made on the basis of the following considerations, which need to be assessed in open electrode tests:

- CO-oxidation activity.
- Corrosion.
- Electrode specificity to CO in the presence of interfering gases, particularly hydrogen. Some work at NCB (Yorks) Laboratories has indicated that H_2 interference is reduced in more concentrated acids.
- Handlability and potential hazards in duty.

7. CONCLUSIONS AND FURTHER WORK.

Experimental laboratory sensors, using sulphuric acid electrolyte and platinum or platinum/gold catalysts have demonstrated very promising performance with good reproducibility, stability and low temperature coefficients. The sensor design embodied a number of features differing from previous practice. A pair of hydrophobic gas diffusion electrodes, manufactured by a foil transfer technique, were mounted in a "disc sandwich" arrangement, with a wicking separator leading from between the electrodes, through a hole in the counter electrode to an electrolyte reserviour. Indications were that attitude stability of the signal was very good and virtually unaffected by wide changes in electrolyte volume due to drying out. Gas access to the sensing electrode was restricted by a gaseous diffusion barrier which resulted in considerably lower temperature coefficients, e.g. about 1/10th the Ecolyser type of cell which is controlled by gas diffusion through an electrolyte film within the electrode structure.

The sensors were operated with both a fixed load resistor and a two electrode potentiostatic circuit of CTL design. The latter circuit ensured a true zero current baseline and gave improved signal response compared to a simple load resistor circuit. The potentiostatic control circuit could be developed into a stable, reliable, low cost signal processing unit for a practical instrument.

Sensor resolutions were better than 1 ppm carbon monoxide. Long term testing was limited and so far there is insufficient data to comment reliably on drift, though one sensor which is now 3 months old has shown encouraging stability. The acid electrolyte system substantially as described above is the one selected for further development. Alternative electrolyte systems were investigated but found to be less suitable. While high carbon monoxide signals can be obtained with gold catalysed electrodes in strong alkaline electrolytes, such systems suffer from severe interference by carbon dioxide. An in-situ gas scrubbing sensor design may overcome this problem, but failing an early demonstration of feasibility, it is not recommended to pursue these electrolyte systems. Electrolytes of near neutral pH were free of carbon dioxide interference but resulted in very

low carbon monoxide oxidation signals using a variety of precious metal catalysts, viz. Au, Pt, Au/Pt, Au/Pd and Au/Fe_2O_3.

An acid electrolyte system was therefore selected, but there remains a final choice of acid type and concentration. This essentially hinges on the choice between perchloric and sulphuric acid systems and whether strong acid is employed or dilute acid containing added salts such as sodium perchlorate or magnesium sulphate to maintain a low solution water vapour pressure. The final choice will be governed by factors such as CO-oxidation activity and selectivity, corrosion, handleability, etc.

Platinum is the basic electrocatalyst choice for acid systems. Gold has insufficient CO-oxidation activity per se, but may impart a synergic effect when intimately mixed with the platinum. This will need to be further assessed in the next phase of the development program, together with other catalyst performance parameters such as corrosion, selectivity etc. Also the electrode structure and composition, particularly the catalyst PTFE ratio, will need to be optimised for maximum CO-oxidation activity and a suitable production method evolved.

The CTL oxygen sensor hardware, based on nickel plated steel, will not be compatible with the chosen acidic electrolyte systems. Consequently the next phase of the program will be largely devoted to the development of suitable acid resistant hardware.

REFERENCES

(1) A.D.S. Tantram, J.R. Finbow; "Oxygen Detector for use in Coal Mines", TCU report, May 1976, NCB Contract Number YB 1350/09/22.

(2) J.P. Hoare; "Electrochemistry of Oxygen", (1968), Interscience, p.46.

(3) A.D.S. Tantram, R. Chan-Henry, B.S. Hobbs, J.R. Finbow; "Oxygen Detector for use in Coal Mines"; City Technology Ltd., Report No. 78/02/001, NCB Contract YB 1350/09/22, July, 1978.

(4) J. Giner; Journal Electrochemical Society (1964) Vol, 111, p.376.

Table 2.1. Solubilities of Various Salts in Water.

	Molecular weight	Solubilities *			
		g per 100 ml		moles l^{-1}	
$NaClO_4.H_2O$	140.46	209 (15)	284 (50)	14.9 (15)	20.0 (50)
$KClO_4$	138.55	0.75(0)	21.8(100)	0.05 (0)	1.6 (100)
NH_4ClO_4	117.50	10.74(0)	42.54(85)	0.91(0)	3.6 (80)
$LiClO_4$	106.40	59.7(25)		5.6(25)	
$Mg(ClO_4)_2$	223.23	49.9(25)	v.s.(hot)	2.2(25)	
$Ca(ClO_4)_2$	238.99	188.6(25)	v.s.(hot)	7.9(25)	
$Ba(ClO_4)_2$	336.27	198.5(25)	v.s.(hot)	5.9(25)	
H_3BO_3	61.84	1.95(0)	39.1(100)	0.32(0)	6.3(100)
$Na_2B_4O_7$ (tetraborate)	201.27	1.49(0)	8.79(40)	0.074(0)	0.44(40)
$NaH_2PO_4.H_2O$	138.01	59.9(0)	427(100)	0.43(0)	30.9(100)
$Na_2HPO_4.2H_2O$	178.01	100(50)	117(80)	5.6(50)	6.6(80)
Sodium Phthalate	210.11	very soluble			
Sodium acetate	82.04	119(0)	170 (100)	14.5(0)	20.7(100)
Na_2SO_4	142.04	4.76(0)	42.7(100)	0.34(0)	3(100)
K_2SO_4	174.27	12(25)	24(100)	0.69(25)	1.4(100)
$MgSO_4$	120.37	26(0)	73.8(100)	2.16(0)	6.13(100)
$NaNO_3$	84.99	92(25)	180(100)	10.8(25)	21(100)
KNO_3	101.11	13.1(0)	247(100)	1.32(0)	24(100)
$Mg(NO_3)_2.6H_2O$	256.43	42.3(18)	58(90)	1.65(18)	2.25(90)
NaCl	58.44	35.7(0)	39(100)	6.1(0)	6.7(100)
KCl	74.56	34.7(20)	56.7(100)	4.7(20)	7.6(100)
$MgCl_2$	95.22	54.3(20)	72.7(100)	5.7(20)	7.6(100)

* Figures in parenthesis are temperatures.

Table 3.1. Results of preliminary catalyst screening tests in alkaline solution (5M KOH).

Catalyst	Fabrication Method	CO-oxidation ($\mu A/ppm/cm^2$)	Corrosion ($\mu A/cm^2$)
Pd/Au 1:1	Deposition	0.0013	0.32
Au	Deposition	0.0002	0.20
Au/Pt 1:1	Deposition	$<10^{-4}$	0.20
Au	Foil Transfer	0.320	0.32
Au/Pd 1:1	Foil Transfer	0.016	0.20
Au/Fe_2O_3	Foil Transfer	0.064	0.32
Au/Pt 1:1	Foil Transfer	nil	0.13
Pt	Foil Transfer	nil	0.20
Au/Fe_2O_3	Mesh Electrode	0.22	0.32

Table 5.1. CO-oxidation activity and background currents of high PTFE content electrodes in $NaClO_4$/borate Electrolyte (pH 7) after exposure to 4M NaOH.

E vs D.H.E. (volts)	i_{CO} (μA)*	$i_{background}$ (μA)
1.000	2	0
1.100	2	1
1.200	4	0.5
1.300	5.5	1
1.400	10	2
1.500	16	5
1.600	20	6.5

* CO-oxidation currents are the net response to a 50 ppm CO in air mixture at an electrode 3.142 cm^2 in area.

Table 5.2. CO-oxidation activity and background currents of PTFE bonded Gold electrodes in neutral (pH 7) $NaClO_4$/borate electrolyte.

E vs D.H.E. (volts)	Au:PTFE ratio 5:1 i_{CO} (μA)	5:1 i_b (μA)	10:1 i_{CO} (μA)	10:1 i_b (μA)	15:1 i_{CO} (μA)	15:1 i_b (μA)
Forward Sweep from air R.P. of 0.96 volts in anodic direction.						
1.100	1	1	7	1	3.5	1
1.300	2.5	2.5	9	2.5	4	3
1.400	3	2.5	11	5	6	6
1.600	9	7	18	10	21	19
1.800	20	49	16	45	19	60
Reverse Sweep						
1.600	-	-	16	1	26	10
1.400	20	1	16	0	21	1
Overnight stand @ air R.P. then retested.						
1.400	19	1	12	1.5	11	3

Note:

i_b = background current.

CO-oxidation currents refer to the net response from 50 ppm CO in air gas mixture from a 3.142 cm^2 electrode.

SIDE VIEW

SIDE VIEW

SIDE VIEW Section on AA'
Showing position of electrolyte bridge/DHE reference electrode.

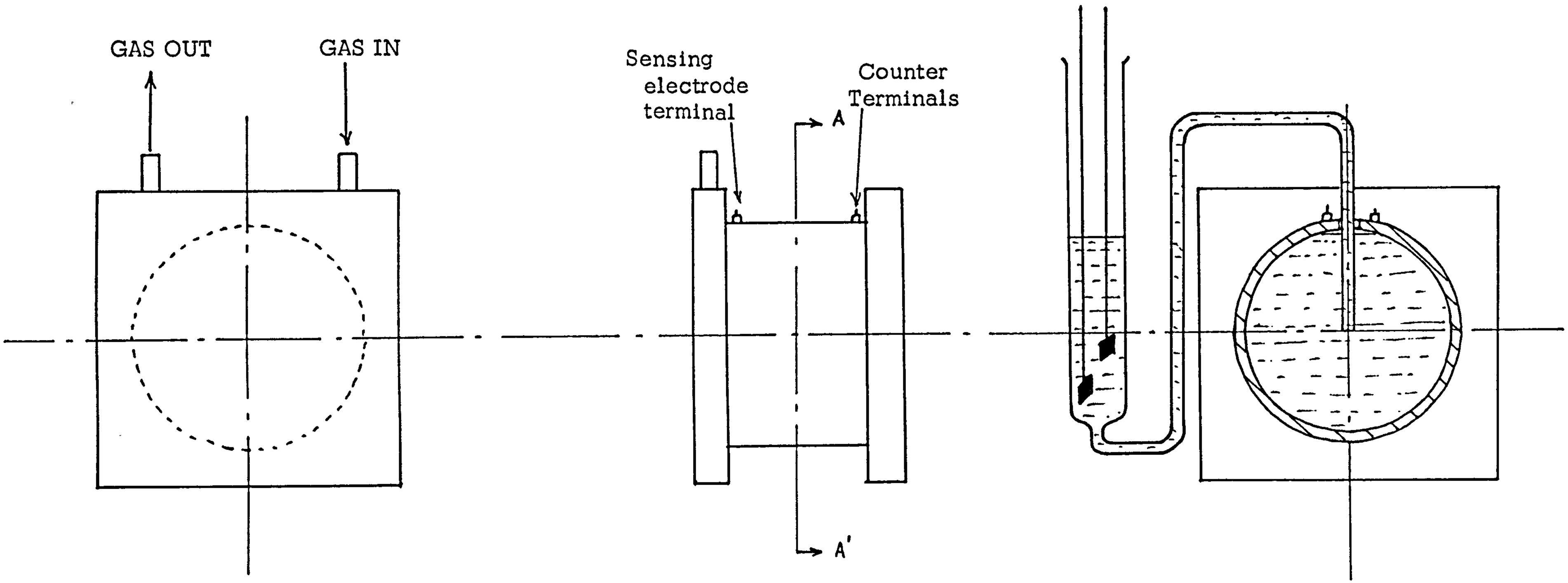

Figure.2.1. Diagram of Ecolyser Test Arrangement.

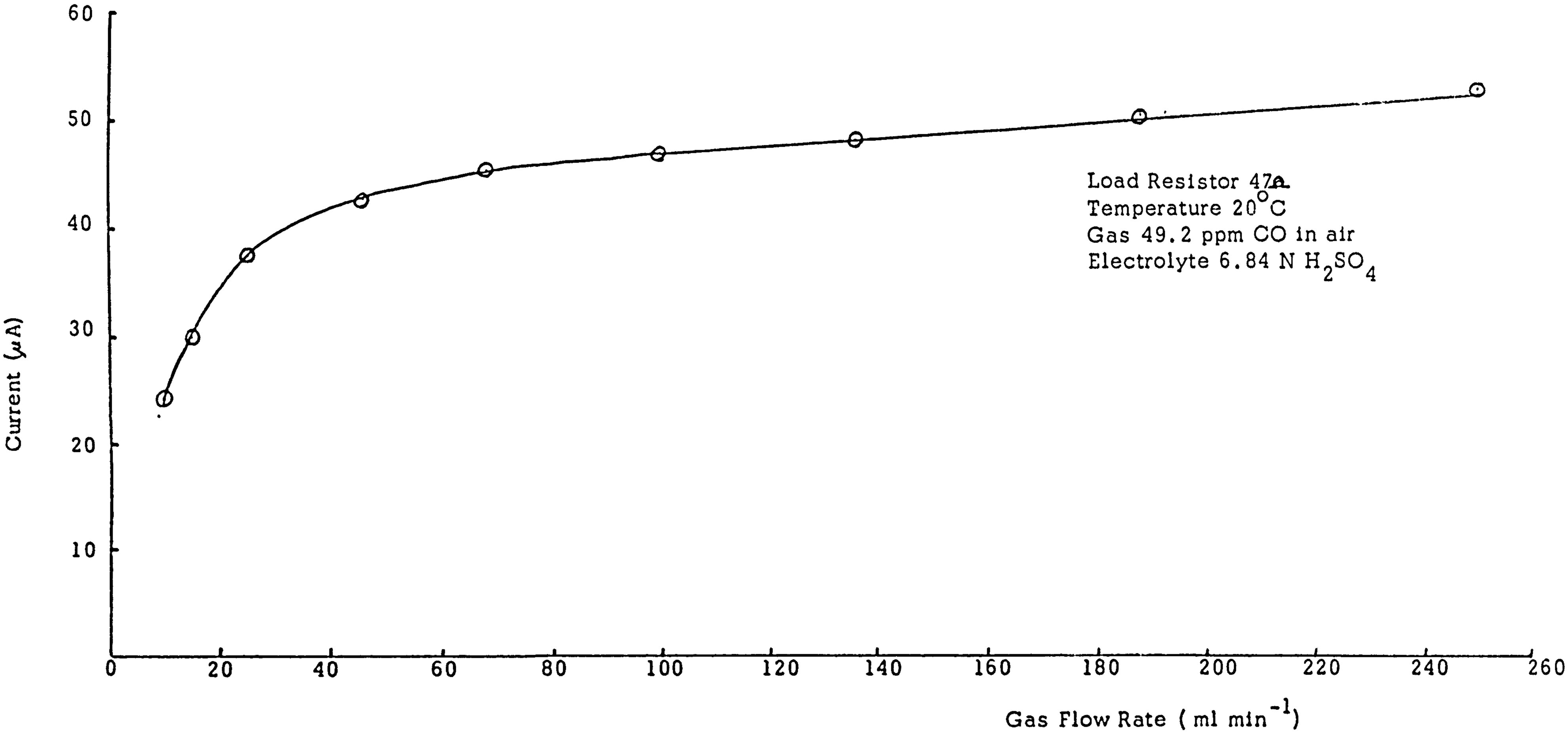

Figure 2.2 Output of Ecolyser Cell on a fixed load as a function of gas flow rate

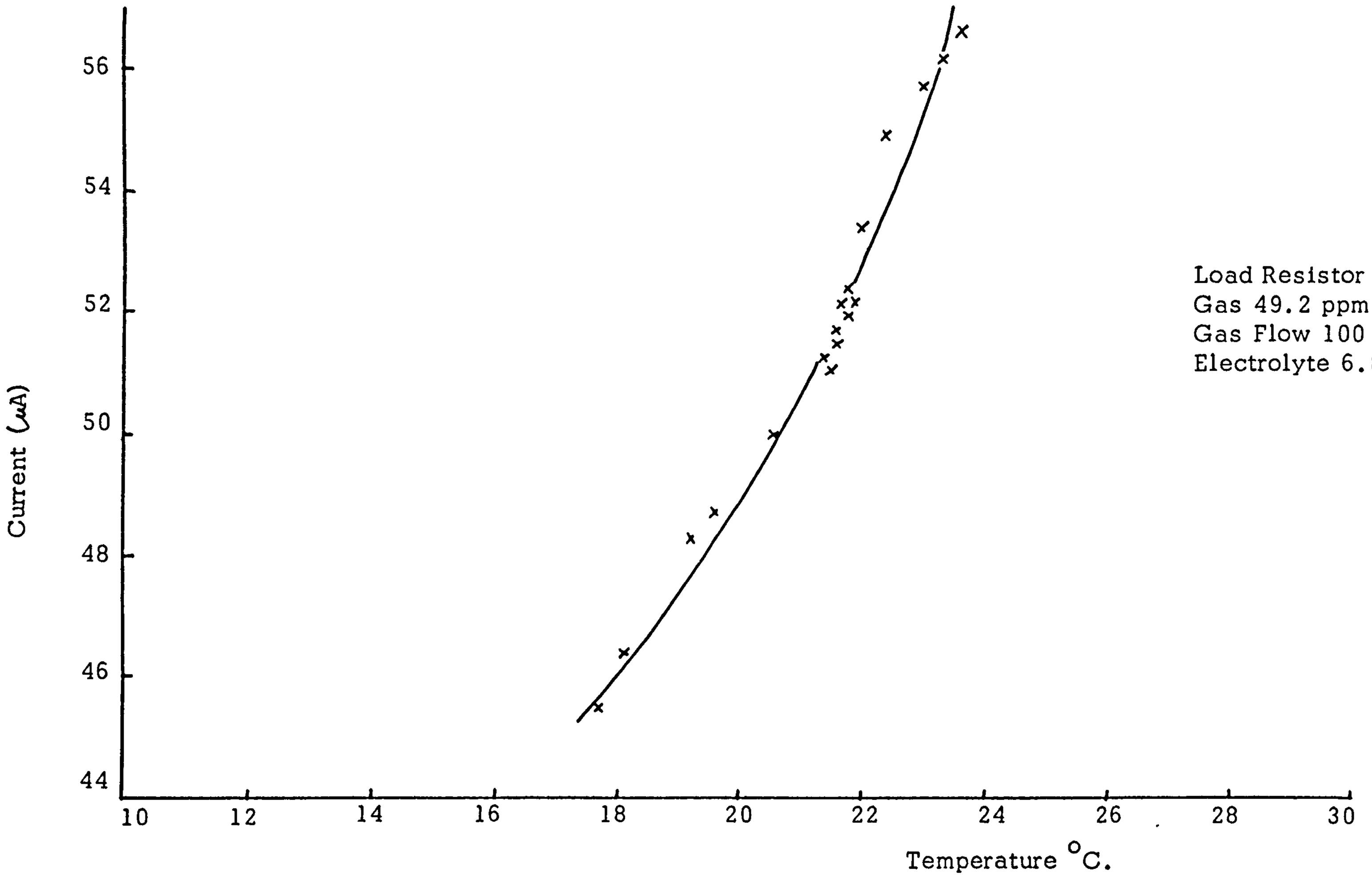

Figure 2.3. Temperature response of Ecolyser Cell.

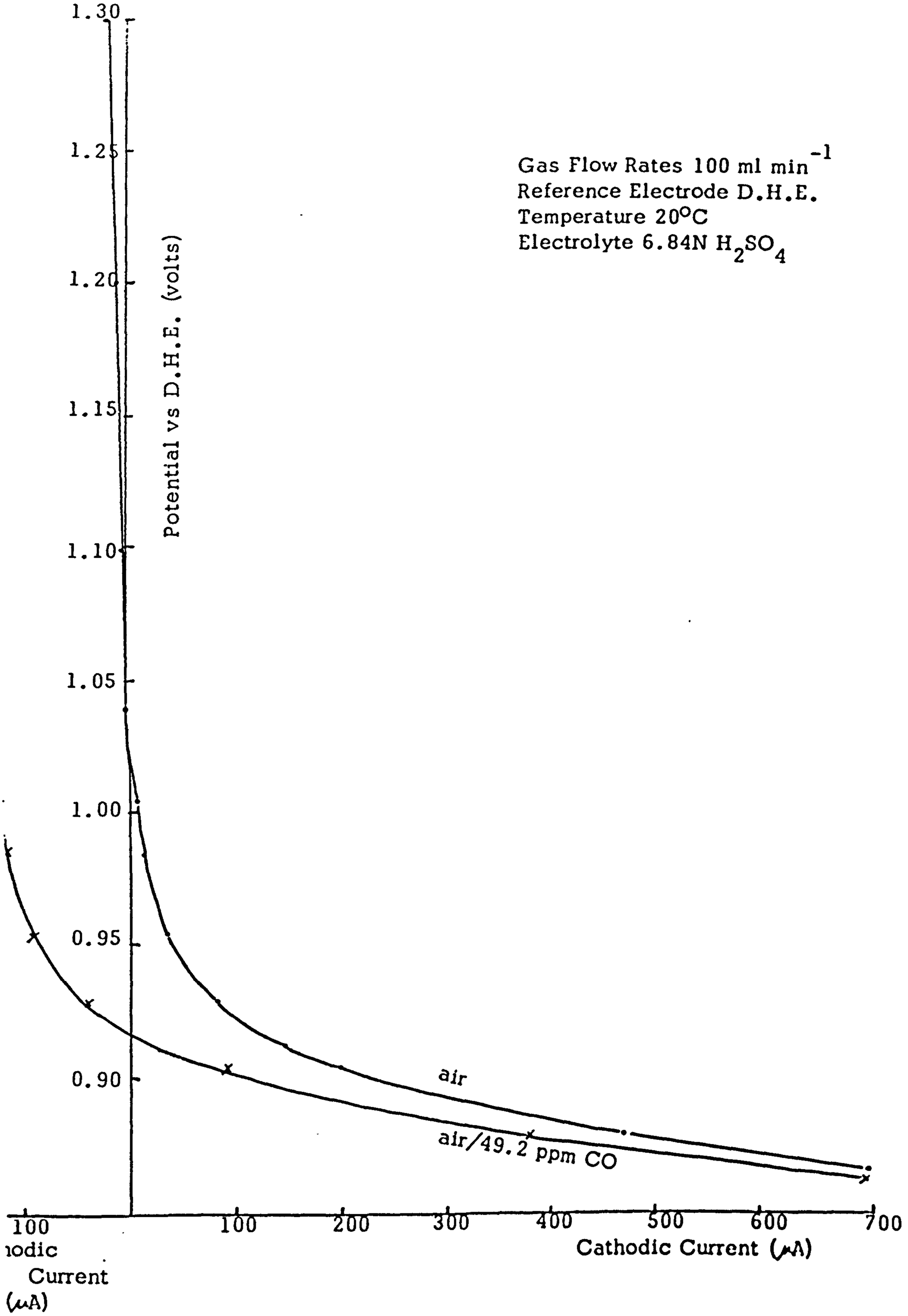

Figure 2.4. i-E curves for Ecolyser Cell with air and air/49 ppm CO.

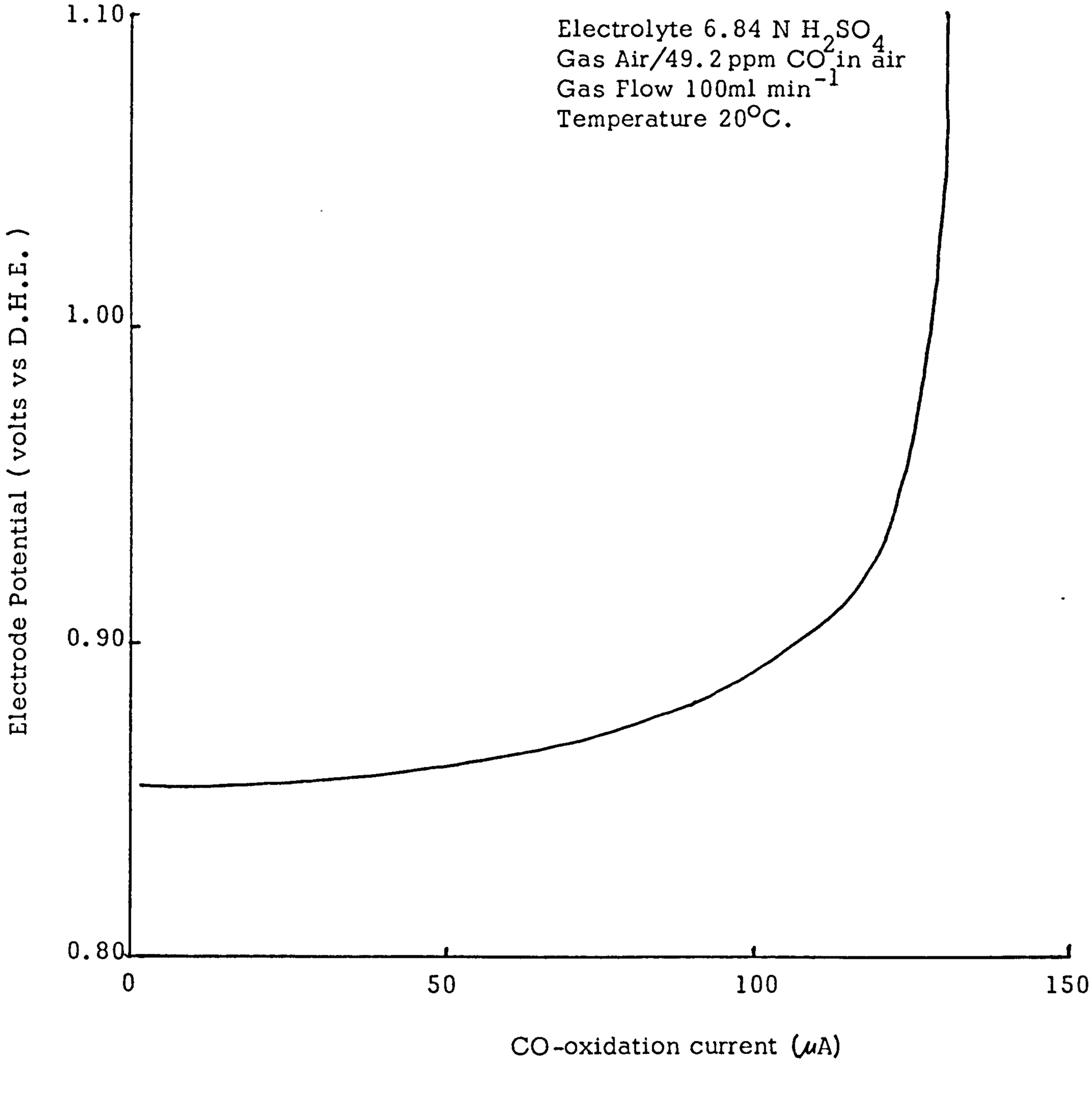

Figure 2.5. Derived CO-oxidation i-E curve for Ecolyser Cell.

Electrolyte 6.84 N H_2SO_4
Gas Flow Rates 100 ml min^{-1}
Gases compressed air Air/49.2 ppm CO
Temperature 20°C

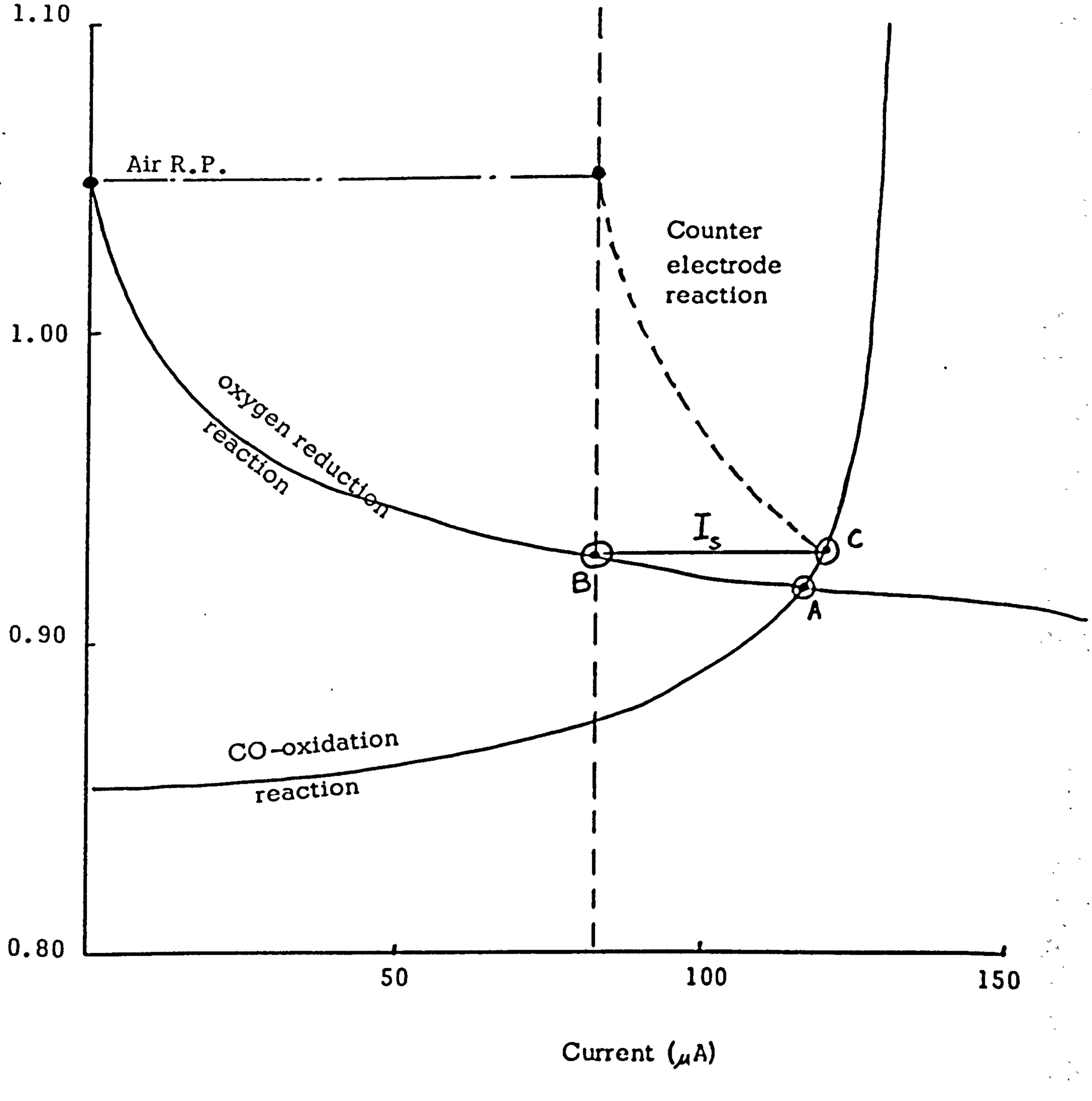

Figure 2.6. i-E curves for sensing electrode local cell and counter electrode in the Ecolyser Cell.

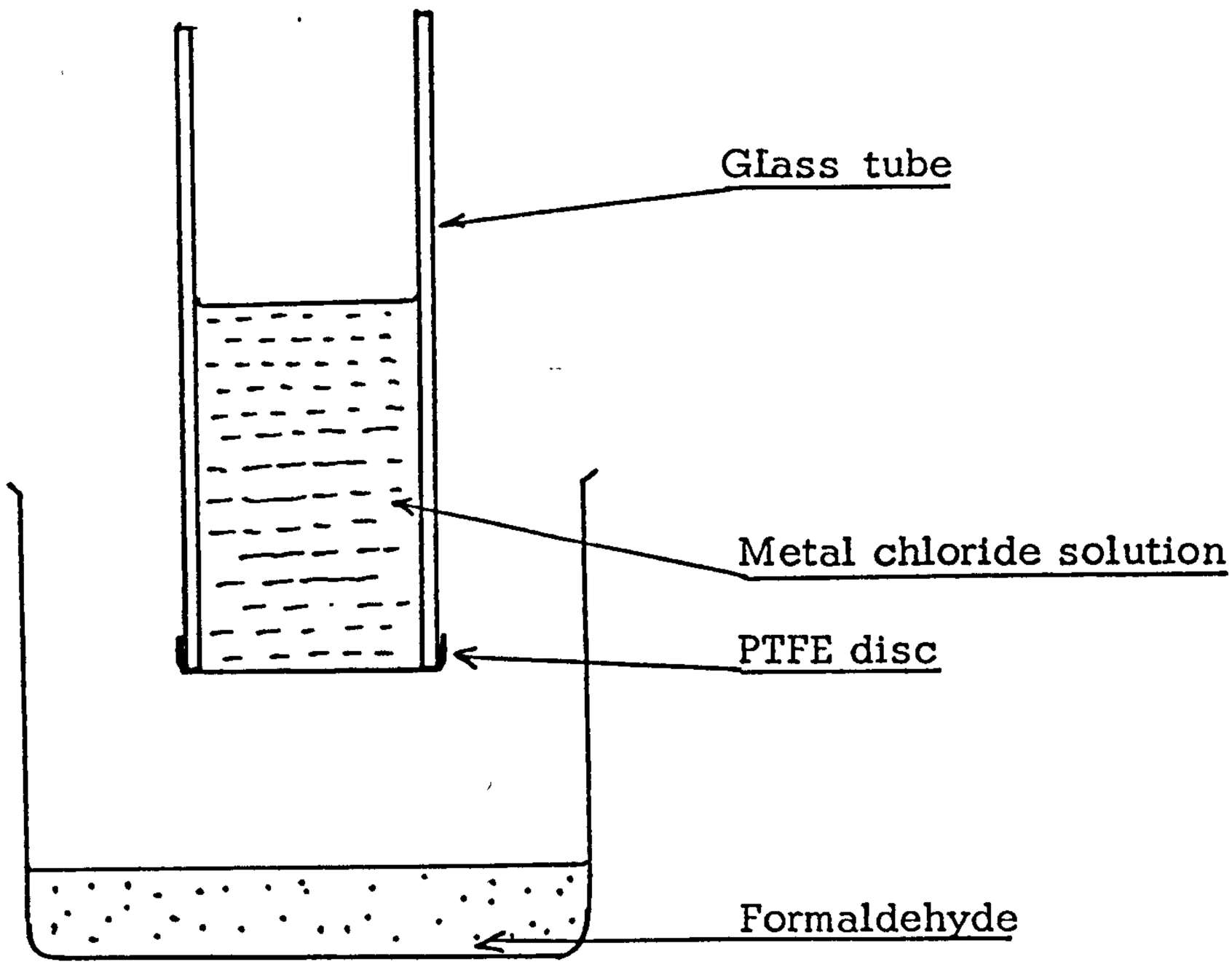

Figure 3.1. Arrangement for direct deposition of precious metals on a PTFE disc.

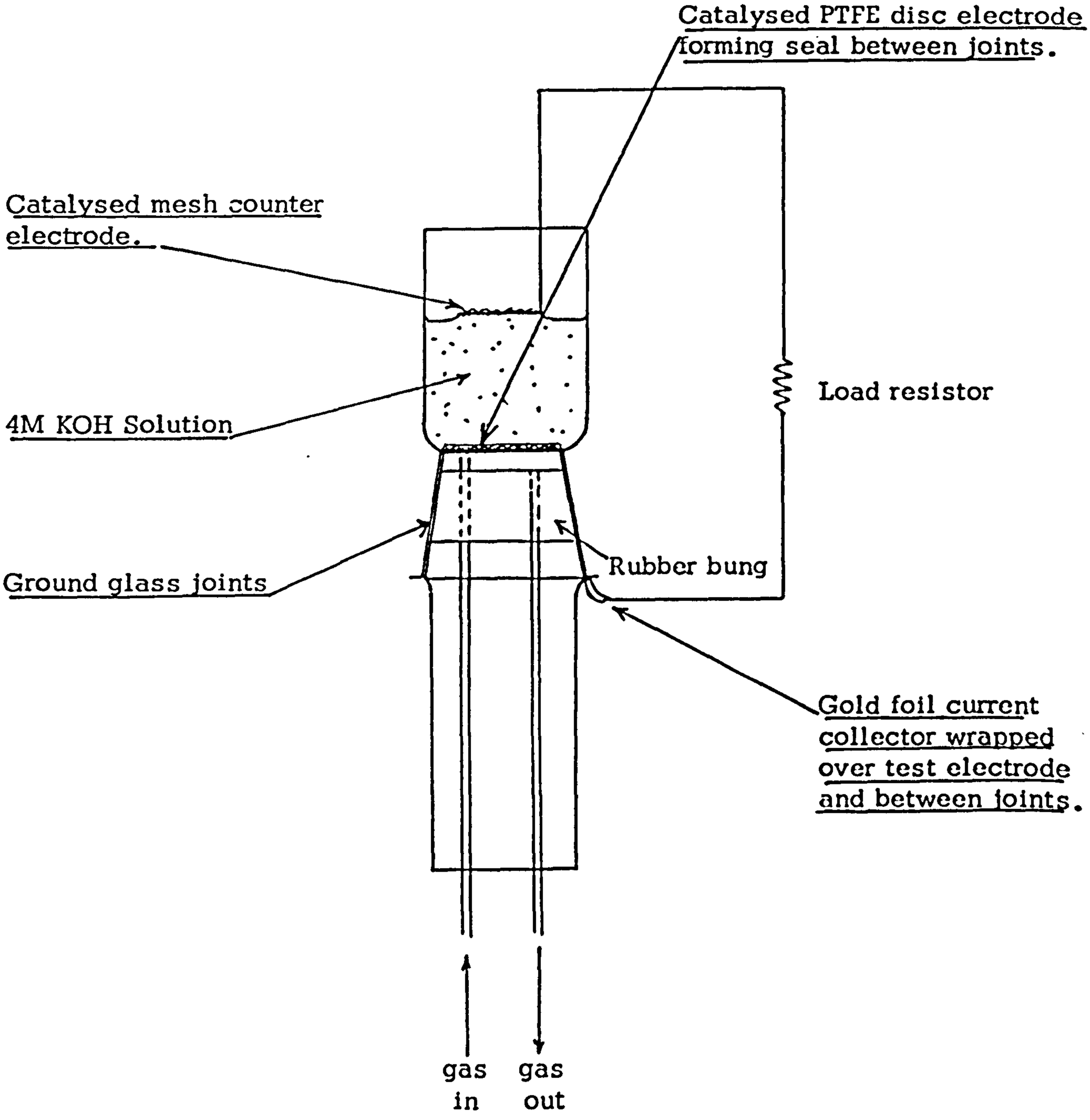

Figure 3.2. Catalyst Screening Test Cell Arrangement.

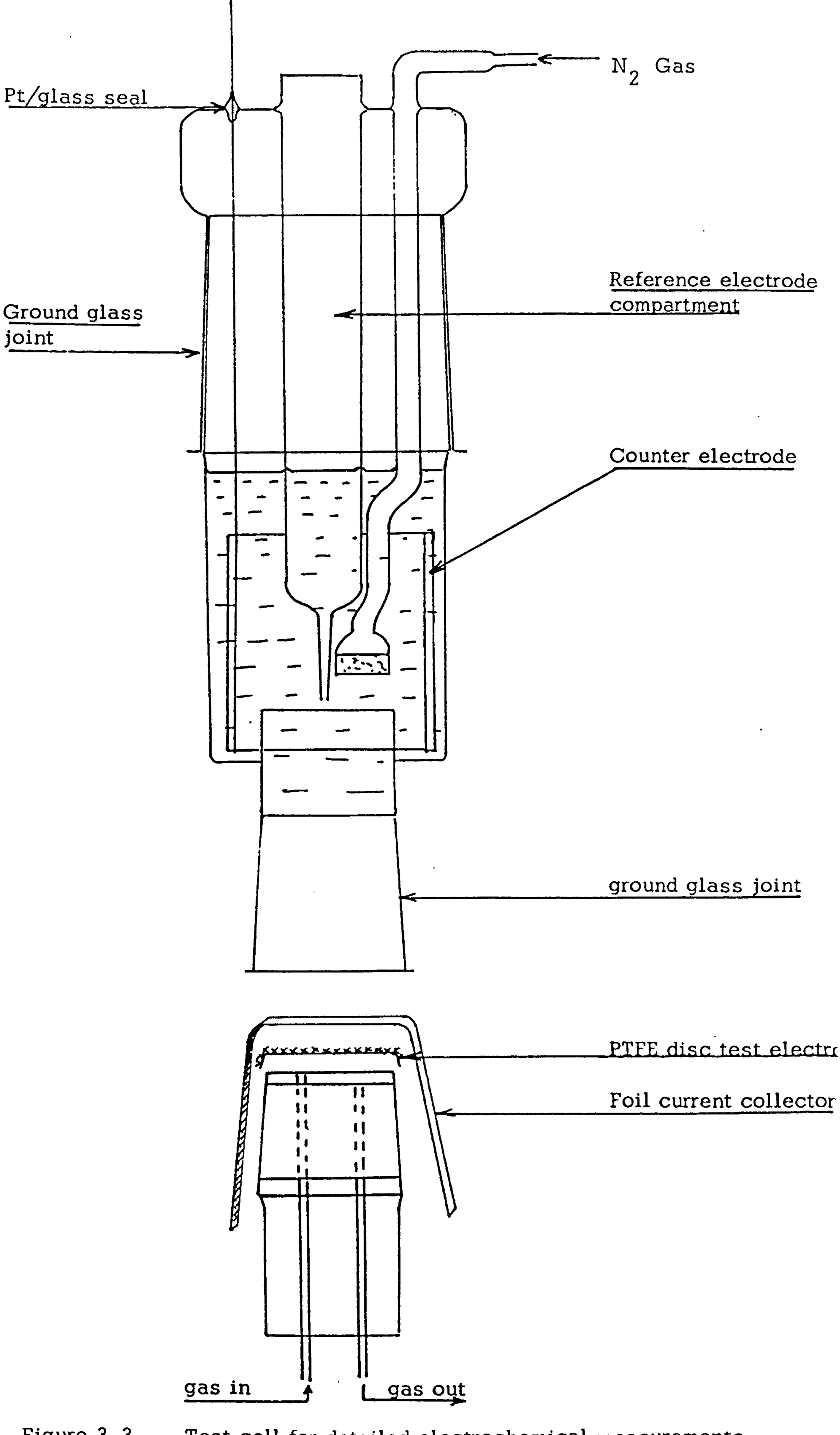

Figure 3.3. Test cell for detailed electrochemical measurements of electrode activity.

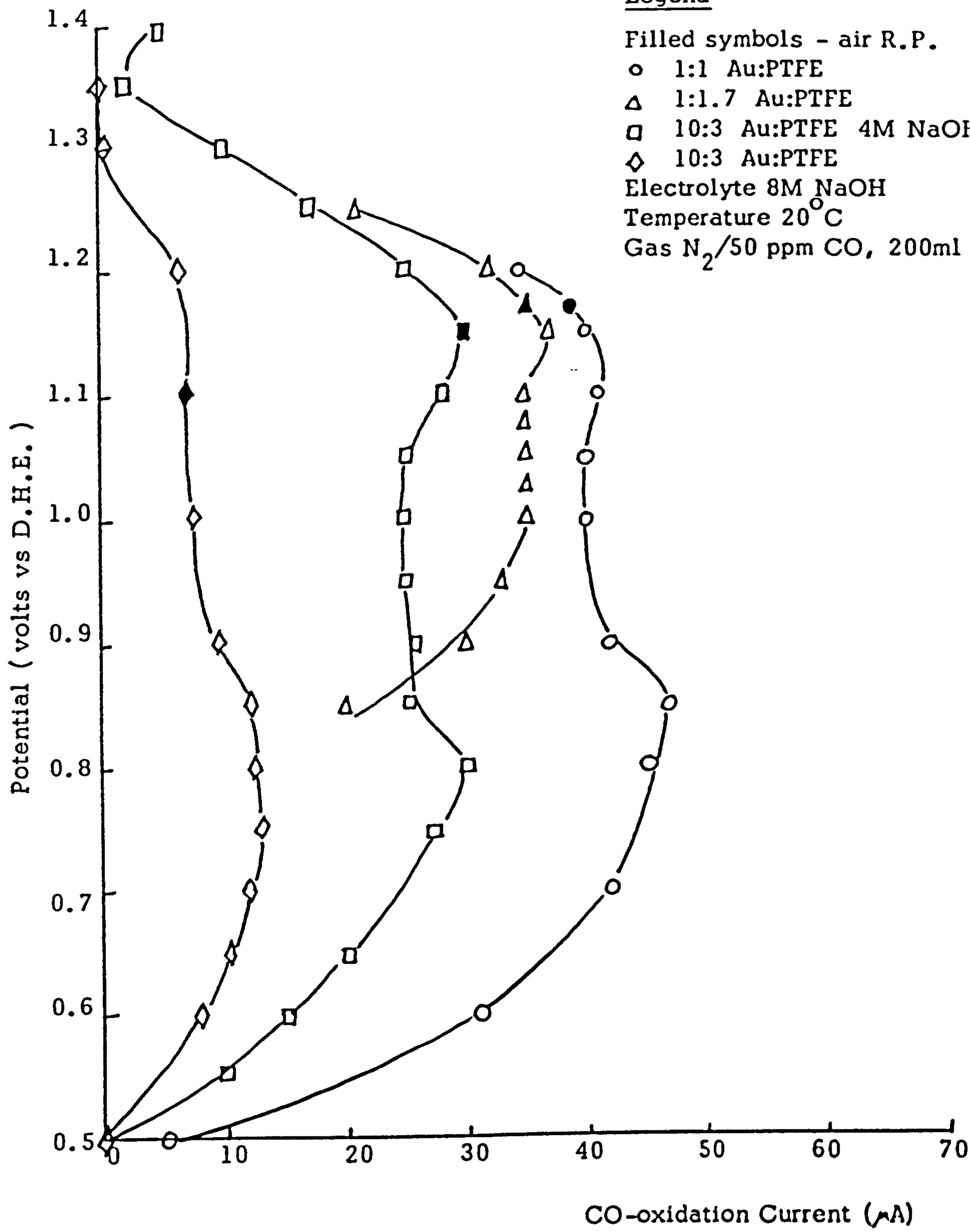

Figure 3.4. CO-oxidation i-E scans for gold electrodes in 8M NaOH.

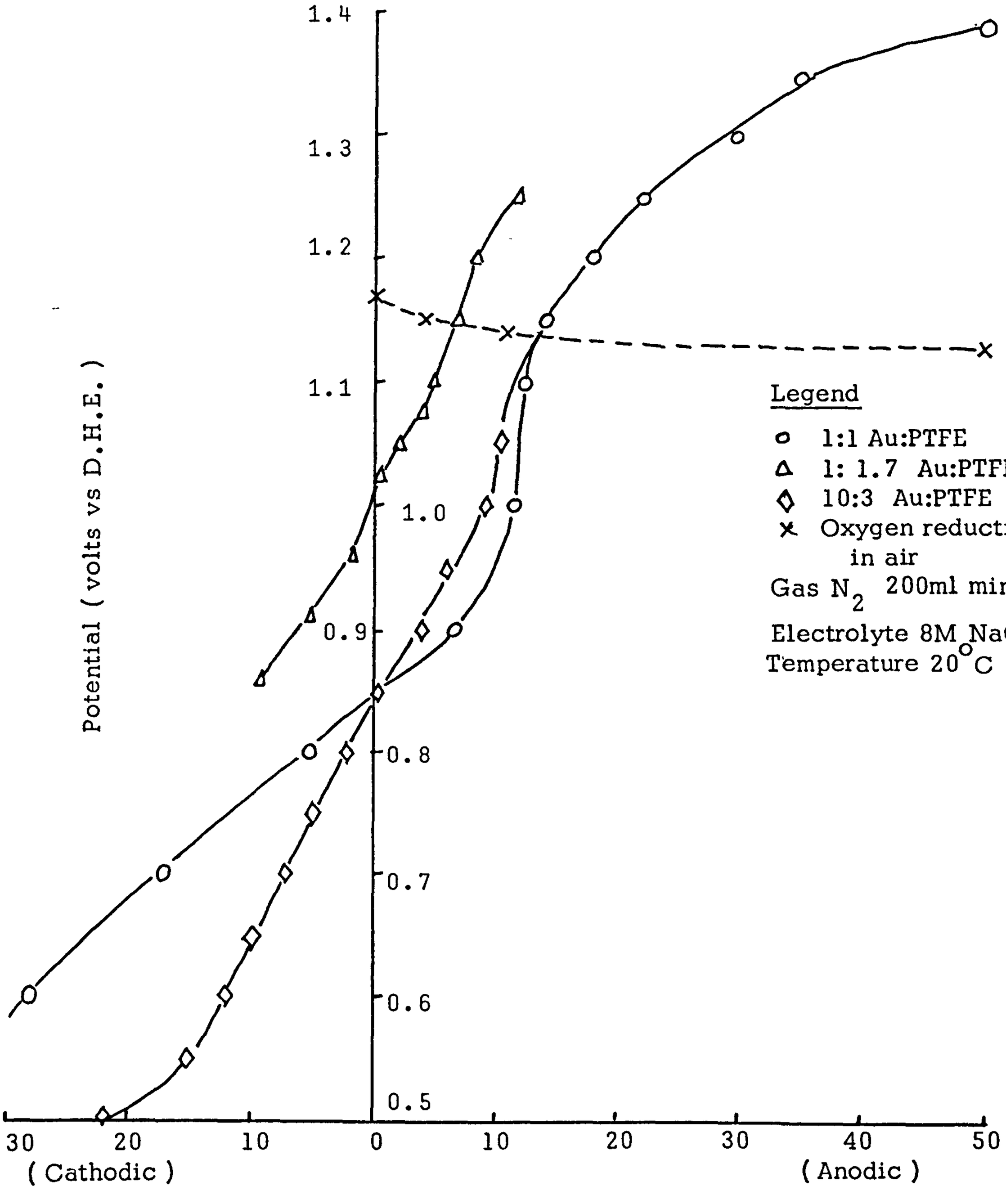

Figure 3.5. Background and oxygen reduction currents for gold electrodes in 8M NaOH.

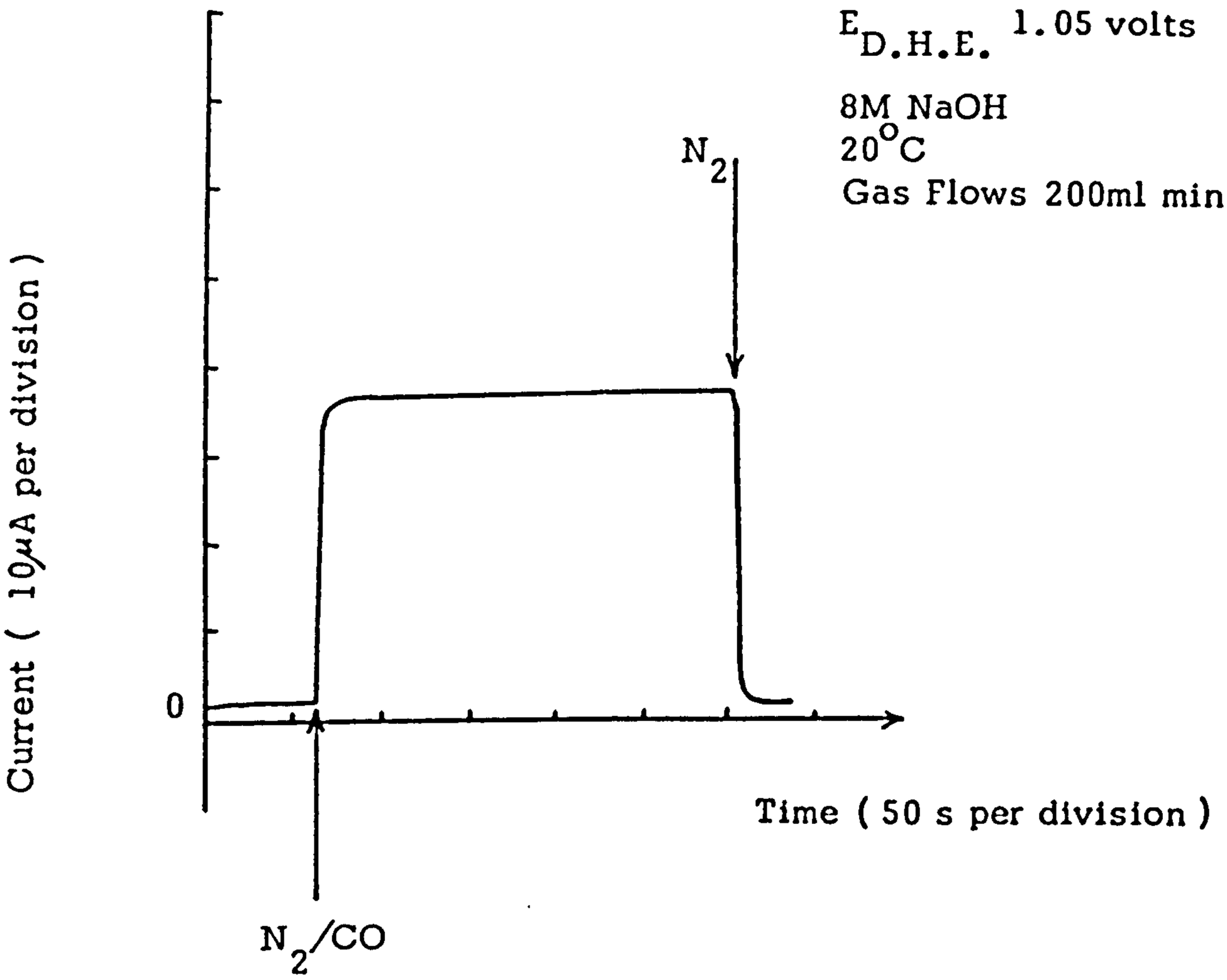

Figure 3.6. CO-oxidation time response of gold electrode in 8M NaOH.

Au:PTFE 1:1.7
$E_{D.H.E.}$ 1.05 volts vs D.H.E.
8M NaOH
20°C
Gas Flows 200ml min^{-1}

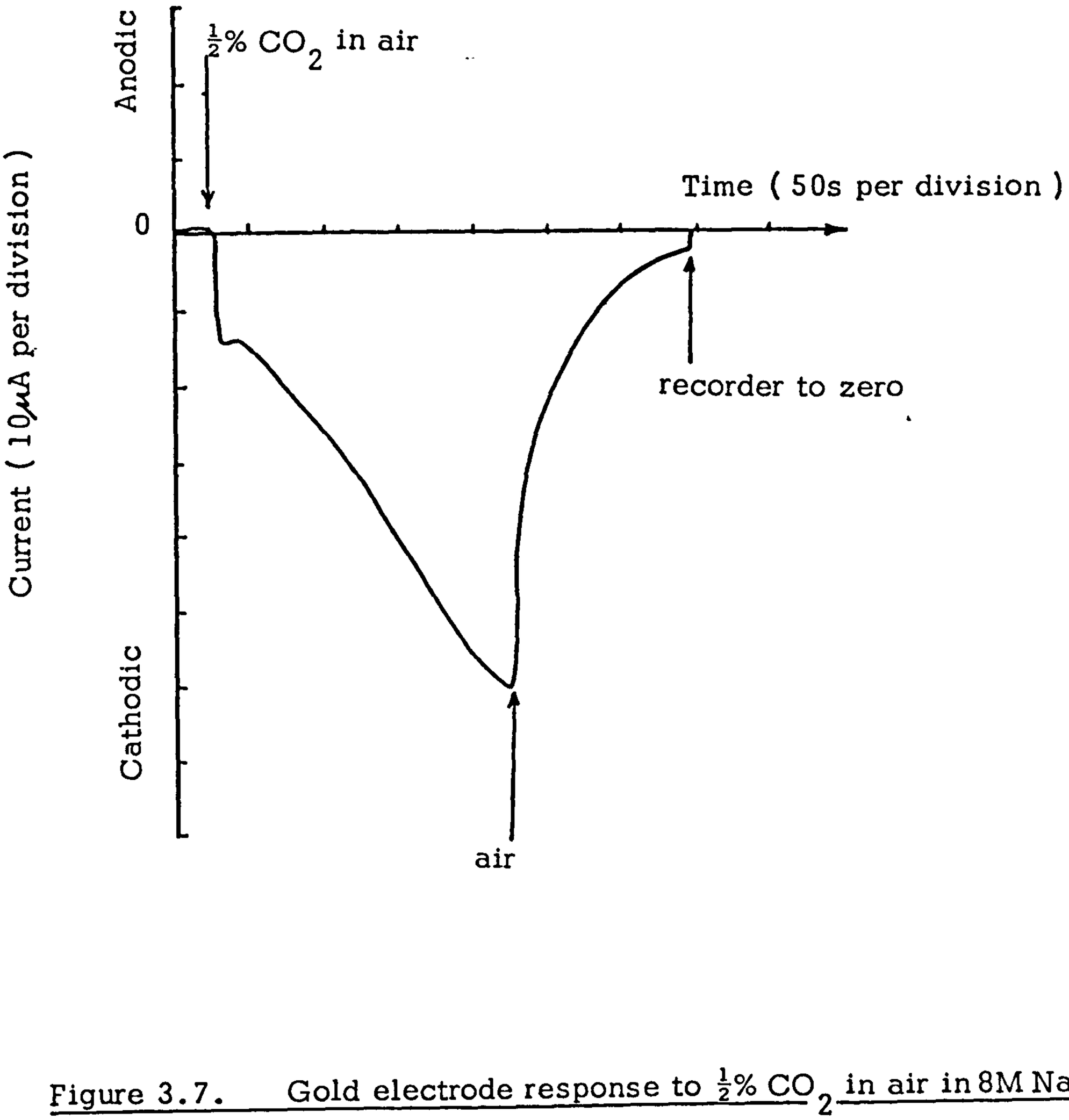

Figure 3.7. Gold electrode response to ½% CO_2 in air in 8M NaOH.

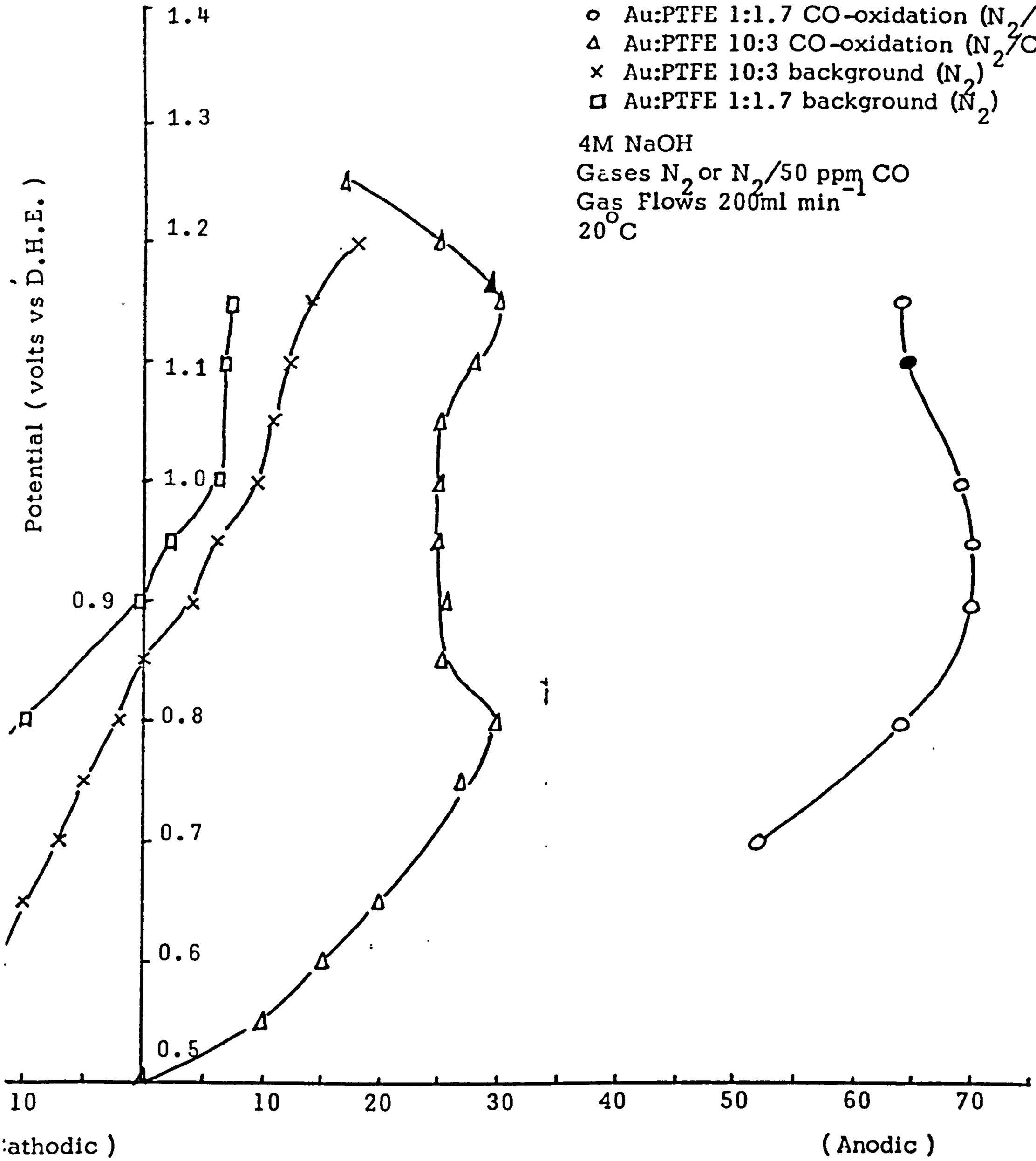

Figure 3.8. CO-oxidation and background i-E scans for gold electrodes in 4M NaOH.

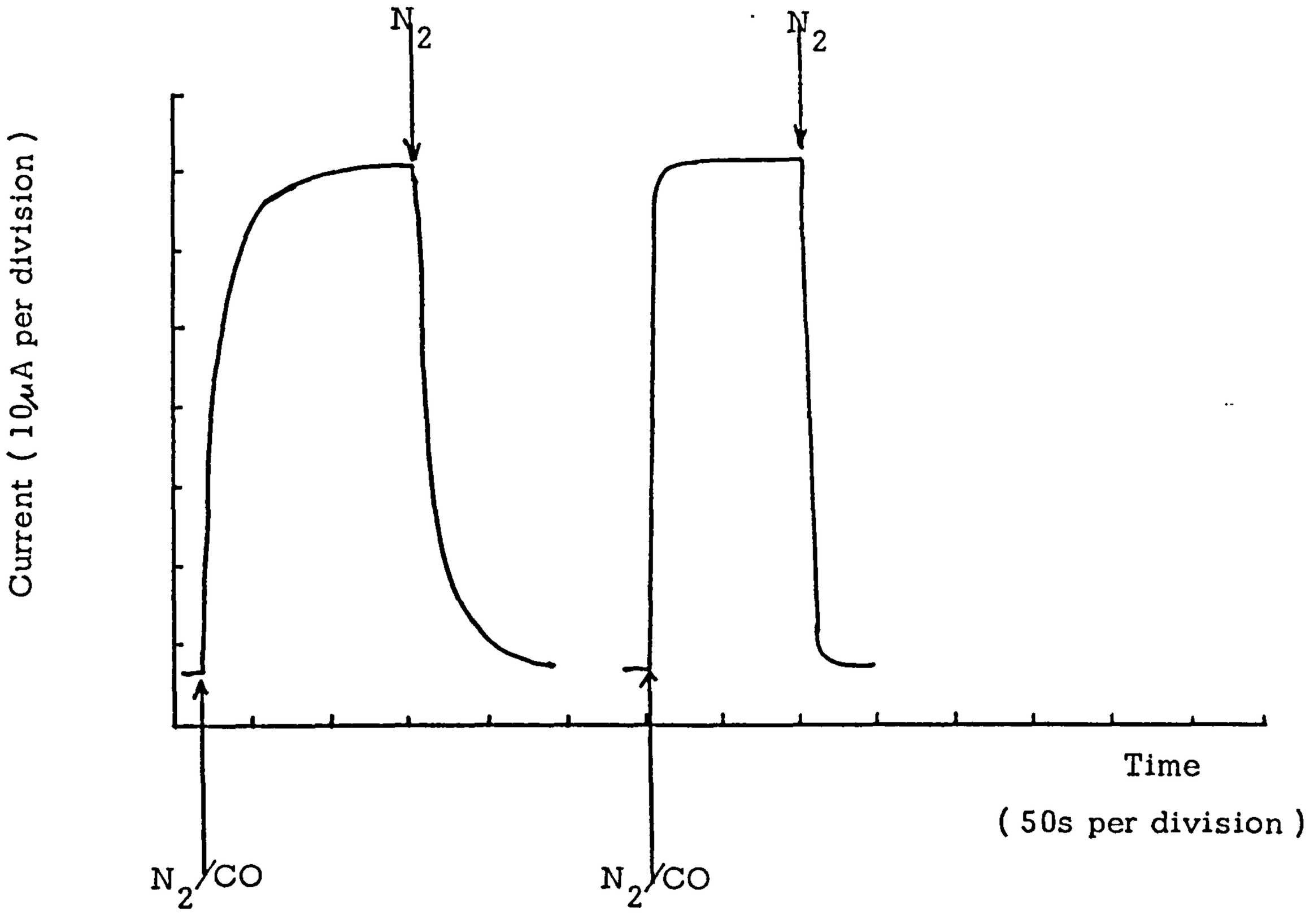

4M NaOH
20°C
$E_{D.H.E.}$ 1.15 volts
Gas Flows 200 ml min^{-1}

Figure 3.9. CO-oxidation response of gold electrodes in 4M NaOH.

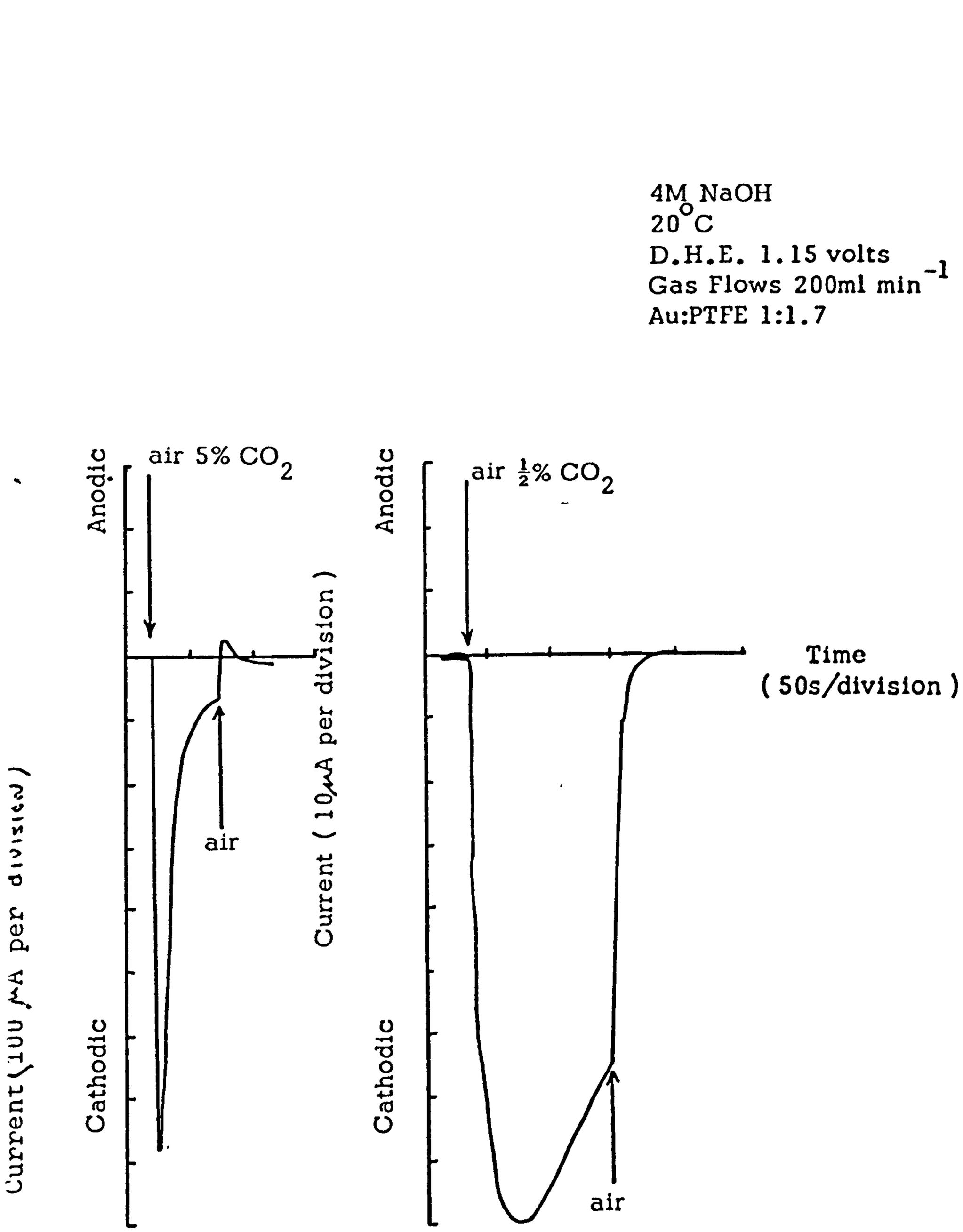

Figure 3.10. CO_2 response of gold electrode in 4M NaOH.

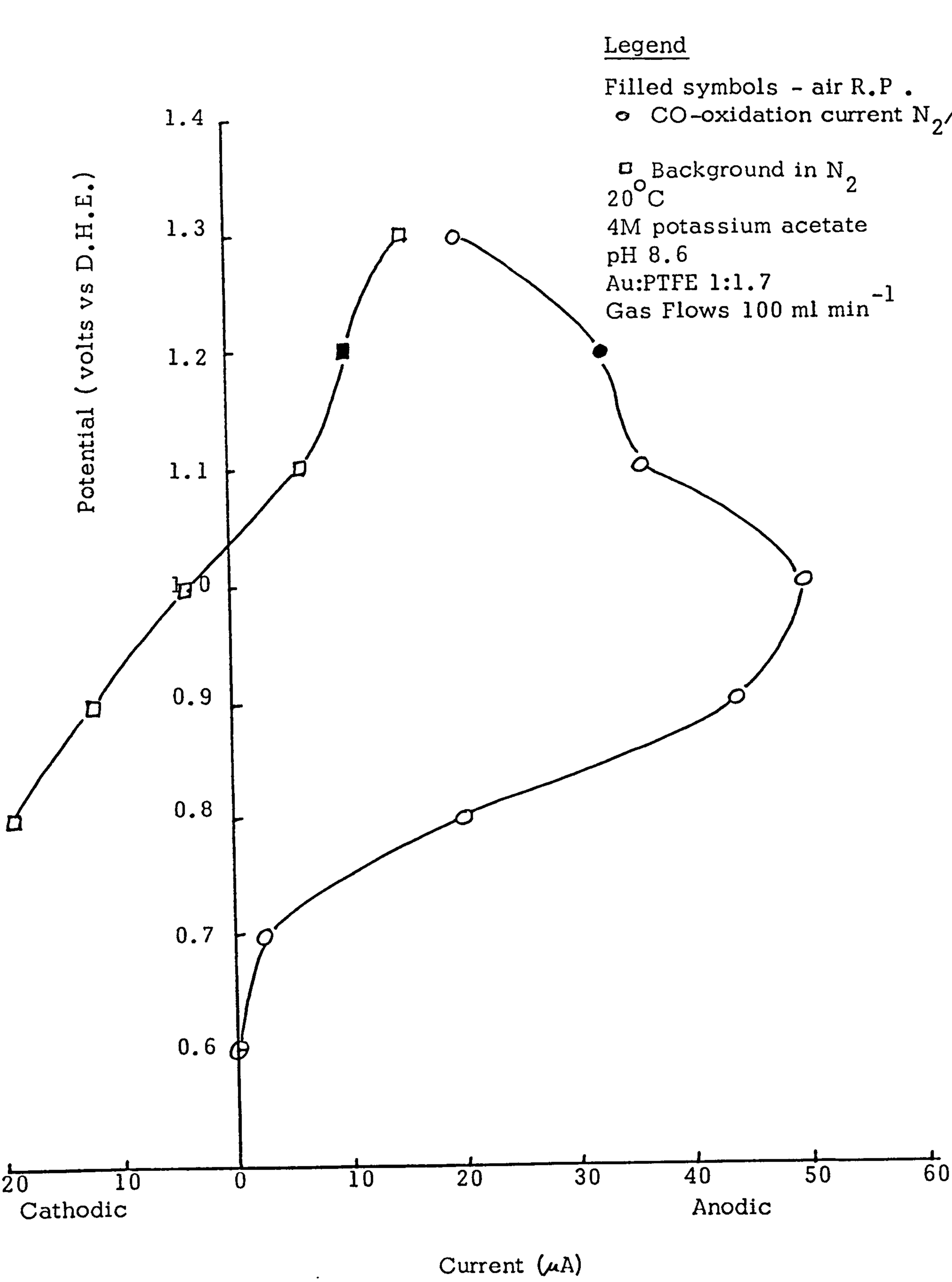

Figure 3.11. CO-oxidation and background i-E curves for gold electrode in 4M potassium acetate solution.

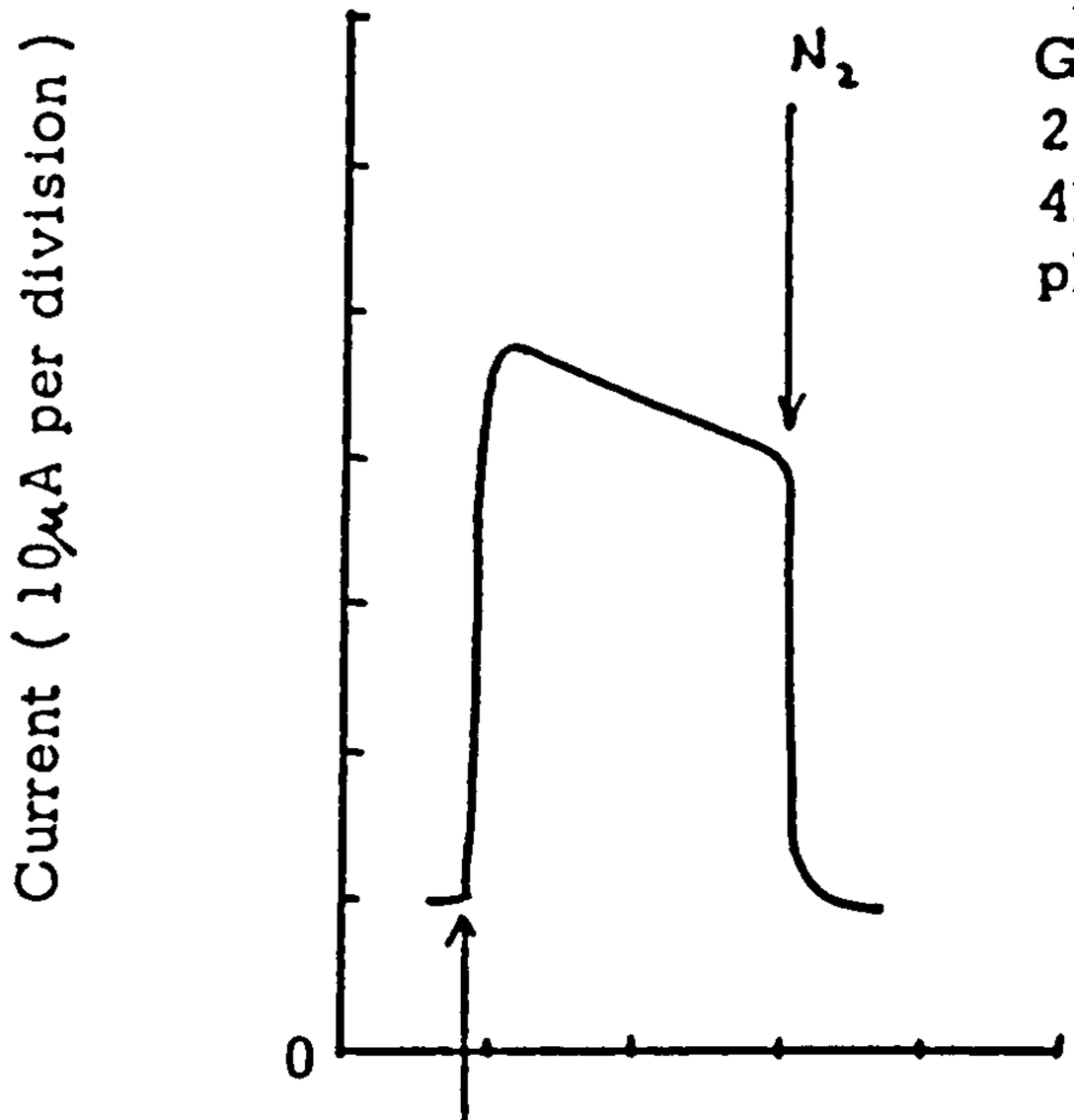

Figure 3.12. CO-oxidation response of gold electrode in 4M potassium acetate solution.

Au:PTFE 1:1.7
$E_{D.H.E.}$ 1.3 volts.
20°C.
Gas Flows 200ml min^{-1}
4M potassium acetate
pH 8.5.

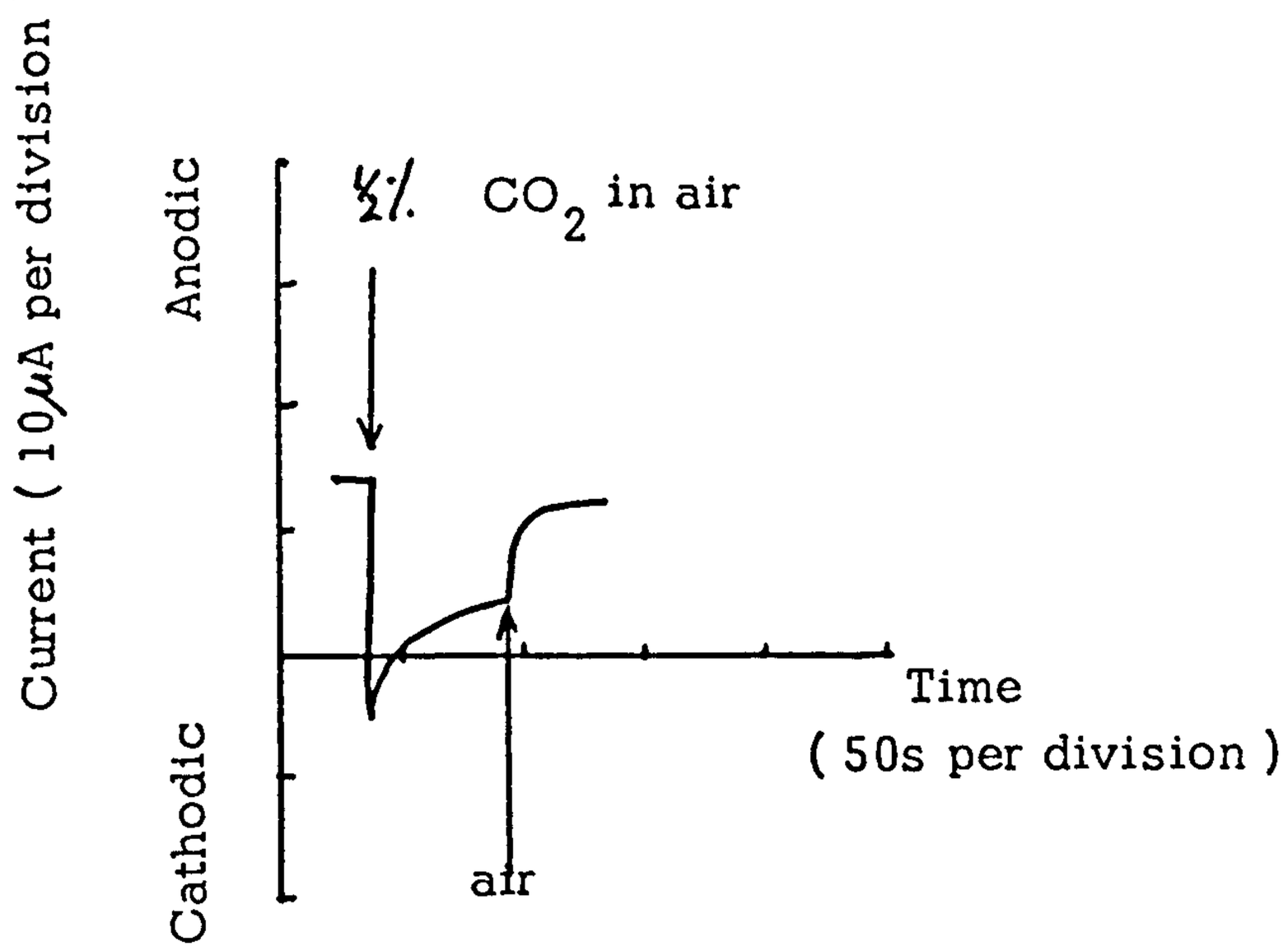

Figure 3.13. CO_2 response of gold electrode in 4M potassium acetate solution.

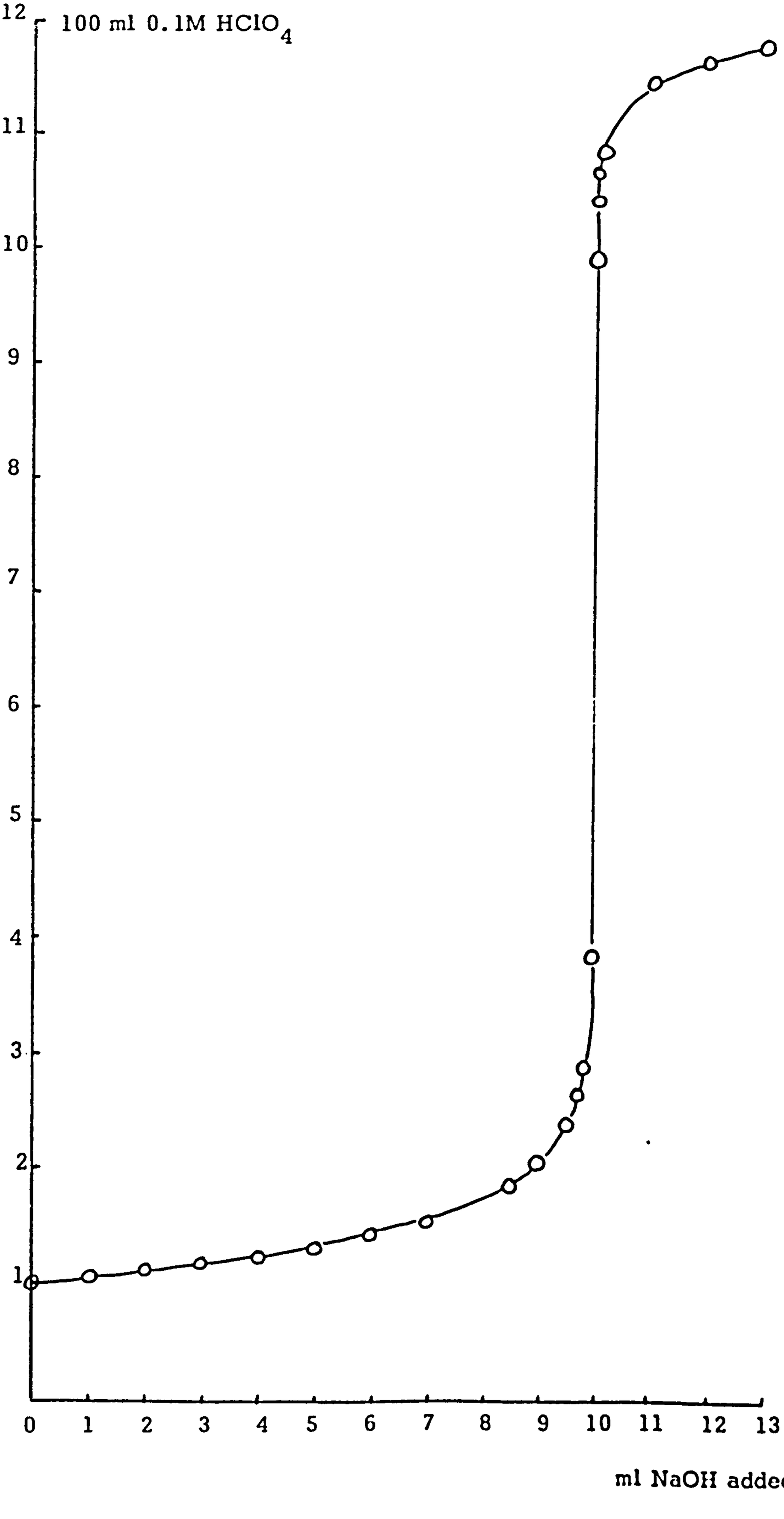

Figure 5.1. Titration curve for perchloric acid neutralisation with NaOH solution.

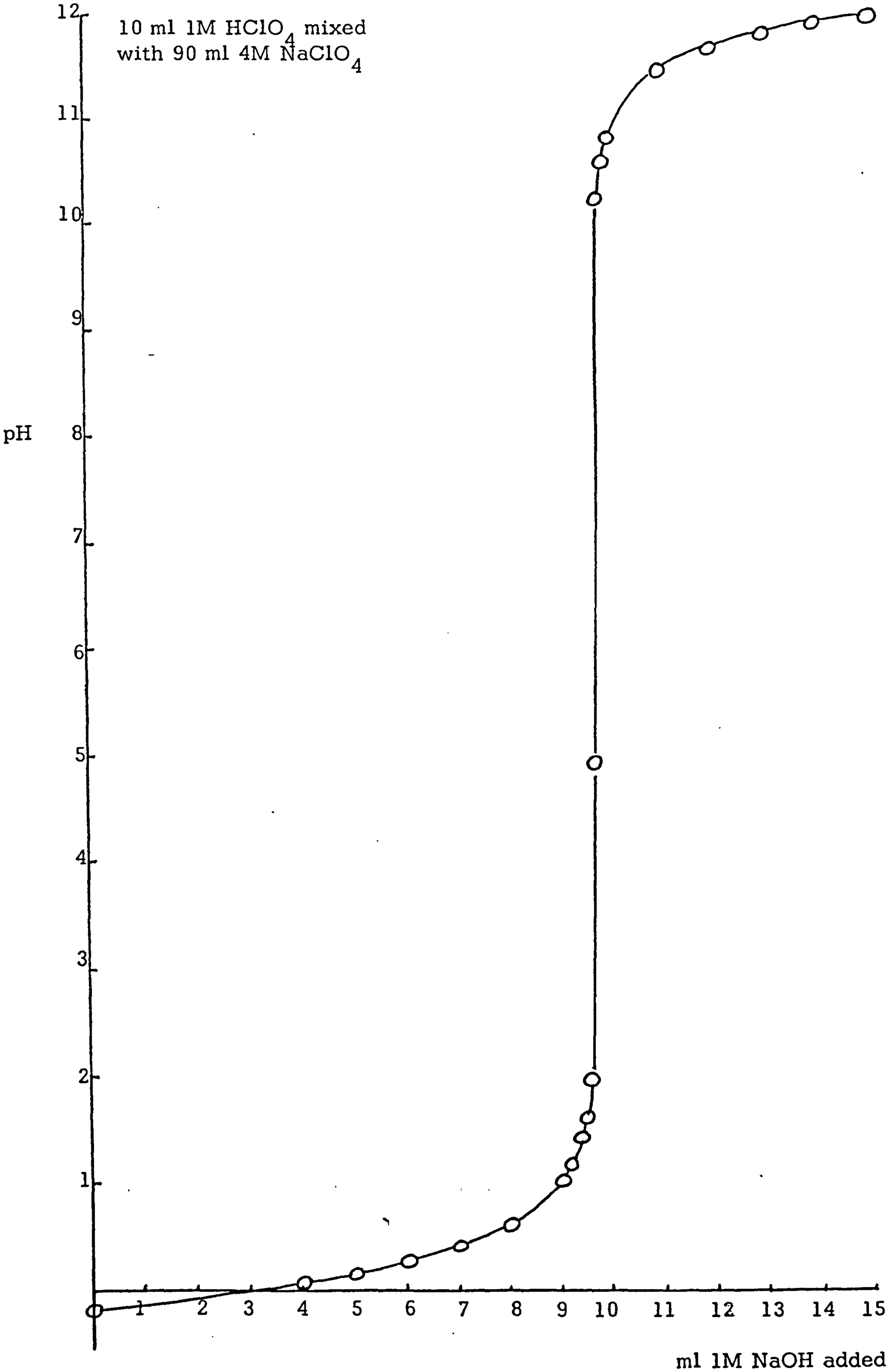

Figure 5.2. Titration curve for perchloric acid/sodium perchlorate neutralisation with NaOH solution.

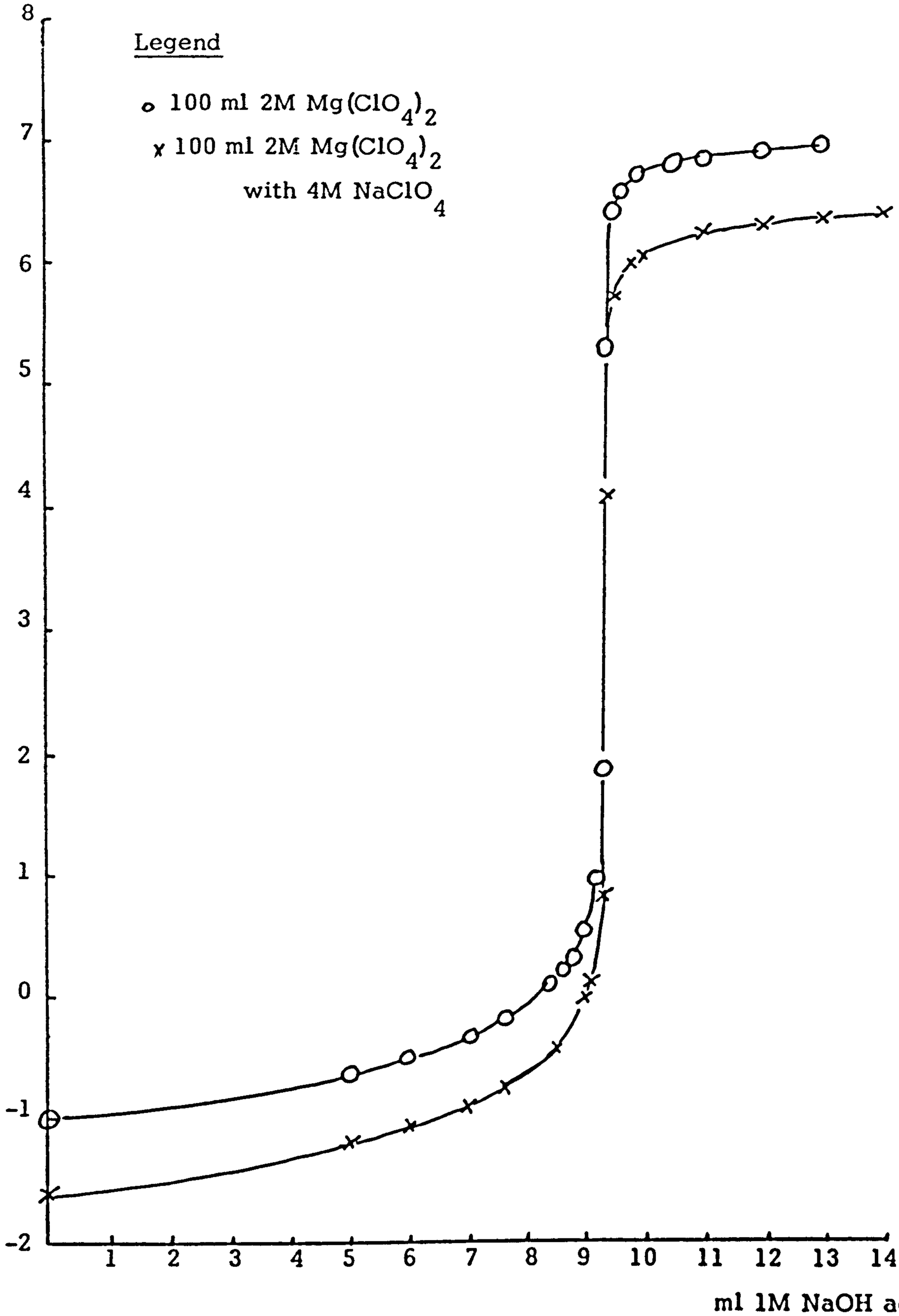

Figure 5.3. Titration curves for $Mg(ClO_4)_2$ solutions.

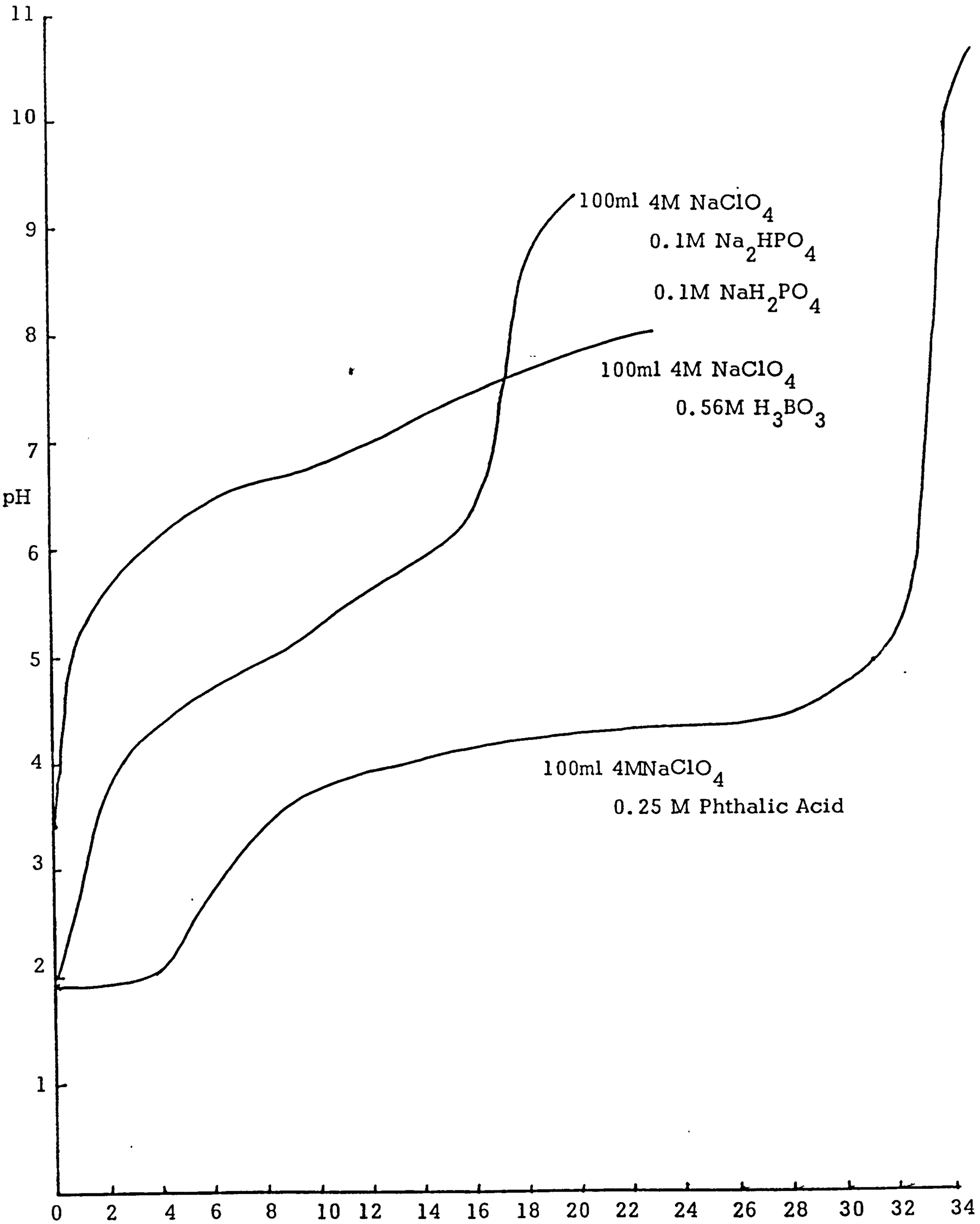

Figure 5.4. Titration curves for buffered sodium perchlorate solutions.

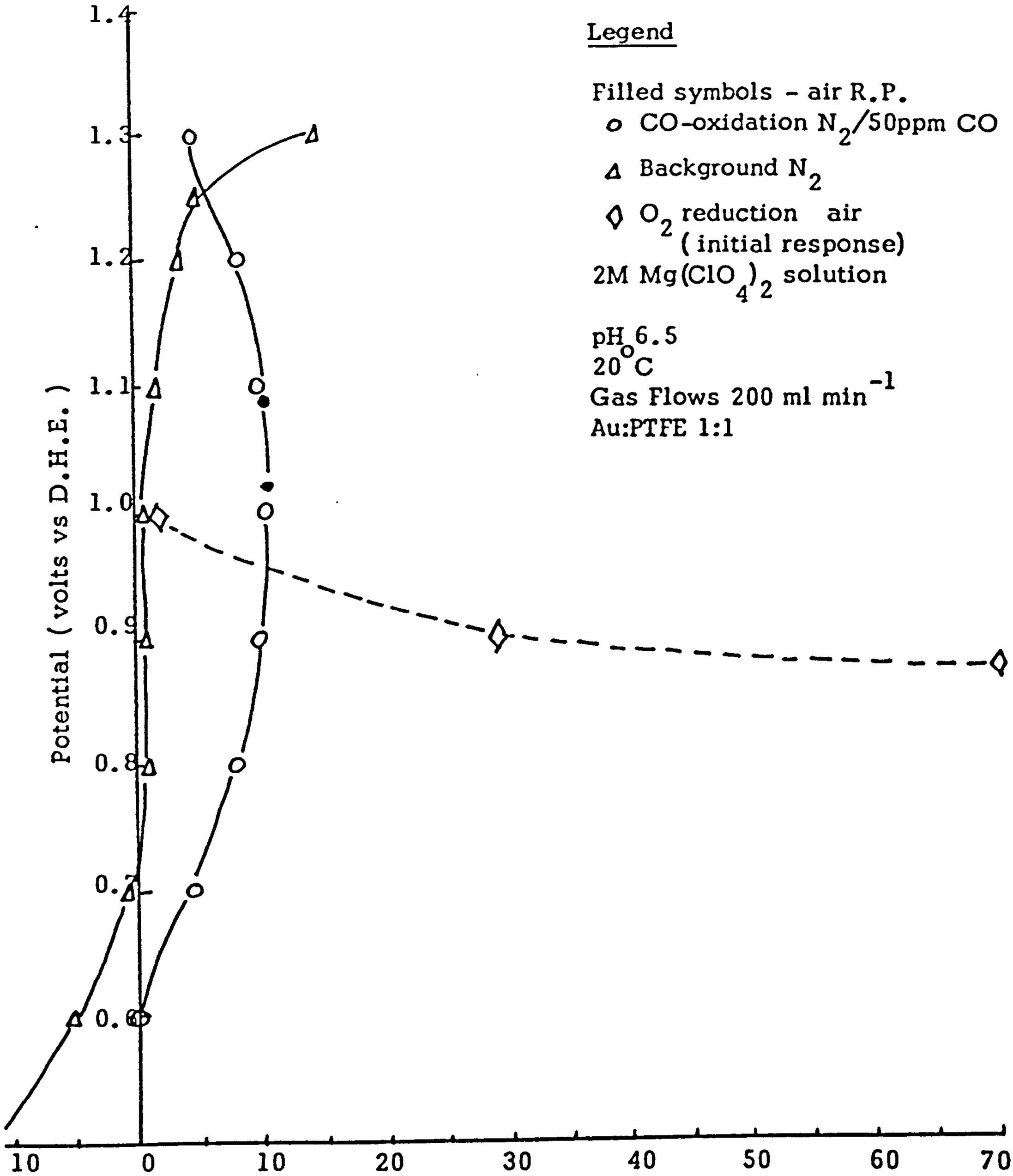

Figure 5.5. CO-oxidation, background and oxygen reduction i-E scans for gold electrode in 2M $Mg(ClO_4)_2$ solution.

TOP VIEW

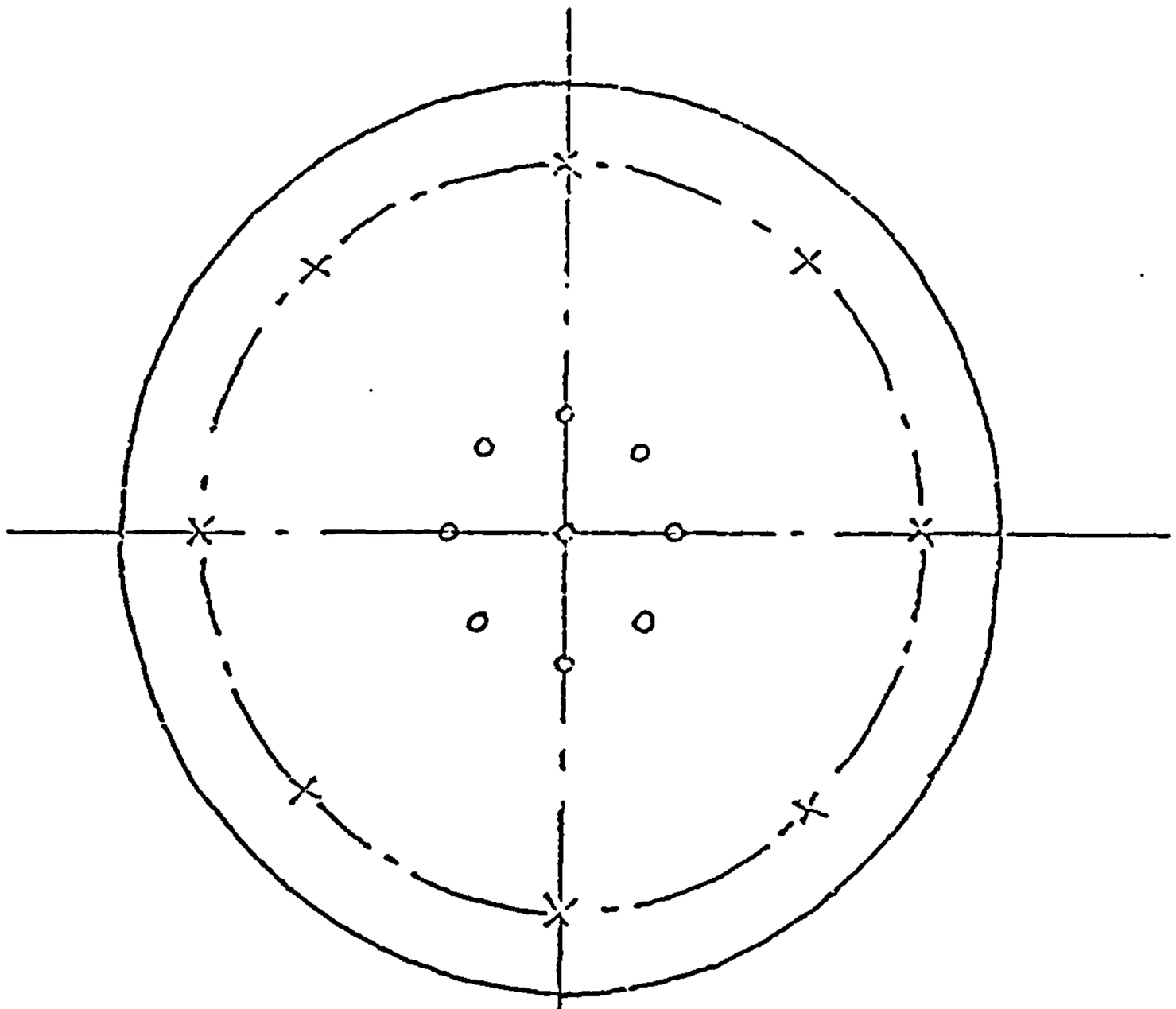

EXPLODED SIDE VIEW

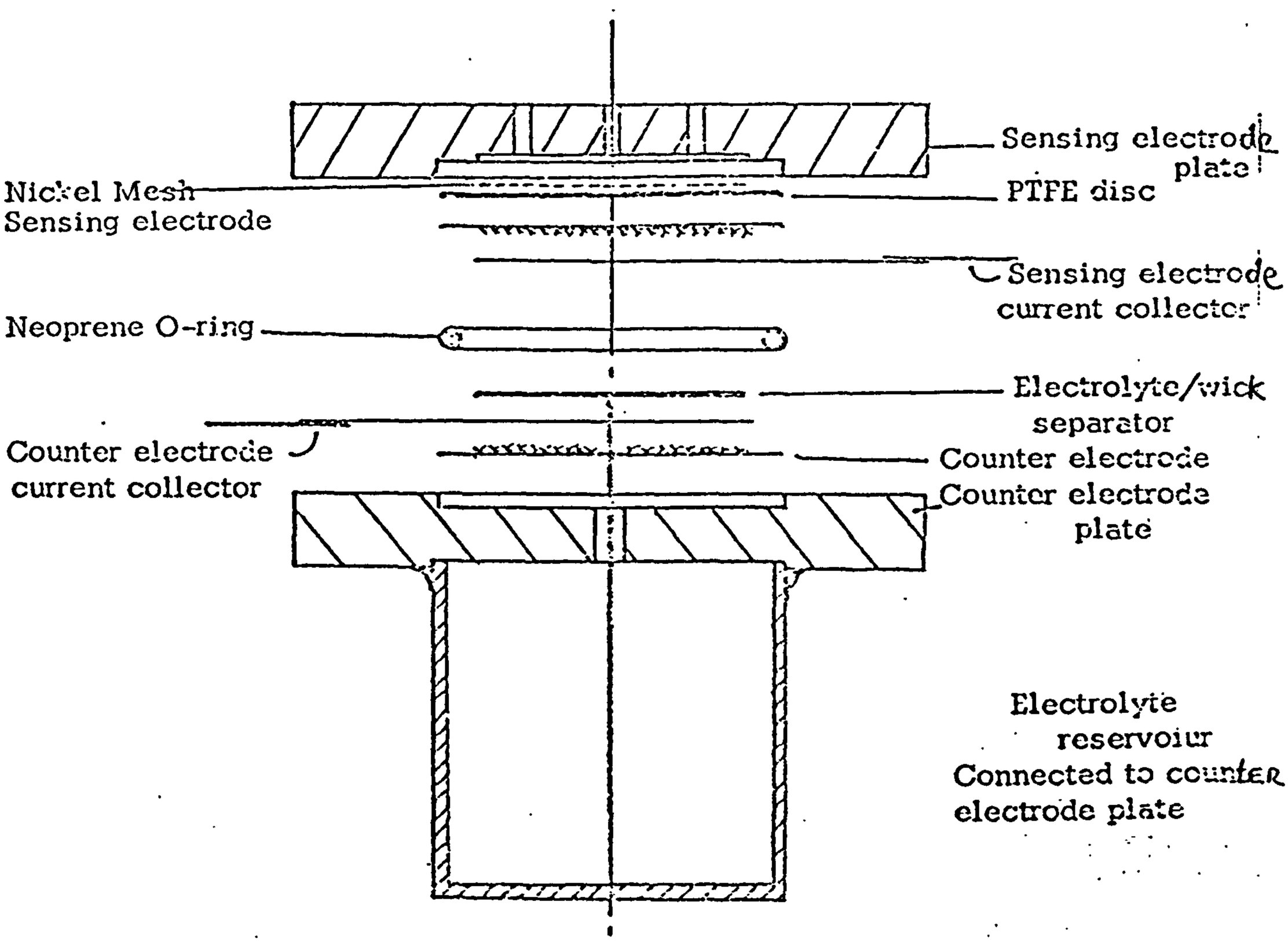

Figure 6.1. General Constructional Features of Experimental Sensors.

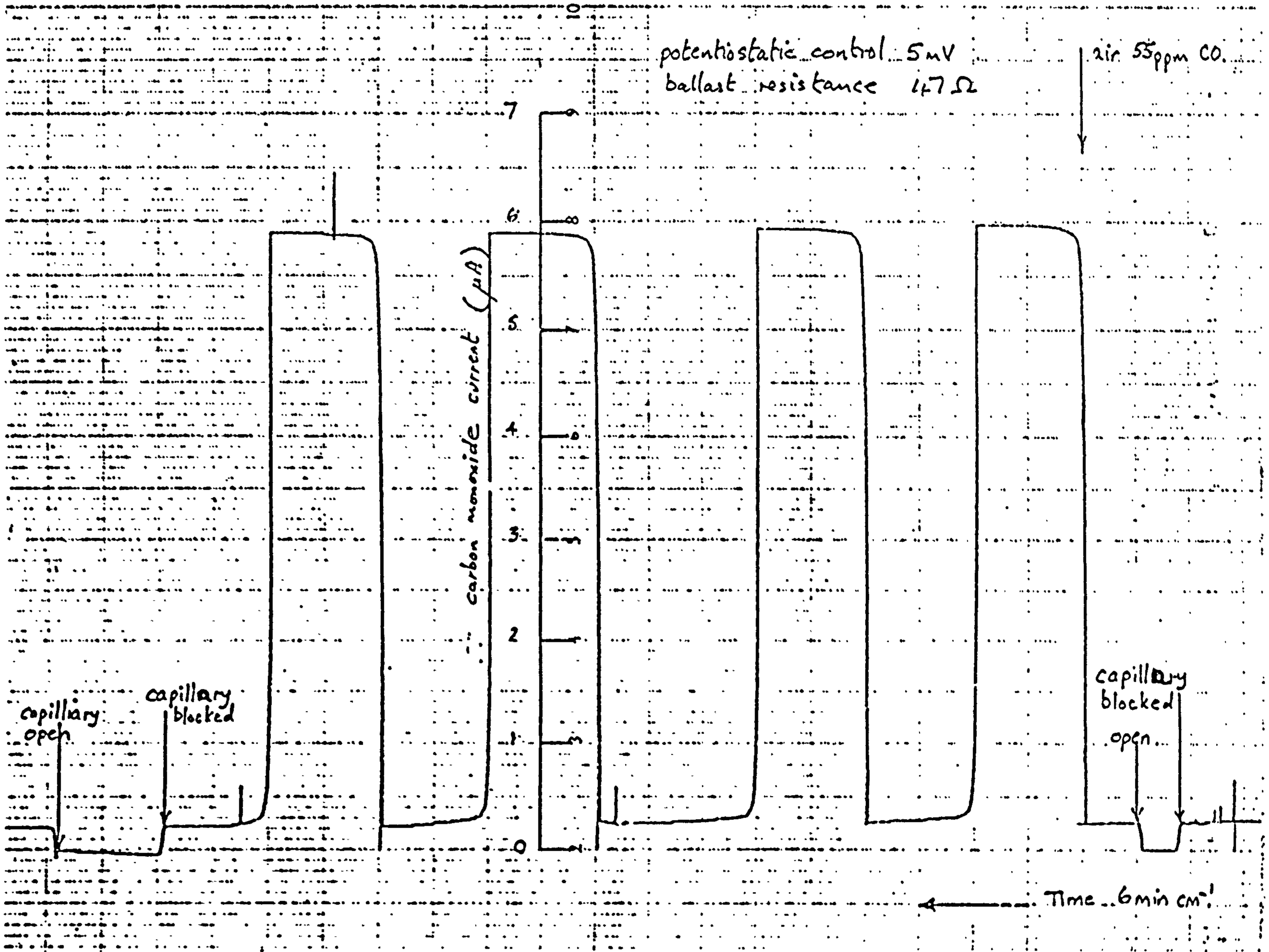

Figure 6.2. Sensor P9 response to carbon monoxide

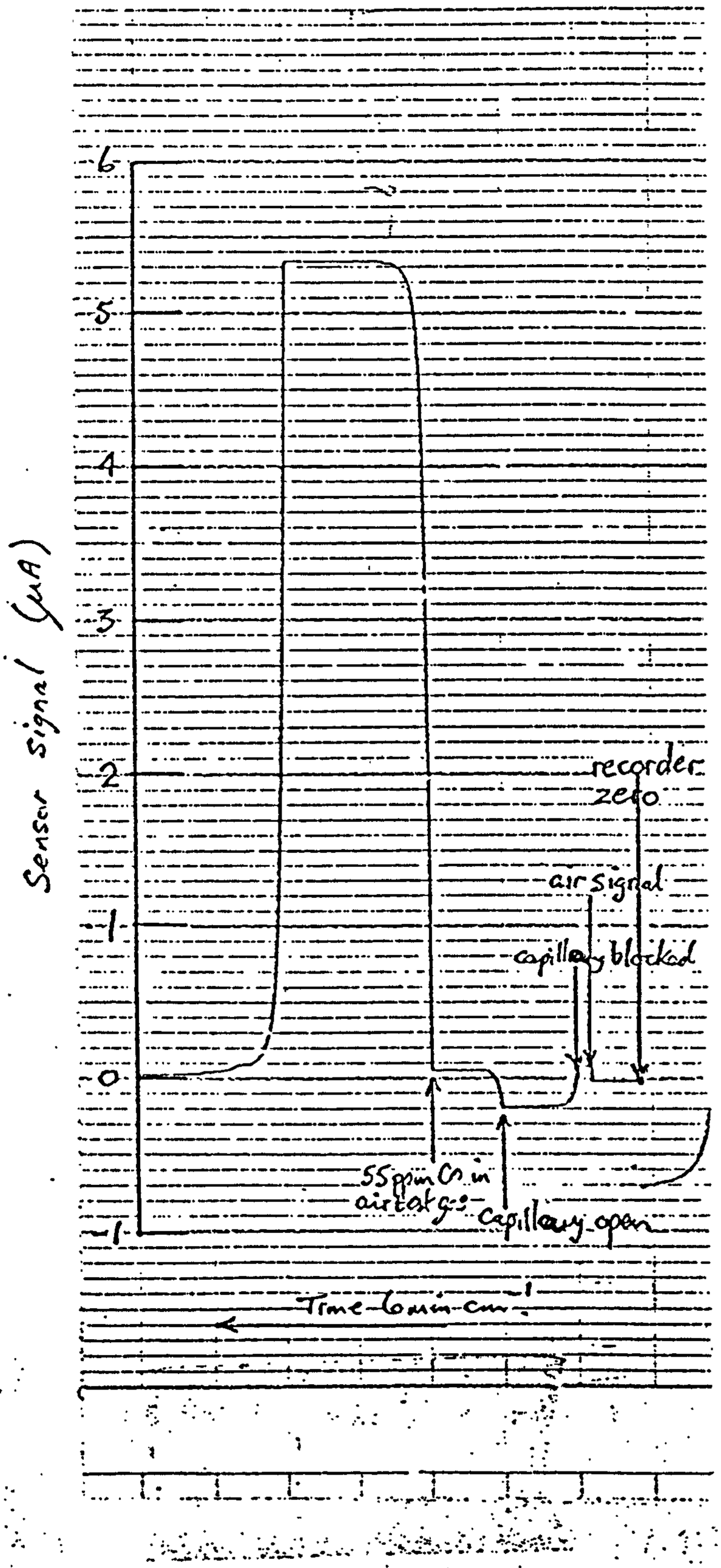

Figure 6.3. Sensor P34 CO response

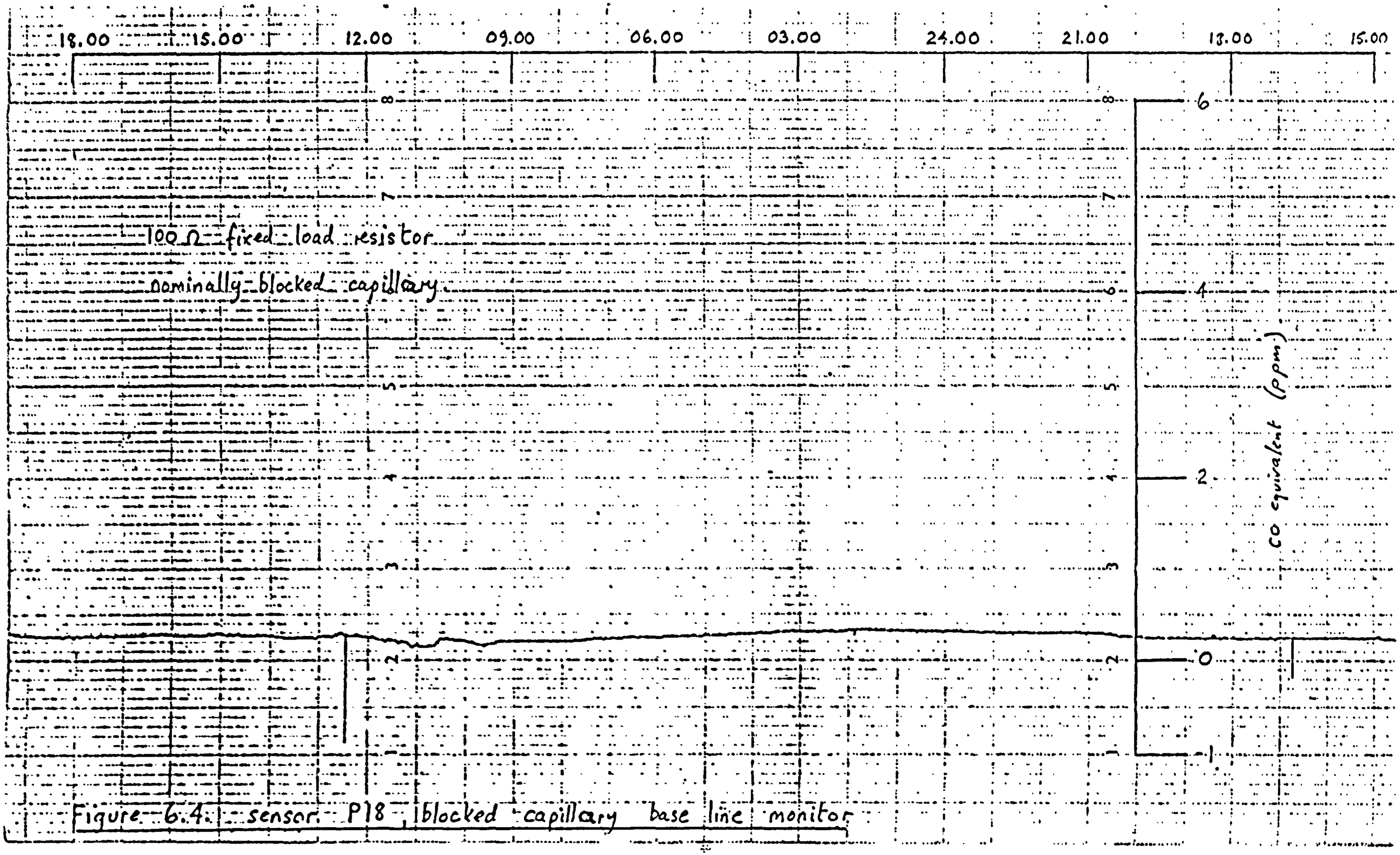

Figure 6.4: sensor P18, blocked capillary base line monitor

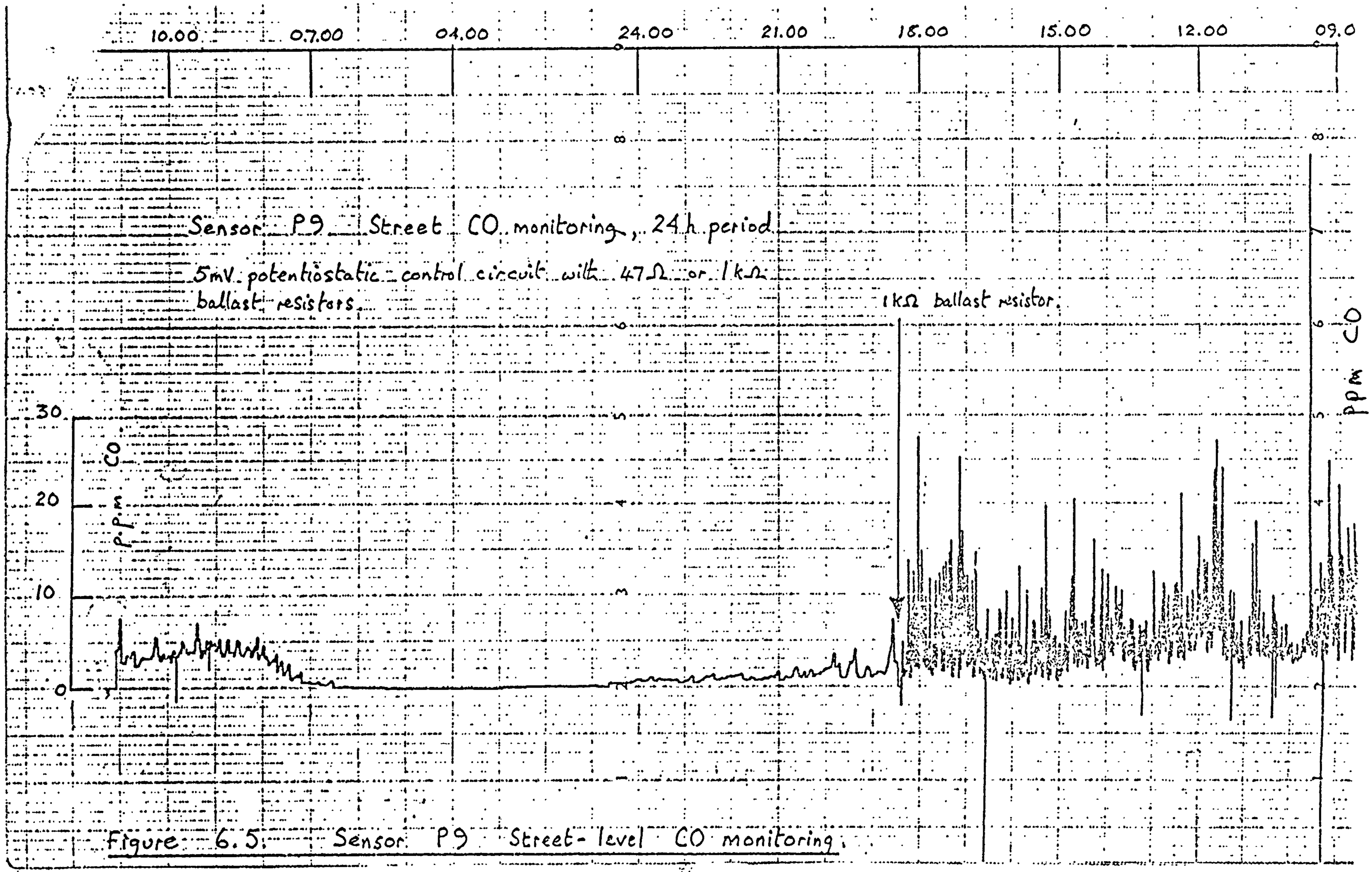

Figure 6.5. Sensor P9 Street-level CO monitoring.

APPENDIX 1.

CARBON MONOXIDE SENSOR ELECTROCHEMISTRY

The carbon monoxide electrode reaction is represented by the equation:

$$CO + H_2O = CO_2 + 2H^+ + 2e \qquad \underline{Equ.1}.$$

The open circuit potential, relative to a standard hydrogen electrode (arbitrary zero) at 25°C is given by the relationship: (1)

$$E = -0.103 - 0.0591\ pH + 0.0295 \log \frac{P_{CO_2}}{P_{CO}} \qquad \underline{Equ.2}.$$

where P_{CO_2} and P_{CO} are the partial pressures of CO_2 and CO respectively and negative signs indicate potentials which are cathodic to the hydrogen zero potential.

The potential relative to a hydrogen electrode in the same electrolyte is then given by:

$$E = -0.103 + 0.0295 \log \frac{P_{CO_2}}{P_{CO}} \qquad \underline{Equ.3}.$$

If a true equilibrium were established at the electrode, the theoretical potential, relative to a hydrogen electrode in the same electrolyte, in the presence of a gas mixture of 1 atmosphere pressure, containing 50 ppm CO, 0.03% CO_2 and the balance nitrogen(or some such electrochemically inert gas) would be $-80\ mV$. Under these conditions then CO is thermodynamically unstable towards water which it would tend to decompose with the evolution of hydrogen:

CO-electrode reaction	$CO + H_2O = CO_2 + 2H^+ + 2e$	$E = -80$ mV
H_2-electrode reaction	$2H^+ + 2e = H_2$	E = zero
overall reaction	$CO + H_2O = CO_2 + H_2$	<u>Equ.4</u>.

However, the carbon monoxide electrode reaction is highly irreversible and approaches equilibrium infinitely slowly at room temperatures, even with precious metal electrolcatalysts of relatively high activity. Consquently measured rest potentials

(1) M. Pourbaix; "Atlas of Electrochemical Equilibria, Pergammon Press (1965), p.452.

of carbon monoxide electrodes are invariably anodic (positive values) relative to a hydrogen reference electrode, i.e. water decomposition (Equ.4.) is not observed.

The anodic oxidation of carbon monoxide proceeds via a "reactant pair" mechanism in which electron transfer occurs between the electrode and a surface intermediate composed of CO and H_2O molecules adsorbed on adjacent surface sites. (2) Precious metal surfaces such as platinum or gold which are normally used as electrocatalysts for the CO reaction, at potentials near or more cathodic to the normal hydrogen electrode, adsorb carbon monoxide strongly with high coverage. Under these conditions the reaction is severly inhibited by the low availability of surface sites for water molecule adsorption to form the reactant pairs. At more anodic potentials the noble metals form surface films of oxides or adsorbed oxygen which have much lower catalytic activity towards the CO-reaction but act as adsorption sites for water molecules. CO-H_2O reactant pairs then form at the metal-oxide interfaces and the electrode can sustain CO-oxidation currents at these potentials.

The onset of surface oxidation occurs at about 0.8 volts on the hydrogen scale for platinum and about 1.30 volts for gold, (3) in sulphuric acid electrolyte. These potentials do not vary to any extent with solution pH, but in alkaline electrolyte adsorption films containing hydroxyl ions form at more cathodic potentials and may modify the kinetics of an electrode reaction. (4)

The surface coverage of a precious metal electrode with oxide increases with potential in the anodic direction. Complete coverage only occurs at considerably more anodic potentials than those quoted above, but when such a condition is reached then the CO-reaction

(2) S. Gilman; J. Phys. Chem. (1964), Vol 68. No.1.pp.70-80.

(3) J.P. Hoare; The Electrochemistry of Oxygen, Interscience, 1968.

(4) ibid; page 29.

will become inhibited by the low availability of suitable adsoption sites for the CO molecule and the electrode is said to be "passivated".

Platinum/gold powders, intimately mixed, might provide a more active catalyst for CO-oxidation than either alone. Gold surfaces are essentially free of oxide up to potentials of 1,3 volts (hydrogen scale) and would provide CO-adsorption sites. Platinum surfaces above 0.8 volts are extensively covered with oxide for water adsorption. The Pt-Au interfaces would then provide a high number of reactant pair sites. Alternatively gold, supported on corrosion resistant oxides (e.g. Fe_2O_3 in alkali electrolytes) could prove a suitable alternative to plain Pt.

Oxygen is an electroactive gas and sets up an electrode reaction on platinum or gold electrodes which can be represented by the following equation in acid electrolytes:

$$2H_2O = O_2 + 4H^- + 4e \qquad \underline{\text{Equ.5}}.$$

The electrode potential relative to a normal hydrogen electrode in the same electrolyte is given by the relationship: (5)

$$E = 1.228 + 0.0148 \log p_{O_2} \qquad \underline{\text{Equ.6}}.$$

The theoretical potential for an electrode in contact with air ($p_{O_2} = 0.20$ atm.) then becomes about 1.22 volts. This electrode reaction is also irreversible and measured values of air electrode rest potentials are about 1.05 volts in acid electrolytes and about 1.15 volts in alkaline media. The potential of a gas sensing electrode, exposed to air containing carbon monoxide therefore, sets up a mixed potential resulting from a local cell between the carbon monoxide and oxygen electrode

(5) M. Pourbaix; "Atlas of Electrochemical Equilibria", Pergammon Press (1965) p. 541.

reactions on the electrocatalyst surface.

$$\text{Oxygen reaction } O_2 + 4H^+ + 4e \rightarrow 2H_2O$$
$$\text{CO reaction } 2CO + 2H_2O \rightarrow 2CO_2 + 4H^+ + 4e$$
$$\text{Overall reaction } O_2 + 2CO \rightarrow 2CO_2 \qquad \underline{\text{Equ.7}}.$$

This can be represented schematically in the following diagram of the current-potential curves for the two electrode reactions.

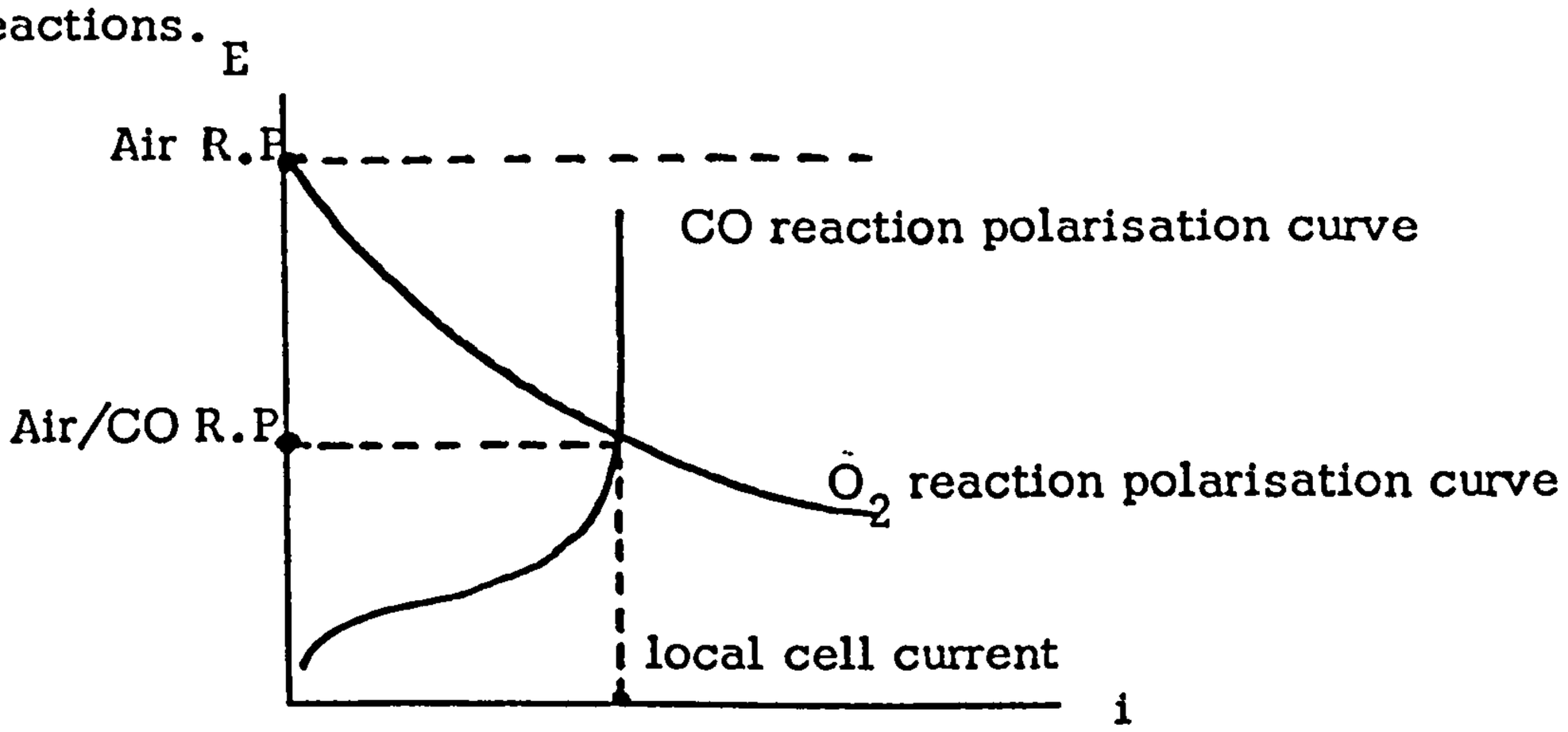

In a sensor the mixed potential sensing electrode is connected via an external load circuit to an oxidising counter electrode. In the NCB and Ecolyser cells this is an oxygen electrode located inside the cell and which is not exposed to the CO in the atmosphere. The cells are designed to oxidise completely any carbon monoxide as it reaches the sensing electrode, but excess oxygen in the air dissolves in the electrolyte and diffuses to the counter electrode where it sets up an oxygen potential; since there is no carbon monoxide in the vicinity of the counter electrode, its potential will be higher than the mixed potential of the sensing electrode. With the load circuit closed, an electron current flows from the sensing to the counter electrode and provides the "signal" of the sensor. The sensor current in the external circuit causes the counter electrode to polarise to a steady potential, slightly above the sensing electrode depending on the load resistance. The counter effectively presents a larger area for the local cell oxygen reduction current at the sensing electrode which therefore depolarises. The situation at a fixed CO concentration in air can be depicted schematically in the following

I_s = signal current

$I_{i.c.}$ = local cell current.

diagram: E

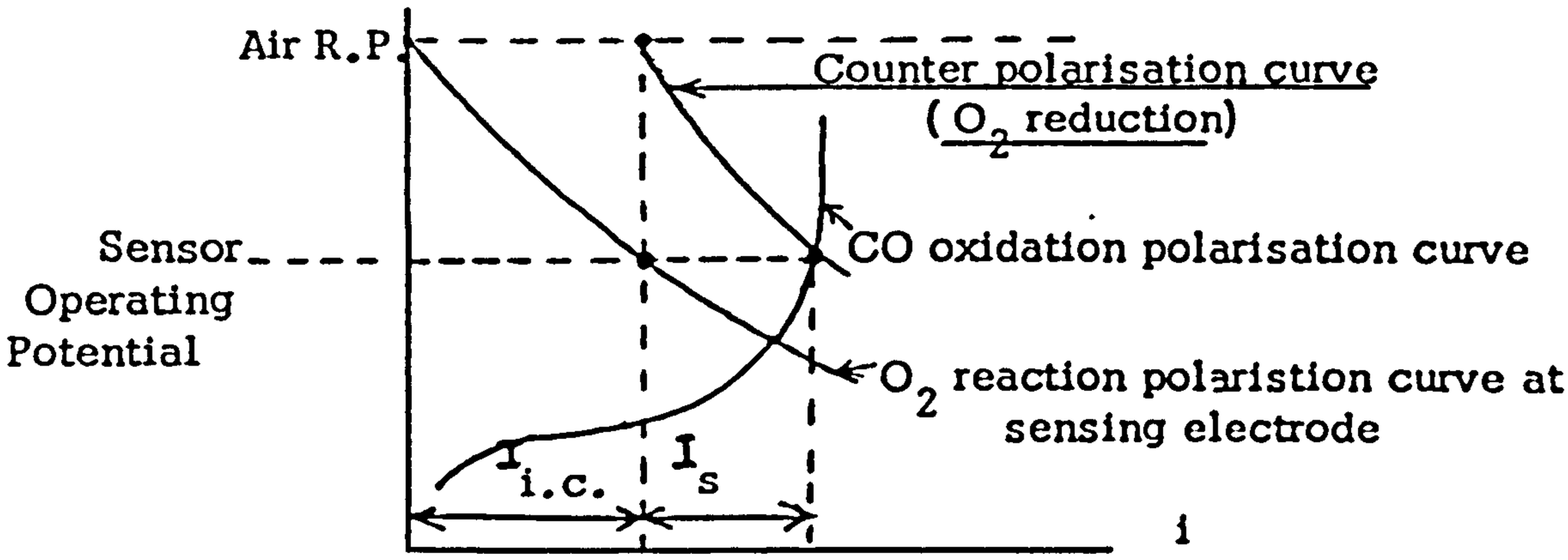

In this design of cell only part of the total CO-oxidation current appears as a signal in the instrument load circuit. The parasitic signal losses caused by the oxygen reduction reaction at the sensing electrode could be eliminated by employing either of three alternative designs as follows:

(a) potential bias circuit.

An external circuit can be used to hold the sensing electrode at a fixed anodic potential difference with respect to the counter electrode. If this p.d. is greater than the counter electrode polarisation at the maximum CO-signal, then the sensing electrode will never experience oxygen reducing potentials and the full CO signal will always be obtained in the sensor load.

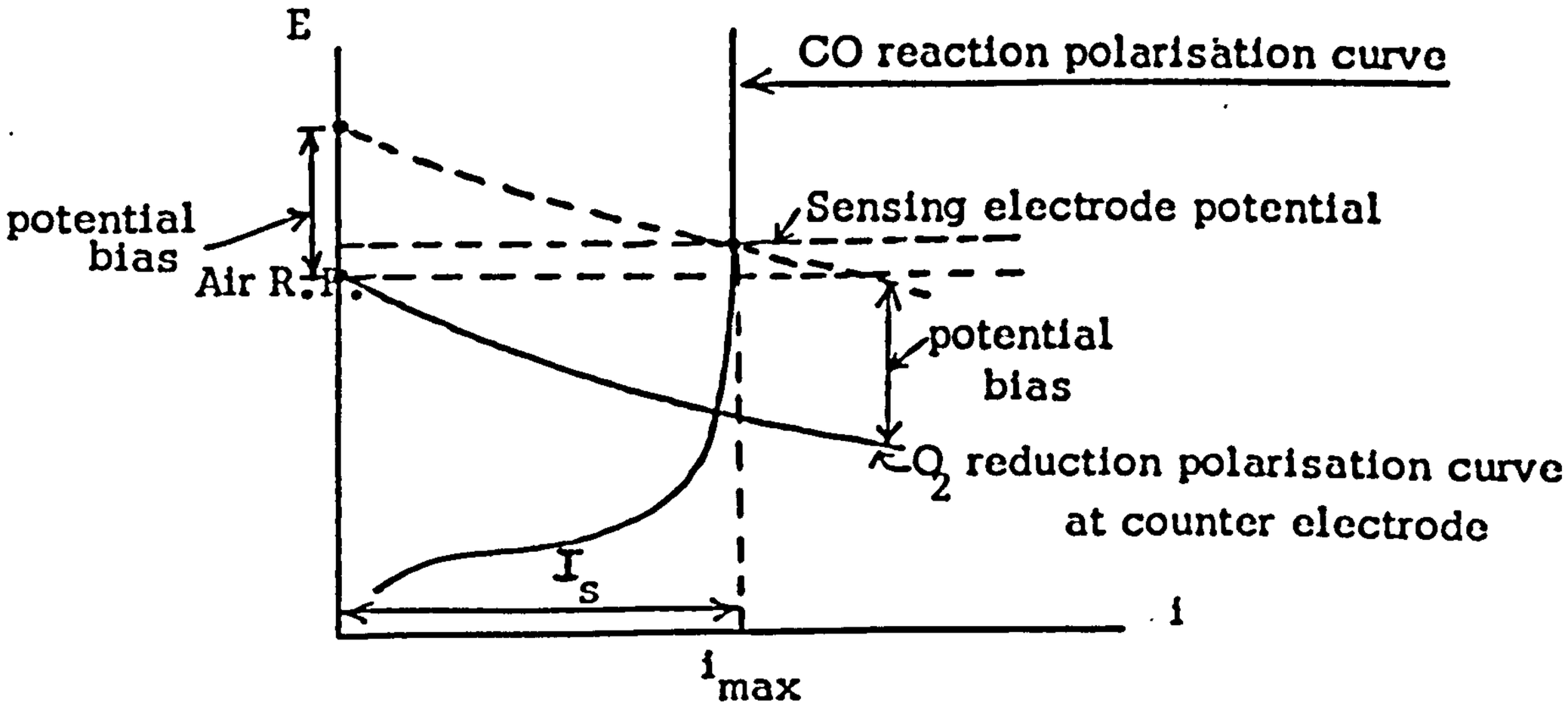

i_{max} is maximum likely sensor current.

I_s is the sensor signal.

The potential bias should not be so great as to drive the sensing electrode into a "passive" region, or cause the oxygen evolution reaction.

(b) battery cathodes.

Battery cathode materials such as NiOOH (in alkaline solution) and PbO_2 (in sulphuric acid solution) may be employed as counter electrodes. These have high potentials above the air rest potential and would be virtually unpolarised at the current density levels in a CO-sensor. Thus these materials will hold the sensing electrode above the air rest potential thus avoiding any local cell action.

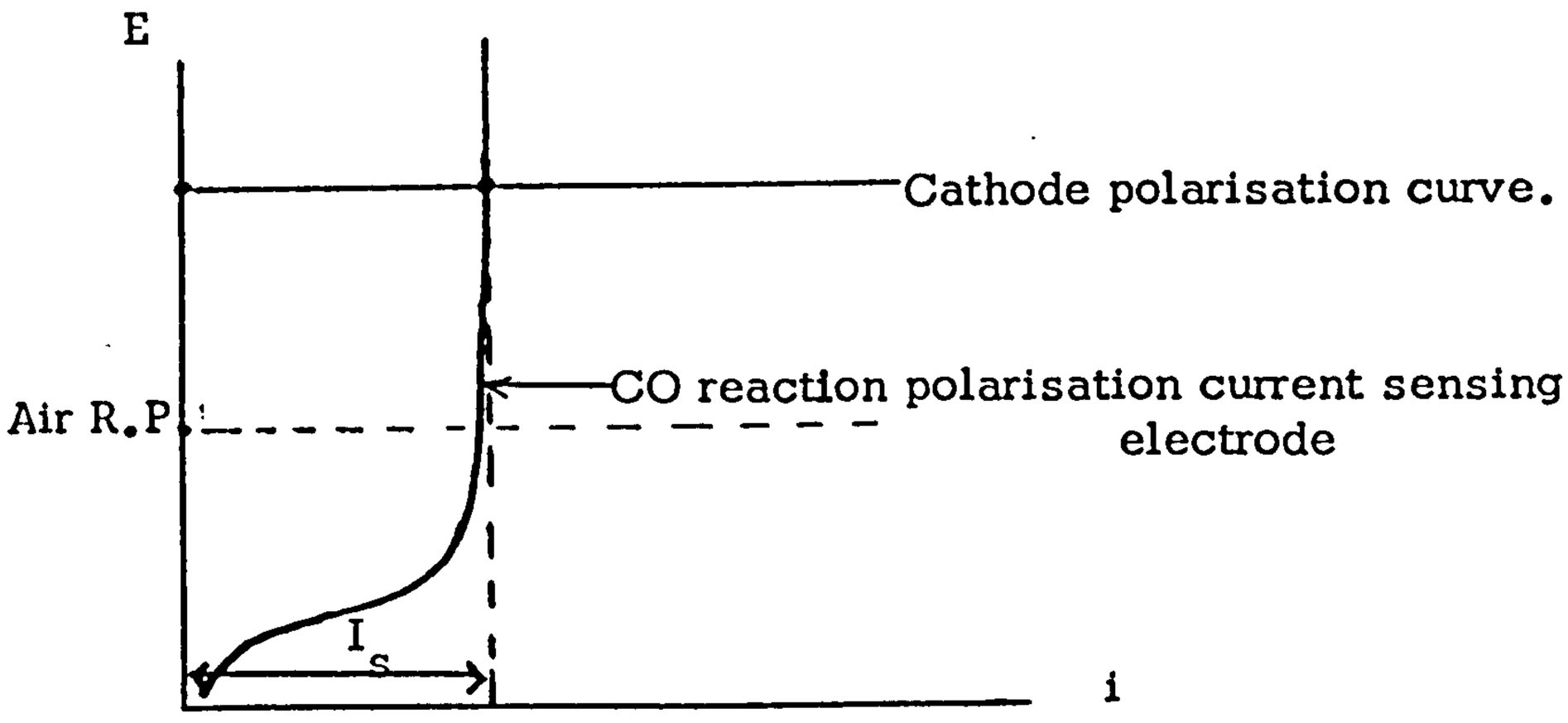

The main drawback with these electrode materials is that they tend to self discharge by reaction with water at their high anodic potentials:

$$4NiOOH + 2H_2O \longrightarrow 4Ni(OH)_2 + O_2 \qquad \text{Equ.8.}$$

$$2PbO_2 + 2H_2SO_4 \longrightarrow 2PbSO_4 + 2H_2O + O_2 \qquad \text{Equ.9.}$$

This can be minimised by suitable design of the cathode structure. But electrode structures used in batteries are normally designed to cope with high current densities and as a consequence they also have relatively high self discharge rates. Such structures would probably not be suitable for gas sensors where shelf life considerations would be of greater importance.

(c) Three electrode potentiostatic control.

A third unpolarised reference electrode, in conjunction with a potentiostatic control circuit, can be used to hold the sensing electrode at potentials above the air rest potential. The Ecolyser cell has provision for this mode of operation by employing a split cathode; one side functions as the reference electrode, the other acts as the cell counter electrode.

APPENDIX 2.

Alkaline " in situ " scrubber sensor.

Alkaline "in situ " scrubber sensor.

The basic idea is to so arrange the diffusion path in the sensor that the gas sees a low "resistance" diffusion path direct to the bulk electrolyte before reaching a relatively high diffusion restriction to the electrode.
In such a case a large proportion of the carbon dioxide could be scrubbed from the diffusing gas before it reaches the active electrode.

The principle is illustrated schematically below:

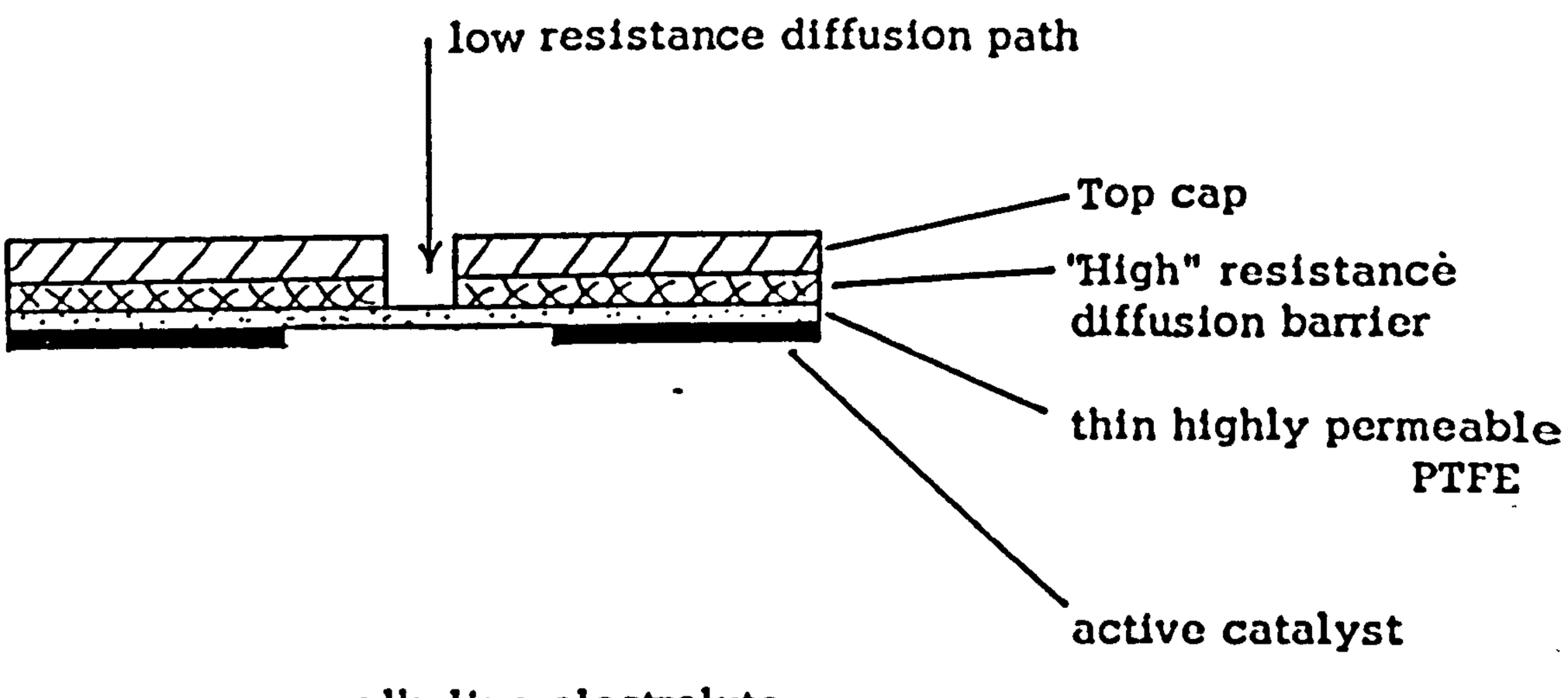

An experimental cell of this type, using components that in the normal sensor arrangement gave a signal of ~ 1μA on 0.5%CO_2, gave no response (certainly less than 0.02μA) on 5% CO_2. However one cannot rely too much on a single test such as this.

Further calculations and experimental tests are required to establish whether it is feasible in practice to achieve the required ratio of diffusion resistances for efficient scrubbing, coupled with a sufficiently high carbon monoxide signal.

Previous calculations had indicated that there should be sufficient adsorption capacity in the standard CTL sensor hardware, using say 5M NaOH, to allow for a life in ambient air of well over 6 months, before one would expect any effect on electrode activity.

Report No. 80/31/003
April, 1980.

City Technology Limited.,
The City University,
Northampton Square,
London, EC1V OHB.

11. CARBON MONOXIDE SENSOR

FOR USE IN COAL MINES

Phase 2.

A.D.S. Tantram.
R. Chan-Henry.
B.S. Hobbs.

Mr. L.R. Cooper,
National Coal Board,
Mining R & D Establishment,
Stanhope Bretby,
Staffs.

NCB Contract Ref. Y 135007/09/21.
CTL Project No. 94.95.31.

CONTENTS

SUMMARY

At the conclusion of phase 2 of the development program the prospects for meeting the Board's requirements on a production sensor look good and there is a high degree of confidence that the remaining problems can be solved in the next development phase.

The original Mark 1 laboratory sensor has been developed and refined to produce the present Mark 3 version, having the following particular features:

1. Matched pair electrode system.
2. Controlled air access to oxygen-reducing counter electrode.
3. Thin sandwich arrangement of electrodes, separator and wick, with O-ring seal external to the electrolyte.
4. Small sensor size.
5. Plastic hardware components designed for simple manufacture.
6. Electrolyte composition chosen for water balance in 63% average relative humidity.
7. Diffusion control to sensing electrode by capillary gaseous diffusion barrier, controlling the signal to about 1/30th the electrodes capability.

Some benefits of this design,deriving in particular from 6 and 7 above, are as follows:

(a) Low temperature coefficient.

(b) Good long term tolerance to wide range of humidity/ temperature operating conditions, i.e. water balance management considerably eased.

(c) Long term stability high because of the large reserve of electrode activity.

(d) Ability to operate over a wide range of CO concentrations.

The cost of these benefits is a relatively low signal level of 0.1μA per ppm. However, the benefits are sufficiently worthwhile to make every effort to accomodate this feature.

In the course of phase 2, 25 Mark 1, 27 Mark 2 and 42 Mark 3 sensors have been made and tested. Two Mark 2 and four Mark 3 types have so far been delivered to the Board for evaluation. To date the longest testing periods have been 7 months for Mark 1 sensors and 3 months for Mark 3. At present 44 sensors are on long term monitoring and the population continues to grow.

The following performance characteristics have been established:

- the sensors seem well capable of discriminating to better than 1 ppm CO in the 0 to 10 ppm range.
- the overall temperature coefficient is about 0.4% signal per ^{o}C. The baseline temperature coefficient is much higher, emphasising the need to achieve a low baseline value for the low ppm range.
- the temperature coefficient and sensor signal are sufficiently different from theoretical values to suggest that some process, in addition to capillary diffusion, is controlling the signal. The most likely cause is local cell, parasitic consumption of CO on the sensing electrode arising from polarisation of the two electrode system to potentials below the air rest potential. This subject will be investigated further in the next development phase.
- after an initial settling-in period, baseline currents have normally been at, or below, 0.1μA (1ppm equivalent). The rate of baseline settling was influenced by pretreatment of hardware components, electrolyte type and the presence and concentration of certain oxidising additives, notably CrO_3 or $KMnO_4$. Further R & D is required in this area to gain a better understanding of the processes involved and to take full advantage of any benefits available.

- a number of sensors, after settling, have shown no measurable signal drift when subjected to regular checks over 6 months. Other sensors have shown some drift, but this generally diminished with time and may be reflecting a greatly extended settling period. There exists some evidence on potential causes, but more work is needed on this topic.

The chosen electrolyte (10N H_2SO_4) will be in balance with an average relative humidity of 63%. This could be adjusted for other likely average humidities. Calculations of water transfer rates indicate that the sensors should cope with continuous exposures to zero or 100% relative humidity at temperatures up to 35^{o}C., for several weeks.

The present hardware design has been kept as simple as possible to allow for the use of machining of a production version. Recently, some stress problems have been evident with this design. To eliminate these, and incorporate a number of other desirable improvements a Mark 4 redesign is proposed. This design would also be suitable for production by moulding which could eventually result in a worthwhile cost saving.

1. INTRODUCTION

This report covers the second phase of a work program to develop a carbon monoxide sensor for use in coal mines. The first phase [1] established a favoured sensor configuration comprising a matched pair of catalysed, gas diffusion electrodes in a "close-sandwich" arrangement, with an aqueous acid electrolyte, drawn from a plastic reservoir by means of a wick. Gas access to the sensing electrode was via a gaseous diffusion barrier and the sensor was housed in plastic hardware with platinum foil current collectors. Platinum and sulphuric acid were selected for the electrocatalyst and electrolyte respectively, but there remained final choices of acid type and concentration and whether Pt or Pt/Au electrocatalysts should be used. There also remained the possibility of employing an alkaline electrolyte, with gold electrodes, provided an insitu CO_2-scrubbing arrangement could be developed.

The main objectives of this second phase were threefold[2]:

- to develop the"Laboratory Model" sensor, from phase 1, to the pre-production, prototype stage and provide NCB with sensors suitable for testing. To achieve resolution better than 1 ppm, with a long term drift of less than 1 ppm per month.
- to carry out the necessary associated back-up characterisation and testing work.
- to tie up the remaining questions concerning choices left open from phase 1., and generate further design data.

2. CELL DESIGN

2.1. General Design Features.

Cell designs can be divided into three broad categories with minor modifications to each of these types:

2.1.1. Mark 1. This design was described in the last report[1] and is shown in figure 2.1. This design was abandoned in favour of alternatives quite early in this phase of the development for the following reasons:

- neoprene 'O'- ring was etched by 10N sulphuric acid, the eventual choice of electrolyte (see section 4). Alternative designs avoided direct contact between the 'O'-ring and electrolyte.

- detailed designs of sensing and counter plates were complex and machining costs would have been high for any production version. This would probably not apply if the production rate justified the use of injection moulding rather than machining to produce components.

- the webril wick and separator material deteriorated after several months in 7N sulphuric acid and completely disintegrated in 10N acid. All later designs employed a glass mat material.

- the maximum cell diameter was reduced in later versions from 45mm to 40mm. The Mark 3 design was also made into a more compact version by incorporating a cavity in the counter plate for the electrolyte reserve, rather than using the cup reservoir as shown in the Mark 1 and 2 designs.

- electrolyte filling in early Mark 1 sensors was affected from the top before assembly. It proved much more convenient to assemble the electrode sandwich first, then fill with electrolyte via a filler hole in the base of the reservoir.

2.1.2. Mark 2. This design is depicted in figures 2.2. and 2.3. The relocation of the 'O'-ring and modified sealing of the cell were common features of both the later designs. In this arrangement the 'O'-ring does not form a primary seal, but merely serves to transmit the clamping pressure to the electrode sandwich. Electrolyte seals were affected between the uncatalysed perimeters of the electrodes and the central PTFE washer and ABS "floor" in the counter plate.

The electrode sandwich was moulded into the cavity formed between the ABS floor and the 'O'-ring,which was compressed from 2.67 mm to 1.35 mm diameter. Mark 2 sensors were either cemented or bolted together. In the cemented versions assemblies were clamped together and Tensol, acrylic cement applied into a machined groove between the perimeters of the sensing and counter plates. When the cement was set, the clamps were removed. There was little to choose between these options but bolting was chosen for the final version in this phase since it could provide a cleaner, more reliable method of assembly. At some later stage however, ultrasonic welding may be considered.

The Mark 2 and 3 designs were virtually identical from the central PTFE washer upwards, the main differences being the design of current collection and counter plate/ electrolyte reservoir.

Platinum foil current collectors in the Mark 2 design were taken through the glued seal between the counter plate and ABS reservoir and soldered to tags bolted to the underside of the counter plate as shown in figure 2.3.

The Mark 2 reservoir comprised a ready-made ABS battery casing, obtained from Ever Ready. This was cut to size and the ABS floor glued into position with Tensol cement. This canister was then cemented into the annular counter plate to form the assembly shown in figure 2.2. The depth of the depression between the ABS floor and the top surface of the counter plate was fixed by assembling the components on a suitable jig. However, under quite moderate temperature

excursions, (up to 30^{o}C), the stresses produced by the cell 'O'-ring compression caused the glued joint between reservoir and counter plate to creep. The gradual relaxation of the electrode sandwich compression resulted in seal failure, as evidenced by the onset of a base line drift.

2.1.3. Mark 3. This design, shown in figures 2.4. to 2.7., was developed to overcome the problems with the Mark 2 arrangement. The figures depict the "flat" sensor version which dispenses with the ABS electrolyte canister. Instead the electrolyte reserve is contained in a cavity in the body of the counter plate. If necessary, a larger electrolyte volume could be carried by glueing the ABS cylindrical container into the cavity.

In this design none of the glued joints are subjected to shearing forces. However, the 'O'-ring compression stresses were still great enough to cause distortion and creep of the ABS sensing and counter plates. For this reason perspex was used which is a more rigid material. It may be that the 'O'-ring compression is greater than necessary and some slackening would be possible to ease the stresses on the hardware. However, further work would be required before this could be instituted, particularly with regard to the longer term effects on sealing, and such steps will need to be included in the following development phase.

Orientation stability was improved in the Mark 3 design by incorporating a double electrolyte wick and an additional glass separator at the counter electrode. This change also eliminated the odd "sluggish" sensor which was sometimes encountered.

Current collection was similar to the Mark 1 arrangement. Platinum foils, pressed against the catalysed surfaces in the "sandwich", were led through slots in the counter plate acrylic ring (figure 2.7.) to solder tabs which were bolted to the topside of the counter plate. The slots in the counter plate ring also provided a means of air access (see section 2.2.) to the counter electrode, via the groove between the ring and the ABS floor of the counter plate (figure 2.4.). The current collector foils were led through

the "sandwich" seal as close as possible to the clamping bolts, where the pressure was highest, to minimise the possibility of electrolyte "tracking" along the metal surfaces. Earlier designs brought the foils through the seal at positions equi-distant from the clamping bolts and sometimes suffered some leakage over extended periods of operation.

2.1.4. Mark 3 sensor specification.

The present specification of components for the Mark 3 sensor design is as follows:

Counter Plate: 40 mm dia., perspex (see figure 2.5.).
Webril Diffuser: 20.32 mm dia., thickness 0.25 mm.
'O'-ring: Edwards VOR 1128, neoprene.
Sensing electrode: 25.857 mm dia., thickness 0.5 mm, platinum catalysed, porous PTFE tape (section 3).Catalysed diameter 20.32 mm
Current Collectors: Platinum foils, 25 mm x 1mm x 0.025m
Sensing Glass separator: Whatman GF/C glass filter paper. 20.32 mm dia., 0.192 mm thickness.
PTFE washer: Porous PTFE as for electrodes, 17.27 mm I.D., 25.857 mm O.D.
Wicks: 2 off GF/F glass matts, 0.457 mm thick.
Counter Glass Separator: 0.254 mm thick, 20.32 mm dia. GF/C glass mat with 3.5 mm dia. hole at centre.
Counter Electrode: same as sensing electrode with 3.5 mm dia. hole at centre.
Floor: 25.4 mm dia., 1 mm thick white ABS sheet with 3.5 mm dia hole at centre.
Counter Plate Ring: made from 30 mm nominal O.D. acrylic tubing (see figure 2.7.)
Counter Plate: 30 mm dia. perspex (see figure 2.6.).

Reservoir (optional): Ever Ready RX14 white ABS cases, machined to size (see figure 2.2.).

Coverslip: 28.5 mm dia., 1 mm thick, white ABS sheet.
Clamping Bolts: 8 B.A. countersunk heads, nickel-plated brass.
Current collection bolts: 8 B.A., domed heads, nickel-plated brass.

2.1.5. Future Developments.

With many Mark 3 sensors the plastic rings cemented to the counter plate fractured under the stress of the 'O'-ring clamping pressure. This did not affect the sensor operation since the ring merely performs the function of spacer and containment for the 'O'-ring. However, such cracking is undesirable and some modifications will be made to the design in the future development program.

Some enquiries have been made with regard to injection moulding costs of the sensor plastic hardware components. These have indicated that mould costs could be covered over the first 1000 sensors with component prices which are comparable to machined components (about £3 per set). Thereafter a set of moulded components would cost only about 1/5th that of machined ones. Also since moulding costs are not affected greatly by design complexity there will be a greater degree of freedom compared to machining. The modified components will therefore, be designed with the view to manufacture by moulding once they have been finalised, rather than machining.

2.2. Gas access to the counter electrode.

A supply of oxygen to the counter electrode is essential in order to maintain the oxygen reduction reaction.

At one extreme, if the oxygen flux to the counter is insufficient to maintain the sensor signal current, then the counter electrode will limit rather than the sensing electrode and the sensor will effectively saturate. Even before this limit is reached any diffusion resistance, sufficient to lower the oxygen partial pressure at the counter electrode, will produce added polarisation and contribute to non-linearity.

The limiting flux of oxygen to the counter electrode therefore, needs to be equivalent to many times the sensor current.

At the other extreme, and in the case where the whole sensor is exposed to the atmosphere under test, if gas access to the counter is too easy, it will also see an appreciable carbon monoxide concentration resulting in a reduction in signal. For example with identical sensing and counter electrodes, having identical gas access, the signal would be zero. The diffusibility to the counter therefore needs to be many times less than that to the sensing electrode.

The treatment below assumes that the sensor is completely diffusion limited, which is not necessarily the case. However, it can still be of some value in setting approximate guide lines.

$$\text{Take Sensor signal } (\mu A) = fx \qquad \ldots(1)$$

where x is the CO concentration in ppm

f is sensitivity in μA per ppm

Assuming diffusion limiting conditions, the electrode in ambient air (21×10^4 ppm of O_2) is given by

$$i_L \text{ (} O_2 \text{ to sensing in } \mu A \text{)} = 42 \times 10^4 f \qquad \ldots(2)$$

(the factor of 2 appears because 1 mol of O_2 is electrochemically equivalent to 2 mols of CO.)

We now put in the condition that the gas flux to the counter should be much less than to the sensing, say at least by a factor b, so

$$i_L \text{ (} O_2 \text{ counter)} \leq \frac{42 \times 10^4}{b} f \qquad \ldots(3)$$

The other condition is that the oxygen flux to the counter should be much greater compared to the sensor current, say at least by a factor 'a',

$$i_L \text{ (} O_2, \text{counter)} \text{ in } \mu A \geq afx \qquad \ldots(4)$$

Equating 3 and 4 we get

$$ax \leqslant \frac{42 \times 10^4}{b} \qquad \ldots(4)$$

or

$$x \leqslant \frac{42 \times 10^4}{a.b.} \text{ ppm} \qquad \ldots(6)$$

We note that these equations are independant of the sensitivity factor f.

The counter will be at its ultimate limit when a = 1, so that the ultimate sensor saturation point is given by

$$x = \frac{42 \times 10^4}{b} \qquad \ldots(7)$$

e.g. if b = 84 the limit would be 5000ppm.

In practice the sensor will suffer appreciably before the ultimate limit is reached, i.e. with a > 1, particularly with the balanced pair mode of operation where relatively small increases in counter electrode polarisation can affect the signal, since the sensing electrode is not truly into a limiting current region because of local cell effects[1].

It was found that the gas supply rate to the counter, via the sensing electrode by dissolution and transport across the electrolyte "sandwich" were insufficient to meet the counter electrode demand, set by the sensor signal, i.e.

$$i_L \text{ (} O_2\text{, counter) by this route } \ll fx$$

All designs of carbon monoxide sensor, based on this principle therefore, need a specially designed air access to the counter electrode. The access must of course be restricted so as to deny any significant access of carbon monoxide in the atmosphere to the counter electrode. The porous PTFE tape, supporting the catalysed electrode, projects beyond the cell seal into the atmosphere; this tape then presents a diffusion path for gases to the electrode[3]. The diffusion path is highly restrictive relative to the

sensing electrode access - measurements indicated oxygen diffusibility rates in air were about 80 times lower relative to the sensing electrode access in the Mark I design (Appendix 2). But, because oxygen is present in much higher concentrations than carbon monoxide, the oxygen supply rate can satisfy the counter electrode without any significant interference from carbon monoxide.

Mark 2 and 3 designs required special air access features for the sensors to operate. This was accomplished by designing a groove between the base plate floor and sides as shown in figures 2.2. and 2.4. Air gained entry to the groove through specially designed slots, and diffused down the counter electrode tape exposed around the groove perimeters.

2.3. Choice of hardware constructional materials.

10N sulphuric acid was the eventual choice of electrolyte and all materials in contact with this medium were required to be resistant to strong acids. For this reason, catalysts and current collectors were restricted to platinum and the sensor body was plastic. The neoprene 'O'-ring, Webril diffuser(sensing electrode gas access), and bolts etc. were not in direct contact with the electrolyte; however, even minor electrolyte leaks (or tracking) caused corrosion of the bolts and solder tags and was soon apparent in causing erratic and drifting signals.

ABS and/or perspex were chosen for the body materials since they can be easily glued - a convenient property at this stage of development. They can also be injection moulded and ultrasonically welded if necessary in the future. Both materials were compatible with the electrolyte system, although there was some evidence that traces of organic matter originating from their surfaces made some contribution to the background current (see section 5) at least in the initial stages of sensor life. This could be inhibited by oxidative pretreatments and/or the use of oxidising additives to the electrolyte (see section 5) but more detailed studies on the wider aspects of these measures are required. Perspex was eventually chosen in preference to ABS for two reasons:

-ABS rod supplies were discontinued although granular material could be obtained for moulding.

-perspex is more rigid and does not undergo creep in the sensor arrangement as did the ABS materials used (see above).

The white ABS used for the baseplate floors, reservoirs and coverslips contained a TiO_2 filler which appeared compatible with the electrolyte. As with perspex however, it is possible that traces of minor constituents and impurities made some contribution to the background currents.

Webril, used as the separator and wick in earlier sensors, proved incompatible in strong sulphuric acid over extended periods of several months. These components were therefore, switched to a glass filter mat material , manufactured by Whatman. The stability of this material has so far proven very satisfactory but the wicking properties were somewhat inferior to the Webril. There was some indication that vacuum filling of the electrode sandwich improved sensor response and orientation stability, but the use of double wicks and extra separators obviated the need for vacuum filling.

2.4. Mark 3 Gas Diffusion Restriction Design.

The top cap assembly, controlling diffusion of the test gas to the sensing electrode was essentially the same for all 3 basic sensor designs. A pattern of 9 x 1.2 mm holes, chosen to achieve a high signal uniformity over the sensing electrode, were drilled in the perspex sensing plate as shown in the figures. No recess was needed to accomodate the gas spreader behind the electrode in the top caps of later designs, since the required space was provided between the compressed 'O'-ring. In the case of Mark 2 and 3 sensor designs, the gas spreader comprised a single Webril disc. Hole lengths in these designs were also increased to 5 mm instead of the 3.68 mm used for Mark 1 sensors[1].

The sensitivity of the capillary diffusion barrier can be calculated from the equation[5]:

$$i = nF \frac{A}{L} D C_g$$

where i is the capillary diffusion current (amps)

L is the capillary length (cm)

n is the number of electrons transferred per mole of reactant gas 'g'.

F is the Faraday Constant (96,494 coulombs per equivalent)

A is the capillary cross sectional area.

D is the gas diffusion constant in air (units cm^2 per s)

C_g is the concentration of the gas 'g'.

$C_g = \frac{P_g}{22.4.10^3}$ at S.T.P. where P_g is the partial pressure of gas 'g' in atmospheres.

The sensitivity of the sensor diffusion barrier, containing 9 capillary holes, then becomes:

$$i\ (\mu A/ppm) = 3.045\ n\ D \frac{d^2}{L}$$

where d is the capillary diameter (mm)

L is the capillary length (mm)

The output varies with the square root of temperature, and at 20^oC. the constant becomes 3.155 instead of 3.045.

For carbon monoxide n is 2 and D is 0.203 $cm^2 S^{-1}$ (Appendix 3) and at 20^oC., the equation becomes

$$i\ (\mu A/ppm\ CO) = 1.420 \frac{d^2}{L}$$

The calculated capillary diffusion barrier sensitivities for Mark 2 and 3 sensors are then 0.369 μA/ppm CO. However, measured sensitivities of sensors were nearer 0.1 μA/ppm CO and, as previously found with the Mark 1 design[1], the capillaries apparently only constituted about 25% of the total signal limitation.

Components located between the capillaries and the electrode, such as the Webril diffuser and PTFE electrode tape, make an additional contribution to the gaseous diffusion resistance. In the standard design of CTL Oxygen Sensor, the much greater reactant concentration gradients present when operating on oxygen from ambient air, compared to the CO sensor, allow a much smaller capillary size to be employed. In this situation the hole provides essentially all the diffusional

resistance and the spreading resistance downstream of the capillary becomes relatively insignificant. Even with the CO sensor design however, these components cannot account for the very large discrepancies between calculated and measured signals - removal of the Webril diffuser resulted in a signal increase of only 10% and the electrode tape/ catalyst composite sensitivity of about 2.7μA/ppm CO, derived from oxygen diffusibility measurements (Appendix 1), would only contribute another 13-14% depression of the calculated capillary signal.

The temperature coefficients of about 0.4% per ^{o}C., were sufficiently high above the theoretical 0.17 % per ^{o}C., to suggest that processes other than gaseous diffusion restrictions were responsible for the limitations in sensor signals. Diffusion through liquid films in the electrode and electrocatalyst activity per se can be discounted in view of the very high sensitivities recorded in open electrode tests (of the order 4μA/ppm CO - section 3). However, counter electrode polarisation under load and the occurrence of parasitic local cells on the sensing electrode, involving CO and O_2 [1], may be exerting some influence. Both effects would have temperature coefficients typical of activated processes of several percent per ^{o}C. This problem will be further investigated in the next development phase.

3. ELECTRODES

3.1. Electrode Manufacture

The method previously described[1] was modified slightly to be more amenable to larger quantity batch production.

Weighed amounts of precious metal catalyst were mixed with measured quantities of PTFE aqueous dispersion (I.C.I. Fluon GP1 dispersion) in an ultrasonic agitator. Isopropyl alcohol was added which coagulated the mixture to a"dough-like" consistency. The dough could be fairly easily divided into approximately equal proportions and applied by means of a spatula into a row of depressions formed in an aluminium foil as described previously.[1] It was found unnecessary to pre-coat the aluminium foil as done in the last report period.[1]

The doughed electrodes were dried with a hair drier and heat cured at 280-290°C., in a circulated air oven, for ½ to 1 hour to remove wetting agents present in the original PTFE dispersion.

The catalysed aluminium foil discs were cut from the main sheet and the cured catalyst layer transferred to porous PTFE tapes using an hydraulic press[4]. Weighing the PTFE discs before and after transfer enabled an exact measure to be made of the catalyst loading.

Acetone was also used to dough the catalyst mix, but the alcohol was preferred, giving a dried mix with fewer, smaller cracks and which foil transferred somewhat better, at lower pressures.

3.2. Selection of electrocatalyst and electrode composition.

3.2.1. Open electrode test method.

To ensure a stable sensor signal over long periods of time, with minimal temperature dependence, it is essential

that the capillary holes present the principal diffusional resistance barrier to the incoming carbon monoxide reactant. In particular the electrode reaction polarisation resistance and diffusional resistance through the electrolyte, should be at least 1/10th to 1/15th the gaseous diffusional barriers, i.e. the electrocatalyst activity reserve should be at least 10 to 15 times the sensor signal.[1][4]

Previous open electrode activity tests had been conducted with catalyst layers, pressure bonded to standard Gore porous PTFE tapes as used in the CTL oxygen sensor. However, diffusibility measurements (see Appendix 1) indicated that this tape would limit at a carbon monoxide current of about 0.9μA/ppm/cm^2, equivalent to a CO signal of about 150μA, on the sensor electrode area of π cm^2 in a 54 ppm CO in air test gas. Measured electrode currents in fact limited at about 70 to 80 μA in this test gas. Whilst this test method suffices to establish whether the electrode activity is above or below the target level of 10 to 15 times the corresponding sensor signal of 5.4μA on the 54 ppm CO in air test gas, π cm^2 area, it cannot distinguish between electrodes having different activities above the 70-80μA level and therefore, cannot be used to optimise electrode activity as a function of catalyst type and catalyst/PTFE ratio. The electrode optimisation work therefore, was conducted with thinner, more porous Gore tapes, having measured diffusibilities greater than 2.5μA/ppmCO/cm^2, i.e. signals in 54 ppm CO in air test gas, and π cm^2 area, of 430μA, or above an 80X factor over the sensor signal.

Some tests were carried out using a fine platinum mesh electrode, into which the catalyst layer was applied by brushing, which could be "floated" on the surface of the electrolyte in a specially designed cell. However, the resultant electrode structure represented too great a departure from that in the sensing electrode. For some reason the mesh electrodes were much more hydrophobic and valid test results were obviously not being obtained from the electrodes.

The thin tape electrodes presented problems when tested in the cell described in the last report.[1] When tested at the bottom of the cell, they sagged under the electrolyte head and broke contact with the current collector. When "floated" in an arrangement similar to that used for the mesh electrodes, gas bubbling occurred on the undersides of the electrodes and upset the current readings. A new test cell was therefore, designed as shown in figure 3.1.

Electrode testing was restricted to measuring currents in aerobic conditions, using a 54 ppm CO in air test gas, at potentials between the air rest potential and up to 100mV anodic overpotential (between about 1000 and 1100 mV on the D.H.E. scale[1]) in ambient room temperature. Potentials were controlled by means of a potentiostat and a Pt/air electrode [1]. In this way no contamination by H_2 from the D.H.E. occurred.

The tests were conducted by allowing the test electrode to settle for about half an hour at the air rest potential in static air. The steady background current was noted and test gas admitted to the electrode at a flow rate of about 200 ml per minute. The response was monitored on a recorder and the difference between background and the steady test gas signal taken as the CO response of the electrode. This procedure was then repeated at 50 and 100 mV anodic polarisation steps.

The following parameters were evaluated using the above procedure:

-effect of platinum/PTFE ratio, using standard Johnson Matthey platinum black in 10N H_2SO_4.
-effect of platinum loading using the standard J.M. black and a near optimum Pt/PTFE ratio.
-effect of platinum black grade and admixture with gold, using a near optimum metal/PTFE ratio.
-effects of ageing various electrode compositions in contact with 10N H_2SO_4.
-effect of H_2SO_4 concentration on various electrode compositions.

3.2.2. Effect of electrode potential on CO signal.

Figure 3.2. shows the effect of electrode potential on the signal obtained from the test gas, over the range 1000 to 1100 mV vs. D.H.E., in 10N H_2SO_4, using freshly prepared, standard J.M. Pt black electrodes. A similar picture exists for aged electrodes[8] and with other grades of Pt black.

The virtual independence of signal with potential indicates that the currents are diffusion controlled, either by the PTFE tape or the electrolyte film, or both. The range of currents measured, 155 to 295 μA, was well above both the standard tape and the sensor limits of 70 and 5.4 μA respectively, in the 54 ppm CO in air test gas.

3.2.3. Effect of Pt/PTFE ratio.

Figure 3.3. shows the variation of signals obtained at 1000 mV (D.H.E.), in 10N H_2SO_4, with freshly prepared standard J.M. Pt electrodes, at different Pt/PTFE ratios between 2:1 and 10:1.

Although there is a hint of an activity maximum at about a 6:1 Pt/PTFE ratio, considering the spread between replicate electrodes, there is little to choose between the measurements between 8:1 and 3:1.

The high spread between replicates could have been due to either variations in the very thin, porous, Gore PTFE tape used, or inherent variations introduced by the electrode preparation method.

The 2:1 electrode had a very sluggish response and was obviously too hydrophobic. A 10:1 replicate electrode was virtually inactive and may have flooded with electrolyte. The preferred range chosen was therefore, 6:1 to 4:1 for the standard J.M. grade of platinum black. Sensor tests are to be conducted within this composition range to define more precisely the desired ratio - some initial tests have indicated that the 4:1 electrodes give a slightly faster sensor response than 6:1 but more work is required on other parameters, in particular temperature coefficient and long

term signal stability.

3.2.4. Grades of platinum black and gold admixtures.

The Johnson Matthey, fuel cell grade platinum black, used in the last development phase[1], is no longer produced, although it could be made available as a "special". As a consequence two other grades of platinum were examined, the Johnson Matthey Standard black and Englehard No. 4 Black.

The Standard J.M. black has a larger particle size (lower specific surface area) than the J.M. fuel cell grade. Although this results in slightly reduced activity, it also imparts a faster response (see section 5.2.) On balance, the standard grade was selected for this phase of the development on the basis of availability, cost and response time; the slightly lower activity is not important since the activity reserve is well above requirement. However, both materials are still being assessed for long term effects in sensors.

The Englehard black has a particle size nearer to the J.M. fuel cell grade. Its activity was about 20% higher than the standard J.M. black in a 3:1 Pt:PTFE electrode, in 10N H_2SO_4. Response times were longer than an equivalent standard J.M. electrode, particularly with higher load resistors. A sensor is on long term test, using this material, which could be used as a fall-back option, instead of the J.M. fuel cell grade black. Since it is produced by Englehard as a standard product, it should be cheaper, more readily available and of more consistent quality than the J.M. fuel cell material produced as a special.

A 1:1 mechanical mixture of platinum and gold was less active than a similar plain, J.M. Standard Pt electrode. In 1N H_2SO_4, with 4:1 metal:PTFE ratios, signals in a 54 ppm CO/air test gas, were 150 and 230 μA for the Pt/Au and Pt electrodes respectively; in 10N H_2SO_4 activities reduced to 50 and 150 μA respectively. Although synergism may be obtained with the correct Pt/Au admixture, the corrosion behaviour of gold in the stronger acid is suspect

and it was not considered worthwhile to pursue this avenue at this stage.

3.2.5. Electrode ageing effects.

A number of electrode variants were stored in contact with 10N H_2SO_4 and periodically retested.The activities of these electrodes over a 30 day period are shown in figure 3.4. They all showed an initial decline over the first week or two of between 18 and 32%, depending on composition. After this period however activities appeared to stabilise.

These tests are continuing and an Englehard electrode has been included for comparison.

3.2.6. Effect of acid concentration.

The effects of H_2SO_4 concentration on the activity of 20-30 day aged, standard J.M. electrodes, and a fresh Englehard electrode, are shown in figure 3.5. Activity decreased linearily with increasing acid concentration over the range 1 to 20N with all electrodes tested. The gradient of each line was practically the same for all electrodes. Even at 20N the electrode signal was above 100μA with electrodes of Pt/PTFE ratio between 6:1 and 4:1, which is within the target specification of 10 to 15 times the sensor signal (5.4μA).

4. ELECTROLYTE

4.1. Selection of acid type and concentration.

Four options were identified for consideration in this phase of the development:

(a) concentrated sulphuric acid (7 to 12 N).

(b) dilute sulphuric acid (0.1 to 1 N) with additions of magnesium sulphate (approx 2M) to lower the electrolyte vapour pressure and reduce water loss.

(c) dilute sulphuric acid with about 4M sodium perchlorate in place of magnesium sulphate as above.

(d) perchloric acid/sodium perchlorate mixtures.

In addition to these we have also examined phosphoric and phosphoric/sulphuric acid mixtures.

The dilute acids containing dissolved salts proved unsuitable; their vapour pressures and hence water evaporation rates were still high, electrode activity was much lower than the straight acid and sensors gave erratic signals. Perchloric acid media were also rejected on the basis of possible fire hazard if a cell dried out.

10N sulphuric acid was selected for most of the work in this phase which has an equilibrium water vapour pressure equivalent to a 63% relative humidity (figure 4.1.). This is roughly in balance with an average laboratory humidity; other acid concentrations could be selected to be in equilibrium with higher or lower average humidities, without affecting the sensor performace significantly (see section 3), e.g. 4N, R_H 92% and 14N, R_H 39%. The variation of solution R_H with sulphuric acid concentration is shown in figure 4.1. - this realtionship is essentially unaffected by operating temperature.

Sensors employing 10N sulphuric acid electrolyte generally required about a month or so to settle to a steady, low level baseline (section 5). Some recent work with phosphoric acid indicated that a shorter settling period was required,

otherwise performance was very similar. There appeared to be no benefit from employing mixed H_2SO_4/H_3PO_4 acids.

4.2. Electrolyte Additives.

The effects on sensor performance of certain oxidising additives such as chromic acid (CrO_3) and potassium permanganate have been studied. The details of these investigations are covered in section 5.

4.2. Water Balance Calculations.

The Mark 3, flat sensor design (section 2), gives satisfactory operation with a minimum liquid volume of 0.5 cm^3; the maximum available space in the liquid reservoir is 2.8 cm^3. Thus, if the cell were initially primed with 1 cm^3 10N H_2SO_4, it could sustain continuous exposure to relative humidities in the range equivalent to 20N H_2SO_4 to 3.6N H_2SO_4, i.e. 14 to 93% R_H (figure 4.1.).

The upper and lower humidity limits for continuous exposure can be extended by adjustments to the priming electrolyte volume and concentration. For example, by using 0.5 cm^3 of 10N H_2SO_4 initially, the sensor can absorb up to 2.3 cm^3 additional water, when the concentration reduces to 1.8 N. In this way continuous exposure to high humidities up to 97-98% is possible, but the sensor will have little tolerance below the 63% R_H of the 10N H_2SO_4 priming solution. Larger volumes of more concentrated acids could be employed where dry atmospheres are likely to be encountered. However, the decline in electrode activity with acid strength above 20N could affect sensor calibration and some doubt exists over the stability of plastic hardware and platinum corrosion resistance in very strong sulphuric acid.

Accepting the 1cm^3, 10N H_2SO_4 primed cell as a fairly flexible option, being capable of continuous operation in R_H's between 14 and 93%, the question remaining is the allowable excursion times in conditions of higher or lower humidity. This will be governed by the water transfer rate

capability of the sensor geometry and will be temperature dependant. High humidities are a more likely condition in mines and therefore attention has been devoted mainly to assessing the water transfer characteristics in 100% R_H.

The water transfer rate from zinc-air cells, under conditions of pure diffusion control, has been shown to obey the relationship[6]:

$$\left(\frac{\partial W}{\partial t}\right)_T = 1.463.10^{-3} A\ i_L\ p_{H_2O}\ (R_{H1} - R_{H2}) \quad ...(1)$$

where: W is the water loss in g.

t is the time in hours

i_L is the oxygen limiting diffusion current in air of the cell configuration, in Amps.

p_{H_2O} is the saturated vapour pressure of water

R_{H1} isthe ambient relative humidity

R_{H2} is the relative humidity of water vapour above the electrolyte

A is a factor which corrects the equation for differences in the geometry for water diffusion compared to oxygen diffusion.

<u>The oxygen limiting diffusion current (i_L)</u>:

Assuming all the diffusion restriction originates from the 9 sensor capillaries, the value for i_L can be calculated from the relationship (see section 2.4.):

$$i_L\ (\mu A/\text{ppm } O_2) = nD\ 3.045\ \frac{d^2}{L} \quad ...(2)$$

In air, containing 21.10^4 ppm O_2, the value of i_L is given by:

$$i_L\ (\text{mA}) = 526.91\ \frac{d^2}{L} \quad ...(3)$$

Capillary hole diameters were 1.2mm for all sensor designs. Hole lengths were 5mm for Marks 2 and 3 and 3.68mm

for Mark 1. Thus the calculated oxygen limiting diffusion currents in air are:

Mark 2 and 3 sensors	152 mA.
Mark 1	206 mA.

The measured currents with a Mark 1 sensor were between 50 and 90mA, but there was some doubt whether these measurements represented a true, diffusion limited condition (Appendix 2). The current-voltage curve shape did not exhibit a well defined limiting current region and was indicative of a process controlled by a high degree of ohmic polarisation. The measured values of current were therefore probably optimistically low.

The discrepancies between measured and calculated sensitivities to CO, discussed in section 2.4., have yet to be resolved and estimates of i_L (O_2 in air) cannot be reliably made from measured CO-signals of sensors. At this stage therefore, water transfer rates were estimated using the calculated value for i_L of 150 mA for the Mark 2 and 3 designs, i.e. total control by the theoretical capillary diffusion relationship. This value should reflect the most pessimistic case. The 'A'-factor in the water transfer equation is assumed to be unity. In the following development phase, it is intended to verify these estimates of water transfer rates in actual water balance experiments. This would also enable an accurate measure to be made of the sensor calibration changes resulting from the acid concentration changes.

The residence time in 100% R_H at any temperature can be obtained by integrating equation 1 above:

$$\int_o^t \partial t_{(T)} = \frac{1}{(1463.10^{-3} i_L p_{H_2O})} \int_{W_1}^{W_2} \frac{\partial W}{1 - R_{H_2}}$$

W_1 = 1 cm^3, 10N H_2SO_4
W_2 = 2.8 cm^3, 3.6N H_2SO_4 (Mark 3, flat sensor design)
R_{H1} = 1
i_L = 150 mA for Mark 2 and 3 sensor designs.

R_{H2} is a function of acid concentration and therefore

water uptake (or loss) - see figure 4.1. However, the relationship is complex and cannot be readily integrated.

A stepwise method was therefore, used in which summation over 6 increments of 0.3 cm^3 was found to give a sufficiently accurate estimate of the residence time.

The equations used for each 0.3 cm^3 increment were as follows:

$$t \text{ (days) } (20^{\circ}C) = \frac{3.248}{1 - R_{av}}$$

$$t \text{ (days) } (40^{\circ}C) = \frac{1.030}{1 - R_{av}}$$

R_{av} is the average electrolyte R_H over the increment of water volume change, determined from figure 4.1.

The results are plotted in figure 4.2. and show that sensors should be capable of exposures to 100%. R_H for periods varying from 23 weeks at 20°C to 7 weeks at 40°C.

Similar calculations for the same sensor configuration in zero R_H show that a residence time of about2 weeks would be required to reduce the electrolyte volume to 0.5 cm^3 (concentration 20N).

Greater tolerance to humidity extremes could be designed by increasing the volume of the electrolyte reservoir, but further development of the wicking system would be required to retain the excellent attitude stability of the sensor.

5. SENSOR TESTS.

5.1. Sensor Stability.

In the course of this phase, 25 Mark 1, 27 Mark 2 and 42 Mark 3 sensors have been made and tested. The longest testing periods have been 7 months for Mark 1, 5 months for Mark 2 and 3 months for Mark 3. The monthly signal records for sensors that have exceeded a 2 month life test period are given in Table 5.1. and figures 5.1. and 5.2. Most of the Mark 2 sensors failed within a few weeks of assembly due to the inherent design fault discussed in section 2.1. Many of the Mark 3 type sensors are of too recent manufacture to be included and are still settling in.

All sensors exhibited an initial settling in period of about 2 months during which signal losses of about 4 and 7% occurred on average with Mark 1 and Mark 3 sensors respectively. Thereafter, the downward drift of signal slowed up considerably, with average signal losses of about 0.7 to 0.8% being recorded between the 2nd and 3rd month with both sensor types. The Mark 1 sensors which have exceeded 3 months testing, appeared to reach a steady signal plateau at about month 4 to 6.

As yet there are no clear relationships between the long term signal stability and the sensor variations, e.g. electrode Pt/PTFE ratios and Pt grades, electrolyte additives, component pretreatments,etc.

5.2. Response times.

Response time data for various types of sensor are given in Table 5.2. and figures 5.3. to 5.6. The major factor responsible for the different responses observed was the electrode composition and grade of platinum. Thus, sensor P112 with J.M. standard platinum electrodes had much the fastest response. This originates from the lower surface area of this catalyst, compared to the fuel cell and Engelhard grades, and hence lower electrode resistance

and capacitance. There was a smaller effect due to Pt:PTFE ratio in which the 10:1 fuel cell grade electrodes of sensor P34 produced a measurably faster response than the 4:1 fuel cell grade electrodes of sensor P 106; the latter electrode conductivity was probably lower due to the higher PTFE content. However, for reasons of electrode activity and consequent signal stability, the high PTFE content is preferred (section 5.1. and 3.2.).

The Engelhard platinum electrode response occupied an intermediate position between the J.M. standard and fuel cell grades of platinum.

5.3. Temperature Coefficients.

The general temperature behaviour was similar for all variants tested and typified by the characteristics listed for sensors P7 and P120 in Table 5.3.

Both sensor signal and baseline vary with temperature. The baseline temperature dependance follows an Arrhenius law, with a measured activation energy of about 18.8 K cal per mole (figure 5.7.). This will add to the signal temperature coefficient and emphasises the need to keep the baseline current at a very low level.

Measured signal temperature coefficients were between 0.35 and 0.40% signal at 20^{o}C. per ^{o}C. (figure 5.8.). This is significantly above the theoretical value of 0.17% per ^{o}C, for the condition whereby the signal is controlled solely by gaseous diffusion. However, the degree of gaseous diffusion control is obviously large since other possible controlling processes, such as diffusion through liquid films, electrochemical reaction and parasitic local cells, would have temperature coefficients about 10 to 20 times that for gaseous diffusion (see section 2.4.). The question of signal control factors and temperature coefficients has still to be completely resolved and will be further studied in the next development phase.

5.4. Effects of pretreatment and electrolyte additives on baselines.

All sensors exhibit a positive baseline which decays with time to a steady low level below 1 ppm CO equivalent ($< 0.1\mu A$). With an untreated set of components and using a plain 10N H_2SO_4 electrolyte, the time taken for the baseline to stabilise to such levels is in excess of 2 months. This time can be considerably reduced by pickling the components in nitric or sulphuric acid and/or adding oxidising agents to the electrolyte. (Table 5.4.).

Hot sulphuric acid leaching of the components has the advantage of not introducing any "foreign" matter into the sensor system and, in the absence of long term results on the effects of additives, this pretreatment is preferred at this stage.

5.5. Signal response to CO in nitrogen gas mixtures.

Parasitic, local cells have been suggested as a possible cause for the apparent loss in CO signal, relative to the calculated capillary diffusion current (section 2.4.). Thus some of the carbon monoxide reacts as follows with oxygen from the air at the sensing electrode:

Anode sites $2CO + 2H_2O = 2CO_2 + 4H^+ + 4e$

Cathode sites $O_2 + 4H^+ + 4e = 2H_2O$

Overall reaction $2CO + O_2 = 2CO_2$

Some preliminary tests were conducted with a 55ppm CO in nitrogen gas mixture. If the signal losses are due to such local cell processes, then anaerobic conditions at the sensing electrode should result in increased signals relative to aerobic conditions.

Increased signals were indeed generally found with the CO in nitrogen test gas, compared to CO in air (see Table 5.5.). The increases in signal varied greatly between sensors of different design and electrolyte concentration and the anaerobic responses tended to creep slowly upwards with time, after an initial fast response. However, these results can only be viewed qualitatively since there remained a reasonably large oxygen access to the sensing electrode via the seals (Appendix 2) and therefore, the degree of anaerobicity was very uncertain. Operation of the sensor in a completely oxygen free environmentis not possible since the counter electrode requires oxygen to operate.

Further, investigations are to be conducted in the next development phase on the effects of potential. biasing of the system above the air rest potential to prevent oxygen reduction at the sensing electrode.(1)

5.6. Hydrogen Response.

Mark 3 sensor responses to a 106 ppm H_2 in air test gas varied between 0.1 and 0.5 ppm CO equivalent, per ppm H_2. Most responses however, were between 0.35 and 0.45. A 10% HNO_3 pickle at 50°C resulted in an increased H_2 sensitivity to 0.4 to 0.8

The hydrogen responses were typified by a slow "creep up" of about 1 to 2μA per hour, following the initial response.

5.7. Orientation effects.

Orientation sensitivity of later Mark 3 versions were minimal. Steady state signals were unaffected by attitude and transient signal changes during inversion amounted to $<$ 0.5 ppm CO equivalent with flat sensors and $<$1 ppm CO equivalent with reservoir sensors.

5.8. Hysteresis.

Mark 3 sensors, exposed to 54 ppm CO in air, for periods up to 1 hour, suffered a slightly positive baseline hysteresis, amounting to $<$1 ppm CO equivalent which returned to normal within

5 minutes of removal of the test gas. This behaviour was the same whether the sensor was completely immersed in the test gas atmosphere or if the sensing electrode plate only was exposed to the gas. Further work is to be conducted on this aspect in the next development phase.

REFERENCES

(1) Phase 1. report; CTL report No. 79/31/002, Sept. 1979, NCB Contract Y 135007/09/21.

(2) CTL proposal for phase 2 of NCB Contract Y 135007/09/21, 10th August, 1979.

(3) "Partial Pressure Oxygen Sensor with Knudsen Diffusion Barrier"; CTL report 79/06/001, August, 1979, NCB Contract YB 1350/09/22.

(4) A.D.S. Tantram, R. Chan-Henry, B.S. Hobbs, J.R. Finbow; "Oxygen Detector for Use in Coal Mines", CTL report No. 78/02/001, NCB Contract YB 1350/09/22, July, 1978.

(5) A.D.S. Tantram, J.R. Finbow: "Oxygen Detector for Use in Coal Mines", CTL report May 1976, NCB Contract YB 1350/09/22.

(6) T.M. Fry,A.D.S. Tantram; "Loss of Water from Zinc-Air Cells by Evaporation", Energy Conversion Limited, Technical Note No. 20, 22nd June 1967.

(7) A.S. Foust, L.A. Wenzel, C.W. Clump, L. Maus, L.B. Anderson; Principles of Unit Operations, John Wiley, (1966) p.106.

FIGURE 2.1.

TOP VIEW

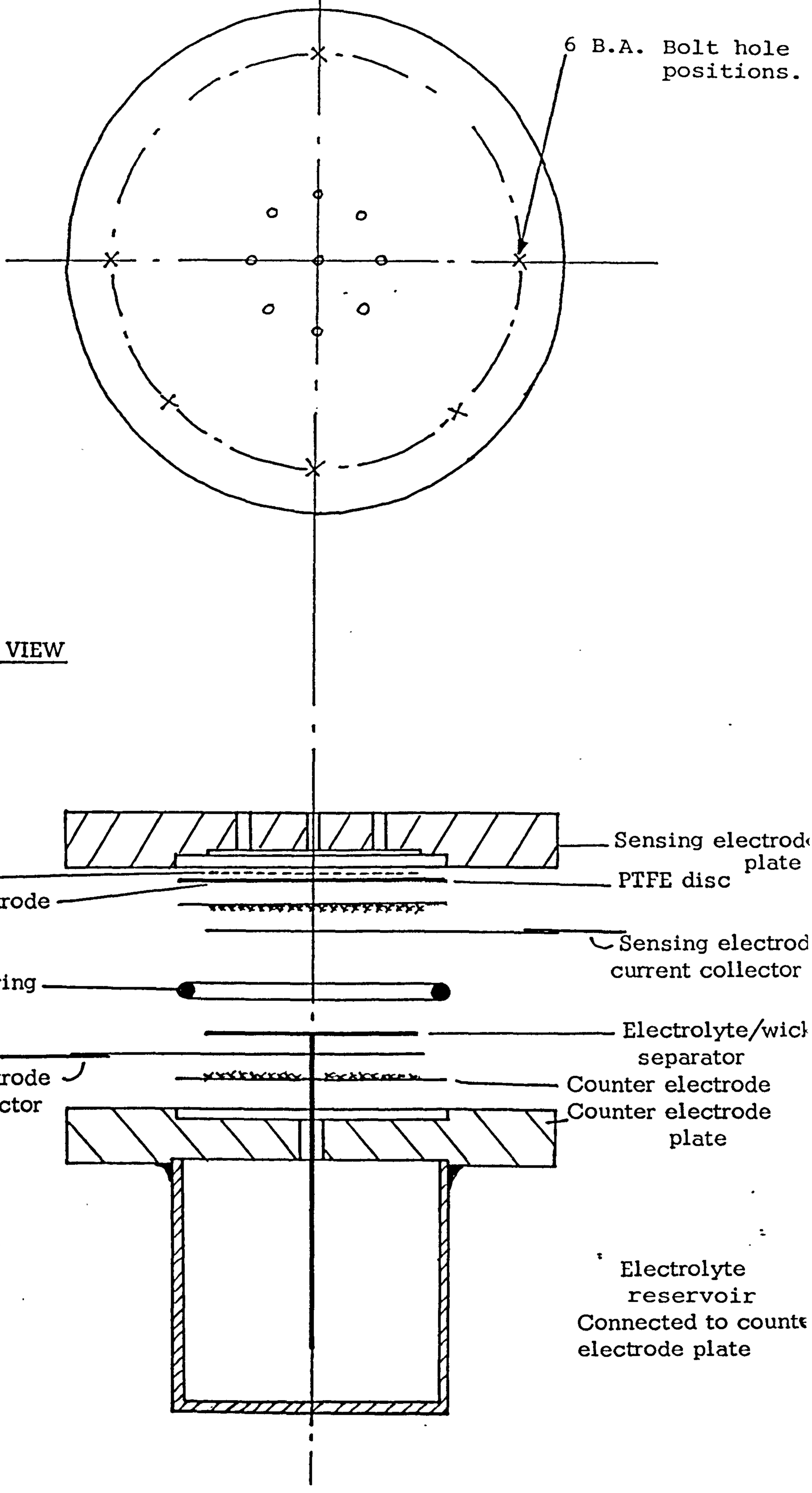

Mark I Sensor Design

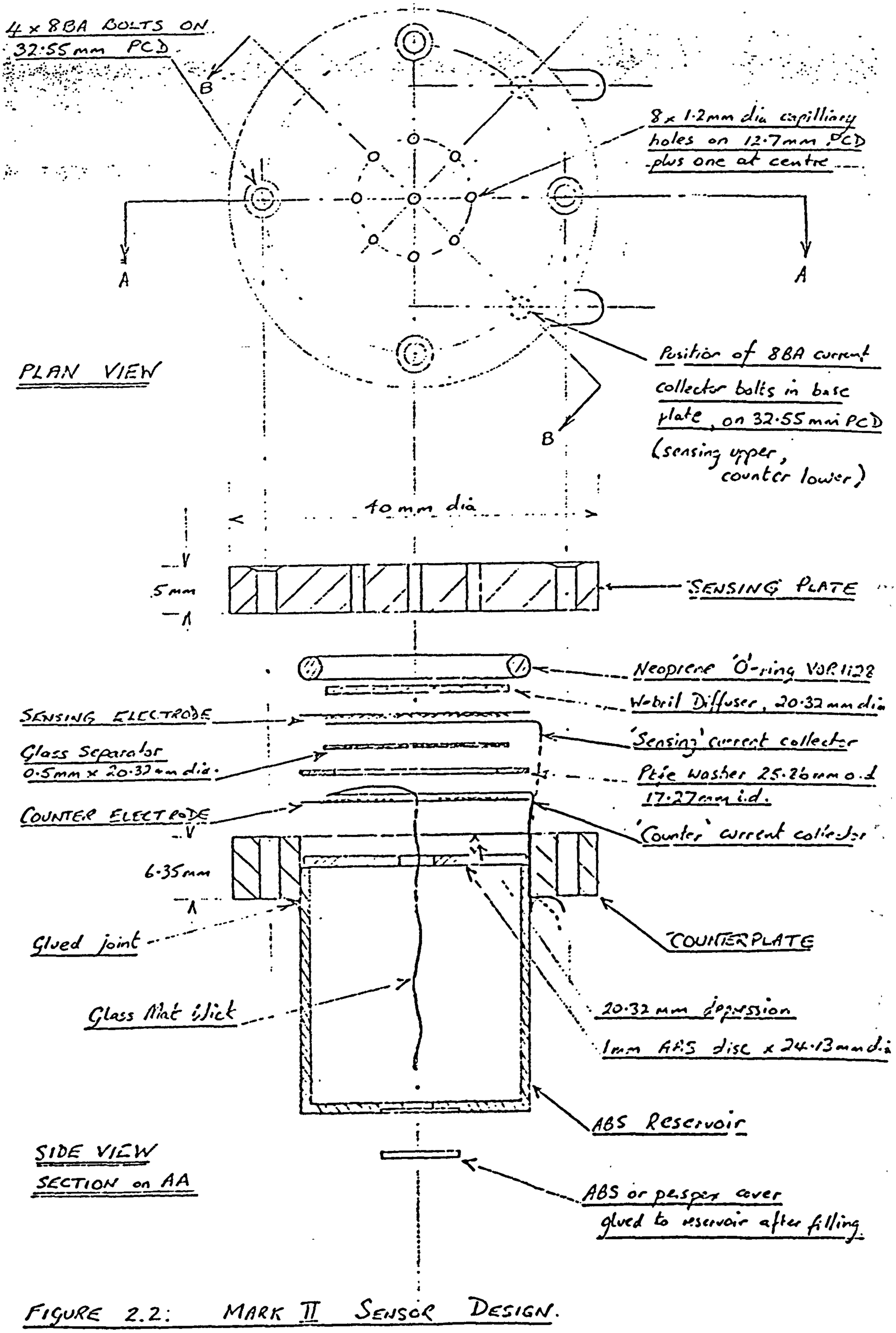

FIGURE 2.2: MARK II SENSOR DESIGN.

FIGURE 2.3.

FIGURE 2.3. MARK II SENSOR CURRENT COLLECTION.

SECTION ON BB, FIG. 2.2.

SCALE : 2×

FIGURE 2.4.

Scale x 2.

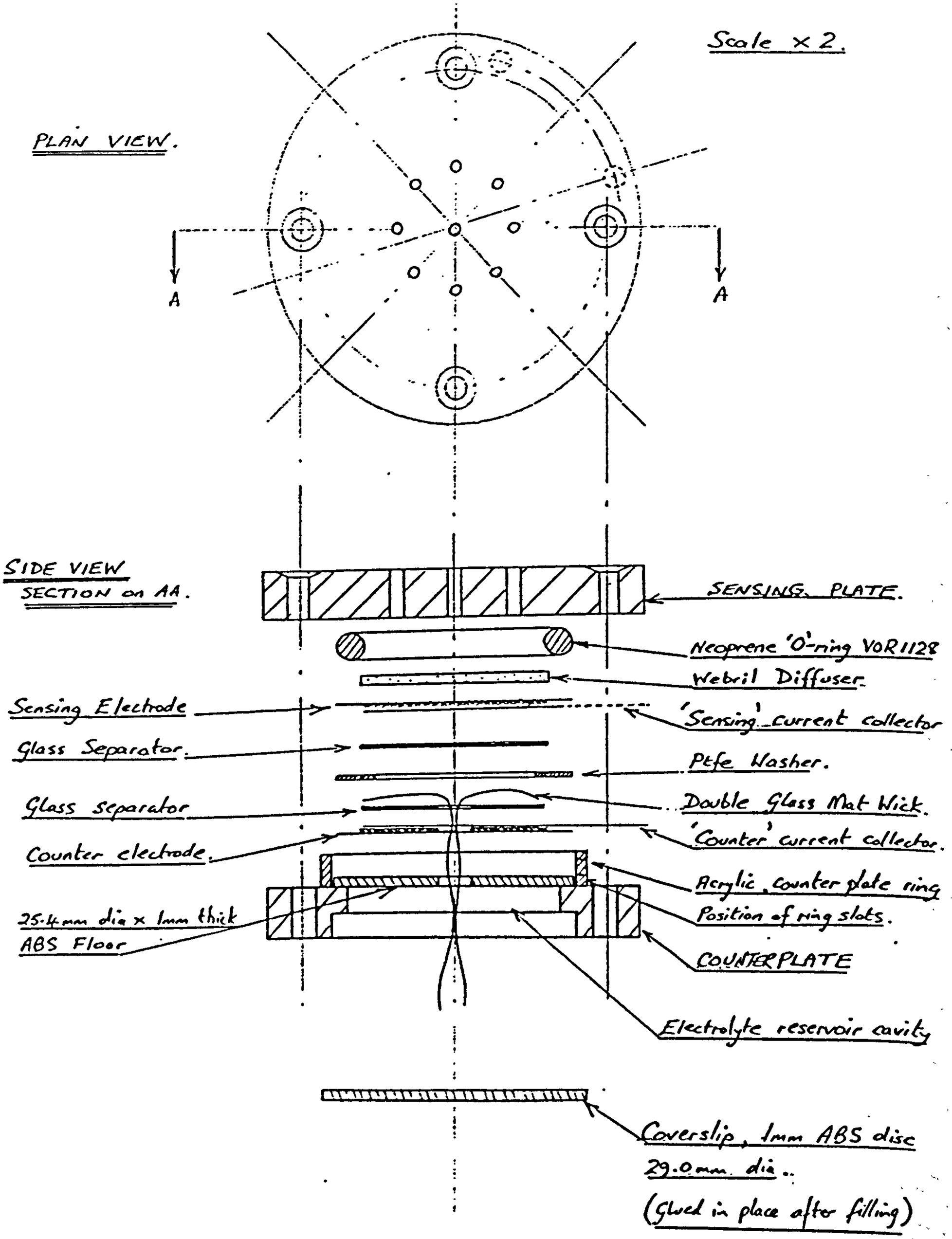

FIGURE 2.3.

CITY TECHNOLOGY LIMITED
THE CITY UNIVERSITY
NORTHAMPTON SQUARE
LONDON ECIV 0HB
Tel. 01-253 3799

SENSING ELECTRODE PLATE.

MARK 3.

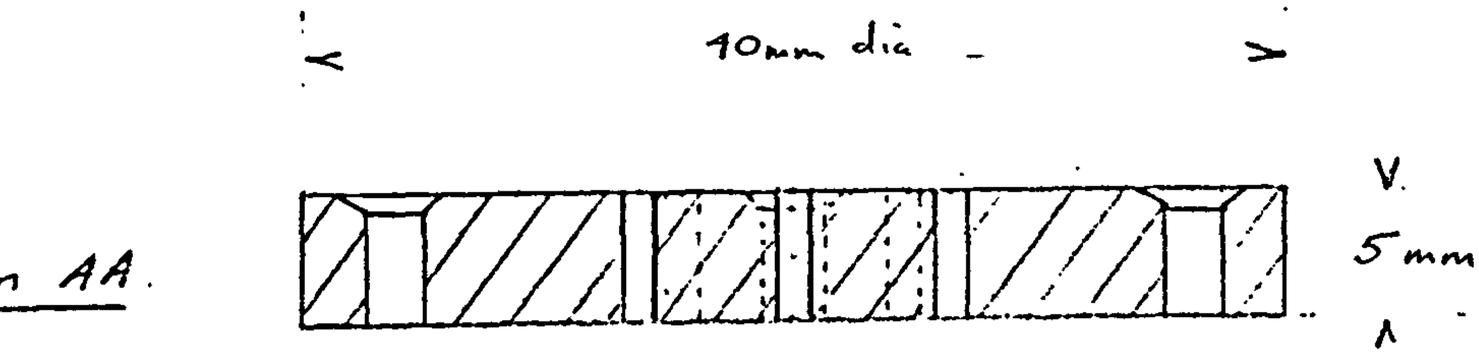

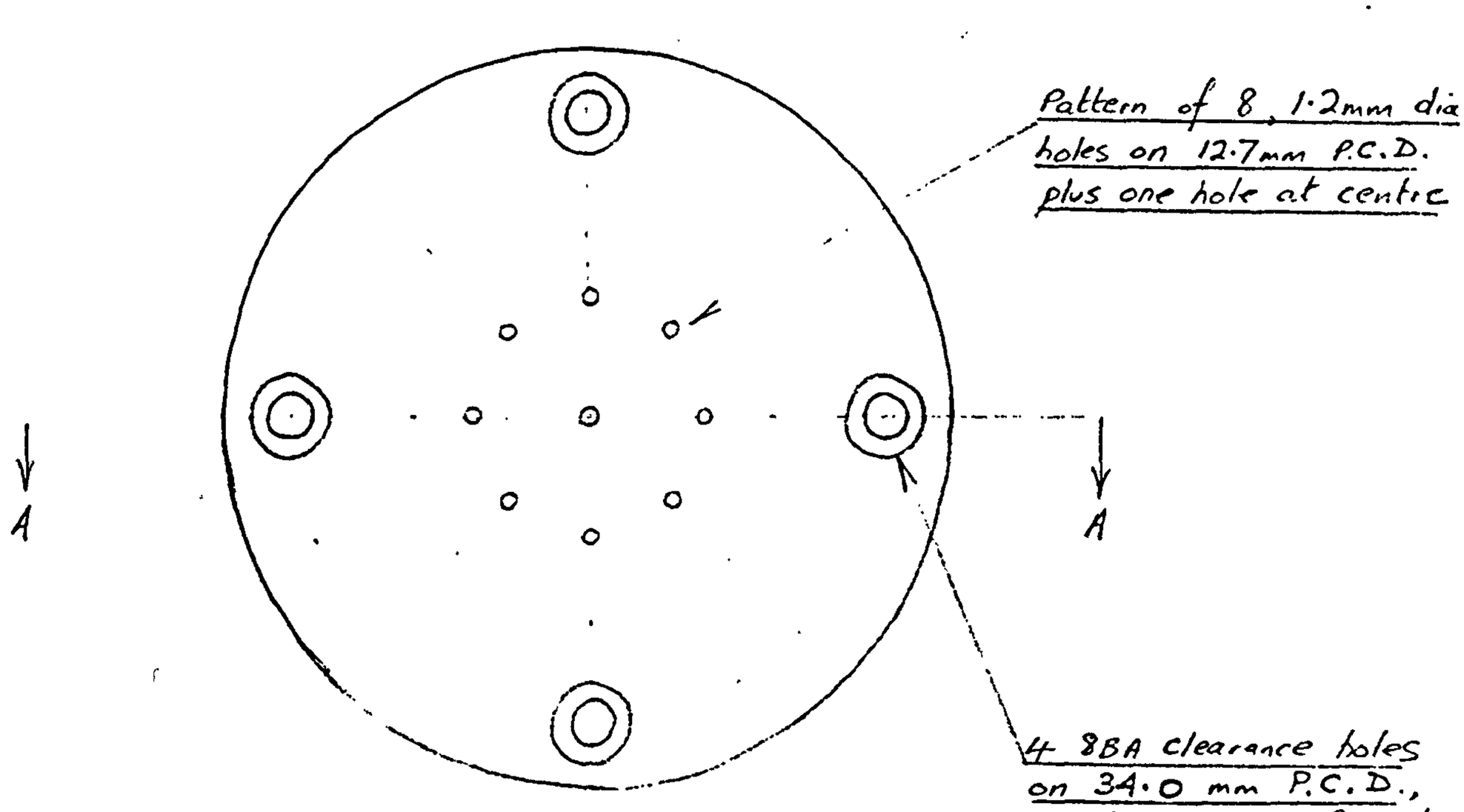

Scale : ×2

Material : Perspex

Ref : BSH/15.2.80.
94.95.31.

FIGURE 2.6.

CITY TECHNOLOGY LIMITED
THE CITY UNIVERSITY
NORTHAMPTON SQUARE
LONDON ECIV OHB.
Tel. 01-253 3799

COUNTER ELECTRODE PLATE,
MARK 3.

SECTION on AA.

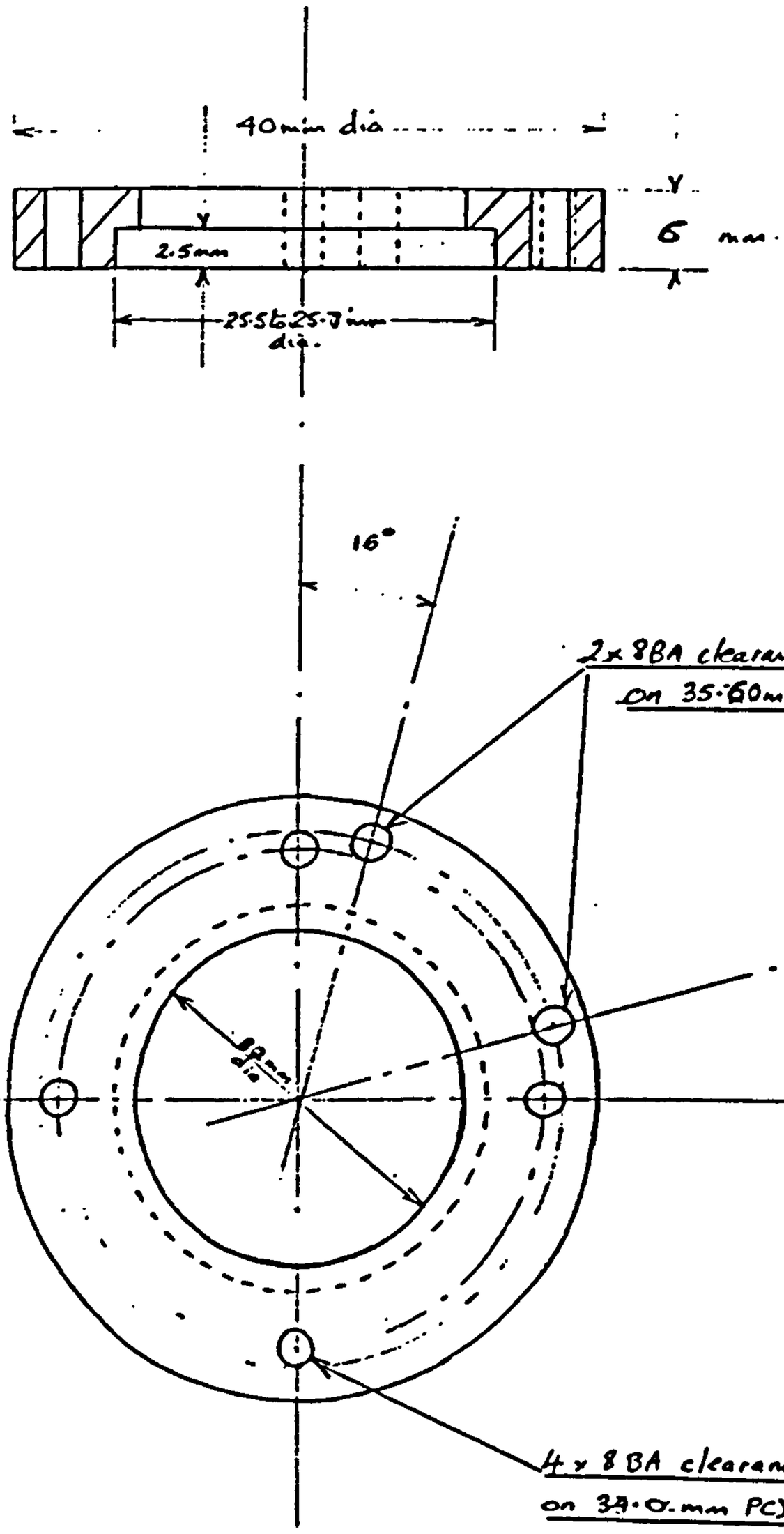

Scale : x2
Material : Perspex.
Ref. BSH / 15.2.80.
94. 95. 31.

FIGURE 2.7

COUNTER PLATE RING.

CITY TECHNOLOGY LIMITED
THE CITY UNIVERSITY
NORTHAMPTON SQUARE
LONDON EC1V 0HB.
Tel. 01-253 3799.

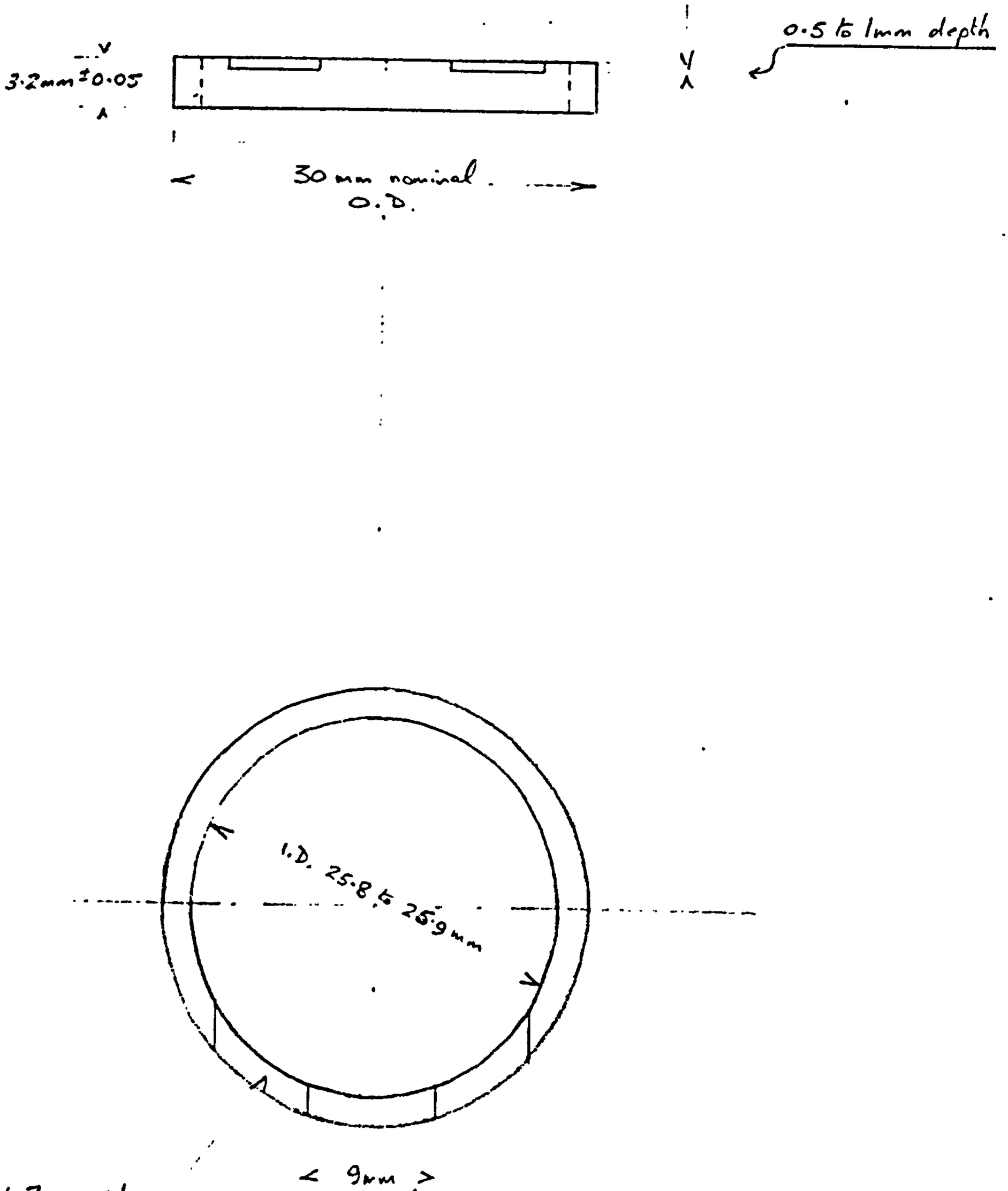

Scale : x2

Material : perspex

Ref : BSH / 15. 2. 80.
94. 95. 31.

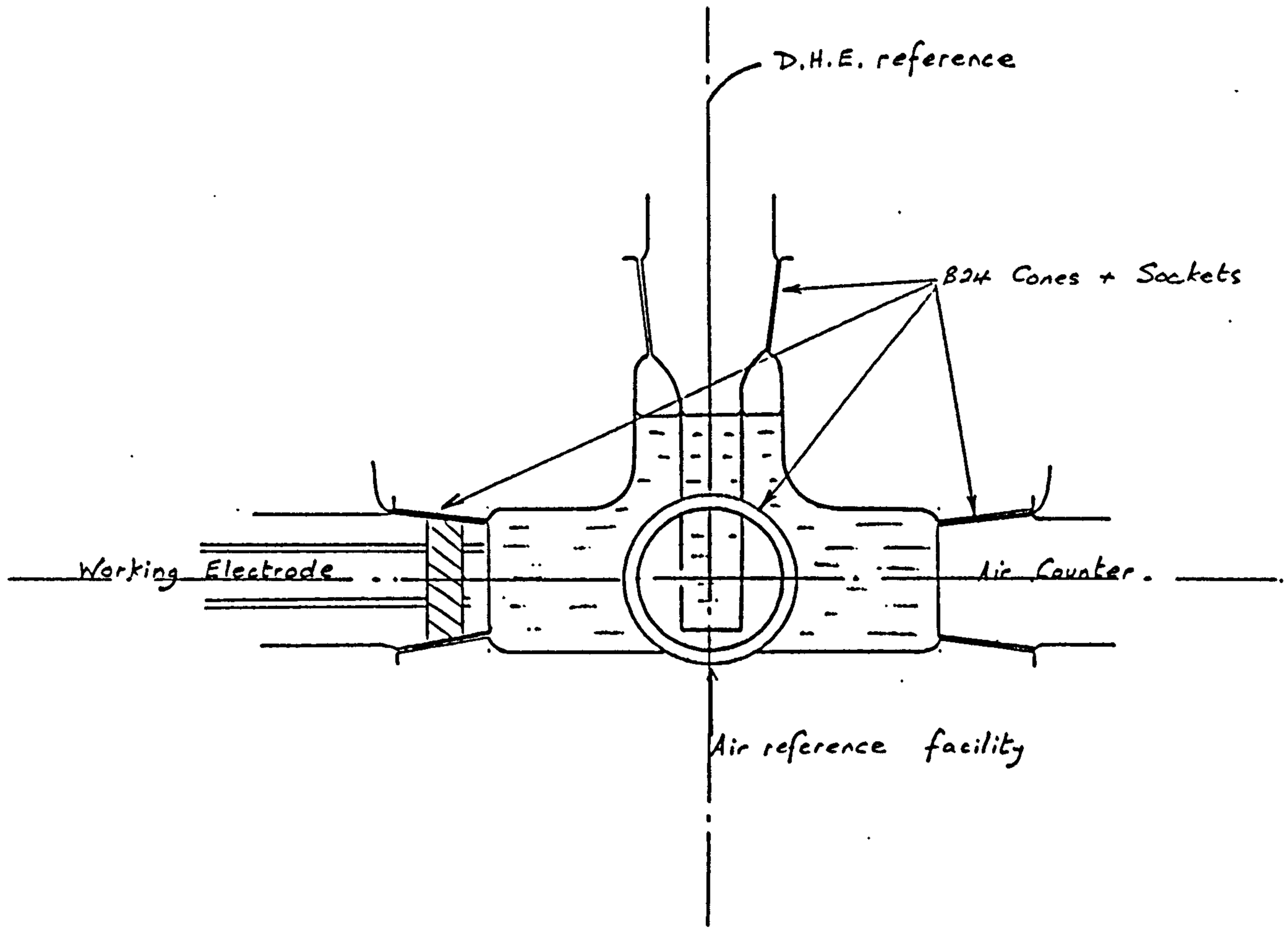

Figure 3.1. Open electrode test cell diagram.

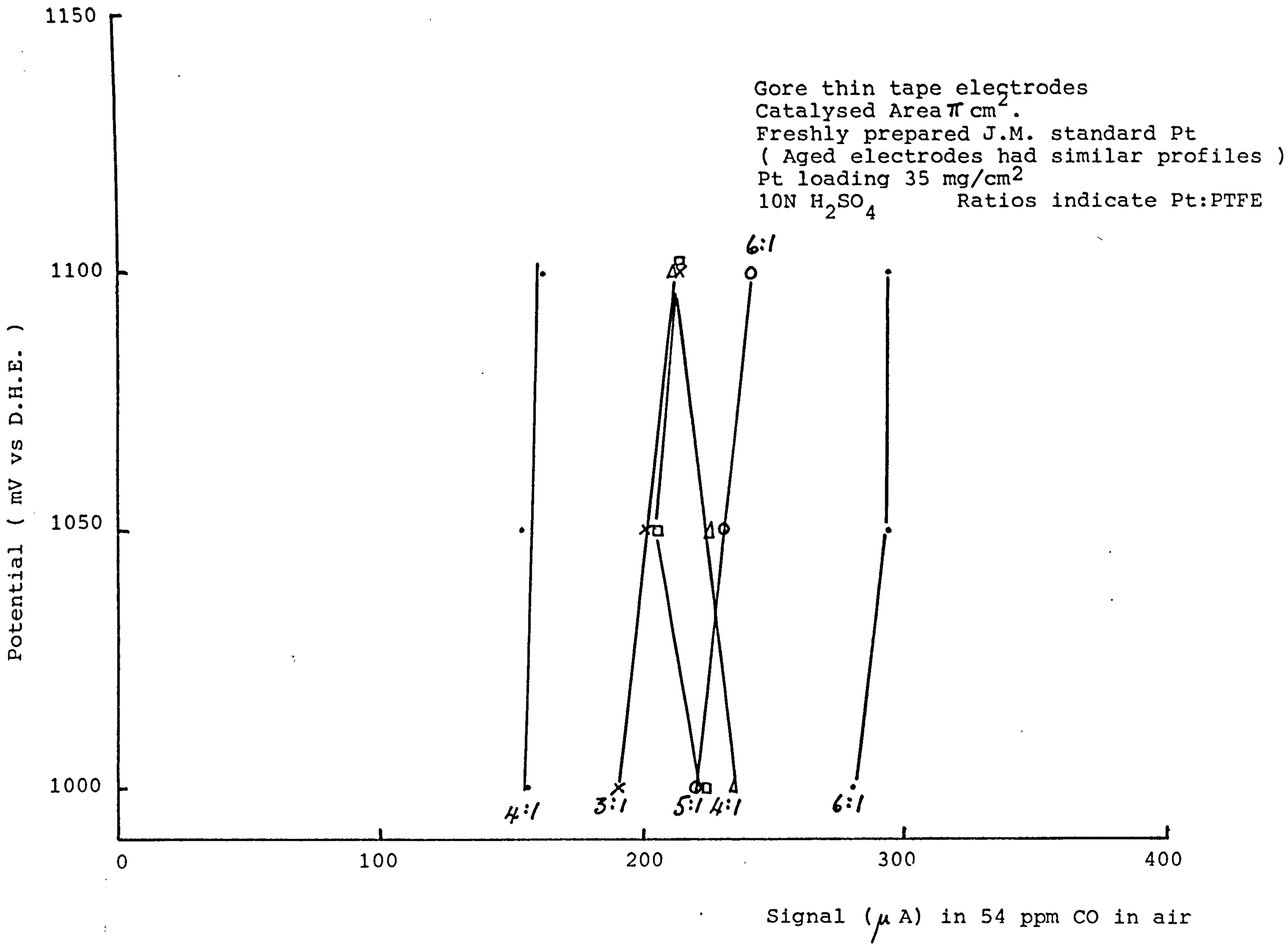

Figure 3.2. Effect of potential on signal of various electrodes.

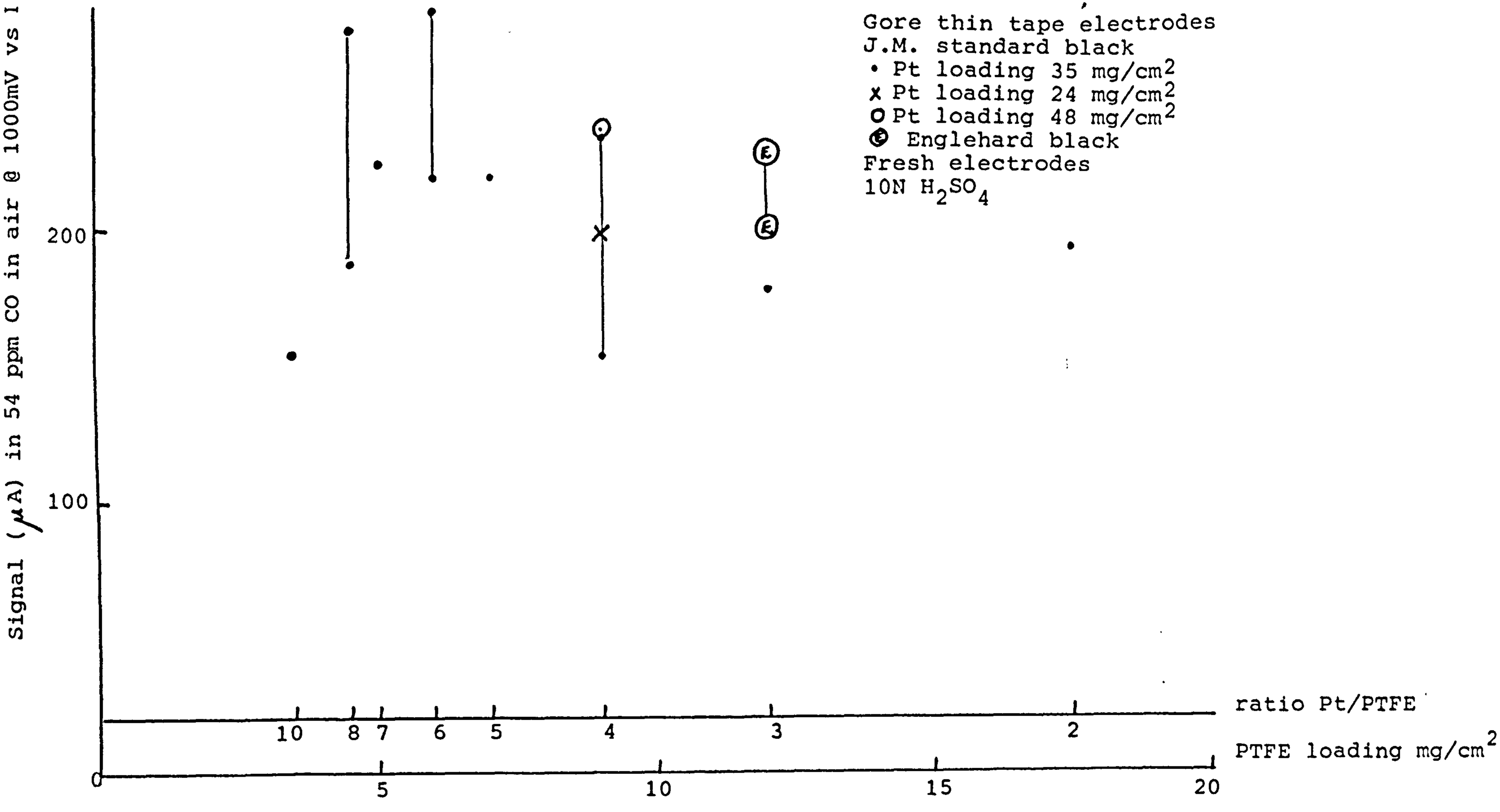

Figure 3.3. Effect of Pt:PTFE ratio on electrode activity.

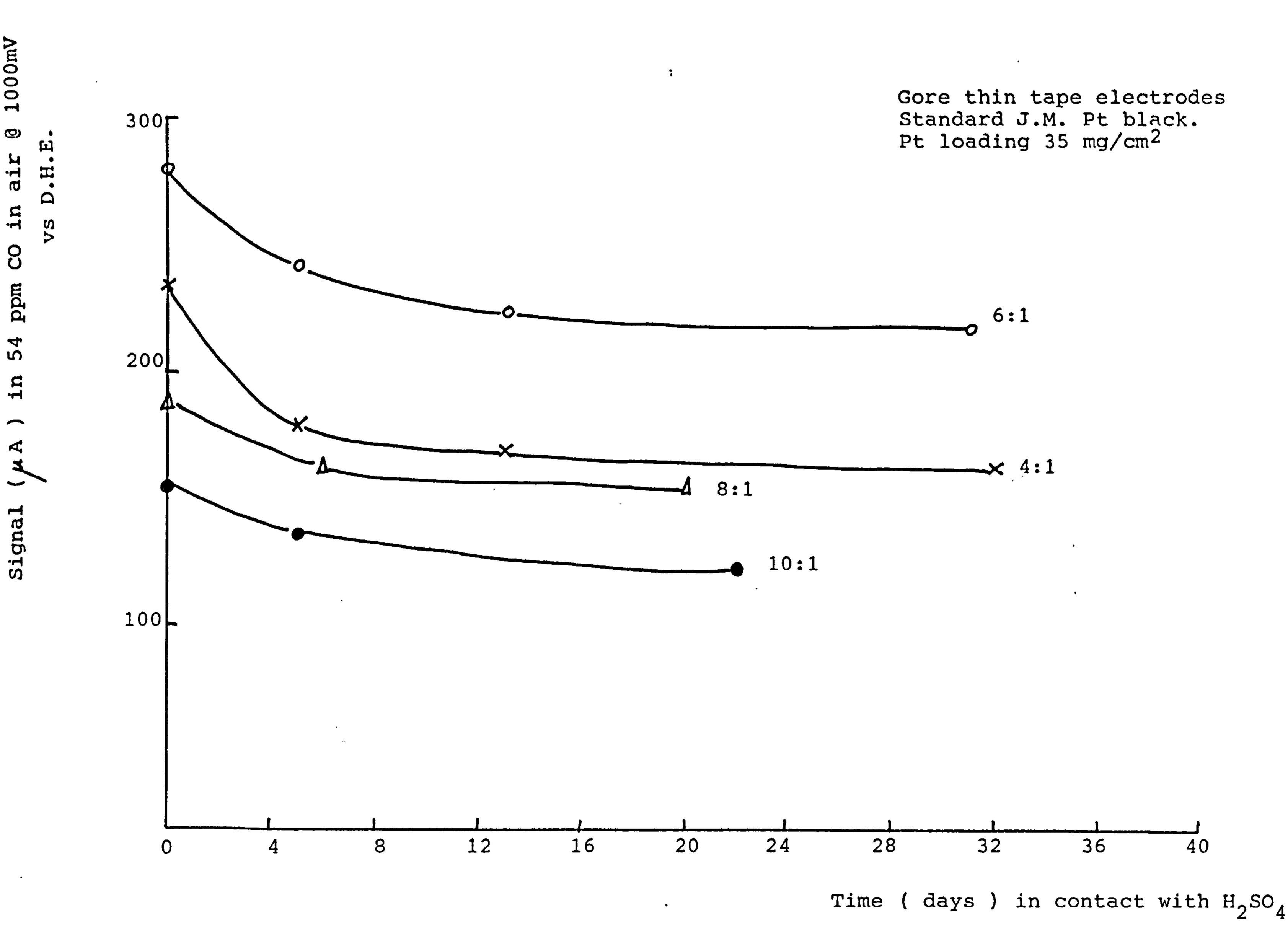

Figure 3.4. Ageing of platinum electrodes.

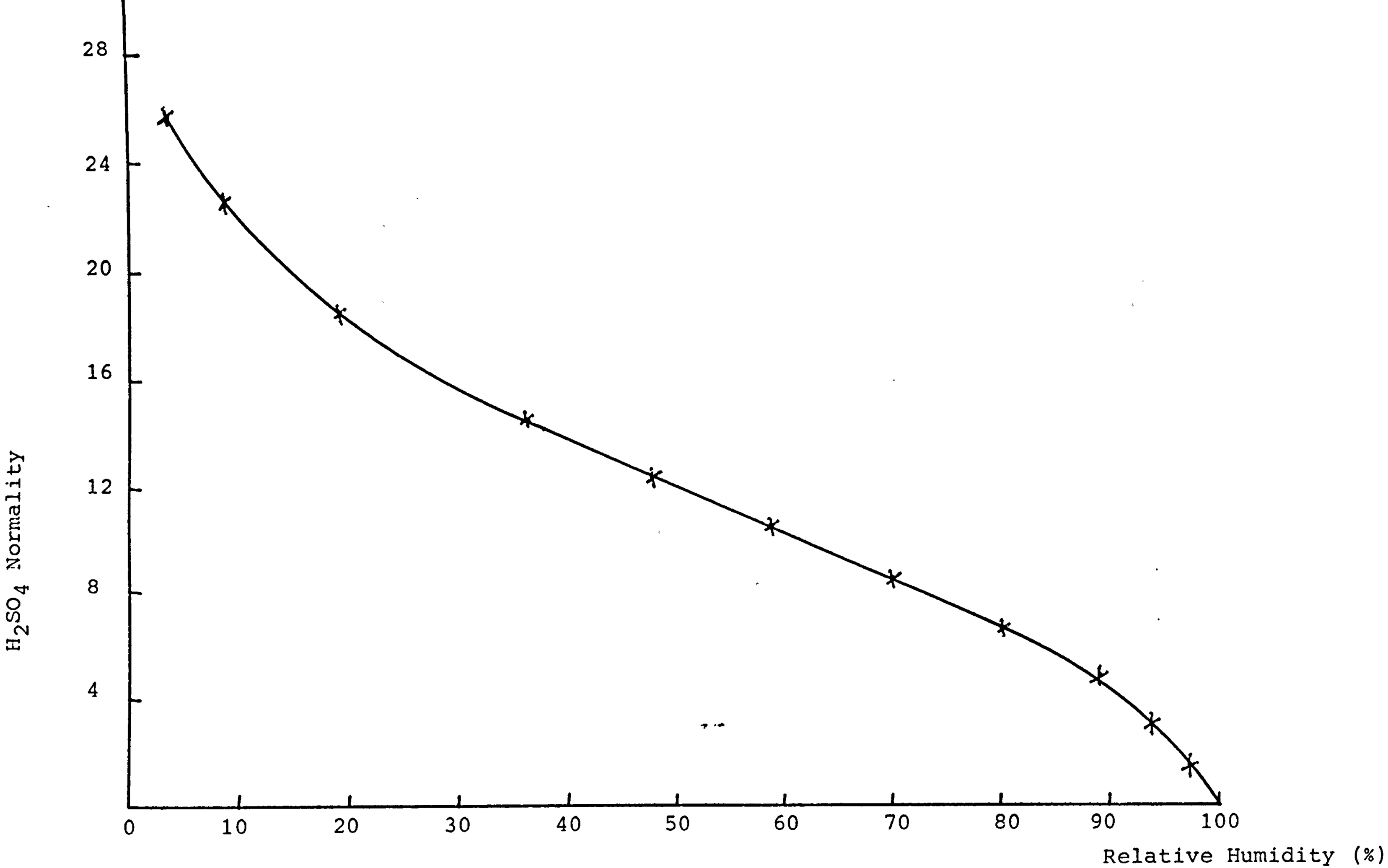

Figure 4.1. Relationship between relative humidity and concentration of aqueous sulphuric acid mixtures.

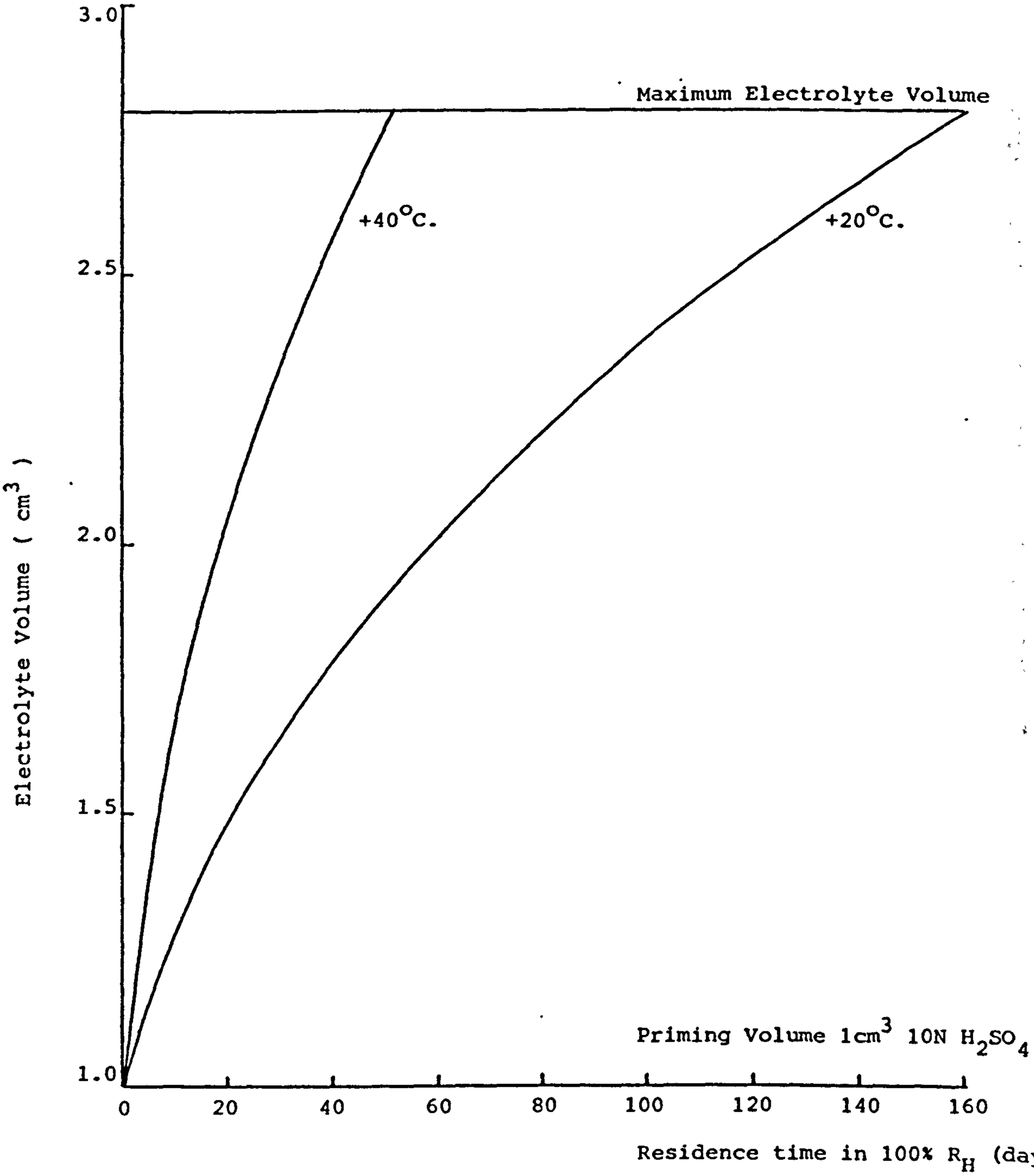

Figure 4.2. Water uptake with time in 100% R...

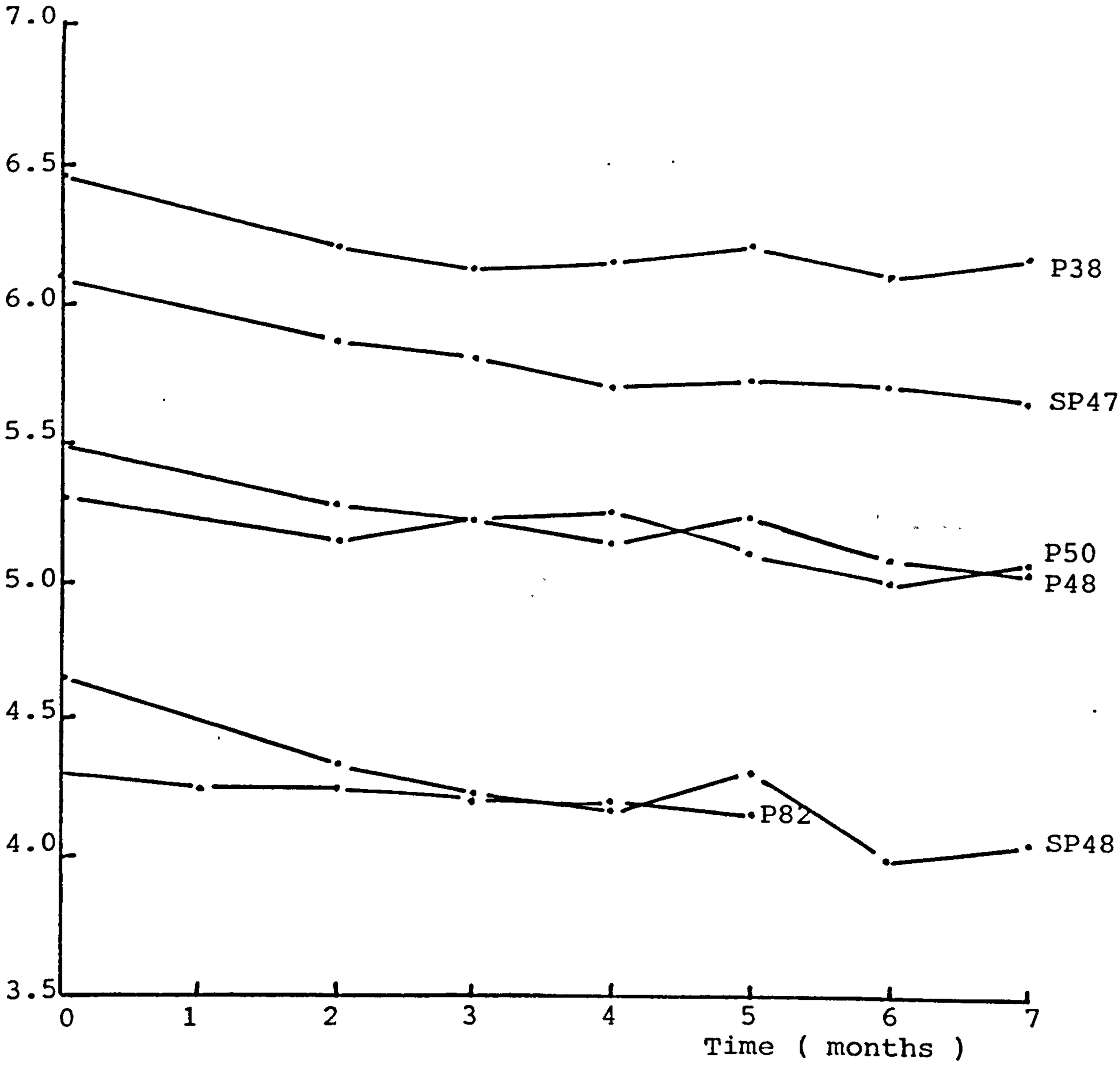

Figure 5.1. Monthly signal record for Mark 1 sensors.

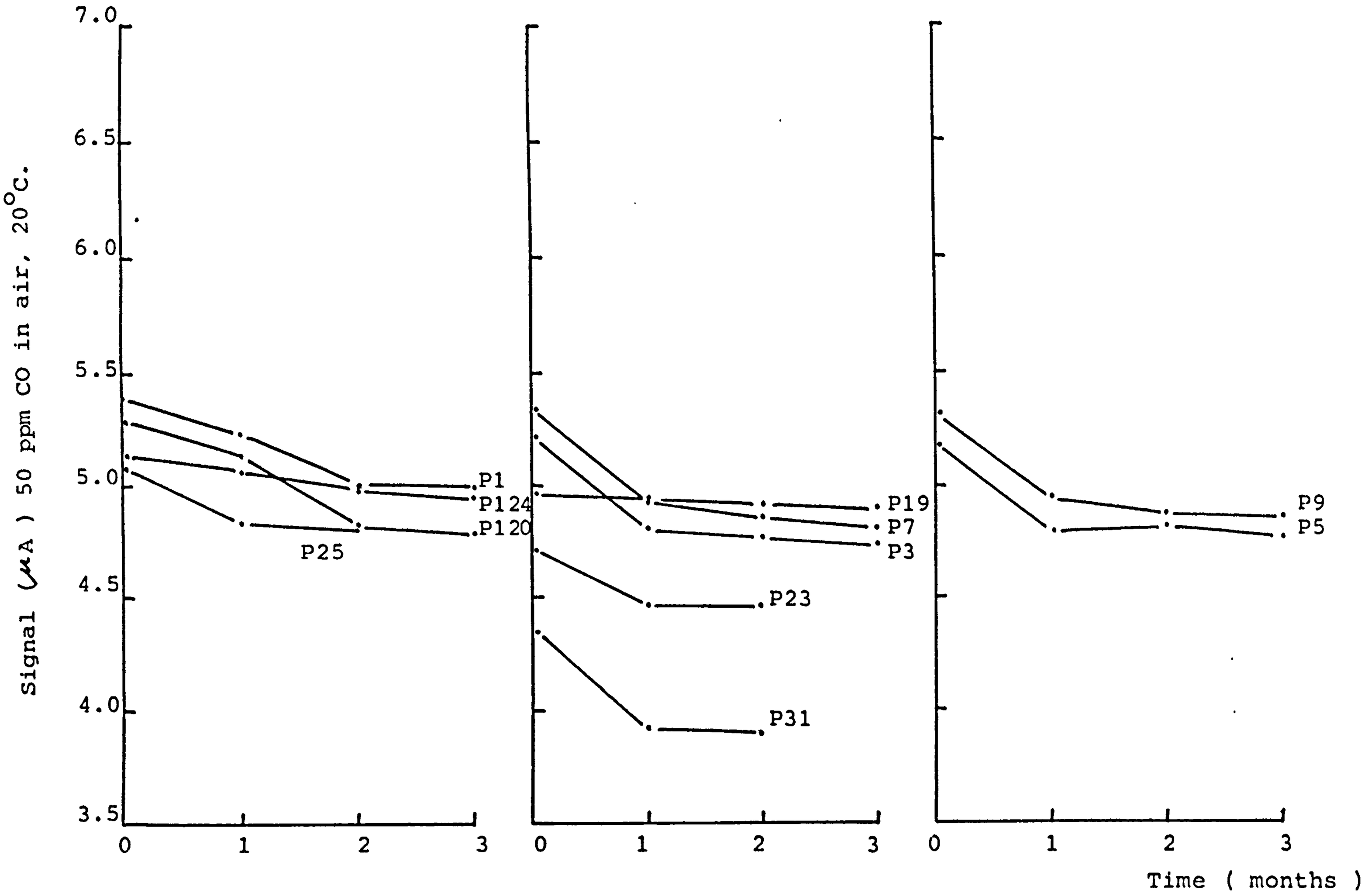

Figure 5.2. Monthly record of Mark 3 sensors.

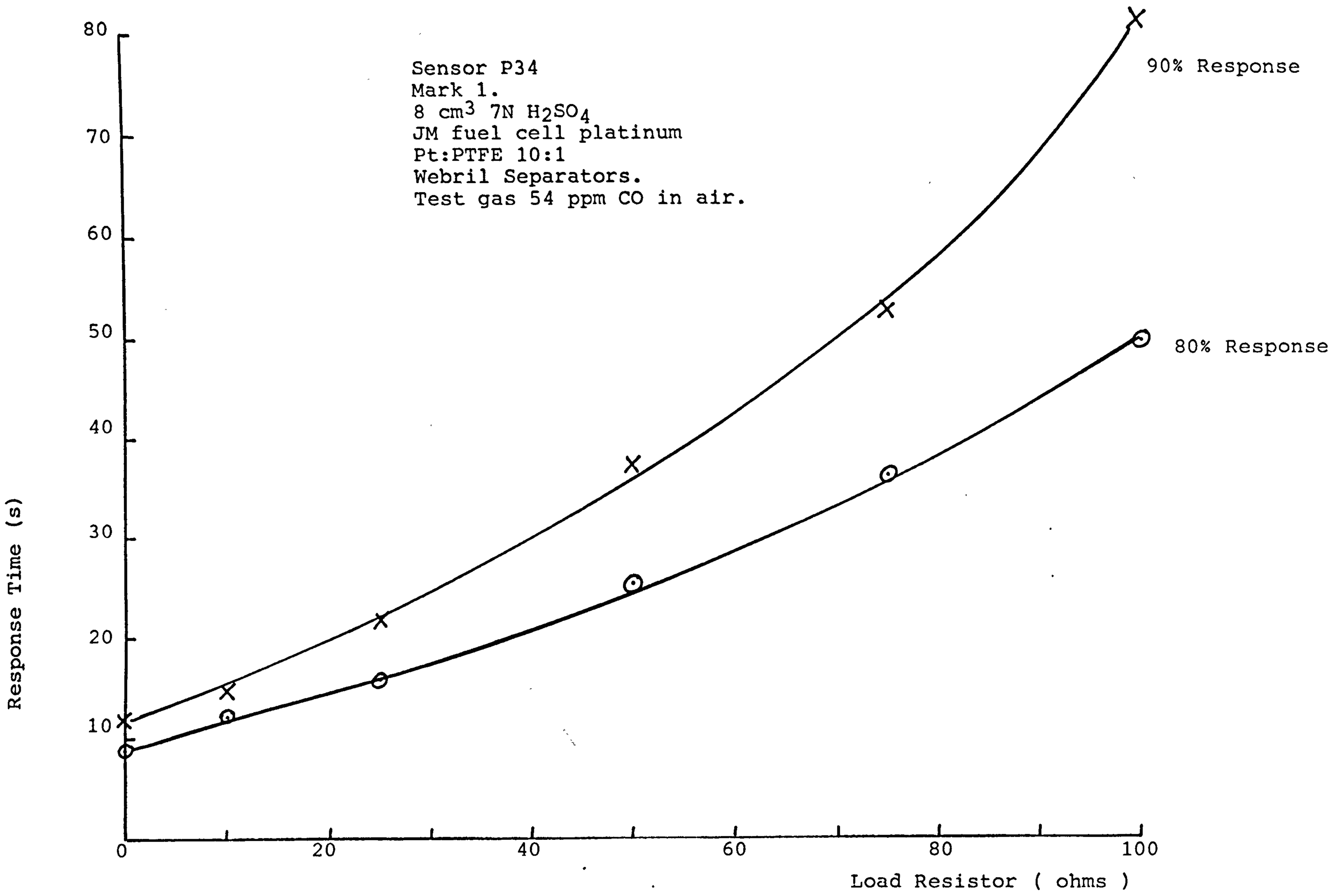

Figure 5.3. Response time/load resistor characteristics for sensor P 34.

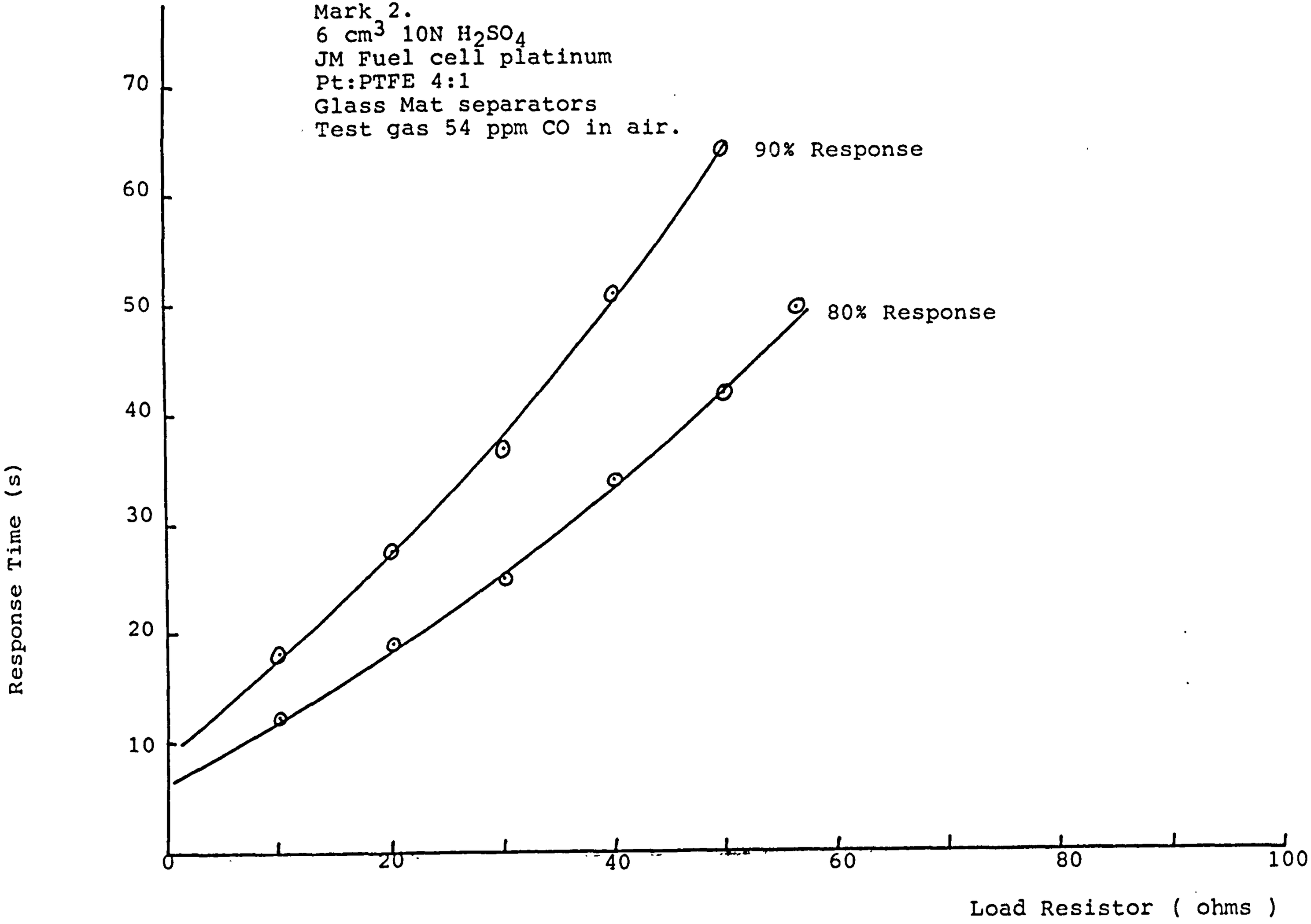

Figure 5.4. Response time/load resistor characteristics for sensor P106.

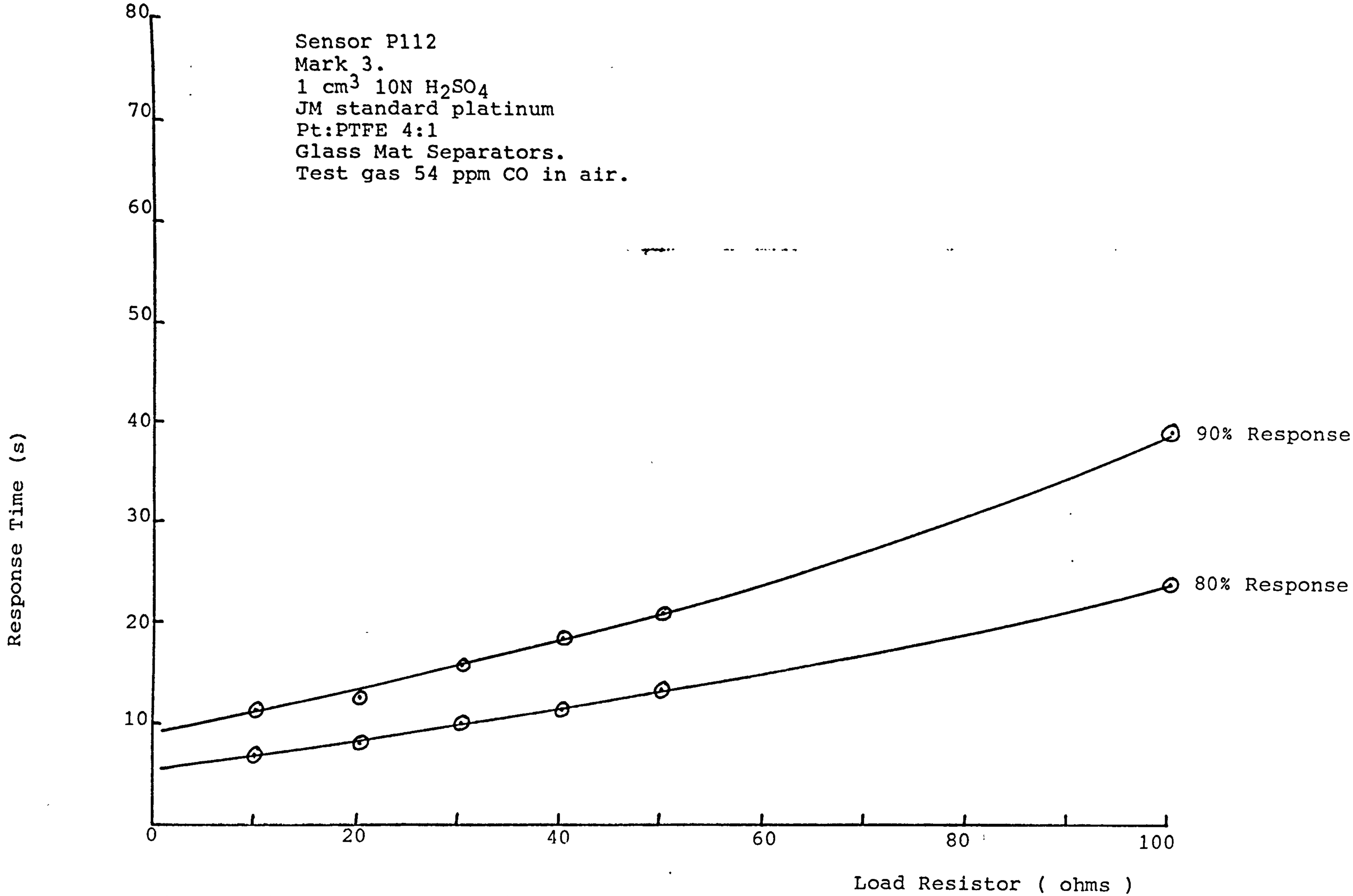

Figure 5.5. Response time/load resistor characteristics for sensor P106.

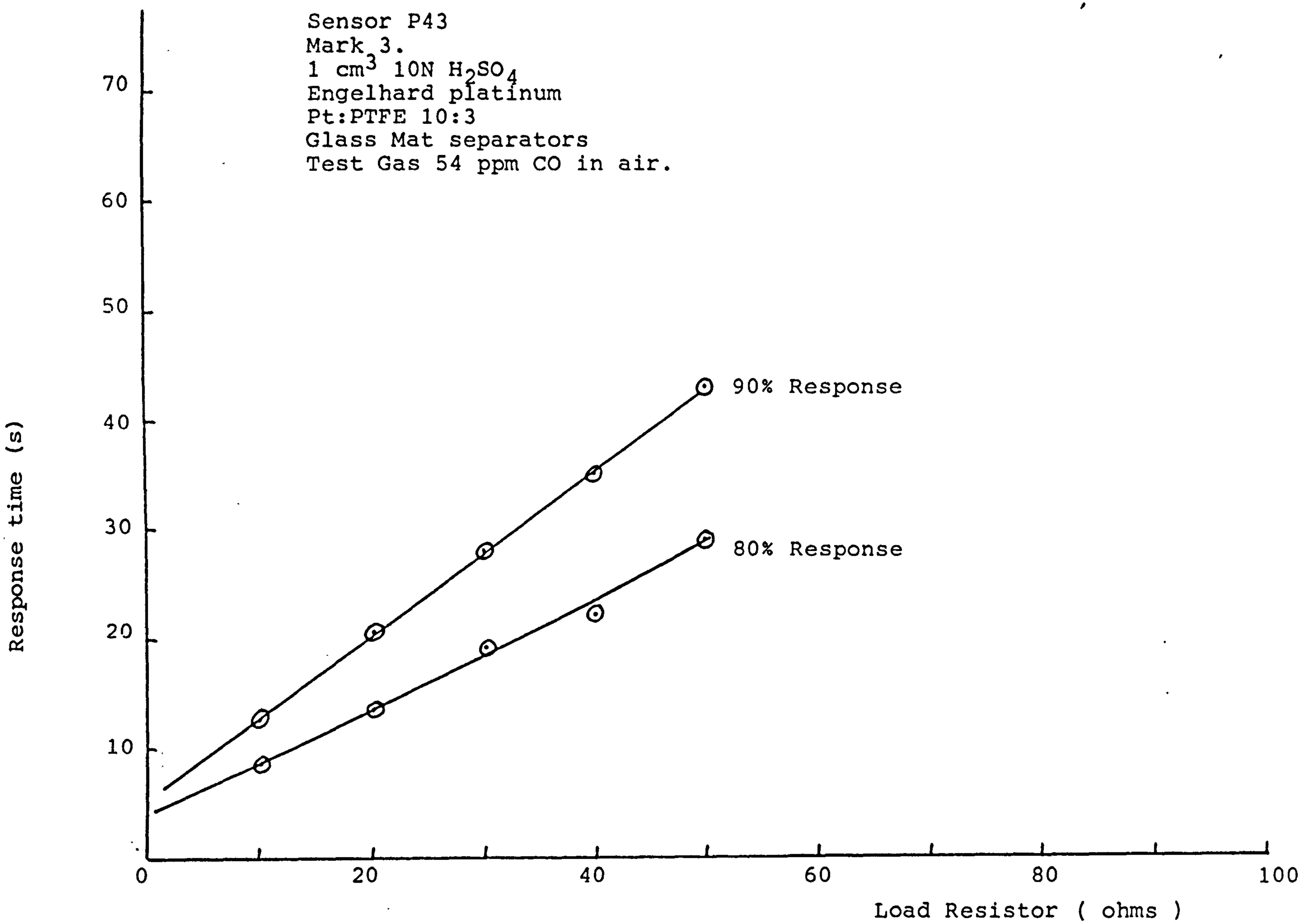

Figure 5.6. Response time/load resistor characteristics for sensor P 43.

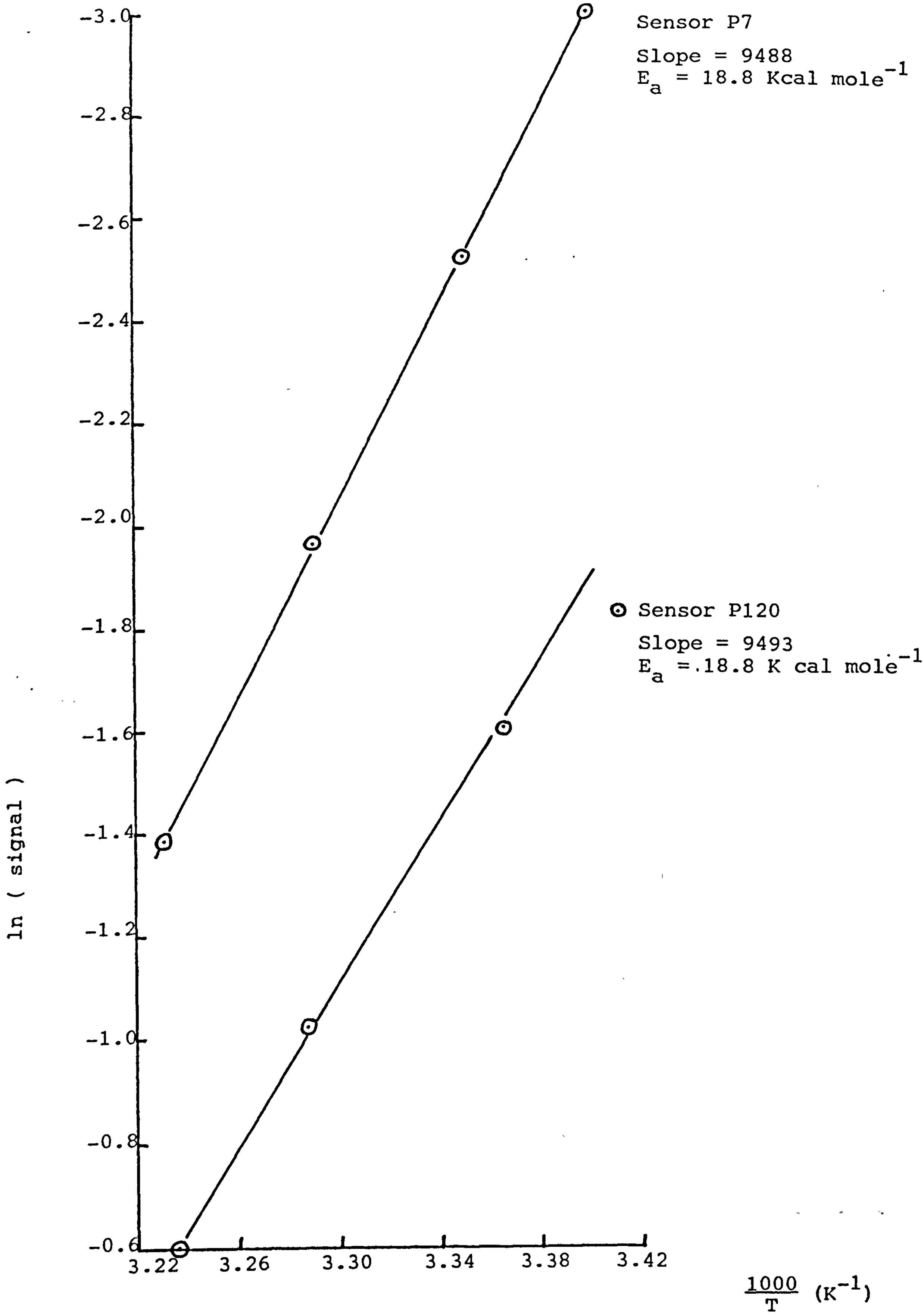

Figure 5.7. Arrhenius plots of sensor baseline currents.

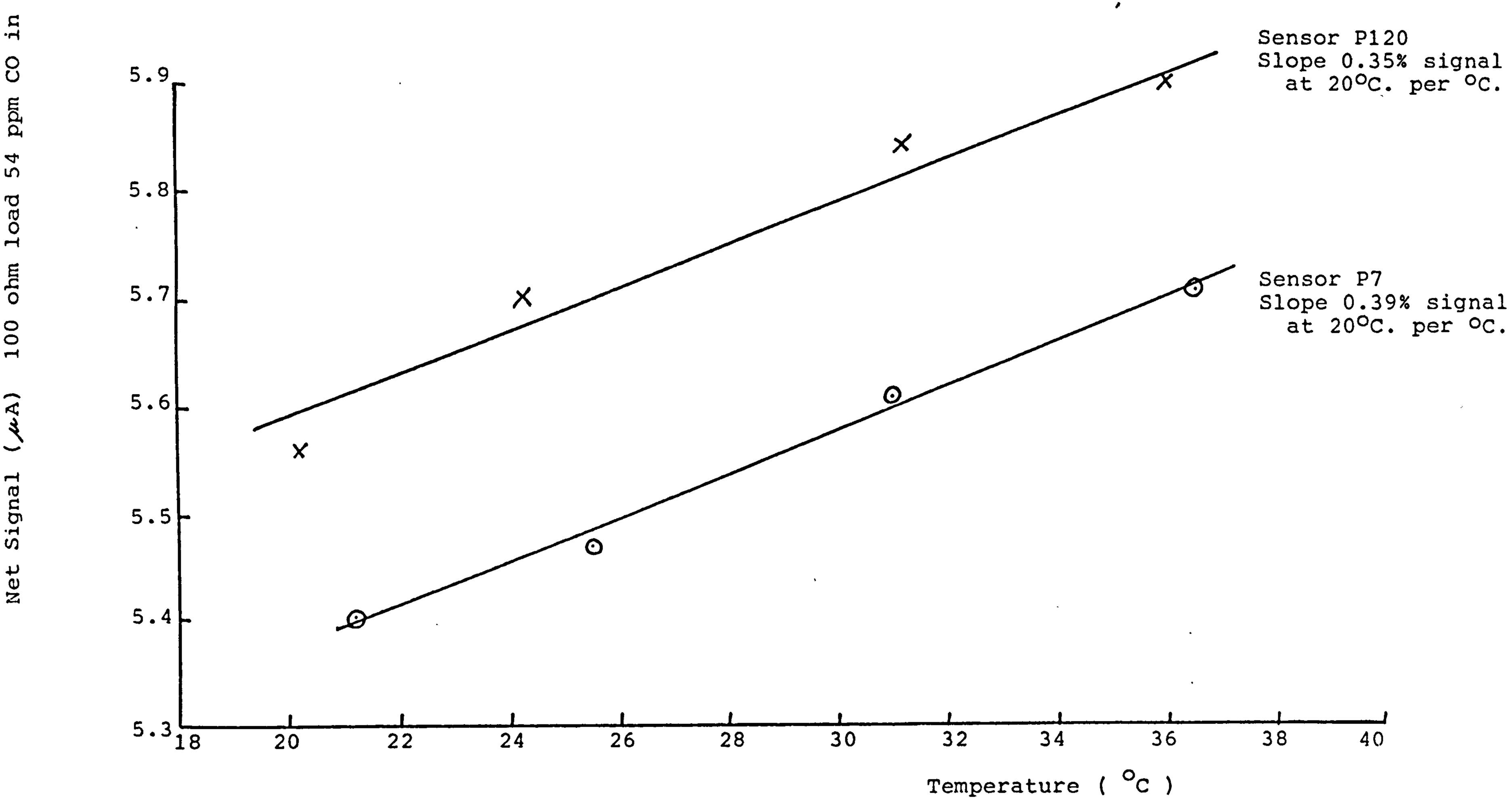

Figure 5.8. Signal temperature dependance of sensors P7 and P120.

Table 5.1.a. Monthly signal records of Mark 1 sensors.

Sensor	Electrodes	Electrolyte Volume and Additives	Component Pretreatment	Sensor Response to 50 ppm CO in air 20°C. Time (months)								% signal drops			
				0	1	2	3	4	5	6	7	0-2	2-3	> 3	Total
SP48	JM Fuel Cell Pt Pt:PTFE 10:1	7 c.c.	None	4.66		4.33	4.23	4.18	4.33	4.00	4.06	7.1	23.	1.0	12.9
SP47	JM Fuel Cell Pt Pt:PTFE 5:1	7 c.c.		6.10		5.86	5.81	5.71	5.74	5.71	5.66	3.9	0.9	0.7	7.2
P38	JM Fuel Cell Pt Pt:PTFE 10:3	7 c.c.		6.46		6.22	6.14	6.16	6.22	6.12	6.18	3.7	1.3	-0.2	4.3
P48	JM Fuel Cell Pt Pt:PTFE 10:3	7 c.c.		5.50		5.28	5.23	5.14	5.23	5.09	5.04	4.0	1.0	0.9	8.4
P50	JM Fuel Cell Pt Pt:PTFE 10:3	7 c.c.		5.33		5.15	5.24	5.25	5.11	5.02	5.07	3.4	-1.8	0.8	4.9
P82	JM Fuel Cell Pt Pt:PTFE 10:3	7 c.c.		4.32	4.25	4.25	4.21	4.21	4.17			1.6	0.9	0.5	3.5

Table 5.1.b. Monthly signal records of Mark 3 sensors.

Sensor	Electrodes	Electrolyte Volume and Additives	Component Pretreatment	Sensor Response to 50 ppm CO in air 20°C. Time (months)								% signal drops			
				0	1	2	3	4	5	6	7	0-2	2-3	>3	Total
P120	JM Std. Pt Pt:PTFE 4:1	5 c.c.	None	5.29	5.14	4.82	4.78					8.9	0.8		9.6
P124	"	5 c.c.		5.13	5.07	4.98	4.94					2.9	0.8		3.7
P1	"	3 c.c.		5.39	5.23	5.00	4.99					7.2	0.2		7.4
P3	"	1 c.c. with 1mM CrO_3		5.22	4.80	4.77	4.73					8.6	0.8		9.4
P5	"	1 c.c. with 5 mM CrO_3		5.18	4.80	4.82	4.76					7.0	1.3		8.1
P7	"	1 c.c. with 20 mM CrO_3		5.33	4.93	4.86	4.80					8.8	1.3		9.9
P9	"	1 c.c. with 10 mM $KMnO_4$		5.31	4.94	4.87	4.85					8.3	0.4		8.7
P19	"	1 c.c. with 10mM $KMnO_4$	30h. at 50°C in 10-20% HNO_3	4.96	4.94	4.91	4.90					1.0	0.2		1.2
P23	"	1 c.c.	"	4.71	4.47	4.47									5.1
P25	"	1 c.c.	"	5.09	4.83	4.82									5.3
P31	"	1 c.c. with 20mM CrO_3	"	4.36	3.92	3.89									10.8

Table 5.2. Response Time data for various sensor types.

Cell Load (ohms)	P34 Response Time (s)		P106 Response Time (s)		P112 Response Time (s)		P43 Response Time (s)	
	80%	90%	80%	90%	80%	90%	80%	90%
0*	8.8	12.0						
10	10.9	14.9	12.3	18.0	6.8	11.3	8.5	12.5
20			19.0	27.5	8.0	12.5	13.5	20.5
25	15.7	21.8						
30			25.0	37.0	10.0	15.8	19.0	28.0
40			34.0	51.0	11.4	18.5	22.0	35.0
50	25.2	37.2	42.0	64.0	13.4	21.0	29.0	43.0
75	36.2	52.6						
100	49.6	80.6			23.6	38.6		
	Mark 1 JM fuel cell Pt Pt:PTFE 4:1 6cm^3 10N H_2SO_4 Glass Mat Separators		Mark 2 JM Std. Pt Pt:PTFE 4:1 1cm^3 10N H_2SO_4 Glass Mat Separators		Mark 3 Engelhard Pt Pt:PTFE 10:3 1cm^3 10N H_2SO_4 Glass Mat Separators		Mark 3 JM fuel cell Pt Pt:PTFE 10:1 8cm^3 7N H_2SO_4 Webril Separators	

* Zero ohm load results obtained by potentiostatic operation.

Table 5.4. Effect on baseline stabilisation times of various component pretreatments and electrolyte additives.

Pretreatment	Electrolyte	Time to stabilise to <0.1 μA baseline.
None	10N H_2SO_4	>2 months
None	10N H_2SO_4 with 20mM CrO_3	1 to 2 months
24 hour immersion in 10% HNO_3 at ambient temp.	10N H_2SO_4	1 to 2 months
24 hour immersion in 10% HNO_3 at ambient temp.	10N H_2SO_4 with 20 mM CrO_3	1 week
24 hour immersion in 10% HNO_3 at ambient temp.	10N H_2SO_4 with 10 mM $KMnO_4$	2 weeks
30 hour immersion in 10% HNO_3 at +50°C.	10N H_2SO_4	< 1 week
15 hour immersion in 10N H_2SO_4 at +40°C.	10N H_2SO_4	< 1 week

Table 5.5. Response of sensors to CO in nitrogen relative to CO in air.

Sensor Type	Electrocatalyst	Electrolyte	% loss in signal in aerobic conditions
Mark 1	JM fuel cell platinum	7N H_2SO_4	30 - 40
Mark 1	JM fuel cell platinum	10N H_2SO_4	15 - 20
Mark 2	JM fuel cell platinum	7N H_2SO_4	20 - 30
Mark 2	JM fuel cell platinum	10N H_2SO_4	3
Mark 3	JM standard platinum	10N H_2SO_4	3 - 7
Mark 3 hot 10% HNO_3 pickle	JM standard platinum	10N H_2SO_4	8 - 18

APPENDIX 1.

DIFFUSIBILITY MEASUREMENTS

The arrangement shown in figure A1.1. was used to compare the oxygen diffusion currents of various electrode materials. Oxygen from the ambient air diffused through the test sample across the 6mm dia. hole, and was electrochemically reduced at the Gould cathode, potentiostatted at zero volts with respect to the lead reference electrode The steady state current between the Gould cathode and lead anode counter electrode was then taken as a measure of the test sample diffusibility.

The data presented in Table A1.1. should be divided by 2 to convert to equivalent carbon monoxide values, since oxygen produces 4 electrons per mole reacted, compared to only 2 electrons per mole for carbon monoxide.

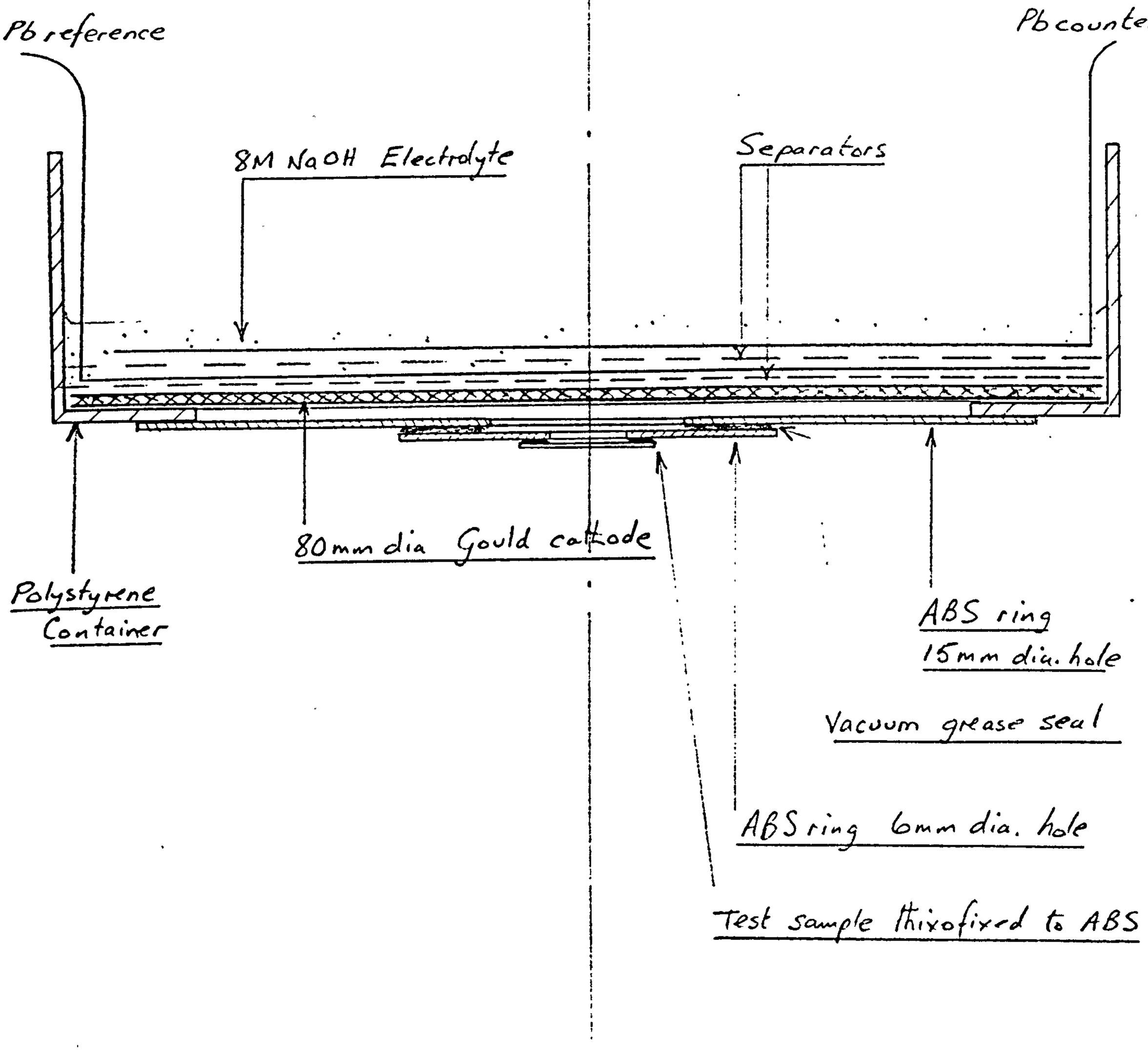

Figure A.1.1. Electrochemical Diffusibility Test Rig.

Table A1.1. Measured oxygen reduction currents in the electrochemical diffusibility rig.

Membrane Sample	Oxygen Reduction current in air (mA/cm^2)	Oxygen Current, (μA/ppm on $\pi^* cm^2$)
Open 6mm diameter hole.	> 2500	> 37.4
Standard Gore Tape	550	8.23
Standard Gore Tape pressed to normal transfer pressures	373	5.58
CTL Oxygen Sensor electrode with Silver catalyst	280	4.19
Used CTL CO anode	360	5.39
Gore fine PTFE tape	> 1000	> 15

* πcm^2 is the area of the catalysed electrode surface in all CTL CO sensors.

APPENDIX 2

SPECIAL SENSOR TESTS

A2.1. Objectives.

A series of steady state current-voltage measurements were conducted with a specially designed sensor to obtain the following information:

(a) To determine the oxygen limiting diffusion current of the sensor configuration for water balance calculations (section 4.3.).

(b) To compare the oxygen fluxes to the counter electrode across the electrolyte sandwich and through the edge seals.

(c) To measure the counter electrode polarisation under likely current loads.

A2.2. Experimental.

The cell comprised Mark 1 sensing and counter plates with an ABS plastic reservoir. A spirally wound assembly, consisting of two lead foil electrodes, isolated from each other by a separator, was located in the reservoir. Electrical connections to these electrodes were made with lead tabs sealed into the reservoir wall, to enable the sensor to be operated in any position without electrolyte leaking out. One lead foil was used as a counter electrode , the other as a lead/lead sulphate reference. The latter took up a steady potential of -313 mV (cathodic) on the D.H.E. scale, within 1 hour or so immersion in the 10N H_2SO_4 electrolyte.

The counter and sensing electrodes were catalysed with J.M. fuel cell grade platinum black in a 4:1, Pt/PTFE mix. Either platinum electrode could be operated as an oxygen reducing cathode, using a potentiostatic circuit and the lead counter and reference electrodes. With this arrangement no gases were generated internally which could have caused damage to the sensor.

Steady state current-voltage curves were recorded by altering the potentiostatic potential in increments and allowing 10-20 minutes to settle before taking a current reading. Measurements were made from the air rest potential,

in a cathodic direction to 400 mV on the lead scale (about 80 mV above hydrogen evolution potentials).

The following sets of measurements were taken:

(a) Sensing electrode current-voltage curve with the capillaries open to ambient air and the sensor inverted. If a well defined oxygen limiting diffusion current could be obtained from this plot, at potentials above hydrogen evolution, then this could be used for water balance equations in section 4.3. The currents were expected to be high - the theoretical capillary current for oxygen in ambient air is about 200 mA (section 2.4.)- and therefore, the sensor was operated inverted to ensure an optimum, low resistance electrolyte pathway between the sensing and lead counter electrodes.

(b) The steady state oxygen current was recorded at 0.400 volts versus lead, with the capillaries blocked off with sellotape to obtain a measure of oxygen access to the sensing electrode via the seal.

(c) The sensor platinum counter electrode current-voltage curve was recorded in both the inverted and upright positions and with the capillaries blocked and open. Comparison of these curves provided a measure of the relative gas access currents through the seals and across the electrode sandwich.

(d) The sensor platinum electrodes were connected via an external load resistor and the platinum counter potential measured against the lead reference, as a function of sensor current, when exposed to gas containing 500 ppm CO in air. In this way the counter electrode polarisation could be measured under likely sensor running conditions. The sensing electrode polarisation can be obtained by including the iR-drop across the load resistor, in addition to the counter electrode polarisation.

A2.3. Results.

A2.3.1. Steady state polarisation of sensing electrode.

The measured curve with open capillaries is shown in figure A2.1. No well defined limiting current was observed which could be reliably used for the water balance calculations. The curve shape was indicative of a high degree of ohmic polarisation which probably originated from the electrode current collection and/or the electrolyte restriction connecting the sandwich and reservoir compartments. To sustain a limiting current of 200 mA was probably asking too much of such a configuration;

When the capillaries were blocked off with the sensing electrode at 0.4 volts on the lead scale, the current fell to a steady 3.4 mA within about 3 minutes. This was a true limiting current, being virtually independant of potential for several hundreds of mV up to about 1 volt on the lead scale. Thus, taking the calculated value of 200 mA as the capillary current, the ratio of gas access to the sensing electrode via the capillaries, to that via the seal was about 60:1.

A2.3.2. Steady state polarisation of counter electrode.

Figure A2.2. shows the air polarisation curve obtained for the sensor platinum counter electrode. This exhibited a limiting current of between 0.68 to 0.87 mA, in the potential region 0.4 to 1 volt on the lead scale, (0.08 to 0.68 volts on the D.H.E. scale). The reduction in limiting current with increasing cathodic polarisation and hysteresis on the return voltage sweep, may have been caused by electrolyte concentration effects arising from the restriction through the wicking hole, linking the platinum and lead electrode compartments.

The polarisation curve was unaffected by the position of the sensor (upright or inverted) or whether the capillaries were open or blocked. Thus, virtually all the sensor counter gas access is via the seals, rather

than across the electrolyte sandwich. The ratio of gas access to the sensing electrode via the capillaries, to the counter electrode gas access is an important design parameter (section 2.2.) and is about 300:1 in this particular configuration. Access of gas through the seals to the sensing electrode was apparently about 4 to 5 times easier than to the counter electrode. This probably indicates that gas access to the counter electrode is confined to diffusion along the length of the counter electrode tape, whereas at the sensing electrode, the gas can leave the tape once it has passed the sealing area and spread over the back of the electrode in the gas compartment beneath the capillary holes.

A2.3.3. Operating potentials of sensor electrodes.

The measured rest potential of the sensor counter electrode in ambient air was 1.23 volts on the lead scale (0.917 volts on the D.HE. scale). When exposed to a 500 ppm CO in air test gas, the sensor current was 50μA across a 1KΩ load resistor. The counter electrode potential fell to 1.210 volts (0.897 volts vs D.H.E.) which would put the sensing electrode at 1.16 volts (0.847 volts vs D.H.E.).

Electrode polarisation of this degree could considerably promote parasitic local cell consumption of carbon monoxide[1], resulting in a depression of signals. It is intended to extend measurements of this sort in the next phase of development with a view to improving the general level and stability of signals by reducing the system polarisation.

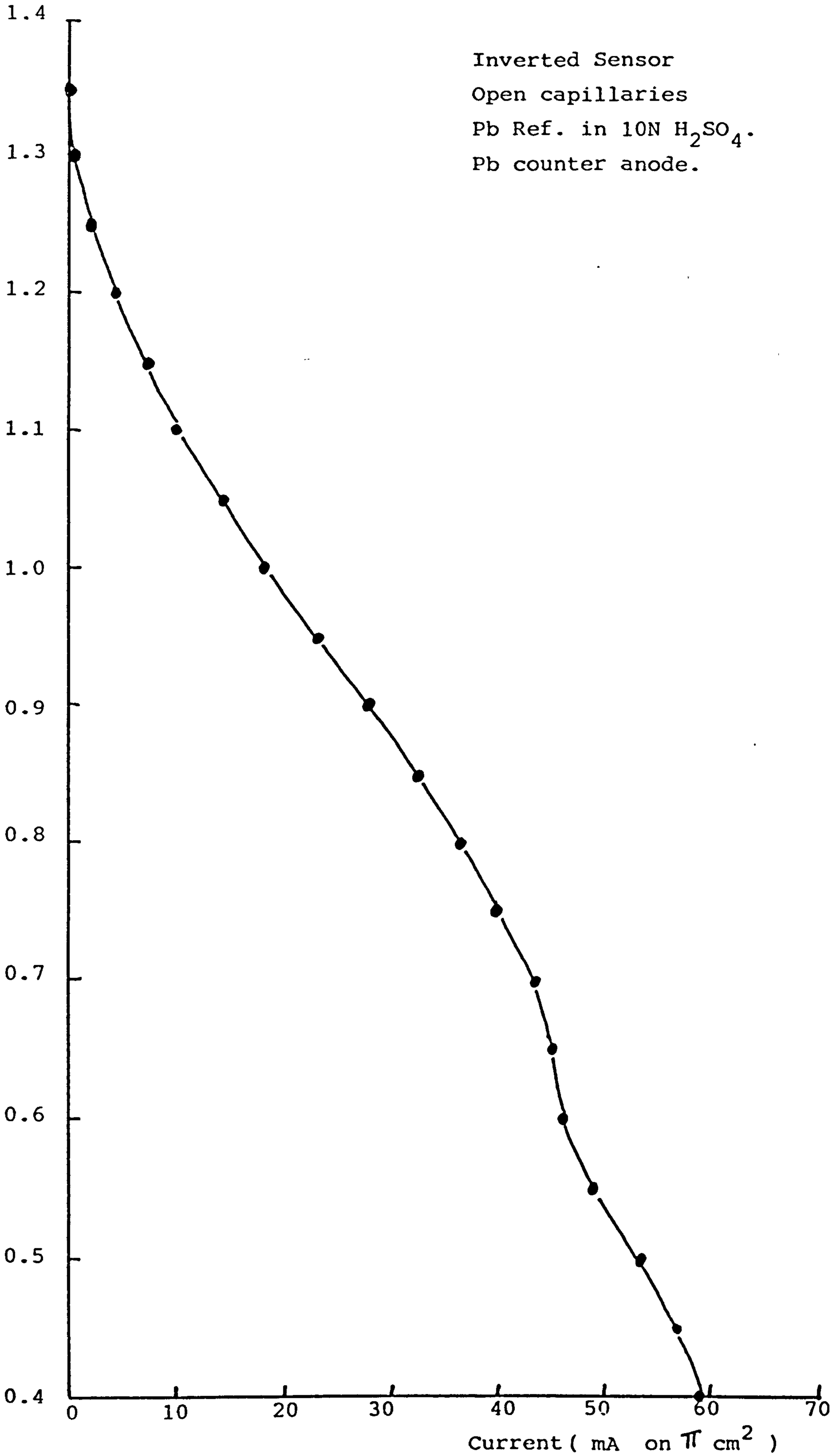

Figure A2.1. Steady state air polarisation curve of sensing electrode

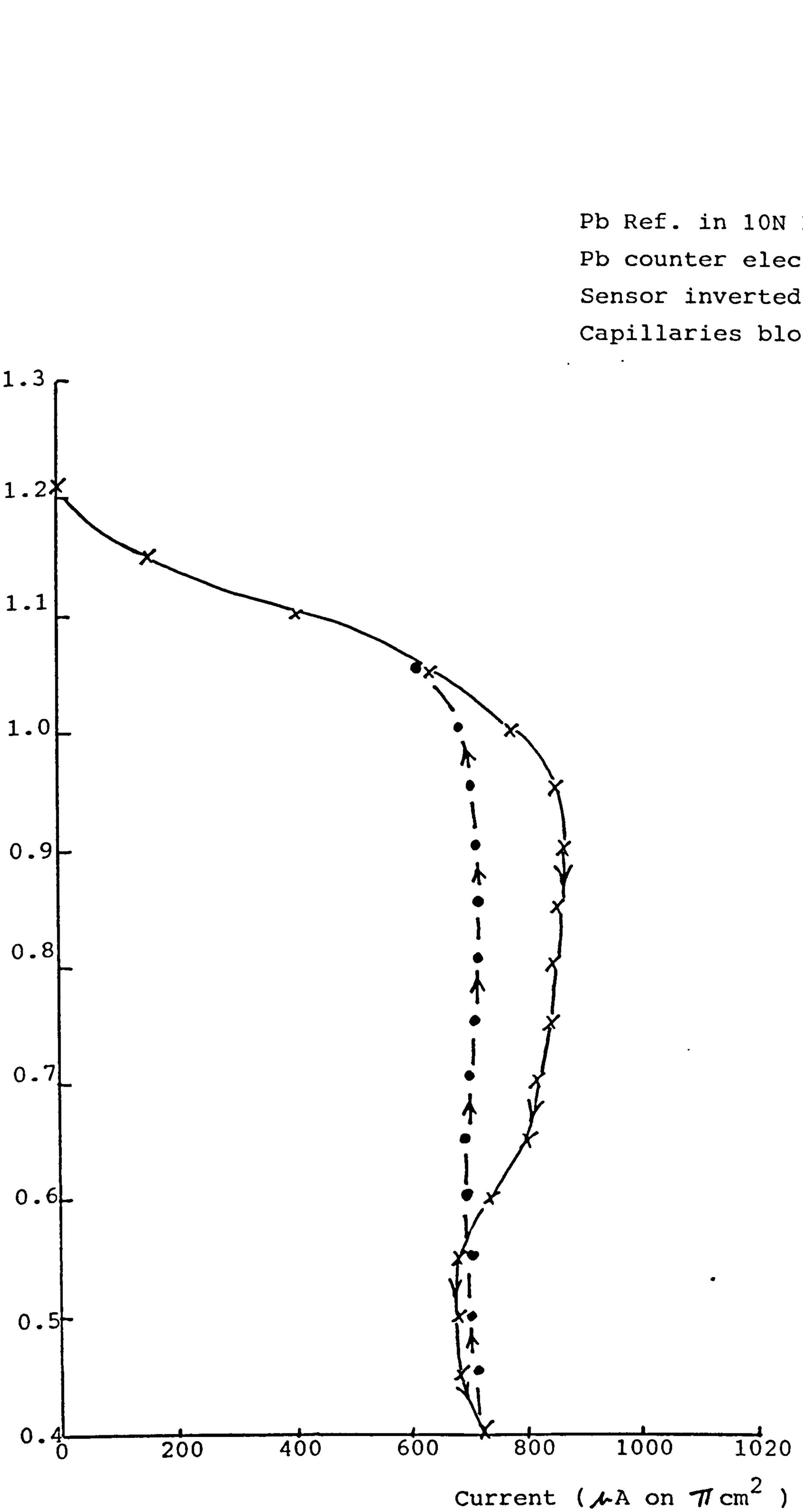

Figure A2.2. Steady state air polaristion curve of counter electrode.

APPENDIX 3.

DIFFUSION COEFFICIENTS

In this report, and the last[1], interconversion of oxygen and carbon monoxide diffusion currents was made on the basis that the diffusion coefficients are the same. This assumption was checked from first priciples as follows:

The diffusion coefficient is given by the equation:

$$D_{ab} = \frac{2.628.10^{-19} \sqrt{T^3 \; 0.5 \left(\frac{1}{M_a} + \frac{1}{M_b}\right)}}{P \; \sigma_{ab}^{\,2} \; \Omega_2}$$

where D_{ab} is the mass diffusibility ($cm^2 \; s^{-1}$).
(diffusion coefficient).

T is the absolute temperature (K)

M_a and M_b are the molecular weights of components 'a' and 'b' respectively.

P is the total pressure (atm)

σ_{ab}, Ω_2 are Lennard-Jones constants.

The latter are obtained as follows:

$$\sigma_{ab} = \tfrac{1}{2} (\sigma_a + \sigma_b)$$

where σ_a and σ_b are the collision diameters of each species (ref.7., Appendix 6), table A3.1.

The collision integral, Ω_2 is obtained from the relationship between Ω_2 and the Lennard-Jones constant, $\frac{"kT"}{\epsilon_{ab}}$ (Table A3.1.) where $\epsilon_{ab/k}$, the 'potential parameter' is given by

$$\frac{\epsilon_{ab}}{k} = \sqrt{\frac{\epsilon_a}{k} + \frac{\epsilon_b}{k}}$$

Values of 'potential parameters' for each gas species are given in Table A3.1.

For carbon monoxide in air at 25°C., 1 atm. pressure,

$M_{CO} = 28.00$ $M_{air} = 28.84$

$\sigma_{CO/air} = 3.6035.10^{-8}$ $\Omega_2 = 0.96$

Hence $D = 0.203\ cm^2s^{-1}$

For oxygen in air, under the same conditions of pressure and temperature,

$M_{O_2} = 32$

$\sigma_{O_2/air} = 3.579.10^{-8}$ $\Omega_2 = 0.93$

and $D = 0.206\ cm^2s^{-1}$

which agrees well with quoted measured values.

Table A3.1. Constants for the Lennard-Jones(6-12) Potential.

(Hirschfelder, Curtiss, and Bird, *Molecular Theory of Gases and Liquids*, John Wiley and Sons, New York, 1954).

Force Constants Evaluated from Viscosity Data

Gas	ϵ/k, °K	σ, 10^{-8} cm	Gas	ϵ/k, °K	σ, 10^{-8} cm
Air	97	3.617	$CHCl_3$	327	5.430
Ar	124	3.418	CO	110	3.590
Br_2	520	4.268	CO_2	190	3.996
CCl_4	327	5.881	CS_2	488	4.438
CH_4	137	3.882	D_2	39.3	2.948
C_2H_2	185	4.221	F_2	112	3.653
C_2H_4	205	4.232	H_2	38	2.915
C_2H_6	230	4.418	HCl	360	3.305
C_3H_8	254	5.061	HI	324	4.123
n-C_4H_{10}	410	4.997	He	10.22	2.576
i-C_4H_{10}	313	5.341	Hg	851	2.898
n-C_5H_{12}	345	5.769	I_2	550	4.982
n-C_6H_{14}	413	5.909	Kr	190	3.61
n-C_8H_{18}	320	7.451	N_2	79.8	3.749
n-C_9H_{20}	240	8.448	NO	91.0	3.599
Cyclohexane	324	6.093	N_2O	237	3.816
C_6H_6	440	5.270	Ne	27.5	2.858
CH_3OH	507	3.585	O_2	88.0	3.541
C_2H_5OH	391	4.455	SO_2	252	4.290
CH_3Cl	855	3.375	$SnCl_4$	1550	4.540
CH_2Cl_2	406	4.759			

* Estimation of the Lennard-Jones constants for gases not given in this table may be made from the following relationships (2):

$$\epsilon/k = 0.77T_c$$

and $$\sigma = 0.841(V_c)^{1/3} = 2.44\left(\frac{T_c}{P_c}\right)^{1/3}$$

or $$\epsilon/k = 1.15T_b$$

and $$\sigma = 1.17(V_b)^{1/3}$$

where T_c = critical temperature, °K
V_c = molar volume at critical temperature, cu cm/gm mole
P_c = critical pressure, atm
T_b = normal boiling point, °K
V_b = molar volume at the boiling point (Appendix D-7)

COLLISION INTEGRALS, Ω_1, Ω_2.

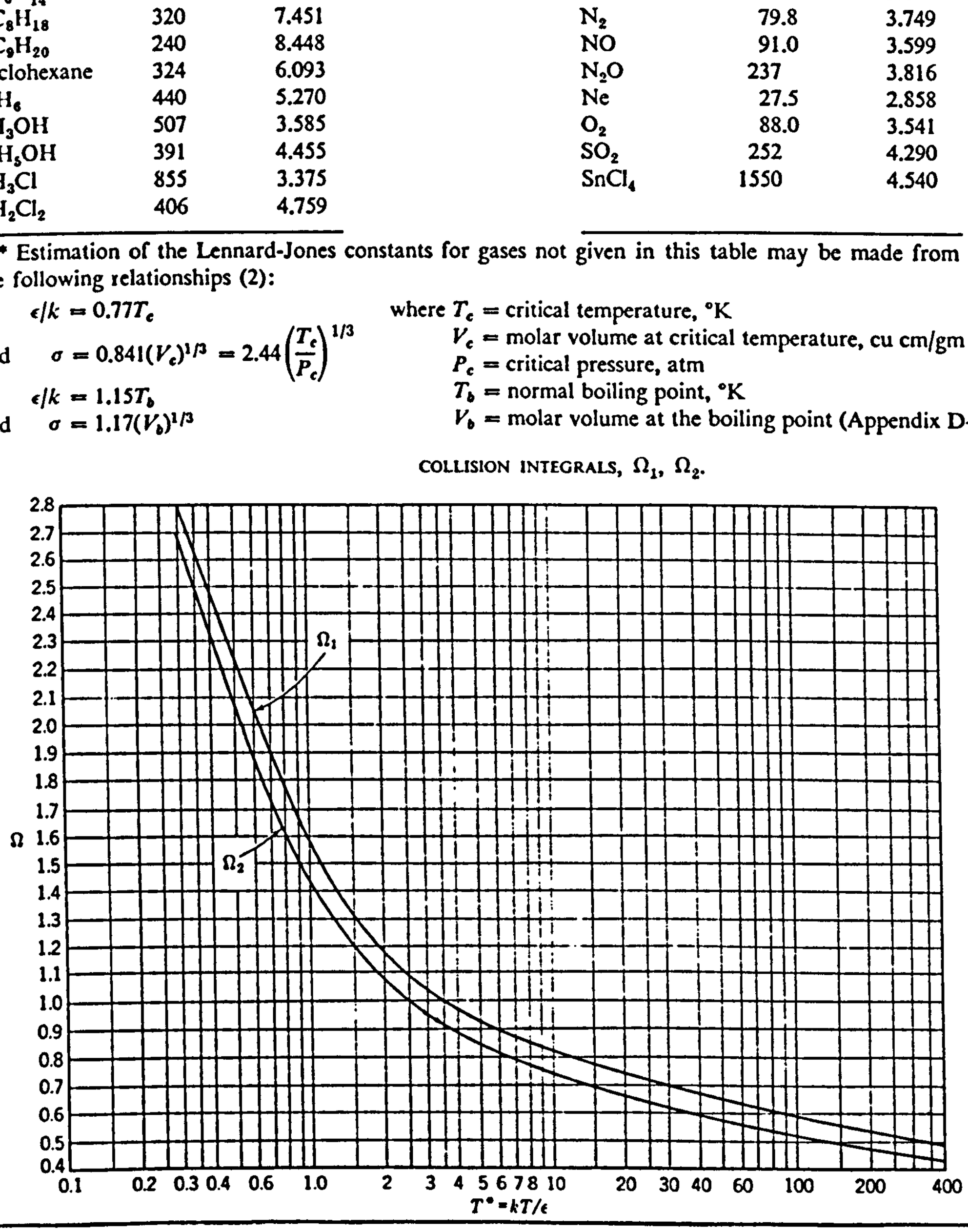

CTL Report No. 81/31/006
July 1980

CITY TECHNOLOGY LIMITED

The City University
17/19 Sebastian Street,
Northampton Square,
London EC1V OHB

12. CARBON MONOXIDE SENSOR FOR USE IN COAL MINES. PHASE 3

Final Report

A.D.S. Tantram

R. Chan-Henry

B.S. Hobbs

Mr. L.R. Cooper
National Coal Board,
Mining R & D Establishment,
Stanhope Bretby.
Staffs.

NCB Contract No. Y 135007/09/21

CTL Project No. 94.95.31

top-plate, behind the sensing electrode, to improve gas distribution to this electrode, and span temperature compensation, using silicone rubber capillary inserts in the top-plate. A commitment has also been made to a new injection moulded hardware design and components should be available for assessment in the second half of the next phase.

Water balance studies have continued during this phase, and the theoretical relationships derived for water transfer rates in the last report, have been substantiated by practical tests. The effects of electrolyte charge on sensor behaviour and the minimum electrolyte volume requirements have also been established during this period.

About 200 sensors have been produced during this phase of which 50 have been passed to NCB for their own testing. Long term monitoring of sensors has continued on 50 sensors from earlier phases of the work and will progress into phase 4. These life tests are providing useful data on endurance aspects of sensor operation and the longest running sensors have so far exceeded 20 months operational life.

The development is now at a stage where sensors, with a performance sufficient to do a very useful job, can be readily supplied for field trial instruments. We consider that it is most important that such field trials are progressed as rapidly as possible. The various sensor options still open do not differ markedly in performance, and we feel that the ultimate choice of the precise trade-offs can only sensibly be made in the light of field experience.

CONTENTS

1. INTRODUCTION

At the end of the second phase of this programme the mark 3 version of the two electrode sensor, with nominally identical anodes and cathodes, was showing a lot of promise. (3)

However, in the early stages of the third phase, which is the subject of this report, an hysteresis problem was identified. This showed up when much longer (e.g. 30 minutes) exposure tests were carried out, particularly at higher carbon monoxide levels (e.g. 100 to 200 ppm). The problem was initially identified by the Bretby and Yorkshire laboratories and confirmed by ourselves. This negative hysteresis behaviour is illustrated below.

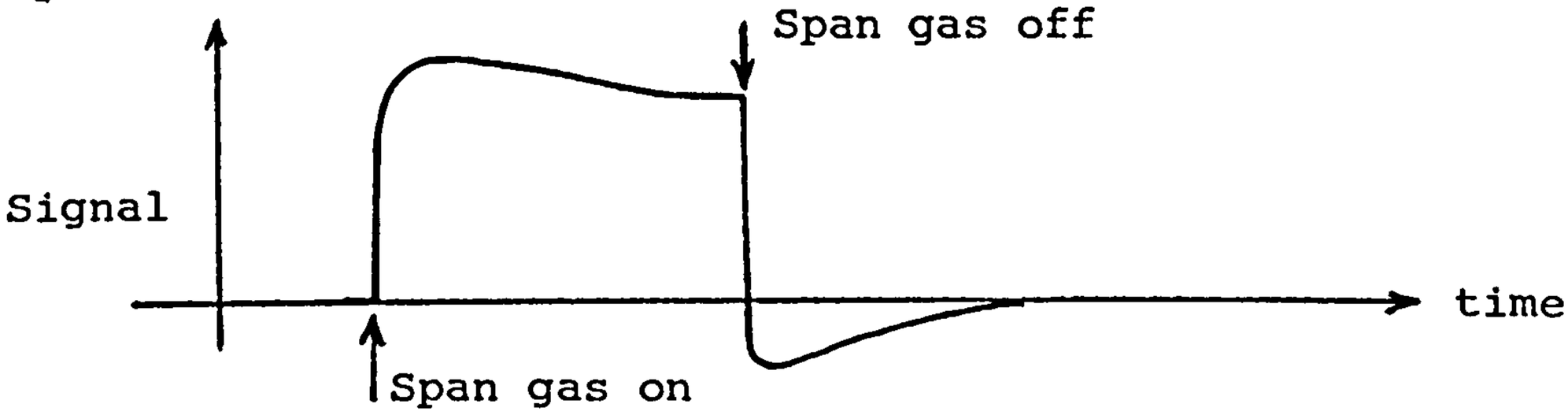

The extent of the hysteresis was dependant on concentration and exposure time and did not show up with short time exposures at the lower concentration levels. It was thought that the level of hysteresis shown by the mark 3 sensor was unacceptable and that a more desirable target would be freedom from significant hysteresis with exposures of 20 minutes at 200 ppm.

An important part of the phase 3 work was therefore to establish the fundamental causes of hysteresis and to try to find a solution. As will be seen, the explanation is concerned with the electrochemistry of "oxide" coverage of the platinum surface as it relates to the working of two-electrode sensors. The work resulted in a much wider and

/Contd.

more detailed understanding which shows that we are inevitably dealing with subtle trade-offs and a fine electrode balancing act. This understanding is important since it helps to define the fundamental limitations of the system and gives guide-lines as to the best compromises within these limitations.

For these reasons this subject will be dealt with in the first section of this report. As will be seen, the Mark numbers have been used to designate the various anode-cathode combinations that have been used to modify the hysteresis behaviour.

Concurrently with this investigation,and independantly of Mark number,there has been a general programme of hardware design improvements and developments. Two specific items concern,(1) the diffusion geometry and,(2) the introduction of temperature compensation,using the differential expansion method with silicone rubber capillary inserts. The theory concerned with these two items is dealt with in the appendices.

During this phase of the work a total of about 200 sensors have been made of which 50 have been passed to N.C.B. for their own tests. We have also had about 50 sensors dating from the earlier phases of the work, which we have continued to monitor periodically. These provide some useful pointers to longer term endurance, the longest running sensor now being 20 months old.

2. PLATINUM/PLATINUM OXIDE ELECTRODE REACTIONS

This section reviews our present understanding of some of the important basic processes that affect sensor behaviour. After initially recalling some fundamentals of two electrode sensor operation, the explanation of hysteresis behaviour is considered in more detail.

(a) The anode determines the current.

(b) The cathode determines the potential.

(c) With the currents we are using (low μA) and relatively low load resistor values (e.g. 100 ohms), the anode potential will always follow, and be very close to, the cathode potential. They will in fact differ by ir, the potential difference across the load resistor, which is unlikely to exceed about 1mV.

(d) We are working under diffusion-limiting conditions. The CO oxidation current, i_{co}, will be dependant on the CO concentration and capillary geometry. At a given concentration and capillary geometry, i_{co} will be a constant. However, the signal (externally measured current) will only equal i_{co} when the anode is at or above its air rest potential. If the potential falls below this, oxygen reduction can occur, producing a cathodic current, i_{O_2}(a), which in part will offset the anodic i_{co}. This local cell action effect, which we have referred to as "scavenging", was described in detail in the previous reports.(1)(3).

The current-voltage curve for a given concentration of CO in air will be of the form illustrated below:

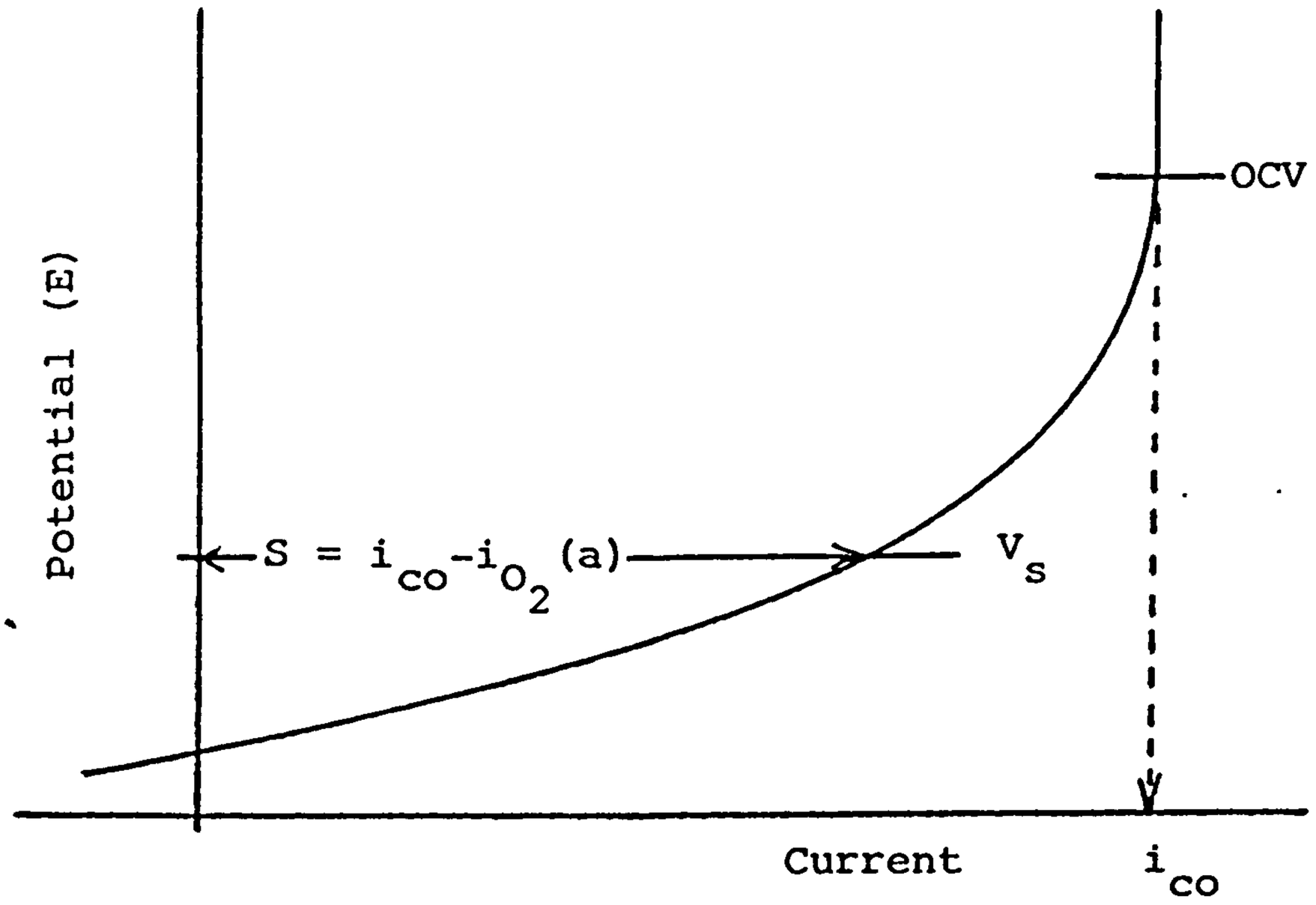

The air rest potential (OCV) will be at the bottom of the vertical limiting current region. If the cathode holds the potential at or above this point then the signal is given by:

$$S = i_{co}$$

If the cathode potential is lower, e.g. at V_s, then:

$$S = i_{co} - i_{O_2}(a)$$

We now have to consider the complications that arise from the time dependance of the electrode polarisation, which is to do with the electrochemistry of platinum and in particular, surface "oxide" films.

At about 850 mV versus the dynamic hydrogen electrode (DHE), platinum starts to react electrochemically with water, laying down a monolayer of "oxide". The equilibrium coverage increases with potential, reaching complete coverage at about 1300mV.

The situation at 20°C. is illustrated below:

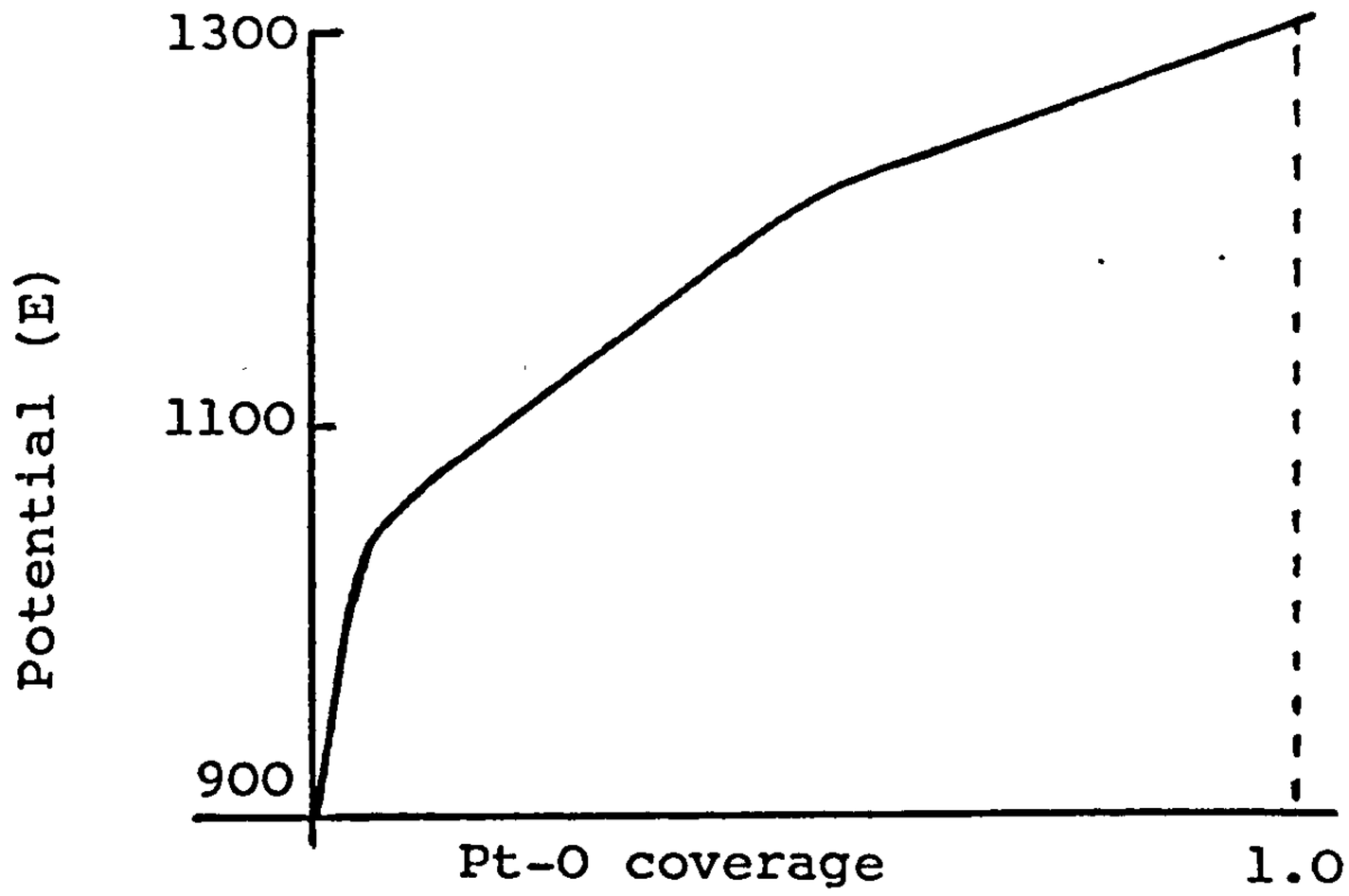

There is still much debate concerning the exact nature of the surface species,e.g. whether it is adsorbed oxy(-O) or hydroxy (-OH) species or even oxygen dissolved in the platinum. The exact species is immaterial to the present considerations, the essential point being that it is an electrochemical reaction involving a faradaic current.

We can write the reaction :

$$Pt + H_2O = Pt\text{-}O + 2H^+ + 2e$$

So within the potential range mentioned, an increase in potential will result in an anodic current i_{Pt}, until the oxide coverage has increased to a new value specific to the new potential. Conversely a reduction in potential will produce a cathodic current, which we will designate i_{PtO}, from the reverse reaction :

$$Pt\text{-}O + 2H^+ + 2e = Pt + H_2O.$$

Note that these are reactions with water. They are quite independant of the presence or absence of oxygen.

The effect is that the platinum has a degree of storage capacity and, for example, with an air cathode, current can be produced from Pt-O reduction as well as from oxygen reduction.

A rough estimate of capacity from "discharge" curves indicates a capacity of about 0.1μA hours per mV. If the sensor has a sensitivity of 0.1μA/ppm, the capacity is therefore about 1 ppm hour per mV. Bearing in mind we can swing about 60 mV, there is a capacity of about 60 ppm hours available. This capacity will of course be dependant on the surface area and the loading of the platinum used. Indications are that at equal loadings, the solvent extracted Engelhard 4 electrodes (see section 4) have about twice the capacity of the J & M Standard 280°C cured electrodes.

The practical consequence is illustrated in Figure 2.1., which shows some actual potential-time curves with an air electrode being run at constant current.

At the start the current will be virtually all from the Pt-O reduction. With time i_{PtO} decays to zero and i_{O_2} increases until finally, in the steady state, all the current comes from oxygen reduction.

We can also see the relatively long times (hours) involved in reaching the steady state condition. So in a sensor, the actual voltage change will be time dependant and will be less for a short exposure than for a long exposure. This can result in different behaviour in these two circumstances. It will be remembered for instance, that hysteresis behaviour was not identified until longer term exposures were used.

In a sensor, the anode and cathode potentials are linked so that the anode potential must follow the cathode potential.

As the cathode potential falls with time,so must the anode potentia and the surface "oxide" on the anode will also be reduced, giving a cathodic current on the anode which will partially offset the anode CO oxidation current.

We can now look in more detail at the practical consequences by considering two extreme cases.

(i) "Creeping" or "Positive Hysteresis"

In the first case we have a high "activity" bias in favour of the cathode, such that the cathode potential never falls below the air rest potential of the anode:

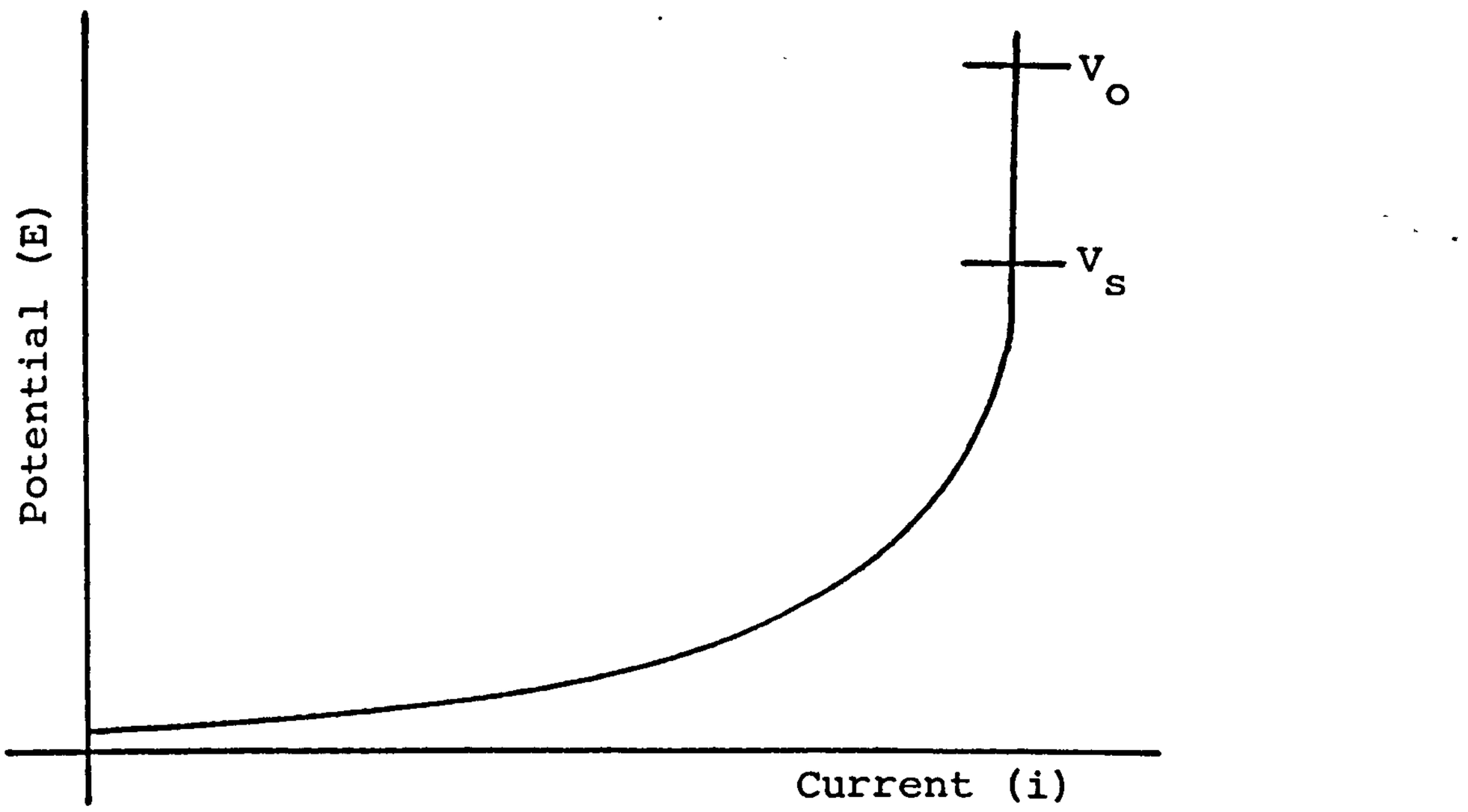

V_o indicates the starting cathode potential and V_s its steady state potential, when all the current is coming from oxygen reduction.

As seen above, it will take time for V_o to drop to V_s and during this period we have the following situation :

ANODE CATHODE

Signal S = $i_{co} - i_{PtO}(a) = i_{O_2}(C) + i_{PtO}(C)$

With time, i_{co} remains constant but $i_{PtO}(a)$ and $i_{PtO}(C)$ decay to zero and $i_{O_2}(C)$ increases until in the steady state:

$S = i_{co} = i_{O_2}(C)$

We can see that these effects will produce a signal that starts too low and will creep up to the full value at steady state as illustrated below:

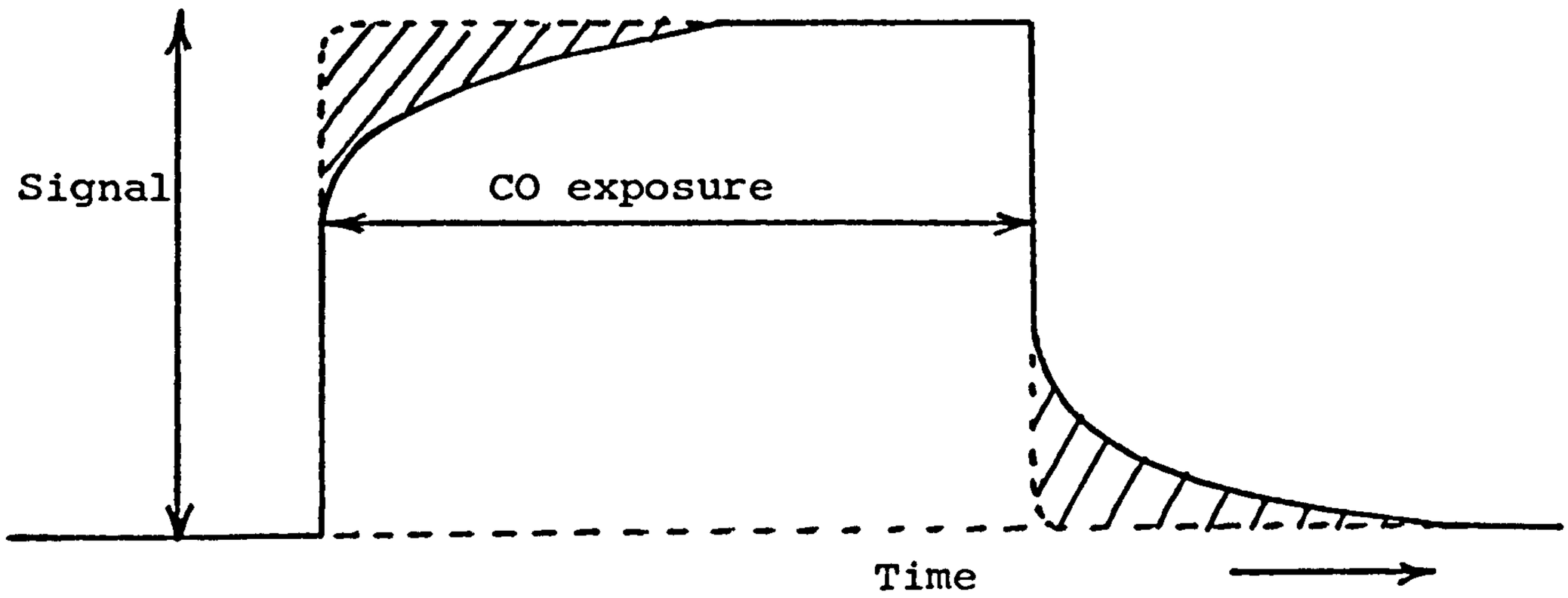

On recovery when the CO is removed, the potentials will rise and the Pt surfaces will reoxidise:

Anode Cathode

$S = i_{Pt}(a) = i_{O_2}(C) - i_{Pt}(C)$

All these currents will decay to zero with time (or at least back to give the net base line current).

As seen in the illustration above, the net signal takes an appreciable time to decay to zero while the anode Pt surface is being re-oxidised. It must follow that at the cathode $i_{O_2}(C) > i_{Pt}(C)$, which is reasonable for an active cathode.

The shaded area in the illustration will be equal to the Pt-O anode capacity for the potential swing in question,

i.e. Shaded area = Anode Pt-O capacity/mV times ΔV

where $\Delta V = V_o - V_s$ (cathode).

The extent of creep-up will be less:

(a) the lower the ΔV, i.e. the lower the cathode polarisation (the more active the cathode) and of course the lower the CO concentration and hence current.

(b) the lower the anode Pt-O capacity,

i.e. the lower its surface area and the lower its loading.

Examples of marked creep up were found with sensors which had relatively high anode loadings, paired with relatively low activity cathodes.

Conversely with the Mark 4 type sensors, with ultra-low loading anodes and active, high loading cathodes, the effect was not evident, as would be predicted from the considerations above. These latter sensors with very low loading anodes were suspect on long term signal stability. There is evidence, however, that we can couple somewhat higher anode loadings with best activit cathodes to give a combination with long term stability and negligible creep up.

(ii) "Signal Decay" or "Negative Hysteresis"

This is the case of nominal matched electrodes.

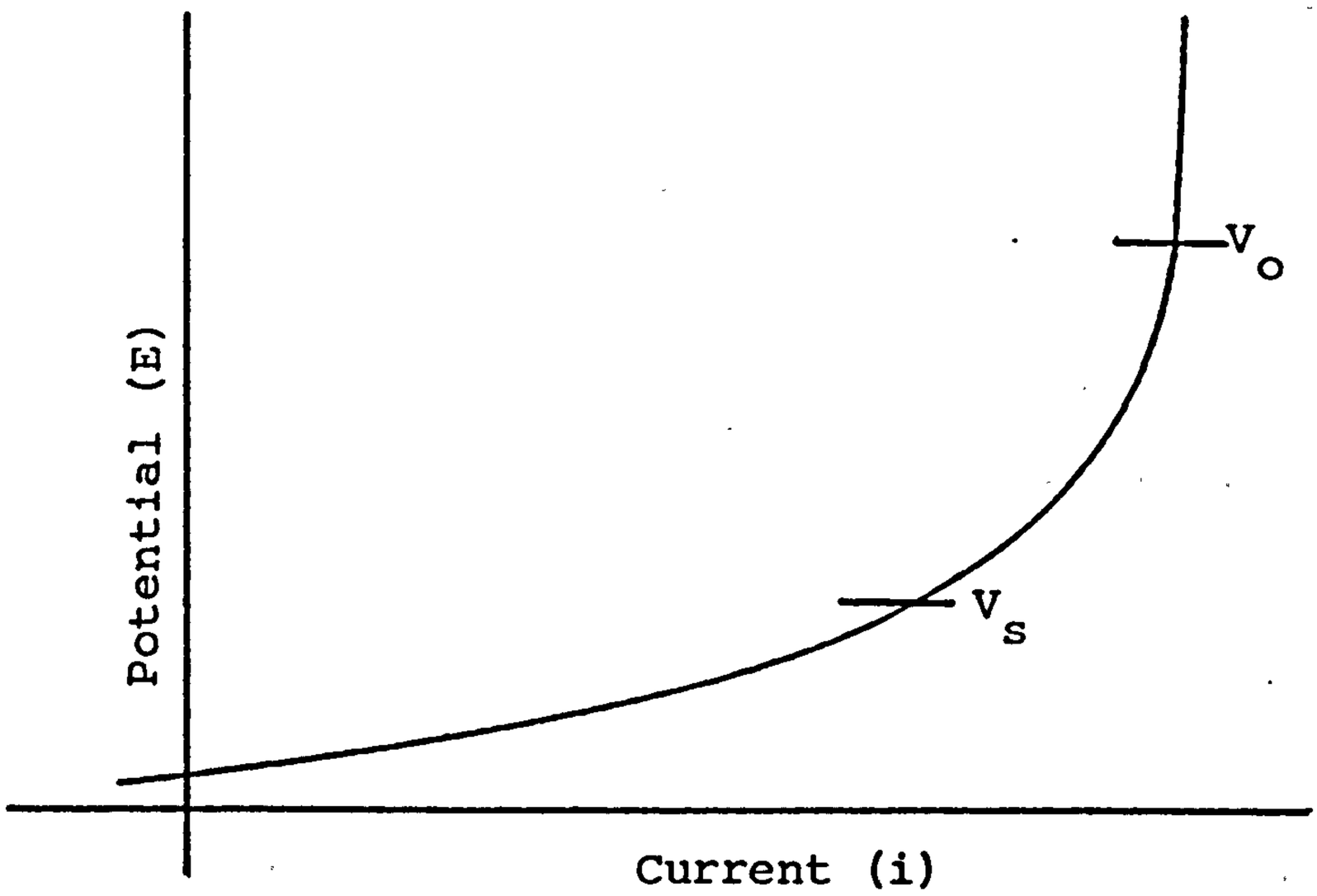

Here we will have a similar creep-up process occurring as in the previous case, but, superimposed on this, will be a reduction in signal ($i_{co} - i_{O_2}(a)$) as we slip down the current voltage curve when the potential falls from V_o to V_s and some oxygen reduction occurs at the anode since we are falling below its air rest potential. The more detailed situation is as below:

	ANODE		CATHODE
S =	$i_{co} - i_{PtO}(a) - i_{O_2}(a)$	=	$i_{O_2}(C) + i_{PtO}(C)$

With time, i_{co} remains constant, both $i_{PtO}(a)$ and (C) decay to zero and both $i_{O_2}(a)$ and (C) increase to a final steady state value. At the steady state:

S =	$i_{co} - i_{O_2}(a)$	=	$i_{O_2}(C)$

The i_{O_2} values being those applying at the steady state potential (V_s).

The steady state signal will be less than the full i_{co}. For Mark 3 sensors the signal was in fact about half the full limiting current value (i_{co}).

The exact shape of the resulting signal versus time trace, depends on the relative rates of change of the i_{PtO} and the i_{O_2} values at each electrode. These rates of change will themselves change with time. In principle it could be possible for these to match completely, with the rate of increase of i_{O_2} always matching the rate of decrease of i_{PtO} at both electrodes. In this case the signal would remain constant with time, although it would of course still be below i_{co}. In practice the more usual behaviour seemed to be that the rates were fairly well matched over a short period, but later became mismatched leading to a response curve of the type below:

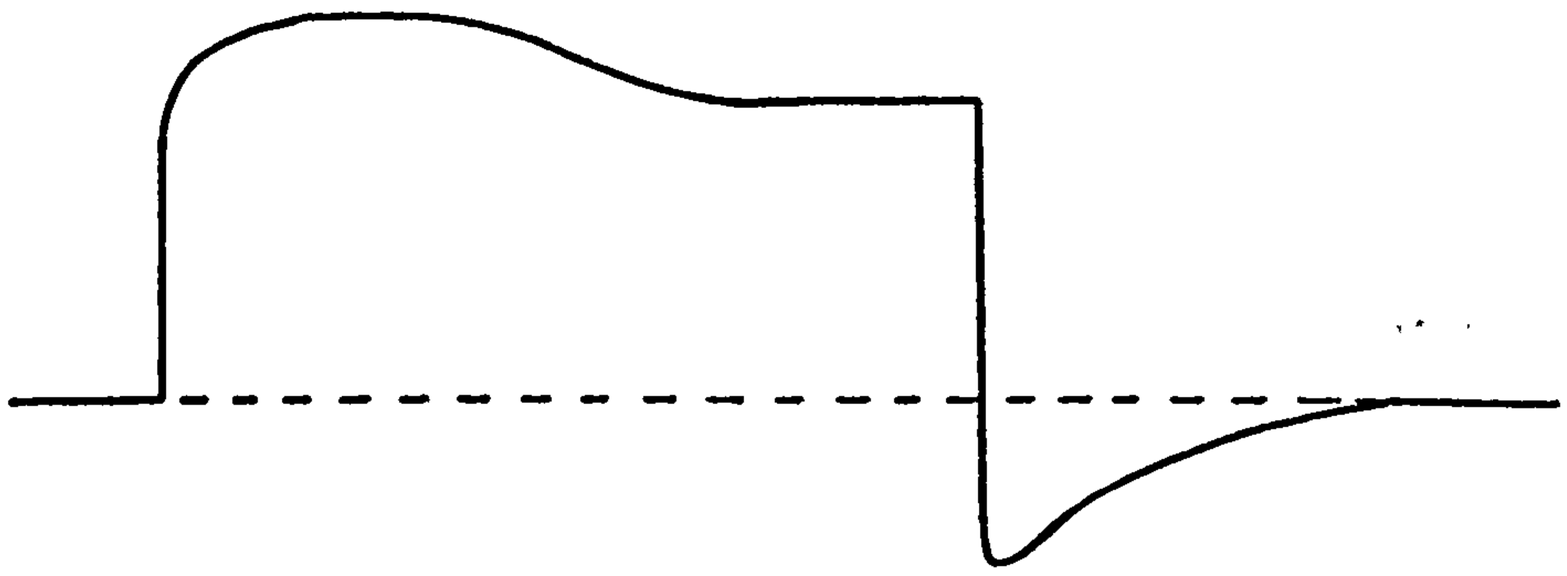

On recovery, with the Pt surfaces being re-oxidised, we will have:

Anode		Cathode
$S = i_{Pt.}(a) - i_{O_2}(a)$	=	$i_{O_2}(C) - i_{Pt}(C)$

All these currents will decay to zero with time (or at least back to give the net base line current).

This type of behaviour shows a negative hysteresis on recovery i.e. with a net cathodic current at the anode and a net anodic current at the cathode. It follows that $i_{O_2}(a) > i_{Pt}(a)$ and $i_{Pt}(C) > i_{O_2}(C)$, but it is difficult to explain why this should be so.

As can be seen from the foregoing treatment, a whole spectrum of behaviour is possible with different electrode combinations giving variations in the $\frac{S}{i_{co}}$ ratio and type and degree of hysteresis.

(iii) Unusual baselines

The relatively high Pt-O capacity in the electrodes and the long time that this takes to adjust to a change in potential, can lead to unusual baseline readings being recorded. If the sensor has been exposed to unduly high ambient CO levels over an extended period and the baseline. is checked by blocking off, the signal will decay rapidly as the CO is used up to an apparently unusually high baseline. If left blocked off long enough,this would slowly return to the more normal value, as measured after the sensor has been in normal low ambient CO levels.

(iv) Air rest potentials

In order to be able to manoeuvre with the two electrode system, one needs to be able to vary the intrinsic air rest potentials of the electrodes. This can be done within limits and the methods are described in section 4.2. Some of the underlying basic points are discussed here.

The theoretical open circuit potential of an oxygen electrode for the oxygen reduction reaction:

$$O_2 + 4H^+ + 4e = H_2O$$

is 1.229 Volts in pure oxygen (1 atm 20°C) and 1.209 Volts in air.

These potentials are versus the standard hydrogen electrode in the same electrolyte. Our experimentally measured potentials were versus the dynamic hydrogen reference electrode (DHE) which is 30 mV negative to the standard hydrogen electrode. The theoretical air potential vs. DHE is therefore 1.239 Volts.

In practice, measured air rest potentials are much lower than this, usually between 1.0 and 1.1V vs DHE. The oxygen reduction reaction is a slow one with a high activation energy. In electrochemical terms this means that it will initially polarise severely, the potential dropping steeply with current in the very low current region. If there is an anodic reaction available, then this can couple with oxygen reduction to form a local cell which results in a "mixed potential" being observed. This situation is illustrated below:

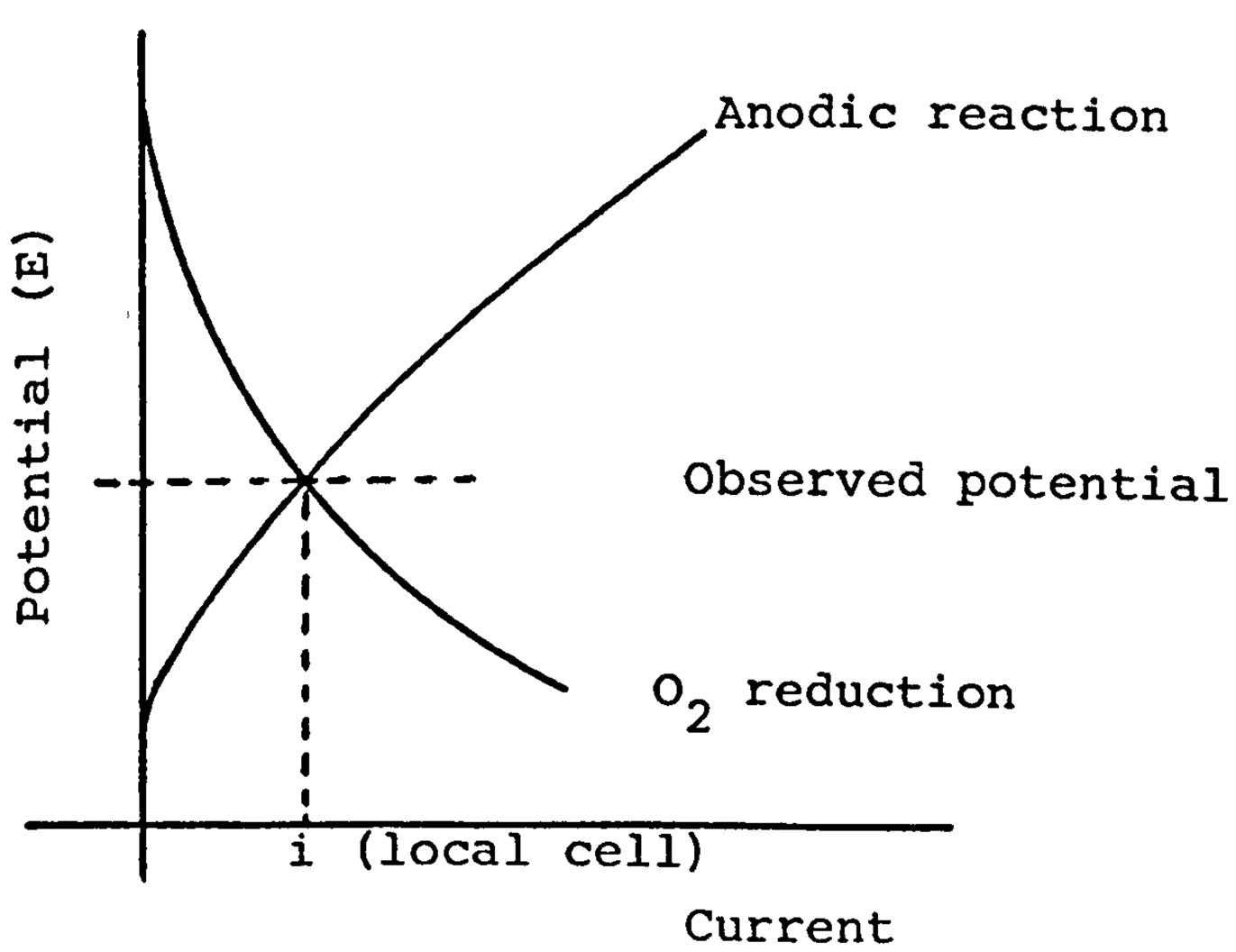

A local cell current as low as about 0.1 to 0.5μA would be enough to reduce the theoretical OCV to the observed values with our type of electrode.

It can be readily seen that even very small quantities of oxidisable impurities can appreciably affect the observed rest potential. In many cases, e.g. if they are organic impurities, these may be oxidised away and the observed potential will wander up to a more stable value.

However, even in the apparent absence of impurities, the air rest potential of platinum remains much lower than theoretical.

It is generally agreed that the local cell, mixed potential explanation is correct, but there is still argument about the anodic reaction concerned in the absence of impurities. One school of thought favours the oxidation of platinum:

$$Pt + H_2O = Pt\text{-}O + 2H^+ + 2e$$

but it is diffucult to see why this does not either grind to a halt or oxidise all the platinum, neither of which appears to happen.

Another suggestion involves the peroxide reactions:

(a) $H_2O_2 = O_2 + 2H^+ + 2e$

(b) $2H_2O = H_2O_2 + 2H^+ + 2e$

but it is difficult to see how the peroxide gets there in the first place for (a) and, at the potentials concerned, the equilibrium peroxide concentration is only about 10^{-13} for either reaction.

All in all there is still no really satisfactory explanation, in spite of decades of academic attention. One must of course remember the very small currents involved which require only

very small amounts of reactant. However, the empirical facts are clear and these are what concern us in practice.

If we couple together in the sensor, two electrodes with different rest potentials, it is not surprising that a current will flow to produce a baseline. What is more surprising is that a baseline can persist apparently permanently, as we would expect the two electrodes to gradually come to a common "equilibrium". In practice it is probably the same mechanisms at work as those which give the persistent lower-than-theoretical air rest potential. As in that case, we cannot properly explain things, but a persistent baseline is an empirical fact that has to be lived with.

As is to be expected, the higher the difference in electrode potentials, the higher the baseline, although it does seem that this eventually plateaus out (see section 7). In practice therefore, we have had to look for a compromise between a combination biased for high cathode activity, and CO tolerance, but with a resultant high baseline, and a low bias combination for low baseline, but with poorer tolerance to high CO levels.

The remarks above apply to "settled in" sensors. Fresh sensors may show enhanced or even negative baselines initially, due to the presence of trace impurities temporarily affecting the electrode potentials as described above.

3. HARDWARE DESIGNS

3.1. Machined Versions

The main hardware design changes since Mark 3 have been associated with gas distribution over the sensing electrode and span temperature compensation.

If the air gap between the capillary holes and the electrode is small, the gap diffusion resistance can become significant relative to the capillary resistance (see Appendix 1). This effect is illustrated by the following example:

> a cavity, 19mm dia. x 2.5mm deep was machined into a perspex sensor top. Five holes of diameter 1.05mm were drilled in the usual pattern. This top, when mounted on a Mark 6 sensor (T9), with the cavity on the inside, had a CO sensitivity of 0.092µA per ppm at 20°C. When the top was reversed so that the air gap was considerably reduced, the sensitivity fell to 0.072µA per ppm.

The signal temperature response of this sensor also altered when the top-plate was reversed (Figure 3.1.). Without the cavity the signal varied linearly over the entire range 0 to 40°C, with a temperature coefficient of 0.30% per °C, with the cavity, a non-linear temperature response was obtained, which for convenience could be divided into two linear segments with temperature coefficients of 0.61% per °C between 0 to 20°C. and 0.34% per °C between 20 and 40°C. This behaviour was typical of uncompensated sensors with cavities and is indicative of a mixed signal contol situation from both capillary diffusion and electrode activity. The

latter varies exponentially with temperature and becomes increasingly significant at lower temperatures. Ultimately, the temperature response curve should limit towards a constant slope of 0.17% per ^{o}C. at some temperature above 40^{o}C. where the electrode contribution to signal control becomes vanishingly small relative to the capillary diffusion resistance. With the T9 sensor top-plate reversed to exclude the cavity in the above example, the air gap would have opened up as the temperature decreased due to the differential contraction between the steel bolts and plastic body, causing a slackening of the clamping pressure. In this specific example, the enhancement of signal due to the resultant decrease in air gap diffusion resistance, apparently fortuitously matched the signal decrease due to the reduction in electrode activity as the temperature was lowered, giving a linear response over the temperature range, 0 to 40^{o}C. However, the air gap geometry is rather nebulous and subject to scatter from sensor to sensor, and to instability during service life. For example, a number of Mark 4 design sensors, having no cavity or Webril packing, had temperature coefficients between 18 and 40^{o}C. of 0.48% per ^{o}C. with a spread of ±0.15 two such sensors had zero coefficients between 18 and 25^{o}C., but between 25 and 40^{o}C. one had a coefficient of -2.0 and the other -4.0% per ^{o}C. Webril packing between electrode and top plate, as used in the Marks 2 and 3 designs achieved more uniform behaviour (temperature coefficients about 0.37% per ^{o}C. ± 0.05) but theoretical considerations of the gap size effects indicated that this design was potentially in a very critical region with regard to the ratio between capillary and gap diffusional resistances (Appendix 1).

Adoption of this arrangement with three-electrode sensors would result in further compaction of the Webril diffuser, creating an even more unstable condition.

Cavities were introduced in favour of the Webril diffuser during the early stages of the Mark 4 design to alleviate this situation. Initially, fairly shallow cavities, 0.5mm deep x 16.5mm dia., were used which gave intermediate behaviour - temperature coefficients of 0.40% per ^{o}C. between 18 and 25^{o}C. and zero between 25 and 40^{o}C. Cavity depths of at least 0.75mm were required to reduce the air gap restriction to insignificant proportions and this was finally enlarged to 19mm dia. x 2.5mm deep by the Mark 6 stage, which has since been adopted as standard.

These cavity sensors gave temperature responses very similar to those shown in Figure 3.1., with maximum coefficients of 0.7% per ^{o}C. in the low temperature region. In the latter stages of Mark 4 design therefore, silicone rubber sleeve compensation was introduced (Appendix 2). The drilled capillary holes in the top plate were enlarged to accept tight fitting lengths of silicone rubber capillary tubing. Due to differential thermal expansion between perspex and the silicone rubber, the resultant capillary holes closed up as the temperature increased and vice versa. The critical parameter governing signal compensation is the wall to bore aspect ratio of the mounted silicone rubber tubing. For sensors without cavities, it was found that an aspect ratio of about 1:1 gave good span temperature compensation. With full top-plate cavities of 2.5mm however,

larger aspect ratios were required. For example, the Mark 6 cavit sensor T9 only achieved partial compensation with an aspect ratio of 1.08, but a second sensor, Mark 5 PR.1., with a ratio of 2.00 exhibited a temperature coefficient of only 0.043 to 0.084% per ^{o}C. (Figure 3.2.). Work is continuing on this aspect of sensor design with the objective of achieving a reliable and reproducible span temperature compensation over the entire temperature range with production size batches of sensors.

3.2. Design for Injection Moulding

Hardware design was sufficiently well established during this development phase to allow consideration of injection moulded designs. Several trial model designs were made in machined perspex before finally committing to the components shown in Figures 3.3. and 3.4. A single impression mould to make the two-component set has been ordered and hardware should be available for evaluation in the second half of the following, 4th phase.

The injection moulded design differs from the current machined version in several aspects:

- the body components, base-plate, floor and 'O'-ring retainer, have been incorporated into a single hardware unit (Figure 3.4.).

- current collector outlets to tabs have been repositioned to the actual securing bolt pressure points to provide maximum sealing pressure and leak resistance. This has necessitated the reversal of the bolting arrangements, namely, nuts countersunk into top-plate and bolt heads into the body.

- securing bolts have been increased from 4 to 6, but with the elimination of separate tab locating bolts, the total number of bolts per sensor is the same for 2-electrode types and is reduced by one with 3-electrode sensors.
- A third electrode tab position is included as standard.
- Additional support and location for tabs is provided by the redesigned body well, slot and lug as shown in Figure 3.4.). This should reduce the possibility of accidentally breaking the tab connections to the platinum foil current collectors.
- Four extra floor holes have been included, in addition to the central wick hole. These holes allow gas access to the cathode ptfe tape and facilitate pressure release of reservoir air resulting from temperature increases, or water uptake in high humidities. The background to this feature constitutes work carried out in the very early stages of the following phase and will appear in later reports. These holes will also be adopted as standard in sensors manufactured from the beginning of the phase 4 stage.
- The injection moulded components have as far as possible been designed to achieve a uniform wall thickness of about 2mm to minimise distortion and moulding time. This accounts for much of the apparently complex shaping and material conservation of both the body and top-plate designs, compared to current machined components.

4. ELECTRODES

4.1. Production Methods

During this report period much effort has been directed towards the continuing development of electrode manufacturing techniques which were both,suitable for scale-up-to volume production,and achieved optimum performance characteristics.

All techniques were based on the "foil transfer" method whereby the catalyst layer was formed on aluminium foil and then transferred by pressing onto a porous ptfe backing tape to give the completed electrode.[1][2] The fabrication methods investigated were mainly concerned with different techniques for depositing the catalyst mix onto the aluminium foil substrate and can be classified as follows:

(i) Spray Method

(ii) Drop Method

(iii) Solvent Extraction

The spray method was originally developed for silver catalysed electrodes, used in the CTL oxygen sensor.[2] It is ideally suited to large scale production and results in good electrode characteristics. However, material wastage is very high due to overspray, offcuts, etc.and overall catalyst transfer efficiencies are at best 40 to 50%. Some attempts were made to improve the platinum utilisation efficiency, but at an early outset the spray method was abandoned in favour of the alternative methods. These were more labour intensive but achieved near 100% platinum utilisation efficiency and were overall more cost effective than the spray method.

The so-called "Drop Method" derives its name from the first stage of the process whereby a free flowing slurry of platinum and ptfe dispersion in aqueous acetone was prepared, which was capable of being measured out in aliquots with a graduated teat dropper into aluminium foil moulds. The exact procedure was as follows:

Platinum black was weighed out and mixed with an appropriate volume of diluted aqueous ptfe dispersion (I.C.I., G.P.1., Fluon dispersion) in an ultrasonic bath. A measured amount of acetone was added to produce a slurry having the required flow characteristics. An homogeneous suspension was maintained by transferring the slurry to a rotating cup, from which aliquots were taken by means of a teat dropper pipette and put into moulds lined with aluminium foil as described in previous reports.[1][3] When using standard Johnson Matthey platinum black, the catalyst moulds were allowed to dry overnight in ambient air. However, the more active Engelhard 4 black was dried by forced air circulation at room temperature for 20 minutes to minimise the contact time between foil and wet catalyst mix. This was necessary as prolonged drying resulted in excessive corrosion of the aluminium, presumably by the formation of an oxygen/metal corrosion cell.

After drying, the moulds were cured in a circulated air oven according to the following cycle:

- 5 minutes 50°C
- 5 minutes 100°C
- 45 minutes 280°C
- removed from oven and cooled in ambient air.

The temperature was raised in stages in order to progressively drive off residual acetone before the mix became too hot. This avoided the possibility of local overheating of the catalyst surface by catalytic burning of any organic vapour. The high temperature stage was necessary to achieve the correct wetting properties of the catalyst by removing a surfactant used to stabilise the ptfe dispersion.

After cooling, the catalyst mouldings were transferred from the foil substrate by pressure bonding onto porous ptfe tape.

With the 'Solvent Extraction Method', the surfactant was removed by leaching the catalyst mix with isopropyl alcohol instead of heating to 280^{o}C on the foil,as with the 'Drop Method'. The procedure was as follows:

A quantity of platinum and ptfe dispersion, sufficient for a number of electrodes, was mixed ultrasonically as in the Drop Method. Excess isopropyl alcohol was then added which coagulated the mix to a loose dough. This dough was transferred to a glass tube having a Whatman GF/A glass mat floor and extracted with iso-propyl alcohol in a Soxhlet apparatus for about one hour. The catalyst mix was at all times flooded in order to avoid catalytic burning of the alcohol. After extraction the mix was eluted with cold water to facilitate handling. The remaining alcohol was then removed by washing with hot water, followed by quenching with cold water, after which the catalyst could be safely exposed to air. The mix was then divided into

portions, put into the aluminium foil moulds and dried at 100°C. for 20 minutes. The catalyst was transferred in the usual manner onto porous ptfe tape by pressure bonding.

4.2. Discussion of Factors Affecting Choice of Electrode Compositions

The choice of anode and cathode compositions was complicated because of the need to satisfy a number of conflicting requirements and the final selection necessitated a number of compromises.

High electrode activity was an important criterion for both anode and cathode. "Activity" in this context refers to both the intrinsic electrocatalytic activity of the platinum black (kinetic factor) and the diffusibility of the electrolyte film in the thinly wetted region between solid catalyst surface, liquid electrolyte and gas phases within the electrode structure (mass transfer factor). Such electrode activities may be measured and compared by experimental determination of the currents generated at a given reactant concentration and polarisation (i.e. difference between rest and operating potentials of an electrode), in the absence of other controlling factors. Experimental methods, using thin Gore backing tapes to support the catalyst layer, were described in the last report.[3]

Generally electrode activity was promoted through the use of higher specific surface area (smaller particle size) platinum black, lower electrode curing temperatures and higher platinum loadings. Thus, the solvent extracted, 100°C. dried, Engelhard 4 catalysts produced the most active electrodes at a given platinum

loading, and J.M. Standard black, 280°C. cured, the least active. Platinum/ptfe ratio also influenced activity, producing broad maxima between about 3:1 and 8:1 for all platinum black types tested; ratios of 4:1 and 6:1 were generally chosen with J.M. Standard and Engelhard 4 blacks respectively, during this phase of the work.

With anodes, an unrestricted (open) electrode activity towards CO-oxidation of at least 10 times the capillary diffusion barrier sensitivity (i.e. the ELECTRODE ACTIVITY RESERVE) was considered desirable to ensure a signal governed predominantly by the capillaries and which is therefore, both stable and of low temperature coefficient.[3] However, an upper limit on the anode activity reserve was imposed by two other considerations:

(i) Sensor response time, being a function of interfacial contact area between anode catalyst and electrolyte, generally increased with steps taken to improve anode activity.

(ii) Parasitic, local cell consumption of carbon monoxide at the anode causes loss of signal sensitivity and may reduce linearity[3]. Suppression of parasitic reactions can be accomplished by enhancing the oxygen reduction capability of the cathode relative to that of the anode. However, measures taken to limit the anode oxygen reduction capability may also affect the CO-oxidation reaction and hence the activity reserve.

Thin tape anodes produced limiting CO-oxidation currents above air rest potentials (i.e. in the absence of oxygen interference) which were apparently insensitive to the fabrication technique but increased fairly linearly with platinum loading in the range 7.5 to 35 mg cm^{-2} (Table 4.1 and figures 4.1. and 4.4.). This probably reflected the fact that diffusion of CO through the thinly wetted area was the dominant controlling mechanism under these conditions. Below 4 to 5 mg cm^{-2} platinum catalyst coverage was incomplete and activity decreased dramatically with loading. Above 35 mg cm^{-2} platinum, CO-oxidation currents became more comparable with the thin tape diffusibility and mixed control set in with an apparent decrease in current per unit platinum loading. Meaningful measurements of activities above 35 mg cm^{-2} would either necessitate the use of ptfe tapes with greater diffusibilities, or the correction of currents for the tape contribution.

Oxygen reduction capability similarly increased with platinum loading but currents were very sensitive to fabrication technique (particularly curing temperature) and prehistory of the electrode (Table 4.1). This was indicative of electrocatalytic activity as the controlling factor, rather than film diffusion.

The final choice of anode composition, prepared from J.M. Standard black by the Drop Method and cured at 280°C., achieved an acceptable compromise between the requirements of CO-oxidation activity reserve on the one hand and response time and oxygen reduction capability on the other. Anodes

prepared in this way, with platinum loadings between 7.5 and 35.0 mg cm^{-2}, on thin Gore-ptfe tape, supported limiting CO-oxidation currents which represented between 10 and 45 times respectively, the 0.1μA ppm^{-1} sensitivity of the capillary hole barrier used with NCB trace CO Sensors.

Note: To express electrode activity in terms of μA ppm^{-1}, the CO-responses given in Table 4.1. (μA ppm^{-1} mg Pt^{-1}) should be multiplied by the loading (mg cm^{-2}) and the electrode area (π cm^2).

Cathode polarisation determines the operating potential of a two-electrode sensor system and therefore, high electrocatalytic activity towards oxygen reduction is necessary:

i) to avoid hysteresis problems associated with changes in platinum surface oxide coverage, arising from excessive polarisation and potential excursions, particularly on prolonged exposures to high carbon monoxide levels above 50 ppm (See section 2).

ii) to suppress parasitic, local cell consumption of carbon monoxide on the anode.

Under galvanostatic conditions, the normal operational mode with sensors exposed to a constant CO concentration, polarisation of the oxygen reduction reaction at the cathode was time dependant, taking up to 3 to 4 hours to achieve a steady state, due to changes in the platinum surface oxide coverage. Figures 4.2. and 4.3. show the potential time behaviour obtained under galvanostatic conditions, in the

current range O to lOμA (O to lOO ppm CO equivalent), of cathodes in mark 4 and mark 6 sensors respectively. These cathodes represent the upper and lower limits, respectively of cathode oxygen reduction activity per unit platinum loading.

Unlike the anode, cathode interfacial area did not influence sensor response time. However, an upper limit was imposed on the differential oxygen reduction activity between cathode and anode due to the need to ensure a minimal sensor baseline in CO-free air. Platinum/air (oxygen) electrodes are so-called polyelectrodes.[4] Their rest potentials in clean air are usually some 150 to 300 mV below the theoretical value of 1.229 volts (normal hydrogen scale) and result from local cell action, involving coupled oxygen reduction and platinum surface oxidation reactions, rather than true thermodynamic equilibrium processes. As such, the measured rest potential values are strongly dependant on the prehistory and catalytic activity and extent of the platinum surface, as demonstrated in the Table 4.2.

As the differential oxygen reduction capability between anode and cathode in a sensor becomes greater, the difference between their air rest potentials will increase and produce a corresponding enhancement of baseline. The baseline, being determined by activated electrochemical reactions, will have a high temperature coefficient (typically 2 or 3% per degree) which will contribute to the overall sensor temperature coefficient.

During this third development phase, three alternative sensor configurations, differing principally in their electrode compositions, were evaluated in an attempt to

overcome the limitations of the Mark 3 version developed by the end of Phase 2. The characteristics of these sensors (Marks 4, 5 and 6), together with the earlier Marks 1, 2 and 3 versions, are summarised and compared in Table 4.3.

Mark 3 sensors used a "matched pair" electrode system of essentially identical anode and cathode, having about 35 mg per cm^2 J.M. Standard black, applied by the "Drop Method". At the end of phase 2 this sensor version was showing a lot of promise. Its response time was considerably improved relative to the Mark 1 and 2 versions due to the replacement of J.M. Fuel Cell black with the much lower specific surface area J.M. Standard black at the anode. Baseline and signal stability in 50 ppm CO were also very satisfactory. However, further investigations in the early part of phase 3 established that the cathode was insufficiently active, resulting in hysteresis effects on prolonged exposures to CO above about 100 ppm (see sections 2 and 7). Parasitic effects were also much in evidence as reflected by the large difference between measured sensitivity and the theoretical value calculated for the capillary barrier, i.e. fractional current limit of only 50% the capillary limiting current. This was also true of other "matched pair" configurations, namely Mark 1 and 2 sensors.

The Mark 4 sensor was designed to overcome these deficiencies in the Mark 3 version. Cathode activity was enhanced by the use of Engelhard 4 black in electrodes made by the solvent extraction method. Anode activity was correspondingly biased downwards by reducing the platinum

loading to 10 mg per cm^2 and retaining the J.M. Standard black with the "Drop Method" of fabrication. Single electrode measurements in sensors indicated that this electrode configuration would result in relatively low cathode polarisation and yield an operational potential well within the limiting current section of the anode current-voltage characteristic (figure 4.5) which should ensure a very stable performance. The Mark 4 objectives were indeed achieved in that CO-tolerance was considerably improved compared to Mark 3, the full capillary signal sensitivity was observed and response was faster. However, the oxygen reduction activity differential between anode and cathode was large and baselines were unacceptably high - difference between air rest potentials of anode and cathode was about 100mV.

Mark 5 and 6 sensors represented compromises between Mark 3 and 4 versions. Each comprised an anode made from J.M. Standard black by the "Drop Method" with platinum loadings in the range 26 to 34 mg per cm^2. Cathodes for both designs were made by the "Drop Method" rather than solvent extraction, to reduce the cathode activity but, whereas the Mark 5 sensors were made with Engelhard 4, Mark 6 cathodes were derated further by using J.M. Standard black. Both cathodes used platinum loadings of 10 mg per cm^2 greater than the anode to bias the activity above the anode. The loading differential of 10 mg per cm^2 was achieved as closely as possible by matching individual anodes and cathodes during manufacture. The resultant characteristics of sensors reflected the compositional compromises, with Mark 5 erring nearer to Mark 4 behaviour than Mark 6 (See Table 4.3.).

Thus CO tolerance and signal achievement for both were down on Mark 4, but better for Mark 5 than Mark 6. Baselines were similar for both Mark 5 and 6 and lay between Marks 3 and 4.

Overall, it was considered that the Mark 5 sensor configuration represented the best compromise of properties and this version was provisionally selected for the NCB application at the conclusion of this phase.

5. ELECTROLYTE

5.1. Water Balance

During this report period, practical tests have been conducted to verify the theoretical relationships previously derived for water transfer rates to and from the sensor electrolyte.[3]

In the last report, the expression for water transfer was derived in terms of the sensor oxygen limiting diffusion current, assuming that the sensor capillaries represent the only factor controlling water access. An equation of the same form is obtained by direct consideration of water vapour diffusion through the capillaries. Thus, the water flux according to Fick's Law is:

$$\text{Water Flux (moles } s^{-1}) = \frac{N \pi d^2}{4\ell} D_{H_2O} (C_1 - C_2) \qquad (1)$$

N is the number of identical capillary holes.

d is the capillary diameter (cm)

ℓ is the capillary length (cm).

D_{H_2O} is the diffusion coefficient of water in air at 1 atm. pressure.

C_1 and C_2 are the water concentrations either side of the capillaries. C_1 will be the ambient air concentration and C_2 the equilibrium water vapour concentration above the sensor electrolyte.

The water concentration differential can be restated in terms of partial pressures at 20°C. :

$$(C_1 - C_2) \text{ (moles } cm^{-3}) = \frac{\Delta P_{H_2O}}{22.4.10^3.760} \cdot \frac{273}{293} \qquad (2)$$

The diffusion coefficient of water at 25°C is 0.256 $cm^2\ s^{-1}$ (A.S. Foust et al; Principles of Unit operations, John Wiley 1966, page 562). This changes in proportion to the 3/2-power of absolute temperature and at 20°C. has the value 0.25 $cm^2\ s^{-1}$.

Substituting values into equational (1) and expressing the water flux in g per day gives:

$$\text{Water Flux } (g\ day^{-1}) = \left(\frac{\partial W}{\partial t}\right)_{20^oC} = 16.713.\ 10^{-3}\ N\ \frac{d}{\ell}^2\ \Delta P_{H_2O} \quad (3$$

The sensors contain silicone rubber capillary inserts in a perspex top, designed to effect temperature compensation of the diffusibility of the capillary system. Assuming this achieves perfect compensation, then equation (3) holds at any temperature provided the correct values of water vapour pressure are used.

ΔP_{H_2O} is given by: $P_{H_2O}\ (R_H - R_{H_e})$

where P_{H_2O} is the saturated vapour pressure of water at the operational temperature (T) and R_H, R_{H_e} are the relative humidities on the ambient air and electrolyte sides of the capillaries respectively.

Substitution into equation (3) and rearranging gives:

$$\int_o^t (\partial t)_T = \frac{\ell}{16.713.\ 10^{-3}\ N\ d^2\ P_{H_2O}} \int_o^W \frac{\partial W}{(R_H - R_{H_e})} \quad (4)$$

Integration of equation (4) gives the variation of water content with time (days) at a fixed temperature (T) and ambient humidity (R_H). R_{H_e} is a function of electrolyte concentration and hence water uptake (or loss). The relationship is complex and integration of the right hand term is not easily accomplished.

A stepwise method is therefore used in which average values of R_{H_e} are taken for a number of small volume increments (∂W) and the estimated times summed separately (see last report CTL No. 80/31/003).

Water uptake experiments were conducted with sensors stored in a chamber at 40°C. and 100% humidity (R_H=1 and P_{H_2O} = 55.324 mm Hg). For simplicity, these were "dummy" sensors excluding current collectors and using uncatalysed tapes, pressed at foil transfer pressures, in place of electrodes. In all other respects they were identical to actual sensors. At regular intervals the sensors were removed and weighed to obtain a measure of water ingress. The sensors each had five capillaries of dimensions 0.105 cm diameter, 0.23 cm length and were primed with 0.5 cm^3 10.3N sulphuric acid. A theoretical water uptake curve was calculated from equation (4) for comparison, using 0.4 cm^3 volume increments, when:

$$\underset{(\text{days})}{t} = \sum_{o}^{W} \left(\frac{1.805}{1 - R_{av}} \right)_{T = 40^{o}C.} \qquad (5)$$

where R_{av} is the mean electrolyte relative humidity for each 0.4 cm^3 volume increment.

The theoretical and experimental data points are compared in figure 5.1. The experimental water diffusion rates were about 20% greater than those predicted by equation (4), but the general curve shapes were identical. In addition to the capillary access, it was estimated from sensor span measurements that "side access" through the sensor seal is at least 10% of that through the capillaries. For example, using a 50 ppm CO in air span gas mixture, sensor signals on the capillaries alone

were about 5μA compared with about 0.2 to 0.5μA on the totally immersed sensors in the gas, with blocked capillaries; the latter, side access, signal represents the difference between cathode and anode side access for CO, which appears as a net sensor signal. The total access available to water at this point therefore would be higher than indicated by these measurements and could approach 15 to 20% of the capillary diffusibility. Within these uncertainties therefore, the correlation between measured and calculated water transfer rates was very good.

Continuing work is being directed towards assessing the effects on sensor operation of prolonged exposures to both high and low humidities.

5.2. Definition of Electrolyte Working Volumes

Standard sensors are currently charged with $1cm^3$ of nominally 1ON sulphuric acid. Very satisfactory operation is achieved with this condition but we need to define the maximum and minimum working electrolyte volumes to accommodate water transfer when operating in humidity extremes. We also need to assess any effects of changes in electrolyte concentration resulting from volume variations due to water transfer in or out of the sensor.

The absolute maximum electrolyte volume is defined by the free internal space of the sensor. This is not so clearly definable since it has been found that the electrode sandwich deforms somewhat, into the top-plate cavity under the influence of hydrostatic pressures in the reservoir. Water uptake measurements have indicated an available volume of about $3.5cm^3$ in the Mark 5, machined design before the membrane bursts- provided

adequate measures are taken to vent any trapped gases in the electrolyte reservoir which may pressurise the system as water is absorbed. This agrees favourably with an estimated volume, based on the dimensions of the reservoir, of about 3 cm^3.

To define the minimum electrolyte volume, a set of 6 Mark 6 sensors were primed with varying amounts of 10N sulphuric acid in the range 0.5 to 1.0 cm^3 (Table 5.1.). These sensors were monitored weekly, according to the usual procedure (Section 6), over a period of 15 weeks. Response times were measured on a 100 ohm load at week 2 and baselines were averaged out over the last 5 weeks and expressed in ppm CO equivalent. Long term stability was assessed by expressing the final, week 15, sensitivity as a percentage of the initial, week 1, sensitivity.

Although there was some scatter in performance parameters from one sensor to another, it was evident (Table 5.1.), that there were no systematic trends with decreasing electrolyte volume down to 0.6 cm^3. At 0.5 cm^3 however, performance did begin to suffer.

Thus, in conditions where sensors are likely to experience prolonged exposures to high humidities, service life could be considerably extended by priming with less electrolyte than the 1 cm^3 currently used (Figure 5.2.). However, this would also reduce the low humidity tolerance of the sensor and precautions should be taken to avoid dessication during storage. The 10.3N acid used in current sensors has an R_H of about 60% which is roughly in balance with mean ambient conditions. A considerable increase in the high humidity tolerance could be achieved by reducing this concentration, but this would necessitate storage in sealed containers to avoid drying out.

The remaining question of the effects on sensor performance when subjected to the acid concentration changes,resulting from the water transfer between the maximum and minimum volume limits,is to be investigated in phase 4.

6. LIFE TESTING OF PRODUCTION PROTOTYPE BATCHES

The two-electrode trace CO sensor has so far evolved over six genetic stages, involving both hardware design changes as well as electrode performance modifications.

Each generation, designated with a Mark number, represents significant modifications in electrode structure in order to achieve the best compromise between opposing requirements for low baselines on the one hand and for CO tolerance on the other. The specification of each Mark is given in Table 4.3.

Since, at each stage, it soon became apparent that further changes were necessary, no substantial batches of any given Mark have been made for long-term monitoring and the data presented in Tables 6.1 to 6.8 represent a range of minor variations within any given Mark.

Unless stated otherwise in the tables, all sensors were charged with $1cm^3$, 10N H_2SO_4. Sensors charged with greater volumes had ABS reservoirs glued to the base plate to accommodate the extra electrolyte. Where chromium and permanganate addivitives were used, the tables indicate the concentrations of these materials in the $1cm^3$, 10N H_2SO_4 charge.

All sensors were permanently loaded with 100Ω resistors and stored in ambient air. Tests were performed once a month by blocking off the capillaries for 5 mins. to obtain the baseline and then checking the span with a 50 ppm CO in air mixture by clamping a hood over the sensor capillaries. The CO test gas was fed from an Aluminium Alloy cylinder at a flow rate of 100 $cm^3\ min^{-1}$.

All sensor baselines were corrected to 20°C., assuming the average energy of activation for the baseline mechanism to be 18.8 kcal mol^{-1}. However, we are now in a position to draw on considerably more data and more detailed analysis suggests that in general, 16.5 ± 2.5 kcal mol^{-1} is a more accurate figure.

Signals of sensors with solid capillaries were adjusted to 20°C assuming an average temperature coefficient of 0.35% signal per °C., whereas sensors with sleeve compensation were not adjusted.

Of necessity, about a third of the sensors made were of a highly experimental nature and did not warrant long-term monitoring, but the data presented in the tables is by and large representative of the long-term stability and of the relative number of failures in the population of sensors.

The oldest sensors (Mark 1) have now exceeded 21 months with no significant loss in CO sensitivity. Most of the other sensor Marks show the same long-term stability, except the Mark 4 sensors, which have low anode loadings (5-15 mg Pt cm^{-2}) and thus have insufficient CO activity reserve to confer long-term stability. This deficiency has been rectified in Mark 5 and 6 sensors, where the anode Pt loadings have been increased to around 30mg cm^{-2}.

Most sensors showed long-term baseline drifts of less than 1ppm CO equivalent, with the exception of Mark 1 sensors, some of which drifted from -2.5 to + 4ppm CO equivalent over the 21 months period. This is probably due to the fact that Mark 1 sensors used synthetic resin-bonded polyamide separators, whereas the subsequent Marks used glass mat wicks. In addition Mark 1 Sensor components were not acid-leached,

a technique which was introduced later and has now been adopted as standard practice.[3]

A significant change in baseline often indicates seal failure; this is illustrated by sensor P38 (Table 6.1.), where the baseline rose to 4.4ppm at month 10 from a normal variation of 1 to 2ppm CO equivalent. One must, however, confirm seal failure by checking for signs of corrosion on the tab terminals or on the metal securing bolts; corrosion on the counter electrode tab would result in a negative baseline deviation and vice versa. If there is corrosion on both tabs, a fortuitous balance might occur and there will be no apparent baseline shift. In general, seal failure does not inhibit sensor response although, in cases of excessively negative baselines, the sensitivity may be diminished due to increased oxygen scavenging at the sensing electrode.

One should also distinguish between an excessive baseline shift due to corrosion and between baseline hysteresis due to prolonged CO exposure at high ambient levels - for example, see sensor P50 (Table 6.1), months 12 and 13. For further details see the following section on hysteresis.

Out of the population of 63 sensors, 5 sensors have suffered seal failure with symptoms of elevated baselines and corrosion appearing on the terminals. Of these sensors, P120 (Table 6.2.) had been subjected to a temperature scan (20-40^{o}C) in month 1 and to overnight heating at 35^{o}C in month 2; failure occurred at month 13. Sensor P97 (Table 6.5.) was subjected to overnight heating at 35^{o}C. when fresh, and failure was detected at month 1. This sensor was assembled with an "O" ring compression of 35% instead of the usual 45%.

Two of the Mark 1 sensors (Table 6.1.) were also lost at month 11 due to cracking of the joint where the reservoir was sealed onto the electrode base plate.

One other sensor (P119 Table 6.6.) was lost at month 6 due to a severed Pt foil current collector.

7. PERFORMANCE PARAMETERS INFLUENCING THE CHOICE OF SENSOR CONFIGURATION FOR TRACE CO MEASUREMENT

7.1. Oxygen Reduction Activity

The correct balance of oxygen reduction activity between anode and cathode proved to be the single, most-important feature in the trace CO sensor design and had important inter-relationships with sensor characteristics such as signal stability and hysteresis, baselines, response times and hydrogen sensitivity.

In a two-electrode galvanic CO sensor, the sensing electrode controls the current whilst the counter electrode determines the operating potential. Platinum is a versatile catalyst, supporting both CO oxidation and oxygen reduction, so that if the sensing electrode polarises appreciably below its air rest potential, some of the CO signal is lost due to local cell action - See sections 2 and 4.2. It is therefore necessary to bias the oxygen activity in favour of the cathode. This can be achieved as described in section 4, either by decreasing the anode surface area using:

(a) minimal platinum loadings,

(b) low surface area powder e.g. J.M. Standard black,

(c) high electrode curing temperatures (280^{o}C.) which lowers the surface area due to partial sintering,

or by increasing the cathode surface area using:-

(a) high platinum loading

(b) high surface area platinum black, e.g. Engelhard No. 4.

/Contd.

(c) solvent extraction with isopropyl alcohol and drying at 100°C to avoid loss of surface area.

Judicious application of these measures provides a means of controlling sensor properties, for example:-

(a) Signal Stability

Because the sensors have a large activity reserve (Section 4.2.) hysteresis behaviour probably does not involve saturation of the catalyst per se. Rather, as there is a potential dependant, equilibrium oxide coverage on the electrode, cathodic polarisation during CO exposure induces an oxide reduction reaction. Sensors in which the anode/cathode surface areas are heavily biased such that the anode operates well into the current limit, where no oxygen scavanging occurs, will then exhibit a "creep-up" effect due to a temporary offsetting signal as the oxide coverage readjusts to the new potential conditions - shaded area.

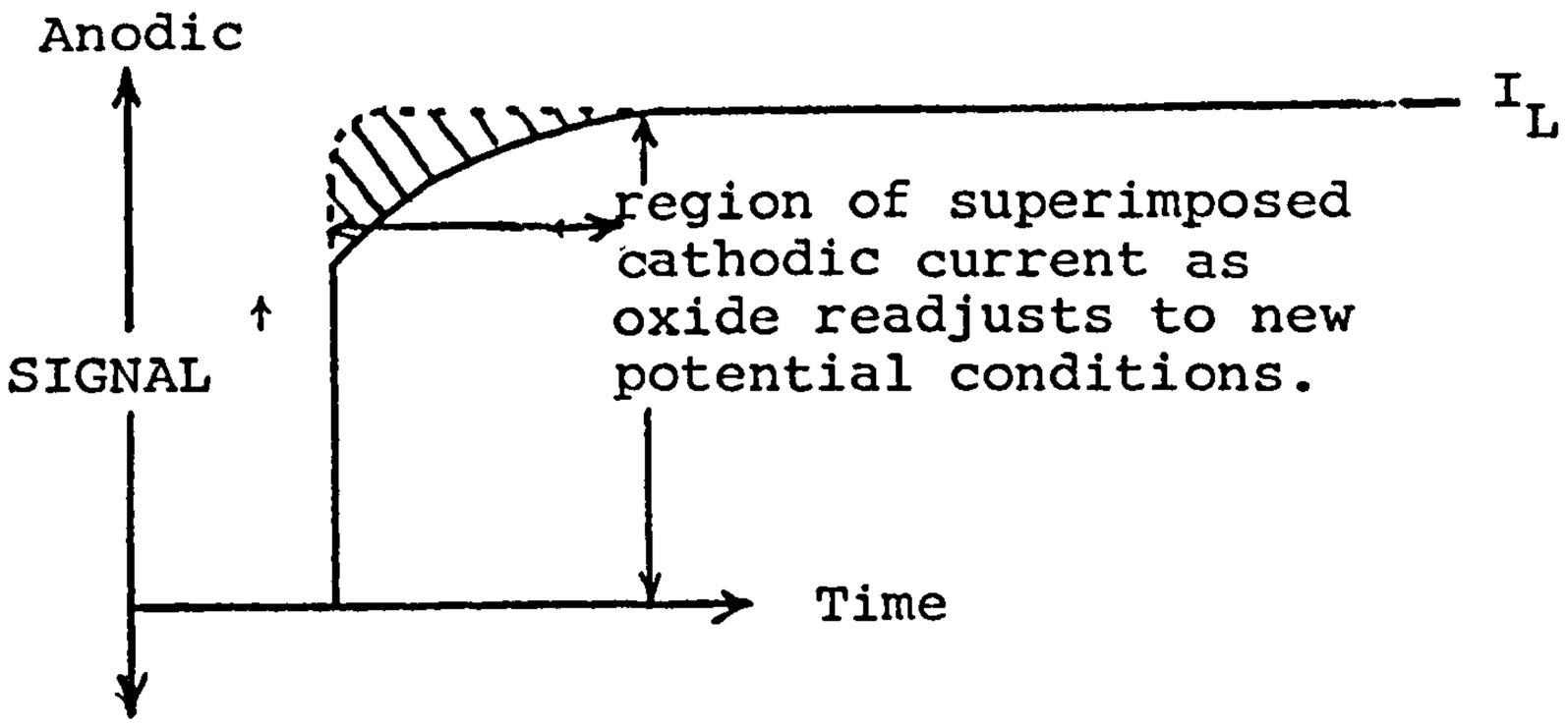

The extent of the signal loss is largely governed by the degree of polarisation and to a lesser extent by the anode loading.

If the sensor anode/cathode surface areas are only marginally biased, the signal may stray off the current limit

and further signal loss would occur due to oxygen scavanging (cross-hatched area).

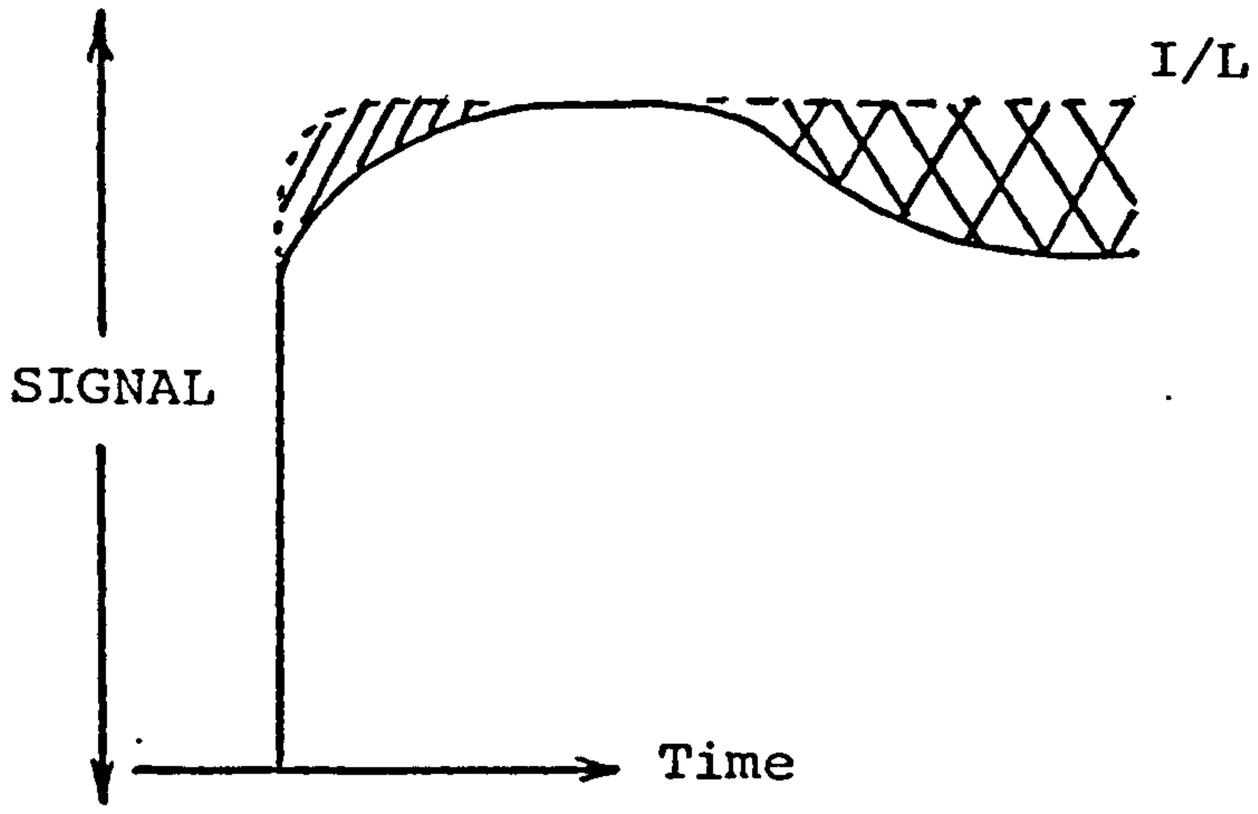

The extent of this signal decay depends not only on the degree of polarization but also on the operating potential.

(b) Baseline Hysteresis

Biasing anode/cathode oxygen activity unfortunately results in increased baselines, see Figure 7.1. and Table 7.1; these results represent the long term average, settled baselines of different sensors, monitored at ambient temperatures close to $20^{o}C$.

Baselines increased almost linearly up to a loading bias of about 10mg Pt cm^{-2}. Between 10 and 20mg cm^{-2}, baselines showed signs of levelling out, although there was a large scatter in behaviour, and no further increase was found at a 25mg cm^{-2} loading bias.

All sensors, despite large disparities in platinum morphology and loading bias, exhibited similar baseline temperature sensitivity, with an average energy of activation of 16.5 ± 2.5 kcal mol^{-1} (Table 7.1.).

Baseline hysteresis after CO exposure was the reverse of the signal effects observed during exposure, as the surface oxide underwent readjustment back to the quiescent condition.

7.2. The Mark 5 Sensor Configuration

Towards the end of this development phase, NCB/CTL jointly selected the mark 5 sensor configuration as the basic design to meet the requirements of trace CO detection. This decision was taken on the basis of the general observations noted above regarding signal stability and baselines, and some empirical data generated by NCB using an agreed regime, involving a 20 minute exposure to 200ppm CO in air and monitoring sensor recovery on removal of the test gas at the 1, 2 and 5 minute points.

The anode utilised J.M. STD. Black (4:1 Pt ptfe ratio) with Pt loadings ranging from 26 to 34 mg cm^{-2} and cured at 280^{o}C. Cathodes used Engelhard No. 4 Pt (6:1, Pt/ptfe) with loadings biased by 10mg cm^{-2} amd were also cured at 280^{o}C. Anodes were screened into four weight categories at 2mg cm^{-2} intervals and cathodes were similarly paired off with a 10mg cm^{-2} bias (Section 4.2.).

Despite the measures taken to maintain a constant loading bias, the resolution of the weight categories, plus the variation in tape weight,probably gave a range of 10 ± 3mg cm^{-2}.

A batch of 16 Mark 5 sensors were made up for further assessment by NCB; Pt loadings were individually recorded to ± 0.1mg cm^{-2} in order to assess behaviour over the likely weight bias range of 7 to 13mg Pt cm^{-2}.

Before these sensors were handed over to NCB, some systematic tests were performed by CTL, but it must be remembered that the sensors were only a week old at this stage and some inconsistency in properties could be expected.

Stability at 200ppm was measured using the agreed regime by subjecting the sensors to total exposure in a partially sealed plastic bag at ambient temperature. Signals were monitored across a fixed load of 50Ω and displayed on a flat-bed recorder. Response times were measured on 50Ω load by exposing only the capillaries, the signal again being displayed on a recorder. Results are summarised in Tables 7.2A and 7.2B.

The loading bias versus baseline plot showed wide scatter but basically bore out the earlier findings that up to 10mg cm^{-2} bias, the baseline increases linearly (Figure 7.2.).

The stability during total exposure to 200ppm CO was assessed by taking the difference in signal at the 5 and 20 minute exposure times. The plot of stability versus baseline indicated that a baseline of 3ppm CO equivalent (i.e. loading bias 10-11mg cm^{-2}) would give optimum stability (Figure 7.2.). Although the optimum baseline was higher than that proffered by YRL, the CTL analysis was based on sensors only 1 week old and when properly settled, the optimum baseline should be closer to 2ppm CO equivalent. The corresponding loading bias of 10-11mg cm^{-2} was in good agreement with that specified for the Mark 5 design.

The 80 and 90% response times both varied linearly with anode Pt weight. At 50Ω load resistance the 80% response time ranged from 20.8s at 26mg Pt cm^{-2} anode loading to 23.9s at 35mg Pt cm^{-2}. The corresponding 90% response time ranged from 29.4s to 34.4s respectively (Figure 7.3.).

Sensor response also showed a linear dependance with load resistance, with the slope and intercept of the 80% response line at 30mg Pt cm^{-2} being 0.31 sec per ohm and 8 sec respectively. The corresponding 90% values were 0.46 sec per ohm

and 10.5 sec. respectively (Figure 7.4.).

7.3. Hydrogen Response

In the past, hydrogen sensitivity has been very variable, not only from one design to the next, but also within the same sensor design (Table 7.3.).

Although the mechanism of hydrogen response is incompletely understood, several trends are apparent. Platinum in its zero valent state is an extremely active catalyst for hydrogen oxidation, which proceeds at low overpotentials of about $\sim$ 100 to 200 mv on the hydrogen scale. On the other hand, platinum operated near its open circuit potential in ambient air gives only a partial response to several hundred ppm H_2 and it is quite likely that the surface oxide at these potentials in some way passively obscures, or more likely actively inhibits, the reaction. One would therefore expect hydrogen sensitivity to be potential dependent, decreasing in some fashion as counter electrode loading, and hence potential, increases. Also, since the hydrogen response is not capillary - controlled, it must also be sensitive to anode loading.

It is possible to partially de-convolute the cathode effect by plotting the product of the hydrogen sensitivity and the cathode loading versus the anode loading (Figure 7.5. and Table 7.4.). Although there was some scatter, plus the odd rogue point, generally the hydrogen sensitivity increased linearly with anode loading up to $\sim$ 30mg Pt cm^{-2}. Above 30mg cm^{-2} there was no apparent dependance on loading.

Similarly, expressing the hydrogen sensitivity in terms of unit anode platinum loading, it was found to decrease reasonably systematically with increasing cathode weight as shown in Figure 7.6. (circled points), albeit with a few rogue points and high scatter above 40mg cm^{-2} cathode loading. At 40mg cm^{-2} cathode loading, the anode loading would be about 30mg cm^{-2}, the point beyond which the hydrogen sensitivity became independant of anode loading. If hydrogen sensitivities on sensors with anode loadings above 30mg cm^{-2} were divided by 30mg cm^{-2} instead of the actual anode loading, then a more consistent plot was obtained for the cathode loading effect (Figure 7.6., crossed points).

The good agreement of these plots suggests that there is indeed a trend with potential and with anode loading. However, the odd points which obviously did not conform indicate that other factors operate which have yet to be defined. As far as hydrogen sensitivity is concerned however, one would like to boost the cathode oxygen reduction performance as much as possible, whilst working with a minimum anode loading. Indeed, sensors recently constructed in this way have shown considerably decreased H_2 sensitivities of about 0.1ppm CO equivalent per ppm H_2.

8. ALTERNATIVE DESIGN OPTIONS TO MARK 5

8.1. Two-Electrode Sensors

Since the NCB/CTL meeting on 22nd May, 1981 we have further clarified our understanding of the factors governing two electrode sensor behaviour, (see discussion in Section 2). In addition we have further empirical results on a wider range of "activity biased" sensors.

At the time of the meeting the highly-biased sensors that had been tested suffered from two alternative disadvantages as well as increased baseline. The first attempts to bias well into the limiting current region used ultra-low loading anodes (10 mg Pt cm^{-2}) in conjunction with high activity cathodes. These sensors showed unnaturally high signal decay with time, which was attributed to the very low loading anode. An increase in anode loading to offset decay was, at the time, also accompanied by a decrease in cathode activity and it was this type of sensor that showed the "creep up" behaviour.

It now seems clear that these two problems can be avoided with an intermediate anode loading, coupled with the best activity cathode. While there would still be the problem of a higher baseline (2 to 3ppm equivalent at $20^{o}C$ as compared to 1 to 2ppm for Mark 5), there are other significant advantages. It therefore seems worthwhile to review these.

With operation at the full limiting current, as opposed to about $\frac{2}{3}$ with Mark 5:

(a) for the same sensitivity, the capillary diameter can be reduced accordingly with a consequent reduction of 33% in water transfer rates and any catalyst poison ingress. The outer silicone rubber sleeve holes, which were uncomfortably large for Mark 5, can also be reduced.

(b) The anode loading can also be reduced in proportion while maintaining the same activity reserve. Since this also drops the anode OCV, it further alleviates the pressure on cathode performance. Proposed anode loading would be $\sim$ 18 mg/cm^2 compared to $\sim$ 30 mg/cm^2 for Mark 5 and $\sim$ 10 mg/cm^2 for Mark 4.

(c) In principle one would expect better long term stability from full limiting current operation. But it must be stated that the fractional limiting current sensors have shown excellent long term stability anyway. However there would certainly be less signal scatter between sensors.

(d) Manufacture is much simpler than Mark 5, since close electrode matching is not required.

The performance advantages are:

(a) The upper CO tolerance range is extended from the nominal 200ppm of Mark 5, to 500ppm (20 minute exposure tests).

(b) Hydrogen interference is significantly reduced, e.g. from about 1:4 for Mark 5, to about 1:10.

In view of these advantages we feel that it is worthwhile considering whether a better overall monitor could not be achieved by accepting the higher baseline and compensating for its high temperature coefficient electronically. The temperature

response is reasonably constant between sensors. The response is exponential with an empirically calculated activation energy of 16.5 ± 2.5 kcal $mole^{-1}$. The most obvious approach would be to include the temperature compensation in off-set zero circuitry.

8.2. Three-Electrode Sensors

As can be seen from section 2, the various hysteresis problems found with 2 electrode sensors derive primarily from the voltage swing resulting from significant cathode polarisation.

A three electrode sensor includes a third, reference, electrode from which negligible current is drawn. In principle, operation with a potentiostatic circuit enables the potential of the sensing electrode to be held at any desired potential with respect to the reference electrode, quite independantly of the potential of the counter electrode as this changes with polarisation.

For patent reasons one cannot operate the sensing electrode at a fixed potential without running the risk of infringing the Energetics Science Patents e.g. G.B. 1,372,245.

However, we have recently discovered that by following an earlier, now lapsed, Patent, GB 1,101,101, one can achieve something very close to the desired effect. The basic circuit is shown in Figure 8.1.

The potential across the sensing electrode plus load resistor R_L is held constant, i.e. between points A and B in Figure 8.1. The signal is taken across R_L. In principle

this potential can be set to any desired value if a reference voltage is included in the circuit, but we recommend that it is held at zero volts, which would be achieved by the circuit shown.

When the sensing electrode is exposed to CO its potential will in fact drop by an amount ΔV, equal to iR_L, where i is the current generated. The change in potential ΔV is effectively used as the measure of concentration.

The swing in electrode potential will, however, be considerably less than occurring in two electrode sensors, e.g. about $\frac{1}{50}$ with a 100 ohm load resistor and about $\frac{1}{100}$ th with a 50 ohm load resistor, and hysteresis effects will be reduced accordingly.

It has previously been the practice to operate three electrode sensors with the sensing electrode held well above its OCV, e.g. 100 to 200mV anodic. While this does help in giving a lower hydrogen sensitivity, it also results in the disadvantages of high baselines and very long settling times after switching on the control circuit. To avoid these disadvantages we propose to control at zero volts, i.e. nominally around the OCV of the sensing electrode. In this case baselines should be similar to those found in our two electrode sensors and, by matching the sensing and reference electrodes, they can in principle be very low. In addition one can short out the reference and sensing electrodes when not in use to help maintain stability and keep start up times to a minimum.

The main advantage of the 3 electrode sensor is the tolerance to very much higher CO concentrations without hysteresis effects being evident. A few initial tests have shown promising results.

The higher complexity of sensor manufacture is offset by the need to take less care in selecting and manufacturing the electrodes, particularly with the cathode.

One potential problem with operating 3 electrode sensors in the diffusion mode is that the reference electrode will "see" the atmosphere under test and its potential will change with CO concentration. The consequences of this need to be checke out in practice.

Again one can envisage the possibility of longer term effects, if the reference electrode potential drifts with time relative to the sensing electrode OCV (CO-free air potential).

The three electrode sensor obviously requires slightly more complicated circuitry, but more to the point is that each sensor must have its separate control circuit. Two electrode sensors therefore have an advantage for multipoint installations.

These are the main obvious considerations concerning the three electrode sensor option. A more detailed and definite comparison can be made, when more testing has been done in the next phase of the programme.

We feel that there will always be a place for both two and three electrode versions depending on the applications, but with the three electrode sensor offering more hope for a single sensor to cover a wide range of concentrations, we would suggest that instrument circuitry is designed to be able to take either two or three electrode sensors, leaving the option open to switch from one to the other at any time.

REFERENCES

(1) A.D.S. Tantram, R. Chan-Henry, B.S. Hobbs; Phase 1 report to NCB Contract Y135007/09/21, CTL Report 79/31/002 (September 1979).

(2) A.D.S. Tantram, R. Chan-Henry, B.S. Hobbs, J.R. Finbow; "Oxygen Detector for Use in Coal Mines", NCB Contract YB 1350/09/22, CTL Report 78/02/001 (July 1978).

(3) A.D.S. Tantram, R. Chan-Henry, B.S. Hobbs; Phase 2 Report to NCB Contract Y135007/09/21, CTL Report 80/31/003.

(4) J.P. Hoare; "The Electrochemistry of Oxygen", Interscience, New York (1968).

Table 4.1. Open Electrode Test Data for Thin Tape Gore Electrodes

Fabricn. Method (All electrodes made with J.M. Black)	Curing Temp. (°C)	Platinum Loading (mg cm^{-2})	Net CO-oxidation limiting current on π cm^2 electrode, above air R.P., on 97.3 ppm CO in air test gas (μA)	CO-oxidation Response (μA/ppm/mgPt)	O_2-reduction current in air at 0.900 volts vs DHE. (μA)	O_2-reduction Response (μA/mgPt)
Sol. Ext.	100	7.5	93	0.041	-690	-29.3
Spray	300	7.6	100	0.043	-3	-0.4
Spray	280	7.7	96	0.041	-26	-3.4
Drop	300*	8.2	75	0.030	-37	-4.5
Spray	280	8.8	132	0.049	-80	-9.1
Drop	280	9.0	98	0.036	-36	-4.0
Drop	300	10.8	117	0.035	-44	-4.1
Spray	300	16.9	178	0.034	-70	-4.1
Drop	300	35.0	378	0.035		
Drop	300	35.0	432	0.040		
Gore thin tape current limit from diffusibility measurements [3]			1127		4712×10^3	

* Platinum Black preannealed at 450°C. before use.

Table 4.2. Air Rest Potentials of Platinum Electrodes

All potentials measured following an overnight contact with electrolyte (10N H_2SO_4), against a dynamic hydrogen reference electrode, at an ambient room temperature of about 20°C.

Electrodes ranked in order of increasing electrocatalytic activity.

Platinum Grade	Electrode Curing temperature (°C)	Pt. loading (mg/cm^2)	Air Rest Potential (Volts vs D.H.E.)
Johnson Matthey Standard	280	2.3	0.932
"	"	4.5	0.961
"	"	8.2	0.973
"	"	12.0	0.992
"	"	31.2	1.072
Engelhard 4	280	3.2	0.957
"	"	10.0	0.980
"	"	11.0	0.983
"	100 (Solvent Extracted)	22.3	1.086

TABLE 4.3. COMPARISON OF PROPERTIES OF CTL TRACE CO SENSORS DEVELOPED FOR NCB

MARK No.		I	II	III	IV	V	VI
SENSING ELECTRODE	Pt GRADE	Johnson Matthey Platinum Black					
		Fuel Cell Grade		Standard Black Grade			
	COMPOSITION	4:1 Platinum to ptfe Ratio					
	Pt LOADING (mg cm^{-2})	∿ 30	∿ 30	∿ 35	∿ 10	26-34	26-34
COUNTER ELECTRODE	Pt GRADE	J.M. Fuel Cell Grade Black Cured 280°C		J.M. Std Black Cured 280°C	Engelhard '4' Pt		J.M. Std. Black Cured 280°C
					Solvent Extract Dried 100°C	Cured 280°C	
	COMPOSITION	4:1 Platinum to Ptfe Ratio			6:1	6:1	4:1
	Pt LOADING (mg cm^{-2})	∿ 30	∿ 30	∿ 40	∿ 25	36-44	36-44
NOMINAL SENSITIVITY		0.1μA per ppm CO					
FRACT. CURRENT LIMIT		∿ 0.5 I_L			I_L	∿ 0.7I_L	∿ 0.6I_L
NO. CAPILLARY HOLES		9	9	9	5	5	5
SPAN TEMPERATURE COMPENSATION		NONE				YES	YES
GAS DISTRIBUTION OVER SENSING ELECTRODE		Woven Ni Mesh	Webril	Webril	Cavity 17mm Dia. 1mm Deep		Cavity 19mm Dia. 2.5mm Deep
AVERAGE BASELINE @ 20°C (μA)	FIRST MONTH	0.02 to 0.08			0.25 ± 0.07	0.11 ± 0.10	0.17 ± 0.06
	SETTLED VALUE	0.02-0.08		0.02-0.08	0.16 ± 0.07		
	AT MTH. NO.	10		16	7		
H_2 SENSITIVITY. ppm CO equiv. per ppm H_2, using 100 ppm H_2 in air.		0.5 - 0.8		0.3-0.6	0.12	0.39 ± 0.16	0.18 ± 0.12
UPPER CO-TOLERANCE LIMIT (ppm CO)		200-500		∿ 100	400-500	∿ 200	∿ 100
RESPONSE TIME ON 100Ω LOAD(S)	80%	∿ 80		20-25	13.5 ± 2	22.3 ± 2	
	90%	∿ 150		30-35	20.2 ± 3	33.6 ± 5	

Table 5.1. Performance characteristics of Mark 6 sensors with varying electrolyte volumes.

Sensor	T19	T20	T21	T22	T23	T24
Electrolyte Volume (cm^3)	1.0	0.9	0.8	0.7	0.6	0.5
Anode Loading (mg Pt cm^{-3})	27	27	29	31	31	27
Cathode Loading (mg Pt cm^{-3})	37	37	39	41	41	37
80% Response time (s)	19.5	22.0	24.5	22.0	23.4	40.8
90% Response time (s)	28.0	32.2	39.0	32.2	35.6	76.8
Average baseline @ 20^{o}C(ppm)	0.6	1.0	0.9	0.6	0.9	2.6
Span stability (%)	98.6	93.9	102.0	98.8	100.0	79.5

Table 6.1. Span sensitivity and baselines of Mark 1 and 2 sensors as a function of age. 'H' denotes 35°C., overnight heat cycle. All cathodes J.M. Fuel Cell Grade Pt, cured 280°C.

Sensor	Pt loading mg cm^{-2}		Initial S µA/ppm	Sensitivity(S) as % init. value & Baseline(B) in ppm CO equiv. vs Age(A) in mths.																				
	Anode	C/Ode		A	1	2	3	4	5	6	7	8	9	10	11	12	13	14	15	16	17	18	19	20
P38	21	23	0.129	S		96	95	96	96	95	96	98	98	97	X		CORROSION ON TERMINALS							
	8 cm^3	H_2SO_4	-	B		-2.4	0.9	0	1.8	1.4	1.1	1.1	0.6	4.4										
p48	22	22	0.110	S		96	95	94	100	93	92	92		96	O		RESERVOIR CRACKED							
	8 cm^3	H_2SO_4	-2.9	B		-2.6	-1.5	-1.5	-0.2	-1.5	-0.9	-0.8	0	0.3										
p50	22	22	0.124	S	97	83	84	84	81	82	83	82	84	86	83	82	83	86		84	86	88	89	87
	8cm^3	H_2SO_4	1.0	B	-0.5	-1.0	-0.7	-0.8	0	0.2	0.1	0.2	0	0.2	0.8	3.0	3.9	0.3		.12	0.7	0.9	0.5	1.1
P82	23	22	0.086	S	98	3H 98	98	97	96	101	98	102	93	101	102	99	99		97	100	107	102	102	
	8cm^3	H_2SO_4	0.0	B	0.5	0	0	0.1	0	0	0.1	0	0.2	0.5	0.5	0.5	0.5		0.7	0.2	0.5	0	0.5	
SP 46	22	23	0.136	S												86	83	87	86		86	89	89	88
	8cm^3	H_2SO_4	-7.4	B												0.9		1.6	2.1		2.7	2.6	2.1	2.0
p47	23	23	0.122	S		96	95	93	94	94	93	97	96	97	99	98	92	99	100		97	103	102	101
	8cm^3	H_2SO_4	2.4	B		-0.9	-0.9	-0.9	-1.1	-1.8	-0.1	-0.1	0	0	0	1.0	-2.4	1.2	1.4		2.6	1.3	1.5	1.6
.P48	22	17	0.093	S		93	91	90	93	86	87	89	90	89	O		RESERVOIR CRACKED							
	8cm^3	H_2SO_4	-7.4	B		-2.9	-1.7	-1.7	-2.2	-2.4	-1.5	-1.7	-1.4	1.2										
P96 Mark 2	23	23	0.088	S	110	112	108	108	112	112	113	113	112	114	X		CORROSION ON TERMINALS							
	8cm^3	H_2SO_4	1.0	B	1.1	0.6	1.6	0.6	0.6	0.7	0	0.7	0.8	0.6										

Table 6.2. Span sensitivity and baselines of Mark 3 sensors as a fraction of age
H denotes 35°C., overnight heat cycle. α denotes temp. scan 0 to 40°C.
Cathodes J.M. Standard, cured 280°C.

Sensor	Pt loading mg cm^{-2}		Initial S µA/ppm	Sensitivity(S) as % init. value & Baseline(B) in ppm CO equiv. vs Age(A) in mths.																			
	Anode	C/Ode		A	1	2	3	4	5	6	7	8	9	10	11	12	13	14	15	16	17	18	19	20
P120	30	36	0.106	S	α 97	H 91	90	95	94	93	95	93	93	95	95		91	X	CORROSION ON TERMINALS					
	$5cm^3$ H_2SO_4		2.0	B	0.5	0.8	0.9	0.6	0	1.0	0.7	0.8	5.0	2.0	2.5		5.5							
P124	29	28	0.106	S	96	94	93	95	96	96	97	95	95	95	96		93	92	97	95	94			
	$5cm^3$ H_2SO_4		1.7	B	H 0.8	0.3	0.7	0.8	0.5	0.3	0.7	0.8	0.9	0.4	0.3		1.1	1.0	0.9	0.5	0.8			
P126	30	29	0.104	S	H 85	79	77	79	84	83	86	83	86	82	78		77		81	83	83			
			4.9	B	2.3	1.5	2.0	1.8	1.3	1.0	0.3	1.4	2.1	0.6	1.7		1.6		1.1	0.7	0.2			
P1	31	31	0.108	S	97	93	92	96	96	95	97	95	95	95	95		92	93	95	94	94			
	$3cm^3$ H_2SO_4		0.0	B	0.8	0.3	0.7	0.4	0.5	0.2	0.4	0.9	1.3	0.4	0.4		1.1	1.1	0.8	0.6	0.4			
P23	33	28	0.094	S	95	95	98	99	100	101	99	98	98	96		95	94	98	96	98				
			3.0	B	0.8	0.8	0.9	0.8	1.5	0.8	0.9	0.9	0.6	0.9		1.2	1.2	1.0	0.8	0.5			
P25	31	30	0.102	S	95	92		91	96	X	CORROSION ON TERMINALS													
			3.1	B	0.5	0.6		-8.0	12.9															
P3	30	29	0.104	S	92	91	95	94	95	96	94	94	94	92		90	91	93	92	95				
	1m Molar CrO_3		0.6	B	0.7	0.6	0.4	0.3	0.5	0.4	0.6	0.9	0.3	0.5		1.0	1.0	0.9	0.7	0.8				
P5	32	31	0.104	S	93	93	96	95	95	98	97	88	94			92	91	94	94	94				
	5M Molar CrO_3		1.0	B	0.9	0.6	0.8	0.4	0	0.4	-2.1	0.4	0			0.9	1.5	0.8	0.6	0.5				

Table 6.3. Span sensitivity and baselines of Mark 3 sensors as a function of age.
'H' denotes 35°C, overnight heat cycle. All cathodes J.M. Standard, cured 280°C.
'α' denotes temp. scan 0 to 40°C.

Sensor	Pt loading mg cm^{-2}		Initial	Sensitivity(S) as % init. value & Baseline(B) in ppm CO equiv. vs Age(A) in mths.																				
	Anode	C/Ode	S µA/ppm	A	1	2	3	4	5	6	7	8	9	10	11	12	13	14	15	16	17	18	19	20
P7	34	34	0.107	S	α 93	91	H 97	97	98	96	†		WITHDRAWN - EXPTL.											
	20m M CrO_3		0.2	B	0.6	0.3	0.6	0.6	0.7	0.2														
P9	35	34	0.106	S	93	92	95	95	95	96	95	95	94	92		92	91	95	95	94				
	10m M	$KMnO_4$	1.2	B	0.8	0.6	0.6	0.6	0.6	0.7	0.8	1.1	0.3	0.7		1.1	1.1	1.2	0.9	1.5				
P19	30	34	0.099	S	100	97	103	103	103	105	104	105	102	100		99	98	102	100	101				
	10m M	$KMnO_4$	6.3	B	1.0	1.2	0.8	0.7	1.4	0.6	1.0	1.4	0.8	0.7		0.9	1.1	1.1	0.8	1.3				
P27	33	31	0.088	S	107	85	85	91	90	92	90	86	86	79		82	78	85	85	86				
	100mM 20mM	CrO_3 $Cr_2(SO_4)_3$	2.8	B	0.7	1.0	0.8	0.6	0.9	0.4	0.5	0.9	0.5	0.4		0.7	1.0	0.5	0.3	0.4				
P29	32	30	0.087	S	98	81	80	85	84	87	85	83	82	78		79	74	83	80	85				
	100m M	CrO_3	-1.1	B	0.4	0.3	0	0	0	0	0	0	0	0		0	0	0	0	-0.1				
P31	42	46	0.087	S	90	89	91	94	102	95	93	93	91				87	92	90	93				
	20mM	CrO_3	1.0	B	0.9	0.9	0.9	0.6	0.7	0.2	0	0.2	0.4				1.1	0.6	0.5	0.2				
P33	40	34	0.098	S	89	96	98																	
	20mM	CrO_3	1.4	B	0.3	0.6	0.4	†	WITHDRAWN - EXPTL.															
P35	39	43	0.100	S	99	103	106	108	108	107	108	107	107	105		105	104	109	106	109				
	20mM	CrO_3	1.8	B	0.8	0.6	0.7	0.6	0.9	0.4	0.4	0.6	0	1.0		1.0	1.6	0.6	1.1	0				

Table 6.4. Span sensitivity and baselines of Mark 4 sensors as a function of age
'H' denotes 35°C., overnight heat cycle. Cathodes Engelhard Pt, Solvent extracted, dried 100°C

Sensor	Pt loading mg cm^{-2}		Initial	Sensitivity(S) as % init. value & Baseline(B) in ppm CO equiv. vs Age(A) in mths.																		
	Anode	C/Ode	S µA/ppm	A	1	2	3	4	5	6	7	8	9	10	11	12	13	14	15	16	17	18	19	20
P109	5	14	0.092	S	H 91	88	80	73		71	58	73	68	64										
			1.5	B	1.6	1.6	1.9	1.9		1.8	2.6	1.3	1.3	2.0										
P111	5	27	0.085	S	95	92	87	79		77	66	76	74	71										
			2.0	B	2.2	1.8	2.0	2.4		2.3	3.7	1.7	1.3	2.6										
P113	8	42	0.096	S	103	101	97	91		87	76	88	84	81										
			2.4	B	2.1	1.5	1.6	1.9		1.8	3.3	1.7	1.5	1.8										
P115	8	40	0.106	S	96	94	86	83		80	72	81	80	77										
			1.8	B	1.8	1.7	1.6	2.2		1.8	2.6	1.3	1.2	1.1										
P117	7	36	0.090	S	96	95	86	84		81	73	82	78	76										
			1.8	B	1.0	1.6	1.5	1.8		2.1	2.7	2.3	1.2	1.4										
P1	6	42	0.096	S	97	94	89	85		82	83	96	79	78										
			3.7	B	2.0	1.8	1.8	1.7		1.8	2.0	1.1	1.2	1.5										
P3	14	27 J.M.Fuel Cell Pt	0.104	S	97	96	91	90		88	81	90	84	84										
			1.9	B	1.9	1.5	1.8	1.8		2.0	3.0	1.5	1.3	2.0										
P5	15	28 J.M.Fuel Cell Pt	0.117	S	97	96	88	87		86	80	90	85	85										
			2.4	B	2.2	2.1	2.3	2.6		2.4	2.9	1.6	1.5	1.8										

Table 6.5. Span sensitivity and baselines of Mark 4 cavity sensors as a function of age. H denotes 35°C. overnight heat cycle. All sensors with 16.5mm dia x 0.75mm deep cavities. Cathodes, Engelhard Pt, solvent extracted, dried 100°C

Senser	Pt loading mg cm^{-2}		Initial	Sensitivity(S) as % init. value & Baseline(B) in ppm CO equiv. vs Age(A) in mths																				
	Anode	C/Ode	S µA/ppm	A	1	2	3	4	5	6	7	8	9	10	11	12	13	14	15	16	17	18	19	20
P91	6	33	0.175	S	H 98	97		97	88	95	89	86												
			1.5	B	1.1	0.9		0.7	0.7	0.5	0.7	0.4												
P93	6	31	0.169	S	H 98	97		93	88	96	92	86												
			1.1	B																				
P95	10	22	0.155	S	H 97	89		79	69	†		WITHDRAWN - EXPTL.												
			2.2	B	2.0	1.7		1.9	2.2															
P97	11	23	0.163	S	H 97	X		CORROSION ON TERMINALS																
			1.8	B	2.2																			
P99	12	24	0.162	S	H 86	81		68	61	65	60	58												
			2.0	B	2.6	1.6		2.1	2.6	1.5	1.7	0.5												
P101	12	25	0.195	S	H 93	87		79	72	77	74	72												
			1.4	B	1.7	1.4		1.9	2.1	1.1	1.4	1.1												
P103	13	23	0.173	S	H 93	90		78	69	76	72	71												
			2.3	B	3.4	1.7		2.5	2.7	1.3	1.5	1.5												
P105	12	27	0.129	S	H 94	82		65	61	67	63	81												
			4.6	B	-0.2	0.2		2.0	2.3	1.0	1.2	0.7												

Table 6.6. Span sensitivity and baselines of Mark 4 sensors as a function of age.
Cathodes: Engelhard (E) and J.M. Standard (SB), solvent extracted (s), drop method (D)

Sensor	Pt loading mg cm^{-2}		Initial S µA/ppm	Sensitivity(S) as % init. value & Baseline(B) in ppm CO equiv. vs Age(A) in mths.																			
	Anode	C/Ode		A	1	2	3	4	5	6	7	8	9	10	11	12	13	14	15	16	17	18	19	20
P107	14	33	0.111	S	101	100		93	87	95	92	92												
	(SB)	D/280°C	1.0	B	0.3	0.5		0.7	0.8	0.3	0.6	0.6												
P113	16	17	0.117	S	122	126		115	104	115	109	105												
	(E)	S/100°C	5.6	B	2.3	2.2		3.7	2.5	1.5	1.5	1.8												
P117	16	23	0.109	S	97	98		91	82	73	70	64												
	(SB)	S/100°C	3.6	B	3.5	3.3		4.6	5.1	10.5	8.4	2.2												
P119	14	24	0.133	S	101	99		92	88	▽	SEVERED Pt FOIL CURRENT COLLECTOR													
	(E)	D/280°C	5.3	B	0.7	0.8		1.8	1.3															
P121	5	25	0.043	S	149	159		127	113	153	143	133												
	(E)	D/280°C	2.6	B	1.2	1.3		4.8	2.3	1.2	1.5	1.6												
P123	10	26	0.161	S	97	96		82	77	87	82	83												
	(E)	D/280°C	0.7	B	0.4	0.5		1.8	1.2	0.9	0.9	0.8												
P125	14	48	0.141	S	117	122		114	96	120	116	115												
	(E)	D/280°C	8.5	B	1.2	1.1		2.9	1.6	0.9	0.9	0.8												
P127	15	34	0.139	S	92	89		83	72	78	73	73												
	(SB)	mix D/S	-	B																				

Table 6.7. Span sensitivity and baselines of Mark 4 sensors as a function of age.
Cathodes: All Engelhard Pt., solvent extracted and heated @ indicated temps.

Sensor	Pt loading mg cm^{-2}		Initial S µA/ppm	Sensitivity(S) as % init. value & Baseline(B) in ppm CO equiv. vs Age(A) in mths.																				
	Anode	C/Ode		A	1	2	3	4	5	6	7	.8	9	10	11	12	13	14	15	16	17	18	19	20
C23	10	22	0.166	S	112		76	74	69	61	60													
		230°C	1.1	B	0.8		1.3	2.0	3.9	2.9	1.5													
C27	10	21	0.163	S			79	74	69	62	62													
		200°C	1.0	B			5.0	3.1	4.8	2.4	-0.4													
C41	16	25	0.131	S	96	98	97	96	92	92														
		230°C	2.0	B	1.9	1.9	1.3	1.7	0.8	1.2														
C45	26	48	0.172	S	112	100	100	101	98	99														
		230°C	0.5	B	0.9	2.0	1.1	1.3	1.0	1.2														
C47	21	50	0.153	S	102	100	99	99	93	95														
		100°C	3.9	B	2.8	2.4	1.8	1.7	2.5	2.1														
C49	20	52	0.121	S	98	94	94	92	91	91														
		230°C	3.3	B	1.6	2.9	1.8	1.6	1.5	1.5														
C51	31	37	0.102	S	100	96	95	96	99	92														
		230°C	2.9	B	2.9	3.1	2.1	1.7	1.8	1.4														

Table 6.8. Span sensitivity and baselines of Mark 5 sensors as a function of age.
Cathodes: Engelhard Pt., solvent extracted, dried 230°C. (N.B. equal cathode and anode loadings this series)

Sensor	Pt loading mg cm^{-2}		Initial	Sensitivity(S) as % init. value & Baseline(B) in ppm CO equiv. vs Age(A) in mths.																			
	Anode	C/Ode	S µA/ppm	A	1	2	3	4	5	6	7	8	9	10	11	12	13	14	15	16	17	18	19	20
T1	32	32	0.092	S	100	100	98	99																
			2.2	B	2.9	2.9	4.0	4.7																
T2	29	29	0.094	S	100	100	97	98																
			2.7	B	2.2	2.3	2.5	2.4																
T3	33	33	0.097	S	98	98		97																
			2.8	B	2.5	2.3		2.8																
T4	31	31	0.097	S	98	98	95	97																
			1.9	B	2.0	2.5	3.5	4.2																
T5	33	33	0.096	S	102	104	102	105																
			0.9	B	0.9	1.6	1.7	2.0																
T6	33	33	0.074	S	99	101	96	99																
			0.0	B	1.6	2.0	2.0	2.2																
T8	32	32	0.086	S	100	100	100	97																
			1.0	B	1.6	2.2	4.6	4.9																
T9	30	30	0.086	S	93	103	98	100																
			-0.7	B	0.1	0.8	1.9	1.2																

Table 7.1. Baseline measurements on various sensor types

SENSOR	Data from log(baseline) vs T^{-1} plot		Platinum Loadings ($mg\ cm^{-2}$)		Loading difference between anode and cathode	Mean baseline current near 20°C (μA)
	Activation Energy ($kcal\ mole^{-1}$)	Linear Correlation Coefficient	Anode	Cathode		
Mark 3						
P7(Cr)	19.0	1.00	34	34	0	0-0.05
P120	15.0	0.99	30	36	6	0.05-0.1C
MEAN	17.0 ± 2.0					
Mark 4						
P7(IV)	16.0	1.00	12.0	28.1	16.1	0.10-0.15
P13	12.6*	1.00	10.6	23.0	12.4	-
P109	16.8	0.99	5.0	14.0	9.0	0.10-0.15
P27	15.1	1.00	9.0	25.8	16.8	-
P25	15.2	1.00	8.7	25.4	16.7	0.10-0.15
P77	13.6	0.99	9.4	23.8	14.4	0.15-0.20
P73	26.0*	0.99	9.2	26.0	16.8	0.20-0.25
P75	16.6	1.00	9.3	23.8	14.5	0.20-0.25
P81	18.1	1.00	7.8	26.1	18.3	-
P85	18.1	1.00	15.9	21.7	5.8	-
P103	18.0	1.00	13.0	23.0	10.0	0.20-0.35
MEAN (*culled)	16.4 ± 2.5					
Mark 5						
T48	16.3	0.917	32.5	43.6	11.1	0.15-0.2C
T51	14.0	0.986	32.6	41.0	8.4	0.15-0.2C
MEAN	15.2 ± 1.2					
Mark 6						
T9	15.6	0.99	33.0	43.0	10.0	0.10-0.15
T19	16.5	0.973	27.0	37.0	10.0	0.10-0.15
MEAN	16.0 ± 0.5					

Table 7.2A. Electrode loadings, response times and baselines of batch of 16 Mark 5 sensors made for NCB.

Sensor	Platinum Loadings (mg cm^{-2})		Weight Difference (mg cm^{-2})	Response Times (s) 50Ω load resistor		Initial baseline (μA)
	Anode	Cathode		80%	90%	
T53	25.8	37.8	12.0	22.2	31.7	
T54	27.4	37.0	9.6	21.0	29.0	0.10
T55	27.8	35.8	8.0	21.3	30.5	
T56	28.6	39.1	10.2	23.0	31.8	0.09
T57	29.2	38.6	9.4	21.0	29.2	
T58	29.5	38.5	9.0	20.5	29.0	
T59	29.7	38.0	8.3	22.5	31.0	
T60	29.9	40.5	10.6	23.3	32.0	
T61	31.1	41.1	10.0	24.2	34.2	0.134
T62	31.9	40.3	8.4	22.0	30.0	
T63	32.2	44.3	12.1	22.6	32.6	0.316
T64	32.3	43.9	11.6	23.5	34.0	
T65	32.8	43.7	10.9			0.168
T66	33.2	43.2	10.0			0.380
T67	34.9	42.9	8.0	23.3	34.7	0.414
T68	34.9	42.0	7.1	23.7	34.2	0.110

Table 7.2B CO-tolerance on 20 minute exposure to 200 ppm CO in air of Mark 5 Sensors made for NCB

* CO-sensitivity based on max$^{m}_{-}$. CO current during 20 min. exposure

Sensor	CO-exposure Net i_{co} (μA)			CO-sensitivity* (μA ppm^{-1})	Stability (ppm) $\left(\frac{i_{co}^{20} - i_{co}^{5}}{\text{CO sensitivity}}\right)$	Recovery Baseline hysteresis (ppm)			
	5 min	10 min	20min			1 min	2 min	5 min	10 min
T54	20.26	20.10	19.50	0.101	-7.5	2.8	-1.2	-2.8	-2.9
T56	19.60	19.52	19.20	0.098	-4.1	6.4	0.7	-1.2	-1.4
T61	19.10	18.91	18.51	0.096	-6.1	11.5	1.5	-0.6	-0.8
T63	17.28	17.28	17.28	0.086	0	10.7	6.1	3.5	2.8
T65	20.35	20.31	19.99	0.102	-3.5	7.8	1.5	-0.8	-1.2
T66	22.94	22.98	23.02	0.115	0.7	12.8	7.4	5.1	4.1
T67	21.11	21.27	21.47	0.107	3.4	15.6	8.5	4.9	3.4
T68	21.01	20.85	20.37	0.105	-6.1	9.6	1.1	-1.3	-1.9

Table 7.3 Hydrogen sensitivities of various sensors exposed to 106 ppm H_2 in air

Sensor	Age (weeks)	H_2 sensitivity / CO sensitivity	Age (weeks)	H_2 sensitivity / CO sensitivity
Mark 3				
P1	2	0.41	29	0.25
P3	1	0.43	28	0.27
P7	2	0.43	28	0.42
P83	1	0.41	15	0.31
P89			14	0.19
P91			13	0.24
P95	1	0.20	12	0.13
Mark 4				
P113	2	0.08	8	0.06
P115	2	0.11	8	0.09
P117	2	0.12	8	0.11
P95	2	0.04		
P99	2	0.02		
P101	2	0.08		
P103	2	0.07		

Table 7.4. Electrode compositions and hydrogen sensitivities of Mark 5 sensors

Sensor	H_2 sensitivity / CO sensitivity	Electrode loadings (mg cm^{-2})		H_2 sensitivity ($\mu A\ ppm^{-1}$) @ 106 ppm H_2	H_2 sensitivity x cathode loading	H_2 sensitivity / Anode loading x 10^3
		Anode	Cathode			
T35	0.18	28.0	39.8	0.0194	0.772	0.693
T36	0.20	28.5	39.6	0.0195	0.772	0.684
T37	0.20	28.8	39.2	0.0212	0.831	0.736
T38	0.22	29.0	38.9	0.0212	0.825	0.731
T39	0.24	29.1	38.6	0.0231	0.892	0.794
T40	0.17	29.5	38.3	0.0163	0.624	0.553
T41	0.26	29.7	38.2	0.0251	0.959	0.845
T42	0.22	29.5	42.6	0.0218	0.929	0.739 (0.727)
T43	0.21	31.0	42.2	0.0224	0.945	0.723 (0.747)
T44	0.17	31.8	42.2	0.0174	0.734	0.547 (0.580)
T45	0.24	32.3	41.5	0.0232	0.963	0.718 (0.773)
T46	0.22	32.8	40.5	0.0229	0.928	0.698 (0.763)
T47	0.21	32.5	43.6	0.0203	0.885	0.625 (0.677)
T48	0.24	32.5	43.6	0.0235	1.025	0.723 (0.783)
T49	0.21	33.1	42.8	0.0212	0.907	0.641 (0.707)
T50	0.24	33.1	42.0	0.0216	0.907	0.653 (0.720)

Figures in brackets refer to anode platinum loadings greater than 30mg cm^{-2} where the ratio H_2 sensitivity to anode loading was replaced by H_2 sensitivity divided by 30 mg cm^{-2} (see text, section 7.3.).

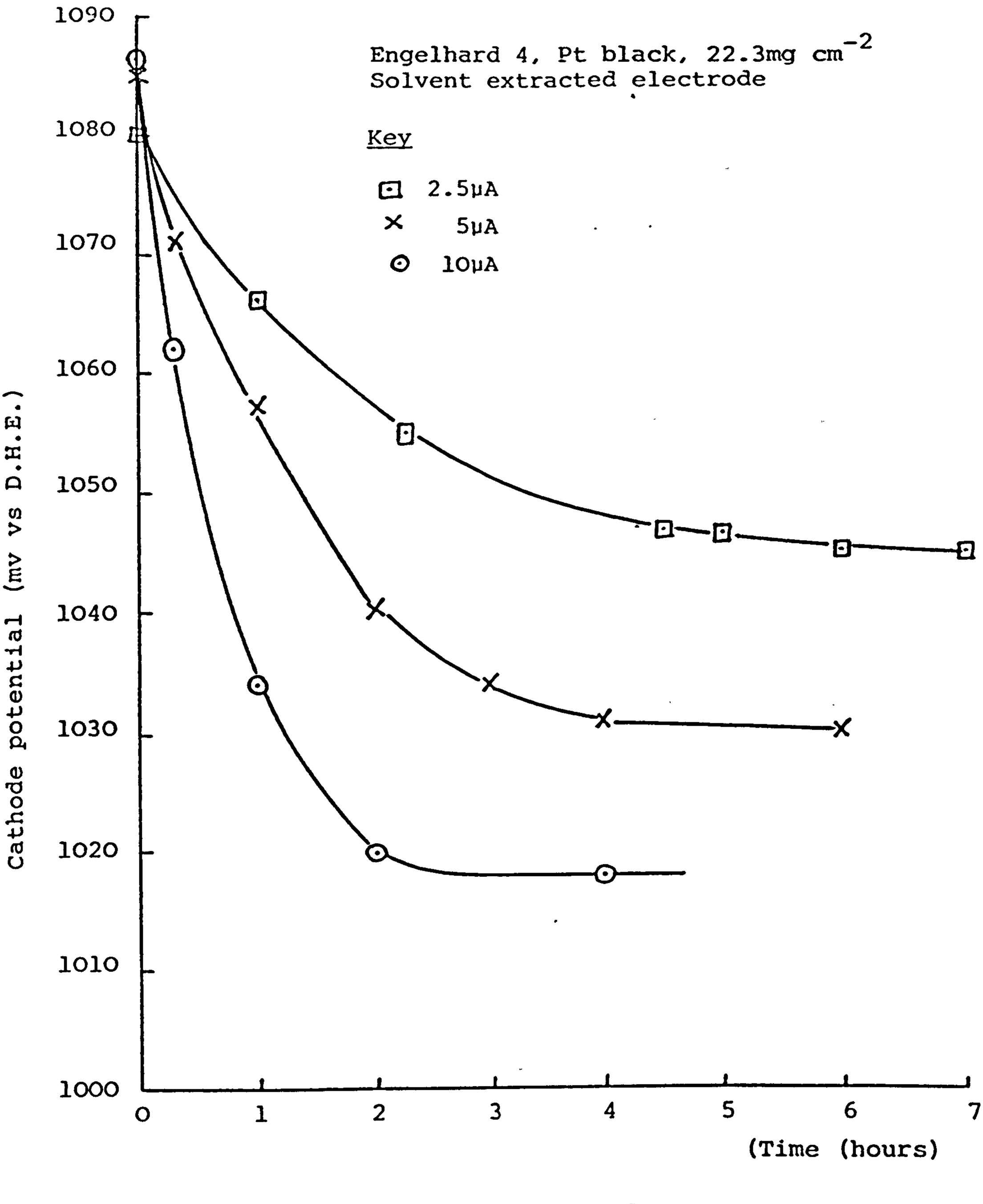

Figure 2.1. Galvanostic air electrode potential-time curves

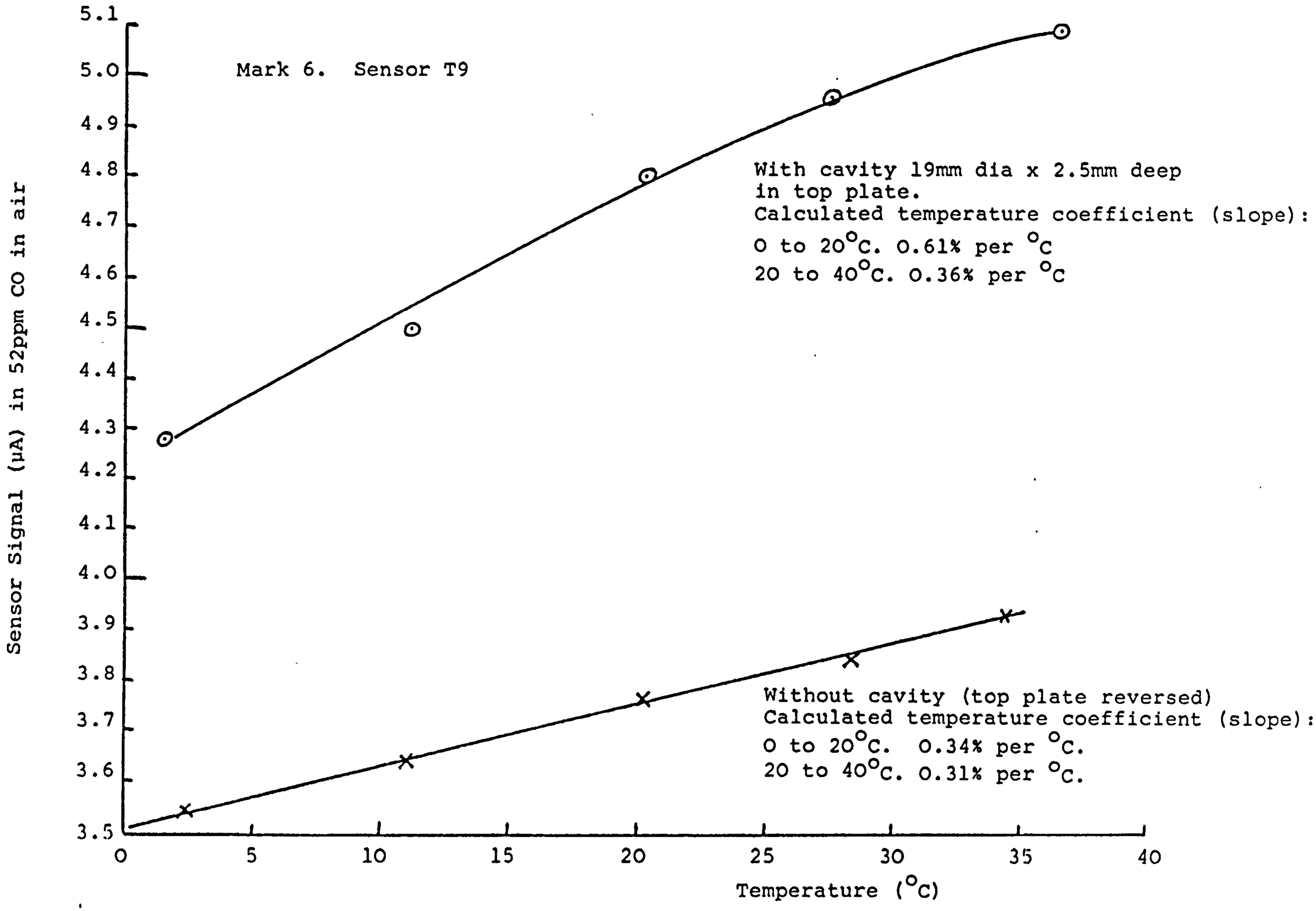

Figure 3.1. Effect of top plate cavity on signal and temperature coefficient of Mark 6 Sensor T9

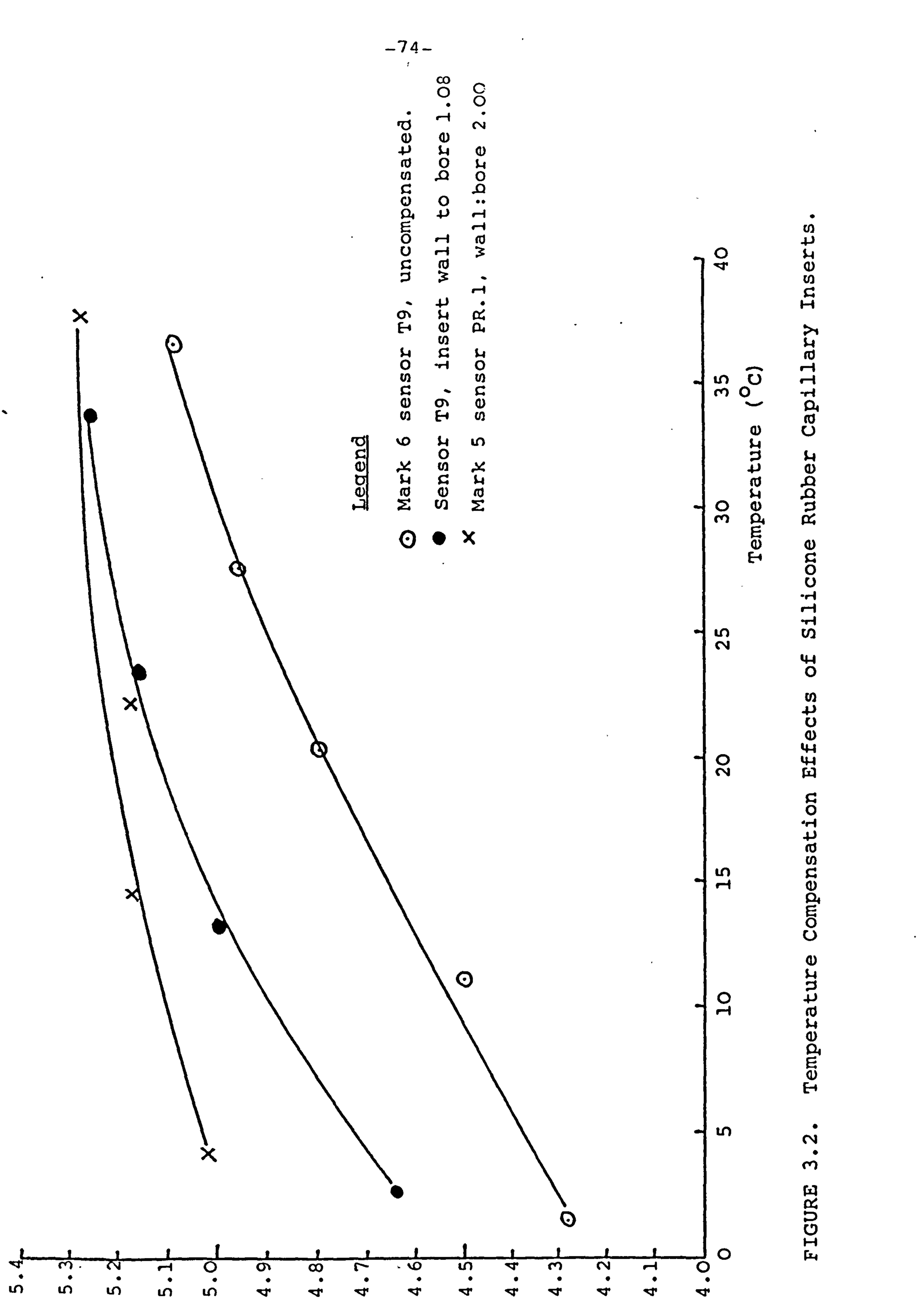

FIGURE 3.2. Temperature Compensation Effects of Silicone Rubber Capillary Inserts.

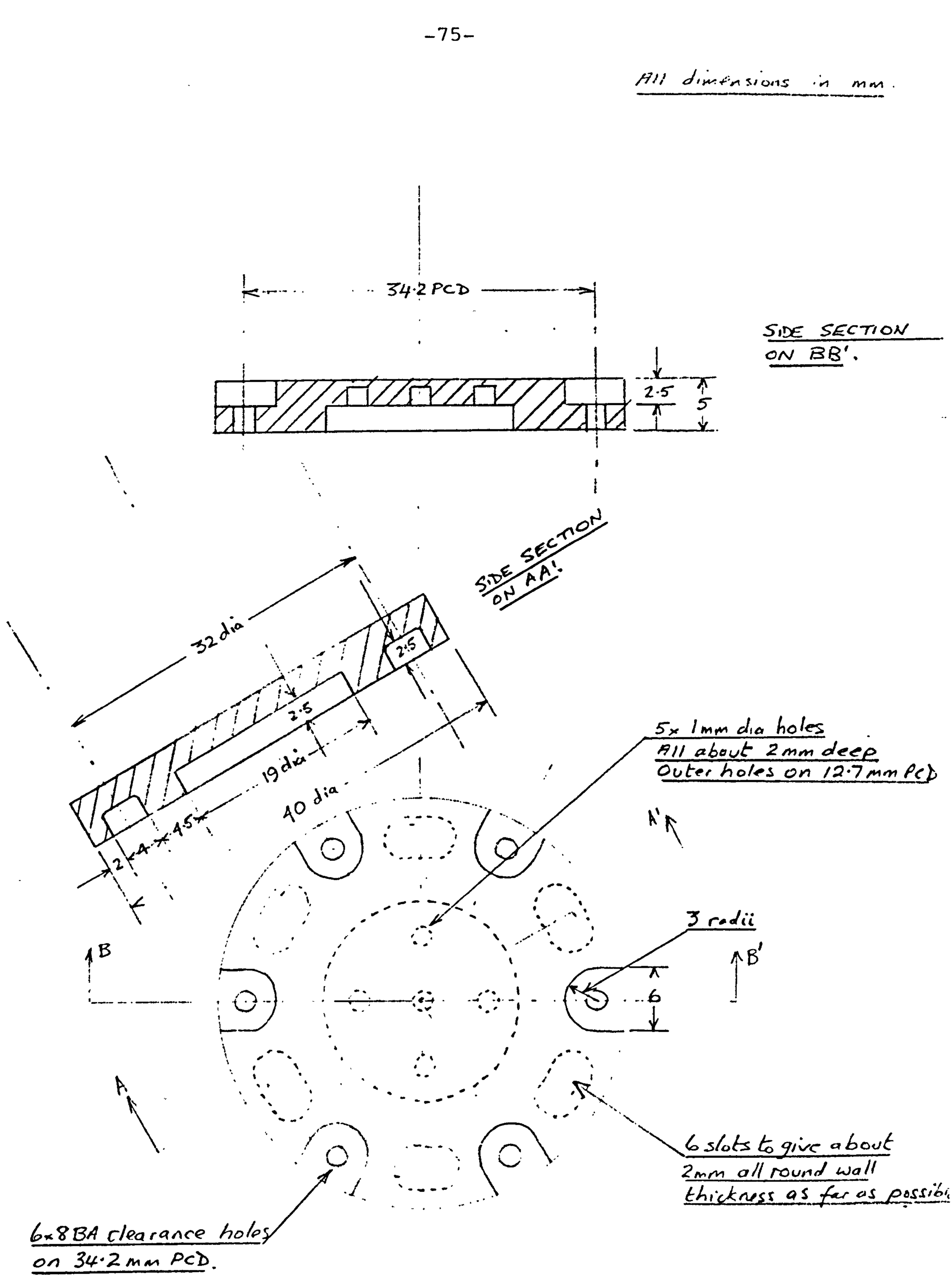

Figure 3.3. Double size, scale drawing of final injection moulding design for CO sensor top-plate.

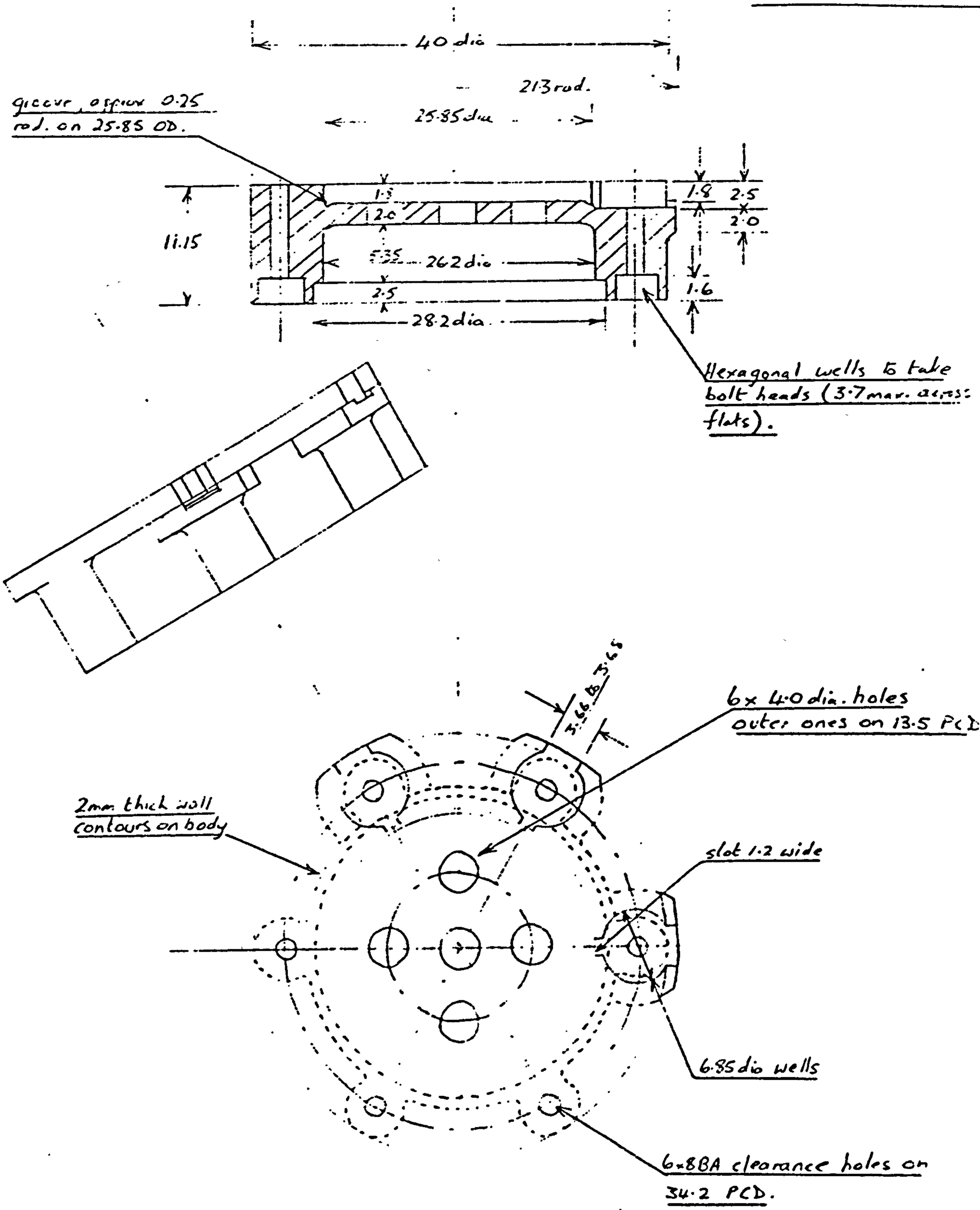

Figure 3.4. Double size scale drawing of final injection moulding design for CO sensor body-plate.

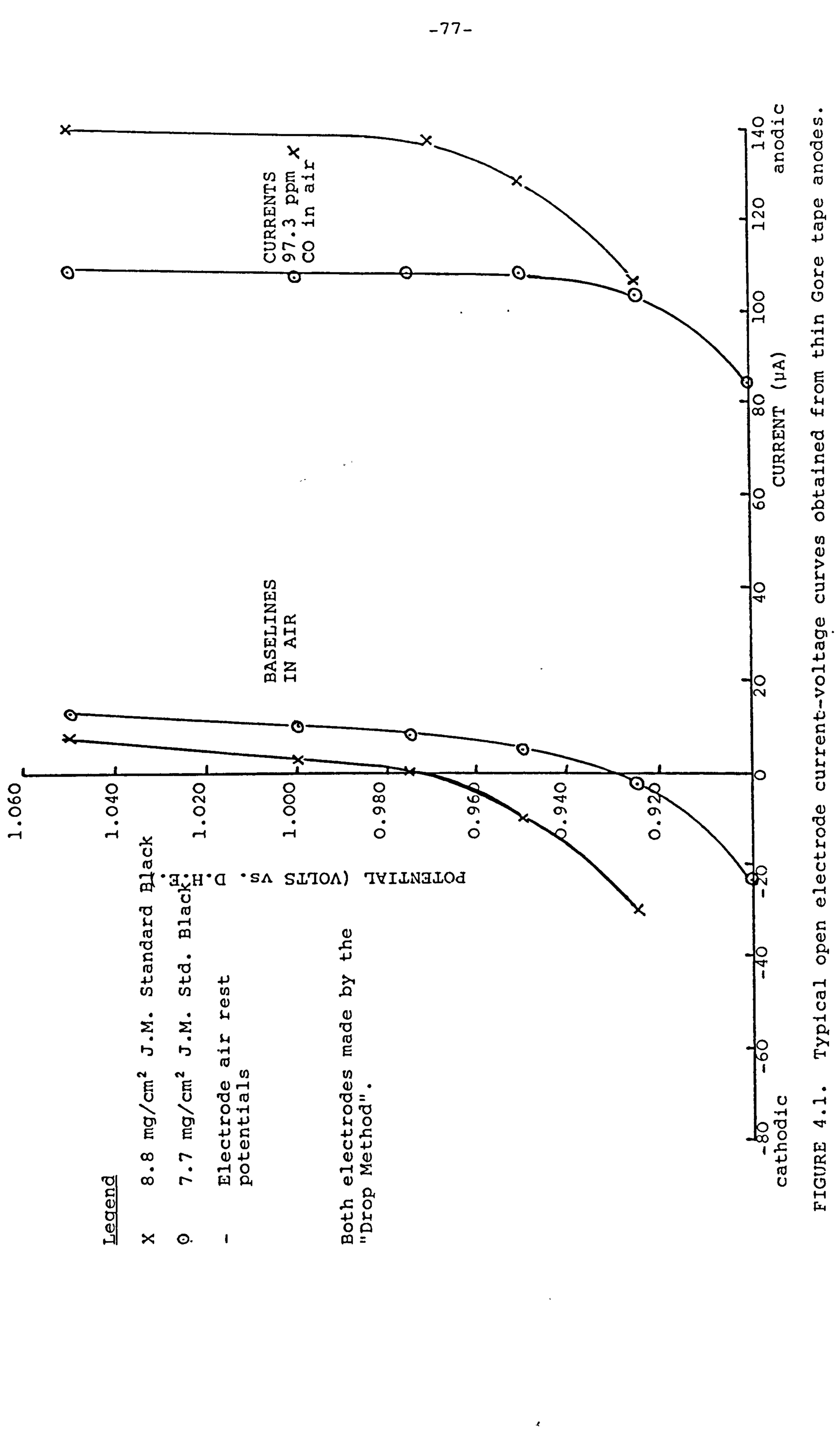

FIGURE 4.1. Typical open electrode current-voltage curves obtained from thin Gore tape anodes.

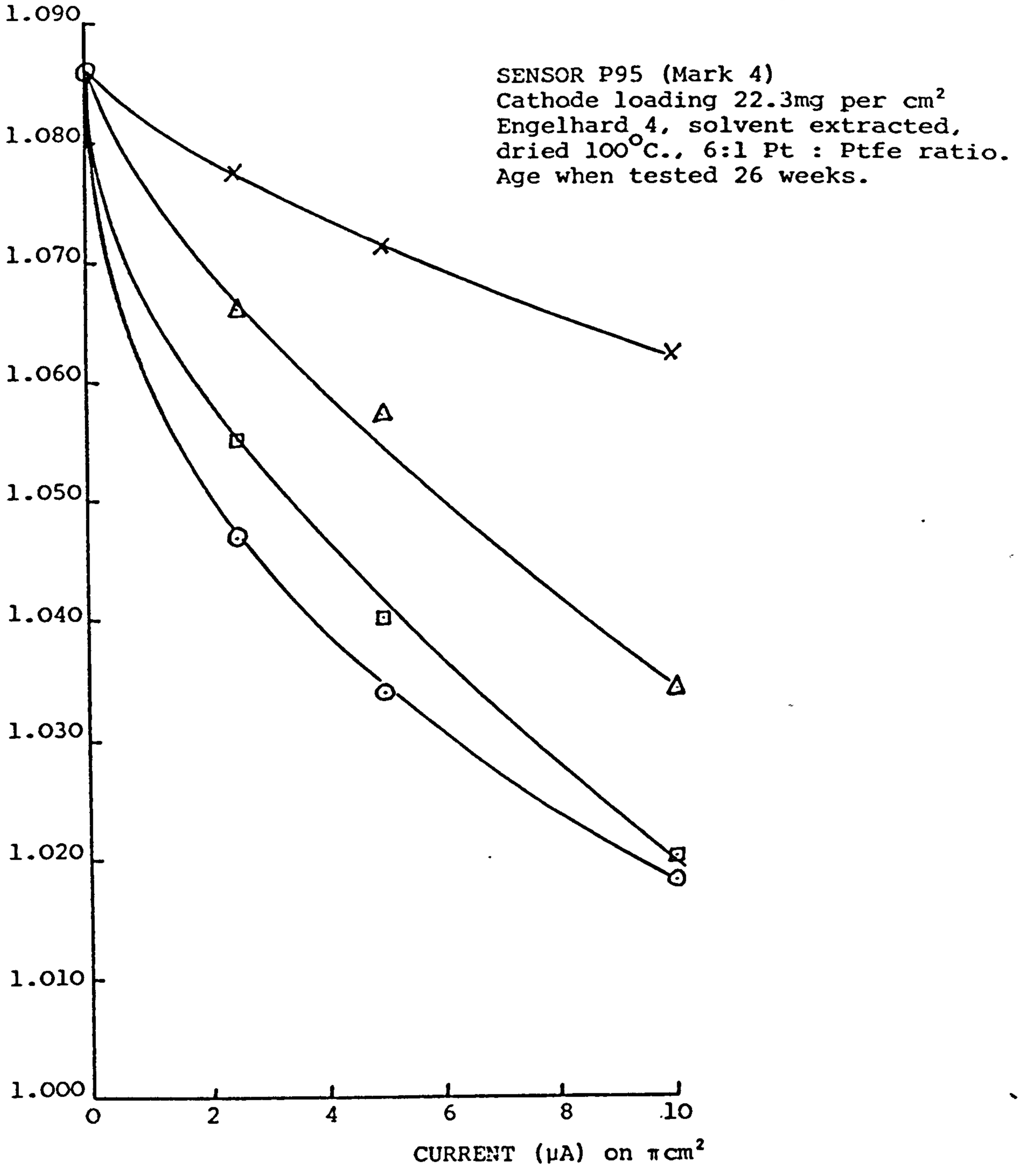

FIGURE 4.2. Time Dependence of Cathode Current-Voltage Characteristic, Derived from Galvanostatic Measurements.

Legend

× 20 minutes
Δ 1 hour
⊡ 2 hours
⊙ 5 hours (∿ steady state)

SENSOR T17 (Mark 6)
Cathode loading 31.2mg per cm^2
J.M. Standard Black, cured 280°C.
4:1 Pt : ptfe ratio.
Age when tested 10 days.

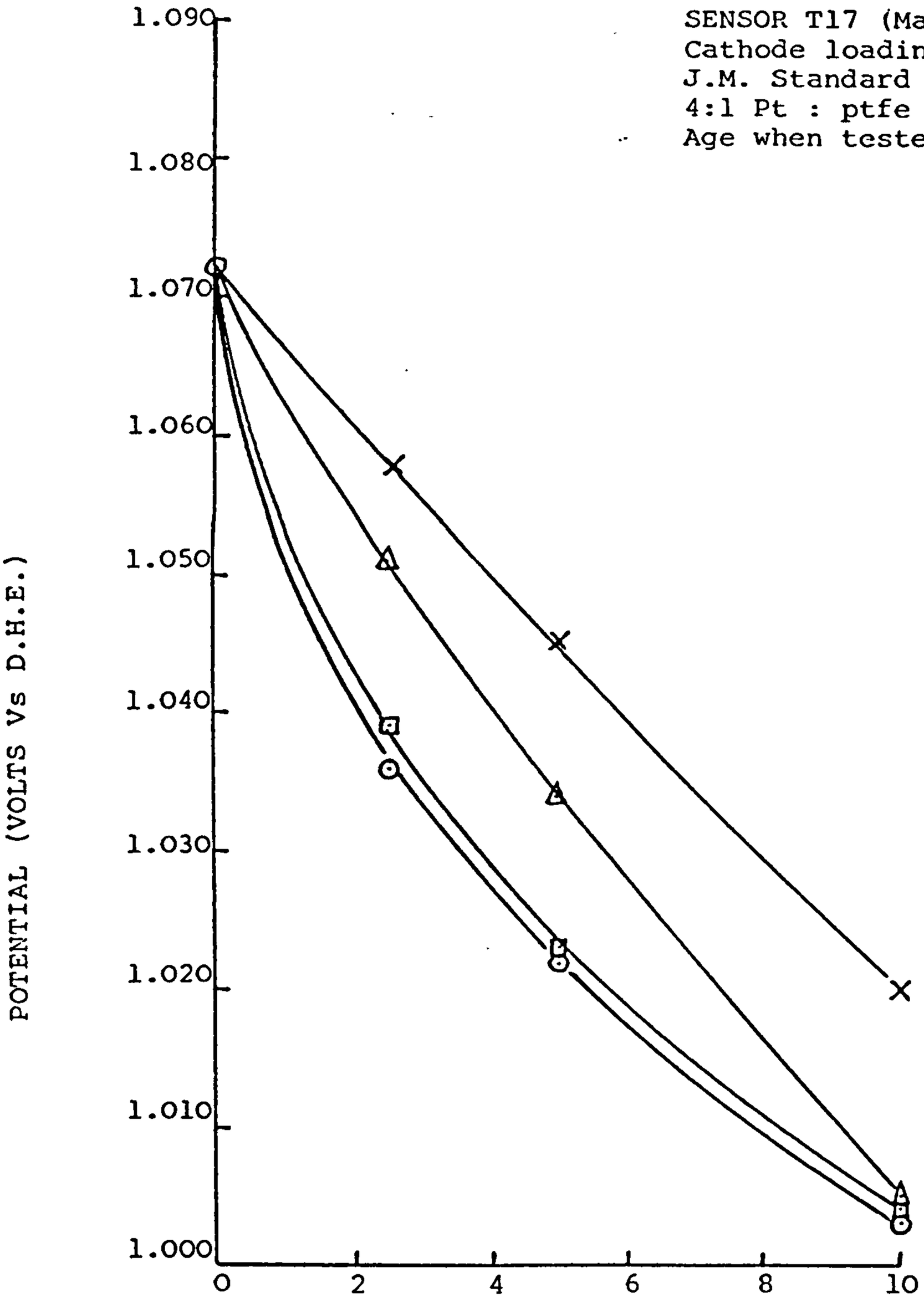

FIGURE 4.3. Time Dependence of Cathode Current-Voltage Characteristic, Derived from Galvanostatic Measurements.

Net CO-oxidation Limiting Current on π cm^2
above air R.P., on 97.3 ppm CO in air (μA)

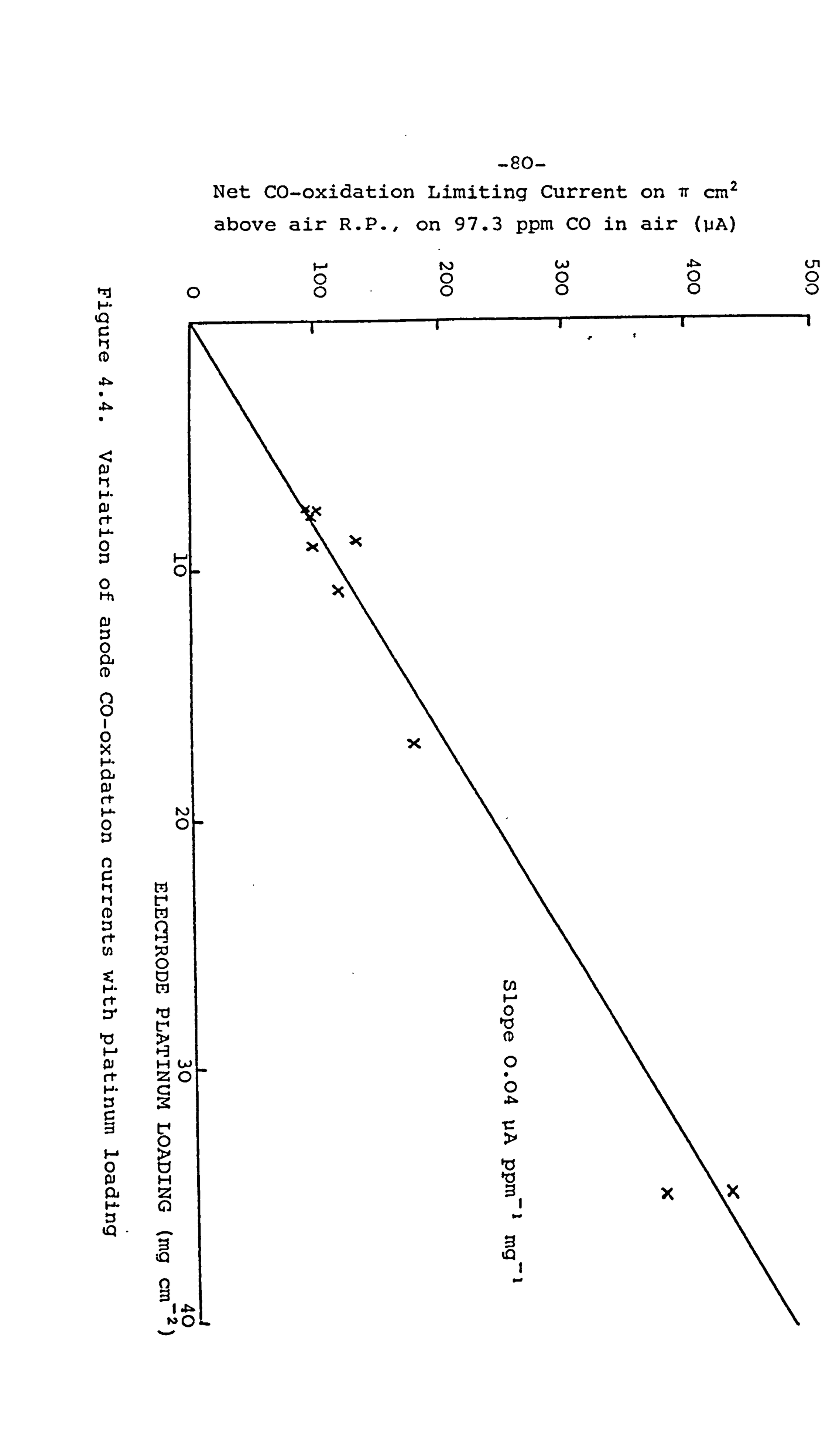

Figure 4.4. Variation of anode CO-oxidation currents with platinum loading

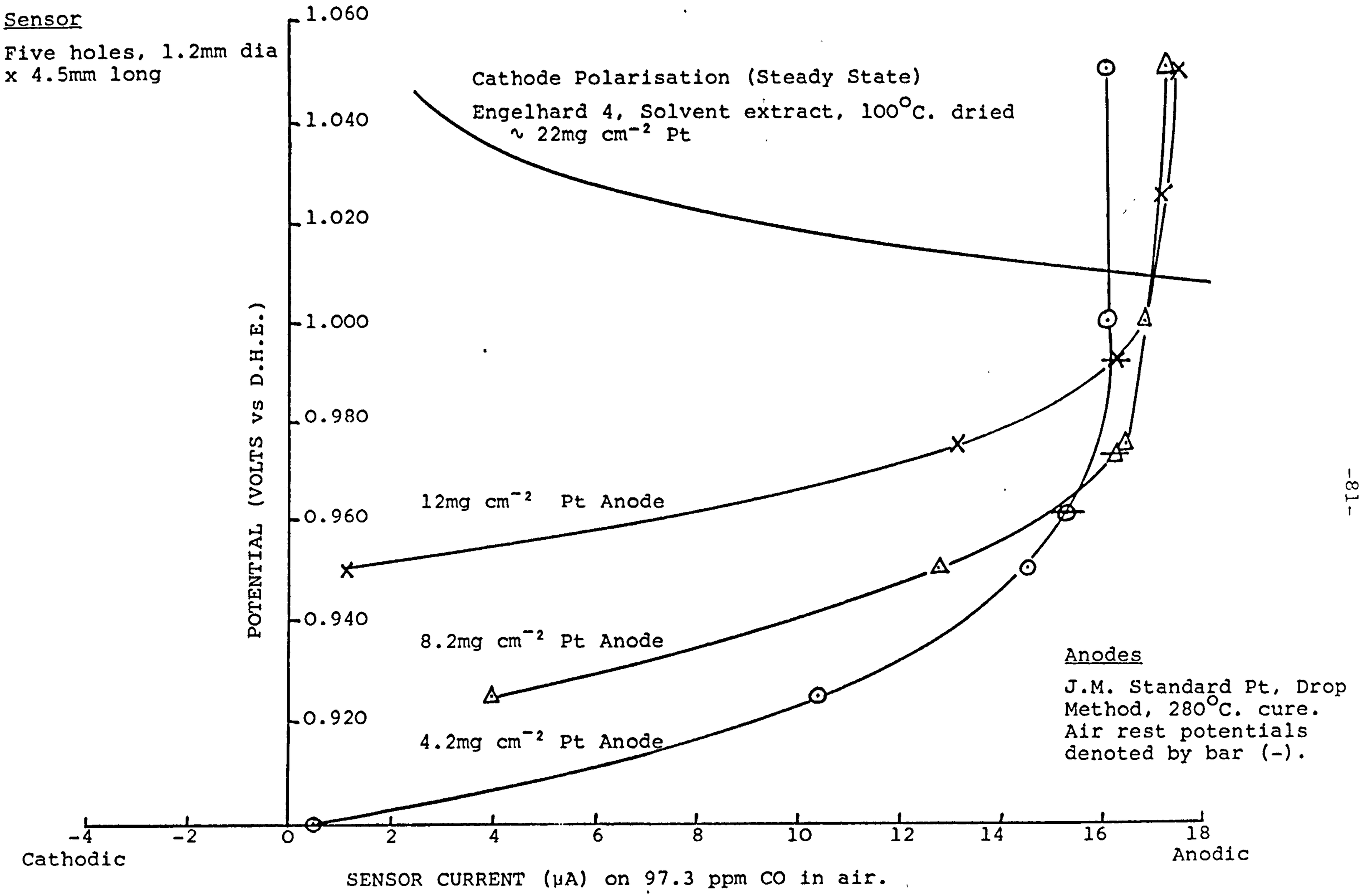

Figure 4.5. Single electrode, potentiostatic polarisation curves in sensors as a function of anode platinum loading.

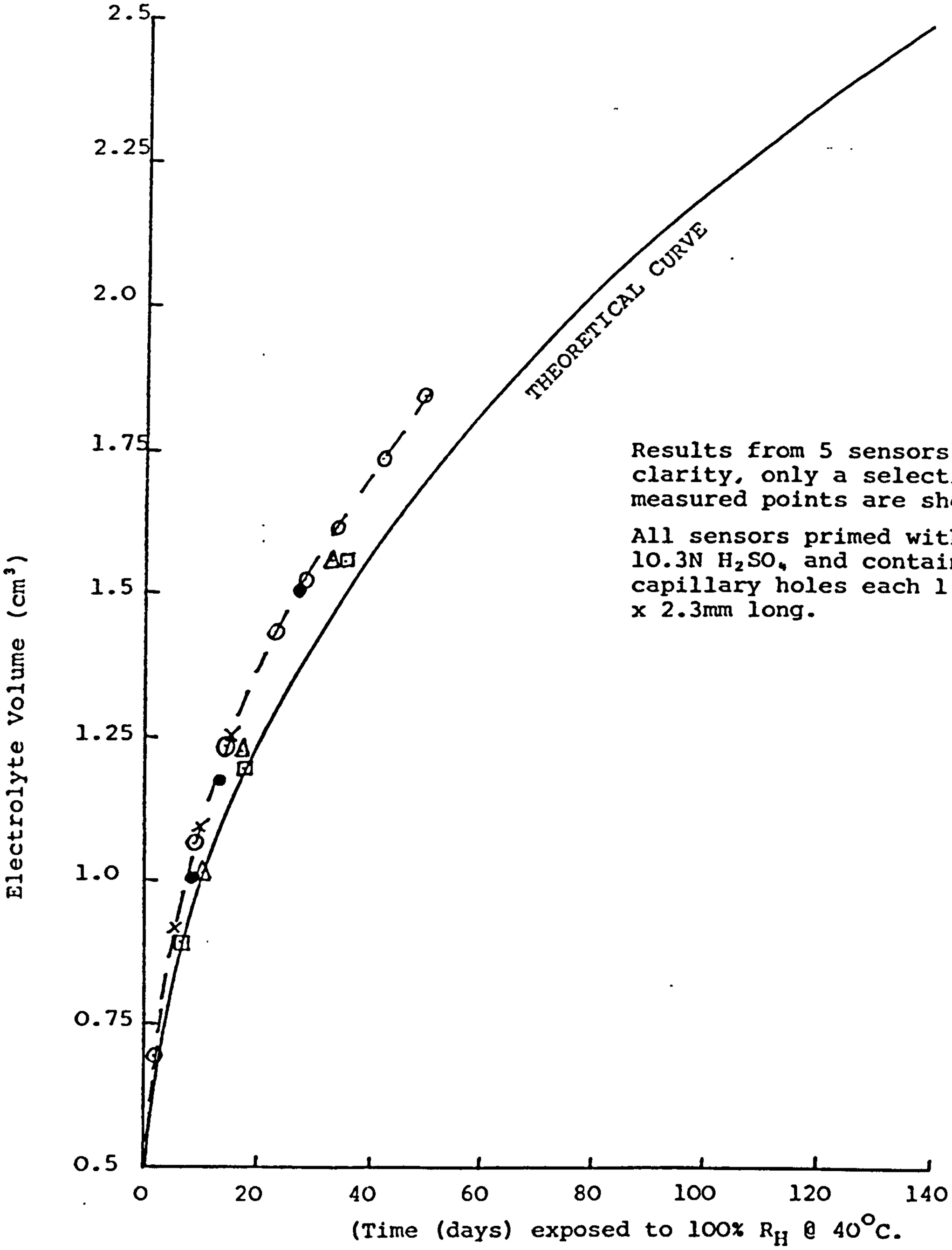

Results from 5 sensors. For clarity, only a selection of measured points are shown.

All sensors primed with 0.5cm³ 10.3N H_2SO_4 and contained 5 capillary holes each 1.05cm dia. x 2.3mm long.

Figure 5.1. Water Uptake Measurements of Various Sensors in 100% R_H, 40°C.

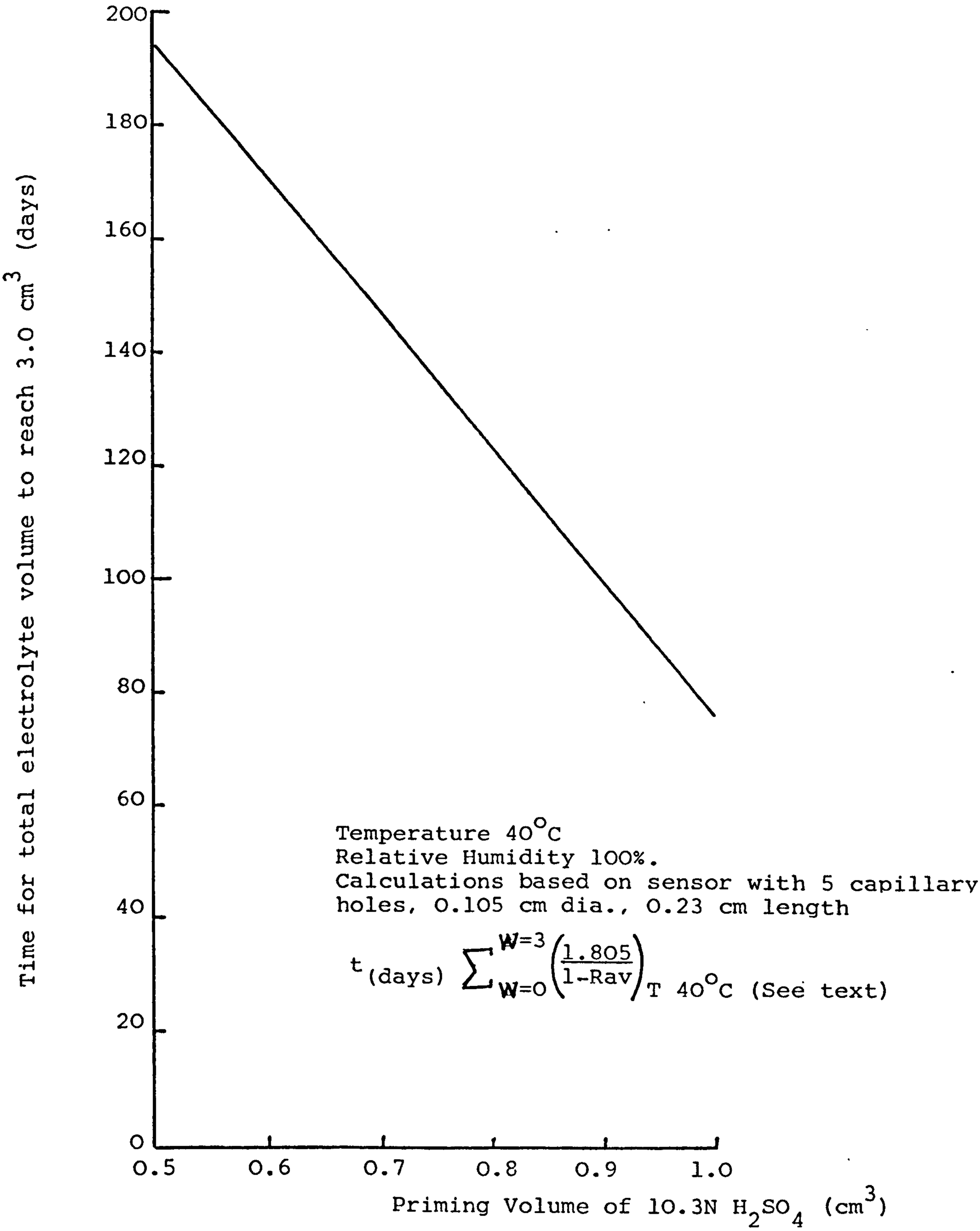

Figure 5.2. Exposure time to reach 3 cm^3 electrolyte volume at 40°C., 100% R_H, as a function of electrolyte priming volume.

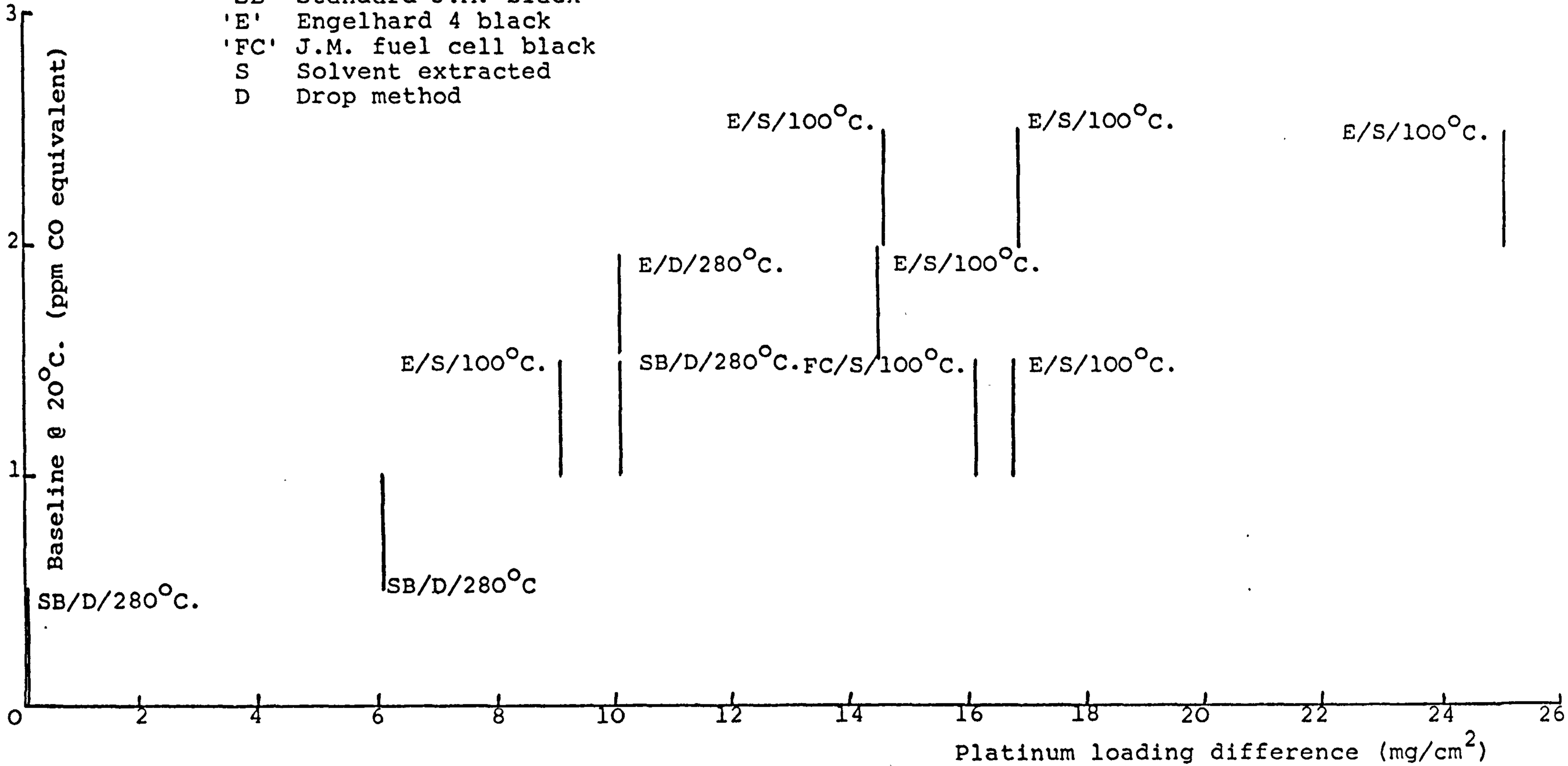

Figure 7.1. Baseline dependance on platinum loading difference between anodes and cathodes in trace CO sensors (indicated baseline ranges are long term results, up to 2 year periods).

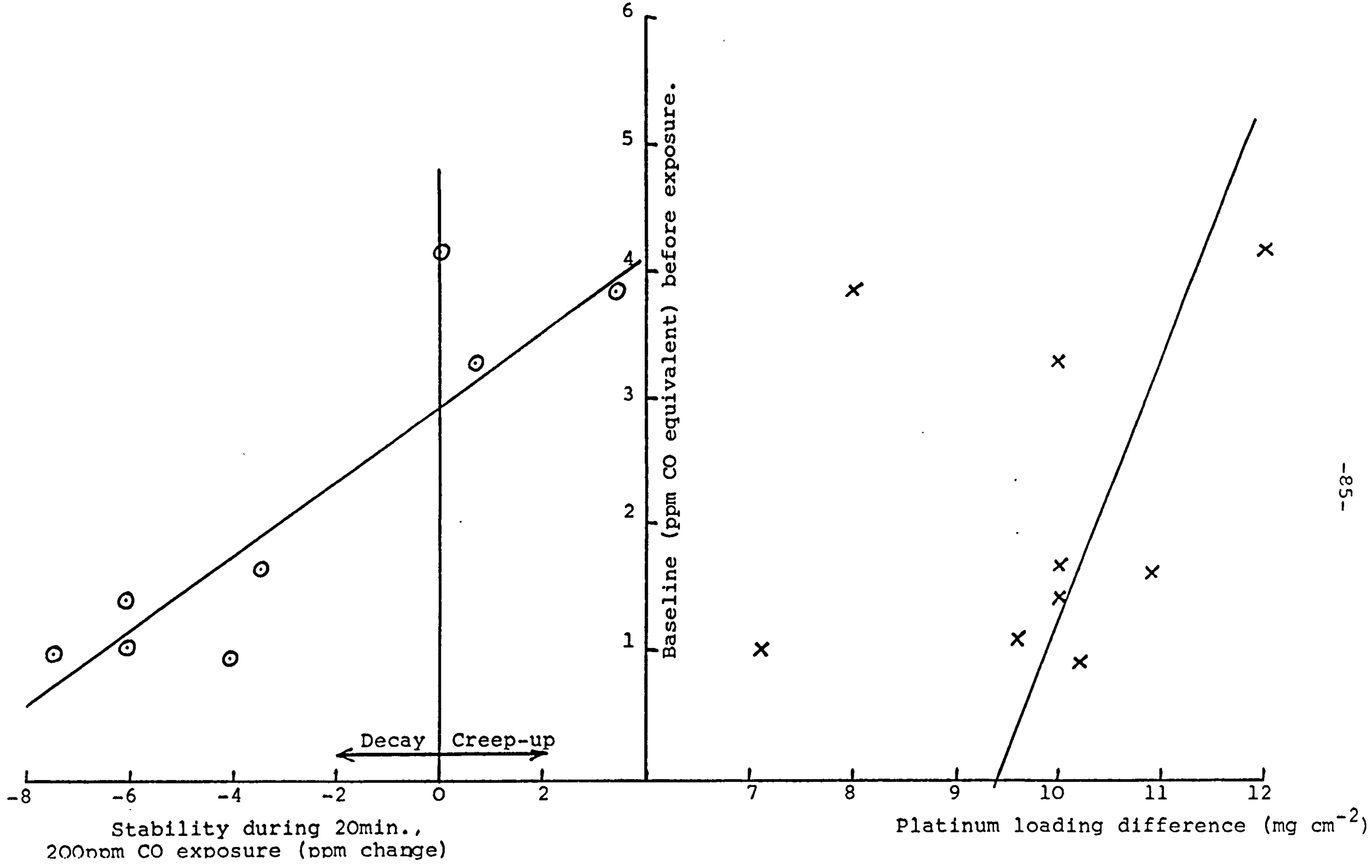

Figure 7.2. Stability during 20 min., 200 ppm CO exposure and baselines of Mark 5 sensors @ age 1 week

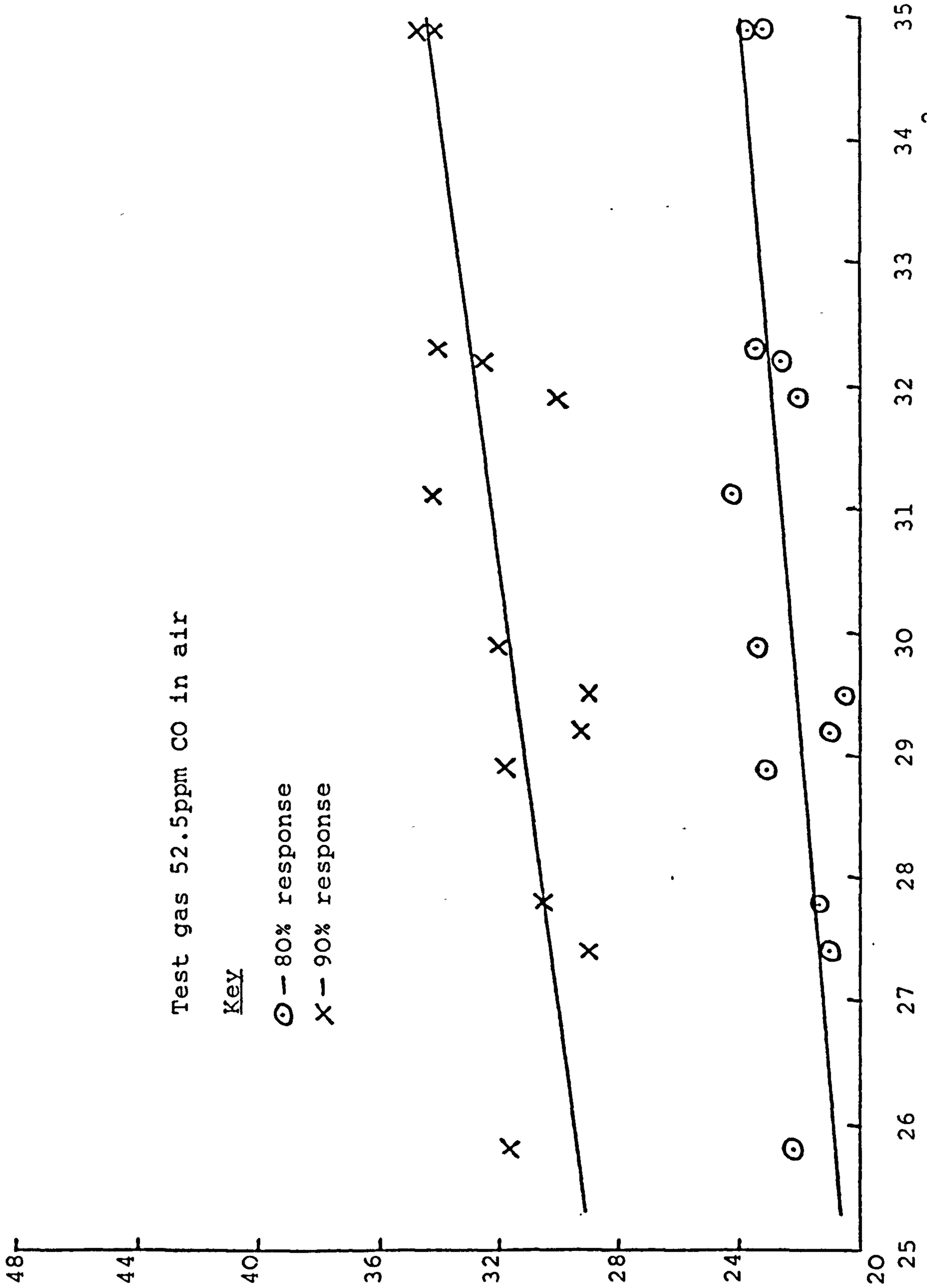

Figure 7.3. Relationship between response time and anode platinum loading for NCB, Mark 5, Trace

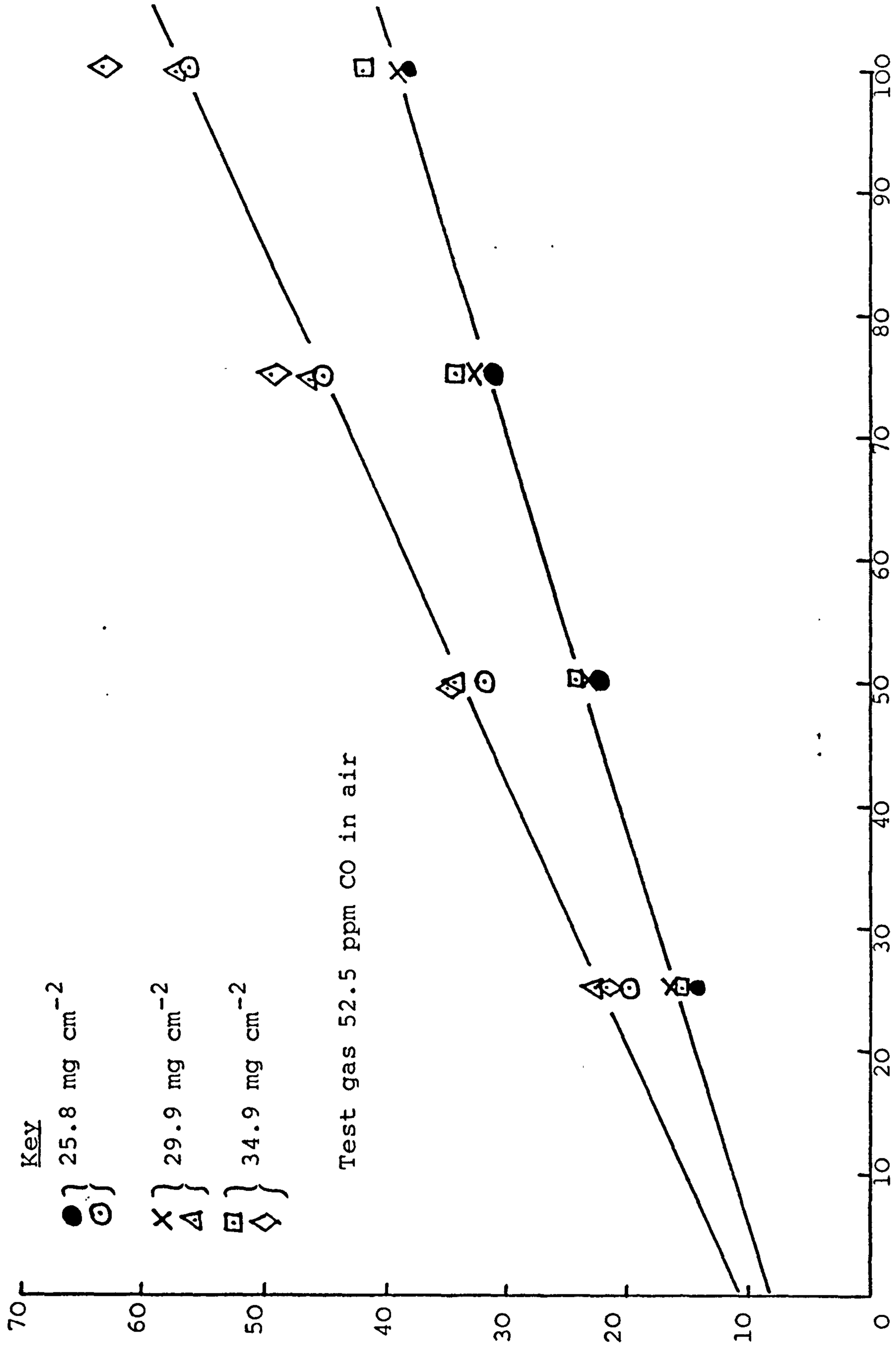

Figure 7.4. Effect of load resistor on response time of Mark 5 Trace CO sensors at three anode loadings.

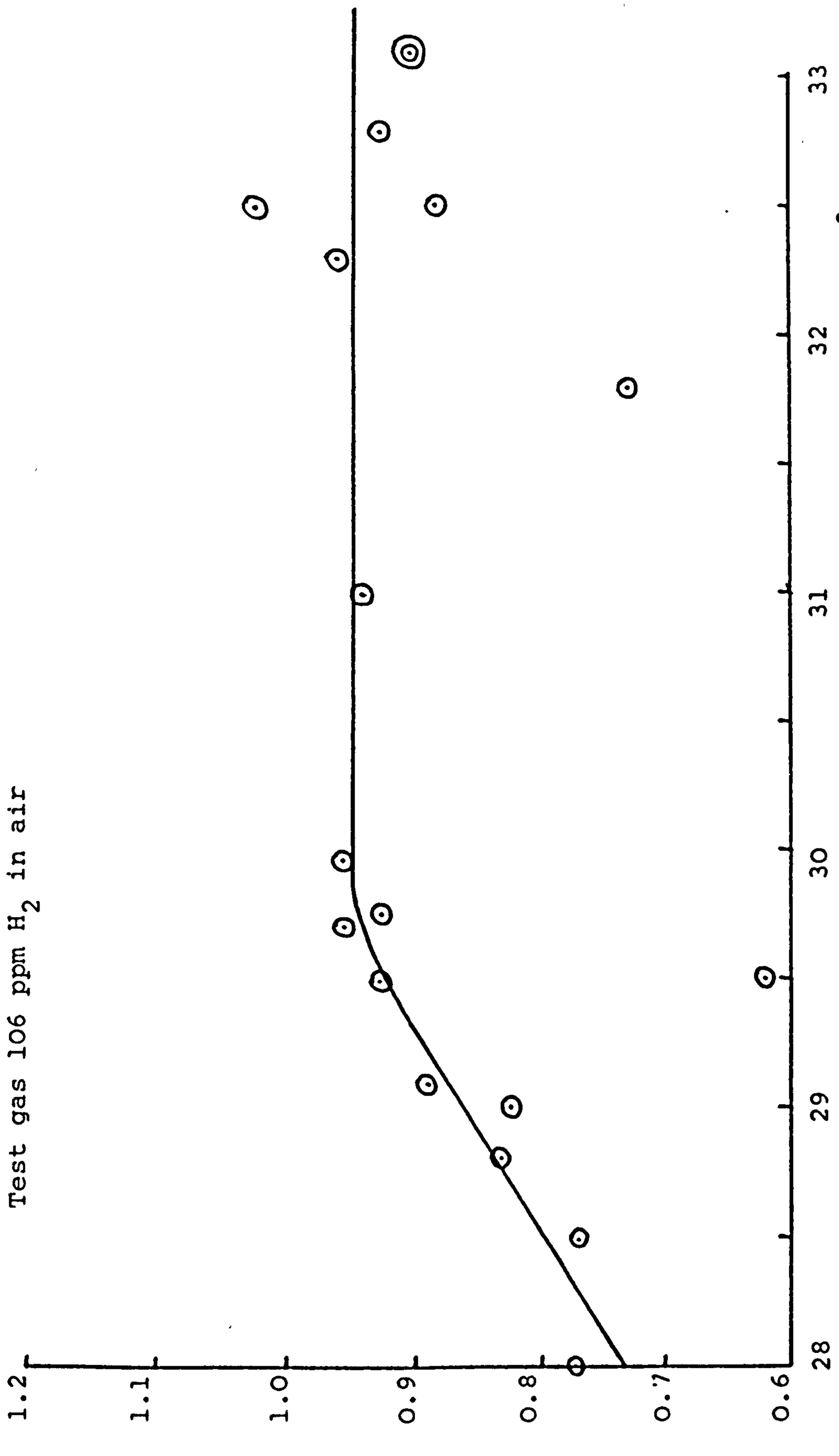

Figure 7.5. Plot of the product of H_2 sensitivity and cathode loading versus anode loading for Mark 5 trace CO sensors.

Product of H_2 sensitivity and cathode loading.

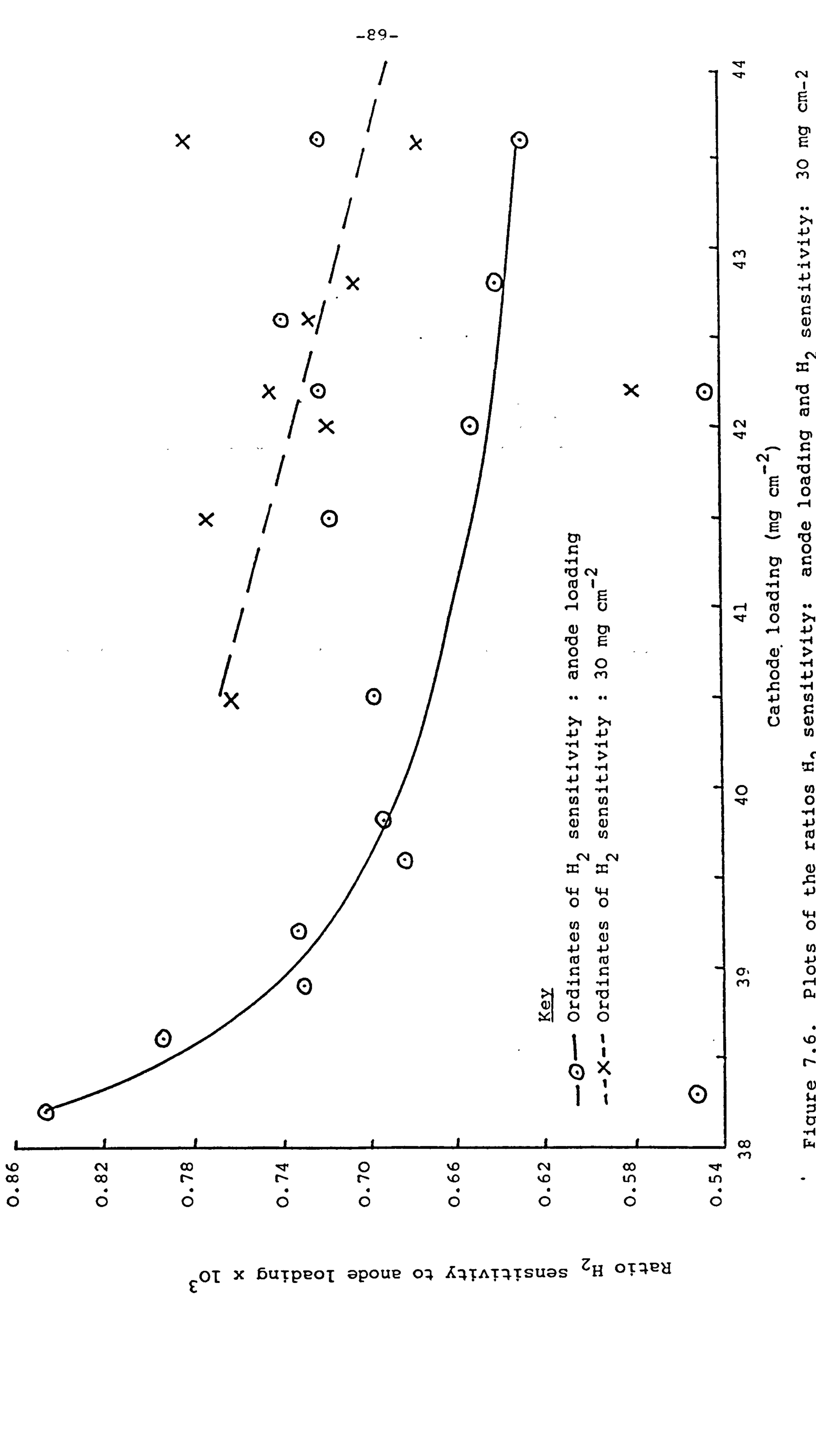

Figure 7.6. Plots of the ratios H_2 sensitivity: anode loading and H_2 sensitivity: 30 mg cm^{-2} loading of Mark 5 trace CO sensors versus cathode loading.

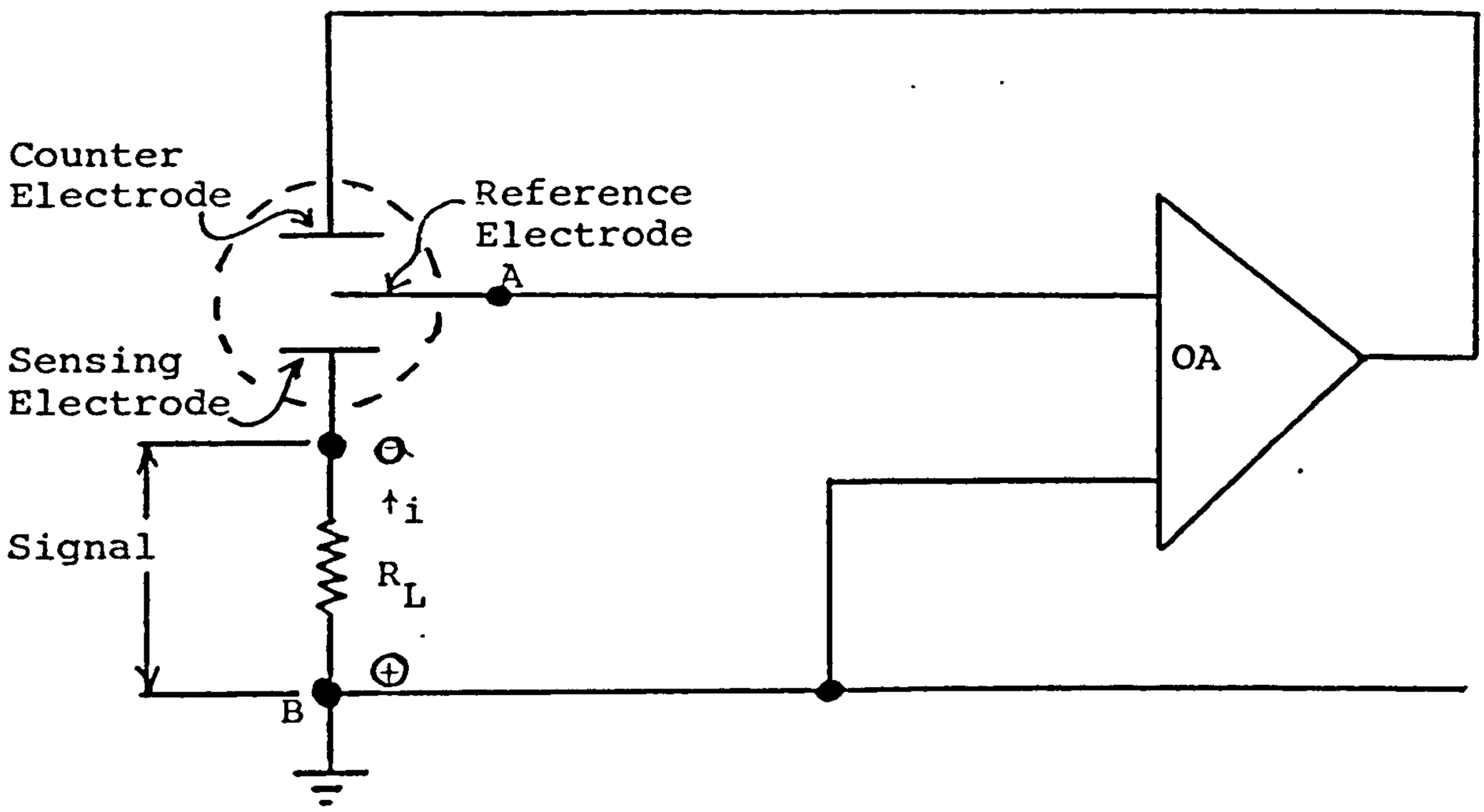

Figure 8.1. Potentiostatic control circuit for 3-electrc sensors.

APPENDIX 1

DIFFUSION SPREADING RESISTANCE

APPENDIX 1.

Diffusion Spreading Resistance

The diffusion paths are illustrated schematically below:

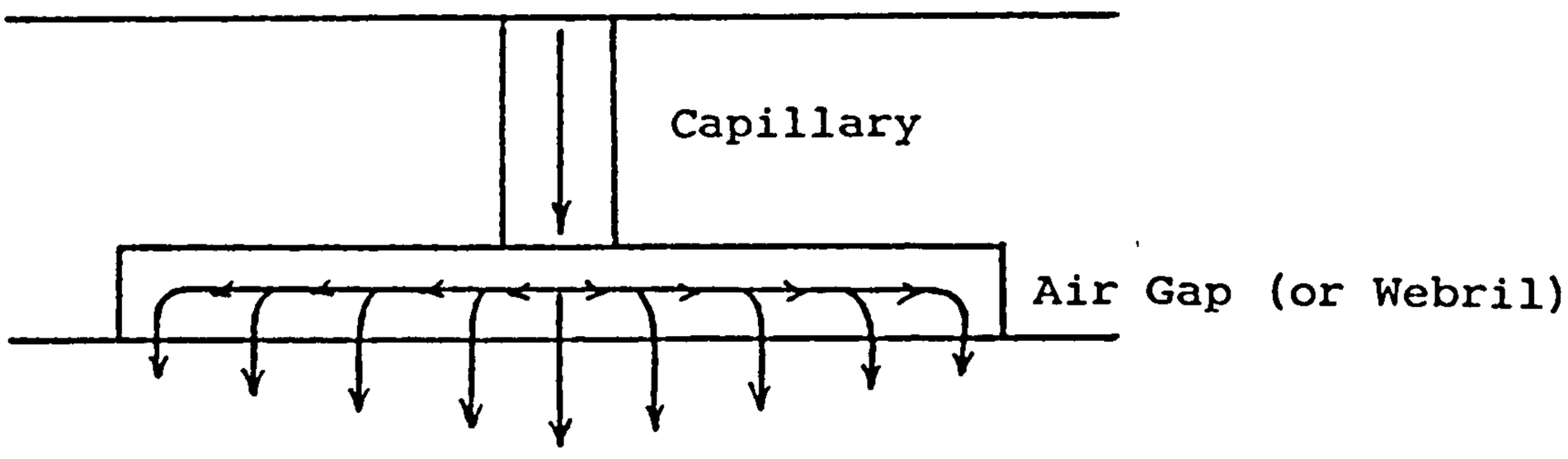

The length of the bottom arrows is intended to indicate the variation in diffusion flux across the electrode. The flux will obviously be highest directly under the capillary and will taper off the further sideways we are from the capillary. So there will be an uneven flux of CO to the electrode and an uneven current density. The degree of uneveness will depend on the sideways diffusion resistance. It is obviously desirable to keep any uneveness within limits and as a guide one can put the criterion that the total sideways diffusion resistance (from capillary to edge), which we will call DRS (diffusion spreading resistance), should be a reasonably small fraction of the capillary diffusion resistance, DRC.

i.e. $DRS \ll DRC$

The equation for DRS is derived below. The drawing illustrates the model used:

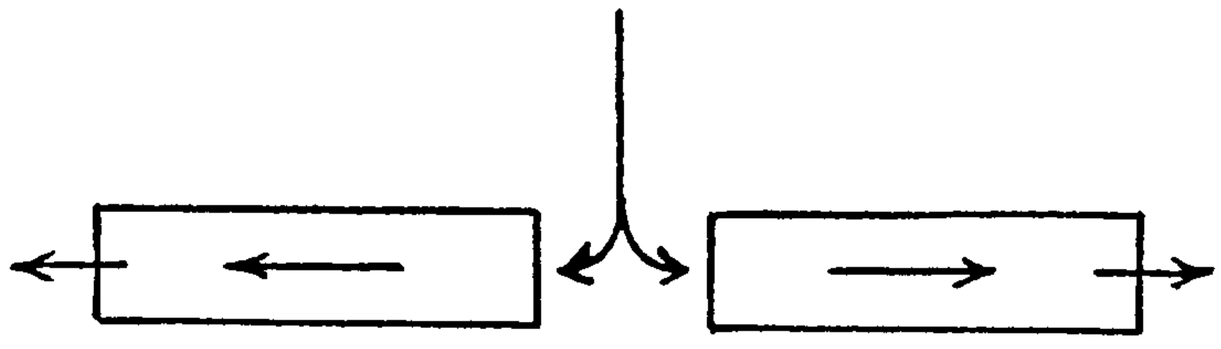

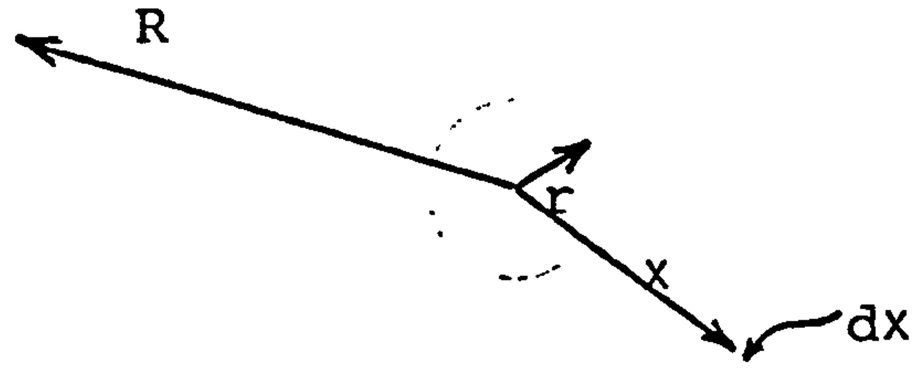

r = radius of capillary (cm)

R = radius of cavity (cm)

t = cavity thickness (cm)

L = path length (cm)

A = cross sectional area of diffusion path (cm^2)

θ = Fractional porosity

τ = Tortuosity

$$\text{Diffusion resistance} = \frac{L\tau}{A\theta} \quad \ldots\ldots\ldots\ldots\ldots\ldots \quad (1)$$

The porosity and tortuosity factors are included to cover the case when a porous packing, such as Webril, is included in the cavity.

At a distance x from the centre :

$$A = 2\pi xt \quad \ldots\ldots\ldots\ldots\ldots\ldots\ldots\ldots\ldots\ldots\ldots\ldots (2)$$

The diffusion resistance (d DRS) of segment dx at this point is given by

$$d(DRS) = \frac{\tau\ dx}{2\pi\ x\ t\theta} \quad \ldots\ldots\ldots \quad (3)$$

Integrating between r and R

$$DRS = \int_{r}^{R} \frac{\tau\ \ dx}{2\pi\ x\ t\theta} \quad \ldots\ldots\ldots \quad (4)$$

$$= \frac{\tau}{2\pi t\theta} \ln \frac{R}{r} \quad \ldots\ldots\ldots \quad (5)$$

For a plain air gap $\theta = 1$ and $\tau = 1$

and the equation simplifies to

$$DRS = \frac{1}{2\pi t} \ln \frac{R}{r} \quad \ldots\ldots\ldots\ldots\ldots \quad (6)$$

The diffusion resistance of the capillary is given by

$$DRC = \frac{b}{\pi\ r^2} \quad \ldots\ldots \quad (7)$$

where b is the length (cm)

$$\text{So the ratio } \frac{DRS}{DRC} = \frac{\tau}{2\pi t\theta} \cdot \frac{\pi\ r^2}{b} \ln \frac{R}{r} \quad \ldots \quad (8)$$

$$= \frac{\tau\ r^2}{2t\theta b} \ln \frac{R}{r} \quad \ldots\ldots\ldots \quad (9)$$

For the simple air gap case

$$\frac{DRS}{DRC} = \frac{r^2}{2tb} \ln \frac{R}{r} \quad \ldots\ldots\ldots (10)$$

Figures A1.1. and A1.2 are plots of the ratio $\frac{DRS}{DRC}$ versus the gap size, t, calculated from these equations.

Fig. A1.1 is for typical values used with early sensors in which there was no machined cavity as such beneath the capillary and a Webril packing was used. The calculations assume the following values.

Porosity $\theta \doteq 0.65$

Tortuosity $\tau = 2$

Capillary radius $r = 0.06cm$

Capillary length $b = 0.5cm$

Outer radius $R = 1cm$ (single hole case).
and $R = 0.33cm$ (9 hole case).

For the 9 hole case, one is making a compromise assumption as to the value of R, the actual diffusion path geometry being much more complex.

Fig. A1.2 is for more typical present day values, with a machined cavity and no webril insert.

Porosity $\theta = 1$

Tortuosity $\tau = 1$

Capillary radius $r = 0.044cm$

Capillary length $b = 0.25cm$

Outer radius $R = 1cm$

Using equation (10) with these values

$\ln \frac{R}{r} = 3:12$ and for a <u>single</u> centre capillary as for the "flue gas" sensor:

$$\frac{DRS}{DRC} = \frac{0.012}{t}$$ to give the plot in Fig. A1.2

For the 5 capillary "trace CO" sensor, the equivalent R is estimated to be about 0.36cms, and, with other dimensions the same, $\ln \frac{R}{r} = 2.1$ and

$$\frac{DRS}{DRC} = \frac{0.081}{t}$$ (See plot in Fig. A.1.2.)

Early sensors had 9 holes and Webril packing and a gap of about 10 thou. It is difficult to be precise about the gap since the electrode sandwich assembly tends to bulge out into the gap.

From Fig. A1.1. we see that a $\frac{DRS}{DRC}$ value of about 60% is indicated at a 10 thou gap, i.e. a very high contribution from spreading resistance. Furthermore we are in a very steep part of the curve, i.e. a small change in the gap will produce a big change in spreading resistance. Operation in a critical region such as this seems undesirable for several reasons.

(a) Very uneven current density across the electrode.

(b) Criticality of dimensions. One would expect large scatters in signal level due to small differences in gap dimensions occuring in practice. Further the gap would be affected by such things as tape thickness so allowing little room for manoeuvre if one wanted to alter such factors for other reasons.

(c) There is a mechanism here for temperature compensation. The gap will tend to narrow as the temperature rises, because of the differential expansion between the plastic hardware and the metal bolts. And indeed, this was quite evidently occuring in these sensors. However, because of (b) a considerable scatter in the degree of temperature compensation might be expected in practice.

All in all it seemed preferable to work in the non-critical, flat part of the curve, where the spreading resistance contribution is low and relatively insensitive to gap widths. The characteristics are then almost wholly determined by the more controllable capillary dimensions. As can be seen from Fig. A1.2., present sensors are in this non-critical region.

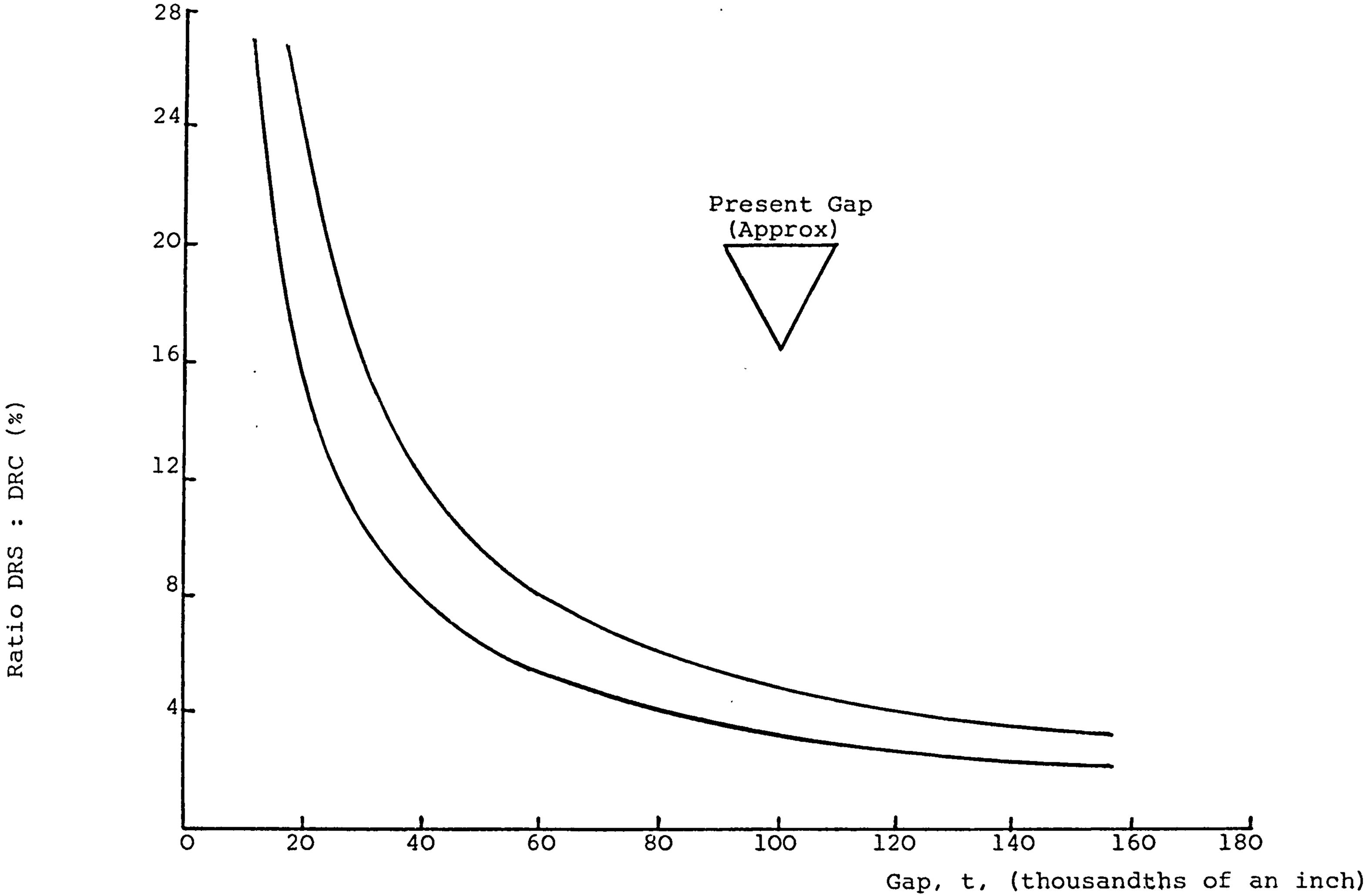

Fig. A1.2. Plot of the ratio DRS:DRC against gap size for later sensor versions.

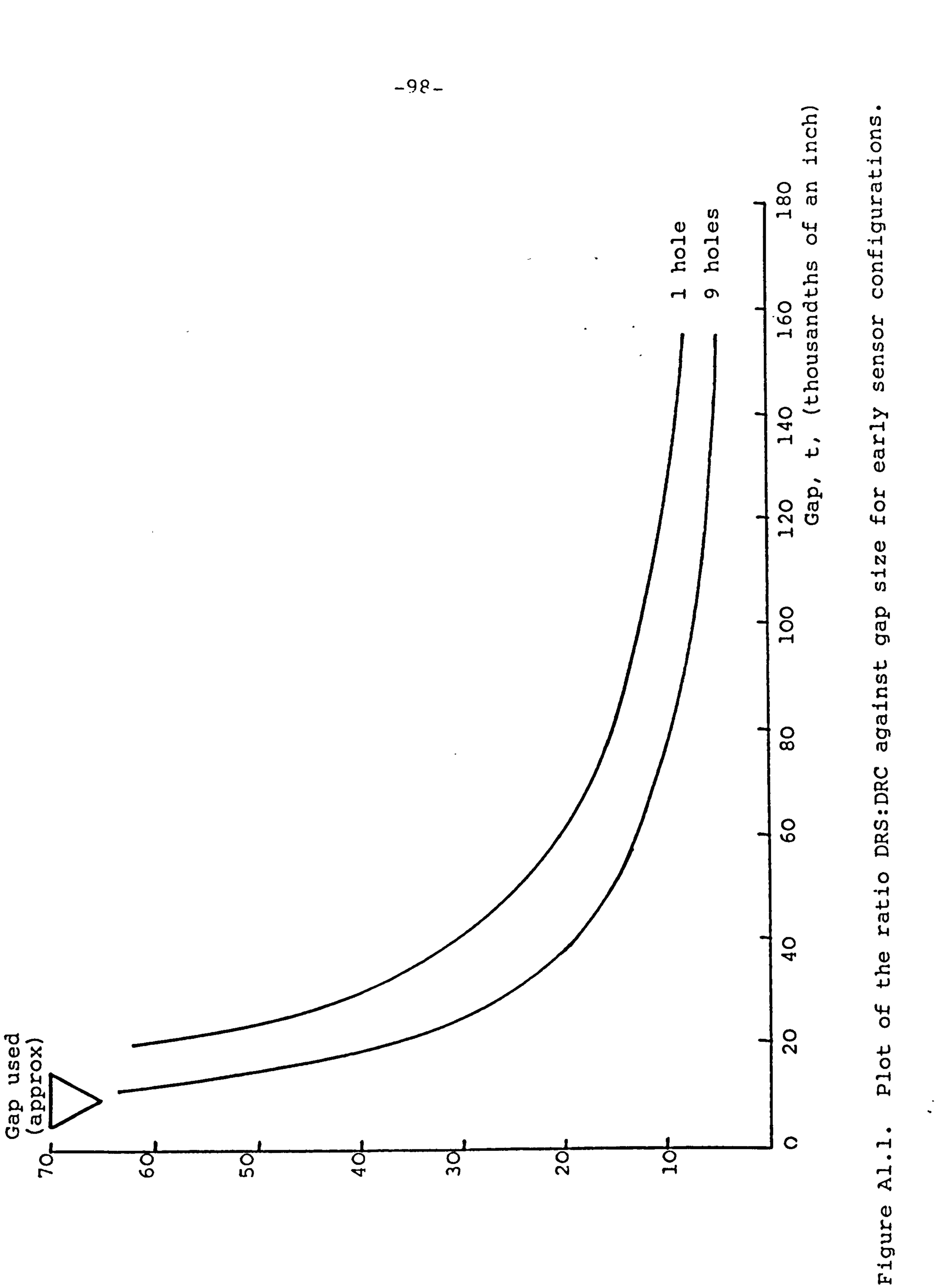

Figure A1.1. Plot of the ratio DRS:DRC against gap size for early sensor configurations.

APPENDIX 2

TEMPERATURE COMPENSATION BY DIFFERENTIAL THERMAL EXPANSION CAPILLARY INSERTS

APPENDIX 2

Temperature Compensation by Differential Thermal Expansion Capillary Inserts

Silicone rubber has a much higher thermal expansion coefficient than perspex. The respective linear expansion coefficients are about:

Silicone rubber 3.10^{-4} per ^{o}C.

Perspex 10^{-4} per ^{o}C.

there is some variation between different stock materials.

With a silicone rubber capillary mounted in perspex, the differential expansion will tend to close up the capillary hole as the temperature increases so running counter to the natural positive temperature coefficient of a normal capillary sensor. With a sensor whose signal is fully limited by capillary diffusion, and in the absence of any thermal expansion effect, the theoretical temperature coefficient is about + 0.17% per ^{o}C. In practice higher temperature coefficients (0.4 to 0.6) are usually found with uncompensated capillary CO sensors, due to the capillary not being fully limiting, so that some contribution from the very high ($\sim$ 3 to 4% per ^{o}C) temperature coefficient of the electrode is seen. With a given sensing electrode the amount of this contribution, and the resulting coefficient,will vary slightly with sensitivity (i.e. with the degree of restriction of the capillary used). In practice we need to compensate for a coefficient of around 0.5% per ^{o}C.

The length of the capillary insert will also increase slightly with temperature, but this is a secondary effect compared to the contraction of the bore and is ignored in the following treatment:

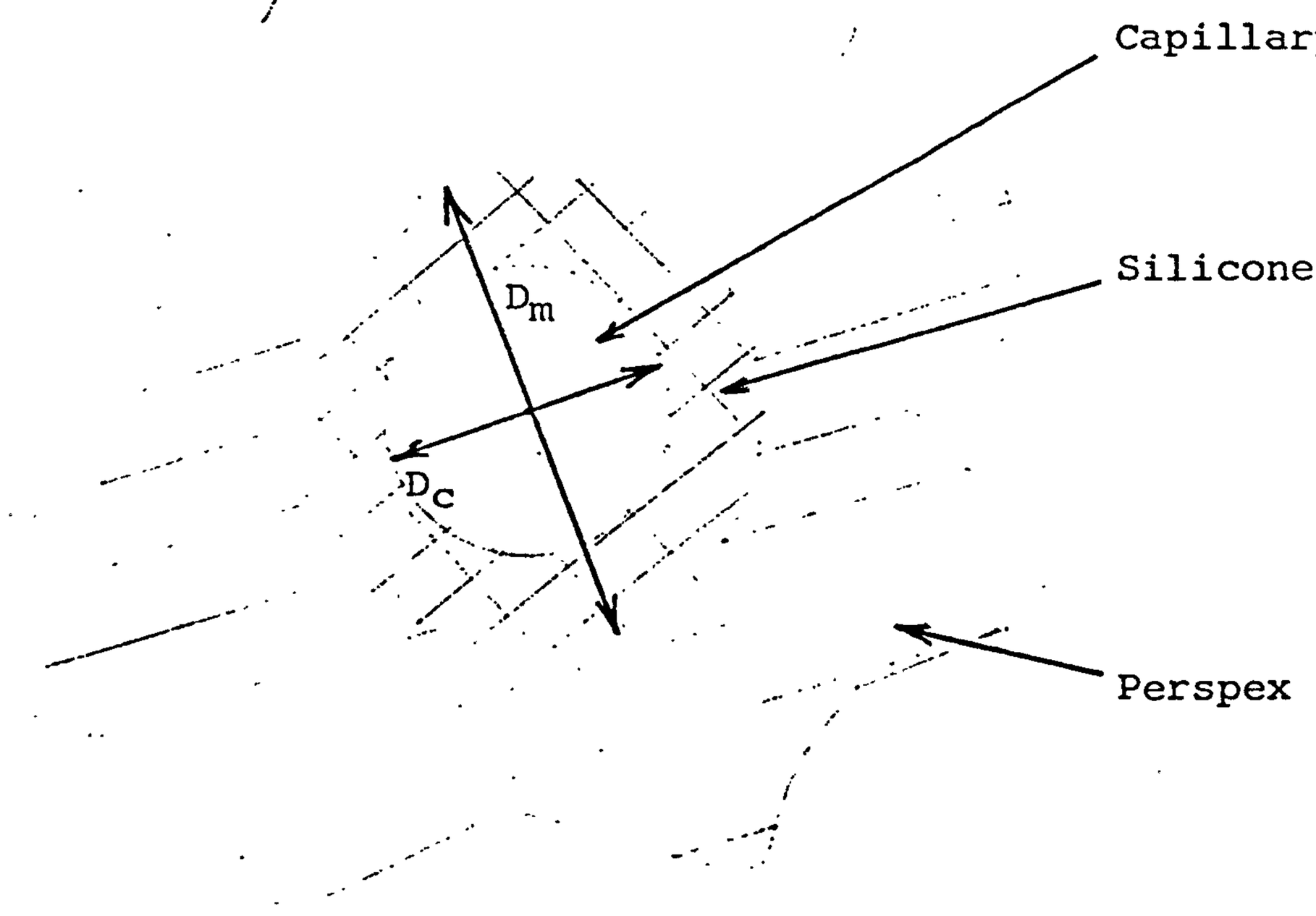

D_c, A_c diameter and area of capillary hole in silicone rubber sleeve.

D_m, A_m diameter and area of the hole in the perspex

A_p cross sectional area of silicone plastic

All changes are taken for a $1^{o}C$. increase in temperature.

α_m is the linear thermal expansion coefficient of the perspex

α_p is the linear thermal expansion coefficient of silicone rubber

The area expansion coefficient is approximately 2 times the linear.

T_c is the fractional temperature coefficient of the assembly on its own, i.e. $100T_c$ would need to be -0.5% per ^{o}C. to compensate for an underlying sensor temperature coefficient of + 0.5%.

The signal is given by:

$S = kA_c$ where k is a constant

and $\Delta S = k\Delta A_c$ ..... (1)

$$T_c = \frac{\Delta S}{S} = \frac{\Delta A_c}{A_c} \quad \text{..... (2)}$$

$$\Delta A_c = \Delta A_m - \Delta A_p \quad \text{..... (3)}$$

$$\Delta A_m = 2A_m\alpha_m \quad \text{..... (4)}$$

$$\Delta A_p = 2 A_p\alpha_p \quad \text{..... (5)}$$

From 3, 4 and 5.

$$\Delta A_c = 2 A_m\alpha_m - 2 A_p\alpha_p \quad \text{..... (6)}$$

From 2 and 6

$$T_c = \frac{2 (A_m\alpha_m - A_p\alpha_p)}{A_c} \quad \text{..... (7)}$$

$$A_p = A_m - A_c \quad \text{..... (8)}$$

From 7 and 8

$$\frac{T_c}{2} = \frac{A_m(\alpha_m - \alpha_p) + A_c\alpha_p}{A_c} \quad \text{..... (9)}$$

or $$\frac{T_c}{2} = \frac{A_m}{A_c}(\alpha_m - \alpha_p) + \alpha_p \quad \text{..... (10)}$$

or $$\frac{T_c}{2} = \left(\frac{D_m}{D_c}\right)^2 (\alpha_m - \alpha_p) + \alpha_p \quad \text{..... (11)}$$

The wall thickness $w = \frac{D_m - D_c}{2}$ ..... (12)

The wall-to-bore ratio $\frac{w}{D_c} = \frac{1}{2}\left(\frac{D_m}{D_c} - 1\right)$ ..... (13)

Whence : $\frac{D_m}{D_c} = 2\left(\frac{w}{D_c}\right) + 1$ ..... (14)

and substituting in (11).

$$\frac{T_c}{2} = \left[\frac{2w}{D_c} + 1\right]^2 (\alpha_m - \alpha_p) + \alpha_p \quad \text{..... (15)}$$

Taking α_m (perspex) as 10^{-4}

α_p (silicone) as 3.10^{-4}

$$\alpha_m - \alpha_p = -2.10^{-4}$$

Then from equation 11:

$$T_c = 2\left[3.10^{-4} - 2.10^{-4}\left(\frac{D_m}{D_c}\right)^2\right] \quad \text{..... (16)}$$

$$= 2.10^{-4}\left[3 - 2\left(\frac{D_m}{D_c}\right)^2\right] \quad \text{..... (17)}$$

$$100T_c = 2 \times 10^{-2}\left[3 - 2\left(\frac{D_m}{D_c}\right)^2\right] \quad \text{..... (18)}$$

Figure A2.1. shows the plot of the resulting temperature compensation versus $\frac{D_m}{D_c}$ (OD to ID) ratio) and also versus

$\frac{w}{D_c}$ wall to bore ratio, $\frac{w}{D_c} = \frac{1}{2}\left(\frac{D_m}{D_c} - 1\right)$

We see, for example, that a wall to bore ratio of 1.5 should give a compensation of - 0.58% per ^{o}C.

These calculations should however only be taken as a guideline. The expansion coefficients assumed are not necessarily accurate. Expansion coefficients of plastics show a spread depending on the actual formulations. Experimental checks are necessary and these indicate that the compensation actually achieved is less than that indicated by Fig. A.2.1., i.e. a somewhat higher wall to bore ratio is required, more like 2 than 1.5.

There is a possibility that, since the silicone rubber is fairly easily deformable, the full ΔA_c is not achieved, the volume change being partially taken up by a lengthwise distortion.

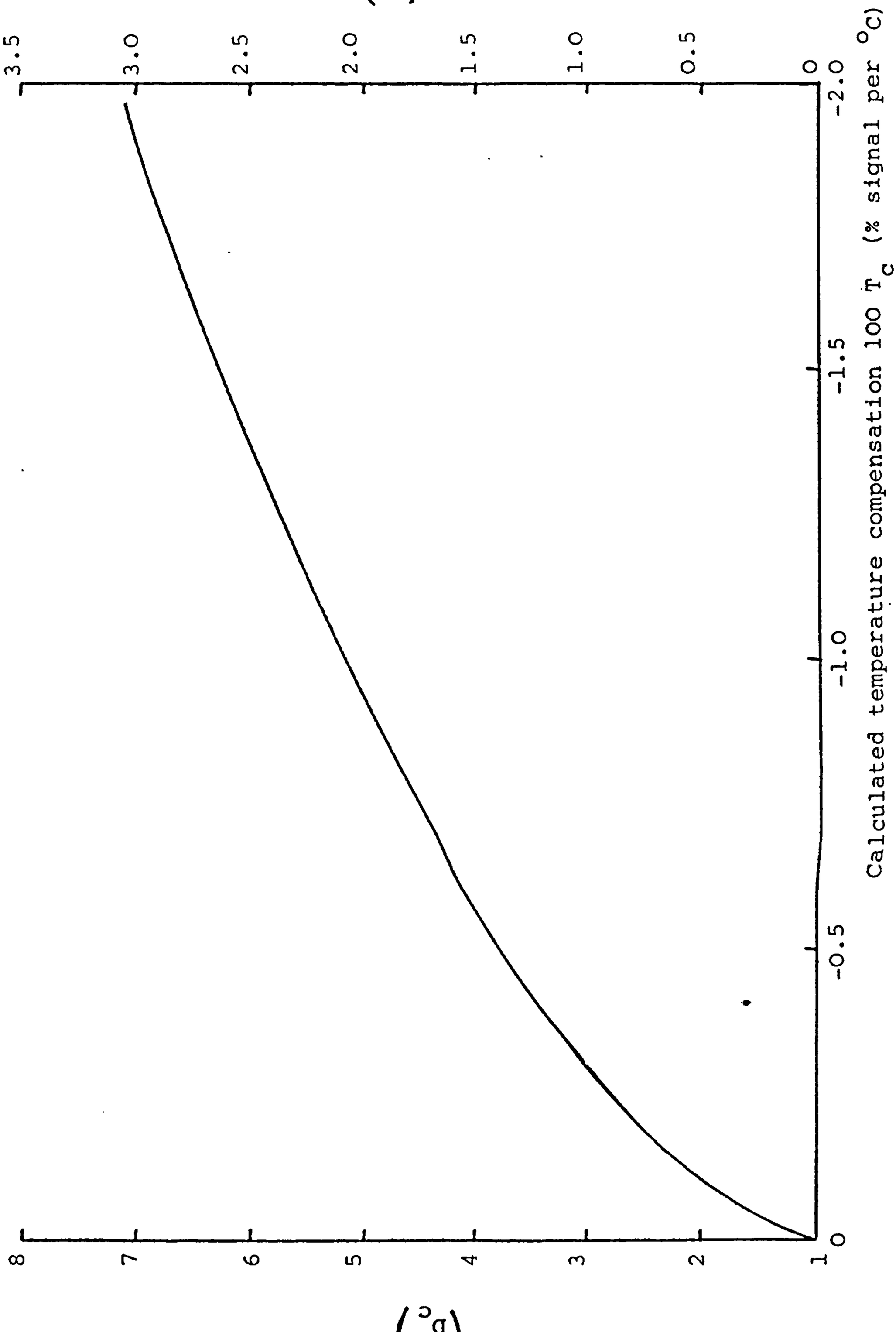

Figure A2.1. Temper

CTL Report No. 82/09/007
September, 1982

CITY TECHNOLOGY LIMITED.

The City University,
17/19, Sebastian Street,
London E.C.1.

13. CARBON MONOXIDE SENSOR FOR USE IN COAL MINES. PHASE 4

Final Report

A.D.S. Tantram
R. Chan-Henry
B.S. Hobbs

Mr. L.R. Cooper,
National Coal Board,
Mining Research & Development Establishment,
Stanhope Bretby,
Staffs.

N.C.B. Contract No. Y 135007/09/21

C.T.L. Project No. 94.09.00

CONTENTS

List of Tables

Page No.

List of Figures

SUMMARY

This report presents the results of the fourth phase of a program to develop a trace carbon monoxide sensor for use in coal mines. The sensor, designed primarily for the fire precaution application, now has the generic title 2T (2-electrode, trace sensor) to avoid the previous proliferation of mark numbers.

Effort during this development phase has been directed along 3 principal lines of investigation, conducted in parallel, as follows:

- Production development and hardware design.
- Electrode optimisation.
- R & D investigations of water balance, temperature compensation and hydrogen sensitivity.

The main hardware development has been a change from machined perspex to injection moulded polycarbonate, which has resulted in much stronger and more durable components. Design alterations have also been made to regulate gas access to the counter electrode, achieve release of internal gas pressures and facilitate interfacing of sensors to instruments. With regard to the latter, additional attachments have been designed and produced which ensure the proper incorporation of sensors

into the "plumbing" systems of total instrument packages. New production techniques and hardware design changes have been introduced which have virtually eliminated leakage problems and sensor losses due to poor internal electrical contact.

At the conclusion of phase 3, the two-electrode system developed had many advantages but was an inevitable compromise between the need to achieve both a low baseline and tolerance to 200 ppm CO. "Fine tuning" of electrode preparation and compositions during the 4th phase has resulted in improvements in performance and consistency. 2T sensors can now be reproducibly manufactured with a 0.5 to 2.0 ppm CO equivalent baseline (20^{o}C) and a capability to operate satisfactorily up to 200 ppm CO. Although no comprehensive program of life testing has been possible in this phase, indications are that the long term behaviour of the latest 2T sensor should at least equal the high degree of stability noted in the best machined perspex sensors.

Water balance studies continued from the last phase, have now reached a fairly comprehensive stage which can be summarised as follows:

- Water transfer rates follow fairly closely the theoretical relationship for control by diffusion through the capillaries.

- The lower limit of liquid volume in the sensor is about 0.4 cm^3, but acid concentrations should not exceed 20N for any sustained period of time.

- The upper limit of liquid volume is close to the available internal space, provided adequate pressure release facilities are available in the electrolyte reservoir.

- Standard sensors, incorporating adequate pressure release facilities should be capable of continuous operation in relative humidities between 20 and 90%. Excursions can be tolerated of several weeks in zero R_H and several months in 100% R_H, although precautions should be taken to avoid progressive water loss or gain, beyond the recommended limits.

A new capillary temperature compensation design has been developed and introduced into 2T sensors which is far more effective than the previous design, producing temperature coefficient values of about 0.4% per degree. This design is very recent and further work will be required to refine and reproducibly establish the technique.

Extensive study has been directed during this phase towards reducing hydrogen cross-interference. The only measure to show any promise was to preanodise the sensing electrode in-situ, after assembly. After such treatment, hydrogen cross-interferences could be reduced to below 10% equivalent CO signal. Studies are continuing to optimise the anodisation conditions and establish the long term stability of the lowered H_2-response following anodisation.

Additional R & D work has been undertaken during this phase on electronic circuits to couple with the sensors and three electrode sensors. The latter offer the prospect of providing a single sensor type, capable of covering all concentration ranges of interest to the NCB in the longer term.

Concurrently with the 2T development program, independent CTL R & D has been conducted on developing sensors for other applications. Where relevant the findings from these programs have been included in this report.

1. INTRODUCTION

During the previous phase (3) of the program the trade-off between baseline and tolerance levels at higher CO concentrations had been explored. While the Mark 5 sensor was the best compromise so far achieved, it was felt that some improvement could still be made by further trimming of the electrodes and their pairings. The objective was to achieve the lowest possible baseline consistent with reasonable tolerance to - and reasonable recovery from -, exposures at the 200 ppm CO level. It was decided to give this type of sensor, aimed primarily at the fire prediction application, the generic title 2T (2 electrode, trace sensor) rather than proliferate mark numbers.

Concurrently with the work on the 2T sensor concerned with the above and other improvements, we have been carrying out our own program on sensors for other applications, in particular for flue gas analysis and for environmental (personnel safety) monitoring (e.g. underground car parks) where the requirements are some-what different. This has resulted in the range of sensors listed below. Any findings from our own program which are useful or relevant to the NCB program are included in this report:

Type	2T	2E	2E	3F
Main application area	Fire detection	Personnel Safety		Flue gas analysis
Nominal sensitivity (μA/ppm)	0.1	0.1	0.1	0.03
Main design range (ppm)	0-30	0-500	0-500	0-1500
Upper CO limit (ppm)	200	500	1000	10,000
Baseline 20°C Equiv. (ppm)	0.5 to 2.0	+1 to +3	-1 to +3	-3 to +10

2T and 2E are two electrode sensors and 3E and 3F are three electrode sensors.

2. HARDWARE DESIGN

2.1. Injection Moulded Design

2.1.1. Design Modifications

During this phase a complete changeover to injection moulded hardware has been made. The design now used for production sensors (Figures 2.1., 2.2., 2.3.) is very similar to that described in the previous report, with some minor modifications as follows:

- the four, 4mm diameter, floor holes on a 13.5 mm PCD around the central wick hole, have been removed. These holes were originally intended to provide pressure equalisation inside the reservoir by ensuring a diffusion pathway to the atmosphere via the cathode ptfe tape. However, as described in section 5.1.3. of this report, the permeability of the diffusion pathway was insufficient to give adequate pressure release and this is now achieved by means of a modified back coverplate and seal design. (Section 2.2. below).

- Three 8BA clearance bolt holes, on a 34.4 mm PCD, have been included for securing the sensor to instrument cases, holders, etc., if required.

- The floor groove around the cathode perimeter has been removed and the current collector gates raised to about 0.5 mm above the floor to reduce gas side access to the cathode (Section 2.3. below).

- The top plate cavity depth has been reduced from 2.5 to 2.0 mm., increasing the capillary lengths from 2.5 to 3.0 mm. This change was intended to reduce both "end effects" with the temperature compensating capillary inserts and the relative errors introduced in cutting the capillary lengths to size.

- The radius of curvature between the floor and reservoir walls was increased from 0.3 to 2.5 mm to strengthen the counter plate at the expense of a small amount of reservoir volume.

2.1.2. Materials

Machined hardware components were made from acrylic (perspex) rod and initial attempts at moulding were also made with acrylic materials. However, the resultant components were very highly stressed and cracked on bolting-up; they were also highly susceptible to crazing and cracking in glued areas where solvent contact occurred. Some subsequent batches of machined components also suffered severe stress effects in glued areas. Acrylics were obviously unsuitable in this application and alternative materials had to be selected.

The following requirements were established in considering candidate materials:

(a) obviously the material had to be a thermoplastic for moulding.

(b) the material had to be capable of joining by glueing in order that existing assembly techniques could be utilised. Techniques such as ultrasonic or thermal welding could not have been adapted within the required timescale and materials such as polypropylene or polythene could not be considered.

(c) the material had to be acid resistant. Specifically it was required to withstand up to 20N H_2SO_4, at temperatures of 40-50^{o}C., at least as well as perspex. This rendered polyamide materials (NYLON) unsuitable.

(d) Superior mechanical properties to perspex were required, particularly, high resistance to stress and solvent crazing. High mechanical strength and toughness were particularly desirable. Some glass fibre reinforced plastics had extremely high strengths but had to be rejected since their moulded surfaces were very rough and could have presented sealing problems with current designs of hardware.

(e) Good machining properties for subsequent operations after moulding, particularly hole drilling, were desirable.

Three materials were selected for evaluation as follows:

- Polycarbonate (PC)
- Polyphenylene oxide (NORYL)
- Acrylonitrile Butadiene Styrene co-polymer (ABS)

All three materials were equally suitable on the first two requirements above of mouldability and glueability.

Material suppliers literature also indicated that they would all have suitable chemical resistance but confirmation tests were needed. Moulded components were immersed for 6 months at 50°C. in 15N H_2SO_4 and subjected to periodic weight checks. None of the materials, including a perspex control, underwent any significant weight change or any other ill-effect during this test. A polycarbonate sensor withstood 20N acid at ambient room temperature for 55 days, without ill-effect (Section 5.1.2.); this test was finally terminated due to failure of the glued seal. It should be noted, that whilst PC is very acid resistant, it is attacked by alkaline media, whereas NORYL, ABS and PERSPEX are resistant to both acid and alkali.

The final selection between the three candidate materials was made on the basis of mechanical properties. All three produced components which were free of stress cracks and solvent crazing. However, the ABS was a rather soft material and mechanical strength was somewhat below that of NORYL or PC. Past experience with ABS, indicated that components could suffer from creep over extended time periods when bolted-up into sensors. There was little to choose between NORYL or PC, except that the latter had a much higher impact resistance and toughness (Figure 2.4.). PC was therefore selected for CO sensors, but if ever the hardware were to be used with an alkaline

electrolyte, then NORYL would need to be substituted for PC.

The actual PC material selected was MAKROLON 2405 which is supplied in a clear form or with various coloured fillers. Some clear components were moulded and gave satisfactory service. However, for the mainstream production sensor, black, carbon-filled material is used since subsequent machining operations such as drilling the capillary insert holes are rather easier in this material than with the clear PC.

2.2. Pressure Release System

2.2.1. Pressure Release System Design

Water uptake and/or heating cause pressurisation of the gas in the electrolyte reservoir which, if not released adequately, can cause electrolyte leakage through the sensor current collector seals - see Section 5.1.3. of this report. The final solution adopted consisted of a pinhole in the back coverplate, protected from electrolyte leakage by a porous ptfe membrane. The detailed design is shown schematically in Figure 2.5. The ptfe membrane also ensures a gas diffusion pathway to the pinhole, even when the hole becomes obscured by electrolyte. The pressure release cannot function if the membrane is totally obscured e.g. if operating in a horizontal position with capillaries

facing upwards. In this position, any free liquid in the reservoir, resulting from excessive moisture pick-up,can form a continuous film over the ptfe and prevent gas release.

The pinholed coverplate assembly sits on a shoulder inside a well in the rear of the sensor counter plate body. The ptfe forms a "wrap-around" configuration which is sealed with Tensol glue as shown in Figure 2.5. - an initial dilute glue is applied to ensure good penetration of the ptfe pores, followed by a concentrated glue layer to form a final seal. A PVC outer coverplate is glued over the sensor rear as shown and is located between the securing bolt pillars (Figure 2.1.). This coverplate affords some protection to the pinhole and also prevents any inadvertant pressurisation of the cell by for example, pressing or clamping directly onto the pinhole coverplate. A slot in the sensor body allows release of gases from the chamber formed between the two coverplates.

2.2.2. Gas access via the pressure release pinhole

A gas access path to the electrode sandwich exists via the pressure release pinhole, into the electrolyte reservoir and through the wick hole. Carbon monoxide entering in this way, particularly during extended and/or high concentration exposures, could interfere with the sensor signal and produce persistent after-effects during recovery, since the reservoir would provide a large store of carbon monoxide.

The following test was conducted to measure any effects caused by rear access of carbon monoxide.

A 2-electrode trace sensor was made, incorporating a pinhole pressure release and a 2E-style electrode combination. The 2E electrode combination comprises a nominal 32mg per cm^2 JM standard Pt sensing electrode and 42 mg per cm^2 Engelhard 4 counter, and allows operation in higher CO concentrations than the 2T electrode pair. Other features, affecting gas accessibilities, were kept similar to 2T sensors. The sensor hardware was machined perspex with full side access. The steady sensor baseline (100 ohm load), with the capillaries and pinhole blocked was recorded before exposing the capillaries to a 500 ppm CO in air test gas in a polythene bag for 30 minutes, firstly with the pinhole blocked (test (a)) and secondly, with the pinhole open (test (b)). After each of these exposures the sensor recovery was monitored in air with both capillaries and pinhole blocked. Any differences between the two recovery curves would then give a measure of the interference from CO which had entered the reservoir during the second exposure.

The results given in table 2.1. in fact show that no significant interference occurred from CO entering by rear access at a 500 ppm concentration.

Further confirmation of this was obtained by allowing the sensor baseline to settle to a steady 0.1μA, with the

capillaries blocked, then exposing the pinhole only to 500 ppm CO in air with the sensor on its side, i.e. maximum gas access through both pinhole and wick hole. No measurable change occurred in the baseline over a 30 minute period.

2.3. Gas Access Routes to Cathode

The principal gas access routes to the sensor interior are:

(a) front access, through the sensor capillaries, directly onto the sensing electrode, where carbon monoxide is oxidised as it arrives. However, oxygen can further diffuse from the sensing electrode cavity, across the perimeters of the electrode tapes where they are in contact with each other, and then radially inwards to the counter electrode.

(b) side access, through the current collector gates in the sensor counter plate (figure 2.1.) and diffusion through the sensing and counter electrode ptfe tapes which protrude beyond the 'O' ring seal area.

(c) rear access from the electrolyte reservoir as described in section 2.2. above.

The latter, by inference from the tests described in section 2.2. above, is highly restricted, i.e. no measurable diffusion of carbon monoxide could be detected

at 500 ppm. However, this route may represent a significant one for oxygen access to the counter when operating the sensor in air and further measurements of the relative, diffusibilities of counter oxygen access routes are proposed, following this report period.

Early investigations[1] with "Mark 1" sensor designs showed that the ratio of front to side access on the sensing electrode was about 60:1 and the ratio of sensing side access to counter side access was about 4 or 5 to one. In this design the 'O' ring separated the two electrodes and formed the sides of an electrolyte compartment. With such an arrangement gas access to the counter was solely via the side, and none occurred from the front, across the electrolyte "sandwich". In these investigations, the reservoirs were filled with electrolyte and there were no rear coverplate pinholes, and therefore, no rear gas access. On the basis of these findings, following designs retained the side access feature of the Mark 1 sensor to ensure sufficient oxygen to meet the counter electrode current demand. However, in all following designs the 'O' ring was located outside the "sandwich", with the sensing and counter ptfe tapes being pressed together to form the electrolyte seal, which provides the additional front access pathway for oxygen to reach the counter electrode.

(1) A.D.S. Tantram, R. Chan-Henry, B.S. Hobbs; Phase 2 report to current NCB contract No. Y135007/09/21, CTL report 80/31/003 (April 1980).

A sensor experiment was conducted to obtain a measure of this front access pathway:

A 2T machined perspex sensor, with 2E-style electrodes was totally encapsulated in epoxy resin, except for the capillaries. Rear access was eliminated by filling the electrolyte reservoir completely before encapsulating. The high linearity and very stable signals, (apart from some creep up at 500 ppm CO - See table 2.2.) obtained with this sensor demonstrate that front access diffusibility easily meets the counter oxygen demand at carbon monoxide concentrations up to 510 ppm in air.

Since front access (and possibly rear access) routes provide an ample oxygen supply for the counter electrode current when operating in air containing up to 500 ppm CO, designs could be considered having much greater restriction of side access. Such designs would have the advantage of producing closer agreement between "top-only" and "total" sensor exposures. Side access causes disagreement between these modes of exposure in two ways:

(a) Carbon monoxide, reaching the COUNTER by the side access route, causes a signal cancellation and reduction in measured sensitivity. Carbon monoxide should be largely removed from front access gases to the counter by anodic oxidation on the sensing electrode. Carbon monoxide produces no interference through rear access up to 500 ppm and could be removed by oxidation catalysts at the pinhole if much higher levels were envisaged.

(b) Side access of carbon monoxide to the SENSING electrode produces additional signal sensitivity in total exposure modes relative to "top-only" modes.

The diffusibility of the counter side access route is several times less than that of the sensing side access route and the net observed effect on total exposure, relative to "top-only" exposure, is usually a signal enhancement. This is illustrated by results from a machined perspex, 2T sensor test as follows:

- baseline 0.03 μA @ 20°C
- span with 52 ppm CO in air on capillaries only, 5.32 μA (0.102 μA per ppm).
- span on total exposure to 52 ppm CO in air, 5.72 μA (0.110 μA per ppm), i.e. about 7½% sensitivity increase in the total exposure situation.

None of the above measurements were affected by blocking or unblocking the rear coverplate pinhole, supporting other findings (section 2.2. above) that CO access to the electrodes by this route is negligible at likely CO concentrations in a trace sensor application.

With the present moulded sensor hardware some steps have been taken to restrict side access by removing the groove in the sensor counter plate, around the electrode peripheries and raising the "gate" levels to 0.5 mm above the counter plate floor (section 2.1.1.). These steps resulted in a 3% reduction in sensitivity of a standard 2T sensor on total exposure,compared to capillary-only exposure:

- baseline 0.1 µA @ 20°C
- span with 52 ppm CO in air on capillaries only, 5.45 µA (0.0973 µA per ppm)
- span on total exposure to test gas, 5.30 µA (0.0946 µA per ppm).

2.4. Carbon Monoxide Sensor Interface Hardware

Two sets of components have been developed for mounting sensors in instruments in either a diffusion mode or flow systems.

2.4.1. Sensor Mounting in Diffusion Mode

The scheme of sensor mounting on an instrument case, using the diffusion mode set of components is shown in Figure 2.6. The collar and plug components are moulded in polycarbonate and detailed drawings of these are shown in Figures 2.7. and 2.8. Two different plugs are supplied with each component set as shown in Figure 2.6. One has a small,machined vent hole in the moulding (Figure 2.6.) and serves to blank-off the sensor when not in use,or to determine the sensor baseline; the vent prevents pressurisation of the sensor when inserting the plug. The second plug is used for calibrating the sensor from cylinders of compressed gas of known concentration.

A bonded ptfe membrane protects the sensor from ingress of dirt, dust, water, etc., and dampens pressure fluctuations and attendant bulk flow effects on the sensor, caused by draughts and gas flows during calibration. However, this membrane is unable to dampen severe pressure fluctuations, such as may be caused by diaphragm pumps. Such pumps should only be used in conjunction with the aspirated mode component set described below, which provides additional damping of gas stream pressure pulses.

The bonded membrane is fabricated from a stainless steel,expanded mesh support, coated with a thin film of Thixofix glue by solution dipping, into which is pressed

a thin (less than 1 thou thick) ptfe tape. Discs of the required diameter are punched from sheets of this composite. Two membrane materials were assessed for this component, a thin Gore ptfe tape and ZITEX (a highly porous, ptfe membrane). Both performed equally well and the former was chosen on grounds of lower cost and better availability. Results of span measurements with a 200 ppm CO in air gas, at 100 ml per minute, 100 ohm load resistor on an experimental 3E (3-electrode) sensor were as follows:

	Span (µA)	Sensitivity (µA per ppm)
Normal Laboratory Hood	13.95	0.0698
Collar and plug with Gore membrane	13.39	0.0669
Collar and plug ZITEX mambrane	13.22	0.0661

Response times were all similar and apart from an expected, slight decrease in sensitivity with the membranes in place, no other changes in sensor characteristics were evident.

2.4.2. Sensor Mounting in Aspirated Mode

The scheme of sensor mounting on an instrument case, using the aspirated mode component set is shown in

Figure 2.9. The hood and chamber components are moulded in polycarbonate and detailed drawings of these are shown in Figures 2.10 and 2.11. A small hole (about 0.7 mm diameter) is drilled in the hood wall at the position indicated in Figure 2.11, before glueing the hood and chamber together; this hole then communicates the 19 mm diameter cavity in the hood with the 25.5 mm diameter cavity of the chamber. Glue seals are indicated on the drawing in Figure 2.10. Such a configuration serves to dampen pressure fluctuations in the feed gas. Additional damping and sensor protection is given by the bonded ptfe membrane as in the diffusion mode of sensor mounting.

There are no significant problems associated with steady, high gas flows, up to 1 litre per minute, aspirated directly to the sensor from pressurised gas cylinders by means of the normal laboratory hood, used for quality control checking and other sensor testing. Inclusion of a ptfe protection membrane extends the flow tolerance to about 2.5 litres per minute (See table 2.3.).

When diaphragm pumps are used in instruments to supply gases to the sensor, the attendant pressure fluctuations in the gas stream produce a considerable enhancement of signal, which is highly flow sensitive, due to bulk flow effects. Under such conditions it would be impossible to obtain meaningful measurements from the sensor (See CTL Technical Note No. 13 reproduced in Appendix 1.) The aspirated mode set of components

however, enable normal, stable responses to be obtained when using diaphragm pumps with flow rates at least up to 1 litre per minute (Table 2.4.).

3. PRODUCTION DEVELOPMENT

3.1. Sealing Procedures with the Injection Moulded Hardware

The main problem area associated with production development during this phase was leakage with the injection moulded hardware. Satisfactory sealing was subsequently achieved by the introduction of the following measures:

(a) "Floor seal"

Leakage across the 'O' ring seal between the counter plate floor (Figure 2.1.) and the cathode ptfe tape was suppressed by glueing a blank ptfe tape onto the floor of the counter plate so that we now have the counter electrode tape sealing onto ptfe rather than onto the polycarbonate floor.

(b) Current collector sealing compound

A light film of fluorinated hydrocarbon grease was applied to the platinum current collector foils in the region of the 'O' ring seal, which acted as an inert, hydrophobic gap filler.

(c) Heat cycle prior to electrolyte charging

Assembled sensors were conditioned at 40^{o}C overnight before priming with electrolyte. This treatment appeared to "bed in" the 'O' ring sealing areas more efficiently before exposure to electrolyte.

Since the full implementation of these three measures very few failures due to leakage have occured with production size batches of sensors after several month's storage. Very long term storage effects have yet to be evaluated.

3.2. Sleeve Compensation Quality Control

The temperature compensating, silicone rubber sleeves, forming the sensor capillaries, produced a high spread in subsequent sensor signals. A prescreening method was therefore developed employing a calibration sensor in a similar way to that used for oxygen sensors. The capillary region of the calibration sensor's top plate was machined out to give an open top, over which the sleeved production plates were positioned and exposed to a test gas from a pressurised cylinder, using the usual laboratory test hood arrangement shown below:

Schematic

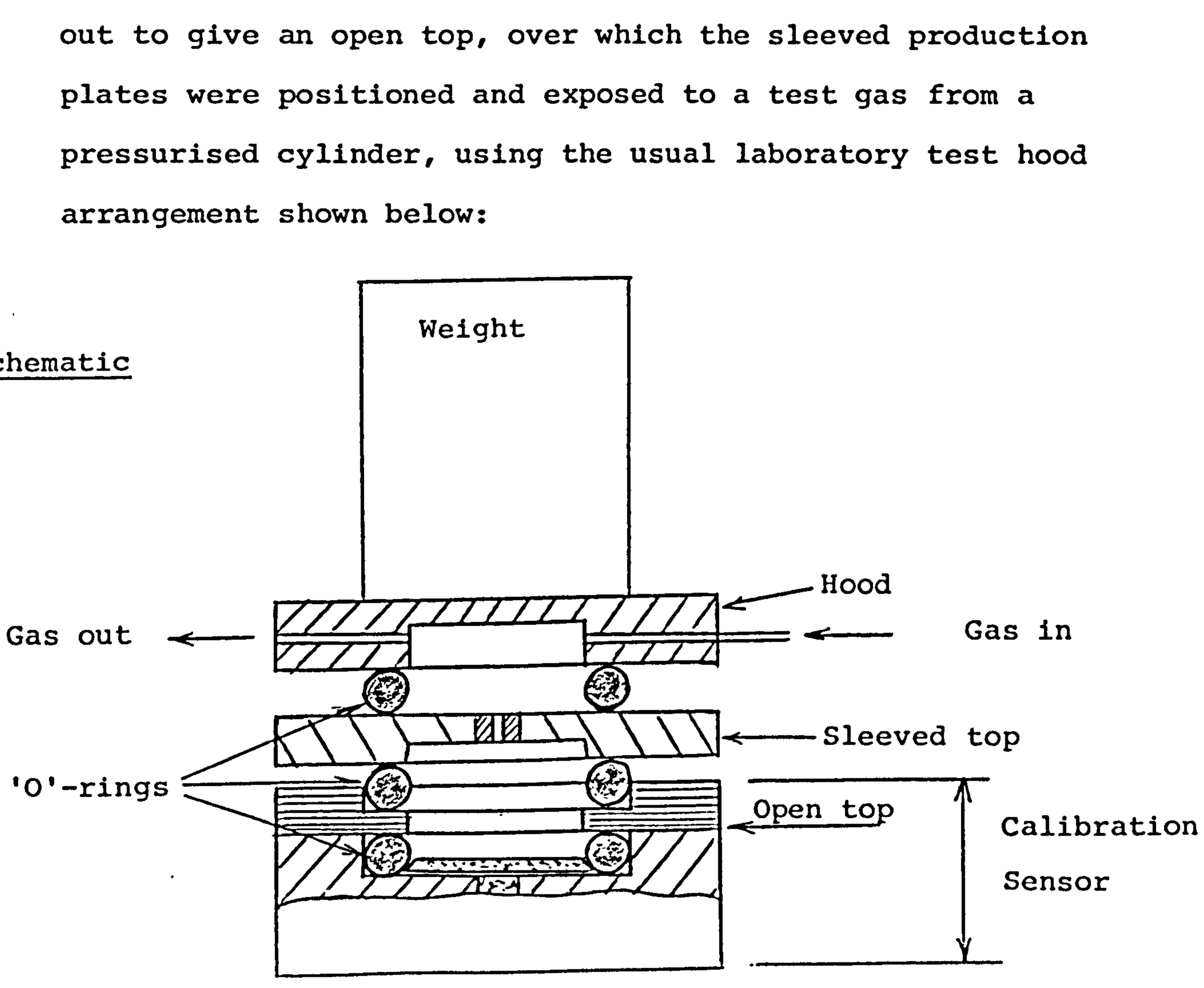

Any tops outside the required span limits could then be rejected before assembly into production sensors.

3.3. Electrode Manufacture

The following electrode compositions have been established for the 2T sensor:

Sensing Electrode (Anode)	Johnson Matthey Standard Black. Pt : ptfe ratio 4:1. Cured 280°C. Loading 20 to 25 mg per cm^2.
Counter Electrode (Cathode)	Johnson Matthey Standard Black. Pt : ptfe ratio 8:1. Cured 280°C. Loading 40 to 48 mg per cm^2.

Techniques developed in the previous phase have proven very satisfactory for production and few changes have been made. The only modification of any consequence is the reduction in platinum to ptfe ratio in the counter catalyst mix from 4:1 to 8:1. The platinum loading in the latest 2T counter electrode is very high (i.e. greater than 40 mg per cm^2) and the ptfe content was reduced to keep the total catalyst bulk within manageable proportions. The sensing electrode composition and general manufacturing techniques are essentially the same as for the Mark 5 and Mark 6 sensors described in the last report but platinum loadings have been reduced by about 20%.

3.4. Current Collection and Electrode Sandwich Support

During the manufacture of production size batches of sensors, it was noticed that the occasional sensor had low signals coupled with a slow response. Detailed investigations of these sensors indicated a partial loss of electrical contact between the current collector foils and electrode faces which most likely developed as a result of the "doming" of the electrode sandwich into the top-plate cavity.

Normal behaviour was restored in these sensors by compressing the dome back, using either Webril packing discs in the top-plate cavity, or incorporating a silicone rubber pillar insert in the centre of the top-plate, with offset capillaries as shown schematically below:

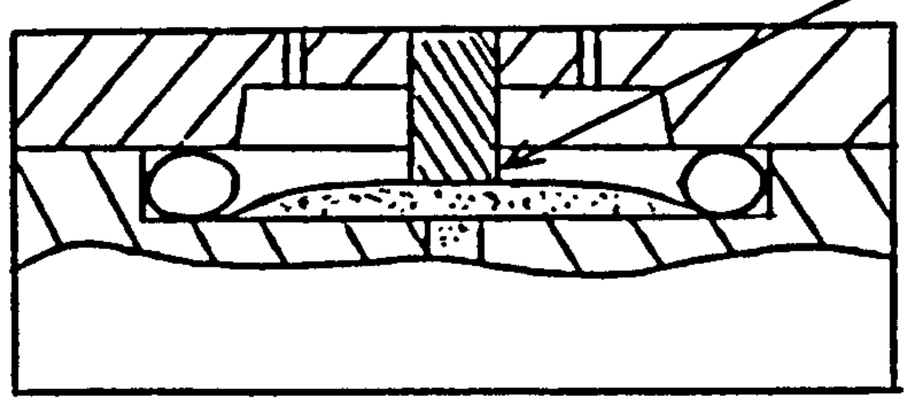

At the time of reporting no final choice between these two support techniques has been made, but either method has totally alleviated the original problem.

4. PERFORMANCE CHARACTERISTICS OF 2T SENSORS

4.1. Background to test program

The injection moulded hardware was introduced about mid-January 1982. About 154 2T sensors were manufactured in the following 7 months, including 43 supplied under this contract to NCB Bretby and Yorkshire Laboratories for their own test programs. All of these sensors would have incorporated the design changes described in Section 2.1.1., the pressure release system (Section 2.2.1) and the measures to improve sealing (Section 3.1.). The modified current collection and electrode support features (Section 3.4.) and the split inserts for improved temperature compensation, were introduced together from about mid-June and were incorporated in about 80 sensors made during the following 2 months.

All of the sensors produced were checked for baseline and sensitivity. Smaller groups of sensors were used for measurements of response times, CO-tolerance, hydrogen sensitivity and temperature coefficient.

Since the current 2T design has only fairly recently been established and committed to production, no comprehensive program of long term testing has been possible in this period. However, indications from recent tests conducted on a few 6-month old 2T sensors, were that long term behaviour should at least be as stable as that obtained with the

machined perspex versions, and a test program can be initiated now that the design is reasonably established.

4.2. Baseline and Signal sensitivity

Baselines and signals (50 ppm CO in air) are checked on sample sensors immediately after assembly and then on all sensors after allowing at least 1 week to settle down. Baseline and signal readings both show some decrease in the first week or so before stabilising to steady values. The following values after at least 2 weeks storage were recorded from a total of 42 sensors, representing 3 batches prepared in January, March and July 1982:

Baselines: mean value 1.20 ppm
standard deviation 0.57 ppm
Spread 0.34 to 3.44 ppm.

Most sensor baselines were below 2.0 ppm, only three had higher values of 2.10, 3.44 and 2.50 in batches 1, 2 and 3 respectively.

Signals: Mean value 0.10 µA/ppm
Standard deviation 0.01 µA/ppm

There were no significant differences between these results and those for the individual sensor batches:

	Batch 1	Batch 2	Batch 3
Age since assembly	17 days	60 days	40 days
Number of sensors	9	20	13
Mean Baseline (ppm)	1.20	1.24	1.15
Standard deviation (ppm)	0.502	0.653	0.466
Mean Sensitivity (μA per ppm)	0.103	0.092	0.110
Standard deviation (μA per ppm)	0.005	0.005	0.005

4.3. Response Time

Response times were not recorded during production quality control and no definitive study of response time has been conducted in the R & D program. However, a great many traces have been recorded in the course of R & D studies in this period and sample readings taken from the January - August 1982 investigations indicate that all sensors have response times of between 23 to 35 seconds for a 90% change on a 50 ohm load. The effects of load resistor on response time, obtained from one sensor (2T 158) are shown in Figure 6.5.

4.4. Carbon monoxide tolerance

Four sensors of the most recent design (June 1982) were subjected to a standard tolerance test with 209 ppm CO in air. Results showed that this design has a useful application range at least up to 200 ppm CO (Table 4.1.).

Table 7.1. shows the result of a tolerance test at 1000 ppm CO on a single 2T sensor. Although drift appeared reasonable, hysteresis on recovery was high and signals during exposure were about 13½% below the expected value.

4.5. Temperature coefficient

A batch of 4 sensors was made to the recent June 1982 design, but without capillary compensation or the electrode sandwich support. Intrinsic signal temperature coefficients were determined on these sensors over the range -30 to + 40°C. Results are given in Table 4.2.

All four sensors produced signal/temperature characteristics typified by that shown in Figure 4.1. Below 20 to 25°C the characteristics were slightly curved, but reasonable straight lines could be drawn through the points from which temperature coefficient values were calculated by regression analysis of 1.0 (± 0.1) % signal at 20°C. per degree change. These values were in good agreement with temperature coefficient measurements on machined perspex 2T-style sensors prior to January 1982. Above 25 to 30°C. the characteristics showed a curvature to much smaller coefficients which is also typical behaviour.

Baselines followed typical behaviour of all measurements made in the past, roughly doubling per 10°C. increase.

No testing in large numbers has yet been carried out on the latest compensated capillary design which has only recently been established. However, on the few sensors tested so far, it would appear that compensated 2T sensor temperature coefficients of 0.4% per degree will be achieved. (Section 5.2.).

4.6. Hydrogen Sensitivity

No definitive testing of this property on large numbers of sensors has yet been carried out. The whole subject of hydrogen sensitivity is still the topic of further research investigation (Section 5.3.). All 2T sensors subjected to hydrogen response so far have had values of between 10 and 30% equivalent CO response at 20^{o}C.

Hydrogen response is probably controlled by both diffusion and electrode kinetics and as such is considerably influenced by temperature, although not as much as doubling for every 10^{o}C. increase:

Temperature (^{o}C)	Sensor hydrogen response (% equivalent CO signal)			
	2T130	2T129	2T128	2T127
-30	4	2	5	4
20	17	15	27	15
30	28	25	47	24
40	41	34	74	37

4.7. Provisional Performance Summary of 2T Sensors

Table 7.2. lists and compares the characteristics of 2T sensors with other versions of CTL CO sensors, based on all testing of recent designs to date. These data are for general guidance only and since all sensor versions are still subject to further development, changes are likely to occur. As regards 2T sensors, it is intended to further investigate the hydrogen cross sensitivity and establish the temperature compensation design in the next phase of development.

5. RESEARCH AND DEVELOPMENT BACKUP

5.1. Water Balance

5.1.1. Introduction

Past work[1] has established two important facts with regard to sensor water balance as follows:

(a) Water transfer rates closely follow the theoretical relationship for control by diffusion through the sensor capillaries.

(b) The limits of workable electrolyte volume for the standard sensor are between 0.5 and 3.5 cm^3., corresponding to acid concentrations of 20N and 2.9N respectively, when primed with 1 cm^3 10N H_2SO_4.

During this report period attention has been focussed on the remaining questions of:

(a) Effects of sensor operation for extended periods at electrolyte CONCENTRATIONS representing these extremes of water loss and uptake.

(b) Effects of the consequent electrolyte VOLUME changes on prolonged exposure to both high and low humidities.

The following investigations were conducted with experimental sensors which were close to the present 2E-version.

The 2T design, finally adopted by NCB for trace CO measurement, has the same nominal sensitivity of 0.1μA per ppm, but has larger capillaries to compensate for the fact that, due to the electrode compositions, it only operates at about 55% theoretical signal, whereas the 2E utilises nearer 90 to 95% theoretical signal. Thus the 2T sensor will be capable of correspondingly greater water transfer rates.

Another consequence of the 2E electrode composition balance is that baselines are generally higher than the 2T and this was reflected in the experimental sensors studied in this work.

5.1.2. Extended Operation at High Acid Concentration and Low Humidity

Test 1. Sensor subjected to continuous zero humidity at ambient Temperature.

Sensor "E4" : Cathode 43 mg per cm^2 Pt (Engelhard No. 4)
Anode 33 mg per cm^2 Pt (J.M. Standard
100 ohm load resistor
Primed 1 cm^3, 10.3N H_2SO_4
(Note: no means provided for internal pressure release - see Section 5.1.3.)

After an initial "settling" period in the laboratory atmosphere, the sensor was placed in a dessicator over silica gel at ambient temperature. The sensor was removed regularly and checked as follows:

(a) Weighed to determine water loss

(b) Baseline measured with blocked-off capillaries.

(c) Span response to CO measured with a nominal 50 ppm CO in air test gas.

The sensor record is given in table 5.1.

The sensor ran satisfactorily for about 4 weeks in zero humidity, during which time the acid concentration increased from 11.7N to 23.2N, representing a water loss of 0.43 cm^3 and a final volume of 0.445 cm^3. There were few signs of performance decline at this point due to electrolyte deficiency. The volume was somewhat below the minimum of 0.5 to 0.6 cm^3 established in previous work, which may reflect a more effective electrolyte distribution on drying out a larger volume compared to priming with a smaller volume.

The water loss rate followed the theoretical relationship closely. An estimated 27 days to reach 23.15N acid from 11.7N (assuming a mean laboratory ambient temperature of 20^{o}C.) compared to 29 days actually measured.

During the 5th week the ABS coverplate and perspex base of the sensor fractured and the test was discontinued. The acid concentration had by then reached 25.3N which was the most probable reason for the plastics failure. The sensor continued to operate reasonably, albeit at a somewhat enhanced baseline and decreased span, although the response

time was essentially unchanged and the electrolyte volume was only about 0.4 cm^3.

Test 2. Continuous operation of a sensor in 20N electrolyte

Sensor "E1" : Cathode 37 mg per cm^2 Pt (J.M. Standard)
Anode 27 mg per cm^2 Pt (J.M. Standard)
100 ohm load resistor
Primed 0.5 cm^3 20N H_2SO_4.
(Note: no means provided for internal pressure release see section 5.1.3.)

The sensor was kept in a dessicator over 20N H_2SO_4 (R_H 14%) at ambient temperature and regularly checked for weight, baseline and span to a 50 ppm CO in air test gas.

The test record is given in table 5.2.

Apart from a somewhat higher variability in baseline and span compared to a standard sensor primed with 10N H_2SO_4, this sensor behaved quite well for a period of 57 days. By day 65 the glued joint of the back coverplate had clearly developed a leak and acid attack on the terminals resulted in a high negative baseline, between 0.5 and 1μA. The test was therefore terminated at this point.

Although the sensor had been stored in a dessicator over its own electrolyte (nominally 20N H_2SO_4), it apparently continued to lose some water, and its concentration over the 65 day test period increased to about 23N.

Tests 3 and 4. Continuous operation of sensors at 15N electrolyte concentration

Results of the two preceding tests indicated that at, or above 20N acid concentration, not only are electrolyte volumes rather close to the lower operational limits but also conditions become too agressive. In particular the glued joints suffer degradation and develop leaks and in certain severe cases the perspex body can fracture. Further life tests were therefore conducted on sensors at the intermediate acid concentration of 15N, as follows:

Sensor "E9" : Cathode 44.2 mg per cm^2 Pt (Engelhard No. 4)
Anode 30.4 mg per cm^2 Pt (J.M. Standard)
100 ohm load resistor
Primed 1 cm^3, 10.3N H_2SO_4.
(Note: pressure release facility in back coverplate).

This sensor was dried over silica gel to about 14N acid concentration, then stored over saturated $MgCl_2$ solution (R_H same as 15N acid). The salt solution achieved better humidity control than 15N sulphuric acid solution.

Sensor "E10" : Cathode 36.7 mg per cm^2 Pt (Engelhard No. 4)
Anode 29.7 mg per cm^2 Pt (J.M. Standard)
100 ohm load resistor
Primed 1 cm^3, 14.4N H_2SO_4.
Stored over saturated $MgCl_2$ solution.
(Note: pressure release as for E9).

The sensor records of weight, baselines and spans are given in tables 5.3. and 5.4.

Both sensors exhibited very stable characteristics for periods between 100 and 200 days with electrolyte concentrations between 14 and 16N H_2SO_4. No plastics degradation, or leaks, were apparent in this time.

Tests 5, 6 and 7, Operation with "new materials" in 2ON acid

3 sensors were made up using moulded NORYL, POLYCARBONATE and ABS components respectively (See section 2.1.). Each sensor was primed with 1 cm^3, 2ON H_2SO_4. All three were kept at a nominal constant weight, and acid concentration, by storing alternately in either the laboratory atmosphere or in a dessicator over silica gel.

The NORYL and ABS sensors developed leaks in their glued coverplate joints within 2 weeks, and had to be discontinued. Since the polycarbonate had by then been selected for the sensor moulded hardware, no further sensors were made with those two alternative materials.

The polycarbonate sensor record is given in Table 5.5. This sensor showed a very stable performance until day 55 when a leak developed in the joint of the coverplate. Acid corroded the "live" bolts of the sensor terminals, causing a high negative baseline, and the test had to be discontinued.

A further polycarbonate sensor, primed with 1 cm^3 15N H_2SO_4, had a very stable performance, similar to perspex sensors, for 200 days. The test was stopped at this point and no serious problems are envisaged with this material, provided acid concentrations do not exceed 20N for any extended period of time.

5.1.3. Extended Operation at Low Acid Concentration and High Humidity

Test 8. Operation of sensor charged with 1.72N acid

Sensor "E5" : Cathode 41 mg per cm^2 Pt (Engelhard No. 4)

Anode 31 mg per cm^2 Pt (J.M. Standard)

100 ohm load resistor

Primed 2 cm^3, 1.72N H_2SO_4.

(No pressure release facilities provided - see section below)

The weight, baseline and span of this sensor were monitored for a 200 day period, stored in a dessicator over 1.72N H_2SO_4. During this time the sensor performance remained very stable (Table 5.6). Although the sensor was stored over its own electrolyte, it did lose a little water over the period and the final electrolyte concentration was about 1.85N.

From day 202, the sensor was kept in the laboratory atmosphere and allowed to dry out. The CO response first showed signs of decline in span at day 235, corresponding to an acid volume of 0.84 cm^3. Thereafter the effect became

progressively more apparent, but did not become too serious until after day 255 when the electrolyte volume fell below 0.4 cm^3 and the CO response underwent a sudden, sharp cut off. The full CO response was restored when the electrolyte volume was returned to > 0.5 cm^3 by putting the sensor in a dessicator over water.

Test 9. Sensor subjected to continuous 100% humidity at ambient temperature

Sensor "E3" : Cathode 43 mg per cm^2 Pt (Engelhard 4)
Anode 33 mg per cm^2 Pt (J.M. Standard)
100 ohm load resistor
Primed 1 cm^3 10.3N H_2SO_4.
(Note: no pressure release facilities provided - see below)

This sensor was "settled" in the laboratory atmosphere, then placed in a dessicator over water. Within 2 weeks of putting in the dessicator leakage occurred at both terminals, identified by a high, erratic, negative baseline, terminal corrosion and acid reaction to pH papers on the tags.

From weight change data the electrolyte volume was estimated to be about 1.3 cm^3. Assuming no pressure release occurred in the electrolyte reservoir, this water uptake would have resulted in an increase of air pressure in the reservoir of about 40 inches water gauge. Even without any water uptake, a temperature change from 20°C. to 40°C. would generate a pressure of about 24 inches water gauge in a

standard sensor, if no release of gases from the reservoir were possible. The region around the platinum foil current collectors would be expected to be most susceptible to leakage caused by back pressures of this magnitude.

Investigations of sensor pressurisation and leakage

A further sensor was made up with a modified coverplate to allow application of a pressure into the reservoir space by means of an adjustable water column. This experiment confirmed that virtually no measurable pressure release occurred over several days under a 40" water pressure head. The only possible pressure release pathway in this sensor would have been by access to the cathode ptfe tape around the wick hole and diffusion through the tape, out of the sensor's side. Two measures were investigated to facilitate pressure release from the reservoir:

(a) Improvement of access to the electrode tapes by drilling holes in the sensor floor. On pressurising such a sensor with a 40" water head a slow, but measurable rate of pressure release was achieved. However, the rates were likely to be too slow to cope with pressurisation caused by a rapid temperature rise.

(b) A small pinhole (about 0.2 mm diameter) was drilled through the centre of the rear coverplate, with a porous ptfe membrane, cemented over the inside of the coverplate,

to prevent electrolyte seepage. The size of the pinhole was restricted to prevent undue amounts of water transfer or CO access to the sensor interior (see sections 2.2. and 2.3.). Pressurised gases within the reservoir would be released by diffusion through the ptfe tape, flow along the channel between tape and coverplate, and out the coverplate pinhole. In this way pressure release would be possible, even if the pinhole area became obscured by electrolyte. Permeability measurements on this configuration confirmed that rapid pressure release was possible, but that a Webril packing disc was necessary between the membrane and coverplate, to prevent the membrane becoming too tightly forced onto the coverplate surface - without this packing, gas release rates actually increased with decreasing pressure in the permeability tests, as the tape relaxed from the coverplate surface and presented a lower flow resistance to the gases. Such a configuration of course will only operate successfully provided the ptfe tape does not become totally obscured by electrolyte, e.g. when operating sensors in a horizontal position with the capillaries facing upwards, or when the sensor reservoir becomes near full. Full design details of the coverplate pressure release system are described in section 2.2.1.

Three sensors were prepared as follows and kept at 40°C, 100% R_H, in a vertical position.

Sensor A: Standard sensor without any pressure release facilities.

Sensor B: Standard sensor with floor holes.

Sensor C: Standard sensor with coverplate pressure release system.

Sensors were removed daily for weighing to estimate water uptake and to assess for leakage by measurements of baseline, visual examination and pH papers.

Sensors A and B developed gross leaks by days 3 and 6 respectively; electrolyte volumes after these times were 1.26 cm^3 and 1.44 cm^3 respectively. Thus, as expected, floor holes gave some pressure relief but this was insufficient to prevent leakage on continuous exposure in high humidities and/or thermal cycling between 20 and 40^{o}C. Sensor C, containing the pressure release coverplate, survived 31 days before leakage was apparent at the current collector seals. At this point the sensor electrolyte volume was 2.02 cm^3, about 60% filled.

Although the coverplate pressure release system resulted in significant improvement compared to the other two sensors, leakage still occurred long before the reservoir filled up. This might have been partly due to the development of large transient pressures on returning the sensors to 40^{o}C after the daily tests. This was confirmed by making another sensor having 5, 2.5 mm holes in the coverplate. Although such a design would have impractically

high water transfer and CO access capabilities, it should be virtually free of any significant pressure transients caused by large step temperature changes. In fact, this sensor virtually filled up completely to 3.4 cm^3 electrolyte volume before finally leaking through the current collector seals after about 30 days at 40°C. in 100%R_H.

Tests 10, 11 and 12. Continuous operation in 100% humidity at ambient temperature of sensors with pressure release coverplates.

Three sensors were made up with pressure release coverplates as follows:

Sensor "E6" : Cathode 43.7 mg per cm^2 Pt (Engelhard 4).
Anode 31.2 mg per cm^2 Pt (J.M. Standard)
100 ohm load resistor
Primed 1 cm^3, 10.3N H_2SO_4.
0.17 mm coverplate hole.

Sensor "PR1" : Cathode 42.3 mg per cm^2 Pt (Engelhard 4)
Anode 31.7 mg per cm^2 Pt (J.M. Standard)
100 ohm load resistor
Primed 1 cm^3, 10.3N H_2SO_4.
0.17 mm coverplate hole.

Sensor "E8" : Cathode 43.9 mg per cm^2 Pt (Engelhard 4)

Anode 30.0 mg per cm^2 Pt (J.M. Standard)

100 ohm load resistor

Primed 1 cm^3, 10.3N H_2SO_4

0.17 mm coverplate hole.

Sensors were "settled" in the laboratory atmosphere, then stored in dessicators over water. Weights, baselines and spans of sensors were monitored regularly. Results are given in tables 5.7, 5.8 and 5.9.

Sensor PR1 developed a leak in the coverplate seal during week 3. This was most likely a faulty seal and not caused by pressurisation; this was the first of the pressure release sensors and improved techniques, now employed in production, have virtually eliminated leakage in this area. Although the sensor was operating perfectly well, the test was discontinued in the 6th week since physical loss of electrolyte by leakage invalidated the water balance record.

Sensors E6 and E8 had very stable characteristics under continuous exposure to 100% humidity, at room temperature, for periods of 250 and 175 days respectively. During these times the sensors liquid volumes increased to fill between 75 and 80% of the available reservoir space without any signs of leakage being detected.

5.1.4. Conclusions

The absolute lower limit of acid volume in the CTL

CO sensor is about 0.4 cm^3*. Below this, complete loss of sensor signal occurs. However, sensors may suffer a progressive decline in signal span with decreasing volume from about 0.8 to 0.7 cm^3 and the electrolyte becomes too aggressive above about 20N concentration (corresponding to 0.5 cm^3 electrolyte volume in the standard sensor), attacking glued joints and seals and in severe cases, inducing cracking and fracture of the plastic hardware. Thus, the practical limits of minimum volume are nearer 0.6 to 0.7 cm^3, corresponding to electrolyte concentrations of 17 to 15N. Within these limits the Standard Sensor can operate continuously in relative humidities down to about 20%, without incurring any water balance problems. Excursions of several weeks at zero humidity can be sustained, but special measures may be necessary to cope with the cumulative water loss when operating for frequent and/or extended periods in very dry conditions. Operating times in dry conditions could be extended by priming with greater volumes and/or using more concentrated electrolyte, but at some point sensors will need to have their water restored by exposure to a moist atmosphere, before any permanent damage occurs through degradation of the plastic hardware, joints, seals, etc.

The upper limit of acid volume is determined by the free space within the sensor reservoir, which is about 2.5 cm^3 in current standard sensor designs. Acid concentration

* Since completing these investigations some additional studies have shown that both temperature coefficient and hydrogen sensitivity, are virtually unaffected by electrolyte volume changes down to 0.4cm^3, below which the signal is sharply cut off.

in a standard sensor, primed with 1 cm^3 10.3N H_2SO_4, at the limit of water uptake, would be about 3N. No measurable changes in sensor performance characteristics (baseline or span) will result from acid dilution to this extent. The increase in liquid volume however, can only be accommodated if adequate means are provided to release the attendant pressure build up within the sensor interior. Pressures caused by thermal cycling must also be relieved if leakage is to be prevented. The pressure release system developed in this report period achieved better than 80% space availability for water uptake and thermal cycling between 20 and 40°C., provided the back of the coverplate was not completely obscured by electrolyte.

Standard sensors incorporating the pressure release system should be capable of continuous operation in relative humidities up to about 93%, without incurring any water balance problems. Excursions of several months (depending on temperature) at higher humidities are possible but, as with very dry conditions, special measures may be necessary to cope with any cumulative water gain when operating frequently or for any extended periods in very moist conditions. Operating times may be extended by priming with smaller volumes of less concentrated electrolyte, but at some stage it will be necessary to restore the water balance by drying out, before permanent damage from leakage occurs.

5.2. Temperature Compensation with Silicone Rubber Inserts

Early sensors which were made with a shallow cavity under the capillaries, had a degree of fortuitous temperature compensation due to differential expansion effects on the appreciable spreading resistance (See Phase 3 report of this contract, CTL Report 81/31/006, July 1980). In the interests of reproducibility and stability the cavity was deepened and the fortuitous compensation was lost. This in turn demanded extra compensation from the silicone rubber capillary inserts. The principle involved is that, since the silicone rubber has a much higher thermal expansion coefficient than the surrounding plastic (polycarbonate in the latest versions), differential expansion will tend to close up the capillary as the temperature rises and so offset the intrinsic sensor temperature coefficient (See Appendix 2 to previous report, CTL 81/31/006, July 1980 for a full description).

In theory the degree of compensation should be proportional to the ratio of silicone rubber to capillary cross sectional areas. In the case of a simple tube configuration, increasing the wall to bore ratio should increase the effect. In practice when this ratio was increased in order to gain the extra compensation now needed for the reasons given above, very little additional compensation was achieved even with substantial increases in wall to bore ratio, i.e. theory was apparently no longer being followed in practice.

It was therefore evident that a substantial part of the differential expansion was being taken up by distortion of the ends of the tube rather than by changing the capillary diameter.

Two factors are probably relevant here:

(1) The radii of curvature of the silicone rubber surfaces. One would expect that the smaller the radius of curvature the more difficult it will be to distort. So distortion of the flat ends of the tube would tend to be favoured over the interior capillary wall with its small radius of curvature.

(2) The relative surface areas of the interior capillary wall and the ends of the silicone rubber. One would expect that the higher the ratio capillary wall area to end area, the more the differential expansion would be taken up by a change in the capillary as opposed to end distortion. If we look at a typical simple capillary insert e.g. 3 mm long, 1 mm bore and 1.6 mm wall, then this ratio is 0.36:1, i.e. the relative areas favour end distortion. The fraction of interior wall area to total exposed area is 0.26 and this is roughly the fraction of the theoretical compensation that was actually achieved.

On these arguments better compensation (nearer the theoretical) should result from building in greater interior wall area of higher radius curvature.

In this direction the following scheme has been briefly tried:

The silicone tube is cut lengthways and a solid core inserted. This results in a configuration in cross section as illustrated below.

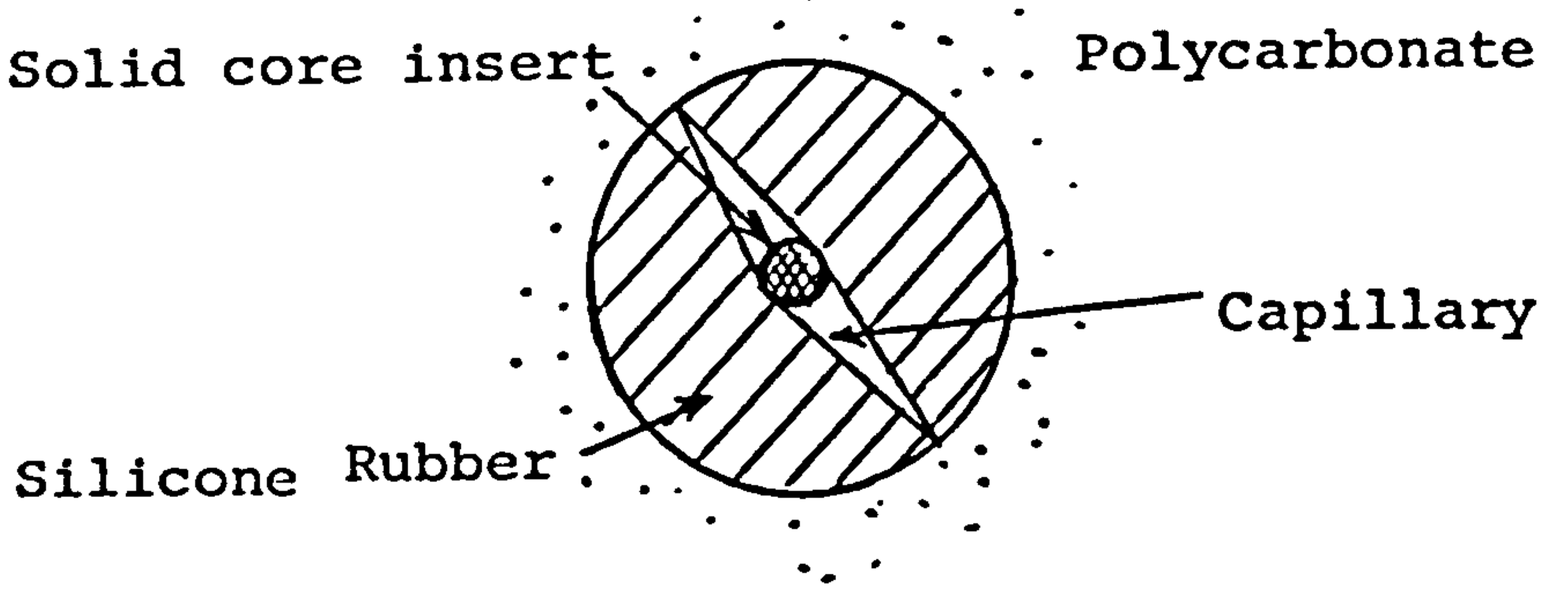

This increases the calculated ratio of interior wall to end surface to 0.74 (in practice a little less as the gap tends to close near the outer diameter). The fraction of interior wall area to total is now 0.42. With two cross splits the calculated ratio is 1.47 and the fraction 0.6.

Initial experiments have indicated improvements roughly consistent with these fractions. For example the 2T sensor intrinsic temperature coefficient is about 0.9 to 1% per degree, compared to about 0.4% per degree, obtained with the latest compensation geometry in the moulded polycarbonate hardware. Further work is required to refine and reproducibly establish this technique.

5.3. Hydrogen Cross-Interference

Three areas of investigation have been pursued in this report period with the objective of reducing hydrogen cross-interference in carbon monoxide sensors:

(a) development of selective sensing electrode catalysts.

(b) development of selective chemical filters.

(c) voltage biasing and anodising of the sensing electrode.

5.3.1. Selective Electrode Catalysts

During this report period studies have been concentrated on a range of precious metals and their alloys with the objective of increasing the CO specificity relative to that of hydrogen. Systems studied included platinum-ruthenium, platinum-gold and platinum-iridium which were evaluated as a function of composition and preparative method.

In addition to greater CO-specificity relative to H_2, it was desirable that any catalyst substitutes be at least as active for CO-oxidation as the currently used platinum blacks. An analysis of the relationships between activity reserve (ratio of open electrode activity to capillary current) and sensor signal and temperature

coefficient revealed that, if anything, electrode activities should be greater than existing electrodes, particularly with 2T sensors. (Appendix 3).

None of the catalysts studied were as active for carbon monoxide oxidation as the currently used platinum blacks and in all cases any decrease in hydrogen response was accompanied by comparable decreases in carbon monoxide activity.

Making a selective CO catalyst by alloying precious metals does not seem feasible at this stage and will not be pursued any further. However, the technique is promising in developing selective H_2S, SO_2 and NO_x catalysts; NCB will be informed should this investigation shed any further light on making a selective CO catalyst.

5.3.2. Selective Chemical Filters

A chemical filtering system, located in-board of the CO sensor capillaries, to remove unsaturated hydrocarbons such as ethylene, using brominated carbon cloth supplied by YRL, has been successfully demonstrated during this report period - See CTL technical Note No. 18, reproduced in Appendix 2. This filter material had no measurable effect on either hydrogen or carbon monoxide.

In principle such a design could be used to increase a sensor's selectivity to carbon monoxide, relative to

hydrogen, provided a filter material were available to remove hydrogen from the gas stream, without affecting the carbon monoxide.

Some investigations were made of platinised and palladised tungsten trioxide materials which are known chemical adsorbents for hydrogen. These material combinations were of particular interest since the hydrogenated forms (hydrogen tungsten bronze oxide) are reoxidised in air to WO_3:

$$H_2 + 2M \rightarrow 2(M\text{-}H) \quad \text{dissociative chemisorption}$$

$$x(M\text{-}H) + WO_3 \rightarrow H_xWO_3 + xM \quad \text{migration/bronze formation}$$

$$2H_xWO_3 + \tfrac{1}{2}xO_2 \rightarrow 2WO_3 + xH_2O \quad \text{regeneration}$$

(where M is platinum or palladium)

However, although the filter was very efficient in removing hydrogen, it also substantially removed carbon monoxide.

In a set of screening tests to select candidate materials for acid gas filtering, measurements were included with H_2 and CO test gases. A wide range of metals and their oxides were evaluated in these tests, e.g. Mn, Cu, Zn, Pb, Co, Ni, Pt and Pd. Most had little or no effect on H_2 or CO and others such as Pt or Pd affected both gases to a similar degree.

As with electrocatalysts, no direct program of research is planned for the immediate future on developing filter

materials for specific removal of hydrogen, but should any lead emerge from the more general studies of filter materials at CTL, NCB will be informed.

5.3.3. Voltage Biasing and Anodising of the Sensing Electrode

The activity of platinum electrodes towards hydrogen oxidation is reduced when the potential is increased to higher anodic values above the normal air rest potential. Under such conditions the platinum surface forms an oxide which is "passive" to the hydrogen reaction.

Baselines (∿ 1μA or 10 ppm CO equivalent) are likely to be too high for the NCB trace sensor to operate at these elevated potentials on the sensing electrode but if the "passive" oxide, once formed, was stable at the normal working potentials, then it should be possible to "precondition" the sensor before use to achieve a low hydrogen sensitivity.

The following investigations were carried out to evaluate the effects on baseline, carbon monoxide signal and hydrogen sensitivity of anodic potential bias on the sensing electrode and to establish the stability of induced characteristics on return to more normal working potentials.

A 3-electrode sensor was used in this work which allowed a better degree of control over the sensing electrode potential than with a biased 2-electrode sensor. The sensor (3F 951) was taken from a production batch of flue gas sensors, manufactured on 2/2/82 and stored with the sensing and reference shorted.

After about 6 weeks storage (19/3/82) the sensor was incorporated into a CTL 3-electrode sensor circuit (see section 6) with its sensing electrode held at zero volts with respect to the reference (Pt/air). A steady baseline of + 0.05μA was obtained within 15 minutes of switching on the potentiostatic circuit; the CO and hydrogen responses were as follows:

CO response (200 ppm CO in air) 0.0338 μA/ppm @ 21°C.

H_2 response (90 ppm H_2 in air) 0.0228 μA/ppm @ 21°C.

H_2 cross interference 67% equivalent CO signal.

The baseline and CO response remained constant over a period of 3 days but the H_2 response decreased over this time to a steady 50% equivalent CO signal.

The sensing electrode control potential was increased stepwise in the anodic direction, allowing at least 3 days for the electrode characteristics to stabilise at each potential step. The measured baseline and H_2 responses at each point, up to + 400mV, and the return to zero mV are shown in figure 5.1. The CO response over the entire potential range remained constant at 0.034 μA/ppm. It was also noticed that the CO response became sharper and less prone to "creep up" after the first few steps of the scan.

The baseline current during the forward potential sweep increased linearly up to about 150mV, then settled to a steady plateau value. At about 350mV, it again increased

sharply with the onset of oxygen evolution. The small hysteresis on the return sweep indicates that true equilibrium was not completely established, even after several days settling at each potential.

Hydrogen response decreased sharply with increasing potential during the forward sweep, going negative above 225mV and plateauing to a steady -10 to -15% CO equivalent above about 280mV. The negative response was caused by excess hydrogen finding a route to the reference electrode. The reference electrode had a polythene protective barrier to screen out hydrogen, but apparently this was not entirely successful. The configuration of the electrode stack was as follows:

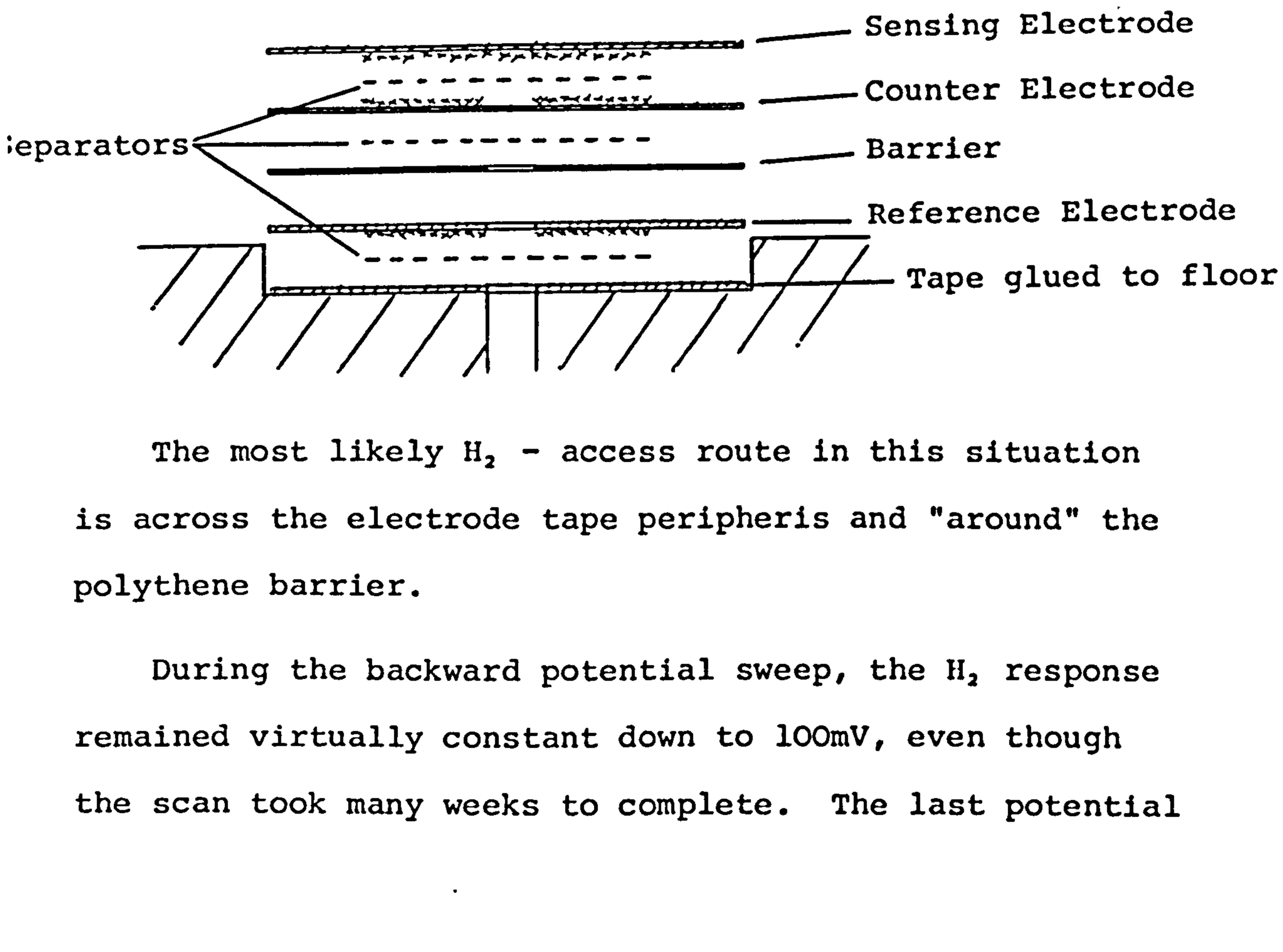

The most likely H_2 - access route in this situation is across the electrode tape peripheris and "around" the polythene barrier.

During the backward potential sweep, the H_2 response remained virtually constant down to 100mV, even though the scan took many weeks to complete. The last potential

step from 100 to zero mV resulted in a change in H_2 response from -10% to zero % over the first 7 days, after which it did not alter over a further 3 day period. At this point the sensor was removed from the circuit and stored with reference and sensing electrodes shorted. It is intended to investigate the stability of the induced H_2-response characteristics of this sensor over longer timescales in the following report period.

Some very recent work with 3-electrode sensors has shown that CO response may be sharpened, whilst reducing H_2 sensitivity and keeping baselines low, by anodising the sensing and reference electrodes together at + 600mV WRT the counter electrode for 3 days. Anodization of 2-electrode sensors would be better carried out by including a third foil electrode which would only be used during the conditioning (Section 7).

Improving H_2 rejection by anodization is under extensive investigation at the moment and long-term performance of these sensors is being monitored.

6. CIRCUITS

6.1. Two-Electrode Circuits

Sensor response times can be considerably shortened by using load resistors of low value, e.g. 90% response times for 2T sensors with 10 and 100 ohm loads are about 20 and 50 seconds respectively (Figure 6.5.). However, with a sensitivity of 0.1μA per ppm for a 2T sensor, signal voltages will only be 1μV per ppm with a 10 ohm load and null drift in conventional voltage amplifiers becomes significant with such small inputs.

Current follower circuits, incorporating a chopper stabilised amplifier, represent a far better technique (See figure 6.1.). The cell current passes through the feedback loop and the gain is determined solely by the gain resistor (R_G):

$$V_o = I_c R_G$$

where: V_o is the amplifier output voltage

I_c is the cell current

R_G is the gain resistance in the feedback loop.

In principle, the cell may be operated with zero load resistance (R_L) but in practice a small, finite load is required to provide sufficient noise rejection.

The circuit shown in figure 6.1. includes a "second order Butterworth low-pass filter" (I.C.2. circuit element) for additional noise rejection. Using this circuit, on a 4.7 ohm load (R_L), the trace shown in figure 6.2. was obtained from a 2T sensor exposed to 63 ppm CO in air.

Chopper stabilised amplifiers cost more than conventional voltage amplifiers, but since they operate on an auto-null principle, there is no need for additional multi-turn potentiometers which are themselves costly and also a source of noise. The chopper stabilised circuit also obviates the need for initial setting-up and subsequent in-service adjustments of the amplifier null.

6.2. Three-Electrode Circuits

With 3-electrode sensors the sensing electrode is controlled against a third, unpolarised reference electrode, thereby eliminating any detrimental effects caused by cathode polarisation which is implicit with 2-electrode sensors.

The three-electrode circuit comprises three amplifier stages (figure 6.3.):

Stage 1. Cell Control (IC 1), the common point is set at the cell reference electrode potential. The sensing electrode is tied to the common point via a load resistor (R_L) so that the only polarisation it suffers is the voltage drop (I_c R_L).

Stage 2. Voltage Amplification (IC 2), the voltage drop I_cR_L is amplified by a conventional voltage-follower circuit.

Stage 3. Low-pass filter (IC 3), as for the 2-electrode circuit.

All IC's are auto-null, chopper stabilised amplifiers,offering the advantages of zero null drift described in Section 6.1. above. Noise rejection and temperature stability are good, for example figure 6.4. shows a trace obtained from a 3-electrode flue-gas sensor (3F 955) using the circuit in figure 6.3. with a 100 ohm load. Temperature coefficient measurements on this circuit,taken with the sensor at ambient room temperature and the circuit in a thermostatted oven, were as follows:

Sensor 3F 955 Load resistor 100 ohm

Test Gas 205 ppm CO in air. Circuit voltage gain 106.5 ± 1.5

Baseline (μA)	Signal (μA)	Span Signal (μA)	Oven temp. (^{o}C)	Room temp. (^{o}C)
0.14	7.36	7.22	6.7	21.8
0.13	7.44	7.31	27.0	22.2
0.15	7.45	7.30	47.8	22.4

The principle of operation of the above voltage-follower circuit in which the signal is taken off the load resistor, is the subject of U.K. Patent 1,101,101, (1964) which has now expired. Improved speed of response has been successfully achieved with lower load resistors down to 20 ohm (figure 6.5.). The alternative technique of replacing the voltage-follower with a current-follower circuit and taking the signal off the gain resistor (see section 6.1. above), runs the risk of infringeing existing Energetics patents on 3-electrode sensor (e.g. U.S.3,776,832 and 1,372,245). In order to avoid any infringement, circuits should conform strictly to the expired U.K. patent in which case signals must <u>NOT</u> be taken off R_G but instead <u>MUST</u> be taken off R_L.

7. THREE-ELECTRODE SENSORS

The sensing electrode in three-electrode sensors is controlled against a third, unpolarised reference electrode (Section 6.2.) and therefore avoids any detrimental effects caused by cathode polarisation which is inherent in the two-electrode mode of operation. Consequently three-electrode sensors possess considerably greater tolerance to high CO concentrations (Table 7.1) and offer the prospect of providing a single sensor, capable of covering all the concentration ranges of interest to the NCB in the longer term.

Additional advantages of three electrode sensors are:

(a) Greater amenability to "conditioning" of the sensing electrode at anodic potentials to reduce the hydrogen sensitivity (Section 5.3.). In a three-electrode sensor the anode and reference are anodised together, using the cathode as counter. After anodising, the anode and reference re-equilibrate at approximately equal rates from a similar condition and baselines are therefore relatively small. With two electrode sensors re-equilibration involves an anodised sensing and cathodised counter which are linked and baselines will be higher. To alleviate this, a third, platinum foil electrode could be inserted in two electrode

sensors which would be used during conditioning instead of the sensor cathode itself.

(b) Since the sensing electrode operates very close to air rest potential, local cell scavenging of carbon monoxide is minimised, i.e. the anode operates near the full current limit. Thus the effective activity reserve is greater than a comparable two electrode situation and intrinsic temperature coefficients should be lower (Appendix 3).

Three-electrode sensors have been developed by CTL., independently of NCB, for flue gas analysis (3F-type) and a large amount of experience has been accumulated in this work which would be directly relevant to any NCB requirement for such a sensor system. However, two areas can be identified in which interests are not directly common to the two applications:

(a) Baselines are not so critical in the flue gas application and values between -3 and + 10 ppm CO equivalent are acceptable. Much lower baseline CO equivalents would be required for NCB applications.

(b) The aspirated mode (Section 2.4.2) is normally used in flue gas applications in which only the capillaries are exposed to the test gas. The question of additional gas access routes to the sensor interior needs to be considered in environmental monitoring where sensors are totally exposed to the test atmosphere.

With regard to the latter, Figure 7.1. shows the "capillary-only" and "total exposure" response of a three electrode, environmental sensor (3E 75) to a 510 ppm CO in air test gas. The signal in the total exposure mode was only depressed by about 1.7% relative to the capillary-only exposure with this sensor. However, there was a slight decay on the total exposure test which was probably caused by CO reaching the reference electrode via side or rear access (Section 2.3.); this effect was almost certainly offset by some additional side access of CO to the sensing electrode.

Further investigations are planned on the subject of access pathways for both two-(2E) and three-electrode (3E) environmental sensors and measures to control CO access, but ensuring a sufficient oxygen supply, by means of low permeability barriers, by physically reducing side access and by placing catalytic filter materials in the gas routes to intercept the CO.

Relatively few 3E sensors have been made and tested to date and the characteristics are therefore not so clearly established as other sensor types such as 3F or 2T. However, Table 7.2. gives some indication of current state-of-art performance of 3E sensors compared to other CTL sensor versions. Baselines of -1 to +3 ppm CO equivalent are still somewhat high, but it is expected that improvements will be made in the next period. Hydrogen cross sensitivities were between 15 and 25% and further improvements on this are

also expected, using the preanodising technique described in Section 5.3. As expected, intrinsic temperature coefficients (uncompensated) were smaller than 2T sensors, i.e. about 0.7% per degree compared to 0.9 to 1% for 2T versions. Flue gas sensors have even smaller values of temperature coefficient because the capillary sensitivity is only about 1/3 that of other sensors and activity reserves will be correspondingly greater (Appendix 3).

TABLES

Table 2.1. Signal Measurements on Pressure Release Sensor

	Test (a) pinhole blocked during exposure	Test (b) pinhole open during exposure
Baseline (μA) (Capillaries and pinhole blocked)	+ 0.09	+ 0.10
Signal on total exposure to 500 ppm CO in air (μA)	48.6	49.5
Recovery (Capillaries and pinhole blocked)		
Time (min.)	(μA)	(μA)
5	- 1.56	- 1.5
10	- 1.4	- 1.38
15	- 1.2	- 1.2
20	- 1.1	- 1.04
25	- 1.0	- 0.96
30	- 0.9	- 0.8
60	- 0.6	- 0.55
90	- 0.4	- 0.4

Table 2.2. Performance tests with encapsulated sensor

(Ambient temperature nominally 22°C)

Baseline	CO Concentration in air (ppm)	Exposure Time (minutes)	Signal Span (μA)	CO Sensitivity (μA/ppm)
0.15	56	5	4.20	0.0750
		10	4.20	0.0750
		15	4.20	0.0750
		20	4.25	0.0759
0.15	205	5	14.80	0.0722
		10	14.80	0.0722
		15	14.80	0.0722
		20	14.80	0.0722
0.15	510	5	36.13	0.0708
		10	36.50	0.0716
		15	36.5	0.0716
		20	36.75	0.0721
		80 steady	39.00	0.0765

Table 2.3. Flow tolerance of CTL Sensors with and without membrane barrier in gas streams from a pressurised cylinder of test gas

Sensor: 3F43 (3-electrode, flue gas sensor).
Test gas: nominal 200 ppm CO in air from a pressurised cylinder at the indicated flow rates.
Temperature: 25°C.
Load Resistance: 50 ohm

Flow rate ml min^{-1}	% signal relative to signal at 100 ml/min. flowrate	
	Without ptfe membrane	with ptfe membrane
5	-	96.9
10	-	97.3
20	-	98.3
40	-	99.0
60	-	99.7
80	-	100.0
100	100.0	100.0
250	100.0	100.0
500	100.3	100.3
1000	102.0	100.5
1500	105.1	101.0
2000	111.1	102.7

Table 2.4. Effect of gas flow from diaphragm pumps on a CO-sensor fitted with aspirated mode set of attachments

Diaphragm pump flow rate ($ml\ min^{-1}$)	% signal relative to calibration using cylinder gas @ 50 $ml\ min^{-1}$	Response times (S)		Back Pressure ($cm\ H_2O$)
		80%	90%	
50	100	20	37	-
100	100	22	28	-
250	100	22	30	2
500	100.6	22	30	7
750	100.7	22	30	13
1000	101.3	22	30	23
Cylinder gas 10 $ml\ min^{-1}$	100	21	29	-

Table 4.1. CO tolerance tests on 2T sensors

All sensors tested on 100 ohm load resistor, 209 ppm CO in air test gas, 21°C. Readings in ppm, for "capillary only" exposures

		Sensitivity µA/ppm	Initial Baseline (ppm)	Exposure (min)				Recovery (min)			
				5	10	15	20	1	2	5	10
Sensor 2T 158		0.098	0.92	208.0	206.0	205.0	205.0	10.7	4.0	1.5	1.0
	Drift (exposure)			0	-2	-2.4	-3.0				
	Hysteresis (recovery)							9.8	3.2	0.6	0.1
Sensor 2T 160		0.106	1.32	208.0	206.0	204.0	203.0	26.4	9.4	3.4	2.4
	Drift (exposure)			0	-2	-4	-5				
	Hysteresis (recovery)							25.1	8.1	2.1	1.1
Sensor 2T 172		0.095	0.95	207.0	205.0	203.0	202.0	25.3	5.3	0.8	0.3
	Drift (exposure)			0	-2	-4	-5				
	Hysteresis (recovery)							24.4	4.4	-0.1	-0.6
Sensor 2T 181		0.103	0.97	199.0	198.0	197.0	197.0	12.7	4.6	2.0	1.4
	Drift (exposure)			0	-1	-2	-2				
	Hysteresis (recovery)							13.7	3.6	1.0	0.4

Table 4.2. Measurements of intrinsic temperature effects on baseline and signal of 2T sensors

All sensors with single 2.6 mm diameter hole drilled in polycarbonate top.
Date of manufacture 10. June 1982
Test gas 56 ppm CO in air.

Sensor	Temperature ($^{o}_{C}$)	Baseline (μA)	Signal (μA)
2T 130	+ 40.0	0.55	4.90
	+ 32.5	0.35	5.60
	+ 22.5	0.15	5.25
	+ 3.5	0.05	4.15
	- 30.0	0.00	1.90
2T 129	+ 41.3	1.35	6.70
	+ 33.4	0.65	6.70
	+ 23.9	0.30	6.40
	- 30.0	0.05	2.25
2T 128	+ 41.5	0.95	6.20
	+ 32.9	0.30	6.30
	+ 21.8	0.15	6.10
	+ 1.0	0.03	5.25
	- 30.4	0.025	2.95
2T 127	+ 40.5	1.30	6.40
	+ 30.5	0.50	6.20
	+ 21.0	0.23	5.88
	+ 1.0	0.08	4.88
	- 30.0	0.025	2.50

Table 5.1 Sensor "E4" monitor in continuous zero humidity at ambient temperature. (primed 1 cm^3 10.3N acid).

Day No.	Weight (g)	Acid Concn. (N)	Baseline @ 20°C (µA)	Signal (µA)	Test Gas (ppm)	Sensitivity (µA/ppm)	Signal as % of initial
0	20.0851	10.3	0.23	5.25	52.0	0.101	100
14	19.9970		0.15	5.11	52.0	0.0983	97.3
21	19.9890		0.14	5.04	52.0	0.0969	96.0
28	19.9730		0.17	4.88	52.0	0.0938	92.9
35	19.9600		0.17	4.90	52.0	0.0942	93.3
49	19.9630	11.7	0.16	4.99	52.5	0.0950	94.1
Placed in a dessicator over silica gel							
55	19.8114	14.18	-0.06	4.79	52.5	0.0912	90.3
62	19.6782	17.37	0.01	4.71	52.5	0.0897	88.8
63	19.6620	17.85	-0.07	4.75	52.5	0.0905	89.6
64	19.6499	18.24	0.01	4.72	52.5	0.0899	89.0
67	19.6197	19.27	0.00	4.64	52.5	0.0884	87.5
68	19.6079	19.70	0.00	4.66	52.5	0.0888	87.9
69	19.5983	20.07	0.03	4.66	52.5	0.0888	87.9
70	19.5908	20.37	0.01	4.67	52.5	0.0890	88.0
71	19.5819	20.73	0.05	4.60	52.5	0.0876	86.8
74	19.5599	21.69	-0.11	4.52	52.5	0.0861	85.2
75	19.5546	21.94	-0.07	4.59	52.2	0.0874	86.6
77	19.5400	22.64	0.15	4.60	52.5	0.0876	86.8
78	19.5300	23.15	0.14	4.61	52.5	0.0878	86.9
82	19.4920	25.30	0.30	4.25	52.5	0.0809	80.1
Coverplate cracked on day 82 and test discontinued.							

Table 5.2. Sensor "E1" monitor in continuous 14% R_H at ambient temperature (primed 0.5 cm^3 20N acid).

Day No.	Weight (g)	Acid Conc. (N)	Baseline @ 20°C (μA)	Signal (μA)	Test Gas (ppm)	Sensitivity (μA/ppm)	Signal as % of initial
0	19.5056	20.0	0.46	4.31	52	0.083	-
8	19.4870	20.8	0.35	3.85	52	0.074	100
15	19.4739	21.4	0.26	3.77	52	0.0725	98.0
22	19.4680	21.6	0.07	4.30	52	0.083	111.7
29	19.4650	21.8	0.21	3.75	52	0.072	97.4
36	19.460	22.0	-0.05	3.50	52	0.067	90.9
43	19.453	22.4	-0.79	4.09	52	0.079	106.0
50	19.447	22.7	0.11	3.36	52	0.065	87.3
57	19.443	22.9	-0.34	3.60	52	0.069	93.6
65	19.440	23.0	-0.5 to-1.0 (leak in coverplate)				

Table 5.3: Sensor "E9" monitored in R_H corresponding to about 15N H_2SO_4 (Primed 1 cm^3 10.3N H_2SO_4, dried to 14.6N H_2SO_4).

Day No.	Weight (g)	Acid (N)	Baseline @ 20°C (μA)	Span (μA)	Span Gas (ppm)	Sensitivity (μA/ppm)	Signal as % initial
0	27.5558	10.3	0.73	5.62	52	0.1080	100
Settled in laboratory atmosphere:							
8	27.4945	11.0	0.20	6.07	52	0.1165	108
28	27.4332	11.7	0.27	5.95	50	0.1190	110
34	27.4153	12.0	0.29	5.72	50	0.1145	105
41	27.4144	12.1	0.18	5.87	50	0.1175	108.6
Stored over silica gel:							
42	27.3741	12.6	0.24	5.81	50	0.1165	107.5
45	27.3053	13.7	0.20	5.82	50	0.1160	107.5
48	27.2600	14.6	0.26	5.58	50	0.1150	103.3
Stored over saturated $MgCl_2$ solution:							
97	27.2881	14.1	0.26	5.53	52	0.1063	98.4
100	27.2835	14.2	0.00	5.89	52	0.1133	104.8
101	27.2807	14.2	-0.17	6.00	52	0.1154	106.8
104	27.2772	14.3	0.22	5.78	52	0.1112	102.9
108	27.2683	14.5	0.16	5.66	52.5	0.1078	99.7
Left in silica gel over weekend, then returned to $MgCl_2$ solution:							
111	27.2088	15.8	0.15	5.85	52.5	0.1114	103.1
118	27.2155	15.6	0.28	5.65	52.5	0.1076	99.6
125	27.2144	15.6	0.32	5.77	52.6	0.1080	101.7
132	27.2136	15.65	0.15	21.82	200	0.109	100.9
139	27.2135	15.65	0.02	6.67	58.0	0.1150	106.4
146	27.2166	15.6	0.14	6.54	58.0	0.1128	104.4
153	27.2169	15.6	0.15	6.66	58.0	0.1148	106.2
159	27.2197	15.5	0.19	6.63	58.0	0.1143	105.8
166	27.2195	15.5	0.48	6.31	58.0	0.1088	100.7
173	27.2249	15.4	0.38	6.48	58.0	0.1117	103.3
180	27.2278	15.3	0.21	6.63	58.0	0.1143	105.8
185	27.2285	15.3	0.05	6.60	58.0	0.1138	105.3
195	27.2296	15.3	0.06	6.87	58.0	0.1184	109.6
201	27.2308	15.3	0.10	6.81	58.0	0.1174	108.6

Table 5.4. Sensor "E.10" monitored in continuous R_H corresponding to about 15N H_2SO_4. (primed 1 cm^3 14.4N H_2SO_4).

Day No.	Weight (g)	Acid (N)	Baseline @ 20°C (μA)	Span (μA)	Span Gas (ppm)	Sensitivity (μA/ppm)	Signal as % initial
0	20.6104	14.5	0.53	5.10	52.5	0.0971	100
6	20.5645	15.2	0.54	5.17	52.5	0.0985	101.4
13	20.5730	15.0	0.59	5.02	52.5	0.0956	98.5
20	20.5743	15.0	0.52	5.10	52.5	0.0971	100.0
34	20.5757	15.0	0.41	19.28	200	0.0964	99.3
41	20.5755	15.0	0.59	5.78	58.0	0.0997	102.7
48	20.5779	14.9	0.52	5.74	58.0	0.0990	102.0
55	20.5792	14.9	0.65	5.70	58.0	0.0983	101.2
62	20.5800	14.9	0.58	5.85	58.0	0.1009	103.9
69	20.5816	14.9	0.85	5.59	58.0	0.0967	99.6
77	20.5810	14.9	0.55	5.71	58.0	0.0984	101.3
85	20.5845	14.8	0.57	5.83	58.0	0.1005	103.5
90	20.5854	14.8	0.52	5.73	58.0	0.0988	101.8
96	20.5877	14.8	0.34	6.00	58.0	0.1034	106.5
102	20.5918	14.7	0.42	5.88	58.0	0.103	104.3
110	20.6044	14.5	0.33	6.05	58.0	0.1043	107.4

Table 5.5. Moulded polycarbonate sensor, monitored in continuous R_H corresponding to 20N H_2SO_4 (primed 1 cm^3 20N H_2SO_4).

Day No.	Weight (g)	Acid (N)	Baseline @ 20°C (μA)	Span (μA)	Span Gas (ppm)	Sensitivity (μA/ppm)	Signal as % initial
0	21.9849	20	1.17	5.57	52	0.1071	100
1	21.9672	20.4	0.87	5.70	52	0.1096	102.3
2	21.9558	20.6	0.70	6.01	52	0.1156	107.9
3	21.9455	20.8	0.72	5.69	52	0.1094	102.2
4	21.9371	21.0	0.75	5.65	52	0.1087	101.5
7	21.9749	20.2	0.71	5.15	52	0.0990	92.4
8	21.9607	20.5	0.46	5.44	52.5	0.1036	96.7
9	21.9450	20.8	0.44	5.58	52.5	0.1063	99.3
10	21.9362	21.0	0.52	5.55	52.5	0.1057	98.7
11	21.9286	21.2	0.50	5.50	52.5	0.1048	97.9
14	21.9607	20.5	0.43	5.68	52.5	0.1082	101.0
15	21.9437	20.9	0.40	5.60	52.5	0.1067	99.6
16	21.9312	21.1	0.46	5.45	52.5	0.1038	96.9
17	21.9141	20.9	0.59	5.26	52.5	0.1002	93.6
18	21.9175	21.4	0.39	5.49	52.5	0.1046	97.7
21	21.9500	20.7	0.41	5.56	52.5	0.1059	98.9
22	21.9308	21.1	0.34	5.52	52.5	0.1057	98.7
23	21.9475	20.8	0.44	5.68	52.5	0.1082	101.0
24	21.9556	20.6	0.35	5.61	52.5	0.1069	99.8
25	21.9362	21.0	0.35	5.41	52.5	0.1030	96.2
28	21.9721	20.3	0.42	5.32	52.5	0.1013	94.6
42	21.9969	19.8	0.22	20.30	200.0	0.1015	94.8
49	21.9113	21.6	0.21	6.10	58.0	0.1052	98.2
55	21.8400	23.4	-0.5	leak at coverplate joint.			

Table 5.6. Sensor "E5" monitored at a constant electrolyte concentration of 1.72N acid, then allowed to dry out. (primed 2 cm^3 1.72N H_2SO_4).

Day No.	Weight (g)	Acid (N)	Acid Volume (cm^3)	Baseline @ 20°C (µA)	Span (µA)	Span Gas (ppm)	Signal as % initial
0	20.7206	1.72	2	0.29	5.5	52	-
7	20.7280			0.24	5.6	52	100
21	20.7120			0.27	5.23	52	93.3
35	20.5770			0.17	5.34	52	95.4
42	20.5950			0.49	5.21	52	93.0
63	20.6207			0.22	5.29	52.5	93.6
77	20.6173			0.14	5.37	52.5	95.0
91	20.6095			0.15	5.35	52.5	94.6
105	20.5943			0.06	5.29	52.5	93.6
133	20.5861			0.08	5.41	52.0	96.6
168	20.5757			0.05	5.25	52.0	95.4
195	20.5807	1.85	1.86	0.23	5.18	50	96.2
202	Sensor kept in laboratory atmosphere:						
203	20.5111	1.92	1.79	0.12	5.31	50	98.6
209	20.3218	2.15	1.60	0.09	5.24	50	97.3
217	20.1002	2.49	1.38	0.06	5.21	50	96.8
223	19.9470	2.80	1.23	0.18	5.11	50	94.9
235	19.5639	4.08	0.84	0.12	5.20	52	92.9
242	19.3847	5.12	0.66	0.26	4.97	52	88.8
249	19.2203	6.88	0.50	0.16	4.98	52	89.0
255	19.1433	8.14	0.42	0.07	4.90	52.5	86.6
262	19.0403	10.76	0.32	-	nil	52.5	-
268	Sensor put in dessicator over water:						
272	19.1294	8.41	0.41	0.14	4.55	52.5	80.5
275	19.1873	7.37	0.47	0.12	4.78	52.5	84.5
288	19.2727	6.23	0.55	0.02	5.83	58	93.3

Table 5.7. Sensor "E6", monitored during continuous exposure to 100% R_H at ambient temperature. (primed 1 cm^3 10.3 H_2SO_4).

Day No.	Weight (g)	Acid (N)	Acid Volume (cm^3)	Baseline @ 20°C (cm^3)	Span (µt)	Span gas (ppm)	Signal as % initial
0	20.4154	10.3	1.00	0.48	6.30	52.5	-
6	20.3720	10.8	0.96	0.37	6.25	52.5	100
14	20.3610	10.9	0.95	0.34	6.17	52.5	98.8
36	20.2915	11.75	0.88	0.31	6.30	52.5	100.8
47	20.2863	11.83	0.87	0.19	6.08	52.5	97.3
Placed in dessicator over water:							
54	20.5020	9.48	1.09	0.58	6.48	52.0	104.7
61	20.6625	8.26	1.25	0.63	6.38	52.0	103.1
68	20.7695	7.61	1.35	0.90	6.14	52.0	99.2
75	20.8524	7.17	1.44	0.54	6.07	52.0	98.1
82	20.9374	6.77	1.52	0.78	5.99	52.0	96.8
89	21.0155	6.43	1.60	0.62	6.00	52.0	97.0
96	21.1555	5.92	1.74	0.56	6.32	52.0	102.1
103	21.2346	5.66	1.82	0.46	6.35	52.0	106.7
110	21.2816	5.52	1.87	0.41	6.26	50	105.2
117	21.3278	5.39	1.91	0.74	6.04	50	101.5
124	21.3910	5.21	1.98	0.44	6.29	50	104.9
131	21.4340	5.10	2.02	0.42	6.02	50	101.2
138	21.4826	4.98	2.07	0.46	6.06	50	101.7
145	21.5127	4.91	2.10	0.38	6.05	50	101.7
156	21.6552	4.60	2.24	0.39	6.04	52	97.6
212	21.9316	4.09	2.52	0.67	22.74	200	95.6
219	21.9040	4.04	2.49	0.86	7.07	58	102.4
233	22.0303	3.94	2.61	0.70	7.05	58	102.2
262	22.1566	3.76	2.74	0.82	6.94	58	100.6
275	22.2122	3.68	2.80	0.87	7.03	58	101.9
300	22.3324	3.53	2.90	0.83	7.15	58	103.6

Table 5.8. Sensor PR.1., monitored during continuous exposure to 100% R_H at ambient temperature (primed 1 cm^3 10.3N H_2SO_4).

Day No.	Weight (g)	Acid (N)	Acid Volume (cm^3)	Baseline @ 20°C (μA)	Span (μA)	Span gas (ppm)	Signal as % initial
0	20.2760	10.3	1.00	0.10	5.11	52.5	-
3	20.2706	10.4	0.99	0.19	5.04	52.5	100
Placed in a dessicator over water:							
10	20.4563	8.7	1.18	0.19	5.00	52.5	99.2
18	20.6244	7.6	1.35	0.10	5.16	52.5	102.4
Coverplate seal leak detected							
25	20.7469	7.00	1.47	0.14	5.18	52.5	102.8
32	20.8206	6.70	1.54	0.09	5.31	52.5	105.4
39	20.9256	6.24	1.65	0.28	5.22	52.5	103.6
42	20.8863	6.40	1.61	0.16	5.29	52.5	105.0

Table 5.9. Sensor "E.8", monitored during continuous exposure to 100% R_H at ambient temperature. (primed 1 cm^3 10.3N H_2SO_4).

Day No.	Weight (g)	Acid (N)	Acid Volume (cm^3)	Baseline @ 20°C (µA)	Span (µA)	Span gas (ppm)	Signal as % initial
0	27.3527	10.3	1.00	0.53	5.64	52	-
7	27.2938	10.9	0.94	0.22	6.10	52	100
22	27.2182	11.9	0.87	0.28	5.73	50	97.7
35	27.1987	12.2	0.85	0.20	5.72	50	97.5
Placed in dessicator over water:							
42	27.4196	9.65	1.07	0.47	5.58	50	95.1
49	27.5544	8.57	1.20	0.38	5.68	50	96.8
56	27.6174	8.14	1.26	0.42	5.62	50	95.8
62	27.7516	7.36	1.40	0.43	5.61	52	92.0
74	27.8931	6.69	1.54	0.38	5.70	52	93.4
82	27.9449	6.47	1.59	0.45	5.85	52	95.9
88	28.0160	6.19	1.66	0.67	5.67	52	93.0
95	28.0961	5.91	1.74	0.34	5.89	52.5	95.6
102	28.1544	5.72	1.80	0.28	6.03	52.5	97.9
109	28.2163	5.53	1.86	0.36	5.81	52.5	94.3
116	28.2800	5.34	1.93	0.28	5.83	52.5	94.7
137	28.4312	4.96	2.08	0.25	6.81	58	100.1
151	28.5387	4.71	2.19	0.24	6.74	58	99.1
165	28.6605	4.46	2.31	0.43	6.52	58	95.8
180	28.7592	4.28	2.41	0.36	6.83	58	100.4
196	28.8494	4.13	2.50	0.44	6.87	58	101.0
210	28.9560	3.96	2.60	0.58	6.87	58	101.0

Test gas 1000 ppm CO in air, "Capillary-only" exposure
Load resistor 10 ohm.
Temperature 22°C.
All readings in ppm CO.

	Signal Sensitivity (μA/ppm)	Initial Baseline (ppm)	Exposure time (min.)				Recovery (min.)			
			5	10	15	20	1	2	5	10
Sensor 2T 158	0.118	0.42	864	863	864	866	12.3	-6.4	-11.3	-9.3
Drift (Exposure)			0	-1	0	+2				
Hysteresis (Recovery)							+11.9	-6.9	-11.7	-9.7
Sensor 3E 120	0.105	1.52	990.5	990.5	990.5	990.5	13.3	8.7	5.3	3.2
Drift (Exposure)			0	0	0	0				
Hysteresis (Recovery)							+11.8	+7.2	+3.8	+1.7

Table 7.1 Comparison of CO tolerance tests on 2T and 3E sensors

Table 7.2. Comparison of performance characteristics of CTL CO sensor versions

Note: The data quoted in this table are for broad guidance only. All sensors are currently subject to further development and testing and changes are likely to occur in the quoted characteristics.

	2T	2E	3E	3F
Concentration range (ppm)	0-200	0-500	> 1000	> 4000
Applications	Trace	Environmental monitoring		Flue gas
Nominal sensitivity (μA/ppm)	0.1	0.1	0.1	0.03
Baseline, pure air, 20°C. (ppm CO equivalent)	+0.5 to +2.0	+1 to +3	-1 to +3	-3 to +10
90% Response time @ 20°C, 50 ohm load (s)	23 - 35	20 - 30	25 - 35	25 - 35
Hydrogen cross sensitivity without any preconditioning (CO equivalent %)	10 to 30	10 to 20	15 to 25	20 to 40
Intrinsic temperature coefficient (% Signal @ 20°C per °C change)	0.9 to 1.0	0.7	0.7	0.5

FIGURES

ALL DIMENSIONS IN mm
DO NOT SCALE

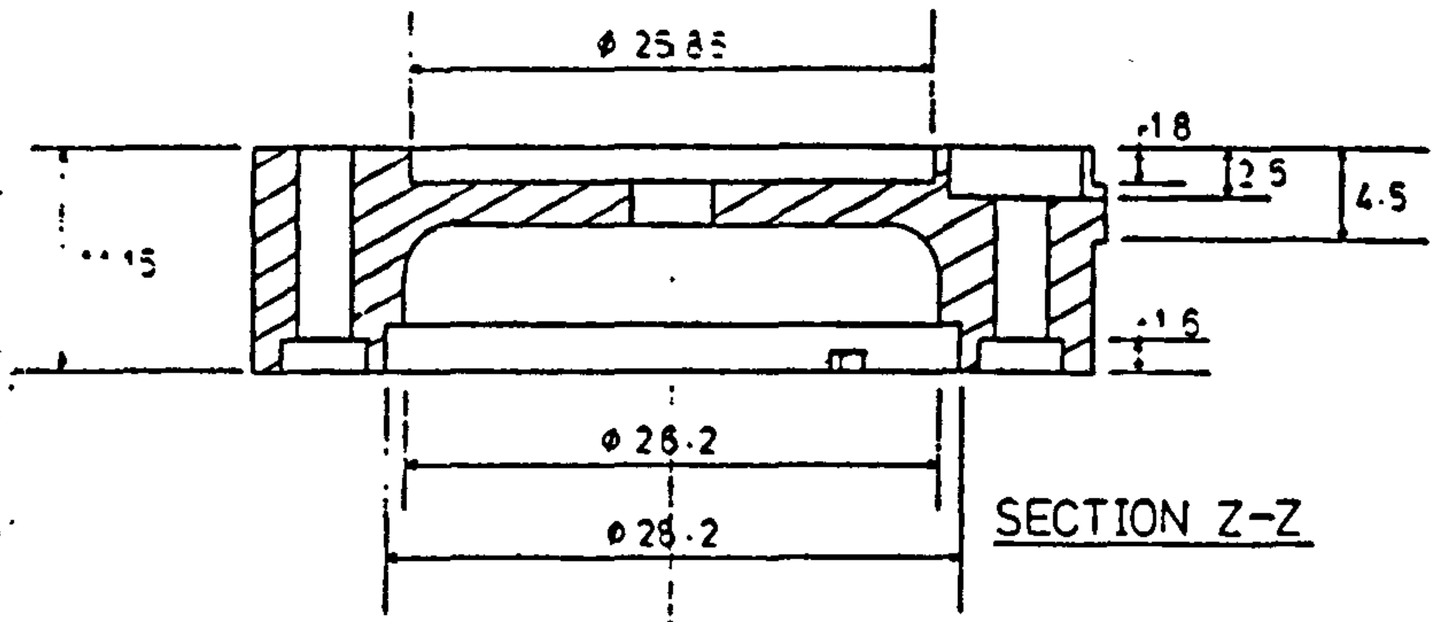

SECTION Z-Z

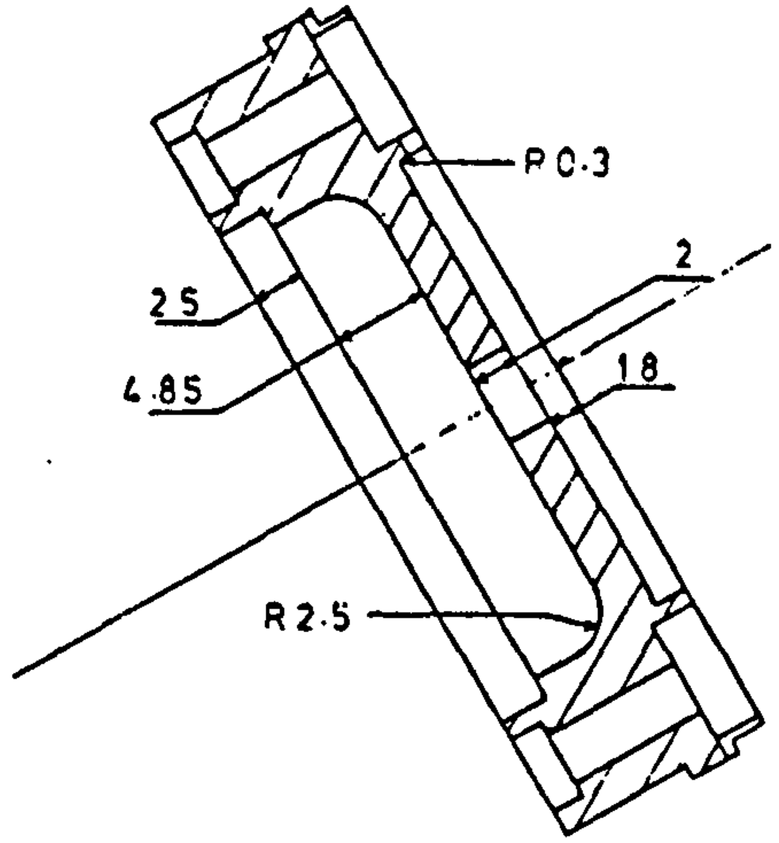

SECTION V-V

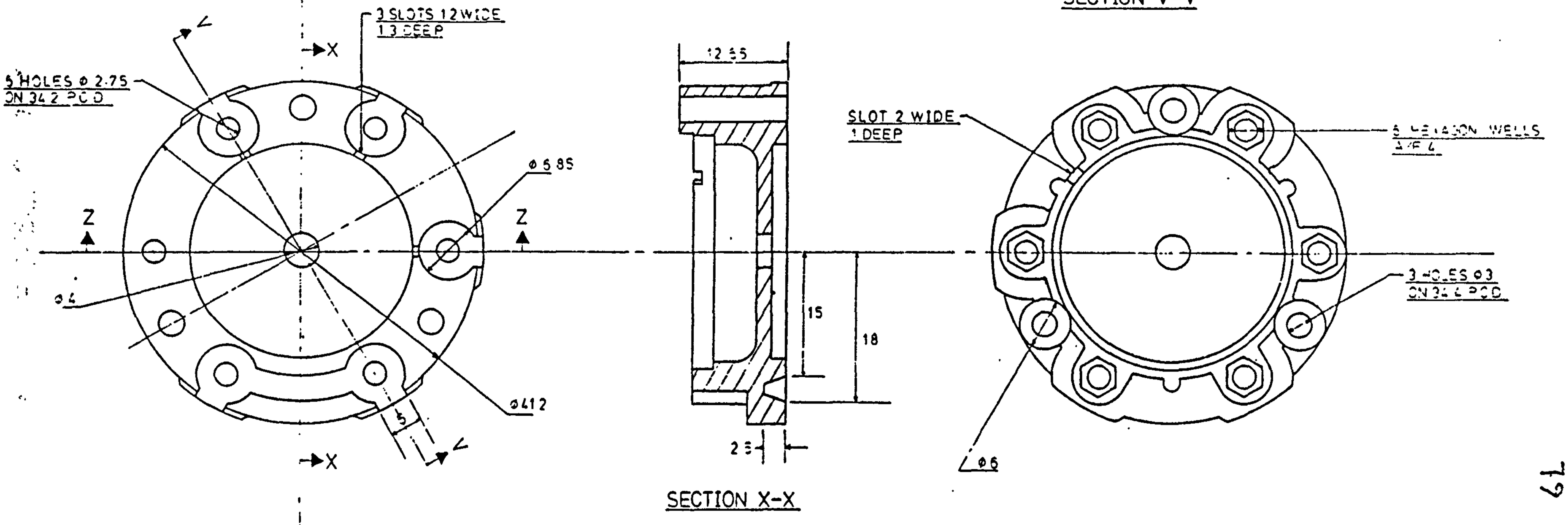

SECTION X-X

FIGURE 2.1 DETAILED DRAWING OF MOULDED COUNTER PLATE

ALL DIMENSIONS IN mm
DO NOT SCALE

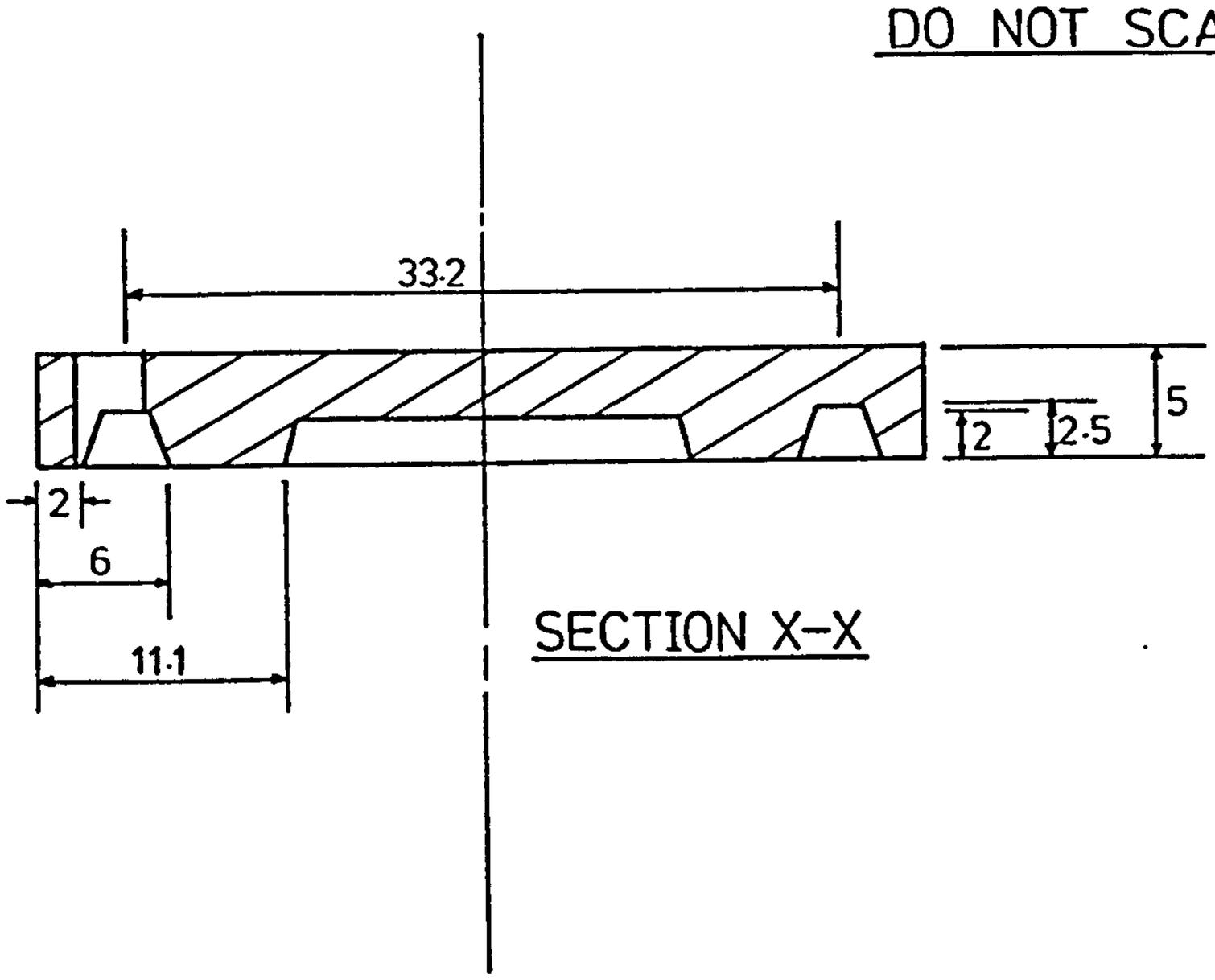

SECTION X–X

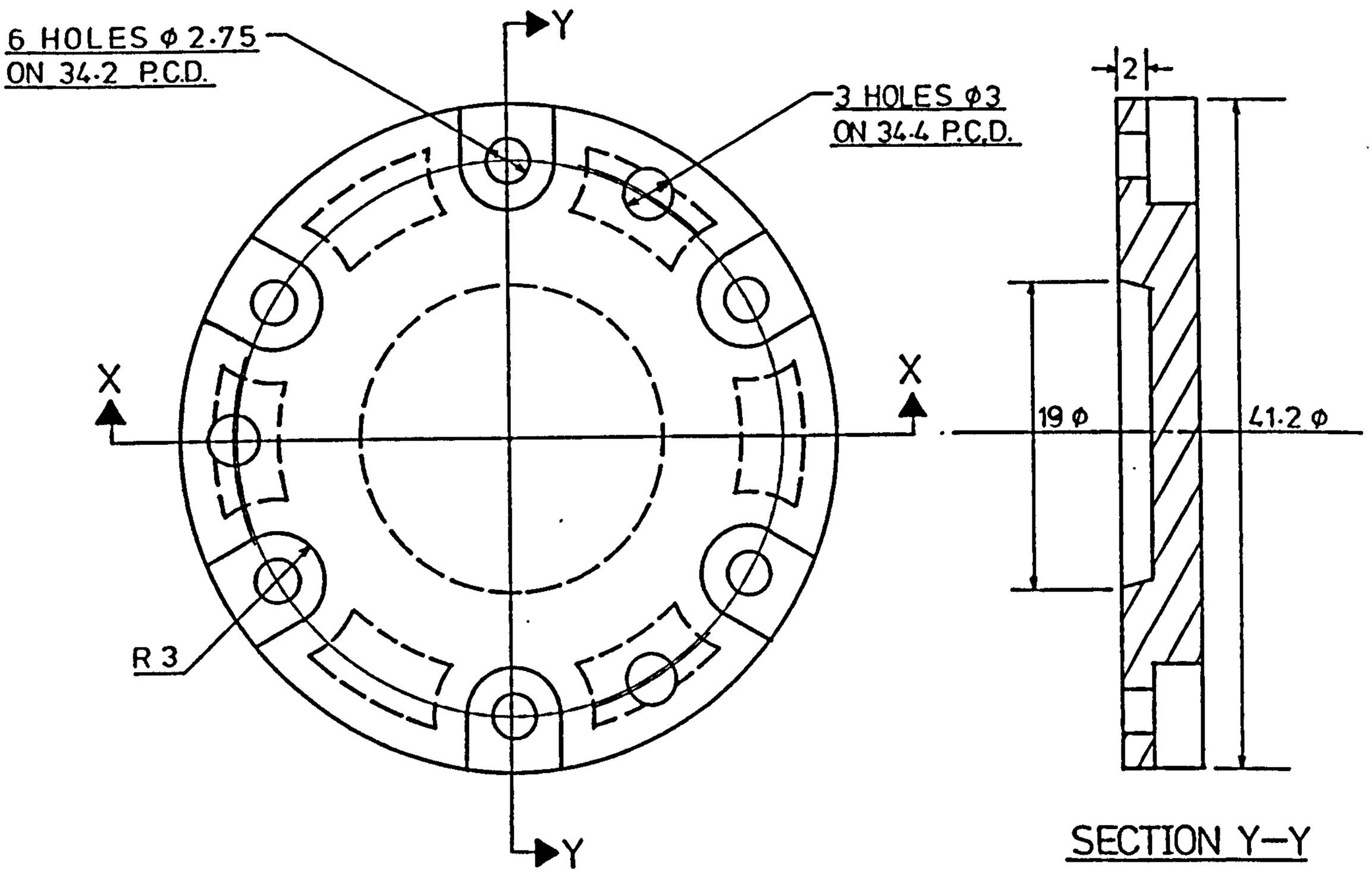

SECTION Y–Y

FIGURE 2·2 DETAILED DRAWING OF MOULDED WORKING PLATE

ALL DIMENSIONS IN mm
DO NOT SCALE

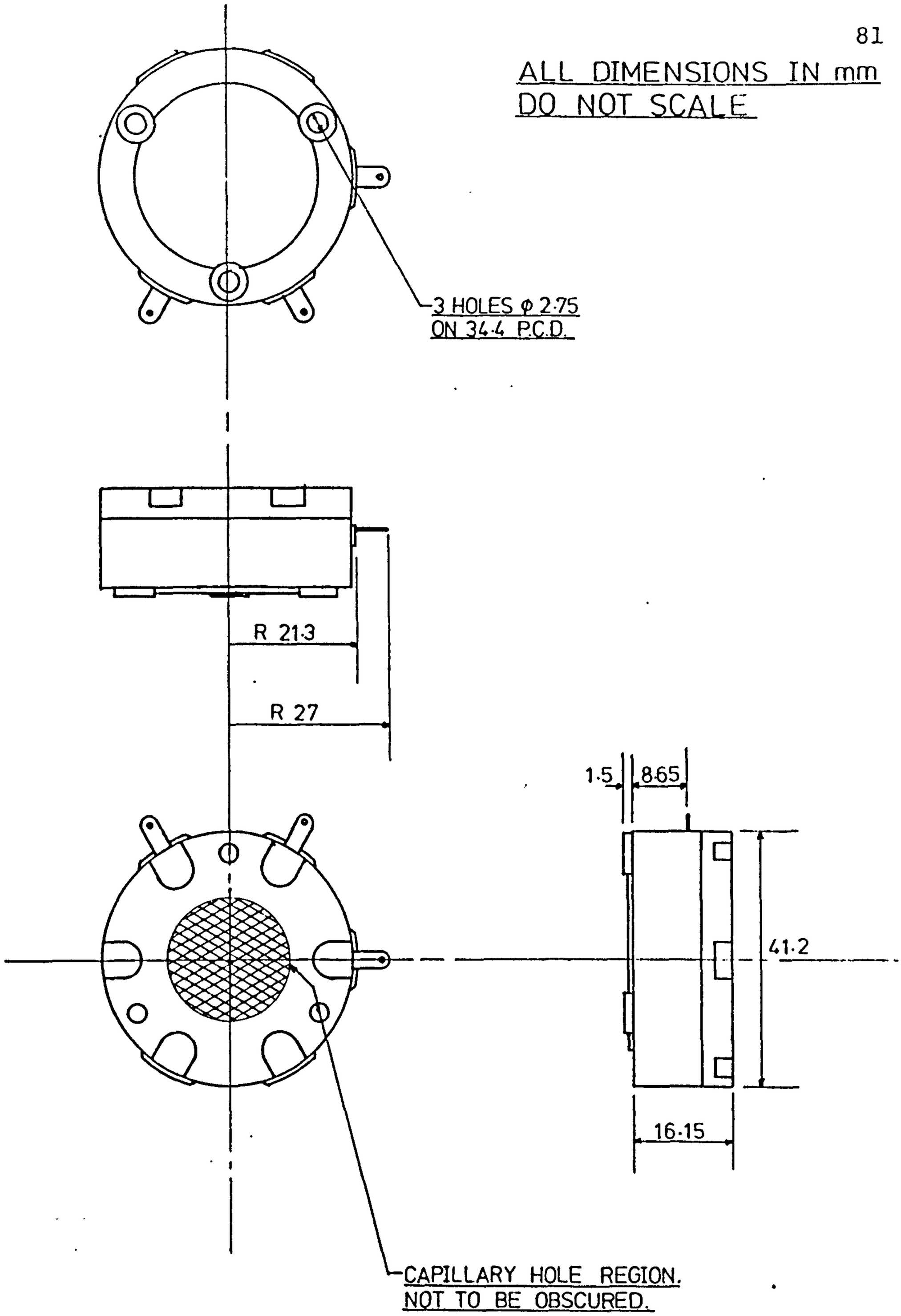

FIGURE 2·3 OUTLINE DRAWING OF MOULDED CO-SENSOR
(3 ELECTRODE VERSION)

NOTCHED IMPACT STRENGTH VS.
TEMPERATURE (ACCORDING IZOD)

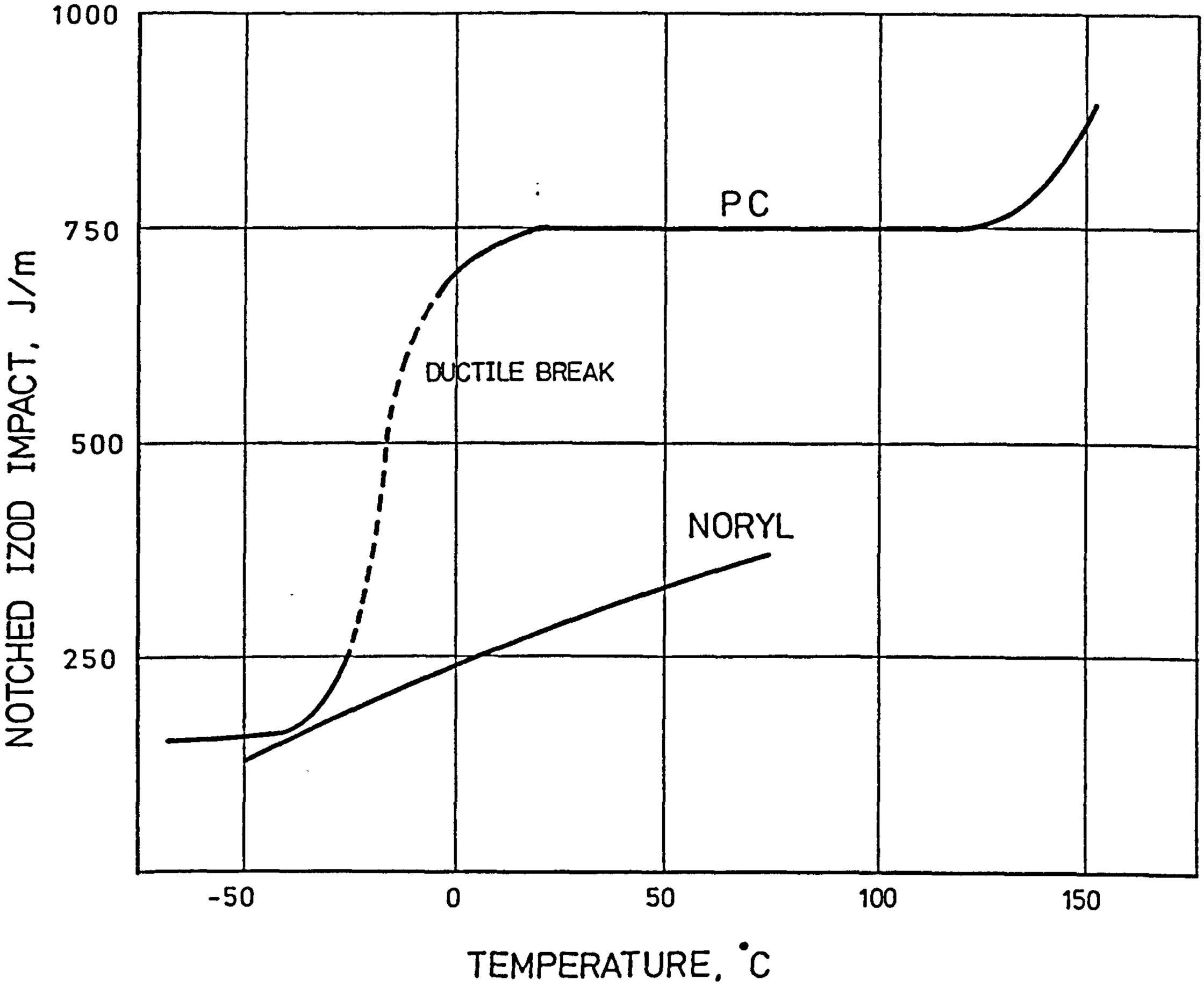

FIGURE 2.4 IMPACT RESISTANCE OF
POLYCARBONATE

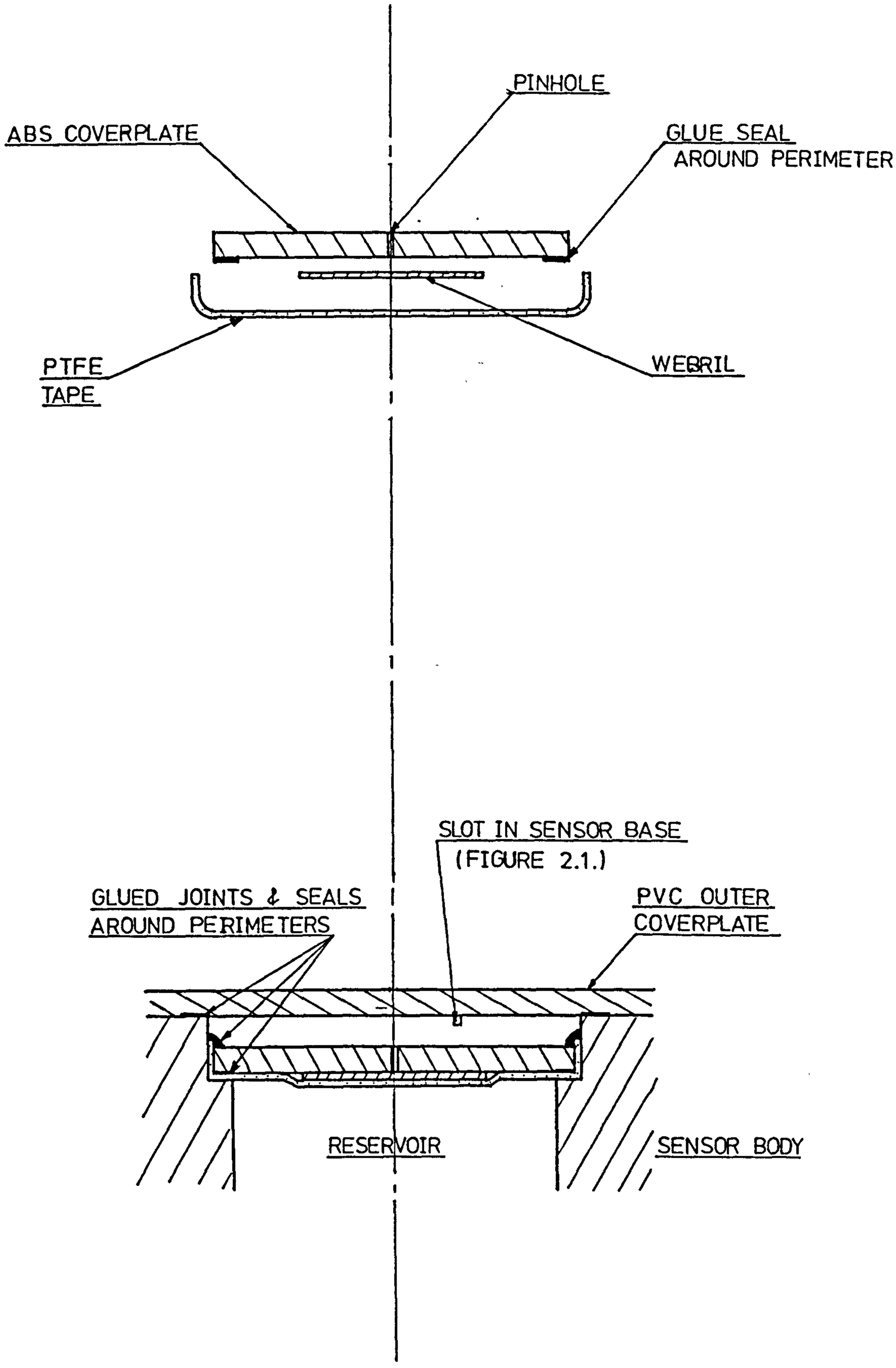

FIGURE 2.5. PRESSURE RELEASE SYSTEM & REAR COVERPLATE SEAL DESIGN (SCHEMATIC)

DRAWN BY :- R.W.STAM
DATE :- 27/5/82

ALL COMPONENTS AVAILABLE
NUTS & BOLT :- M2

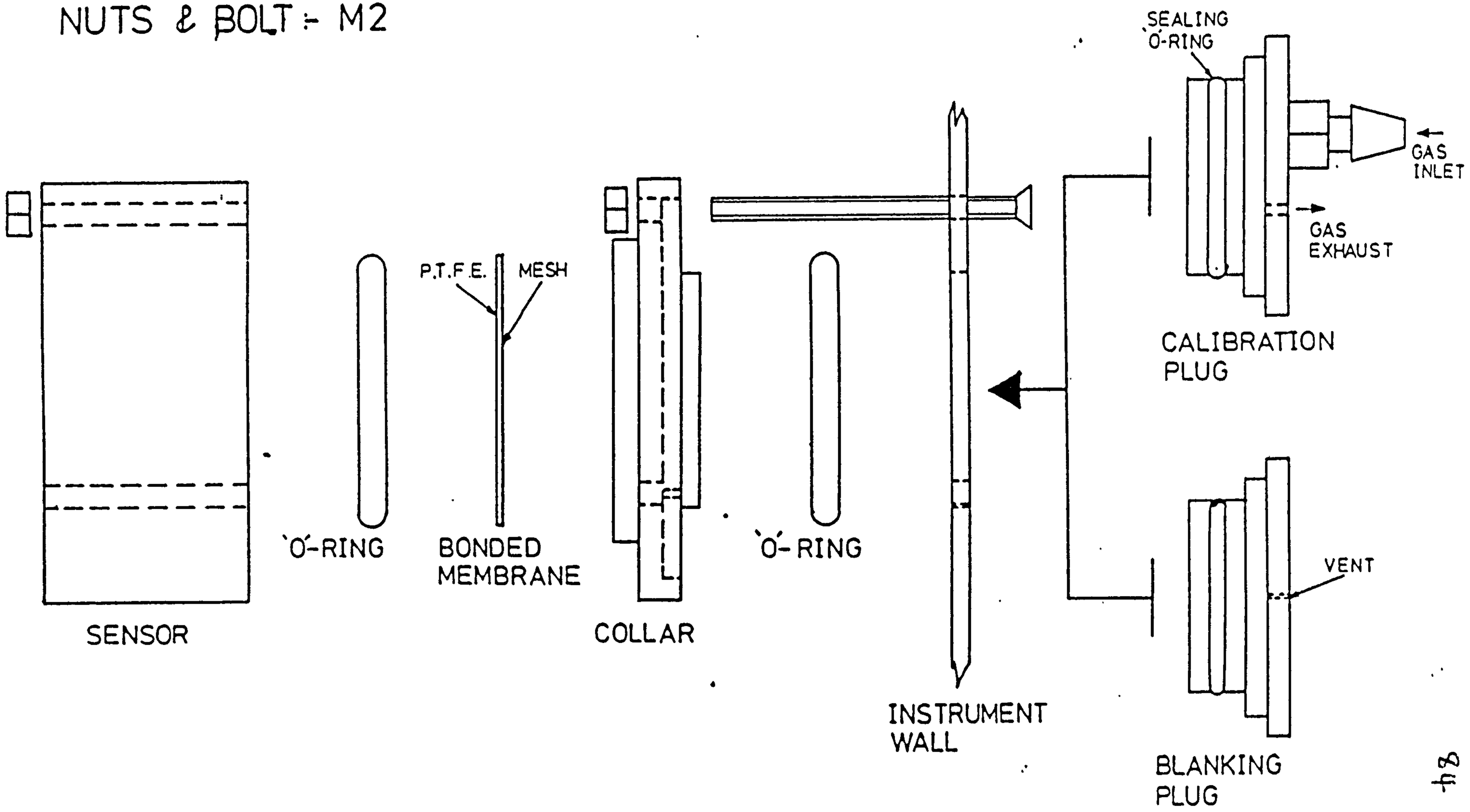

FIGURE 2.6 INSTRUMENT MOUNTING SCHEME FOR SENSORS IN THE DIFFUSION MODE.

SCALE~2X DO NOTSCALE ALL DIMENSIONS IN mm MATERIAL : POLYCARBONATE

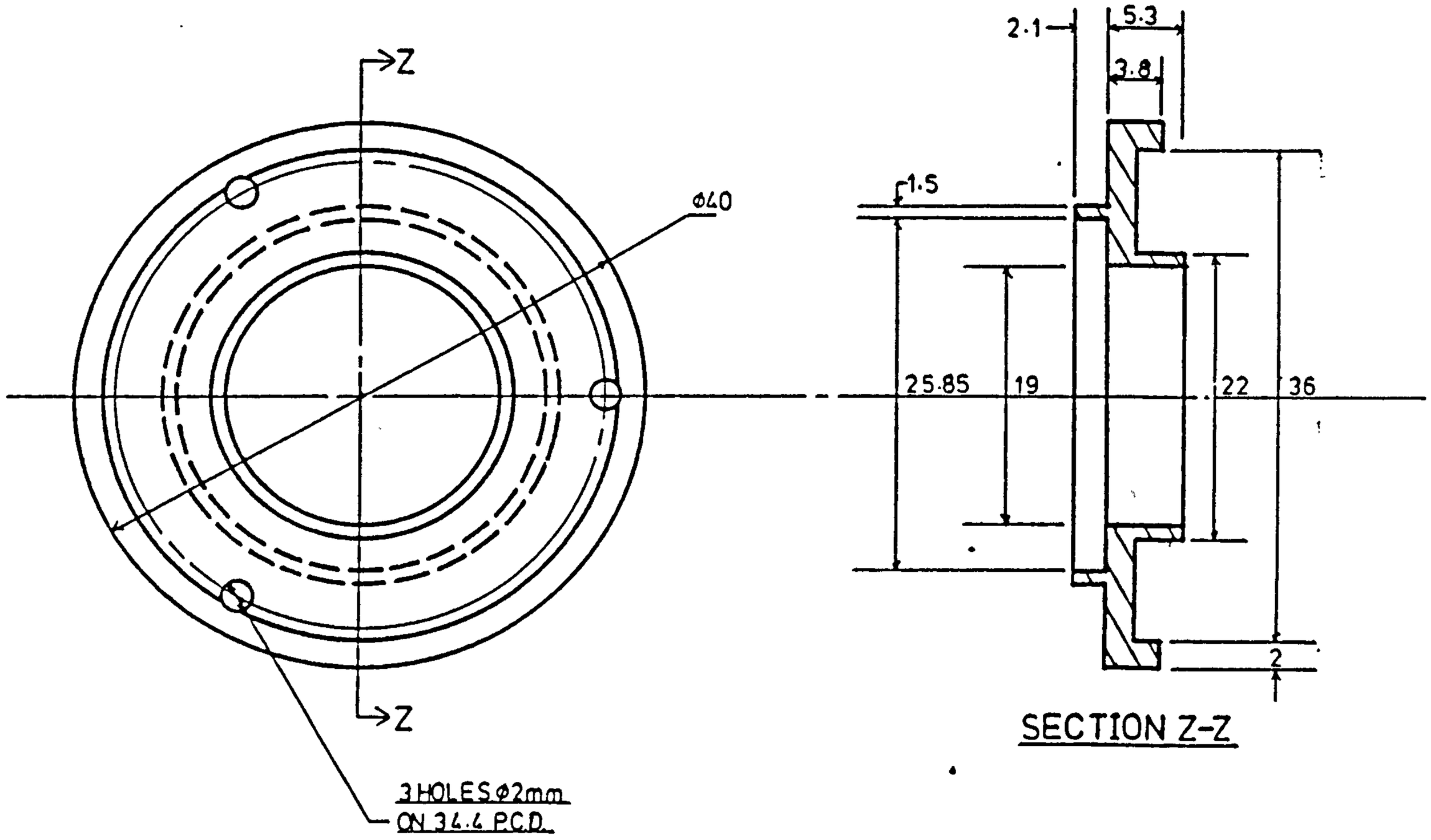

FIGURE 2.7 COLLAR MOULDING FOR DIFFUSION MODE SENSOR MOUNTING.

SCALE - 2X DO NOT SCALE ALL DIMENSIONS IN mm MATERIAL : POLYCARBONATE

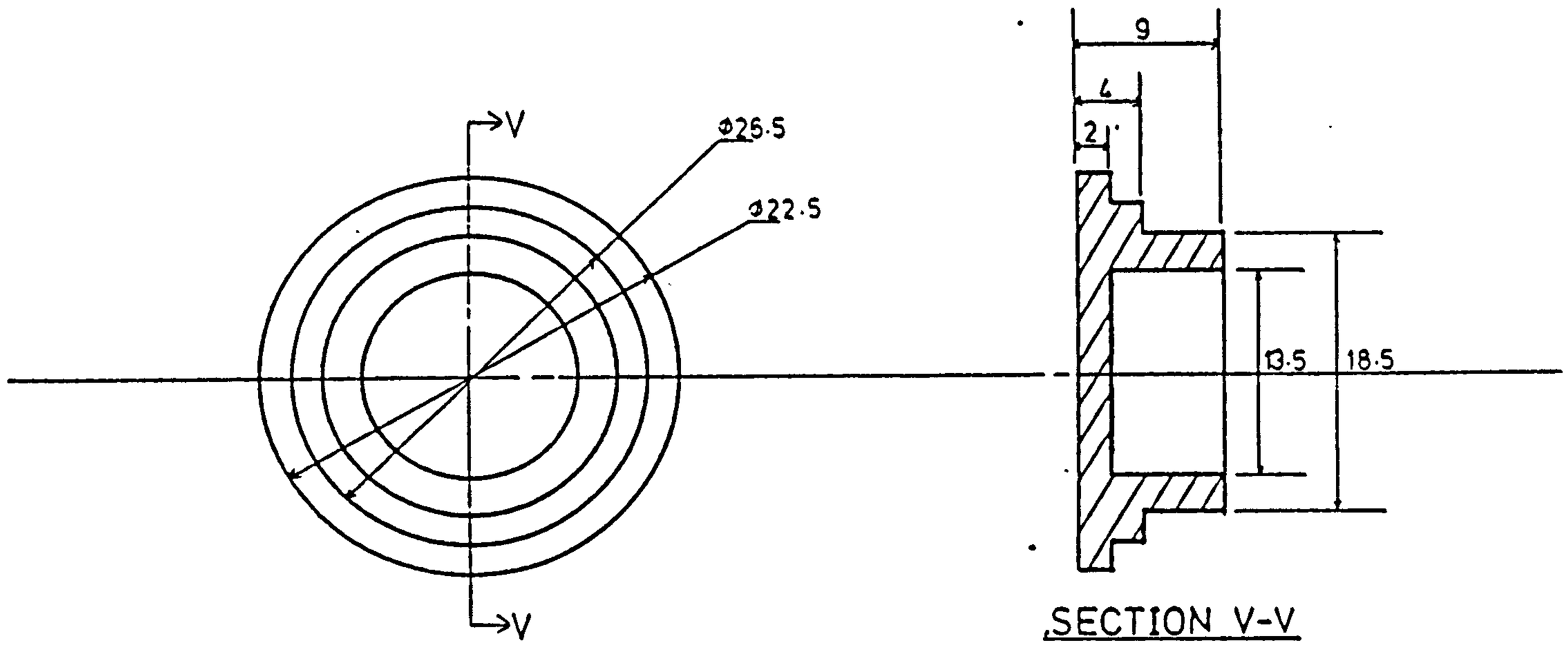

FIGURE 2.8 PLUG MOULDING FOR DIFFUSION MODE SENSOR MOUNTING.

DRAWN BY :- R.W.STAM
DATE :- 21/5/82

ALL COMPONENTS SUPPLIED
NUTS & BOLTS:- M2

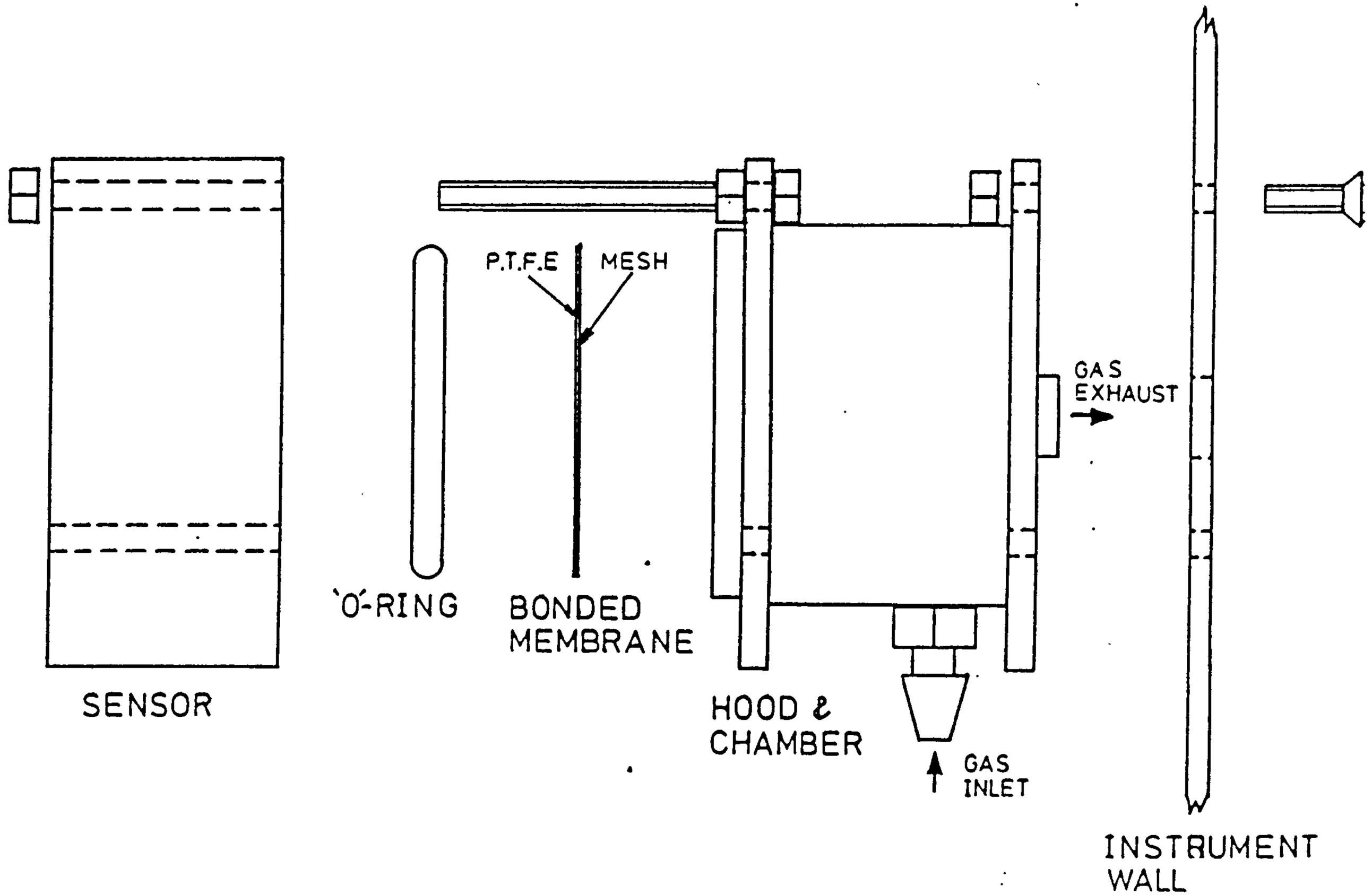

FIGURE 2.9 INSTRUMENT MOUNTING SCHEME FOR SENSORS IN THE ASPIRATED MODE.

SCALE~2X DO NOT SCALE ALL DIMENSIONS IN mm · MATERIAL : POLYCARBONATE

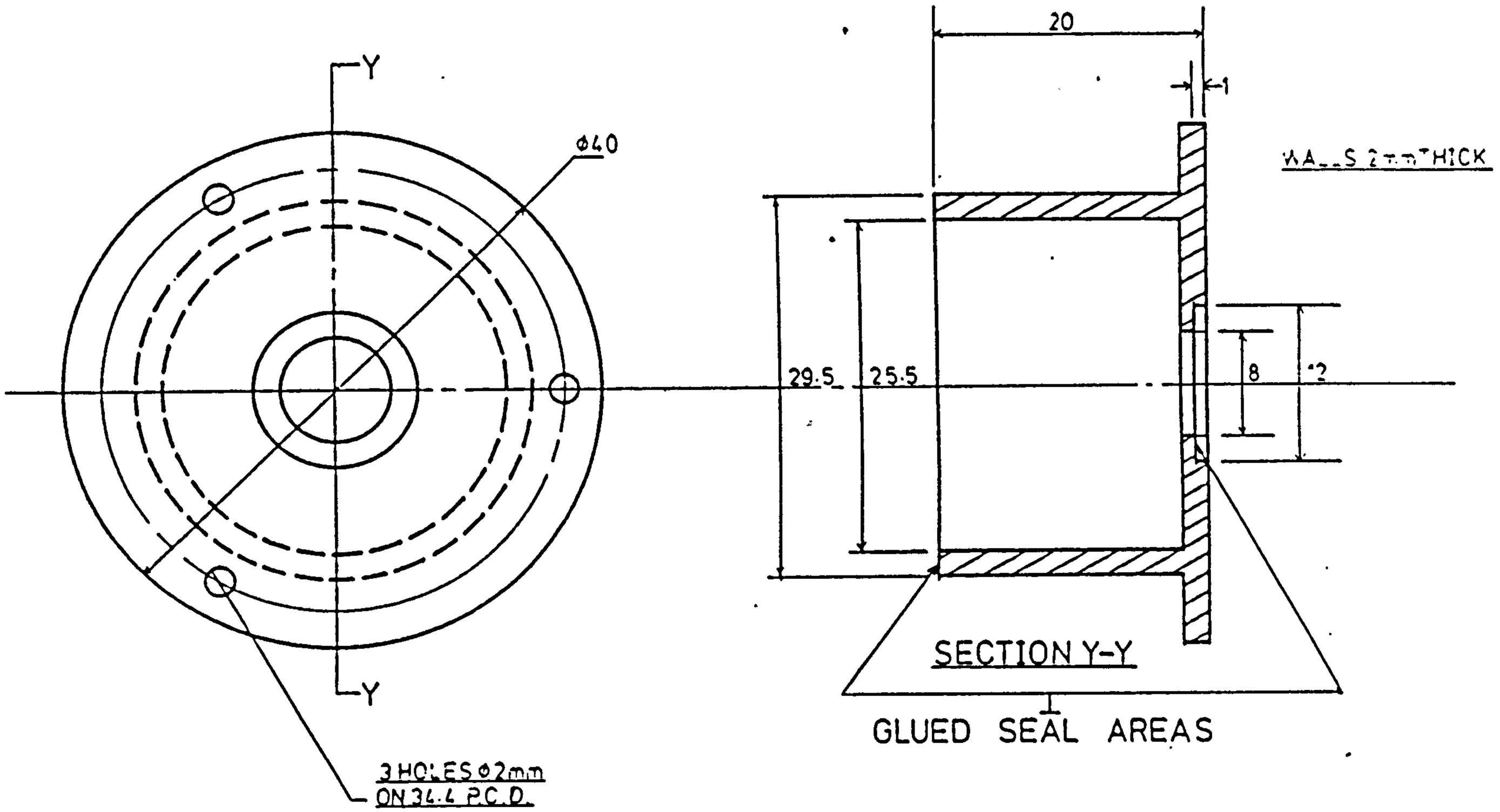

FIGURE 2.10 HOOD MOULDING FOR ASPIRATED MODE SENSOR MOUNTING.

SCALE-2X DO NOT SCALE ALL DIMENSIONS IN mm MATERIAL : POLYCARBONATE

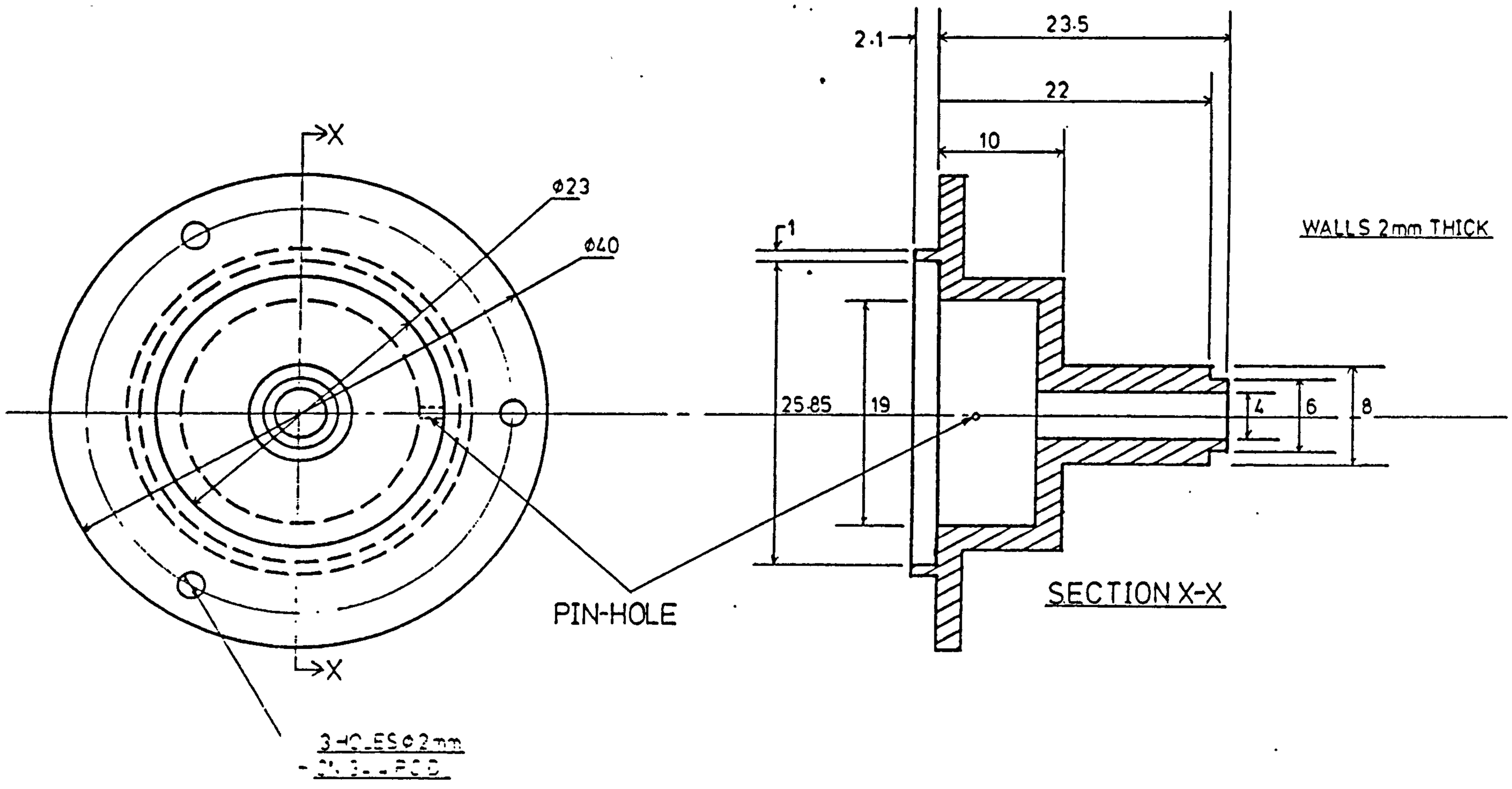

FIGURE 2.11 CHAMBER MOULDING FOR ASPIRATED MODE SENSOR MOUNTING.

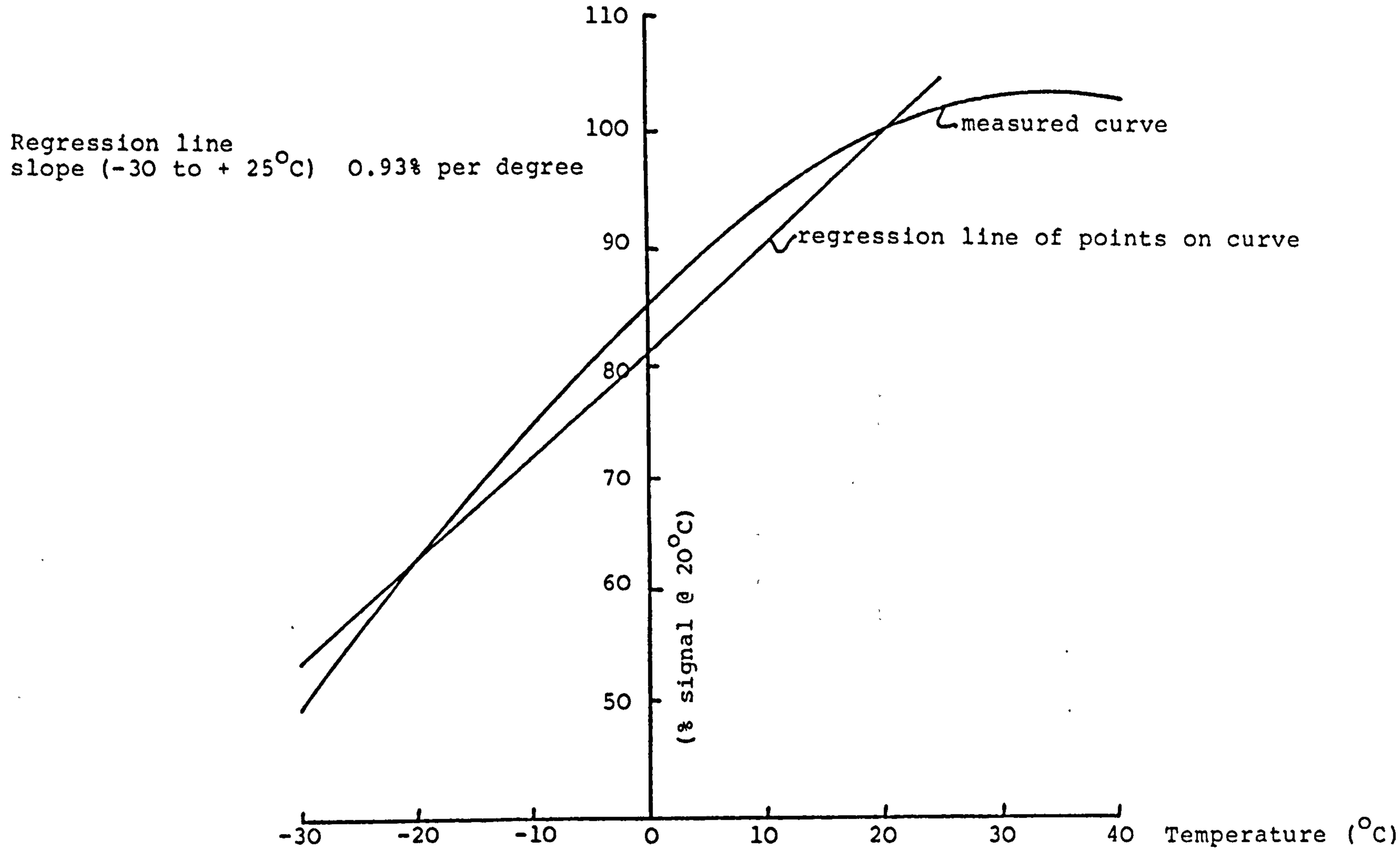

Figure 4.1. Typical intrinsic signal temperature characteristic of 2T sensors.

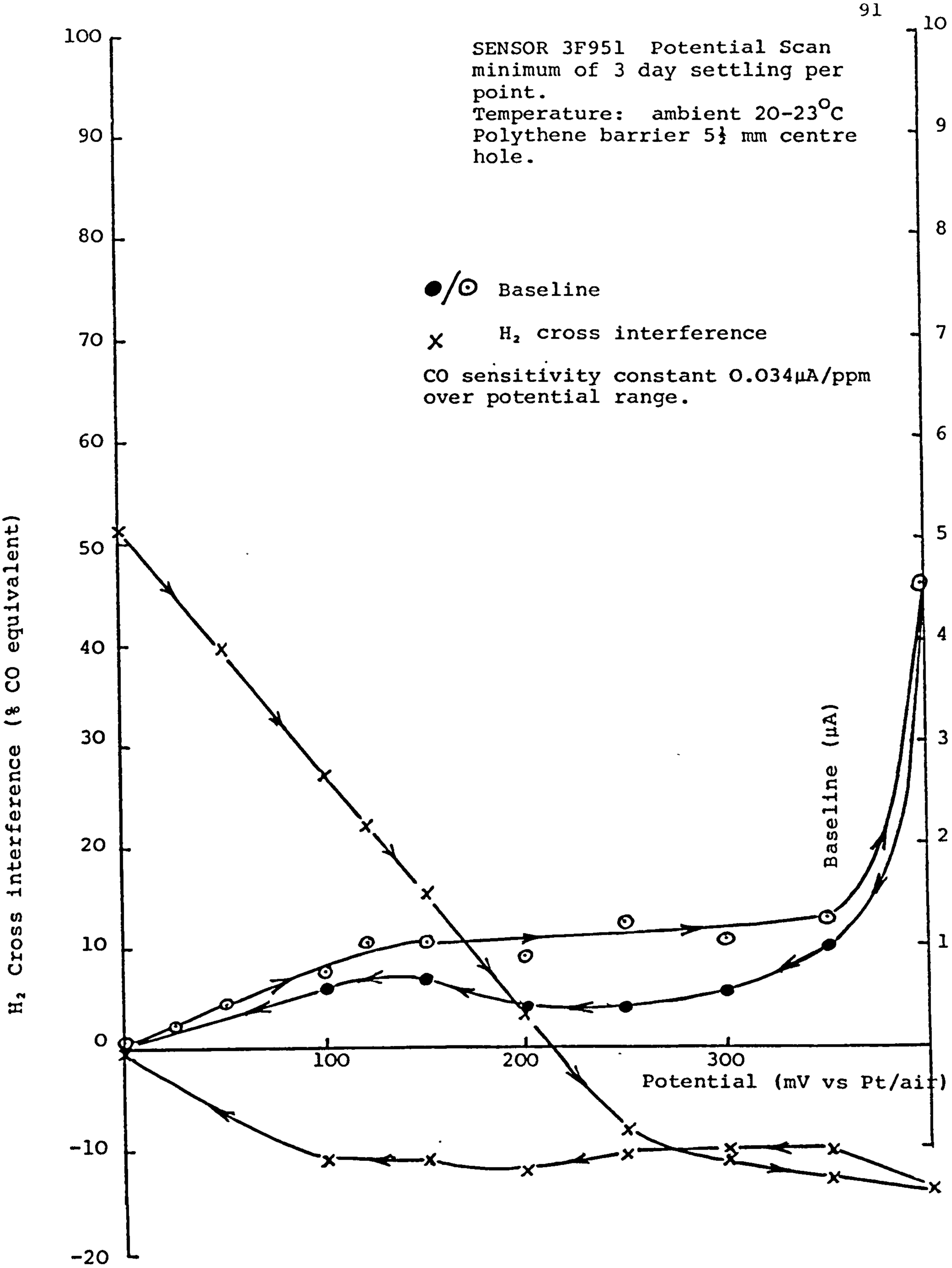

Figure 5.1. H_2-response and baseline of sensor 3F 951 as a function of sensing electrode potential.

J.H.GILBY.
4/2/82.

2- Electrode Circuit

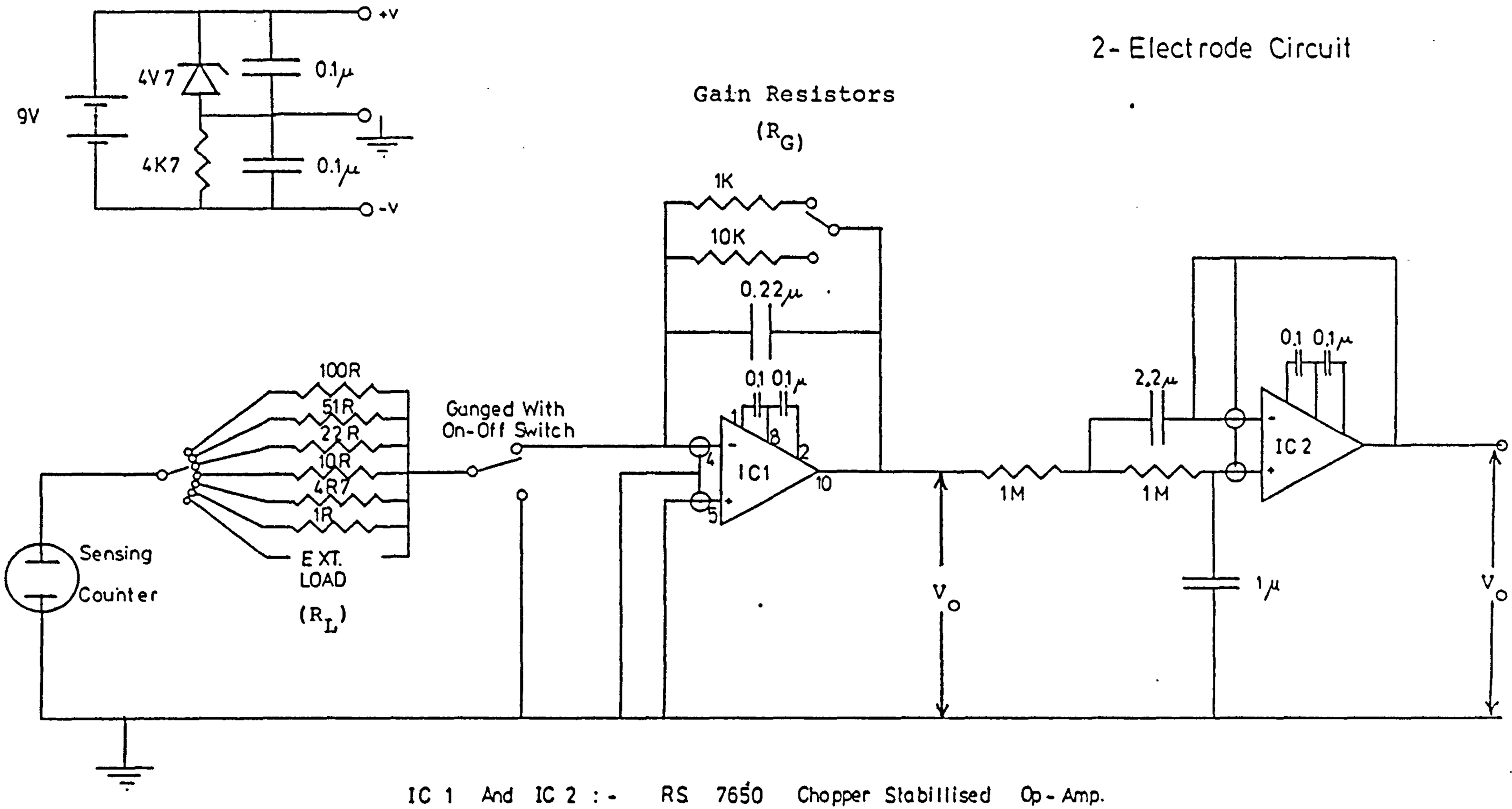

IC 1 And IC 2 :- RS 7650 Chopper Stabillised Op-Amp.

Figure 6.1. Current-Follower circuit for use with two-electrode sensors

SENSOR 2T 158

Test gas 63 ppm CO
in air

R_L 4.7 ohm

R_G 10k ohm

100 mV FSD

Timebase 5 min cm^{-1}.

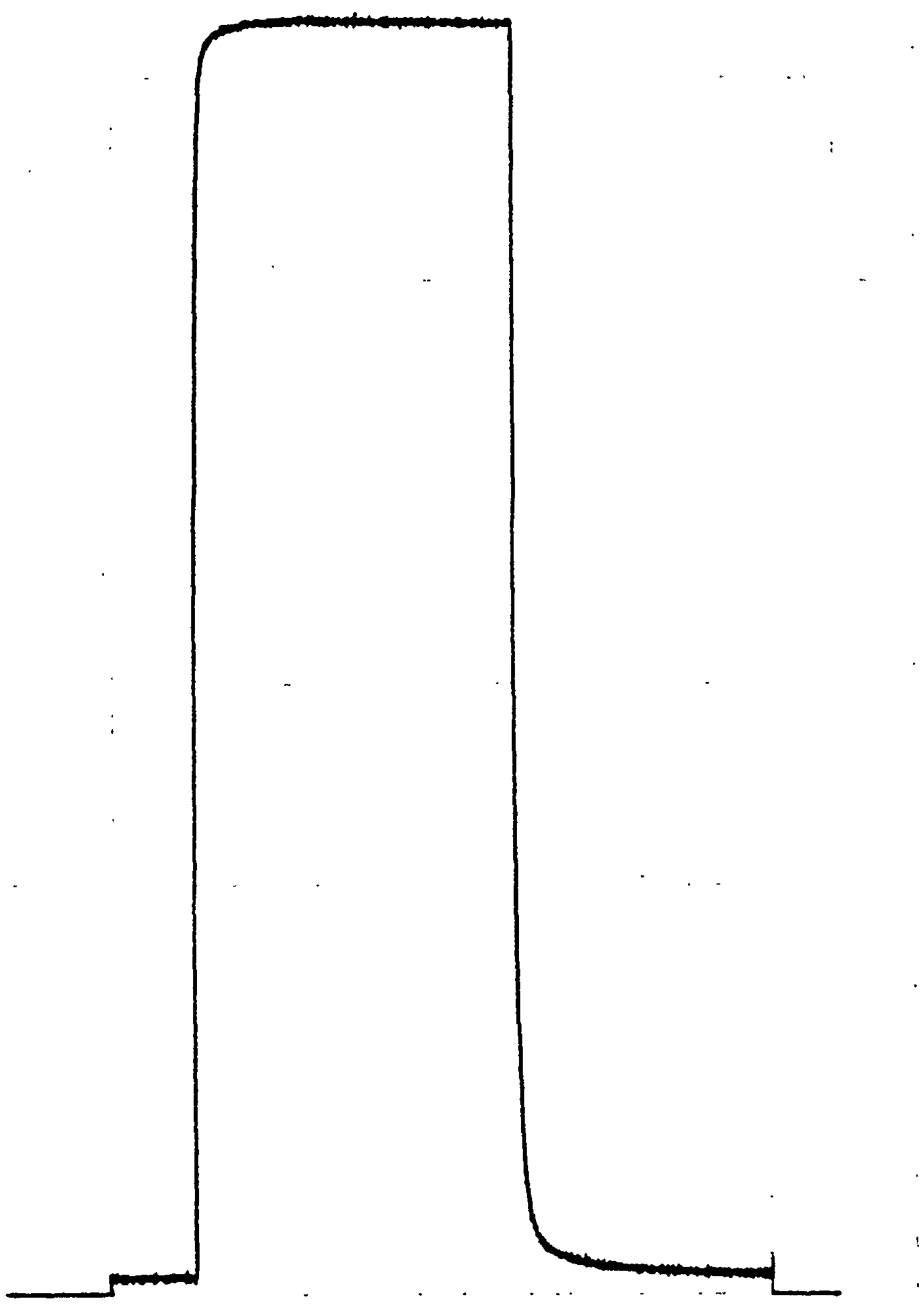

Figure 6.2. 2T Sensor trace obtained with current follower circuit

IC 1, 2 & 3 :- RS 7650 Chopper Stabilised Op-Amps.

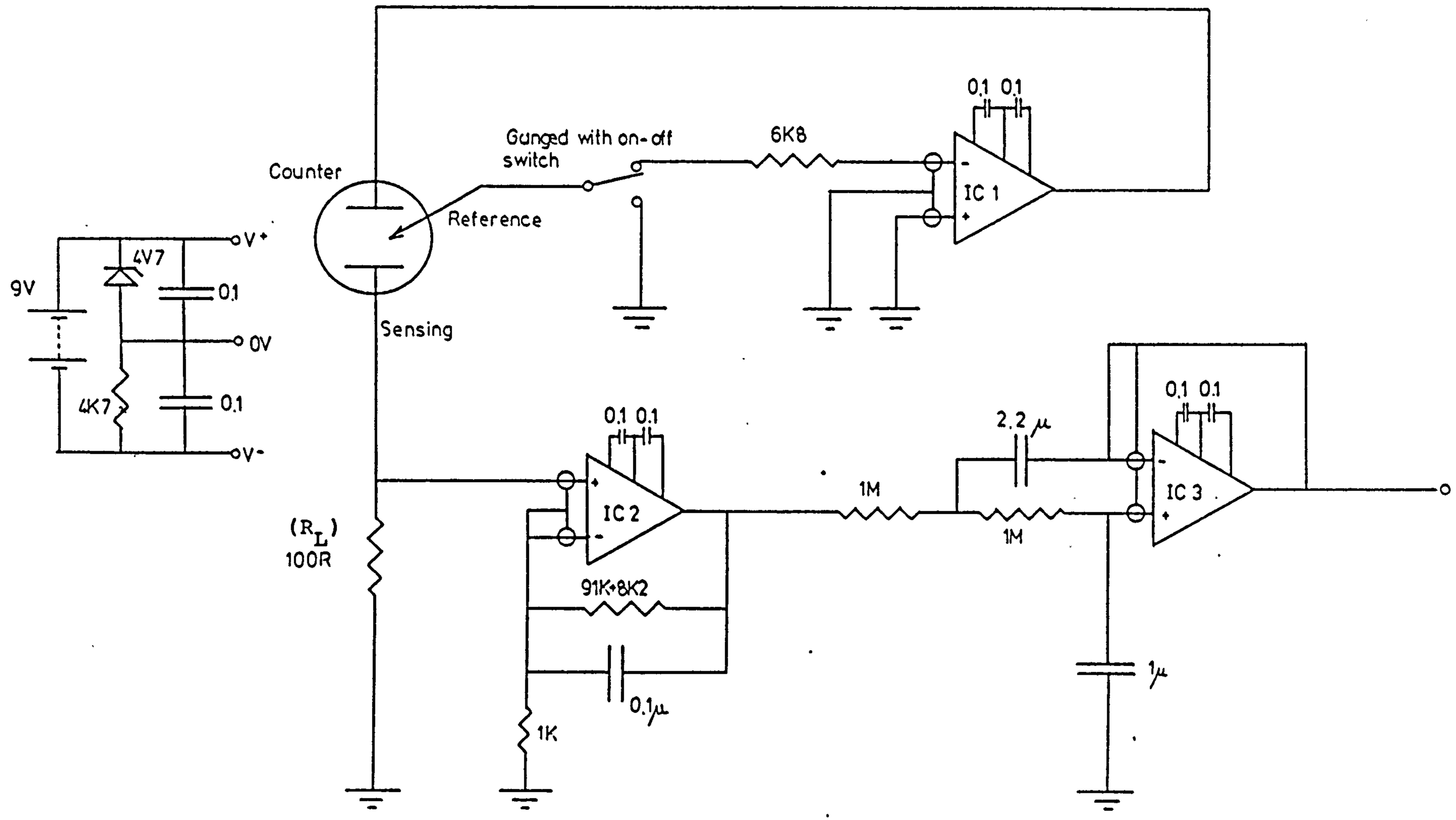

Figure 6.3. Circuitry for use with three-electrode sensors.

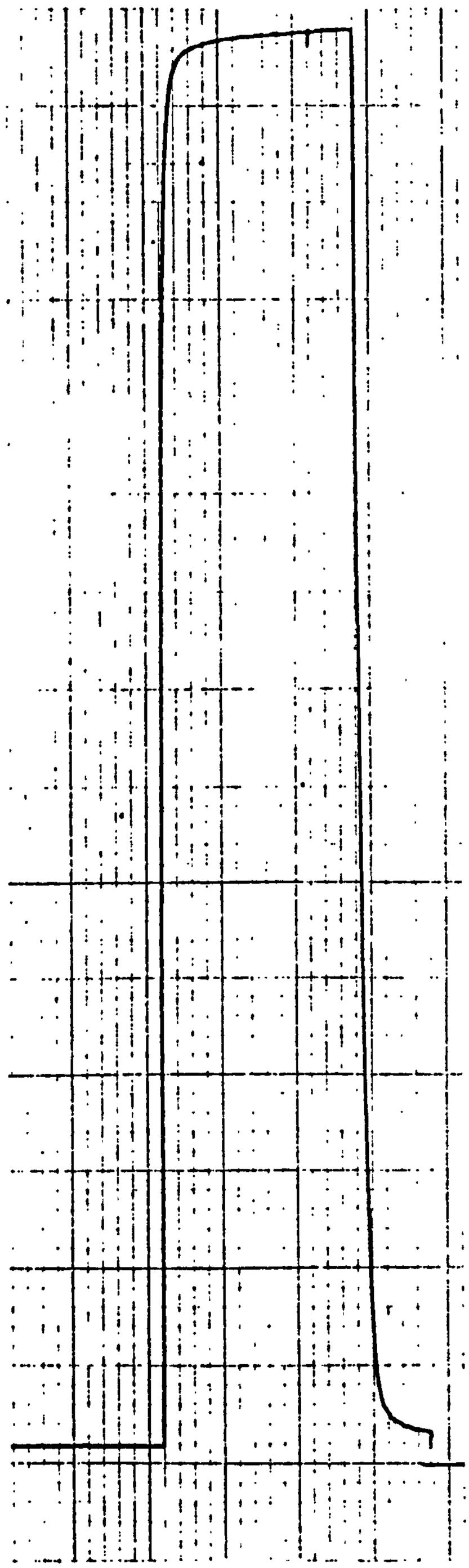

Figure 6.4. 3F Sensor trace obtained with 3-electrode circuit.

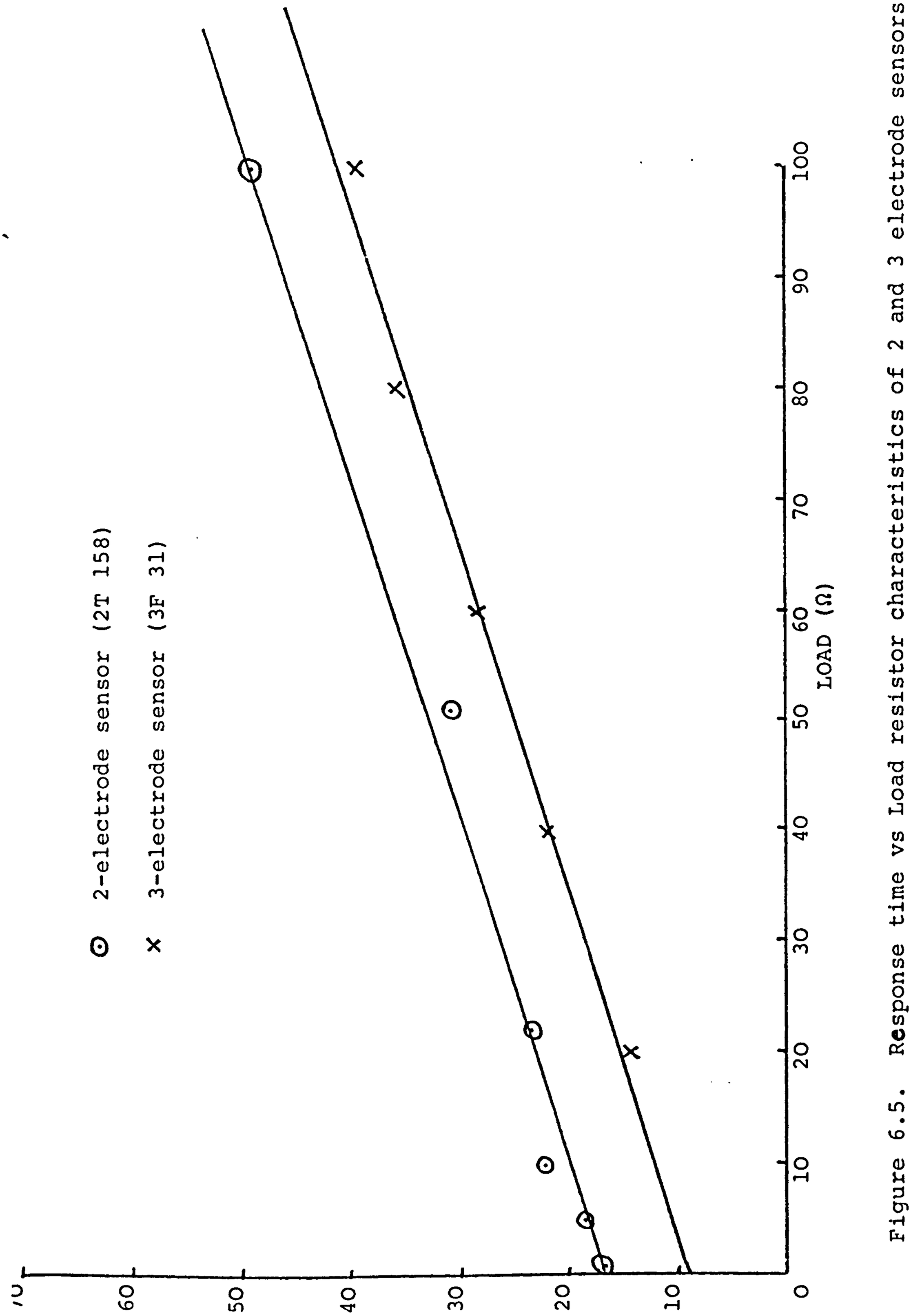

Figure 6.5. Response time vs Load resistor characteristics of 2 and 3 electrode sensors.

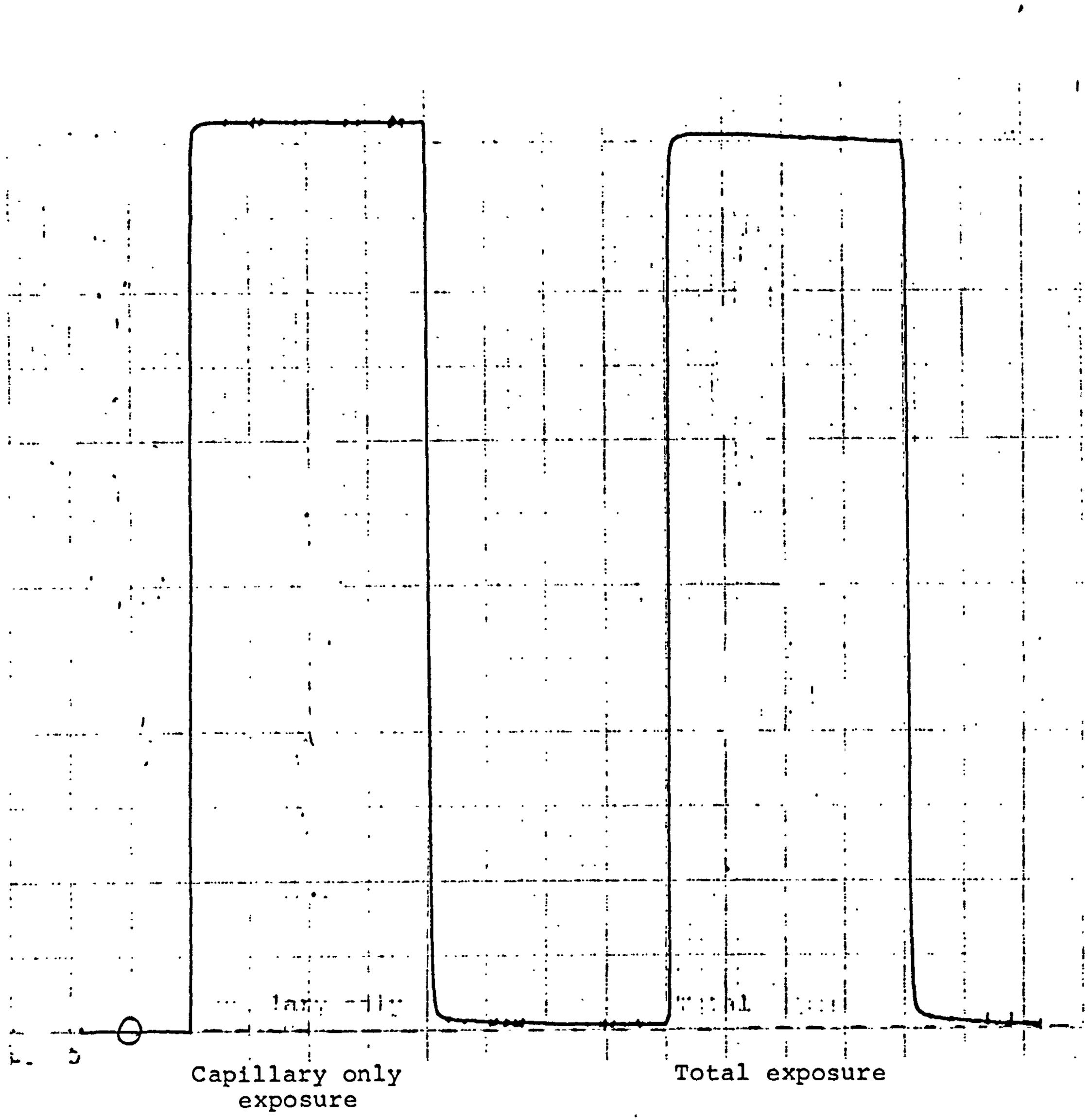

Sensor 3E 75

R_{gain} 1k ohm

R_{load} 100 ohm

510 ppm CO in air test gas

Timebase 5 min cm^{-1}

Signal 1µA/division

Temperature 21.6°C

Figure 7.1. Capillary-only and total exposure CO-tolerance tests on Sensor 3E 75

APPENDIX 1

GAS FLOW EFFECTS WITH CTL CARBON MONOXIDE SENSORS

TECHNICAL NOTE No. 13

CTL Carbon Monoxide Sensor. Gas Flow Effects

A flow test was made using gas from a cylinder with a cross flow head as below at flow rates varied from 100 to 2500 mls/min.

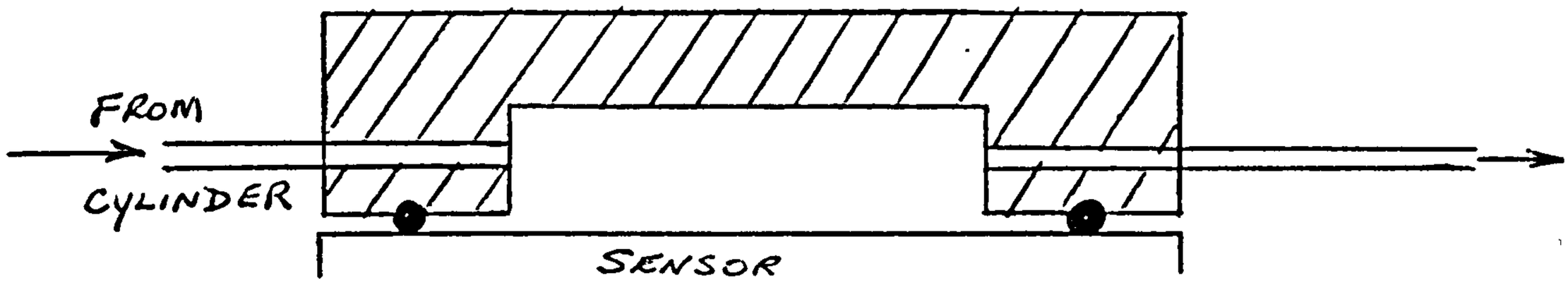

Only a relatively small flow sensitivity was found with the sensitivity increasing linearly with flow rate at a little less than 0.4% of signal per 100 mls/min. increase. The back pressure was 2.6 cms water per 100 mls/min. The effect may be less with lower back pressure, but this has not yet been checked.

When a pump is used in the flow system, particularly if it is a diaphragm pump, pressure oscillations are introduced into the gas stream, which can markedly affect the signal by "pumping" extra gas through the diffusion capillaries into the sensor. Not only will this be a "false" signal, but it is also likely to be apparently flow dependent since the pressure pulse frequency will change with pump speed.

Anything,e.g. baffles, restrictions included upstream,that helps damp out the oscillations will be helpful, but by far the most important and effective thing is to ensure that the downstream back pressure is as near zero as possible. One is then effectively using the "infinite" baffle capacity of the ambient air.

The only thing to ensure is that there is insufficient back diffusion from the ambient air to affect the signal.

This is not a real problem with the CO sensor. Since one is measuring in the ppm range, the concentration difference for back diffusion is also effectively only in the ppm range.

As a guide we have found in a test with 2000 ppm CO, at the low flow rate of 50 mls/min. that, with a 4.4 mm I.D. outlet tube, back diffusion only just becomes detectable when the length of the outlet is reduced to 8 mm. Back diffusion will be less the higher the flow rate and the lower the CO concentration.

One should also note that, since the diffusion rate varies as d^2 (d = tube diameter) while the back pressure varies as $1/d^4$, the widest possible diameter should be used to minimise the back pressure. In general a wider but longer tube is better than a shorter but narrower tube. Clearly also the back pressure will be less the lower the flow rate.

With attention to these points it should be possible to eliminate the effect of pressure oscillation induced by the pump. But since different pumps will have different characteristics these must be individually checked.

The vent from the sensor should be taken outside the instrument, so that the gas does not reach the side of the sensor, which might affect the signal.

A.D.S.T.
11.8.81

Addendum (1) to Technical Note No. 13.

CTL Carbon Monoxide Sensor. Gas Flow Effects

In technical note No. 13 the effect of pump-induced oscillations in the gas stream was discussed. In particular it was recommended that the back pressure downstream of the sensor be kept as low as possible.

Appreciable additional benefit may be obtained by including an expansion chamber after the pump, followed by a restriction (e.g. a length of narrow bore tubing) as shown schematically below.

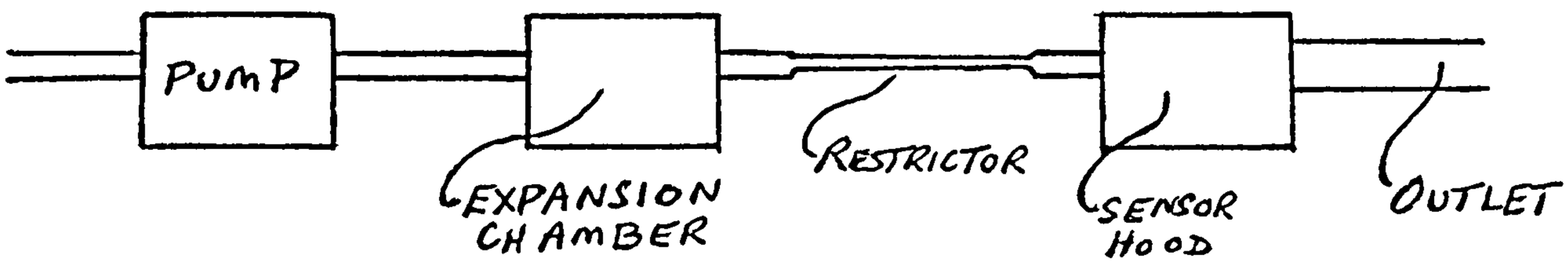

Outlet tube. As unrestrictive as possible to give lowest possible back pressure without significant back diffusion (the larger the bore the better).

Restrictor · The more restrictive the better.

Expansion chamber The larger the volume the better.

There will, of course, be practical limits as to how far one can move in the desired directions with the components above and some experimentation will be required to find the best compromise for a particular instrument.

The expansion chamber will have no significant effect without the restrictor. The higher the expansion chamber volume the less can be the restriction and vice versa (indications are that these are roughly in proportion to achieve the same effect. e.g. if you halve the volume you need to double the restriction for the same effect).

As a starting guide an expansion chamber of about 10 ccs volume with a restrictor consisting of about 20 cms of 1.5mm bore tubing seemed to largely eliminate the oscillation effect from a diaphragm pump in a crude test (smaller bore tubing would enable this length to be significantly decreased.

A.D.S.T.
10 September, 1981.

APPENDIX 2

PRELIMINARY INVESTIGATIONS OF IN-BOARD FILTERS TO REDUCE ETHYLENE CROSS-SENSITIVITY OF 2T CARBON MONOXIDE SENSORS

City Technology Limited

17/19 Sebastian Street, London. EC1V 0HB

Telephone 01-253-3799. Telex 263896

TECHNICAL NOTE NUMBER 18

Preliminary Investigations of In-Board Filters to Reduce Ethylene Cross-Sensitivity of 2T CO Sensors

B.S. Hobbs

6 July, 1982

Preliminary Investigations of In-Board Filters to Reduce Ethylene Cross-Sensitivity of CTL Carbon Monoxide Sensors

Specificity of gas sensors can be improved by the use of selective chemical filters to remove interfering constituents from the gas stream. Ideal filter materials are those which undergo spontaneous regeneration, for example by catalytic oxidation in aerobic conditions, thus reducing the need for maintenance. However, since most materials are non-regenerative, it would be advantageous to locate the filter downstream of the diffusion barrier of the sensor where the cumulative total exposure to reactants is considerably lower than in the main gas stream.

This concept of "in-board" chemical filtering has been demonstrated with CTL capillary-limited carbon monoxide sensors, particularly for the removal of acid gases such as SO_2, and is covered by provisional patents. This work was undertaken to examine further the use of in-board filtering to selectively remove ethylene with brominated carbon cloth.

Ethylene produces a cross-interference at platinum electrodes in carbon monoxide sensors where it undergoes a 2-electron oxidation to ethylene glycol:

$$C_2H_4 + 2H_2O = C_2H_4(OH)_2 + 2H^+ + 2e.$$

The diffusion coefficient of ethylene in air is 0.157 cm^2s^{-1} @ 25°C, 1 atm. pressure, compared to 0.203 for carbon monoxide. Since both gases undergo 2-electron oxidations, the theoretical cross-sensitivity should be 77 ppm CO. equivalent per 100 ppm ethylene.

NCB (Yorkshire Labs.) had found that bromine impregnated carbon cloth can remove ethylene interference without affecting the carbon monoxide signal to any great extent. Presumably the unsaturated double bond reacts to form the relatively stable brominated adduct:

$$C_2H_4 + Br_2 = C_2H_4Br_2$$

Plain and brominated carbon cloths were supplied by NCB (Yorkshire Labs.) for these tests.

A CTL sensor, incorporating an in-board filter system was made by bolting an additional spacing component between the counter and capillary plates as shown schematically in Figure A2.1. The filter chamber was made from a capillary top-plate component by machining out the centre portion as shown in Figure A2.1. The filters were backed with 0.18mm thick, porous ptfe tape in order to keep the electrodes clean. Tests were conducted with a Type 2T trace CO sensor, moulded in black NORYL (polyphenylene oxide). A 100ohm load resistor was soldered across the terminals and the sensor was left in ambient air for 1 month before testing. Baselines and responses to air test gases containing CO(58ppm), H_2 (90ppm) and ethylene (96ppm) respectively, were measured on a recorder at 10μA FSD and 5 minutes per cm chart speed.

The measured span and response time on a 58 ppm CO in air test gas were not materially affected by the filter cavity, but the porous ptfe tape decreased the CO sensitivity by 3 to 4%, although no detectable change in response time was apparent.

The results of these tests are summarised in Table A2.1. Apart from a slight reduction in H_2-sensitivity with a brominated carbon cloth filter, the CO and H_2 responses were all quite normal. Ethylene responses of both the controls, with and without a plain carbon cloth filter, consisted of a rather sluggish rise to a peak which fell short of the expected signal level, followed by a steady decline in current (Figure A2.2.Recovery on removal of the test gas was drawn out and approached the normal baseline as a limit, without actually going negative. Such behaviour is indicative of insufficient electrode activity to oxidise all the hydrocarbon as it reaches the sensing electrode. The excess reactant eventually gets to the counter, causing further signal depression.

With a brominated carbon filter the sensor's ethylene response was very low and stable (See figure A2.2 indicating significant removal of hydrocarbon on the filter and complete reaction of the residue as it reached the sensing electrode. The filtration efficiency was not significantly improved by using 2 cloth discs instead of one.

The efficiency of ethylene filtration gradually decreased with time when the sensor was left in ambient air, e.g. the results in Table A2.3 shows increase in ethylene cross-sensitivity of the test sensor from 0.09 ppm CO equivalent per ppm ethylene to 0.236, over a 3 week period. One filter left out on the laboratory bench was almost completely deactivated over the same period.

Brominated carbon filters produced a slight negative response on the baseline, probably due to bromine reduction at the sensing electrode. This could be eliminated by interposing a plain carbon cloth between the filter and electrodes, without any adverse effects on other aspects of the sensor operation.

Table A2.1 Results of cross-sensitivity tests on a 2T sensor with in-board chemical filter.

(All readings taken at a nominal 20°C. ambient temperature)

Filter	Baseline	Sensitivites (μA/ppm x 10^3)			ppm CO equivalent per ppm of interfering gas	
	(μA)	CO	H_2	C_2H_4 (peak)	H_2	C_2H_4 (peak)
Blank	+ 0.10	83.6	27.8	50.0	0.333	0.598
Plain Carbon cloth	+ 0.15	82.8	26.7	56.7	0.322	0.685
Br_2/Carbon cloth	- 0.35	86.2	22.2	4.2	0.258	0.049
Double Br_2 cloth	0.00	86.2	22.2	3.1	0.258	0.036

Table A2.2 Effect of Time on ethylene cross sensitivity of a 2T sensor with brominated carbon cloth filter

Day No.	Baseline (μA)	Sensitivities (μA/ppm x 10^3)		ppm CO equivalent per ppm C_2H_4
		CO	C_2H_4 peak	
1	-0.10	81.0	7.3	0.090
3	+0.10	76.7	10.4	0.136
4	+0.10	76.7	9.4	0.123
8	+0.05	75.9	13.0	0.171
22	+0.15	75.0	17.7	0.236

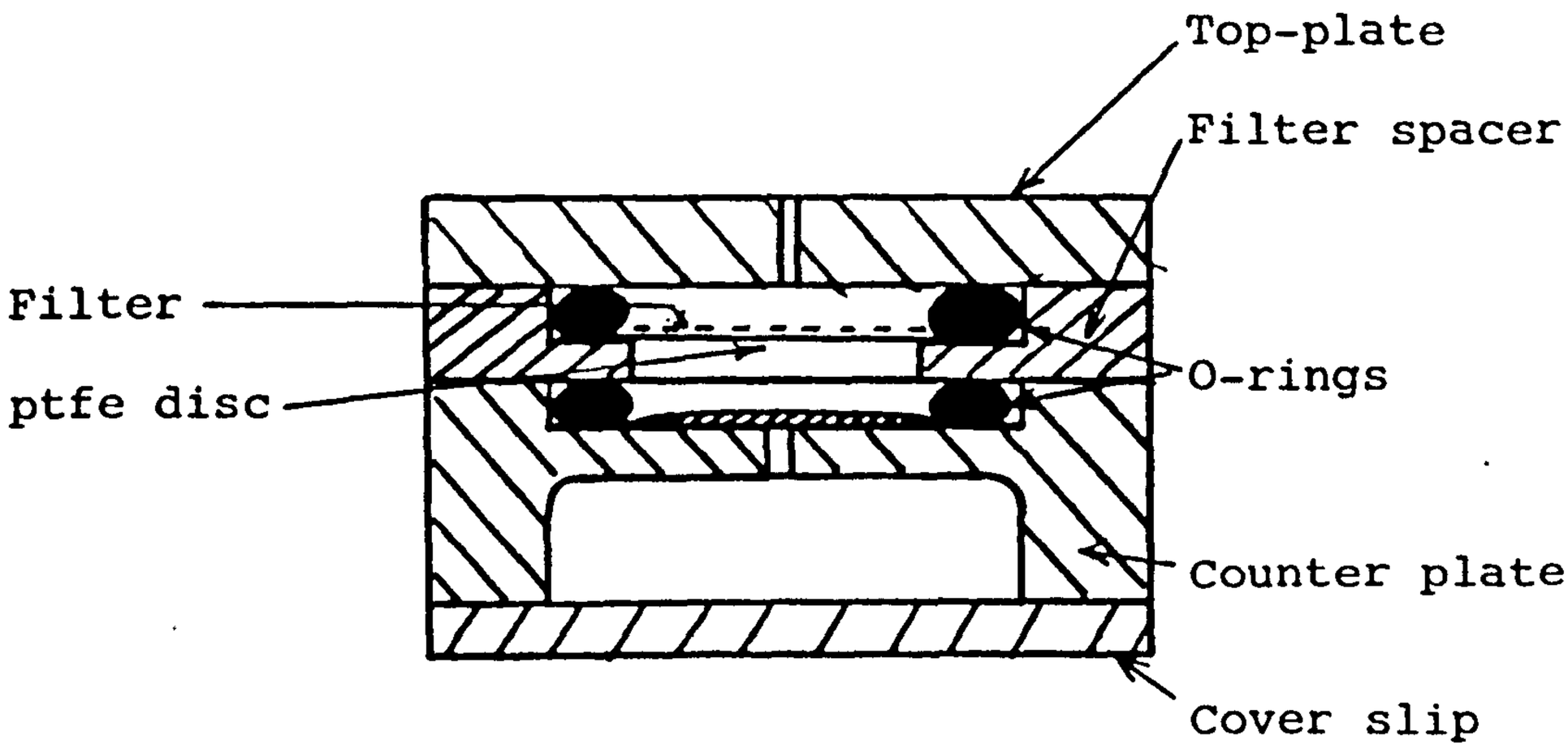

Figure A1.1.Schematic diagram of modified 2T sensor with in-board filter attachment.

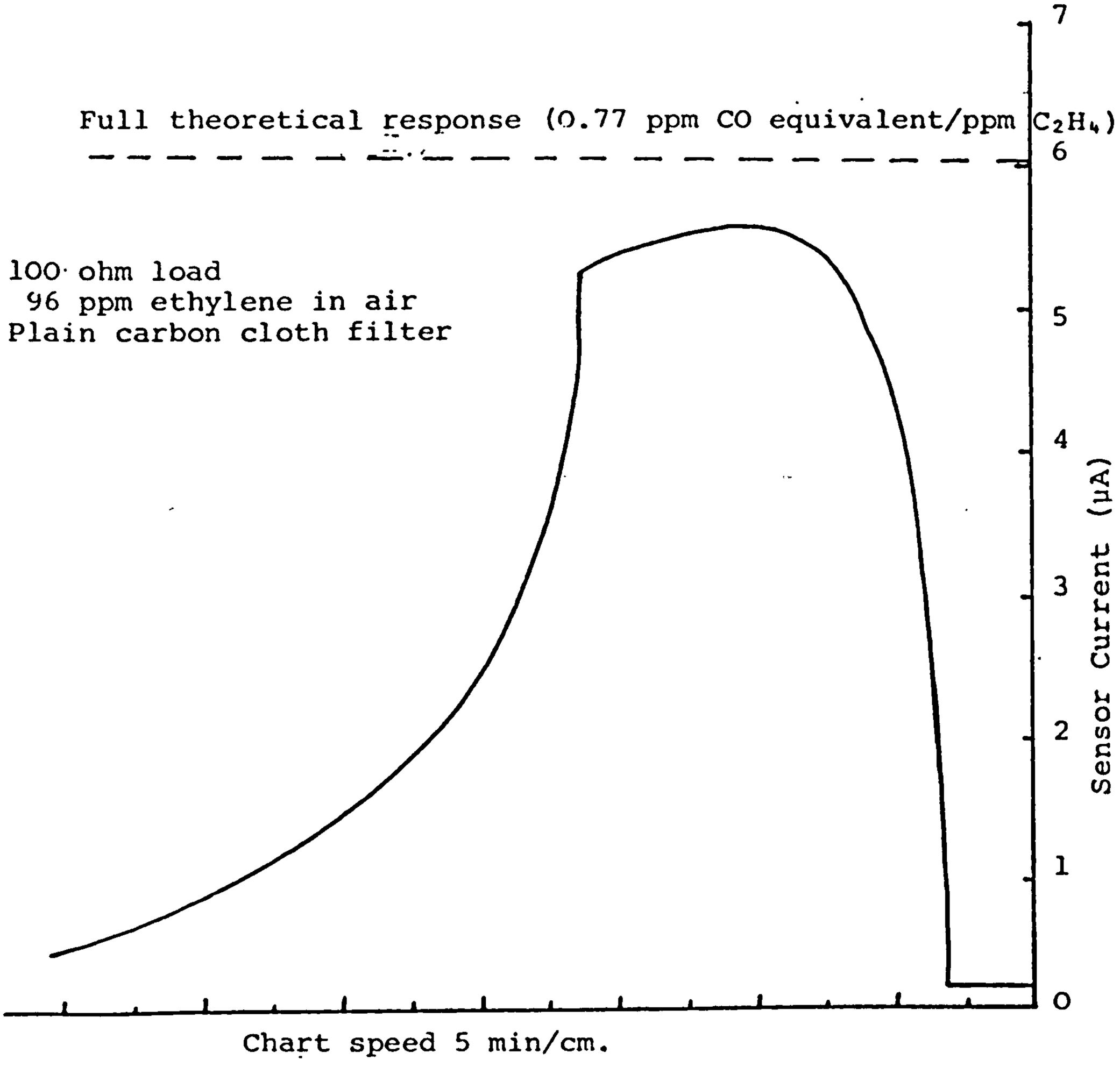

Figure A2.2.Typical Ethylene response of 2T sensor, with or without plain carbon filters.

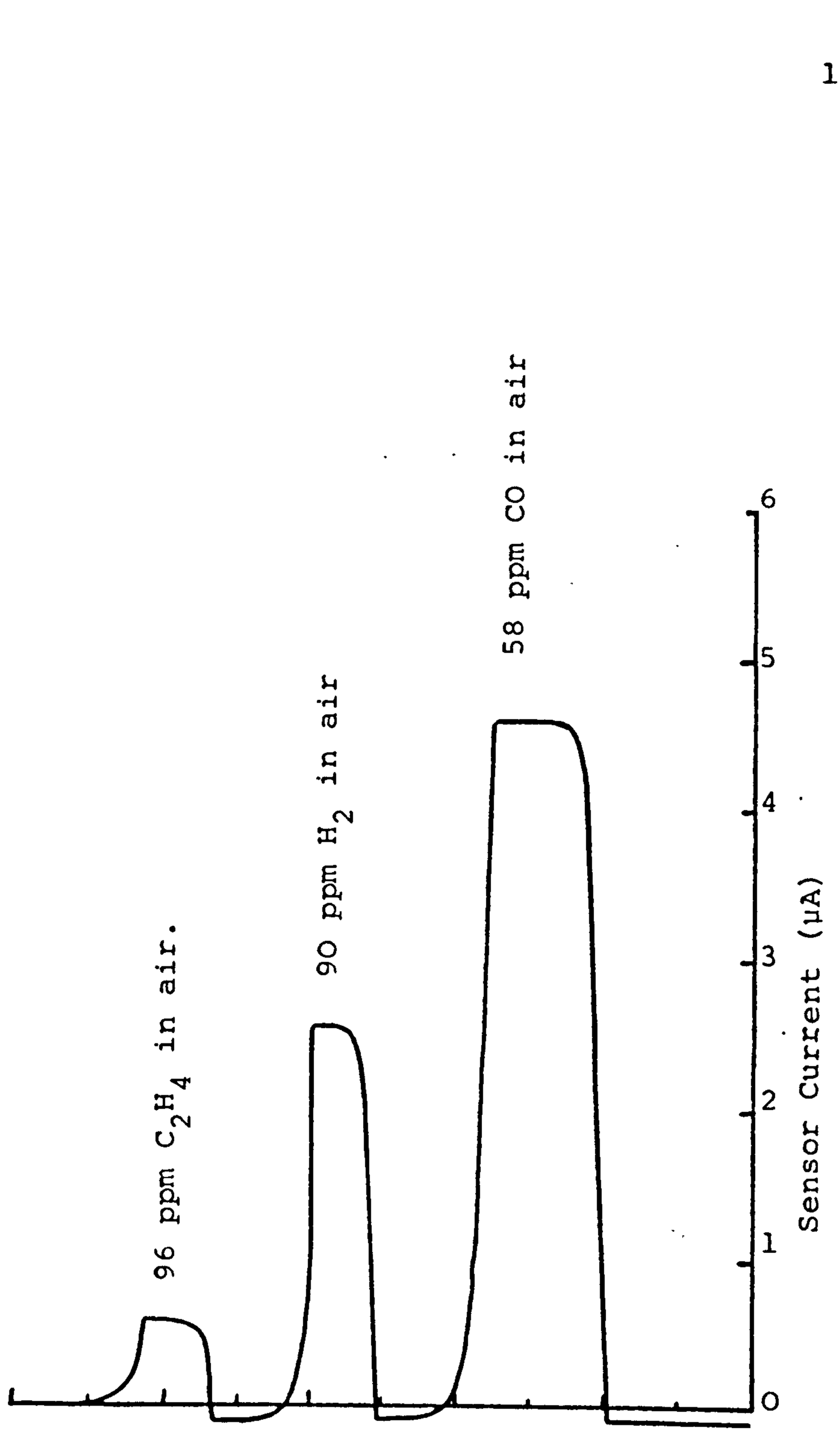

Figure A2.3.Typical responses to CO, H_2 and C_2H_4 of a 2T sensor with a fresh brominated carbon cloth filter.

APPENDIX 3

RELATIONSHIPS BETWEEN ELECTRODE ACTIVITY RESERVE AND SENSOR SIGNAL AND TEMPERATURE COEFFICIENT

Ideally one would like the signal current to be controlled totally by the capillary diffusion barrier. In this case the $T^{\frac{1}{2}}$ law should be followed giving a temperature coefficient (uncompensated) of 0.17% signal per ^{o}C at $20^{o}C$ (0.183% at $0^{o}C$ and 0.159% at $40^{o}C$).

In practice the electrolyte film in the sensing electrode may also provide a significant diffusion resistance. As shown below this will (a) depress the true capillary signal (b) increase the sensor temperature coefficient, since diffusion of gas through the electrolyte film follows an exponential law resulting in a high temperature coefficient, 2 to 3% of signal per ^{o}C at $20^{o}C$. Because of the exponential law the coefficient will also be strongly temperature dependant, higher at low temperature and lower at high temperature.

The sensor characteristics will therefore depend on the relative contributions of these two diffusion resistances:

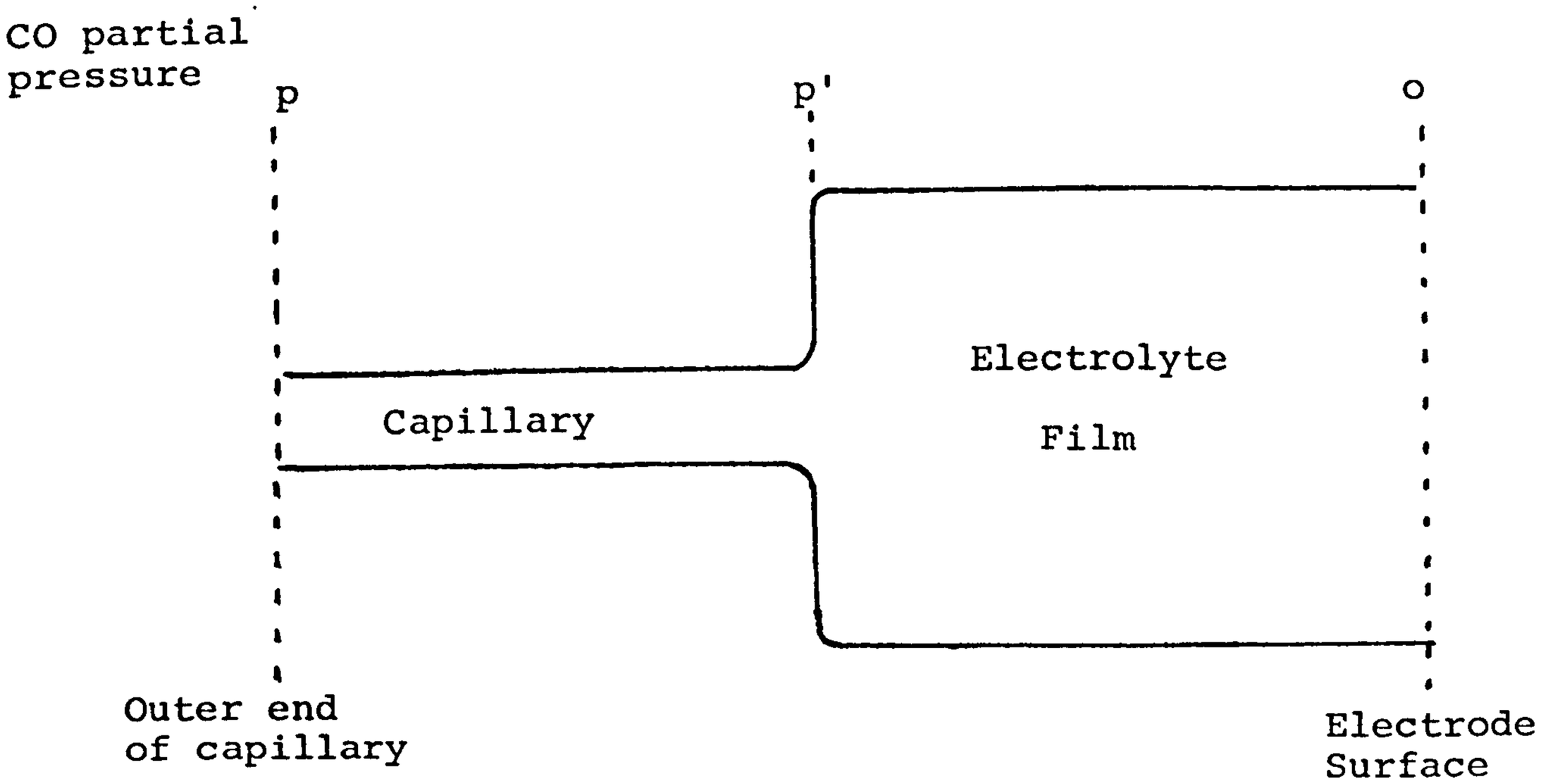

The flux of CO through the capillary expressed as a current (i_s) is given by:

$$i_s = k_c (P-P') \quad \ldots\ldots\ldots\ldots\ldots\ldots (1)$$

where k_c includes the diffusion constant, geometric factors and conversion factor from mass flow to current.

Similarly for the electrolyte film:

$$i_s = k_e P' \quad \ldots\ldots\ldots\ldots\ldots\ldots (2)$$

Substituting in (1) for $P' = \frac{i_s}{k_e}$ from (2):

$$i_s = k_c\left(P-\frac{i_s}{k_e}\right) \quad \ldots\ldots\ldots\ldots\ldots\ldots (3)$$

Rearranging:

$$i_s = \frac{k_c k_e}{k_c+k_e} P \quad \ldots\ldots\ldots\ldots\ldots\ldots (4)$$

For the capillary on its own:

$$i_c = k_c P \text{ hence } k_c = \frac{i_c}{P}$$

For the electrolyte film on its own:

$$i_e = k_e P \text{ hence } k_e = \frac{i_e}{P}$$

Substituting in (4) gives:

$$i_s = \frac{i_c i_e}{i_c+i_e} \quad \ldots\ldots\ldots\ldots\ldots\ldots (5)$$

It is convenient to talk in terms of activity reserve (R) defined as:

$$R = \frac{i_e}{i_c}$$

i.e. the ratio of the current capability of the electrode on its own (open electrode current) to the current with 100% capillary limitation.

Substituting for $i_e = Ri_c$ in (5) gives

$$i_s = \frac{i_c R}{1+R} \quad \ldots\ldots\ldots\ldots (6)$$

and $i_s \rightarrow i_c$ as $R \rightarrow \infty$

The relationship is depicted in figure A3 where it is seen that even at an activity reserve of 20, there is a measurable element of electrode control in the sensor signal. Electrodes used in current sensor designs generally have lower activity reserves, and greater degrees of electrode control as follows:

Sensor Type	Activity Reserve (S_E/S_C)	Signal as percentage of theoretical capillary current
2T	3 to 4	78
2E	5 to 6	85
3E	6 to 7	87
3F	~ 20	95

The effect on temperature coefficient may be derived as follows:

If the activity reserve is R, then the relative contributions to the signal are R from the capillary, compared to 1 from the electrode. An amount R is subject to the capillary temperature coefficient (α_c) and an amount 1 to the electrode temperature coefficient (α_e). The resulting sensor temperature coefficient α_s will be the resulting mean, so:

$$\alpha_s = \frac{R\alpha_c + \alpha_e}{R + 1} \quad \text{..... (7)}$$

Rearranging: $$\alpha_s = \frac{R}{R+1} \left[\alpha_c + \frac{\alpha_e}{R}\right] \quad \text{..... (8)}$$

The theoretical capillary temperature coefficient (α_c) is 0.17% per degree and measured values of α_e for CO oxidation on platinum electrodes are about 2.5% per degree. Substitution of these values into equation (8) and its solution produces the relationship shown in figure A3.

Estimated intrinsic temperature coefficients from equation 8 for current sensor designs are in fair agreement with measured values as follows:

Sensor Type	Activity Reserve	Estimated temperature coefficient (% per degree)	Measured temperature coefficient (% per degree)
2T	3 to 4	0.7	0.9
2E	5 to 6	0.5	0.7
3E	6 to 7	0.5	0.7
3F	∿ 20	0.3	0.5

Note The above is a simplified treatment to illustrate the order of magnitude of the effects. Two points should be noted:

(1) The capillary diffusion is actually proportional to $\frac{P}{P_t}$, where P is the partial pressure and P_t is the total pressure, since the diffusion constant is proportional to $\frac{1}{P_t}$. The electrolyte film diffusion will be proportional to P and independent of P_t. A strict treatment should take this into account. At very high values of R (capillary dominated signal) the sensor will be a true concentration (volume %) sensor, with zero pressure coefficient. At low values of R there is an element of partial pressure response, which will result in a finite pressure coefficient when treated as a concentration sensor.

(2) The treatment has implied temperature coefficients independent of temperature. For the capillary's $T^{\frac{1}{2}}$ law the deviation from this assumption is not large, but it is much more significant for the electrolyte films' exponential law. The effect of this is that with low values of R the resulting temperature coefficient, expressed as % signal per ^{o}C, will be higher the lower the temperature as illustrated below:

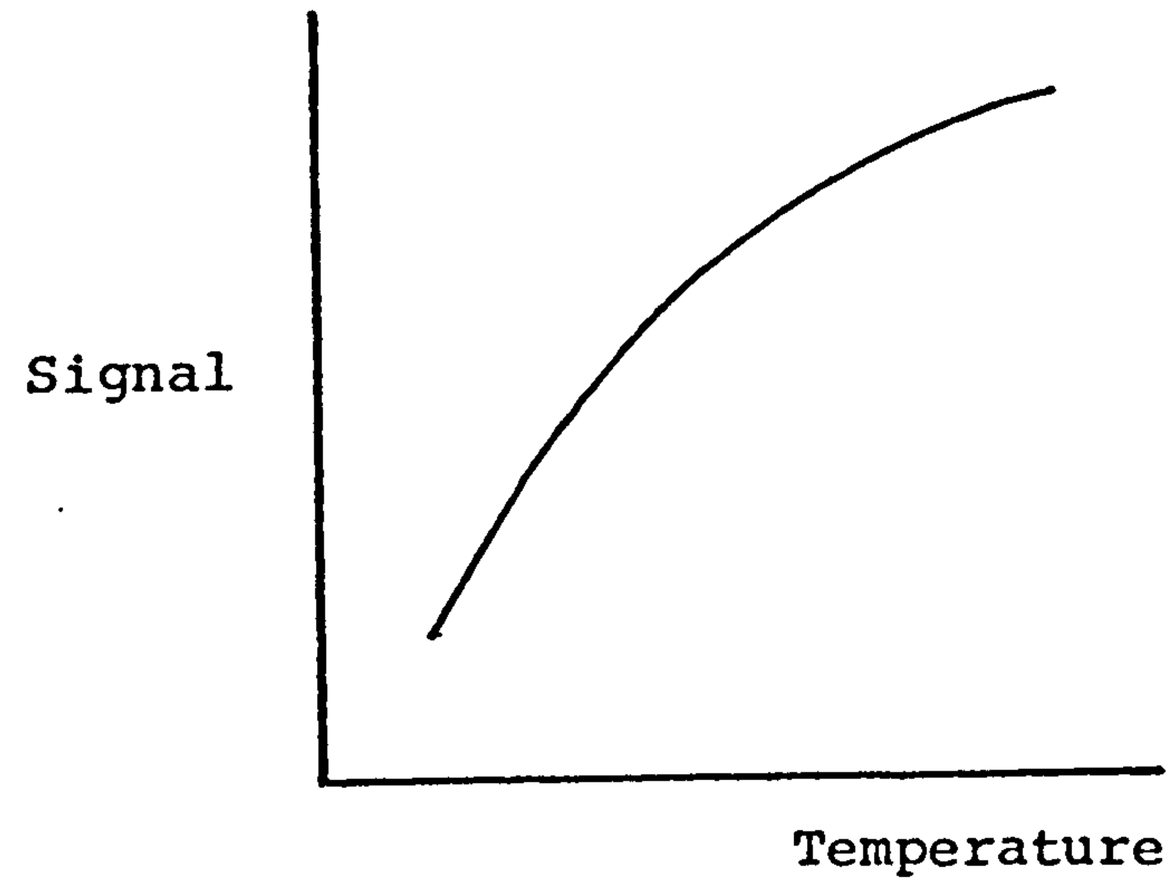

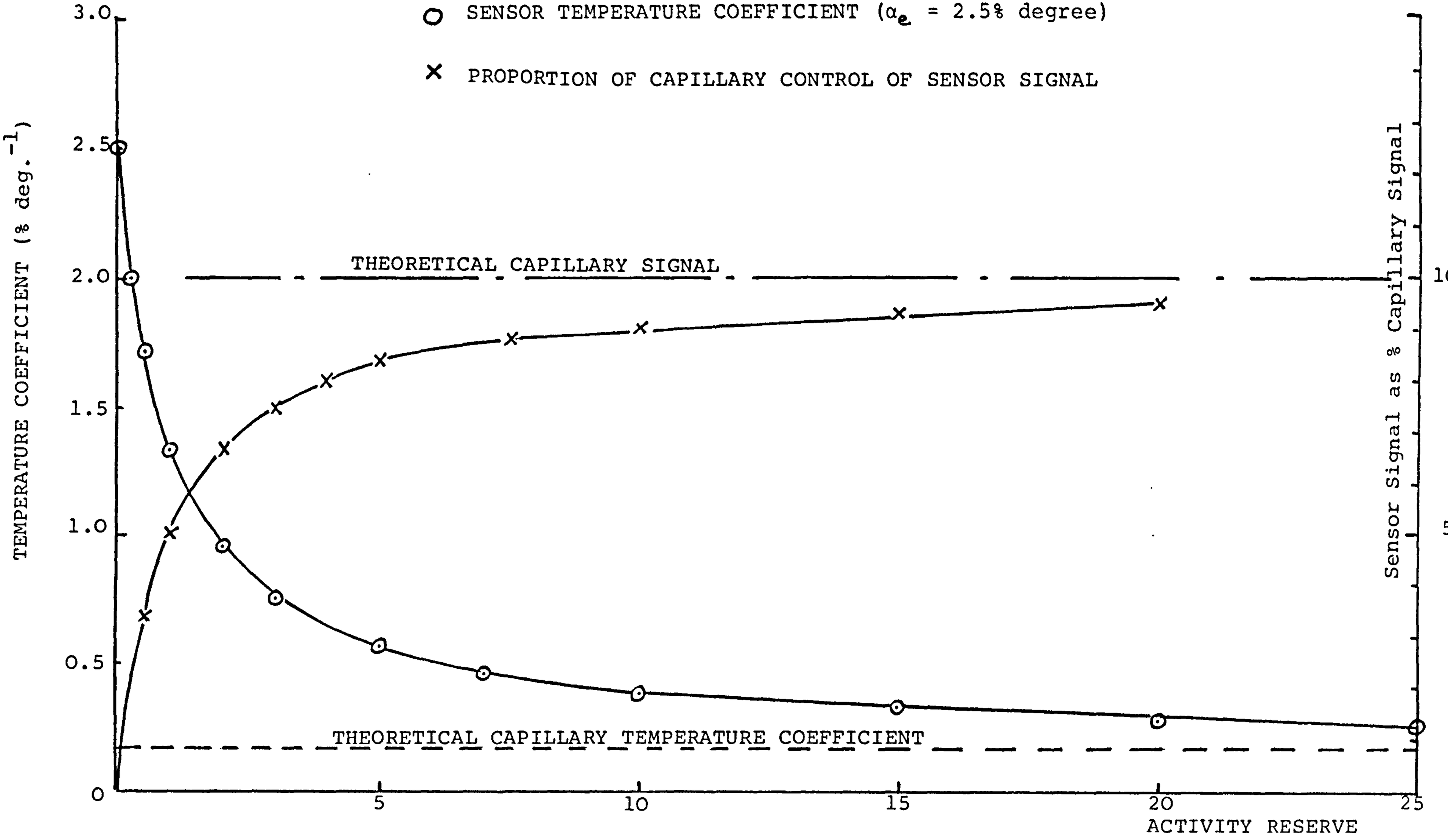

Figure A.3. Relationships between "Activity Reserve" and sensor signal and temperature coefficient.

CTL Report No. 83/09/008

July 1983

CITY TECHNOLOGY LIMITED,
The City University,
17/19, Sebastian Street,
London EC1V OHB

14. CARBON MONOXIDE SENSOR FOR USE IN COAL MINES : PHASE 5

Report

A.D.S. Tantram
R. Chan-Henry
B.S. Hobbs

Mr. L.R. Cooper,
National Coal Board,
Mining Research and Development
Establishment,
Stanhope Bretby,
Staffs.

NCB Contract No. Y 135007/09/21

CTL Project No. 94.09.00

CONTENTS

CONTENTS (Contd.)

List of Tables

List of Figures

List of Figures (Contd.)

Summary

This report presents the results of a fifth phase of a program to develop a trace carbon monoxide sensor for use in coal mines.

Effort during this phase has been directed in the following principal areas:

- hardware design development for both 2 and 3 electrode sensor versions.
- characterisation of the latest 2T (2-electrode, trace) sensor design.
- further investigations of hydrogen cross sensitivity.
- chemical filter hardware and materials development.
- water balance calculations in high humidity conditions.

Apart from some minor changes to the electrolyte wick and electrical connections, the only major design modifications have been to reduce gas side access through the current collector gates, which was shown to be excessive in previous designs of environmental sensors, and to introduce changes in the composition and configuration of the electrode stack in 3-electrode sensors to optimise CO signal response and shield the reference electrode from partially reacting gases at the sensing electrode, particularly hydrogen.

2T sensor characterisation has been extended to designs with the new, split sleeve, capillary to achieve improved temperature compensation. Results of a separate study on transient, short circuit signals with 2T sensors has also been undertaken (see appendix).

The following measures to reduce hydrogen cross sensitivity have been investigated:

- potential biasing of the sensing electrode.
- preanodisation of sensing and reference electrodes before use.
- electrolyte additives.

Biasing of 2-electrode sensors tended to reduce CO-tolerance and could only be considered with present designs if some reduction in the upper CO concentration limit were accepted. Further work has therefore been suspended.

No such disadvantages were incurred with 3-electrode sensors and characteristics under bias were investigated in more detail, including "start-up" times on interrupting the bias for various periods. A bias potential of + 300mV (sensing relative to reference) was the preferred condition. This produced a hydrogen cross sensitivity of about 5% with current designs and a baseline of below 1μA, i.e. below 10 ppm CO equivalent with 3E sensors. Below + 300mV, higher hydrogen responses were incurred with only marginal reductions in baseline. Baselines increased sharply at potentials greater than + 350mV due to the evolution of oxygen at the sensing electrode.

Preanodisation of sensing and reference electrodes reduced hydrogen cross sensitivities with current designs to 15 to 30% for 3E sensors and 20 to 50% with 3F sensors. More work however, is required to both obtain a fuller understanding and to optimise this procedure. Anodisation may also be used with 2-electrode sensors but conditions will need careful selection to avoid prejudicing the CO tolerance.

The addition of soluble redox couples to the electrolyte was examined to reduce hydrogen sensitivity by effectively chemically biasing the sensing electrode to higher working potentials. With this approach it appeared that the conditions required to achieve the desired suppression of hydrogen interference, also produced undesirable side effects and it was concluded that a satisfactory solution would not be possible, at least with the present system geometry.

In-board chemical filters, introduced in the last report, have been further developed. Two hardware configurations are available, one with higher filter capacity but with a slower response, the other with a fast response but lower filter capacity. Materials have been developed for removing SO_2 and organic molecules in CO sensors and for removing CO to produce a hydrogen sensor.

The theoretical model derived in previous reports for water transfer between the interior of a sensor and its surroundings was used to estimate the possible endurance times of 2T sensors in high relative humidities at 35°C. The effects of interior space utilisation together with primary acid concentration and volume were considered over a range of relative humidities between 90 and 100%.

1. INTRODUCTION

The original objectives during this 5th phase of a program to develop a carbon monoxide sensor for use in coal mines were as follows:

(a) To provide a backup service to the NCB, dealing with enquiries, providing additional technical data, etc., arising from NCB field trials with 2T sensors.

(b) To develop and characterise 2T sensors incorporating an improved span temperature compensation design based on split capillary inserts.

(c) To investigate the possibility of reducing hydrogen cross interference in both 2 and 3 electrode sensors by anodic potential biasing or preanodisation of the sensing electrode.

(d) To continue development of in-board chemical filters to improve CO specificity.

In addition to these topics, additional work has been undertaken in the following areas:

- further development, modifications and improvements to sensor hardware designs.
- an investigation of gas access pathways to the sensor interior.
- reduction of hydrogen cross sensitivity by chemical biasing of the electrodes using soluble redox additives in the electrolyte.

- adaptation of in-board chemical filtering to remove CO in hydrogen sensors based on CTL hardware designs.
- extended calculations of 2T sensor water balance in conditions of high humidity.
- study of transient, short circuit signals from 2T sensors.

2. HARDWARE DESIGN

2.1. Modifications to Wick Arrangement

A modified wick arrangement has been introduced as shown in Figure 2.1. which is more amenable to production assembly. In the new arrangement a standard sub-assembly is produced, comprising the ptfe tape glued to the floor, the central wick, tacked in place with a spot of glue over this tape and the cupped wick in the electrolyte reservoir. Appropriate Electrodes and separators are then inserted afterwards, depending on the type of sensor required.

This proved simpler to assemble compared to the older method of threading the wick through the electrode.

In order to ensure contact between wick and separator, the central hole in the counter electrode was increased from 3.5 to 7.0 mm.

2.2. Rear Electrical Connections

Rear connections via bolts (Figure 2.2.) are now offered as a standard alternative to side tag connections (Figure 2.3.) with all sensor types.

2.3. Moulding Modification to Current Collector Gates

In the last report the current collector gates had been raised by 0.5 mm to restrict gas side access which caused discrepancies between capillary-only and total exposure tests. This proved insufficient and gates had to be further built-up with perspex cement which was a difficult and time-consuming operation in

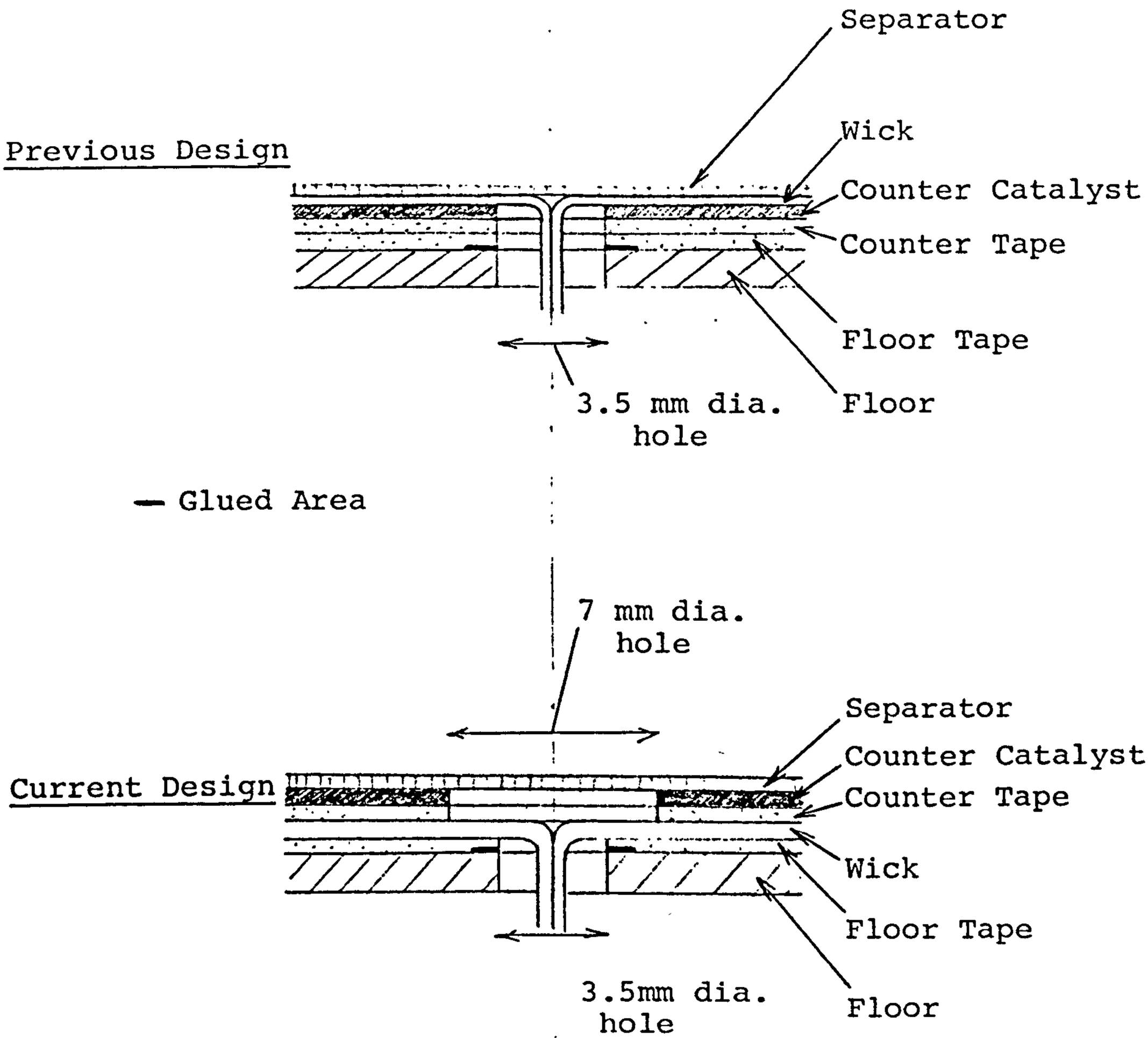

Figure 2.1. Schematic diagram of modified wick arrangement.

City Technology Limited

17/19 Sebastian Street, London. EC1V 0HB

Telephone 01-253-3799. Telex 263896

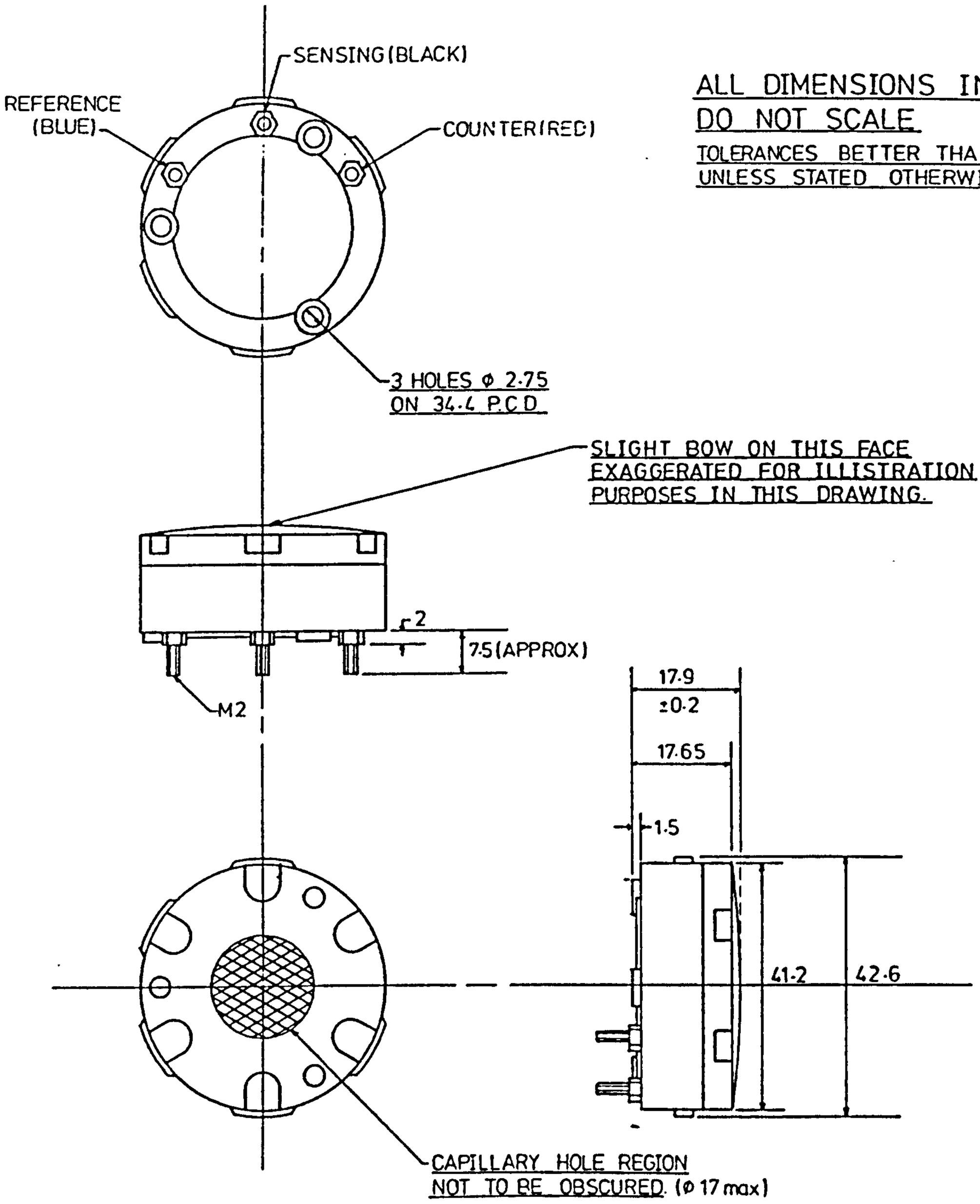

ALL DIMENSIONS IN mm
DO NOT SCALE
TOLERANCES BETTER THAN 0·08 UNLESS STATED OTHERWISE.

Figure 2.2. Outline Drawing Of Moulded Gas Sensor Design With Rear Terminal Connections

City Technology Limited

17/19 Sebastian Street, London. EC1V 0HB

Telephone 01-253-3799. Telex 263896

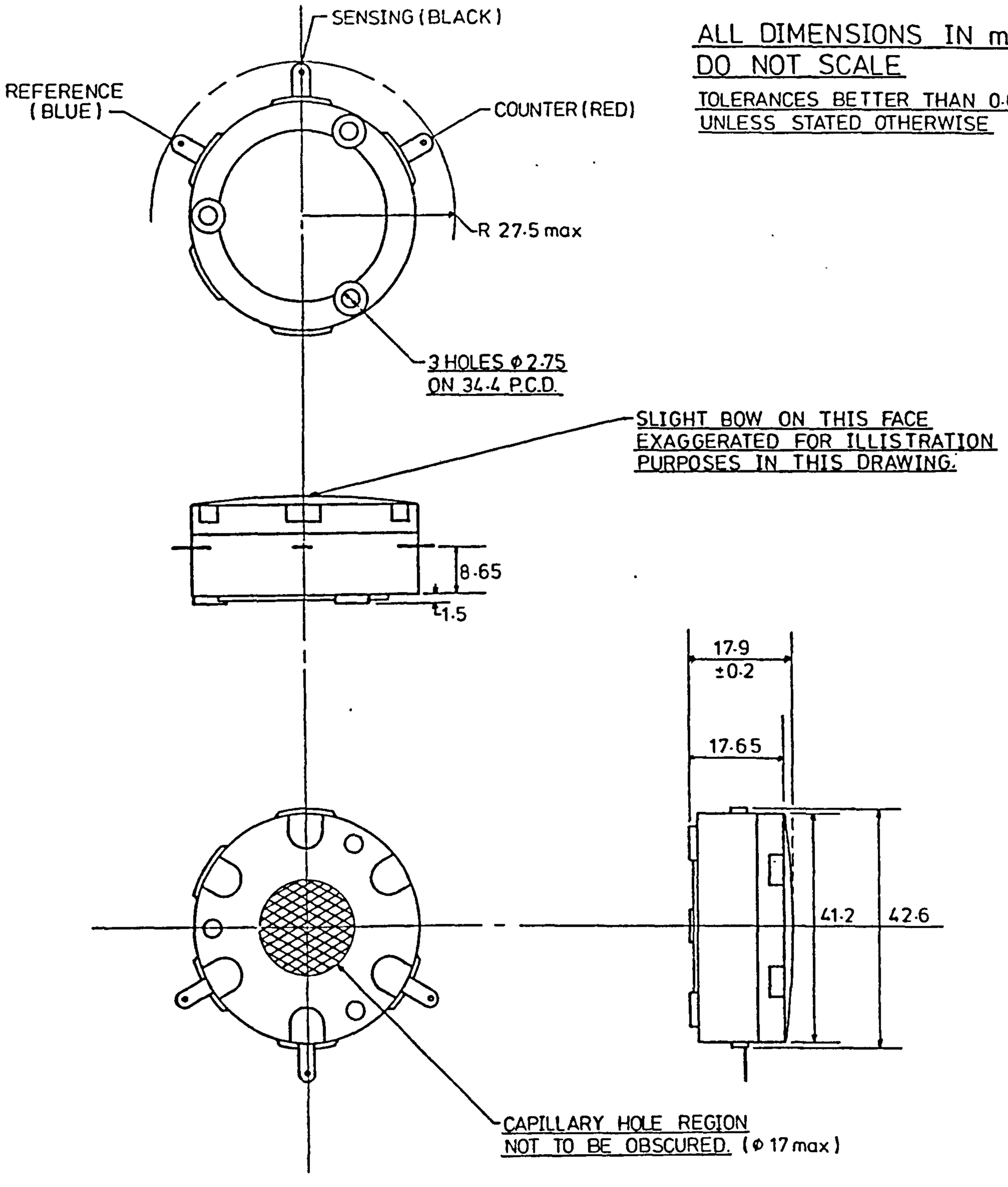

ALL DIMENSIONS IN mm
DO NOT SCALE

TOLERANCES BETTER THAN 0.08 UNLESS STATED OTHERWISE

Figure 2.3. Outline Drawing Of Moulded Gas Sensor Design With Side Terminal Connections

Enlargement of modification to all 3 gates. Raised gates shown as shaded area.

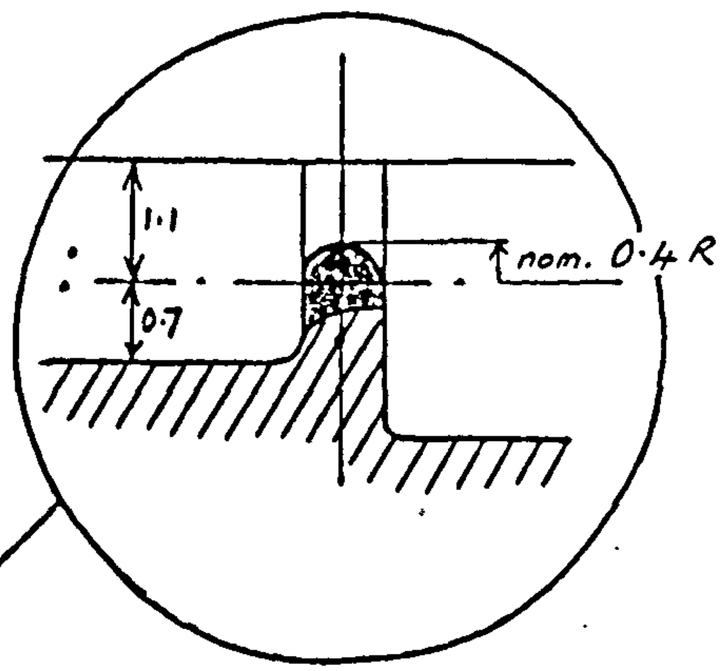

ALL DIMENSIONS IN mm
DO NOT SCALE

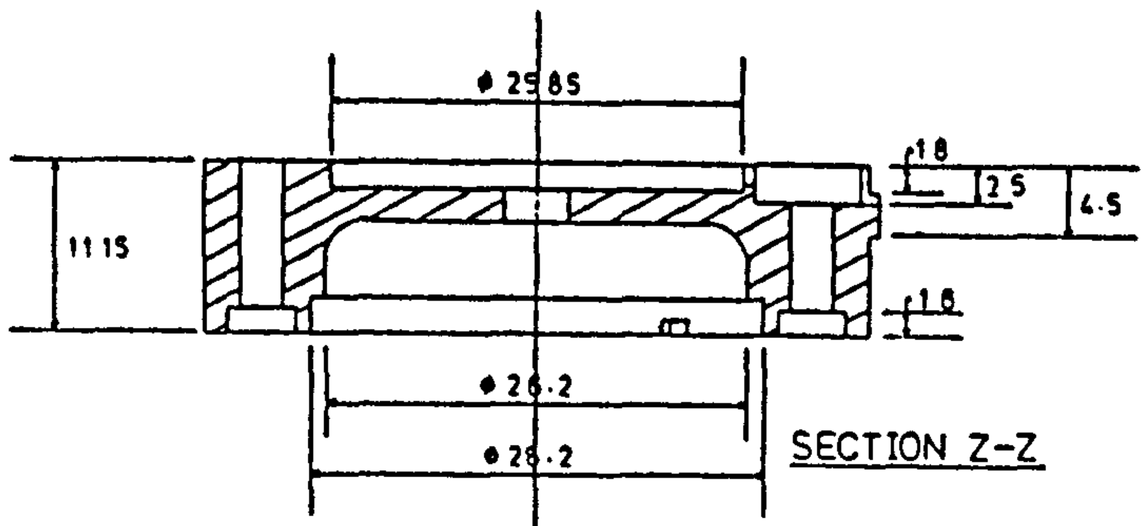

SECTION Z-Z

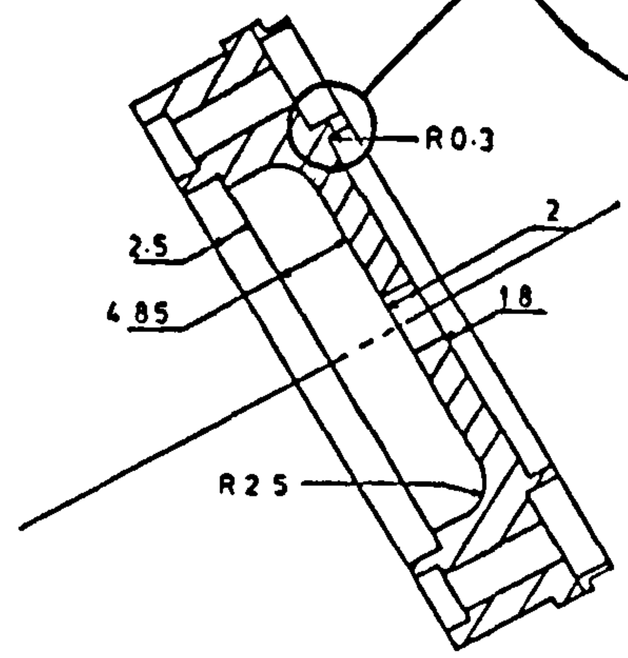

SECTION V-V

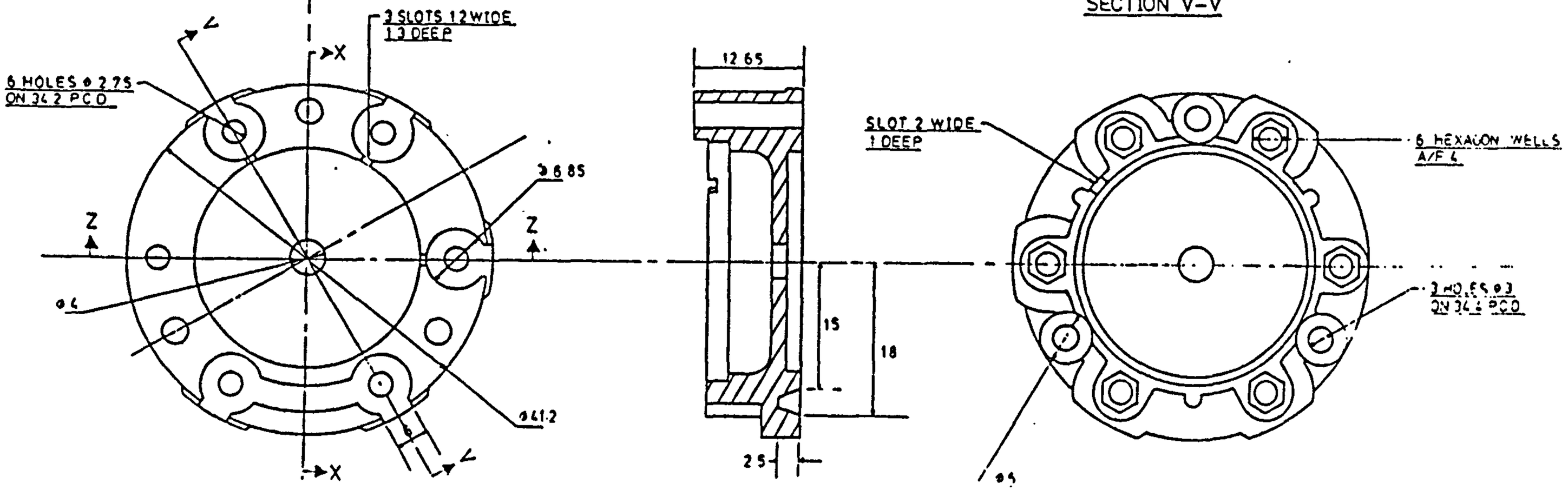

Figure 2.4. Drawing of gate modification to sensor baseplate.

production with potentially variable effect. The baseplate moulding has now been further modified as shown in Figure 2.4. to produce components with shallower gates which now have satisfactory levels of gas side access for sensors in environmental monitoring situations (See Section 3 below).

2.4. Three-Electrode Sensor Design Changes

There have been some fundamental changes in the electrode configuration of three-electrode sensors during this report period. The original electrode STACK configuration described in the last report was as follows:

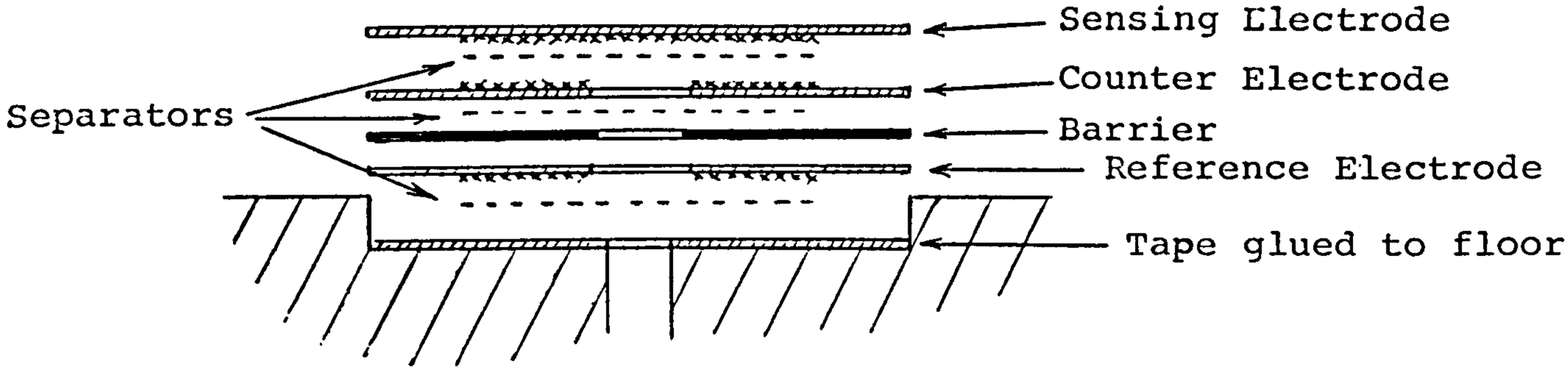

Sensors of this style were found to undergo a fortuitous signal cancellation when exposed to hydrogen due to the gas accessing the reference electrode, across the ptfe tapes, from the sensing electrode. This access pathway was highly variable from sensor to sensor and hydrogen cross sensitivities recorded on large numbers of 3F (flue gas) sensors were between -20 and +40% carbon monoxide equivalent.

A low permeability polythene barrier had been introduced by the last report point which had reduced hydrogen access to the reference sufficiently to eliminate negative hydrogen responses - typical values for 3E and 3F hydrogen cross interferences were 15 to 30% and 20 to 40% carbon monoxide equivalent, respectively. However, some hydrogen access to the reference persisted (see last report; CTL report 82/09/007, September 1982, p.52) and many sensors exhibited an initial low signal on exposure to carbon monoxide, followed by a slow creep-up to the full limiting current. The latter effect was in some unknown way, related to the stack geometry and in particular to the position of the reference electrode.

The following ANNULAR RING REFERENCE design was introduced in which the reference was relocated between the counter and sensing electrodes:

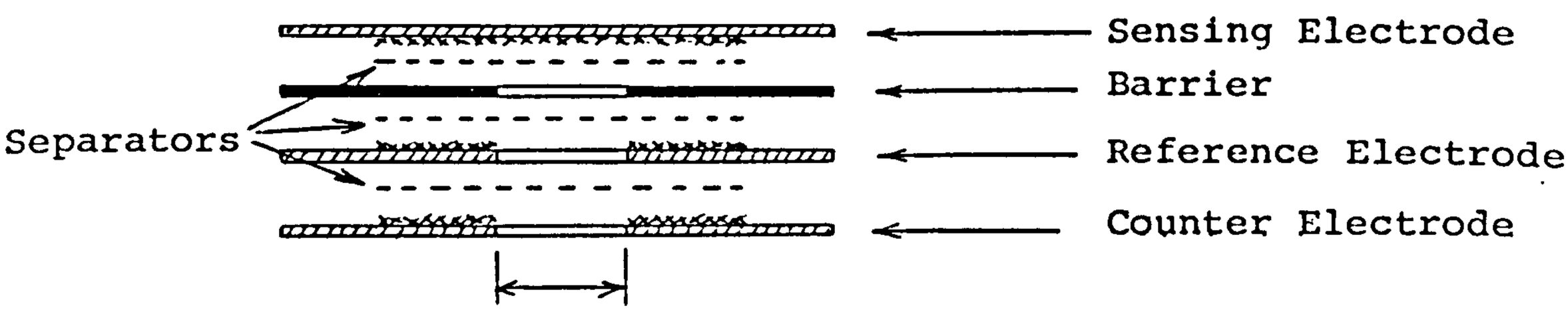

This design neither suffered the adverse carbon monoxide signal response to previous STACK designs nor negative hydrogen signals. However, operation of 3F sensors in a mixture containing 500 ppm of each of H_2 and CO resulted in some signal decay with an associated amount of baseline hysteresis during the recovery due to the persistence of some hydrogen access to the reference. This is undesirable and was finally eliminated by the introduction of the latest DISC REFERENCE design:

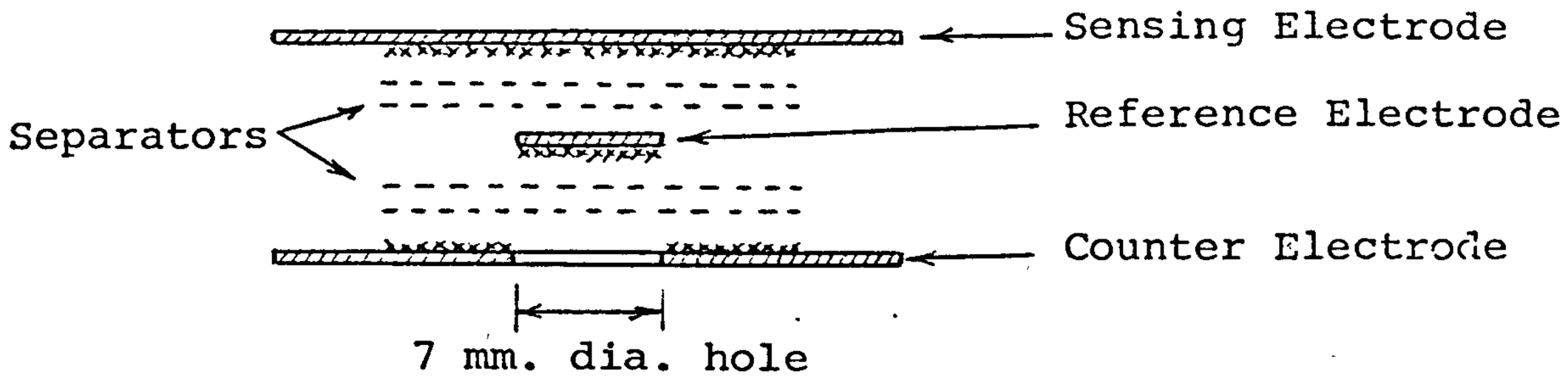

A high performance reference electrode catalyst (i.e. high anodic air rest potential) is now used in both 3E and 3F sensors, containing solvent extracted Engelhard No. 4 platinum black, in an 8:1 metal to ptfe mix, dried at 100°C. (i.e. effectively a 2E counter composition). Even so, the hydrogen cross sensitivities of untreated sensors are very high, typically:

3E Sensors 50 to 100% CO equivalent

3F Sensors 100 to 200% CO equivalent

due to the virtually complete elimination of hydrogen access to the reference. Preanodisation is therefore essential with these sensors (see Section 5.4. below) and currently optimised regimes reduce the hydrogen interferences to levels close to thosequoted in the last report for the STACK configuration:

3E (after preanodisation) 20 to 35% CO equivalent

3F (after preanodisation) 20 to 50% CO equivalent

3. COUNTER ELECTRODE GAS ACCESS

3.1. Introduction

The three gas access routes to the sensor counter electrode were considered in the last report as follows:

(a) FRONT ACCESS, through the sensor capillaries, diffusion across the perimeters of the sensing and counter electrode tapes where they are in contact and then radially inwards to the counter electrode catalyst. Since the sensing electrode oxidises virtually all carbon monoxide as it arrives at its surface, this access route will be open only to oxygen (note: other gases such as hydrogen, which are not completely oxidised by the sensing electrode may also access the counter by this route).

(b) SIDE ACCESS, through the current collector gates in the baseplate and diffusion through the sensing and counter electrode tapes which protrude beyond the 'O' ring seal area. Both oxygen and carbon monoxide can access the counter electrode by this route when the sensor is totally exposed to test gas as with environmental monitoring situations. Differential diffusibilities of carbon monoxide towards sensing and counter electrodes via the side access route, produce discrepancies between capillary-only and total exposure tests. Differences can be either positive or negative with respect to the sensor signal.

(c) REAR ACCESS, via the rear pinhole, through the electrolyte reservoir free space and the wick hole. Previous tests have indicated negligible gas access by this route.

Discrepancies between capillary-only and total exposures have now been reduced to less than 2% by further increasing the current collector gate heights as described in section 2 above.

With such designs the counter electrode oxygen demand becomes more reliant on front access and a series of experiments were conducted to measure actual oxygen diffusion rates via side and front-access routes with various sensor designs.

3.2. Experimental Details

The basis of these experiments was to measure the oxygen limiting current to a silver catalysed cathode in the counter electrode position with all gas access paths blocked except the one under investigation. The electrolytic cell was completed by a silver anode at the normal sensing electrode position, which underwent oxidation to silver oxides and avoided any interference from oxygen evolving at this electrode. Since silver electrodes are used, an alkaline (4M NaOH) electrolyte had to be used; although polycarbonate is subject to attack by alkaline conditions, the rate proved slow and no deleterious effects were observed over a period of several days, during which measurements could be completed. A third silver-silver oxide, reference electrode was used,

in conjunction with a potentiostat, to hold the cathode potential in an oxygen limiting current region, but above hydrogen evolution potentials. The anode/reference potential was also monitored to ensure that no oxygen evolution occurred on the anode.

All silver electrodes consisted of ptfe bonded Johnson Matthey flake silver (FS6) catalyst, applied to a porous ptfe tape in the usual way for platinum CO-sensor electrodes. Anodes had loadings of 36 mg/cm^2 catalyst and reference and cathodes 18 mg/cm^2.

In measurements of SIDE ACCESS, sensors were fitted with blank top plates, without any capillary holes, to eliminate direct front access.

In FRONT ACCESS measurements the sensor was potted in epoxy resin, to block any side access.

In the last report rear access rates were shown to be negligible compared to front and side access rates. However an additional test was run in this work to provide confirmation of this in which cathode oxygen currents in air of two potted sensors, with blocked capillaries, were compared, one sensor having the standard 1 cm^3 electrolyte, the other being completely filled with electrolyte.

Current-voltage scans on an old-style (open gate) sensor with blocked front access and a new-style (raised gate) sensor with blocked side access, both yielded oxygen reduction, limiting currents in the cathode potential range -700 to -1000 mV vs the silver-silver oxide reference. A potential of -1 volt is above hydrogen evolution potentials and was used to measure limiting

currents in all subsequent measurements.

In measuring oxygen limiting currents the sensors were soaked in an oxygen-free nitrogen atmosphere until a stable background current was established at -1 volt control potential. The sensors were then brought into air and the current remeasured when fully stabilised.

3.3. Results

Counter electrode oxygen limiting currents in air for various sensor configurations are shown in Table 3.1.

Side access measurements were made on both old-style (low gates) and new-style (raised gates) sensor hardware. The old-style mouldings were tested with all gates open and one, two and three gates closed respectively with perspex cement. The new-style mouldings were tested "as moulded" and with one gate clipped out with cutters. The latter is a quick and effective production method which may be necessary if it is envisaged that the sensor will operate in an aspirated mode for extended duration in high carbon monoxide/low oxygen atmospheres, e.g. some flue-gas conditions, when the front oxygen supply could be insufficient to meet the counter electrode demand. This is an extremely unlikely situation in environmental monitoring.

The test results show that the total oxygen side access rate in air for an old-style moulding, without any cementing of the gates, amounts to about 5 or 6 mA, compared to 0.6 mA for the built-up gate design of the new mouldings. The older-style environmental sensor design, with all three gates cemented had an oxygen side access leakage of about 2 mA, much higher than the new-style gate design. Clipping

Table 3.1. Counter Electrode, Oxygen Access Measurements with Various Sensor Configurations

HARDWARE	GATE DESIGN	BACKGROUND CURRENTS IN N_2 (mA)	OXYGEN CURRENTS IN AIR (mA)
Old-Style Mouldings	3 open gates	0.022	5.6
Side Access Configuration	1 cemented gate	0.021	3.7
(blocked Capillaries)	2 cemented gates	0.020	3.7
	3 cemented gates	0.021	2.2
	Potted terminals	0.025	0.021
	Potted terminals (filled with electrolyte)	0.008	0.008
New-Style Mouldings	As moulded	0.028	0.60
Side Access Configuration (blocked Capillaries)	1 clipped gate	0.022	2.5
New-Style Moulding		0.015	1.8
Front Access Configuration (potted sides)			

one gate in the new-style moulding resulted in an oxygen side access rate about equal (2.5mA) to the old-style environmental sensor with cemented gates.

Background currents in nitrogen of about 0.02mA were obtained with all sensors charged with $1cm^3$ electrolyte. One sensor filled with electrolyte, however, had a background of only 0.008mA which indicates that a small REAR ACCESS route exists for oxygen, amounting to about 12μA in air.

Front access does not depend on gate design and only one hardware design therefore, needed to be tested. The results showed a front oxygen access rate in air of 1.8mA, equivalent to the oxygen demand in a 1.8% CO mixture at a sensor sensitivity of 0.1μA per ppm. which represents an ample safety margin for any likely environmental monitoring situation.

4. PERFORMANCE TESTING OF 2T SENSORS

4.1. Introduction

During this report period testing has been concentrated on characterising span temperature compensation using the split capillary design introduced towards the end of the last report period. Extra data has also been collected on baselines and response times, confirming the picture presented in the last report and pressure coefficient measurements have been made.

A separate investigation of "Transient Short Circuit Signals in CTL 2-Electrode Trace Sensors", relevant to the N.C.B. interests is given in Appendix 1.

4.2. Span Temperature Compensation

The temperature response of a batch of 12 2T sensors, incorporating the split capillary design, is summarised in Figure 4.1. Best linear fit values of temperature coefficient between 10 and 40^{o}C., compared with cylindrical capillaries and uncompensated sensors, are as follows:

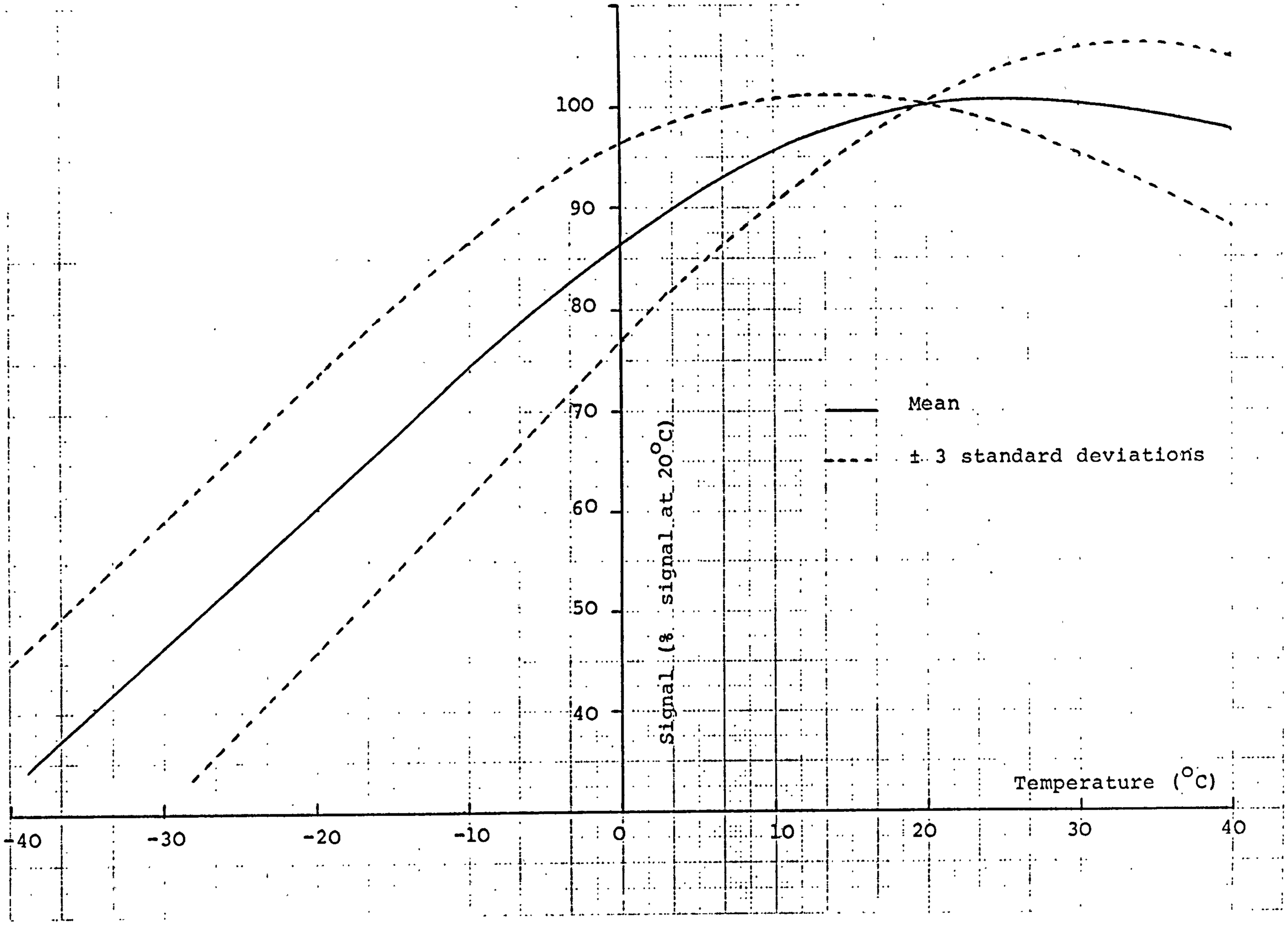

Figure 4.1. Temperature Response of a Batch of 12 2T Sensors

Sensor Type	No. in batch	Temperature Coefficient (%signal at 20°C per °C)	Standard Deviation
Split Sleeves	12	0.27	0.17
Cylindrical Sleeves (previous report)		0.90	
Uncompensated	4	1.20	0.13

Clearly the split sleeves give much more effective temperature compensation than the previous unsplit cylindrical sleeve design, and they have been used in production sensors since July 1982.

4.3. Baselines

The baseline data obtained on the above 12 sensor batch with split sleeves, is similar to previous baseline characteristics as follows:

Temperature (°C)	+ 3	+ 22	+ 40
Baseline (ppm equiv)	0.00	0.60	3.4
Standard Deviation	0.20	0.50	1.2

4.4. Response Times

The 90% response time versus load characteristic for a batch of 5 2T sensors is shown in Figure 4.2. The curve is almost linear up to about 50 ohm load with a slope of 0.3 s per ohm and an intercept at zero load of 15.5 s. Above 50 ohm load the slope increases progressively to higher response times. The reported behaviour is for relatively fresh sensors (nominally 1 month). There is some evidence that response times are subject to an ageing effect although there is no systematic data to quantify this.

4.5. Pressure Coefficient

The CO responses of 12, 2T sensors were measured over a range of pressures from ambient (764 torr) to 1100 torr, using a 49.3 ppm CO in air test gas.

All sensors gave linearly increasing outputs with pressure of slopes between 0.043 to 0.018% per torr. The mean pressure coefficient value was 0.03% per torr and the standard deviation 0.006.

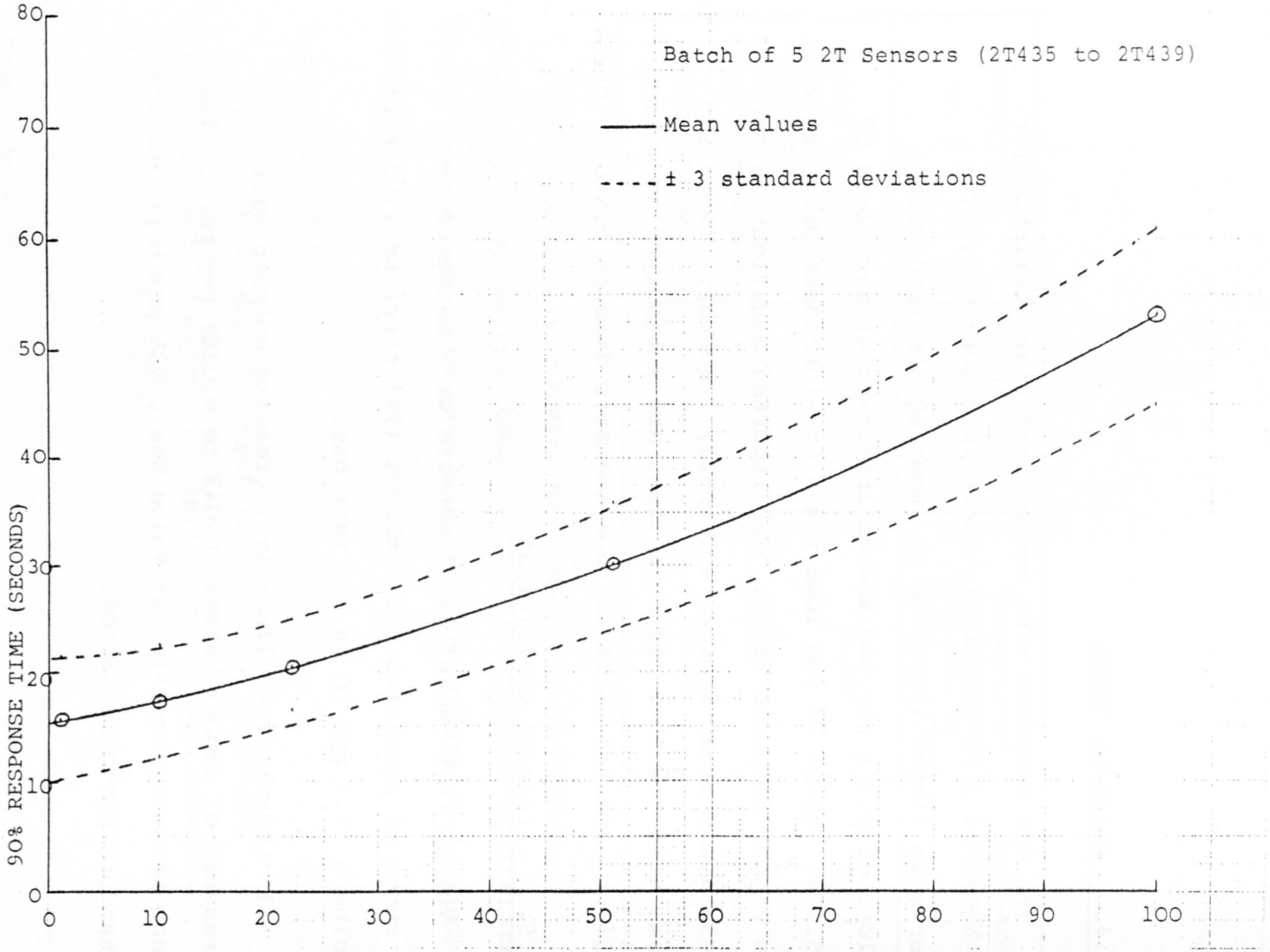

Figure 4.2. Response time vs load resistance characteristics of 2T sensors

5. HYDROGEN CROSS SENSITIVITY

5.1. Introduction

Standard 2T sensors have hydrogen cross sensitivities of between 10 and 30% carbon monoxide equivalent at 20°C. Hydrogen interference could be reduced if alternative, more specific electrocatalysts, or chemical filter materials, could be found. So far no suitable candidate materials have been identified.

Voltage biasing of 2T sensors can reduce hydrogen interference by operating the sensing electrode at a more anodic potential. The greater degree of platinum oxidation at these potentials results in a surface which is less active towards hydrogen oxidation. Certain difficulties can be envisaged with biased sensors which may limit applications, e.g. relatively high baselines, reproducibility of behaviour and start-up times after switching off the bias and uncertainties of behaviour of platinum electrodes when biased at anodic potentials for long periods of time. The effects of voltage biasing have been explored with two-electrode sensors during this report period in order to clarify the practical pros and cons of biasing for low hydrogen sensitivity.

Hydrogen interference is greater with the three-electrode sensors with shielded, disc reference electrodes and voltage biasing has also been investigated with both 3E (3-electrode environmental) sensors, which have direct relevance to NCB applications, and 3F (3-electrode flue gas) sensors, which have been developed independently at C.T.L.

The surface oxidation and reduced hydrogen sensitivity experienced by platinum electrodes at anodic bias potentials is partly irreversible and persists when the electrode is returned to normal operational potentials (CTL report 82/09/007, September 1982, pp. 50 to 53). Anodic biasing can therefore, be used as a PRETREATMENT to reduce hydrogen cross sensitivity and progress on the development of this technique is reported.

Another approach investigated in this report period was to CHEMICALLY bias the sensing electrode to higher potentials where hydrogen interference is inhibited by the addition of soluble redox couples to the electrolyte.

5.2. Biased Operation of Two-Electrode Sensors

Table 5.1. summarises the behaviour of two 2E sensors when operated under anodic bias conditions.

Sensor 2E 563 was taken from production stock and had been stored for 3 months with its terminals shorted. When tested at zero bias, it produced a very stable response in a 200 ppm CO in air test gas, with negligible baseline hysteresis on removing the test gas. Hydrogen cross sensitivity in a 100 ppm H_2 in air test gas was 18.5% CO equivalent.

Application of a +150mV bias to this sensor produced a zero hydrogen cross interference but also induced a CO signal creep up, coupled with a significant and very

Table 5.1. Behaviour of 2E Sensors under anodic bias conditions

SENSOR	Bias Voltage (mV)	Time on bias	Baseline (μA)	CO-response @ 200 ppm (μA/ppm)	Creep-up 5 to 20 min (ppm)	Hysteresis		Hydrogen Cross interference (%)
						5 min (ppm)	20 min (ppm)	
2E 891	Zero	6 days	0.60	0.119	-	-	-	17.6
	zero	8 days	0.50	0.119	4.3	4.2	3.8	19.3
	25	3 days	0.65	0.119	4.2	3.0	2.5	14.3
	25	5 days	0.65	0.117	8.5	3.0	2.5	13.7
	50	6 days	0.65	0.119	4.2	3.0	3.0	11.3
	50	11 days	0.50	0.116	2.6	2.6	2.6	11.3
	50	20 days	0.80	0.124	8.0	5.6	3.2	12.6
	100	7 days	0.90	0.118	11.0	9.3	6.8	9.4
	100	13 days	0.85	0.120	6.3	6.7	5.4	8.4
	100	20 days	0.75	0.116	6.5	7.3	5.4	7.1
	150	7 days	0.95	0.117	10.2	17.0	14.0	6.1
	150	14 days	0.65	0.113	5.2	7.4	5.2	5.3
	150	21 days	0.70	0.110	4.5	6.4	4.5	4.2
	300	7 days	1.20	0.109	13.8	8.7	5.0	0.8
	300	21 days	0.75	0.102	5.9	7.4	4.6	Nil
2E 563	Zero	3 months	0.35	0.124	Nil	0.8	0.8	18.5
	150	8 days	0.90	0.117	8.5	9.0	8.5	Nil
	300	12 days	1.75	0.115	7.0	8.7	7.0	Nil
	300	20 days	1.00	0.106	7.5	5.7	4.7	Nil
Recovery	Zero	15 days	0.30	0.097	- 4.1	Nil	Nil	7.7
	Zero	40 days	0.20	0.095	- 3.5	Nil	Nil	10.0
	Zero	58 days	0.22	0.094	- 7.5	- 1.3	- 1.3	9.0

persistent, positive baseline hysteresis on removing the test gas.

After 8 days at +150mV, the bias potential was increased to +300mV. Hydrogen interference and creep up were similar to the +150mV bias, but the hysteresis appeared to be reducing with time. However, even after 20 days at +300mV the hysteresis was still considerably greater than at zero bias on commencing these investigations.

On returning to zero bias after 20 days at +300mV, the hydrogen interference partially recovered to a steady 10% or so. The CO-tolerance, measured by the CO signal stability and hysteresis, improved although, relative to the initial behaviour at zero bias, the signal suffered some decay and negative hysteresis, even after 58 days at zero bias. Another consequence of the biasing was a reduction in the signal sensitivity on returning to zero bias of about 25%.

The other sensor, 2E 891, was subjected to a progressive increase in bias potential, in steps up to +300mV, allowing 3 weeks between each step for the sensor to 'settle'.

Hydrogen cross sensitivity of this sensor decreased with increasing bias potential, reaching zero at + 300mV.

Even at zero bias, on commencing these investigations, the CO-tolerance at 200 ppm was not as good as the previous sensor, the signal suffering some creep-up and hysteresis on removing the test gas. There were some changes in creep-

up and hysteresis with potential, but they were small and did not appear to conform to any well-defined trend. If anything, increasing the bias potential resulted in poorer CO-tolerance, as observed with the previous sensor, but no further conclusions were possible on the basis of the behaviour of this single sensor.

The tendency to lower CO-tolerance on biasing two-electrode sensors is probably associated with surface platinum oxide electrochemical reactions, resulting from cathode polarisation, which are more evident at elevated (more anodic) potentials. In view of this, further work on permanently biased two-electrode sensors was not considered worthwhile pursuing, although the possibility remained of improving H_2 cross interference by preanodising - see section 5.4. Even this can reduce CO-tolerance and conditions will require careful selection.

There is the possibility that the creep and hysterises effects induced by biasing are not significant at lower CO levels. This was not however investigated since reasonable tolerance to 200 ppm CO seems to have become an established requirement.

Three-electrode sensors do not suffer reductions in CO-tolerance on biasing since the cathode has no influence on the sensing electrode polarisation. Potential biasing therefore, is of greater interest to three-electrode systems and was investigated in greater detail (see section 5.3. below).

5.3. Biased Operation of Three-Electrode Sensors

5.3.1. Report of Results from 3F Sensor Development Program

3F sensors are intended for flue gas analysis. They differ from 3E sensors principally in their capillary sensitivity which is nominally 0.03μA per ppm CO, compared to 0.1μA/ppm for 3E sensors. The consequences of this are that 3F sensors can operate in higher CO concentrations but have a correspondingly greater hydrogen cross sensitivity and ppm CO equivalent baseline - baselines are virtually unaffected by the capillary hole size and hydrogen is only partially controlled by the capillaries. Apart from these differences, other aspects of operating 3F sensors under biased conditions, such as settling times, stability of performance and start-up characteristics after switching off the bias, are relevant to 3E operation and therefore the results from the 3F program are included in this report.

Two 3F sensors (3F/2562 and 3F/Ex1), with "disc reference" construction, but with normal Johnson Matthey catalyst performance (see section 2.4. above) were manufactured without pre-anodising and settled for about 1 week at zero bias to establish an initial set of performance parameters, namely baseline, carbon monoxide sensitivity and hydrogen sensitivity. Sensor 3F/Ex1 had a detachable capillary plate so that open electrode responses to test gases could also be measured.

A +300mV bias potential between reference and sensing was applied and the sensor performance characteristics at this potential were monitored periodically. Results are presented in Figures 5.1. to 5.4. for the first month's operation at bias. Five additional sensors, including one with a detachable top-plate, were put on a +300mV bias at the same time and tested less frequently - the behaviour of these sensors confirmed that of the two tested in more detail.

(a) Baselines: Steady values were approached within 3 to 4 weeks following the initial application of +300mV bias to fresh sensors (Figure 5.1.). Values were 0.8μA ± 0.2 at 20°C. For a 3F sensor this would represent a CO equivalent of about 27 ppm (±7). Baselines should be similar with 3E sensors when the value would represent 8 ppm (±2) CO equivalent.

(b) Hydrogen cross sensitivity: Hydrogen cross sensitivities decreased to steady values of 3.5% (±3) CO equivalent within 3 to 4 weeks (Figure 5.2.).

(c) Carbon monoxide sensitivity: A linear decrease of about 5% in carbon monoxide sensitivity occurred over the first month following the application of the +300mV bias (Figure 5.3.). This correlated with a loss of open electrode activity towards carbon monoxide oxidation and hence a reduction in activity reserve (Figure 5.4.) - see

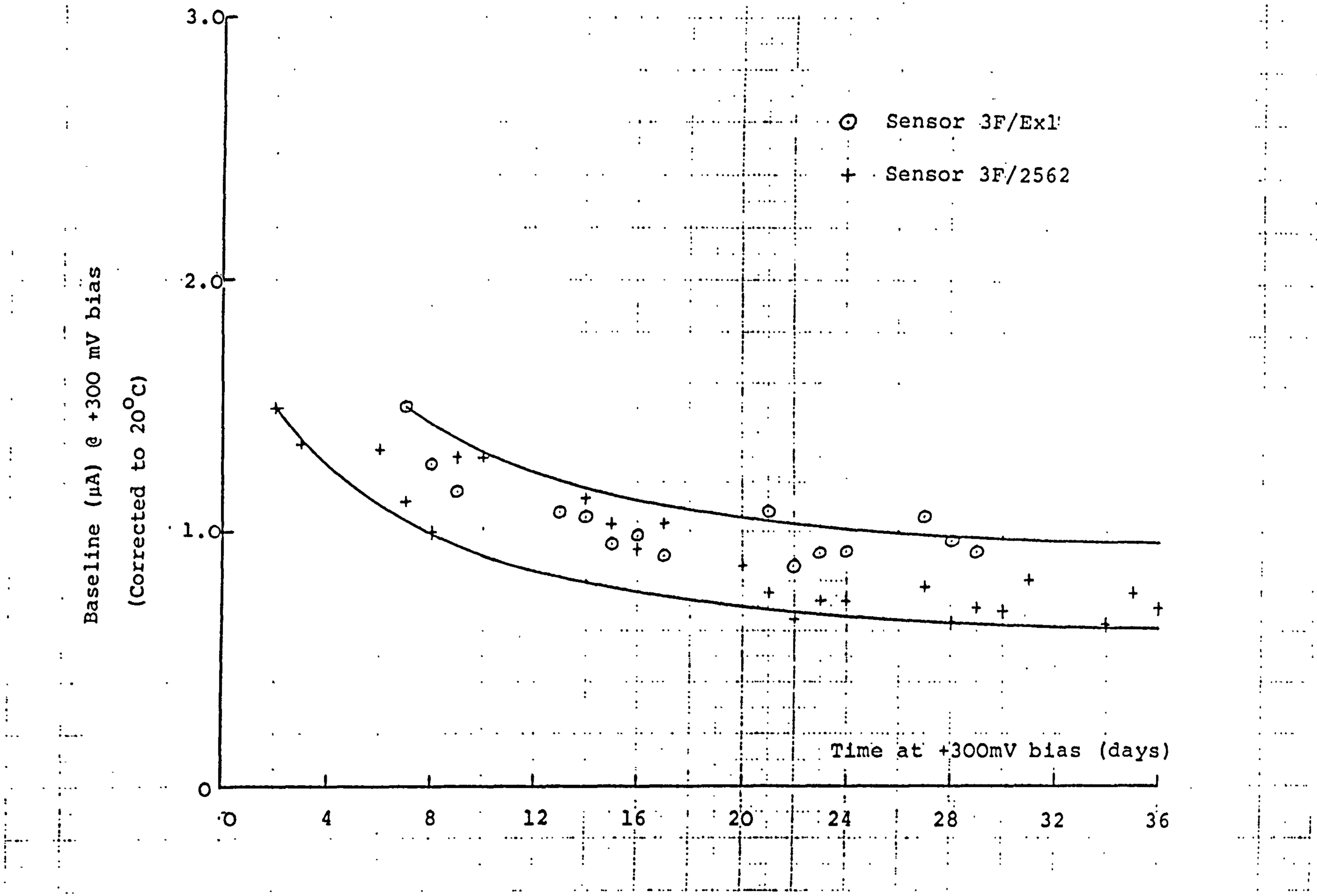

Figure 5.1. Baseline behaviour of 3F sensors at +300 mV bias potential

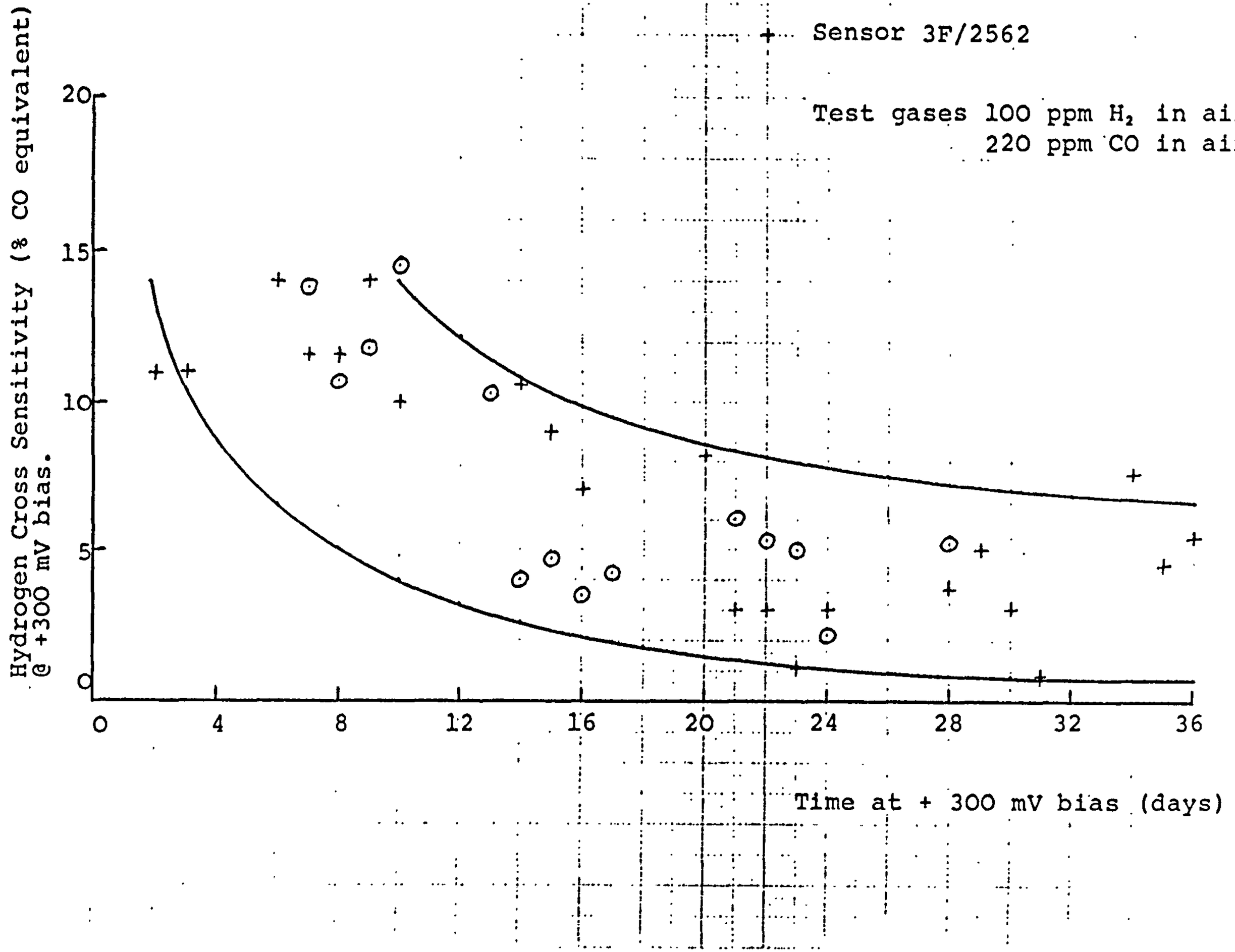

Figure 5.2. Hydrogen cross sensitivity of 3F sensors at +300 mV bias potential

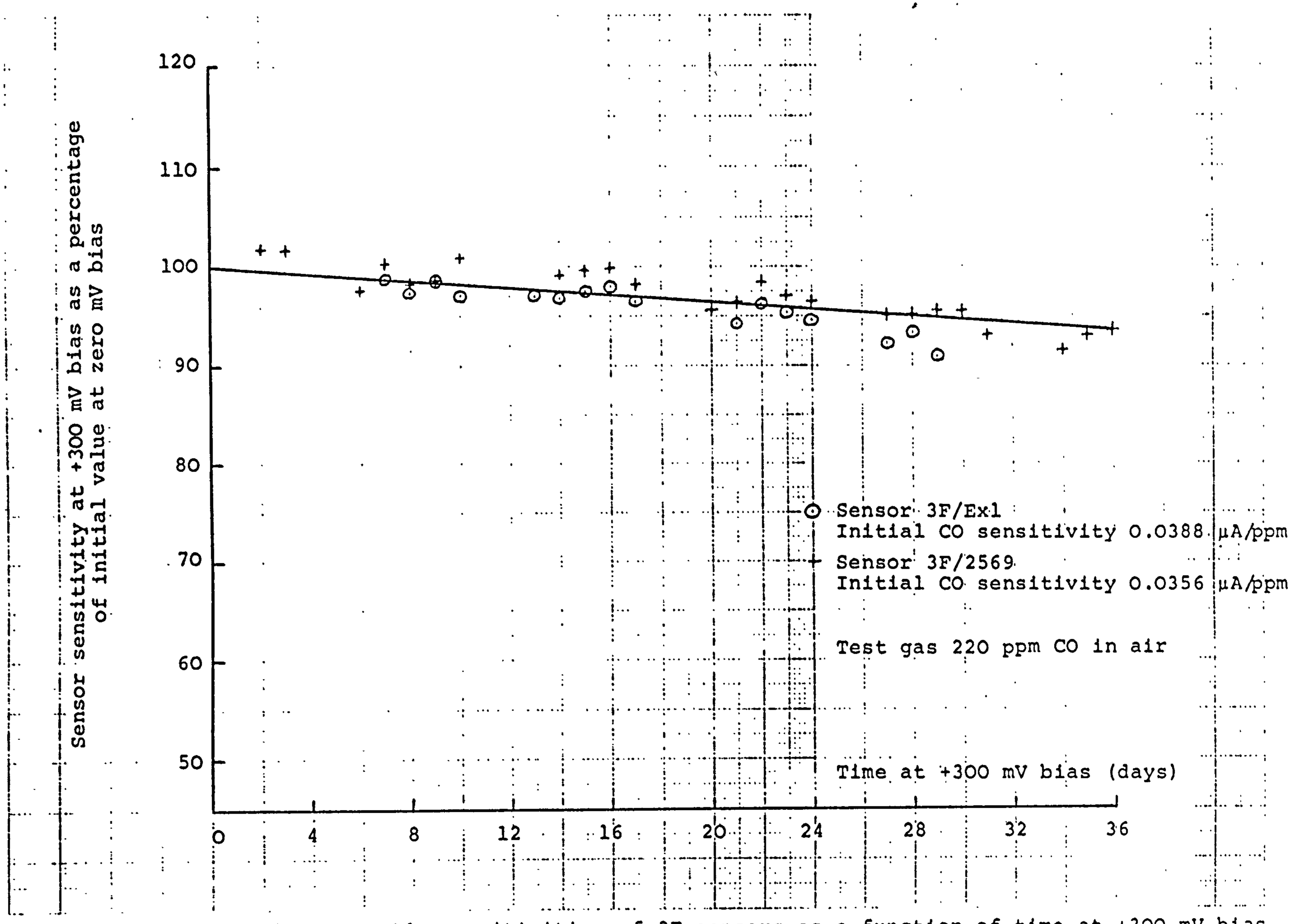

Figure 5.3. Carbon monoxide sensitivities of 3F sensors as a function of time at +300 mV bias

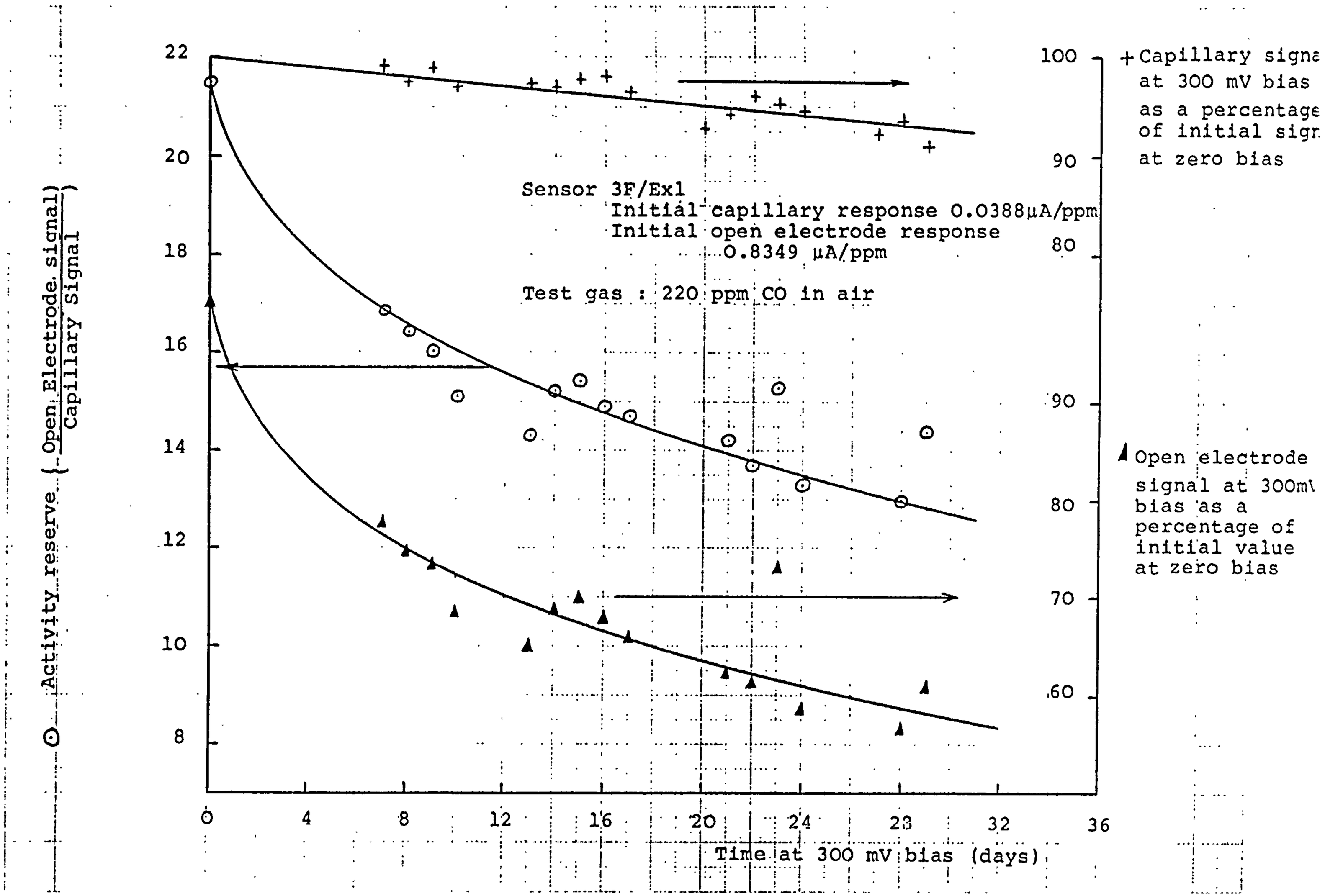

Figure 5.4. Capillary and open electrode CO responses of sensor 3F/Ex1 at +300 mV bias

last report (Appendix 3) for a discussion of the relationship between capillary signal and activity reserve. Although there was some indication that the rate of electrode deactivation could be slowing down, the process was clearly continuing well beyond one month's operation on bias.

The parallel 3E studies reported below were continued for longer periods and included a control sensor operated at zero bias.

(d) Start-up: After 36 days the sensor 3F/2562 was switched off bias, with electrodes open circuit, for various periods and the recovery times measured on resuming the bias for the parameters,baseline, carbon monoxide sensitivity and hydrogen sensitivity. Results are given in Table 5.2. and figures 5.5. to 5.7.

When shut-off periods were no greater than 2 or 3 hours, recovery times on start-up were fairly rapid, within minutes of resuming the bias (Figure 5.5.). For longer shut-off periods the CO and H_2 sensitivities generally recovered within an hour or so, significantly faster than the baseline. Baseline recoveries were measured in hours for off periods of several hours to overnight (Figure 5.6.) and in days or weeks for longer off periods (Figure 5.7).

Start up characteristics of biased 3E sensors have not been measured in this report period, but they should be similar to the 3F results.

Table 5.2. Start-up Characteristics on +300mV Bias of 3F Sensor 2562

Time off bias	Recovery times for CO and H_2 sensitivities	Time to original baseline
½ hr.	1 to 3 minutes	1 to 3 minutes
2½ hr.	3 to 5 minutes	3 to 5 minutes
6 hr.	< 1 h.	1 to 2 hours
Overnight	< 1 h.	3 to 5 hours
Over weekend	Several hours	7 to 10 days
2 months	Overnight	12 to 16 days

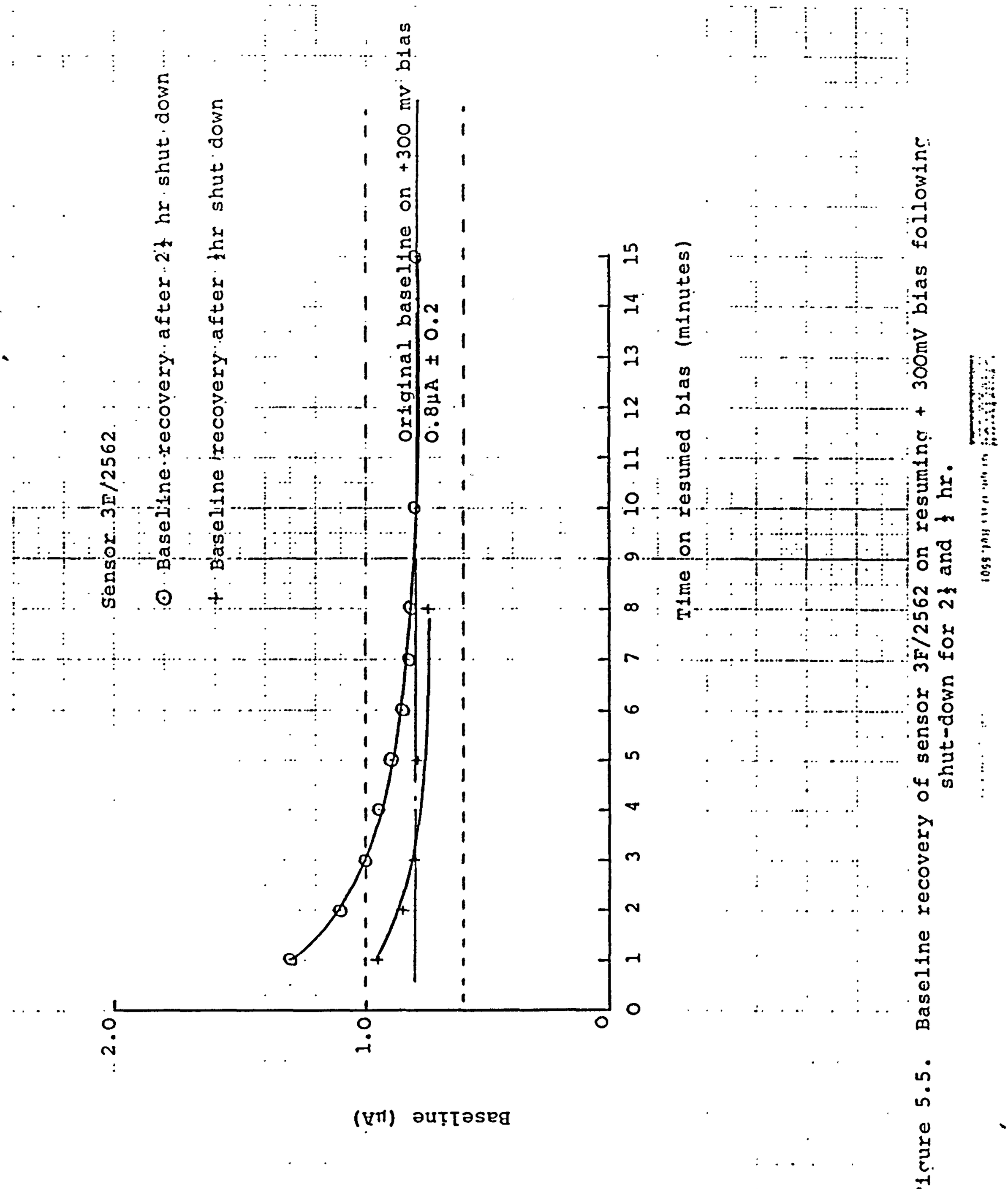

Figure 5.5. Baseline recovery of sensor 3F/2562 on resuming + 300mV bias following shut-down for 2½ and ½ hr.

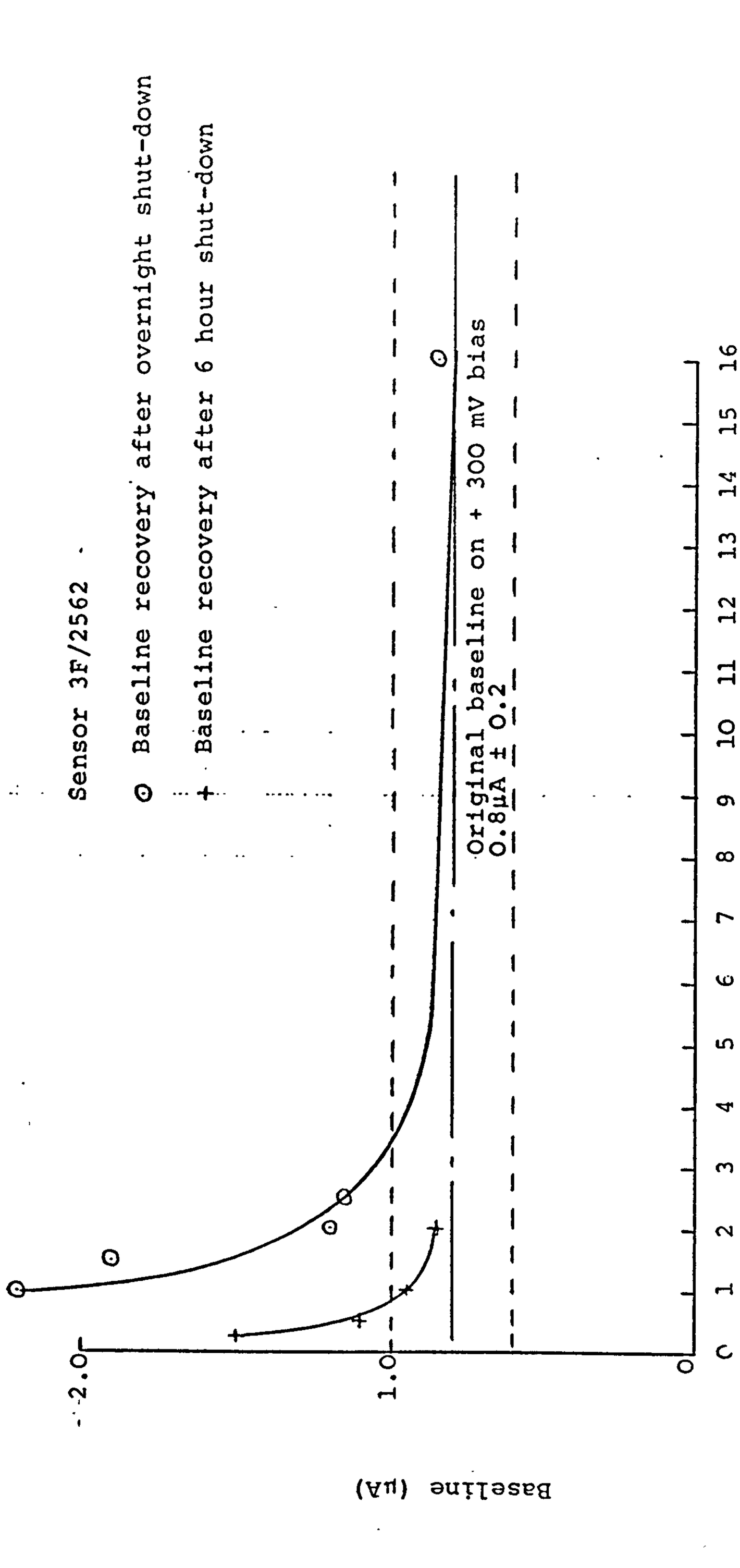

Figure 5.6. Baseline recovery of sensor 3F/2562 on resuming + 300 mV bias following shut-downs for 6 hours and overnight.

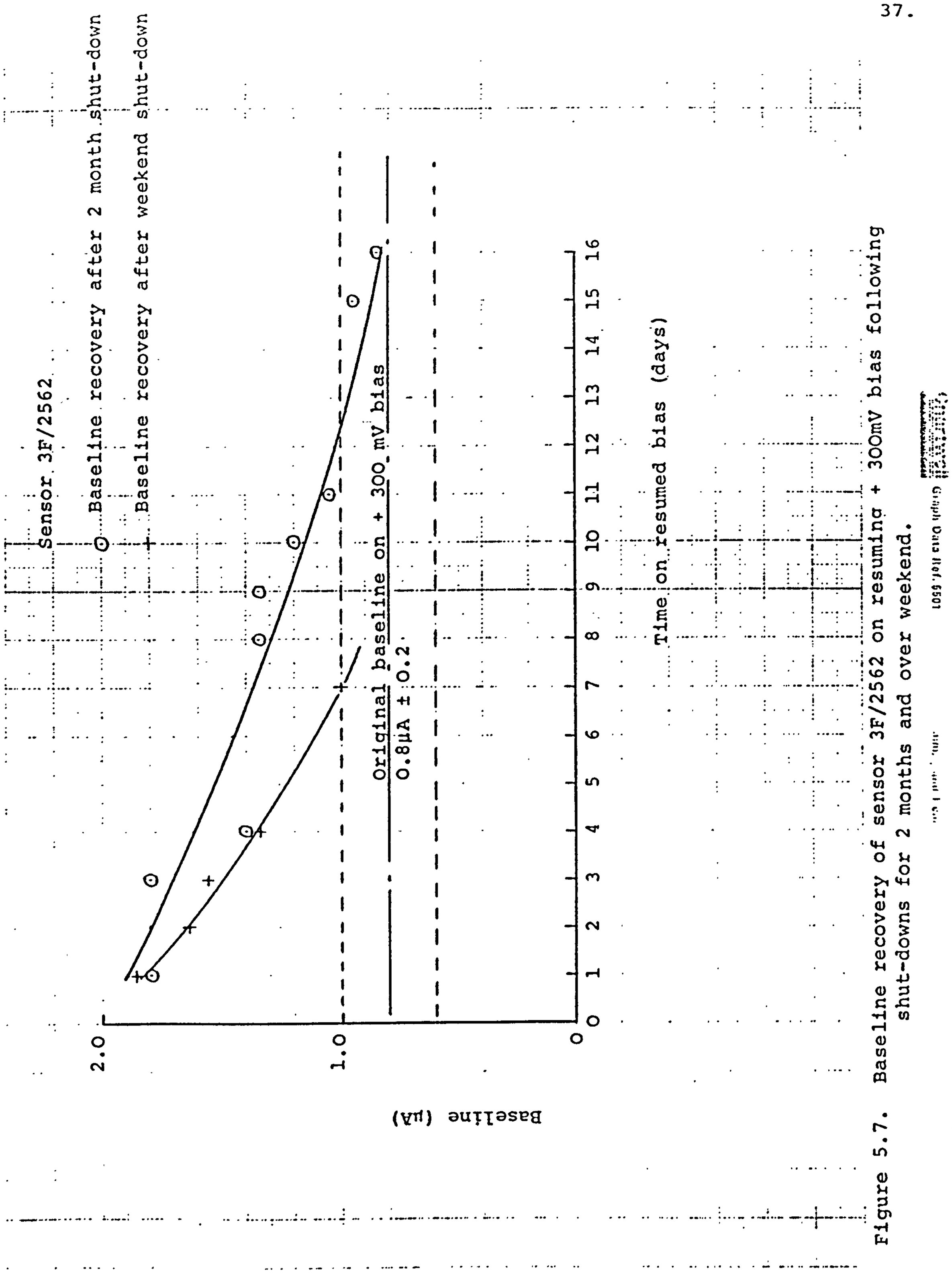

Figure 5.7. Baseline recovery of sensor 3F/2562 on resuming + 300mV bias following shut-downs for 2 months and over weekend.

5.3.2. Biased Operation of 3E Sensors

Four 3E sensors (3E/ExB1 to 3E/ExB4) with high performance catalyst, disc reference electrodes were manufactured without pre-anodising and settled for 15 days at zero bias (sensing and reference electrodes shorted) to establish an initial set of performance parameters, namely baseline, carbon monoxide sensitivity and hydrogen sensitivity. All sensors were fitted with detachable capillary plates to enable measurements to be made of open electrode responses.

After settling, one sensor was set at each of the bias potentials 50, 150 and 300mV, with the remaining sensor kept at zero bias to act as a control. Performance characteristics were monitored regularly and the results for the first 2 months on bias are presented in figures 5.8. to 5.13.b.

(a) Baselines: All 4 sensors achieved steady baseline values of between 0.2 and 0.4μA at 20°C. during the 15 day settling period at zero bias (figure 5.8.).

On applying the bias potentials, the sensors resettled to steady baselines within about 5 to 6 weeks (figures 5.9., 5.10 and 5.11). The control sensor, 3E/ExB1, at zero bias, remained at a steady, 0.3μA baseline throughout these tests (figure 5.8.).

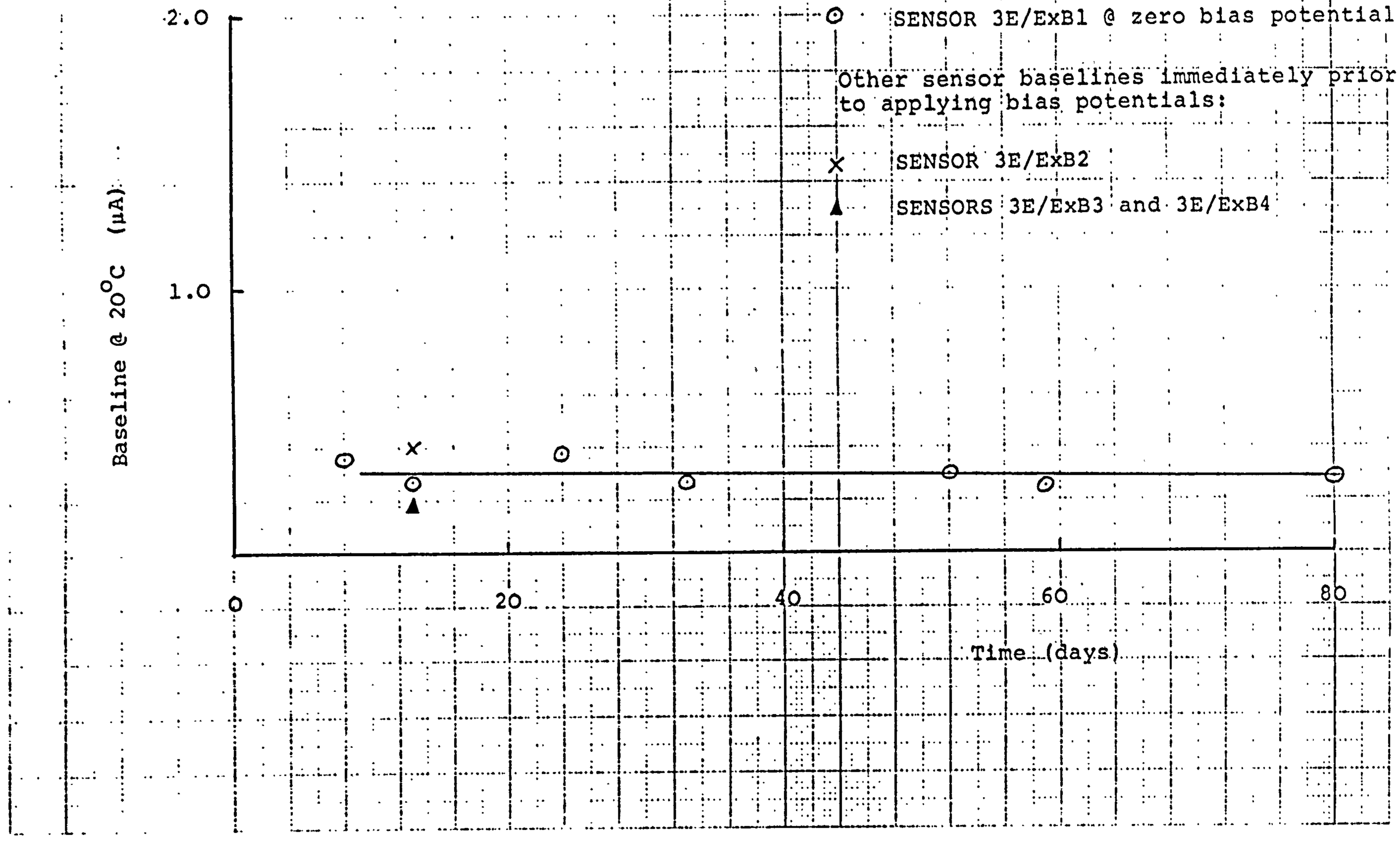

Figure 5.8. Baseline behaviour of control sensor 3E/ExB1 at zero bias potential.

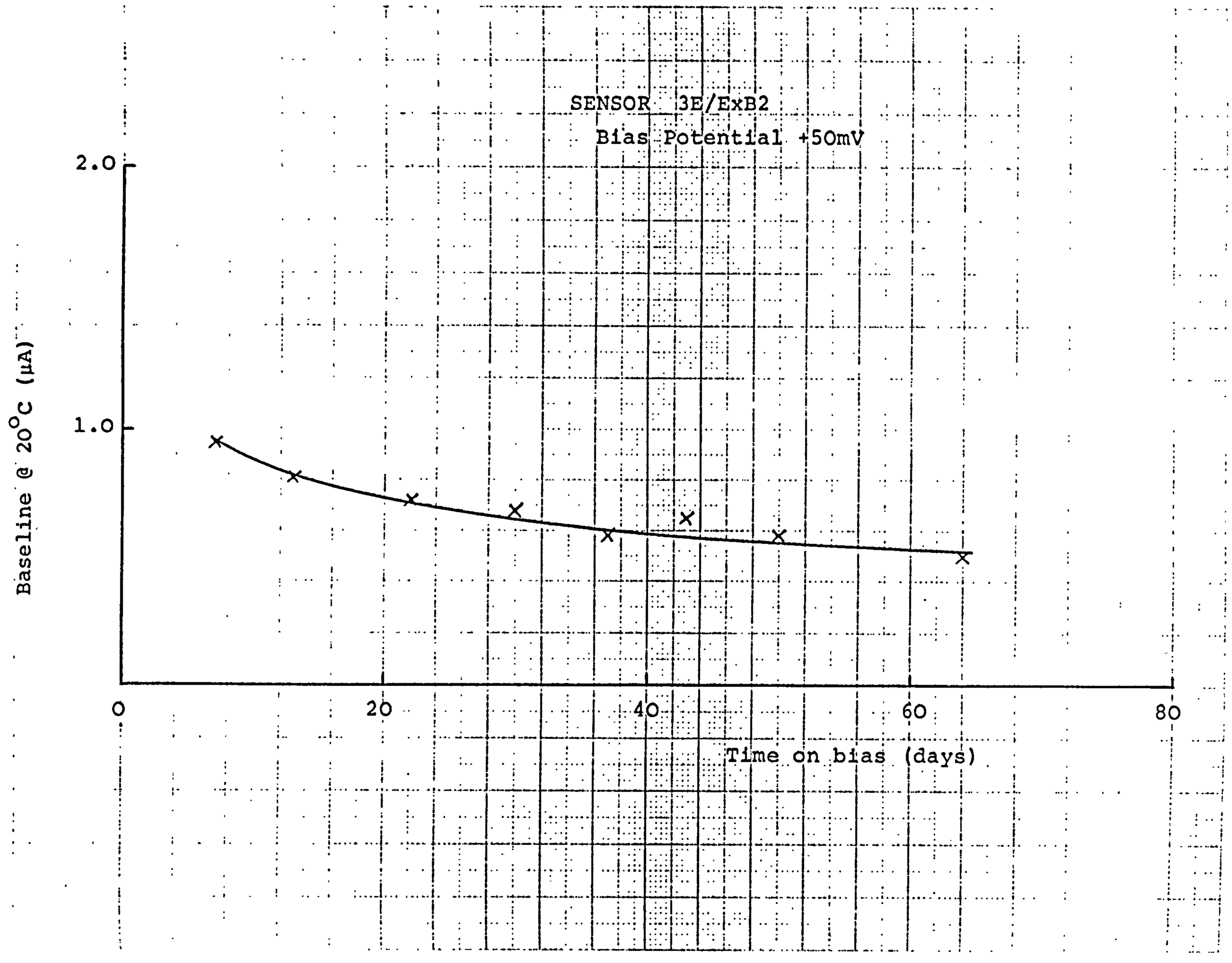

Figure 5.9. Baseline behaviour of sensor 3E/ExB2 at +50mV bias potential

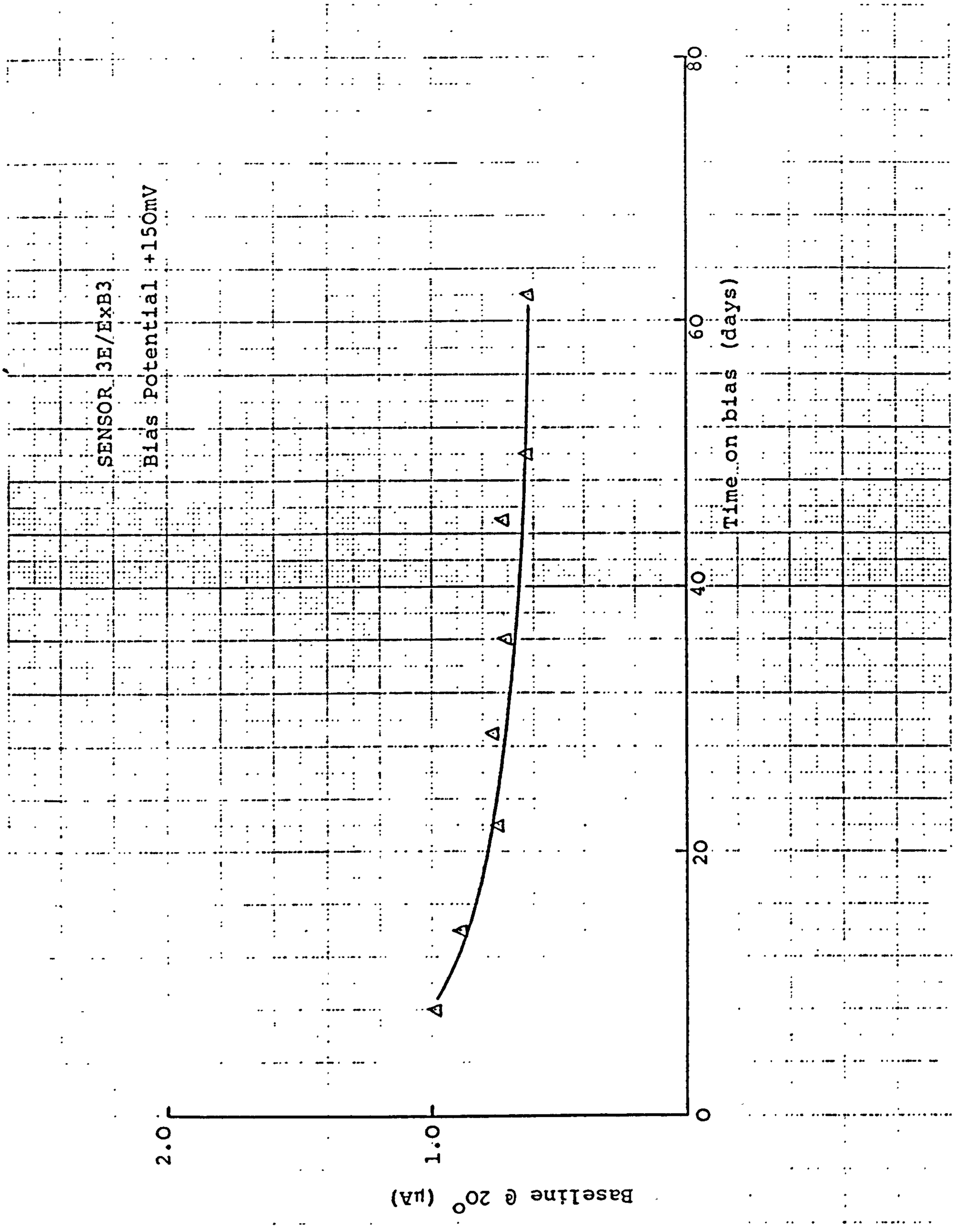

Figure 5.10. Baseline behaviour of sensor 3E/ExB3 at +150 mV bias potential

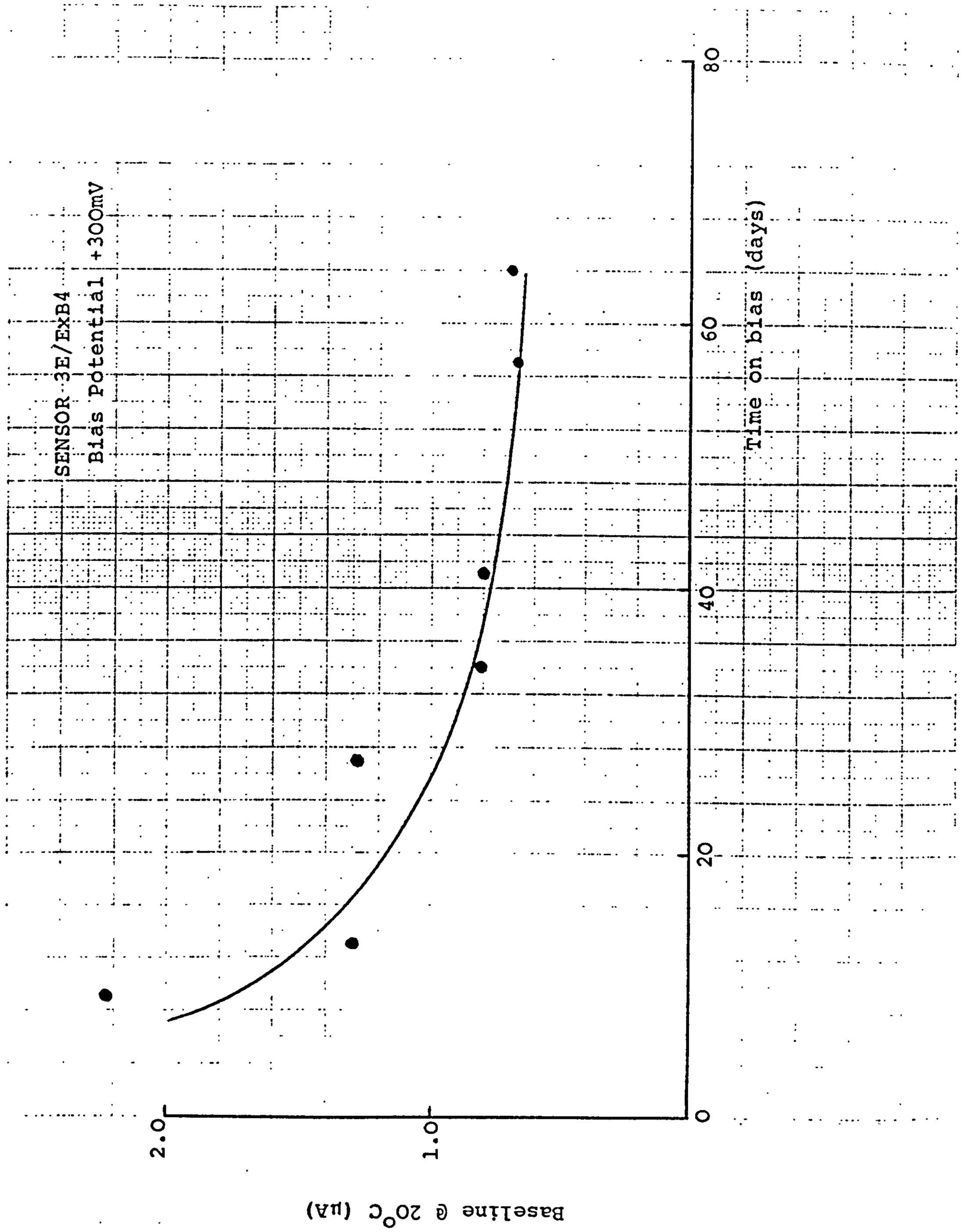

Figure 5.11. Baseline behaviour of sensor 3E/ExB4 at +300mV bias potential.

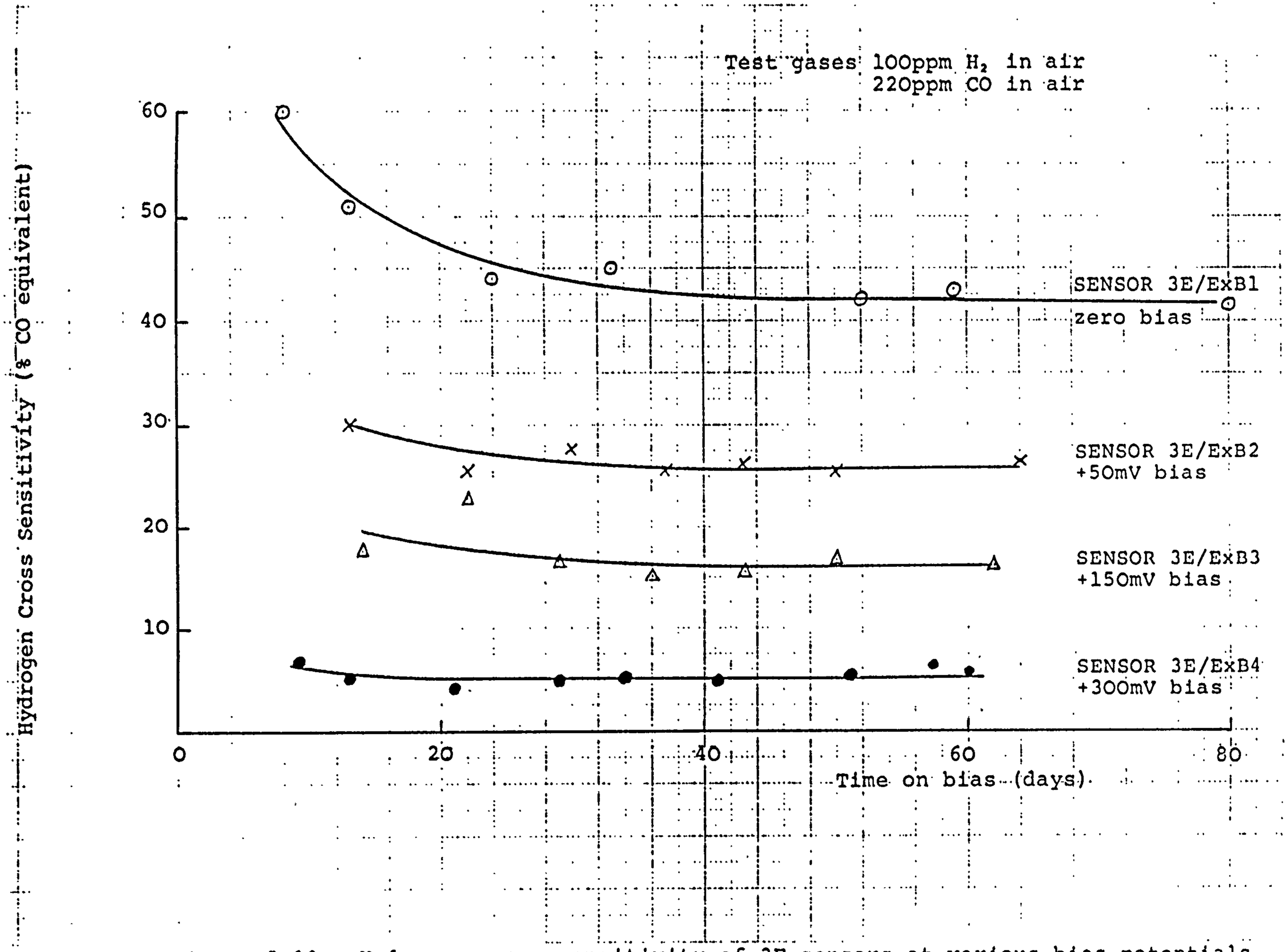

Figure 5.12. Hydrogen cross sensitivity of 3E sensors at various bias potentials.

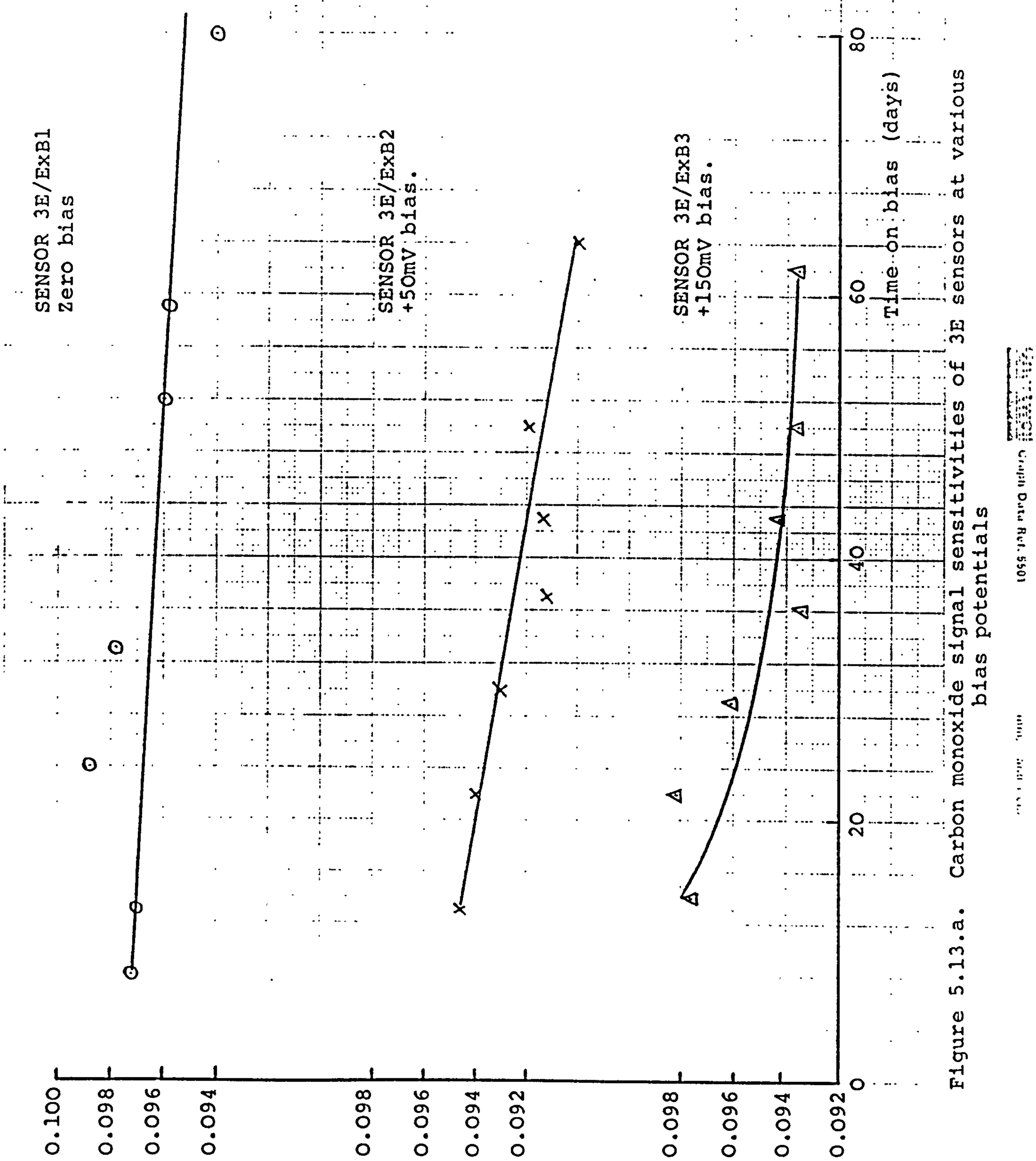

Figure 5.13.a. Carbon monoxide signal sensitivities of 3E sensors at various bias potentials

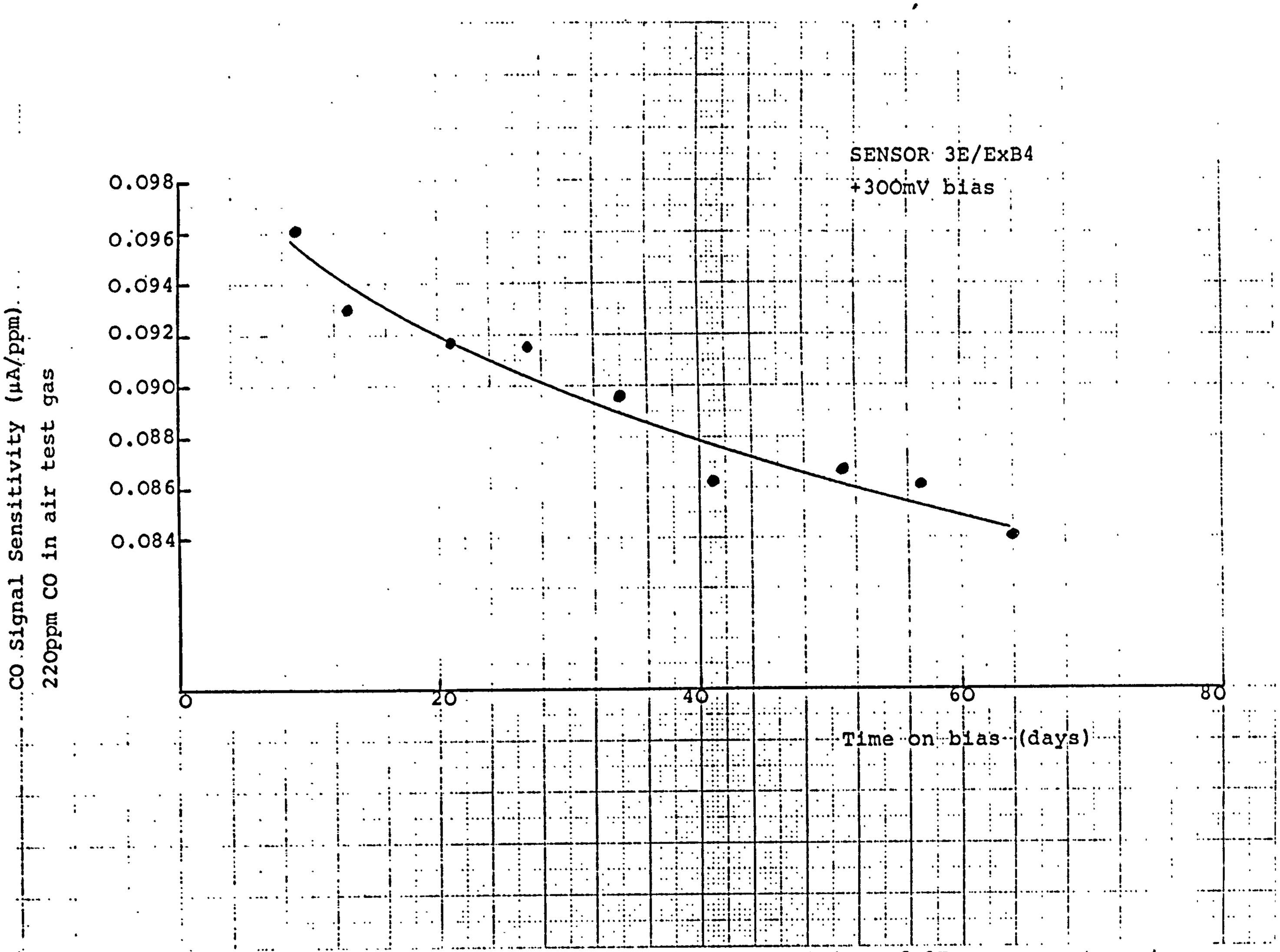

Figure 5.13.b. Carbon monoxide signal sensitivities of 3E sensors at various bias potentials.

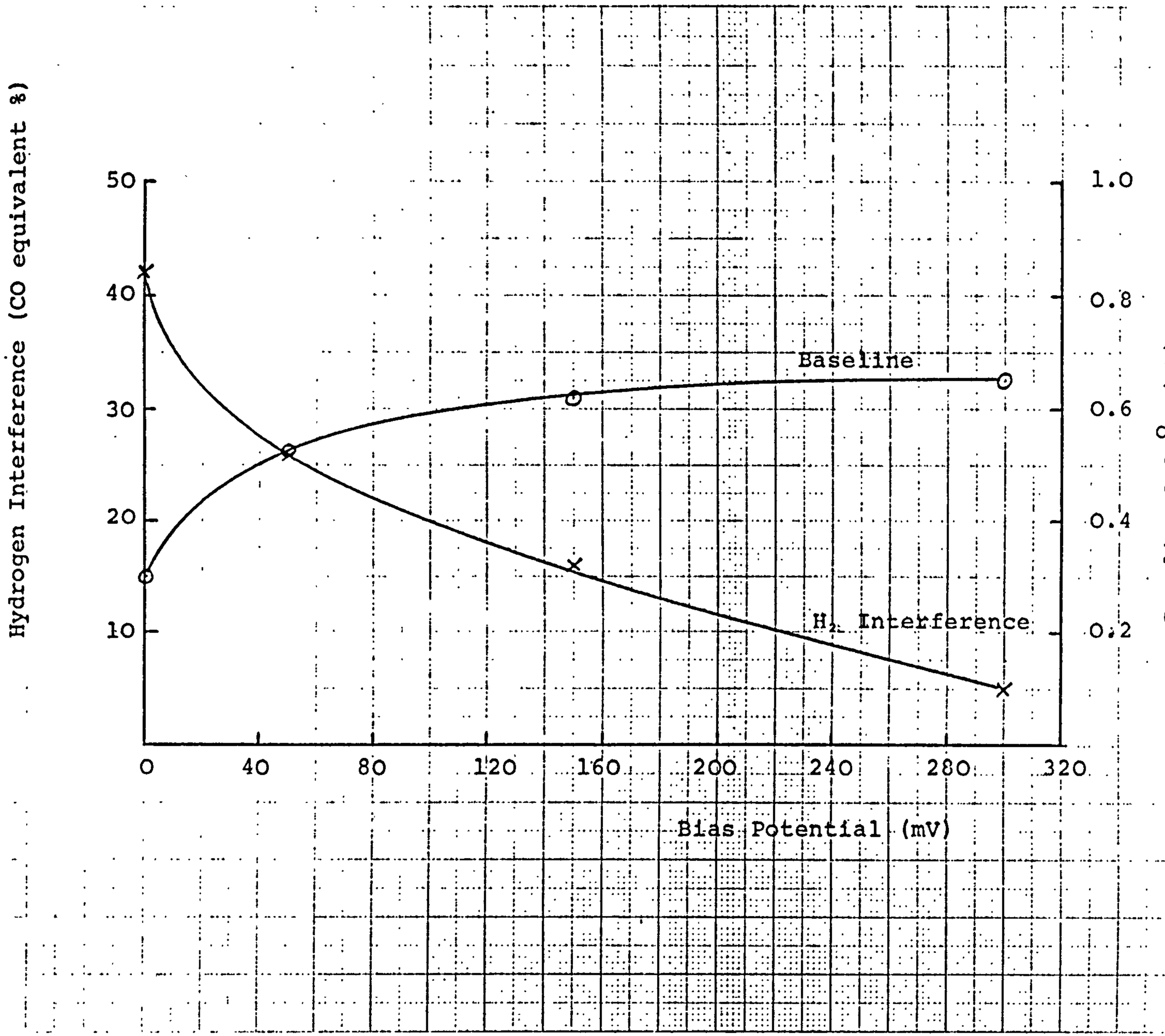

Figure 5.14. Baseline and hydrogen cross sensitivity of 3E sensors as a function of bias potential.

Figure 5.14. shows the effect of bias potential on settled baselines, taken 50 days after application of the bias. Evidently baselines increase sharply with small bias potentials above zero, but limit at about 0.6 to 0.7μA over the potential range 50 to 300mV. In past work, baselines were found to increase sharply at potentials much above +350mV when oxygen evolution sets in (see CTL report 82/09/007, September 1982, figure 5.1.) and therefore, no tests were conducted above +300mV.

(b) Hydrogen cross sensitivities: Hydrogen interference achieved steady values within about 3 to 4 weeks of application of the bias potential for all sensors (Figure 5.12).

Figure 5.14 gives the measured hydrogen interferences after 50 days at bias as a function of bias potential. Hydrogen interference decreased progressively with increasing potential from about 42% at zero bias to about 5% at + 300mV. In view of the small baseline change over the bias potential range of 50 to 300mV, the higher bias potential would be preferred to achieve the maximum hydrogen suppression. CO-sensitivity underwent a greater initial decrease at higher bias potentials, but indications were that a new steady state is achieved after about 60 days on bias (see below).

(c) Carbon Monoxide Sensitivity: Sensor signal sensitivites to a 220 ppm CO in air test gas are shown as a function of time, following the initial 15 day

settling period, in figures 5.13.a and 5.13.b.

The control sensor at zero bias and sensor 3E/ExB2 at 50mV bias, both had very stable CO signals throughout the test period.

Sensors 3E/ExB3 and 3E/ExB4, at 150 and 300mV bias respectively, underwent an initial signal loss of about 4 and 8% respectively (see table 5.2.a.) over the first 50 days on bias, corresponding to the point of this report. However, the signals were apparently stabilising by this time and the sensors will continue to be monitored.

The signal variations noted with time on bias correlated closely to the measured changes in the open electrode activities. (Table 5.2.a.). The effect became more apparent as potential increased since surface oxide coverage of the platinum increased and partially deactivated the CO electrode reaction. Given time, the platinum surface should achieve a new equilibrium depending on potential, when the signal would be expected to stabilise once again.

(d) Start-up: This topic was not investigated with 3E sensors during this report period. However, the times to reach a steady state on resuming a bias potential, following a shut down period, should closely resemble those measured with 3F sensors in section 5.3.1. above.

Table 5.2.a. CO Signal Stability and Activity Reserve of Biased 3E Sensors

A	Bias Potential (mV)	ZERO	50	150	300
B	CO-sensitivity @ zero bias after settling (µA/ppm)	0.097	0.093	0.098	0.095
C	CO-sensitivity @ bias after 50 days (µA/ppm)	0.096	0.092	0.094	0.087
D.	Change in sensitivity (%)	- 1.0	- 1.1	-4.1	-8.4
E	Activity Reserve @ zero bias after settling	6.7	5.2	6.4	5.7
F	Activity Reserve @ bias after 50 days	5.8	4.8	5.7	4.5
G	Theoretical * capillary sensitivity after settling (µA/ppm)	0.114	0.115	0.117	0.116
H	Theoretical * capillary sensitivity after 50 days on bias (µA/ppm)	0.116	0.116	0.115	0.112

* Theoretical signals were calculated from the measured signals and activity reserves, using the relationship derived in the last report (CTL report 82/09/007, September 1982, Appendix 3). The theoretical signals should be the same for the settled condition (G) and the 50 day on bias (H) condition if the measured signal changes were caused by changes in activity reserve. The above data indicates this to be true, within the accuracy limits of the measurements.

5.4. Preanodisation

In the last report period the sensing electrode of a 3F sensor was subjected to a slow stepwise potential scan from zero, with respect to the reference electrode, up to +400mV and back to zero, allowing at least 3 days for conditions to stabilise after each voltage increment (CTL Report 82/09/007, September 1982, pp. 50 to 53). Hydrogen cross sensitivity underwent a significant decrease with increasing anodic potential during the forward potential scan which persisted during the return scan to zero potential. On holding at zero the hydrogen interference increased over 7 to 10 days from about -10% to a steady 10 or 12% (compared to an initial value of 67% before the scan). Since then, the hydrogen cross interference has remained constant for 12 months to the time of this report. This sensor was an old-style stack design, and some hydrogen signal cancellation was evident (See Section 2.4. above) - above +200mV., hydrogen responses were actually negative. Nevertheless the anodic potential scan had achieved a significant and permanent decrease in the hydrogen cross interference.

This behaviour was also apparent with sensors taken from the voltage bias investigations of sections 5.2. and 5.3. above, e.g. the recoveries of sensors 2E 563 and 3F/Ex1 on returning to zero bias were monitored for periods of 1 month and more, after terminating the tests at +300mV.

Results were as follows:

Sensor	Time on +300mV bias (days)	Steady H_2 index before +300mV bias (%)	Steady H_2 index > month after + 300mV bias (%)
2E 563	20	18.5	10.0
3F/Ex1	30	166	55.0
(disc reference)			

The time taken for a sensor to re-settle to a steady baseline and hydrogen sensitivity after anodising the sensing electrode, was typically between 1 and 2 weeks. However, later investigations with 3-electrode sensors revealed that steady baselines resulted almost immediately if the sensing and reference electrodes were anodised together; the sensing and reference electrodes were shorted and a potential applied from a potentiostat between this pair and the counter electrode, the latter being made the cathode and the electrode pair the anode.

Hydrogen cross sensitivities still required 1 to 2 weeks to approach steady values but these proved reasonably predictable from the measurements taken a day or two after anodisation. The actual anodic potentials experienced by

the sensing/reference electrode pair during such anodising treatments, depends on the counter electrode polarisation at the cell current flowing. This could introduce an element of variability into the results achieved, but this has been far outweighed in practice by the ability to test sensors soon after pretreatment for quality control during production and the greater ease of anodising batches of sensors using a 2-electrode potentiostatic technique.

With the introduction of the disc reference sensor designs, which have very low levels of H_2-signal cancellation (see section 2.4. above), it was necessary to employ preanodisation to achieve practically low H_2 cross-sensitivities, in advance of any detailed fundamental investigations of the process. Early empirical work established that a pretreatment voltage of > 600 mV for several days was too severe and produced undesirable side-effects on other performance parameters, suggesting a drastic reduction in CO activity reserve, e.g. poor CO tolerance, high temperature coefficient, low CO sensitivity. On the other hand, 300 mV proved too low to be effective enough within reasonable timescales. Current production practices are therefore based on a 450mV, 24 hour regime for 3E sensors and 450mV, 72 hour for 3F sensors.

With the latest cell designs and high performance, disc reference electrodes (Section 2.4. above) this generally

achieves a 15 to 30% hydrogen index with 3E sensors and 20 to 50% with 3F sensors. Significant numbers of production sensors however, are found to have much higher hydrogen sensitivities and one or more additional anodising treatments are frequently necessary. The reasons for this are yet unclear and current research is aimed at an improved understanding of the anodising process.

One fact is certain, that the decrease in hydrogen sensitivity after anodising is accompanied by some loss in carbon monoxide activity reserve. This is illustrated by the recovery at zero bias of sensor 3F/Ex1 (Table 5.3.) which had been operated with its sensing electrode at +300mV bias with respect to its reference electrode for 30 days (Section 5.3.1. above). The initial CO open electrode signal before biasing was 0.8342μA/ppm, representing an activity reserve of 21.5. On returning to zero bias the sensor approached a steady state after about 1 week with an activity reserve of 12.4. Corresponding hydrogen cross interferences were 166% initially and 53% after anodisation. A second sensor (3F/1) was subjected to a sequence of anodisation treatments of both sensing and reference electrodes together, beginning with two, one week periods at 300mV and followed by two, three day periods at 450mV. Baselines, capillary and open electrode responses to both H_2 and CO were measured during the recovery periods at zero bias (sensing to reference) between each anodisation.

Table 5.3. Performance characteristics of 3F sensors after various anodisation pretreatments

Sensor	Anodising Voltage (mV)	Anodising Time (days)	Recovery Time (days)	Baseline (μA)	Capillary CO signal (μA/ppm)	Open electrode CO signal (μA/ppm)	CO activity reserve	Capillary H_2 Signal (μA/ppm)	Open electrode H_2 signal (μA/ppm)	H_2 Cross interference (ratio H_2 to CO capillary signals as a %)
3F/Ex1 (sensing electrode only anodised)	Initial unanodised		-	-0.26	0.0388	0.8324	21.5	0.0644	0.1760	166
	300	30	7	0.10	0.0348	0.4315	12.4	0.0186	0.0320	53
3F/1 (sensing and reference anodised together)	Initial unanodised		-	0.04	0.0342	0.5850	17.1	0.0416	0.0800	122
	300	1st x 7	14	0.15	0.0337	0.4570	13.6	0.0206	0.0393	61
	300	2nd x 7	18	0.20	0.0334	0.3004	9.0	0.0172	0.0320	51
	450	1st x 3	4	0.03	0.0329	0.2940	8.9	0.0106	0.0187	32
	450	2nd x 3	3	0.05	0.0320	0.2425	7.6	0.0060	0.0100	18.6
			6	0.07	0.0316	0.2299	7.3	0.0086	0.0121	27.3

Table 5.4. Open electrode activity measurements on 3F sensors after various anodising treatments

	Anodising Voltage (mV)	Anodising Time	Recovery Time	Open electrode CO activity (μA/ppm)	Electrode CO activity corrected for tape limit (μA/ppm)	Corrected CO activity as a fraction of initial activity (μA/ppm)	Open electrode H_2 activity (μA/ppm)	H_2 activity as a fraction of initial activity (μA/ppm)
SENSOR 3F/1	Initial unanodised		-	0.5850	0.700	1.00	0.080	1.00
	300	1st x 7 days	14 days	0.4570	0.521	0.74	0.039	0.49
	300	2nd x 7 days	18 days	0.3004	0.327	0.47	0.032	0.40
			85 days	0.3080	0.336	0.48	0.035	0.44
	450	1st x 3 days	3 days	0.2773	0.300	0.43	0.014	0.18
			4 days	0.2940	0.319	0.46	0.019	0.23
	450	2nd x 3 days	3 days	0.2425	0.260	0.37	0.010	0.12
			6 days	0.2299	0.245	0.35	0.012	0.15
SENSOR 3F/Ex1	Initial unanodised		-	0.8342	1.077	1.00	0.176	1.00
	300	30 days	7 days	0.4315	0.488	0.45	0.032	0.18

The results are given in Table 5.3. and again illustrate the deactivation of both CO and H_2 electrode activities as a consequence of anodisation. It is apparent from these initial results however, that the hydrogen sensitivity of both sensors was affected to a much greater extent by anodisation than the CO sensitivity, even after correction for the effects of electrode tape limitation[(a)] (See Table 5.4.).

(a) Note: Open electrode sensitivities quoted in Table 5.3. include two limiting factors - the ptfe backing tape and the catalyst layer; the latter further comprises both diffusion limitation through the electrolyte film and kinetic limitations at the electrocatalyst surface. A correction can be made for the tape diffusion limitation, from a knowledge of its diffusibility, to yield an electrode catalyst activity value, although it is not possible to further resolve this into the electrolyte film and kinetic components. Measurements of tape diffusibility gave values of 3.7 μA/ppm for CO and 13μA/ppm for H_2. Correction of open electrode sensitivities for tape limitation can then be made using the relationship:

$$\frac{1}{I_e} = \frac{1}{I_c} + \frac{1}{I_T}$$

where I_e, I_c, I_T are the electrode, catalyst and tape sensitivities respectively.

With H_2, the tape diffusibility is large and tape limitations could be ignored in the measured open electrode currents of Table 5.3. With CO however, the tape limitation is significant and corrections were necessary to produce the comparative data in Table 5.4.

5.5. Electrolyte Redox Additives

These were conceived as a method of chemically biasing the sensing electrode to a higher potential where hydrogen interference would be reduced.

For example a platinum electrode in a saturated solution of MnO_2 in sulphuric acid has a potential of about 1.4V and from the results of the electronic biasing tests we would expect hydrogen interference to be very low at such a potential. So the question was, can one achieve the same effect by including a redox couple in the electrolyte to set up the required potential?

The experiments covered a fair range of additives and concentrations. The results tended to be somewhat erratic and for this reason are not described in detail, but the main findings are given below. The bulk of the experiments were made with 3F sensors.

Initially solutions of chromic acid or ceric sulphate in concentrations ranging from 5 to 100 millimolar, in 10N sulphuric acid were tried. These did indeed reduce the hydrogen interference and, above about 15 millimolar,

usually to a low level. However the effect tended to wear off with time, particularly at lower concentrations of additive whilst greater additive concentrations usually produced high persistent base lines which were often accompanied by signal decay and hysteresis during exposures to CO at or above 50 ppm.

MnO_2 solutions surprisingly had only a relatively minor effect in spite of the observed potential mentioned earlier, but, while baselines tended to be slightly increased, no other undesirable side effects were usually produced.

It was clear that low concentrations became depleted, e.g. the oxidised species will tend to become reduced both by reduction by the platinum surface and by reduction by any oxidisable impurities present or even by CO from ambient air and test gases. We therefore tried the use of medium concentrations of 10 to 20 millimolar, chromic oxide or ceric sulphate, which had given good hydrogen suppression without excessive base lines, coupled with a reserve of solid manganese dioxide in the electrolyte reservoir. The idea was that the manganese dioxide would continually reoxidise the soluble redox couple back to the 1.4 volt potential equivalent. This approach did in fact keep the hydrogen interference low, but problems with high baselines and hysteresis at higher CO levels were still present.

The source of these problems can be explained in general terms as follows.

The soluble redox couple is of course all-pervading and will raise the potentials of the counter and reference electrodes as well as the sensing. At say 1.4 volts the counter electrode cannot work off oxygen reduction and so perforce has to work off the redox couple, which will be reduced, the reduced species can then diffuse to the reference electrode and lower its potential. The reference is controlling the sensing electrode potential so this is lowered and leads to side reactions e.g. surface oxide reduction or redox additive reduction at this electrode which will give cathodic currents subtracting from the anodic CO oxidation current, i.e. one will get a decaying signal and negative hysteresis on recovery. It will also be seen that any differences in the oxidation state of the redox couple between the sensing and reference electrodes can lead to a high baseline.

It can also be seen that the more active the redox couple (i.e. the faster its oxidation/reduction reaction) the more marked can be these perturbations. It is significant that the manganese redox reaction is very slow and the manganese addition on its own did not produce significant side reaction effects; the chromium and cerium couples are very much faster and did.

In general one seems to be caught between conflicting requirements. A slow couple will not give the desired suppression of hydrogen interference, a fast couple will, but will produce the undesirable side effects mentioned.

It was therefore concluded that this approach would not give a satisfactory solution to the hydrogen interference problem at least with the present system.

6. IN-BOARD CHEMICAL FILTER

6.1. Introduction

The concept of in-board chemical filtering was introduced in the last report (CTL report 82/09/007, September 1982, pp. 48 to 50) and is the subject of CTL patent applications (e.g. European patent application No. 83302609.9). During this report period effort has been concentrated on developing suitable hardware and filter materials. No suitable candidate materials have yet emerged for the selective removal of hydrogen in the presence of CO, but selective filters have been developed for sulphurous gases (i.e. SO_2 and H_2S) and a hydrocarbon filter is under evaluation by the N.C.B. Filter materials have also been developed which selectively oxidise CO for use in a hydrogen sensor.

6.2. Hardware

6.2.1. "Interposed Segment" Design

This design, which was intended to be fully demountable for servicing the filter, is shown schematically in Figure 6.1. An extra annular section is bolted between the baseplate and capillary plate of a standard sensor as shown. Filter material is contained within this segment between the electrode sandwich and a ptfe membrane, pressure bonded to

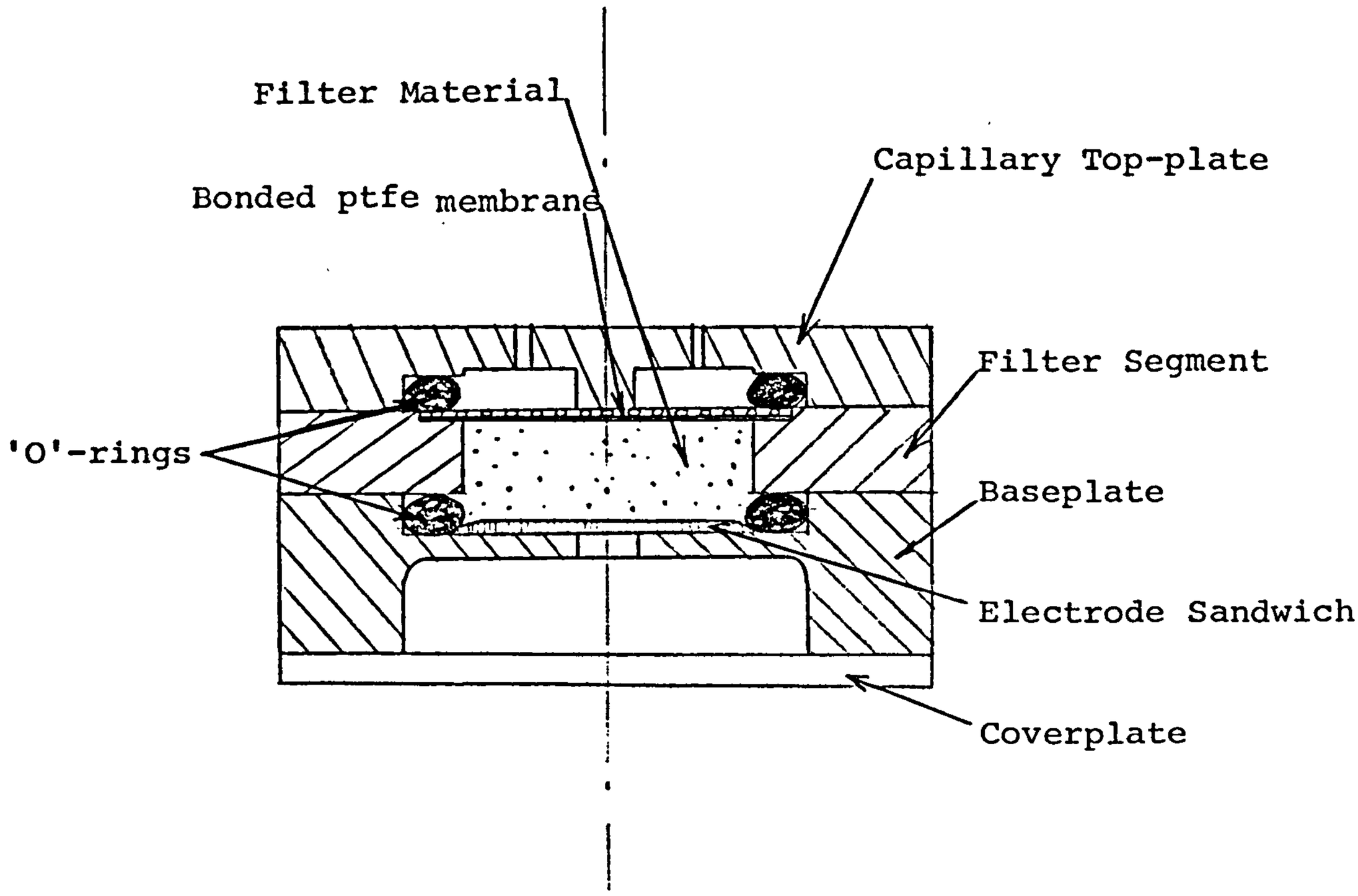

Figure 6.1. Schematic Diagram of Interposed Segment In-Board Filter Design

a nickel mesh. The capillary top-plate can be unbolted and detached to service the filter, without loosening the segment/baseplate bolts which maintain the electrode sandwich seal.

In their present form, sensors would need to be returned to CTL for servicing of the filters, since great care must be exercised in removing and replacing the filter material in order to avoid damaging the electrode sandwich. User servicing would be possible if the filter material could be contained in a suitable replaceable cartridge.

This filter design introduces a significant amount of dead volume into the space between the capillaries and electrodes which results in extended response time, for example (See Table 6.1.a.).

Sensor 2T/X34, fitted with a standard top plate, containing 5 x 1.05mm diameter capillary holes, had a 90% response time of 17 seconds on a 1Ω load, with a slope of about 0.22 seconds per ohm between 0 and 51 ohms.

The same sensor, fitted with a filter segment, without any filter material, had a 90% response time of 42 seconds on 1Ω load with the same slope of 0.22 seconds per ohm between 0 and 51 ohms.

The response time was unaffected on filling the filter segment with an MnO_2 catalyst.

Table 6.1.a. Response time measurements on sensor 2T/X34 with in-board chemical filters

Sensor 2T/X34 : - top-plate 5 x 1.05 mm dia. capillary holes
- interposed segment filter, 1g of 10:1 MnO_2 to ptfe mix (i.e. 0.91g MnO_2)
- age when tested, 2 weeks

Sensor Configuration	Baseline (μA)	CO-sensitivity @ 53.3 ppm (μA/ppm)	Load Resistor (Ω)	90% Response Time (s)
As above	0.12	0.087	1	42
	0.12	0.088	10	43
	0.20	0.088	22	46
	0.12	0.087	51	52
MnO_2 mix removed	0.22	0.090	1	42
	0.21	0.089	51	53
Bonded ptfe membrane removed	0.23	0.091	1	42
	0.21	0.090	51	53
Segment and top plate replaced with standard top plate only	0.21	0.094	1	17
	0.20	0.092	51	29
Top plate replaced with cavity filter, containing 0.55g of 10:1 MnO_2 to ptfe (0.50g MnO_2), 6 x 1.28 mm holes	0.22	0.092	1	17
	0.22	0.092	51	28

Table 6.1.b. Response time measurements on
Sensor 2T/X33 with in-board chemical filters

Sensor 2T/X33: - top-plate 5 x 1.05 mm dia. capillary holes

- interposed segment filter, 0.65g of 10:1 active carbon to ptfe mix (i.e. 0.59g carbon)
- age when tested, 2 weeks

Sensor Configuration	Baseline (μA)	CO sensitivity @ 53.3 ppm (μA/ppm)	Load Resistor (Ω)	90% Response Time (s)
As above	0.10	0.094	1	60
	0.10	0.094	10	62
	0.05	0.095	22	65
	0.10	0.094	51	70
Carbon mix removed	0.17	0.097	1	36
	0.12	0.097	51	45
Bonded ptfe membrane removed	0.13	0.098	1	36
	0.11	0.098	51	46
Segment and top plate replaced with standard top plate only	0.15	0.101	1	13.5
	0.12	0.101	51	27
Top plate replaced with cavity filter containing 0.395g of 10:1 carbon to ptfe (0.36g carbon), 6 x 1.28 mm holes	0.20	0.126	1	27
	0.20	0.125	51	38

A second sensor, 2T/X33 produced the following characteristics (See Table 6.1.b):

90% response time when fitted with a standard top plate, 13.5 seconds on a 1Ω load, with a slope of about 0.22 seconds per Ω.

90% response time when fitted with a blank segment filter, 36 seconds on a 1Ω load, with a similar slope.

On filling the segment with an activated carbon filter the response time further increased to 60 seconds on 1Ω load, unlike the MnO_2 material which had no effect. (See section 6.3.4. for a discussion of the effect of filter material on response time.)

Another design option consists of bonding the filter material to a ptfe membrane. This arrangement can produce a faster response and could be user-serviceable, but lacks filter capacity.

6.2.2. Top-Plate Cavity Filter

In this design the filter material is lightly tamped into the top-plate cavity. Thin ptfe tape lines the cavity to protect the capillaries from blockage and another membrane on the top-plate underside contains the filter material within the cavity.

This design produces a much faster response than the "Interposed Segment" type, for example (See tables 6.1.a. and 6.1.b):

Sensor 2T/X33, fitted with a filter segment, containing 0.59 g activated carbon, had a 90% response, on a 1Ω load of 60 seconds. On replacing the filter segment with a cavity, top plate filter, containing 0.360 g activated carbon, the measured response time was 27 seconds.

Sensor 2T/X34, fitted with a segment filter, containing 0.91 g MnO_2, had a 90% response, on a 1Ω load of 42 seconds. Replacement of the segment with a cavity filter top plate containing 0.50 g MnO_2, resulted in a response time of 17 seconds, identical to the standard top plate without any filter (See Section 6.3.4. below).

Both sensors' response times varied virtually linearly with load resistor between 0 and 51 ohm, with a slope of about 0.20 to 0.30 s per ohm.

The cavity filter design however, has the following disadvantages when compared with the segment filter design:

(a) About half the filter capacity

(b) Is not readily demountable, since removal of the top-plate may loosen the electrode sandwich seal.

(c) Not readily compatible with temperature compensation sleeves.

6.3. Filter Materials

6.3.1. Formulation of filter materials

Filter materials were blended with ptfe dispersion, dried and cured at 280°C. The ptfe binds and immobilises the loose powders and produces a composite with improved diffusibility. Powder to ptfe ratios were normally 10:1.

A great deal of filter material evaluation has been conducted during this report period and for the sake of brevity only the more successful results are reported here.

6.3.2. Removal of sulphurous gases

Originally developed for flue gas sensors where SO_2 interference is a problem, but may also have some relevance to 2T applications. Filters comprise MnO_2 as the active element which removes SO_2 and H_2S by oxidation and salt formation. A number of possible chemical reactions may occur, for example:

(i) Formation of Mn(III) oxide and sulphate

$$3\ SO_2 + 6\ MnO_2 \rightarrow 3\ SO_3 + 3\ Mn_2O_3$$

$$Mn_2O_3 + 3\ SO_3 \rightarrow Mn_2(SO_4)_3$$

$$3\ SO_2 + 6\ MnO_2 \rightarrow Mn_2(SO_4)_3 + 2\ Mn_2O_3$$

(ii) Formation of Mn(III) oxide and sulphite

$$SO_2 + 2\,MnO_2 \rightarrow SO_3 + Mn_2O_3$$

$$Mn_2O_3 + 3\,SO_2 \rightarrow Mn_2(SO_3)_3$$

$$4\,SO_2 + 2\,MnO_2 \rightarrow Mn_2(SO_3)_3 + SO_3$$

(iii) Participation of aerial oxygen

$$8\,SO_2 + 4\,MnO_2 + 3\,O_2 \rightarrow 2\,SO_3 + 2\,Mn_2(SO_4)_3$$

$$\text{or } 3\,SO_2 + 2\,MnO_2 + O_2 \rightarrow Mn_2(SO_4)_3$$

(iv) Catalytic oxidation via Mn(II) compounds

$$2\,Mn_2O_3 + 2\,SO_2 \rightarrow 4\,MnO + 2\,SO_3$$

$$4\,MnO + O_2 \rightarrow 2\,Mn_2O_3$$

$$2\,SO_2 + O_2 \rightarrow 2\,SO_3$$

On the basis of the first 3 reactions above, filter capacity would be determined by an SO_2 : MnO_2 stoichiometric ratio of between 0.5 and 2 to 1. If the latter Mn(II) reactions occur to any significant extent, filter capacity would be considerably greater in aerobic conditions.

A 3F sensor was assembled with a top-plate cavity filter, containing 0.45g of 10:1 mixture of MnO_2 and ptfe (i.e. 4.7 millimoles MnO_2) and subjected to continuous exposure to a 1000 ppm SO_2 in air gas stream. The theoretical capacity based on 100% MnO_2 utilisation, according to reaction (i) above, was 244 days in 1000 ppm SO_2 (calculated capillary current for SO_2 at this concentration was 22μA).

Considerably longer filter life would be expected if any of the other reactions were involved to any significant extent. So far the sensor has completed 63 days at 1000 ppm SO_2 without any significant signs of SO_2 breakthrough (Table 6.2.).

6.3.3. Removal of CO (Hydrogen Sensor)

Whilst a selective H_2 - removal filter material has not yet been found, several materials selectively remove CO in the presence of H_2. Such a filter, incorporated in a sensor, can then form the basis of a specific H_2 sensor. A silver oxide/MnO_2 mixture (1:1 by weight) was finally selected for use in a sensor, which appears to catalyse the oxidation of CO by air in much the same way as Hopcalite, but which has considerably more resistance to deactivation by water vapour absorption. Precious metals such as Pt and Pd or platinised and palladised alumina are equally effective substitutes to the silver oxide, but are considerably more expensive.

Examples of hydrogen sensor characteristics are as follows:

(a) Three-electrode sensor 3HY(P3)

- Top-plate : 4 x 1.05 mm dia. uncompensated capillaries, no centre support.
- Filter : Interposed segment, containing 0.873g mixture of 1:1 by weight Ag_2O/MnO_2 with ptfe in the ratio 4:1.

Table 6.2. Endurance test of sensor 3F/P99 on continuous exposure to 1000 ppm SO_2 in air

Time (days)	SO_2 concentration (ppm)	SO_2 exposure (ppm SO_2 days)	Baseline (μA) (μA/ppm)	CO - sensitivity @ 227 ppm		H_2 - sensitivity @ 100 ppm		SO_2 - sensitivity @ 1000 ppm	
				(μA/ppm)	% initial	μA/ppm	% cross interference	μA/ppm	% cross interference
0	-	-	-0.32	0.0361	100	-	-	-	-
9	500	4,500	-0.23	0.0356	99	-	-	-	-
16	500	8,000	-0.16	0.0368	102	-	-	-	-
20	500	10,000	-	-	-	-	-	-	-
34	1,000	24,000	-0.10	0.0352	98	0.027	77	-	-
58	1,000	48,000	0.00	0.0338	94	0.026	78	0.0003	0.9
66	1,000	56,000	-0.02	0.0344	95	0.026	75	0.0004	1.2
73	1,000	63,000	+0.10	0.0350	97	0.029	84	0.0006	1.8
76	1,000	66,000	+0.10	0.0350	97	-	-	0.0007	2.0

- Sensing electrode: 2T anode
- Reference: 10mm dia. disc cut from 10mg Pt/cm² material.
- Counter: 10 mm dia. central hole

Sensor behaviour, 4 days after manufacture (Sent to NCB Scottish Regional Laboratory for further evaluation)			
Baseline @ 20°C (μA)	H_2 Sensitivity measured @ 100 ppm (μA/ppm)	CO Cross sensitivity measured at 227 ppm (% H_2 equivalent)	CO cross sensitivity measured at 539 ppm (% H_2 equivalent)
- 0.8	0.063	0.7	3.3

(b) Two-electrode sensor 2HY(P5)

- Top plate: 4 x 1.05mm dia. uncompensated capillaries, no centre support.
- Filter: Interposed Segment, containing 0.850g 1:1 by weight Ag_2O/MnO_2 with ptfe in the ratio 4:1
- Sensing electrode: 2T anode
- Counter electrode: 2T anode (7mm dia. central hole)

Sensor behaviour, 4 days after manufacture Sent to NCB East Midlands Laboratory for further evaluation			
Baseline @ 20°C (μA)	Hydrogen Sensitivity measured at 100 ppm (μA/ppm)	CO cross sensitivity measured at 227 ppm (% H_2 equivalent)	CO cross sensitivity measured at 559 ppm (% H_2 equivalent)
0.09	0.0220	0.4	4.0

Note: The counter electrode could not be completely protected from hydrogen access and some cancellation occurred, even with polythene barriers between the electrodes. This cancellation, together with scavenging and oxide reduction effects due to cathode polarisation, and a less reactive sensing electrode surface due to a positive baseline, would account for the much lower hydrogen sensitivity, compared to the 3-electrode sensor 3HY(P3).

(c) Batch of five two-electrode sensors

All five sensors (2HY1 to 2HY5) were constructed as sensor 2HY(P5) above. The characteristics of each sensor, monitored with time in a laboratory atmosphere, are given in Table 6.3.

Carbon monoxide cross sensitivities of hydrogen sensors were low up to concentrations of 500 to 600 ppm: no tests

Table 6.3. Characteristics of Two-Electrode Hydrogen Sensors as a Function of Age

(Hydrogen sensitivities measured @ 100 ppm, CO sensitivities @ 227 ppm)

Sensor	Characteristic	Week No. from manufacture					
		0	1	2	3	4	5
2HY1	Hydrogen Sensitivity (µA/ppm)	0.0240	0.0234	0.0223	0.0175	0.0203	0.0193
	Hydrogen Sensitivity (% initial)	100	98	93	73	85	80
	CO cross sensitivity (% H_2 equiv.)	0.8	nil	0.6	2.9	1.7	1.6
	Baseline (ppm H_2 equiv.)	2.5	1.3	nil	nil	nil	-1.0
2HY2	Hydrogen Sensitivity (µA/ppm)	0.0281	0.0250	0.0228	0.0197	0.0235	0.0194
	Hydrogen Sensitivity (% initial)	100	89	88	70	84	69
	CO cross sensitivity (% H_2 equiv.)	2.2	1.0	2.0	6.7	3.6	5.0
	Baseline (ppm H_2 equiv.)	2.1	2.0	0.9	nil	nil	-0.9
2HY3	Hydrogen Sensitivity (µA/ppm)	0.0290	0.0263	0.0247	0.0218	0.0228	0.0210
	Hydrogen Sensitivity (% initial)	100	91	85	75	79	72
	CO cross sensitivity (% H_2 equiv.)	1.1	1.5	1.6	4.0	3.5	2.8
	Baseline (ppm H_2 equiv.)	4.5	2.7	0.8	0.9	1.0	1.4
2HY4	Hydrogen sensitivity (µA/ppm)	0.0253	0.0232	0.0194	0.0192	0.0197	0.0182
	Hydrogen sensitivity	100	92	77	76	78	72
	CO cross sensitivity (% H_2 equiv.)	0.7	1.3	1.8	2.5	2.7	2.7
	Baseline (ppm H_2 equiv.)	3.6	1.7	1.0	1.0	nil	1.1

Table continued .....

Sensor	Characteristic	Week No. from manufacture					
		0	1	2	3	4	5
2HY5	Hydrogen sensitivity (µA/ppm)	0.0230	0.0230	0.0194	0.0187	0.0197	0.0180
	Hydrogen sensitivity (% initial)	100	100	84	81	86	78
	CO cross sensitivity (% H_2 equiv.)	2.3	1.7	4.1	7.0	5.8	5.0
	Baseline (ppm H_2 H_2 equiv.)	5.4	3.9	2.1	1.6	3.0	2.2

have yet been conducted at higher CO concentrations.

Hydrogen responses included a large measure of electrode activity control, i.e. activity reserve factors were very low see CTL report 82/09/007, September, 1982, Appendix 3). This would account for the abnormally high signal decay in the first few weeks of service. Hydrogen responses were also fairly sensitive to ambient temperature, as expected with a low activity reserve, although no actual measurements of span temperature coefficient have yet been made.

Hydrogen activity reserve, and hence the amount of capillary control on the signal, can be increased by using smaller, more restrictive capillaries, which in turn reduces the sensitivity. Also electrode activity may be enhanced, for example by optimising electrode composition and running at a negative baseline. Any increase in electrode activity reserve by either restricting the capillaries or boosting electrode performance would result in more complete hydrogen oxidation at the sensing electrode and reduce signal cancellation due to hydrogen accessing the counter.

6.3.4. Active Carbon Filter

Active carbon has been shown qualitatively to remove some organic vapours, e.g. alcohols. It may also remove some unsaturated hydrocarbons, sulphurous gases and oxides of nitrogen. No specific tests have yet been conducted at CTL with this material, but sensors incorporating active carbon

filters have been supplied to NCB East Midlands for evaluation.

The active carbon used for filters in CTL CO sensors produces a lengthening in response time, probably as a result of adsorption reactions introducing a significant retention time into the filter. For example (See Tables 6.1.a and 6.1.b):

Sensor 2T/X33, fitted with segment and cavity filters, containing 0.59 and 0.36g carbon respectively, had 90% response times, on a 1Ω load, of 60 and 27 seconds respectively. The corresponding responses with empty segment and standard top plate were 36 and 13.5 seconds respectively.

Sensor 2T/X34, fitted with segment and cavity filters, containing 0.9l and 0.50g MnO_2 respectively, had 90% response times, on a 1Ω load, of 42 and 17 seconds respectively. Corresponding responses with empty segment and standard top plate were also 42 and 17 seconds respectively.

Thus it would seem that the carbon material introduces something of the order of 35 to 40 seconds per gram.

MnO_2 had no apparent effect on response time. However, the powder must have represented some restriction to gas diffusion which exactly balanced the dead space effect in the sensor without filter material (See Section 6.2.1.).

7. OPERATION OF 2T SENSORS IN HIGH RELATIVE HUMIDITY

This study was undertaken at the request of the N.C.B. and was reported in C.T.L. Technical Note Number 22 which is reproduced below.

City Technology Limited

17/19 Sebastian Street, London. EC1V 0HB

Telephone 01-253-3799. Telex 263896

TECHNICAL NOTE NUMBER 22

Operation of 2T Carbon Monoxide Sensors in High Relative Humidity

B.S. Hobbs
G.G. Amabilino

1 November 1982

Operation of 2T Carbon Monoxide Sensors in High Humidities

In conditions of high humidity, sulphuric acid electrolyte absorbs water until its vapour pressure equals that of the atmosphere. The relationship between sulphuric acid concentration and relative humidity is shown in Figure 1.

Water uptake by a sensor only has a harmful effect if the volume increase exceeds the available free space in the sensor reservoir when leakage may occur. Standard 2T sensors are primed with $1cm^3$ of 10.3N sulphuric acid and are fitted with a pressure release system to expel displaced air as the sensor absorbs moisture[1]. The free space within the sensor reservoir amounts to about $2cm^3$ and if this were fully utilisable, continuous operation would be possible in relative humidities up to about 93.5%. The sensor can tolerate excursions at higher humidities for times governed by the rate of water ingress into the electrolyte reservoir.

Water transfer rates between the interior of CTL sensors and the outside environment follow fairly closely the theoretical relationship for control by diffusion through the sensor capillaries[1]:

---

(1) A.D.S. Tantram, R. Chan Henry, B.S. Hobbs; Phase 4 Report to NCB Contract No. Y135007/09/21, CTL Report No. 82/09/007 (September 1982)

$$t_{(T)}\,(\text{days}) = \frac{1}{16.713.10^{-3}\ n\ d^2\ p_{H_2O}} \int_o^W \frac{\partial W}{R_H - R_{H_e}} \qquad (1)$$

where: t is the time in days to transfer a volume of water W cm^3 at a constant temperature T

l is the capillary length (cm)

n is the number of capillaries

d is the capillary diameter (cm)

p_{H_2O} is the saturated vapour pressure of water at temperature T (torr)

R_H is the external environment relative humidity

R_{H_C} is the sensor electrolyte relative humidity

The law governing the relative humidity of aqueous sulphuric acid solutions is complex (Figure 1) and integration of the right hand term in equation (2) is not easily accomplished. Instead a stepwise method is used in which average values of R_{H_e} are taken for a number of small volume increments (∂W) and the estimated times summed separately.

A "Basic" program was written for a Commodore PET 8032 microcomputer, to estimate maximum residence times of CTL 2T sensors using equation (1) above, in both moist and dry conditions - in the latter case water loss limits are set by the need to maintain at least 0.4cm^3 electrolyte for the sensor to operate and to avoid electrolyte concentrations greater than 20N to prevent deterioration of the glued seals

---

(2) A.D.S. Tantram, R. Chan Henry, B.S. Hobbs; Phase 3 Report to NCB Contract No. Y135007/09/21, CTL Report No. 81/31/006 (July 1981)

and plastic hardware[2]. The computer program was menu-driven, requesting values of the various parameters, from which it calculated the time to reach a given condition of water loss (or gain) from an initial starting point. Individual parameters could be altered and times recalculated. Results could be stored and printed out as required. Solutions of equation (1) were made assuming the sensor was fitted with capillary inserts which achieved perfect temperature compensation. In this situation p_{H_2O} was the only temperature dependent term.

Calculations of 2T sensor residence times in high humidities were carried out with the following fixed parameter values:

Capillary length	3mm
Capillary diameter	1.5mm
No. of capillary holes	5
Temperature	$35^{o}C$
Water vapour pressure (p_{H_2O})	42.175 torr
Initial electrolyte volume	$1cm^3$
Number of volume increments (∂W)	100

Residence times were estimated as a function of atmospheric relative humidity between 90% and 100% for initial concentrations of 10.3N (Standard), 7N and 5N and assuming (a) 80% available space utilisation (final volume $2.6cm^3$) and (b) 95% utilisation (final volume $2.9cm^3$). The results, depicted graphically in Figure 2, indicated that a standard sensor

could withstand 100% relative humidity, at 35°C, for a period between 43 and 60 days, depending on the utilisation of available space. By priming with more dilute electrolyte the 100% humidity residence time could be increased, eg. up to 165 days with $1cm^3$ 5N acid, at 95% space utilisation. Continuous exposures up to 96% and 97.5% R_H may be possible with $1cm^3$ of 7 and 5N priming acids respectively.

5N sulphuric acid is the most dilute electrolyte which could be used without incurring any storage problems at normal ambient humidities of about 50%. At such humidities the sensors would lose water until the electrolyte achieved about 12N concentration. The electrolyte volume of 5N, $1cm^3$ charge would then be $0.42cm^3$, just enough to enable the sensor to operate. The time to reach this condition at 20°C is estimated to be about 28 days. Extended operation in 100% R_H would be possible by using more dilute electrolyte charges, but precautions would be needed to prevent drying-out on storage, or in the event of periods of low humidity during operation. For example, a sensor charged with $1cm^3$, 2N acid would have a life in excess of 1 year at 35°C, 100% R_H, but would cease to operate within about 12 days if stored at 20°C in 50% R_H. Dried out sensors can be restored to operation by re-exposure to moist conditions[2].

The only other way to extend residence times in high humidity would be to build in extra reservoir volume. However, this would mean redesigning the sensor hardware.

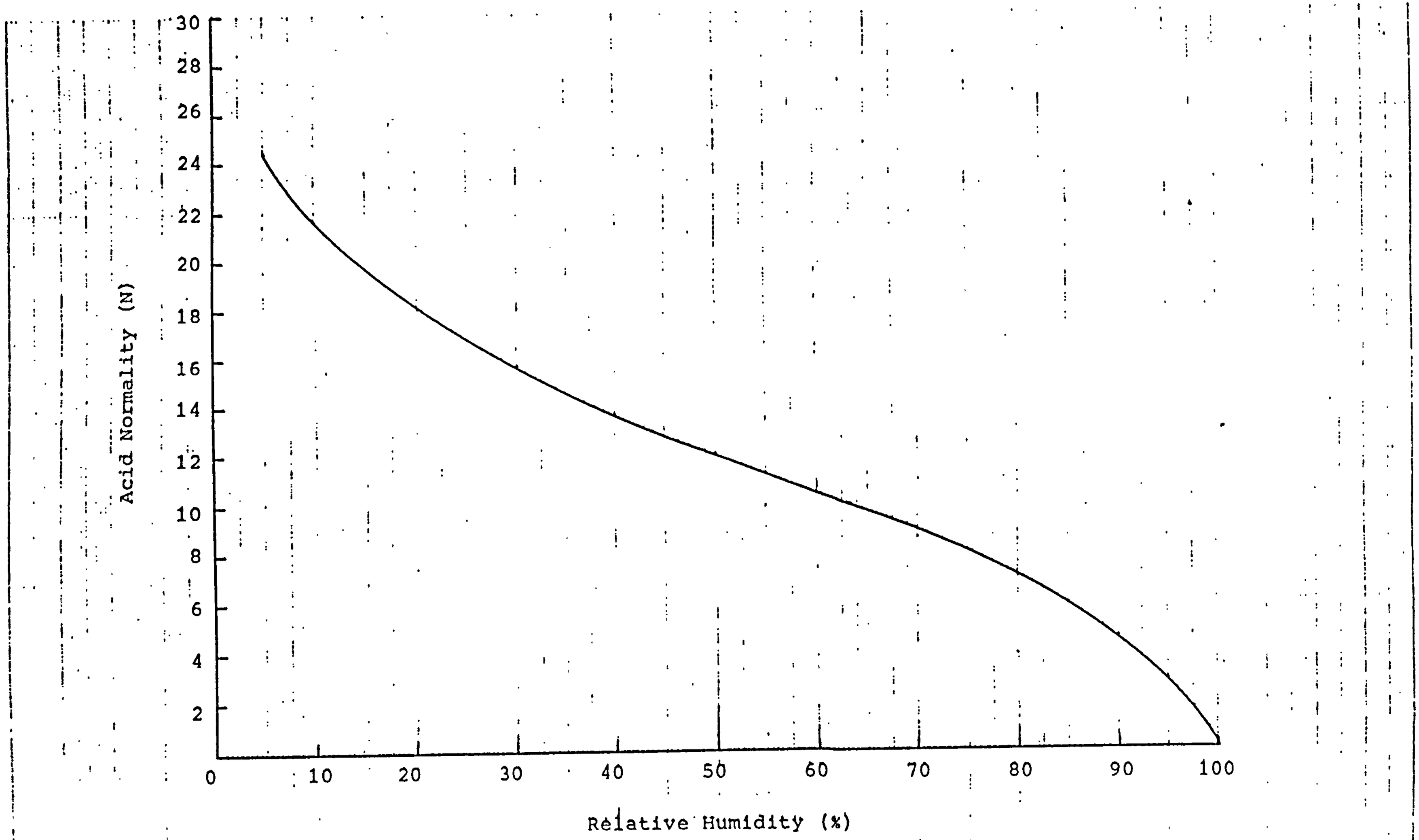

Figure 1. Relative Humidity of sulphuric acid solutions as a function of composition.

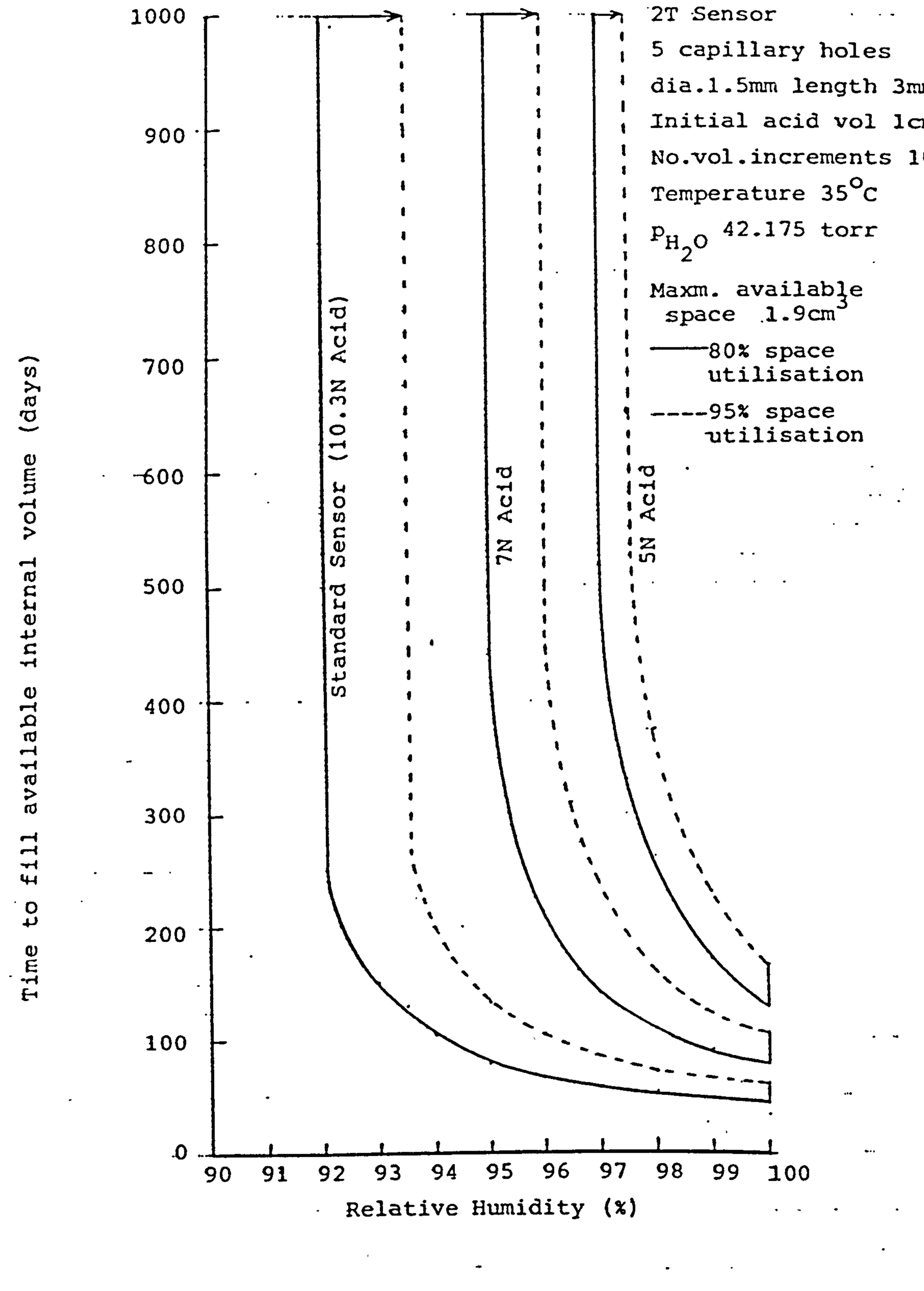

Figure 2. Residence times of 2T sensors in high humidity at 35°C.

APPENDIX

TRANSIENT SHORT CIRCUIT SIGNALS IN CTL 2-ELECTRODE TRACE SENSORS

City Technology Limited

17/19 Sebastian Street, London. EC1V 0HB

Telephone 01-253-3799. Telex 263896

TECHNICAL NOTE NO. 17

"TRANSIENT SHORT CIRCUIT SIGNALS IN CTL

2-ELECTRODE TRACE SENSORS"

J.H. Gilby

July 1982

Abstract

A Preliminary investigation of the transient voltages and currents produced by a CTL Trace sensor, which has been exposed whilst open circuit to carbon monoxide, when it is shorted out.

Background

BS5501 Relates to the construction and testing of electrical apparatus for use in potentially explosive atmospheres. Paragraph 1.3 of the General requirements states that:-

"Devices in which, according to the manufacturers specifications, none of the values 1.2V, 0.1A, 20μJ or 25 mW is exceeded need not be certified or marked".

Obviously it is of interest to establish whether the CTL Carbon Monoxide sensor will meet these requirements. The worst case envisaged is that the sensor is exposed to carbon monoxide whilst open circuit in which case the potential across it will rise. Whilst in this condition it is shorted out.

Testing Details

A 2-electrode Trace Sensor is exposed to carbon monoxide via its capillaries. The Potential across the sensor rises and when it is at a maximum the terminals are shorted out using a Potentiostat. A Mercury wetted relay triggered via a toggle switch was used as a bounce free switch to load the sensor with the Potentiostat. The sensor

current and voltage were monitored using a Datalab DL902 Transient recorder. This can take 2048 8-bit samples with a maximum sample rate of 1µsec per sample. The Potentiostat was a "Ministat" made by H.B. Thompson (s/n 07379/9).

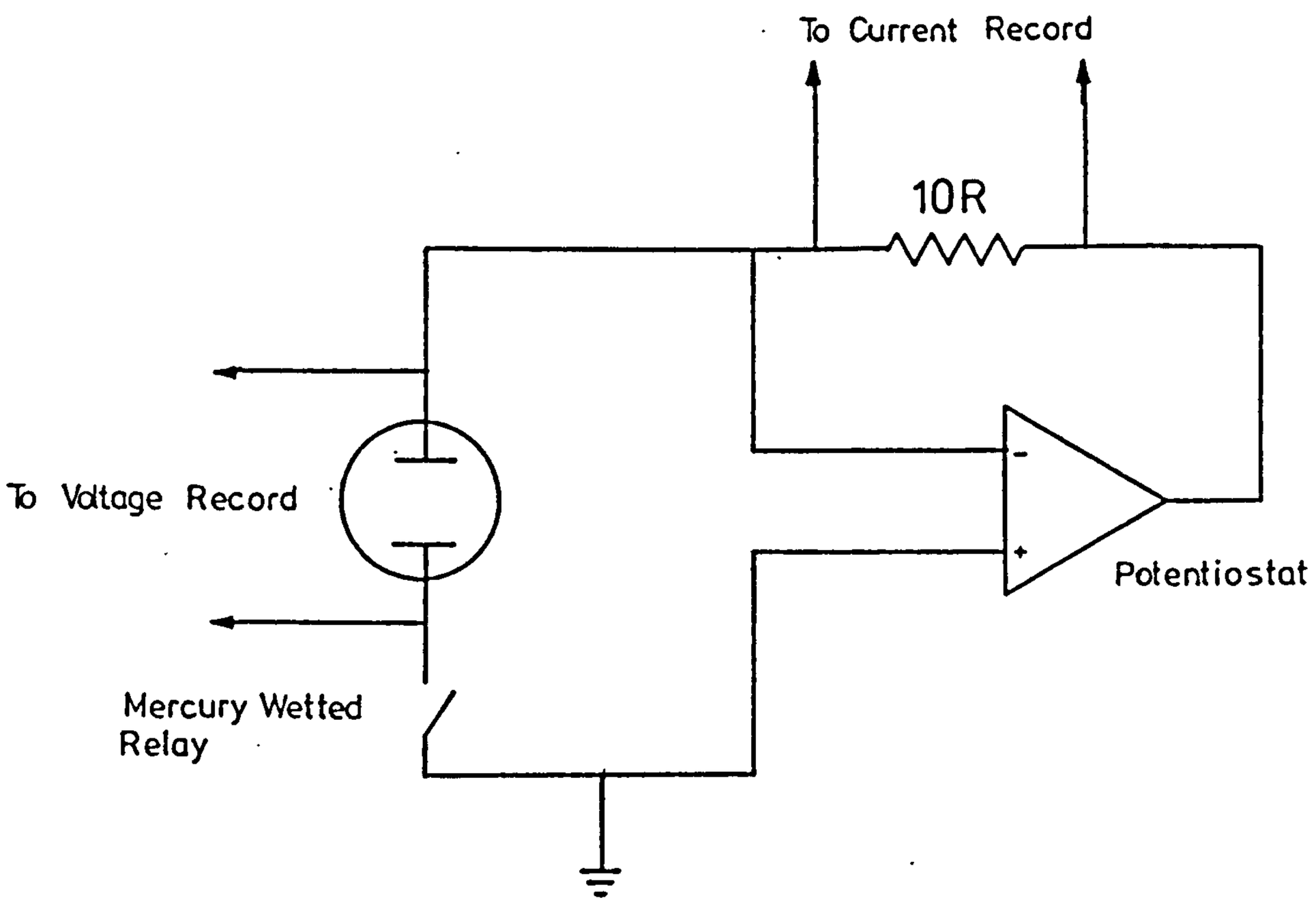

Results

The Potential across the sensor rises with increasing gas concentration. At 1000 ppm values of approximately 120mV were measured. On continual long exposure the potential drops away as carbon monoxide filters through to the Counter Electrode (See Graph 1 for example). In view of this the run was made at the point of maximum OCV.

Graphs 2 to 6 show typical results at a resolution of 0.2 milliseconds per sample. Graph No. 7 is taken at the maximum resolution of 1 μsec per sample to check that no sudden transient signals have been missed.

As can be seen the voltage is at a maximum at the same time as the current so these maximum values have been multiplied together to give the peak power.

The total energy that can be transfered into any external load is the product of the voltage across the load, the current through it and the time. Since the short circuit eventually produces zero volts across the sensor it does not matter that a current is still flowing since this cannot do any work across a zero potential difference. The values of energy transferred in the table below have been calculated by simpsons rule from the product of the instantaneous voltages and currents.

Table of Results

Sensor No.	Peak Current (mA)	Peak Voltage |Equals OCV| (mV)	Peak Power (mW)	Energy Transfer into Short (mJ)	Test Gas (ppm)
2T P62	47	54	2.5	-	500
2T 141	104	100	10.4	0.13	1000
2T 140	144	118.6	17	0.11	1000
2T 139	120	115	13.8	0.11	1000
2T 138	88	119	10.5	0.084	1000
2T 137	175	151	26.4	0.25	5000

Finally in order to check that no transient currents had been overlooked a run was made using the fastest sampling rate available (1 μsec per sample) and this is presented as Graph No. 7.

Conclusion

The values of instantaneous voltages found are well below the value of 1.2V quoted in BS5501. However the values of instantaneous current and power and the Total energy transferred are likely to exceed the quoted values if the gas concentration is sufficiently high. Graph 1 shows that the potential across the sensor will drop steadily after reaching its initial maximum, whilst Graph 7 confirms that the sampling rate used for the runs was not masking any short duration transient signals.

GRAPH NO 1

2/7/82

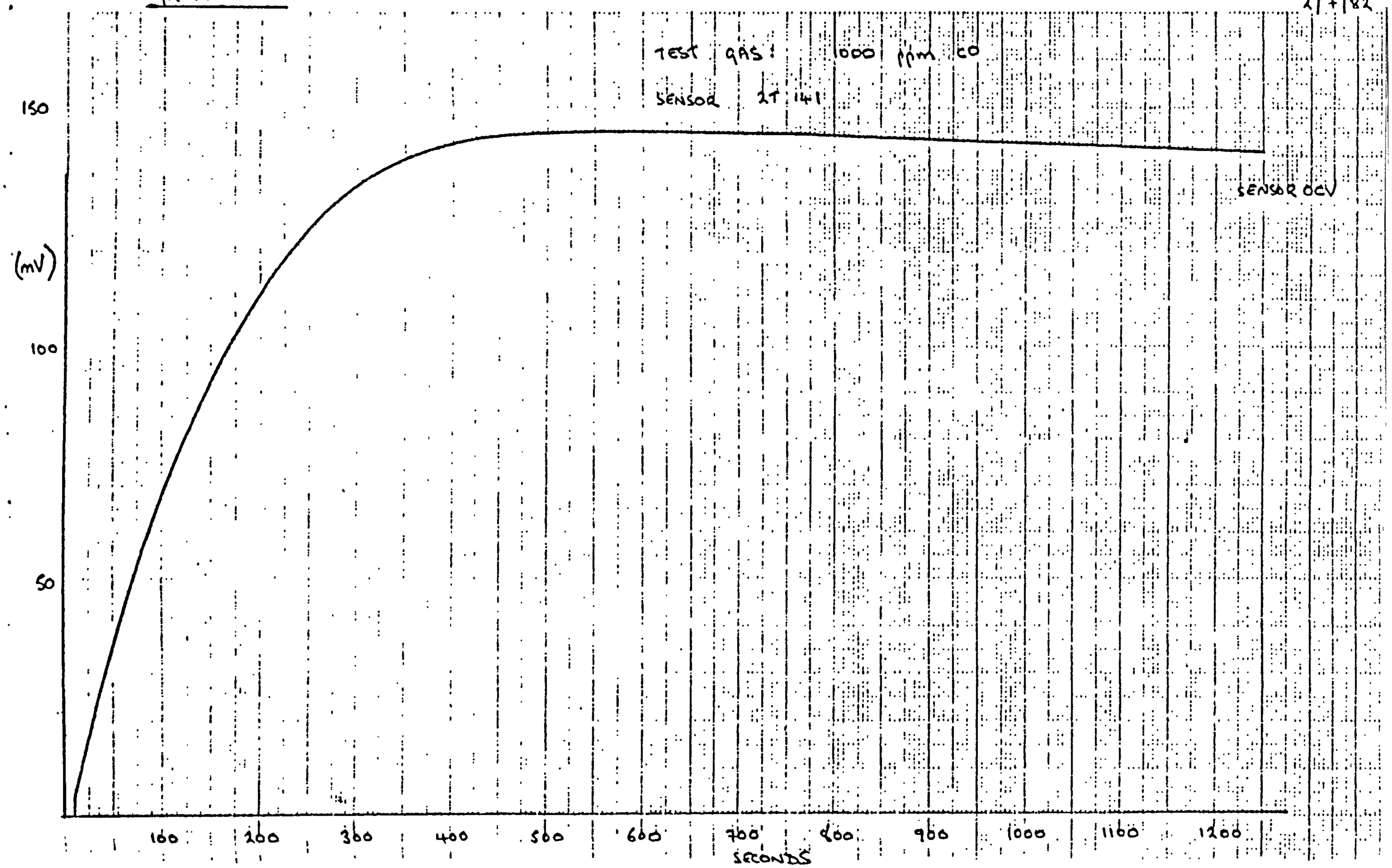

GRAPH NO 2

1/7/82

SENSOR : 2T 141
TEST GAS : 1000 ppm
SAMPLE INTERVAL : 0·2 msec

OCV = 100mV

20mV/cm

100mA

PEAK CURRENT = 104 mA

410msec

GRAPH NO 3

11/7/82.

SENSOR : 2T 140

TEST GAS : 1000 ppm CO

SAMPLE INTERVAL : 0.2 msec

OCV = 118.6 mV

20 mV/cm

100 mA

0

PEAK CURRENT = 144 mA

410 msec

GRAPH NO 4

1/7/82

SENSOR 2T139

TEST GAS : 1000 ppm CO

SAMPLING INTERVAL : 0.2 msec

OCV = 115 mV

20 mV/cm

100 mA

PEAK CURRENT = 120 mA

410 msec

GRAPH NO 5

1/7/82

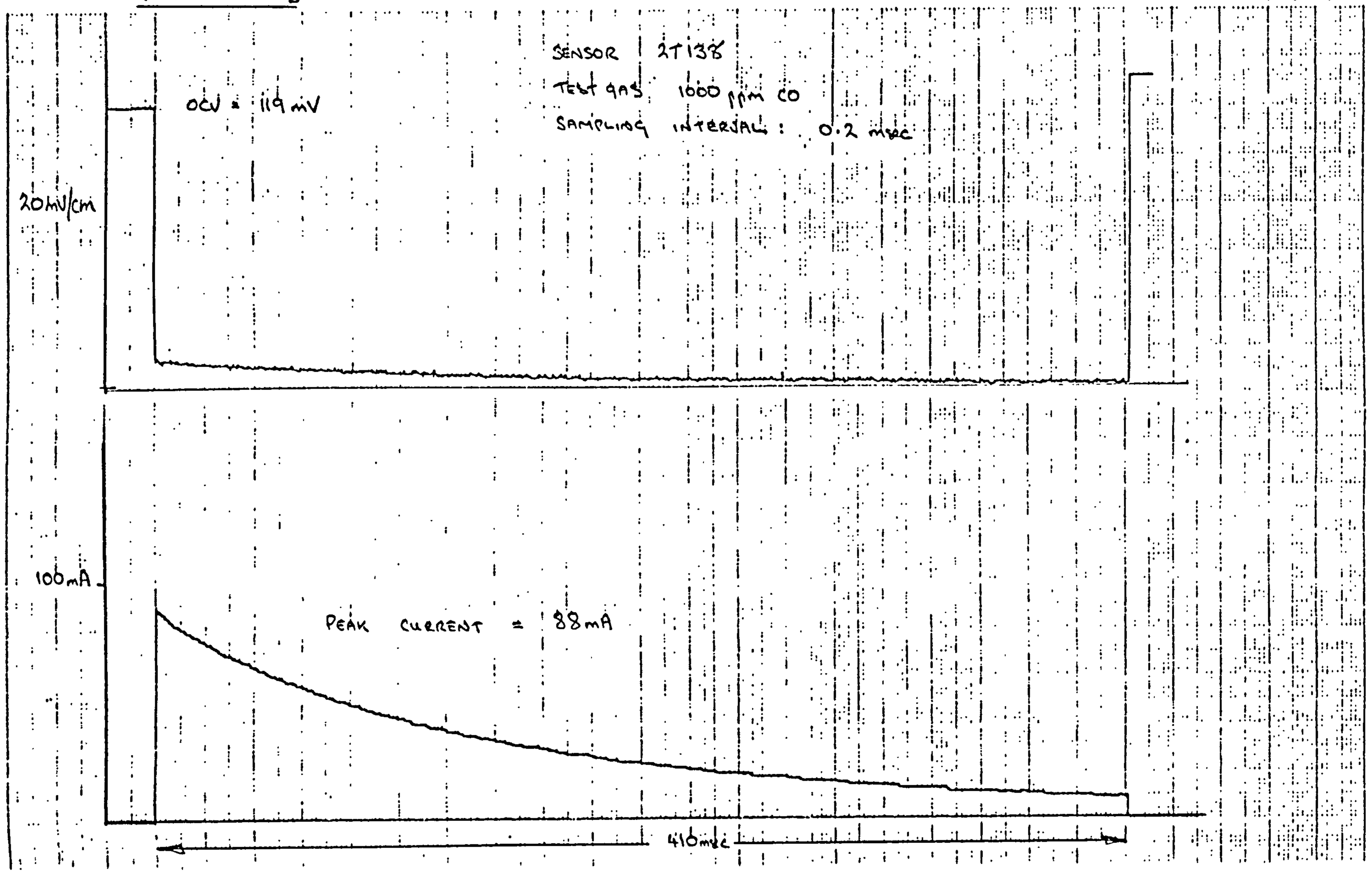

GRAPH NO 6

1/7/92

SENSOR NO : 2T137

TEST GAS : 5000 ppm CO

SAMPLING INTERVAL : 0.2 mSec

OCV = 151 mV

20mV/cm

200

(nA)

100

PEAK CURRENT = 175 mA

410 mSec

GRAPH NO 7

EXPANDED TIMESCALE 1/7/82

SENSOR : 2T141

TEST GAS : 1000 ppm CO

SAMPLING INTERVAL : 1 μsec